Identification of potential novel drivers and biomarkers of CDK4/6 inhibitor resistance in metastatic breast cancer

DISSERTATION

To obtain a doctoral degree (Dr. rer. nat.)

at the Department of Biology

Faculty of Mathematics, Informatics and Natural Sciences

University of Hamburg

Submitted by

Leonie Florence Ott

Hamburg, 2022

This study was conducted from December 2017 to March 2022 at the Institute of Tumor Biology at the University Medical Center Hamburg-Eppendorf under the direction of Prof. Dr. Klaus Pantel and the co-supervision of Prof. Dr. Julia Kehr.

1st Reviewer: Prof. Dr. Klaus Pantel

2nd Reviewer: Prof. Dr. Julia Kehr

Date of oral defense: 06.07.2022

Contents

Summary

Inhibitors of cyclin dependent kinases 4 and 6 (CDK4/6i) have become part of the standard first-line therapy of patients with hormone receptor-positive (HR+) metastatic breast cancer. Despite initial response to the therapy of approximately 90% of patients, resistance is almost inevitable eventually. The search for reliable biomarkers, either predicting therapy response or facilitating response monitoring and indicating emerging resistance early enough to switch to a more effective therapy overcoming this resistance is ongoing. Amplification of the *CCND1* gene or loss of the CDK inhibitor p16 were promising candidates but were not associated with progression-free or overall survival in any clinical trial. Solely loss of the retinoblastoma RB protein or *RB1* mutations are associated with primary and secondary resistance, but they emerge only in a minority of patients with HR+/HER2-negative breast cancer, receiving CDK4/6i therapy (4.7%) [1]. Thus, this thesis aimed to unravel resistance mechanisms and to identify putative new biomarkers to recognize patients not beneficiating from CDK4/6i therapy.

For that purpose, cell culture models were established, providing the opportunity to analyze resistant cells *in vitro* and to identify transcripts, proteins and microRNAs (miRNAs), potentially associated with or involved in the development of resistance. MCF7 cells and a CTC (circulating tumor cell)-derived cell line, CTC-ITB-01, were cultured under contiguous treatment with increasing concentrations of ribociclib for 18 months, and resistance was validated by functional assays, such as cell cycle profiling and identification of IC_{50} values by colony formation and viability assays.

To identify novel biomarker candidates for resistance to ribociclib, whole transcriptome sequencing was performed on parental and ribociclib-resistant cell lines and selected mRNAs or encoded proteins, respectively, as well as one miRNA, were successfully validated. Additional to qPCR, an *in situ* hybridization (ISH) assay for the detection of miRNAs was established, to reliably detect miRNAs and assess spatial heterogeneity of miRNA expression. The compatibility of this ISH assay with immunofluorescent staining and its single cell resolution made it a helpful tool to investigate miRNAs on cultured parental and resistant cells and even on CTCs.

Some deregulated targets, so far not associated with CDK4/6i resistance, such as *SOX9*, miR-146a-5p and a significant number of transcripts, related to epithelial-mesenchymal-transition (EMT) and cancer stemness, were shared by both resistant cell lines. Yet, a higher number of unique deregulated transcripts and miRNAs such as *CDK14*, *ALDH1A1* and miR-205-5p in CTC-ITB-01 cells or *CD44* and miR-675-5p in MCF7 cells were found in each resistant cell line, demonstrating the variety of different processes associated with resistance to ribociclib. Interestingly, potential networks promoting ribociclib resistance were identified for both resistant cell lines. In resistant CTC-ITB-01 cells a potential posttranscriptional regulation of *CDK14* mRNA levels by miR-205-5p cells and a SOX2-SOX9-SLUG axis in resistant MCF7 cells were implied. However, these findings require future experimental validation.

Compared to their parental cells, ribociclib-resistant MCF7 and CTC-ITB-01 cells had also gained mutations, some of which have not been published yet. These included for example mutations in *NF1* and *MAP3K5* in CTC-ITB-01 cells or *NOTCH3* in resistant MCF7 cells.

Cell adhesion was one GO (Gene Ontology) gene set identified to be enriched in resistant MCF7 and CTC-ITB-01 cell line cells. Indeed, the expression of various genes encoding cell adhesion or adhesion-related molecules was deregulated in the ribociclib-resistant cells. In resistant versus parental CTC-ITB-01 cells, amongst others, expression of *LGALS1*, *ICAM1*, *MUC13* and *CLDN1* genes was upregulated, whereas in resistant MCF7 cells, the expression of *ALCAM* and *MUC1* was increased. Expression of *DSC2* was decreased in resistant CTC-ITB-01 and MCF7 cells. Since former microfluidic experiments had already demonstrated a very strong capacity of CTC-ITB-01 cells to adhere to endothelial cells, the adhesive capacity of resistant versus parental cells to endothelial HUVEC cells was compared. While the number of cells adhering to the HUVECs was increased in resistant versus parental MCF7 cells, surprisingly less resistant than parental CTC-ITB-01 cells adhered to the HUVECs. The differences regarding the adhesive capacity of resistant CTC-ITB-01 and MCF7 cells shall be investigated in future experiments.

Moreover, genes encoding EMT- and cancer stemness-related transcription factors such as *SOX9*, *RUNX2* or *OVOL2*, and kinases as for example *AXL*, *DLCK1* or *LYN* with differential expression in resistant versus parental cells were identified. Many kinases represent druggable targets and their inhibition may thus represent a potential treatment option for patients who developed ribociclib resistance.

Since most patients with breast cancer develop resistance to CDK4/6i therapy, finding subsequent therapy options is of great importance. Thus, combined treatment of ribociclib with fulvestrant was tested. The addition of fulvestrant did not influence the viability of CTC-ITB-01 cells and had only a moderate impact on that of MCF7 cells, while the clonogenic growth of parental and resistant CTC-ITB-01 and MCF7 cells was efficiently suppressed.

Mutations in the *PI3KCA* gene encoding the phosphoinositide 3-kinase p110-isoform (PI3Kα) are frequent in HR+ breast cancer and are a precondition for the treatment of these patients with the PI3Kα inhibitor alpelisib. Both MCF7 as well as CTC-ITB-01 cells harbor *PIK3CA* mutations. Thus, inhibition of PI3Kα by alpelisib was tested in parental and ribociclib-resistant cell lines, to find out whether the efficacy of this treatment would be impeded by ribociclib resistance. Treatment with alpelisib as a mono-therapy could effectively reduce cell viability. The combination of both drugs, ribociclib and alpelisib yielded high suppression of not only cell viability but also of clonogenic growth.

Morphological changes to a rounder and apoptotic phenotype implied higher cytotoxicity of alpelisib than that of fulvestrant and ribociclib. Ribociclib arrests cells in G1, resulting in a moderate reduction of cell viability and stronger inhibition of clonogenic growth. Testing β-galactosidase activity by X-Gal staining revealed induction of cellular senescence in parental MCF7 cells upon treatment with solely ribociclib and in combination with alpelisib, whereas only the combination of ribociclib and fulvestrant induced senescence in resistant MCF7 cells. No treatment, tested in this study, induced senescence in any CTC-ITB-01 cell line, suggesting rather induction of reversible quiescence, a characteristic feature of stem cells. Since the ribociclib-resistant cells did not differ in terms of sensitivity to PI3Kα inhibition, the combination of alpelisib and ribociclib apparently represents an effective therapy option in this setting and resensitizes also ribociclib-resistant cells to CDK4/6 inhibition.

In the present study, several candidate biomarkers with potential relevance to indicate resistance to CDK4/6 inhibitors and to characterize CTCs were identified. However, for application in the CellSearch® system (CS), suitable antibodies, positive and negative controls, fluorescence dyes and appropriate concentrations and exposition times have to be tested before clinical application is feasible. While assays to detect SOX9 and CDK6 are still in development, vimentin (VIM) expression can already be determined with the CS [2]. Since ribociclib-resistant cells have gained features characteristic of EMT, CTCs from a heterogeneously treated cohort of patients with metastatic breast cancer of different molecular subtypes were analyzed for the expression of VIM, an early indicator of EMT, with the CellSearch® system. Positivity of VIM identifying epithelial/mesenchymal hybrid cells was detected in blood samples from 67 of 201 patients (33.3%) while 134 of 201 patients (66.7%) only had VIM-negative CTCs. Vimentin-positive CTCs were more frequently detected in patients with triple negative and HER2-positive primary tumors than in patients with HR+-positive metastatic ones ($p=0.0167$). CTCs with mostly weak intensity of VIM-specific immunofluorescence were more frequently observed in blood samples with ≥5 CTCs/7.5 mL blood compared to those with <5 (1-4) CTCs ($p=0.0003$). Interestingly, the percentage of VIM-positive CTCs was not increased during treatment including therapy with CDK4/6 inhibitors. In future studies, CTCs and vimentin expression of CTCs have to be analyzed on larger patient cohorts followed after first-line therapy including CDK4/6 inhibitors.

In conclusion, a set of candidate transcripts, proteins, gene mutations and microRNAs potentially associated with resistance to ribociclib was identified ready to use for further *in situ* and functional characterization as well as validation in clinical liquid biopsy samples.

Zusammenfassung

Inhibitoren der Zyklin-abhängigen Kinasen 4 und 6 (CDK4/6i) sind heutzutage Teil der Standardtherapie beim metastasierten Mammakarzinom. Allerdings ist trotz eines initialen Ansprechens auf die Therapie bei ca. 90% aller Patientinnen das Entstehen einer Resistenz gegenüber diesen Therapeutika nahezu unausweichlich. Daher wird nach zuverlässigen Biomarkern gesucht, die den Erfolg der Therapie vorhersagen oder entstehende Resistenz früh genug anzeigen können, um den Wechsel zu einer wirksamen Therapie zu ermöglichen. Amplifikationen des *CCND1*-Gens oder der Verlust des CDK-Inhibitors p16 galten als vielversprechende Kandidaten, konnten klinisch jedoch nicht mit progressionsfreiem- oder Gesamtüberleben assoziiert werden. Lediglich der Verlust des Retinoblastomproteins (RB) oder Mutationen im *RB1*-Gen sind eindeutig mit primärer oder sekundärer Resistenz gegenüber einer Therapie mit CDK4/6-Inhibitoren assoziiert, wobei die Frequenz der *RB1*-Mutationen, insbesondere bei Patientinnen mit Hormon-Rezeptor-positiven (HR+)-/HER2-negativen Mammakarzinomen unter CDK4/6i Therapie gering ist (4.7%) [1]. Daher war es Ziel dieser Arbeit, Resistenzmechanismen aufzudecken und neue potenzielle Biomarker zu etablieren, mit deren Hilfe Patientinnen, die nicht von einer entsprechenden Therapie mit CDK4/6i profitieren, identifiziert werden können.

Zu diesem Zweck wurden Zellkultur-Modelle etabliert, die die umfassende *in vitro*-Charakterisierung von Zellen, die eine Resistenz gegenüber Ribociclib entwickelt haben, ermöglichen. Dabei sollten Transkripte, Proteine und Mikro-RNAs (miRNAs) identifiziert werden, die in die Entstehung der Resistenz einbezogen oder damit assoziiert sind. Die Zelllinien MCF7 und CTC-ITB-01, die aus zirkulierenden Tumorzellen (circulating tumor cells – CTCs) einer Patientin mit metastasiertem Mammakarzinom generiert wurde, wurden über 18 Monate mit ansteigenden Konzentrationen von Ribociclib kultiviert. Die Ribociclib-Resistenz wurde durch funktionelle Experimente, wie die Analyse der Zellzyklusprofile, Koloniebildungs- und Viabilitäts-Assays, bestätigt.

Zur Identifizierung neuer potenzieller Biomarker für Resistenz gegenüber Ribociclib wurde das gesamte Transkriptom der resistenten und parentalen Zelllinien durch RNA-Sequenzierung analysiert, und die Deregulation ausgewählter Transkripte beziehungsweise der kodierten Proteine sowie einer miRNA wurden experimentell bestätigt. Zusätzlich zur Validierung mithilfe der quantitativen „real time"-PCR (qPCR) wurde eine *in situ*-Hybridisierung (ISH) zur Detektion von Mikro-RNAs (miRNAs) auf Einzelzellebene und zur Erfassung der räumlichen Heterogenität der miRNA-Expression etabliert. Kompatibilität mit Immunfluoreszenz-Färbungen und mRNA-Detektion machen diesen Assay zu einem wertvollen Werkzeug zur Detektion von miRNAs nicht nur in kultivierten Tumorzellen, sondern auch in CTCs.

Einige der deregulierten Zielmoleküle, beispielsweise *SOX9* oder miR-146a-5p sowie eine signifikante Anzahl von Transkripten, die mit der epithelialen-mesenchymalen-Transition (EMT) und Tumorstammzelleigenschaften assoziiert sind, wurden in beiden resistenten Zelllinien detektiert und sind bisher nicht im Kontext der Resistenz gegenüber CDK4/6-Inhibitoren beschrieben worden. Allerdings wiesen beide Zelllinien auch eine Vielzahl individuell deregulierter Transkripte und miRNAs auf, wie z.B. *ALDH1, CDK14* und miR-205-5p in den resistenten CTC-ITB-01- oder *CD44* und miR-675-5p in den resistenten MCF7-Zellen, was auf eine Vielzahl möglicher Resistenzmechanismen schließen lässt. Potenzielle Interaktionen, die die Ribociclib-

Resistenz beeinflussen können, wurden für beide resistente Zelllinien vorhergesagt. In resistenten CTC-ITB-01-Zellen könnte *CDK14*-mRNA post-transkriptionell durch miR-205-5p reguliert werden, und in resistenten MCF7-Zellen könnte eine SOX2-SOX9-SLUG-Achse bestehen. Diese Annahmen müssen jedoch durch experimentelle Untersuchungen bestätigt werden.

Im Vergleich zu den parentalen Zelllinien weisen die Ribociclib-resistenten CTC-ITB-01- und MCF7-Zellen zusätzliche Mutationen auf. Einige dieser Mutation wurden bisher noch nicht in der Literatur beschrieben. Dazu zählen z.B. Mutationen in *NF1, MAP3K5* sowie *NOTCH3*, die in den resistenten CTC-ITB-01- bzw. -MCF7-Zellen detektiert wurden.

Durch Vergleich der bei Ribociclib-Resistenz deregulierten Gene mit der „Gene Ontology (GO)"-Datenbank konnten signifikant beeinflusste Signaltransduktionswege vorhergesagt werden. Neben anderen war der Signalweg „Zelladhäsion" sowohl in den Ribociclib-resistenten CTC-ITB-01- als auch in den -MCF7-Zellen signifikant beeinflusst. So war in den resistenten CTC-ITB-01-Zellen u.a. die Expression von *LGALS1*, *ICAM1*, *MUC13* und *CLDN1* erhöht, während in den resistenten MCF7-Zellen u.a. *ALCAM*- und *MUC1*-Expression verstärkt exprimiert wurden. Dahingegen war die Expression von *DSC2* sowohl in den resistenten CTC-ITB-01- als auch in den MCF7-Zellen signifikant schwächer als in den jeweiligen parentalen Zellen. Da sich CTC-ITB-01-Zellen durch außerordentlich starke Fähigkeit zur Adhäsion an endotheliale Zellen (HUVEC) auszeichnen, wurde in Mikrofluidik-Experimenten die Adhäsionsfähigkeit parentaler und resistenter Zellen an HUVEC-Zellen verglichen. Während die Anzahl adhäsiver Ribociclib-resistenter MCF7-Zellen gegenüber der parentaler adhäsiver Zellen erhöht war, zeigte sich überraschenderweise eine Verringerung der Anzahl adhäsiver Zellen in resistenten gegenüber parentalen CTC-ITB-01-Zellen. Die Ursachen für die Unterschiede zwischen resistenten CTC-ITB-01 und MCF7-Zellen sollen in weiteren Experimenten aufgedeckt werden.

Neben deregulierten Genen, die EMT- und Tumorstammzell-assoziierte Transkriptionsfaktoren, wie *SOX9*, *RUNX2* oder *OVOL2*, kodieren, wurden auch Gene, die EMT-assoziierte Kinasen, wie *AXL*, *LYN* oder *DLCK1* kodieren, in resistenten und parentalen Zellen differenziell exprimiert. Viele Kinasen repräsentieren Proteine, die zielgerichtet therapeutisch inhibiert werden können und somit potenzielle Therapieoptionen für Patientinnen mit CDK4/6-Inhibitor-Resistenz bieten.

Da die große Mehrheit der Mammakarzinom-Patientinnen, die mit CDK4/6-Inhibitoren behandelt werden, eine Resistenz gegenüber diesen Therapien entwickelt, wird intensiv nach therapeutischen Optionen gesucht, von denen die Patientinnen auch bei Vorliegen der Resistenz profitieren. Zu diesem Zweck wurden die Zelllinien mit Ribociclib und Fulvestrant behandelt. Jedoch hatte die Zugabe von Fulvestrant keinen Einfluss auf die Viabilität der CTC-ITB-01- Zellen und beeinflusste die Viabilität der MCF7-Zellen nur moderat. Dagegen wurde das klonogene Wachstum Ribociclib-resistenter und parentaler CTC-ITB-01- und MCF7-Zellen, das anhand von Koloniebildung getestet wurde, effizient supprimiert. Somit könnte die Behandlung mit Fulvestrant zusätzlich zu Ribociclib eine weitere Therapieoption darstellen.

Im nächsten Schritt sollte getestet werden, ob durch zusätzliche Gabe von Alpelisib eine Reduktion von Viabilität und Koloniebildung in den Ribociclib-resistenten Zellen erzielt werden kann. Mutationen im *PIK3CA*-Gen stellen eine Voraussetzung für die Behandlung von HR+-Mammakarzinom-Patientinnen mit Alpelisib dar. Sowohl MCF7- als auch CTC-ITB-01-Zellen

weisen Mutationen im PIK3CA-Gen auf und sind deshalb für Untersuchungen zur Effektivität der Alpelisib-Behandlung geeignet. Durch Zugabe von Alpelisib sollte getestet werden, ob die Effizienz der Therapie durch Resistenz gegenüber Ribociclib behindert wird. Alleinige Behandlung mit Alpelisib verringerte die Viabilität der Zellen deutlich. Die Kombination beider Inhibitoren supprimierte nicht nur die Viabilität, sondern konnte auch das klonogene Wachstum effektiv reduzieren. Da sich die resistenten Zelllinien in Viabilitäts- und Koloniebildungs-Assays hinsichtlich ihrer Sensitivität gegenüber Alpelisib nicht von ihren parentalen Zellen unterschieden, könnte die Kombination von Alpelisib und Ribociclib eine wirksame Therapieoption darzustellen.

Morphologische Veränderung hin zu einem runden, auf Apoptose schließenden Phänotyp legen eine höhere Zytotoxizität von Alpelisib im Vergleich zu Fulvestrant oder Ribociclib nahe. Ribociclib arretiert die Zellen in der G1-Phase des Zellzyklus. Daraus resultieren eine moderate Reduktion der Zell-Viabilität und eine stärker ausgeprägte Inhibition des klonogenen Wachstums. Die Analyse der β-Galactosidase-Aktivität durch kolorimetrische X-Gal-Färbung zeigte Induktion zellulärer Seneszenz in parentalen MCF7-Zellen nach alleiniger Behandlung mit Ribociclib sowie nach Ribociclib- und Fulvestrant- oder Alpelisib-Kombination. In den resistenten MCF7-Zellen konnte Seneszenz nur durch die Behandlung mit Ribociclib und Fulvestrant induziert werden. Keine der in dieser Arbeit getesteten Behandlungen induzierte Seneszenz in den CTC-ITB-01-Zelllinien, was die Vermutung nahelegt, dass nicht Seneszenz, sondern eher reversible Quieszenz, eine für Stammzellen charakteristische Eigenschaft, induziert wurde.

In der vorliegenden Arbeit wurden verschiedene Kandidaten für potenzielle Biomarker, die CDK4/6-resistente Zellen identifizieren könnten, detektiert. Ein Ziel der Arbeit bestand darin, derartige Biomarker auch auf CTCs im CellSearch®-System zu testen. Jedoch müssen vor einer Anwendung an klinischen Proben verschiedene Parameter getestet und validiert werden, wie Positiv- und Negativkontrollen sowie geeignete Fluoreszenz-markierte Antikörper und deren Konzentrationen. Während sich Tests zur Detektion von CDK6 und SOX9 noch in der Entwicklung befinden, kann Vimentin (VIM) in CTCs bereits detektiert werden [2]. Da Ribociclib-resistente Zellen EMT-indikative Eigenschaften erworben haben und VIM als früher Indikator für EMT und das Vorliegen von epithelial-mesenchymalen Hybridzellen angesehen werden kann, wurde die VIM-Expression in CTCs von Patientinnen mit metastasierten Mammakarzinomen im CellSearch®-System analysiert. Die Mammakarzinome waren hinsichtlich ihres molekularen Subtyps heterogen, und die Patientinnen erhielten verschiedene Kombinationstherapien in unterschiedlicher Behandlungslinie. Vimentin-Positivität wurde in 67 von 201 untersuchten Patienten (33.3%) detektiert, während 134 der 201 Patientinnen (66.7%) nur VIM-negative CTCs aufwiesen. CTCs mit überwiegend schwacher VIM-spezifischer Immunfluoreszenz wurden häufiger in Blutproben mit ≥5 CTCs/7.5 mL Blut beobachtet als in Proben mit <5 (1-4) CTCs/7.5 mL Blut ($p=0.003$). Der Prozentsatz VIM-positiver CTCs veränderte sich nicht signifikant unter Therapie, inklusive einer Therapie mit CDK4/6-Inhibitoren. In zukünftigen Studien sollten CTCs und Vimentin-Expression der CTCs an einer größeren Kohorte von Patientinnen mit metastasiertem Mammakarzinom vor und nach Erstlinien-Therapie und während der Folgetherapie, inklusive einer CDK4/6-Inhibitortherapie, detektiert werden.

Zusammenfassend lässt sich schlussfolgern, dass in der vorliegenden Arbeit eine Reihe von Transkripten, Proteinen, Genmutationen und miRNAs identifiziert werden konnten, die potenziell

mit der Resistenz gegen Ribociclib assoziiert sind und für weiterführende *in situ*- und funktionelle Analysen sowie Validierung an klinischen Flüssigbiopsie-Proben zur Verfügung stehen.

1. Introduction

1.1 Breast cancer

According to the GLOBOCAN 2020 data, 20% of all people will develop cancer eventually. In women, breast cancer (BC) is accounting for nearly one quarter (24.5%) of all cancers diagnosed worldwide, followed by colorectal and lung cancer [3]. Despite a very high 5-year survival rate of 99% for noninvasive breast cancer, the survival probability drops to 86% for regional disease and only 29% for patients with distant metastases in the United States (US). However, since approximately two-thirds of cases (63%) are detected early, the overall 5-year survival rate is rather high with 90.3% between 2011 – 2017 [4]. Factors, increasing the individual risk for breast cancer are female gender, age over 40, obesity, long exposure to hormones or radiation, and alcohol abuse. Additionally, family history, in particular mutations in the breast cancer genes 1 & 2 (BRCA1&2), increase the risk for breast cancer significantly [5].

1.1.1 Classification of breast cancer

At diagnosis, only 20% of breast cancer cases are *in-situ* or non-invasive carcinomas. Histologically, a majority of approximately 80% out of the remaining cases is characterized as invasive ductal carcinoma (IDC), followed by around 10% of invasive lobular carcinoma (ILC). These cancers have already invaded adjacent tissue and bear the capacity not only to spread to nearby lymph nodes but also to distant sites [6]. Furthermore, carcinomas of the breast can be histologically graded from I (low) – III (high), based on the level of differentiation with a low grade indicating a higher likelihood of survival [7].

Carcinomas of the breast can be further classified by their molecular subtypes. In 2000, gene expression profiling of 65 breast cancer tissue samples was performed. Albeit a striking heterogeneity of expression profiles was described, four distinct molecular subtypes, namely "ER+/luminal like, basal-like, *Erbb2*+ and normal-like" could be determined [8]. This classification has been discussed, refined, and updated numerous times, resulting in four to six major subgroups used today [9–15]. An overview of the respective subtypes can be found in Table 1.

Additionally, breast cancer can be stratified by clinical parameters, including the primary tumor, involvement of adjacent lymph nodes, and presence of distant metastases (TNM staging). Since the 1970s, the American Joint Committee (AJCC) publishes guidelines for staging. In the latest (8^{th}) version, T1 – T4 describe the size of the primary tumor and its grade of local invasiveness. Lymph node involvement is evaluated in clinical and pathological categories, resulting in cNX – cN3c (clinical category) and pNX – pN3c (pathological category). Metastases can similarly be classified either by clinical imaging or histological analysis. While M0 represents the absence of distant metastases, cM1 and pM1 indicate their presence. Taking all three parameters together, patients are stratified into stages I – IV, albeit patients with a cM1 or pM1 classification are always classified as stage IV, independently of the other parameters [16]. Micrometastases and isolated tumor cells or tumor cell clusters in lymph nodes can be separately described as stages pN1mi and pN(i+), respectively [16]. In the 8^{th} edition of the AJCC recommendations, a prognostic staging protocol was

introduced, combing TNM staging with molecular subtypes and tumor grade, to stage patients individually and specifically. In individual cases, evaluation of a multigene panel may support the stratification [17].

Table 1: Overview of BC molecular subtypes. Adapted and modified from [18–20].

Subtype	Expression Profile	Frequency
Luminal A	ER+, PR±, HER2-, Ki67 low (< 14%)	~70 % [18,19]
Normal-like	ER+, PR±, HER2-, Ki67 low (< 14%)	Rare [18,19]
Luminal B	ER+, PR±, HER2 ±, Ki67 high (≥ 14%)	10-20% [18,19]
HER2+ enriched	ER-, PR-, HER2+, Ki67 high (≥ 14%)	5-15% [18,19]
Triple negative	ER-, PR-, HER2-, Ki67 high (≥ 14%)	15-20% [18,19]
Claudin-low	ER-, PR-, HER2-, Ki67 high (≥ 14%)	1.5-14% [12]

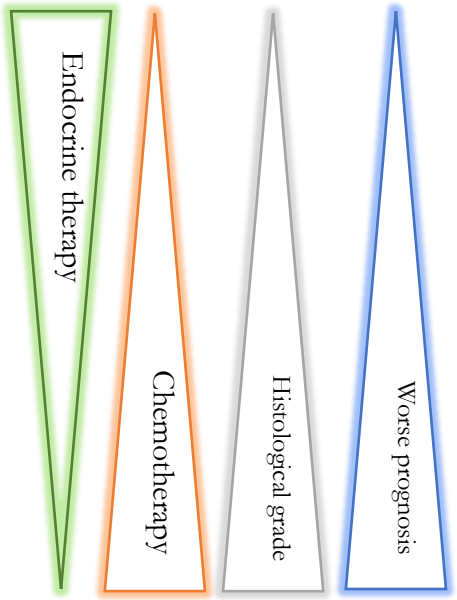

1.1.2 Treatment of hormone receptor positive breast cancer

Generally, local breast cancer is considered a curable disease, and more than 90% of cancers are diagnosed at either localized or local-infiltrative stage. Hence, therapy aims to eradicate the primary tumor and prevent relapse and metastasis. In addition to surgical removal of the tumor or combined surgery and radiotherapy, systemic therapy represents a major component of breast-conserving therapy. The therapy regime is directed by the patients' individual staging, but particularly by the molecular subtype of the primary tumor [21]. More than two-thirds of all cancers diagnosed are either luminal A or B and thus express either the ERα and/or progesterone receptor (PR) [21,22]. The second most frequent molecular marker is the human epidermal growth factor receptor 2 (HER2), overexpressed or amplified by around 20% of breast cancer cases. Patients with a HER2+ tumor usually benefit from a HER2-targeted therapy which includes small molecule inhibitors like lapatinib or neratinib, targeting the tyrosine kinase domain of HER2 and thereby preventing signal transduction [21]. Alternatively, HER2 can be targeted externally with anti-HER2 antibodies such as trastuzumab [23] or pertuzumab [24]. Triple-negative breast cancer accounts for approximately 15% of all breast cancer cases diagnosed and is characterized by a lack of hormone receptor (HR) and HER2 expression. Hence, targeted therapy options are limited for these patients, making chemotherapy the primary treatment option currently [25]. However, targeting drugs are under current investigation, such as poly-ADP-ribosyl polymerase (PARP) inhibitors, a protein involved in the homologous end-joining repair of DNA double-strand breaks, inhibition of phosphoinositide 3-kinase (PI3K), or immune checkpoint inhibitors [26].

ERα is a nuclear, ligand-dependent transcription factor, that upon activation binds to estrogen-responsive elements in target gene promoters [27,28]. Tumors, with at least 1% positivity for ER or

PR immunohistochemical staining are classified as hormone receptor-positive (HR+) [29], and practically all of them are treated with endocrine therapy. The selective estrogen receptor modulator (SERM) tamoxifen competitively binds to ERα and is administered virtually by default for five years in pre-and postmenopausal women, reducing the risk of recurrence and death for up to 15 years [29]. In postmenopausal women, or women, who developed resistance to tamoxifen, aromatase inhibitors (AI) such as exemestane, letrozole, or anastrozole, that reduce or prevent estrogen production upon binding to the aromatase [30] represent alternative treatment strategies [31]. However, if the patients are deemed to have an increased risk of relapse within 10 years, they might be treated with adjuvant or neoadjuvant chemotherapeutic agents, such as anthracyclines like epirubicin or taxanes such as paclitaxel [32].

1.1.3 Treatment of metastatic HR+ breast cancer

Despite the high efficacy of all treatment options, even of low-risk patients (T1N0), 13% of patients relapse with distant metastases within 20 years after five years of endocrine therapy [33]. In contrast to local disease, metastatic breast cancer (mBC) currently is considered an incurable disease, and therapy merely provides palliation. Surgery cannot provide complete removal and thus, chemotherapy or if available endocrine therapy are important components of the therapy in a metastatic setting [34]. Similar to localized breast cancer, HR+ positive cancers can be treated with tamoxifen or AIs. Additionally, the selective estrogen receptor degrader (SERD) fulvestrant, poses another option for the treatment of mBC patients [31,35]. All of these therapeutics can be given sequentially until progression and can be complemented with ovarian suppression by gonadotropin-releasing hormone agonists (GnRH) such as goserelin for premenopausal women [13].

1.1.4 CDK4/6 inhibitors in the treatment of mBC patients

Yet, virtually all mBC patients develop endocrine resistance eventually [36]. Thus, targeted therapy has been implemented into the treatment regime of mBC patients. The most important novelty are inhibitors of the cyclin-dependent kinases 4 and 6 (CDK4/6i). In 2015, the first CDK4/6i palbociclib was FDA approved as a first-line therapy agent in combination with letrozole, followed by ribociclib and abemaciclib in 2017. All three inhibitors are also approved for combined treatment with fulvestrant. However, abemaciclib is the only one, that is also approved as a monotherapeutic agent [37–39].

All CDK4/6i were evaluated in multiple clinical trials and are approved as first-line treatment in combination with any AI or first and second-line treatment combined with fulvestrant in women with any menopausal status [38–40]. On average, seven clinical trials demonstrated a prolongation of 8.8 months in progression-free survival (PFS) of any CDK4/6i with endocrine therapy versus placebo plus endocrine therapy, independently of any clinicopathological parameter [40]. More specifically, as first-line therapy in combination with an AI, PFS increased for approximately 10 months vs AI therapy alone. As a second-line agent, it can improve PFS for up to 5 – 7 months vs fulvestrant only [41]. Adverse events are mainly neutropenia for palbociclib and ribociclib, which can be counteracted by a drug holiday and dose reduction due to its reversibility. Moreover, nausea, diarrhea, fatigue, and increased liver toxicity and infections are observed regularly [38].

CDK 4/6 inhibitors act by interrupting the transition of the G1 phase in the cell cycle to the S phase which is mediated by the cyclin D1/CDK4/6 complex interaction with the retinoblastoma protein (Rb). Presumably, by binding to the ATP-binding pocket of CDK4/6, the CDK4/6i prevent downstream phosphorylation of RB [42]. Thus, RB stays dephosphorylated and thereby activated and tightly bound to the transcription factors E2F that normally induce transcription of further cell cycle relevant genes such as cyclins and CDKs, enabling the transition from late G1 phase to S-phase [43,44] and stages beyond thus impacting cell proliferation through various ways [45]. The mode of action is depicted in Figure 1.

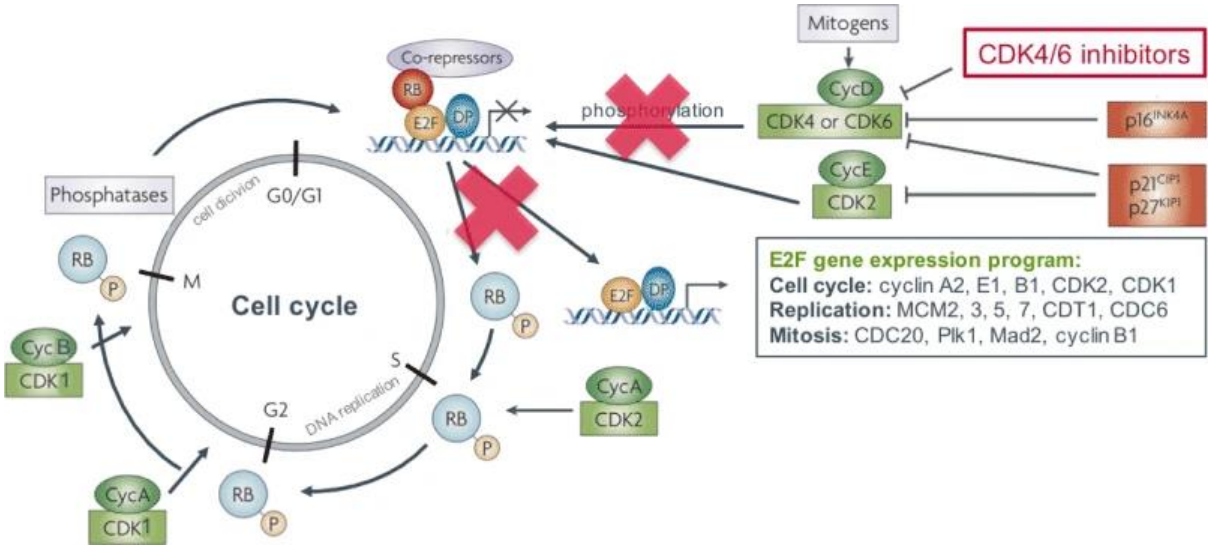

Figure 1: Overview of key proteins in cell cycle progression. CDK4/6i inhibit CDK4 and 6 similarly to the endogenous inhibitors p16, p21, and p27. Hence, phosphorylation of Rb is prevented, Rb remains inactive and bound to the E2F transcription factor complex. Since the transcription of E2F induced genes such as *CCNA2*, *CCNE1*, *CCNB2*, *CDK2*, and *CDK1* is not initiated, the treated cell is arrested in the G1 phase [44].

By acting downstream of the pathway inhibited by endocrine treatment, the addition of CDK4/6i can circumvent endocrine resistance [46]. ER-targeting therapy was shown to increase cyclin D1 levels [47] which confers resistance to treatment with ER agonists as was shown experimentally [48] and evaluated clinically [49]. Generally, endocrine therapy merely results in tumor regression in around 30% of patients and it can stabilize disease in approximately 20% of patients, whereas the other half progresses after a short time [50]. Since elevated cyclin D1 levels do not imperatively impede effective CDK4/6i treatment, these inhibitors represent an ideal therapeutic option in the endocrine-resistant setting [46,51].

In summary, the oral availability, manageable adverse effects, and high efficacy make CDK4/6i an important component in the therapy of HR+ mBC patients [52].

1.2 Resistance to CDK4/6i and common resistance mechanisms

1.2.1 Cell cycle-related

Generally, resistance is a major problem in cancer and HR+ mBC in particular. As mentioned before, endocrine resistance is extremely common and despite the initially great efficacy of

CDK4/6i plus endocrine therapy in mBC patients, the majority of patients also eventually encounter therapy resistance [53,54]. In clinical trials, that finally led to the approval of CDK4/6i, at least one-third of all patients progressed under therapy within two years [55]. Albeit, in cell culture experiments, functional RB seems to be a relevant factor to induce cell senescence, its expression or proficiency is not mandatory for acute Cdk 4/6i efficacy. However, the long-term efficacy of CDK4/6i is higher in RB competent cells, which might be attributable to a concordant decrease of $p21^{CIP1}$ and $p27^{KIP1}$ and elevated p107 levels in RB-deficient cells [43]. $P21^{CIP1}$ and $p27^{KIP1}$ are intrinsic inhibitors of cell cycle progression. Their binding to CDK/cyclin complexes inhibits CDK signaling [56,57]. Strikingly, in cell culture experiments $p21^{CIP1}$ and $p27^{KIP1}$ levels were regulated post-transcriptionally and not on the RNA level [43]. They are not only targeting the CDK4/6/cyclin D1 complex but also the CDK2/cyclin E1 complex, which is also phosphorylating Rb [44]. Hence the loss of $p21^{CIP1}$ and $p27^{KIP1}$is also associated with Cdk 4/6i resistance.

$P16^{INK4}$ represents another biological inhibitor of CDK4 that prevents binding of cyclin D1. It induces a negative feedback loop upon inactivation of Rb, diminishing CDK4 expression. In RB deficient cells, $p16^{INK4}$ is increased, which might be a consequence of oncogenic stress [58]. Although its primary function is to induce cell cycle arrest, high $p16^{INK4}$ levels are indicating reduced sensitivity towards CDK4/6 inhibition, since CDK4 expression and respective activity are already strongly reduced and low $p16^{INK4}$ levels were shown to be associated with higher sensitivity to palbociclib treatment [46,59]. Nonetheless, two clinical phase II studies could not show any predictive value for PFS of elevated $p16^{INK4}$ levels [60,61]. Increased p107 levels are attributable to E2F promotion and can compensate RB deficiency partly since p107 similarly interacts with E2F as Rb [43,62]. However, its suppressive capacity is comparatively moderate in the presence of palbociclib compared to Rb proficient cells and cannot fully prevent palbociclib evasion [43]. If loss of RB is accompanied by additional E2F-dependent induction of *CCNE1* transcription or amplification, this results in increased resistance to CDK4/6i [63,64]. In combination with loss of suppression of $p21^{CIP1}$ and $p27^{KIP1}$ on CDK2 this mechanism might be able to circumvent dependency of cell cycle progression on signaling of the Cdk 4/6 complex, ultimately resulting in resistance to CDK4/6i as was demonstrated in CDK4/6 deficient AML cell lines [65]. Also in breast cancer cell lines results were implying that aberrant CDK2 signaling is a way to evade cell cycle progression by Cdk 4/6i [43] that is not completely inhibited by CDK4/6i. Only inhibition of CDK2 with a specific inhibitor re-sensitized resistant cells to inhibition of CDK 4 and 6 [66,67] and was similarly effective in resistant cell lines as in parental ones [54]. All these aberrations are eventually attributable to deviant E2F signaling, as CDK2 and cyclin E1 are amongst the targets of E2F transcriptional activation. Cell culture experiments proved that increased E2F expression was sufficient to completely bypass inhibition of CDK4/6, independently of the Rb status [43]. Summarized, these results imply an important role of E2F and the cyclin E1/CDK2 axis for CDK4/6i bypassing since the loss of RB itself is not sufficient, to convey resistance to CDK4/6 inhibition. Thus, inhibition of CDK2 or other downstream targets of E2F in RB-deficient tumors might represent an interesting treatment option [68].

Furthermore, in another preclinical model, abemaciclib-resistant derivates of breast cancer cell lines were characterized by increased CDK6 levels due to *CDK6* gene amplification. Concomitantly, cyclin E1 was overexpressed, and reduced ERα mRNA was observed, resulting in cells not only resistant to CDK4/6 inhibition but also with reduced sensitivity towards endocrine treatment. This

observation was congruent with data from a small cohort of patients, that switched from ER+ subtype to ER- subtype under CDK4/6i therapy [53]. Interestingly, in a lymphoma model, it was also demonstrated that CDK6 can induce transcription of the *CDKN2A* ($p16^{INK4}$) gene in a kinase-independent manner [69]. This has not been shown in breast cancer so far but might play a role in an increase of $p16^{INK4}$ levels in a CDK4/6i resistant situation. Strikingly, preclinical studies demonstrate, that even CDK4/6i-resistant cell lines derived from a common parental cell line develop unique resistance mechanisms, stressing the individual response and heterogeneity of resistance mechanisms also of each patient to therapy [54].

1.2.2 Non-cell cycle-related

Apart from cell cycle-related resistance mechanisms, other aberrations are correlated with Cdk 4/6i resistance. For instance, around 45% of all luminal A and 29% of luminal B breast cancer tissues carry an activating mutation in the *PIK3CA* gene, encoding the catalytic subunit p110α of the phosphatidylinositol-3-kinase (PI3K) [14]. Alterations of the PI3K/mTOR pathway reportedly promote endocrine resistance as well as resistance to CDK4/6 inhibition [68,70]. Furthermore, loss of PTEN, a negative regulator of the PI3K/mTOR axis, has been described to stimulate CDK4/6i resistance by preventing the transport of $p27^{KIP1}$ to the nucleus. Thus, interaction with its targets is impeded and leads to increased CDK2 and CDK4 activity, supporting CDK4/6i bypassing [71]. Indeed, dual-target inhibition of the PI3K/AKT/mTOR axis and the CDK4/6 signaling pathway with a PI3Ki and a CDK4/6i, increased apoptosis of tumor cells in vitro compared to CDK4/6i alone, however, PI3K inhibition alone cannot overcome CDK4/6i resistance and re-sensitize cells [64]. Interestingly, on the other hand, CDK4/6 inhibitors are an effective treatment option to re-sensitize PI3K inhibitor-resistant cell lines to PI3K inhibition [72]. Furthermore, combined CDK4/6 and PI3K and mTOR inhibition was proposed as a treatment strategy to avoid the early emergence of CDK4/6i therapy resistance [64,73]. In the case of established CDK4/6i resistance, cell culture experiments indicate that inhibition of the mammalian target of rapamycin (mTOR) is a treatment option since resistant breast cancer cell line cells showed high sensitivity to such a treatment [73]. The synergistic effect of PI3K and CDK4/6 blockage has also already been demonstrated in clinical trials [74]. Despite the implication of PI3K mutations in the development of resistance to CDK4/6 inhibition, their presence only has a non-significant impact on the PFS of HR+ mBC patients and their benefit of combined treatment of fulvestrant plus CDK4/6i [75].

Mutations in the fibroblast growth factor receptor (FGFR) are also frequent in HR+ breast cancer (15%) [76]. Normally, FGFR signaling is required for mammary gland development, but aberrant signaling promotes breast cancer progression and is associated with worse PFS. Breast Cancer cell culture models demonstrate that increased FGFR expression correlates with reduced sensitivity to palbociclib. Mechanistically, this might be, at least partially, due to increased induction of *CCND1* (cyclin D1) by FGFR. Noticeably, FGFR amplification often is concordant to cyclin D1 overexpression and approximately 30% of tumors with *FGFR1* amplification additionally harbor a *CCND1* amplification. Treatment with an FGFR inhibitor could re-sensitize cells to treatment by fulvestrant plus CDK4/6i. This triple combination proved also to be highly efficient in patient-derived xenografts (PDX), making this treatment scheme an option for CDK4/6i resistant tumors

[76]. However, no clinical trials for FGFR inhibition in an HR+ CDK4/6i resistant setting exist so far.

Resistance to CDK4/6i is bringing a demand for subsequent therapy options. As mentioned previously, inhibiting the activity of CDK2, the PI3K/mTOR axis, and perhaps also FGFR might represent such alternatives. The utility of PI3K/mTOR inhibition in addition to endocrine therapy and CDK4/6i is currently under investigation in clinical trials [55]. Moreover, CDK4/6i resistance did not impede sensitivity to commonly used chemotherapeutic agents in cell culture experiments, meaning that chemotherapy could be also a treatment line succeeding targeted therapy [54].

Resistance mechanisms to CDK4/6 targeted therapy are multifactorial and complex in HR+ mBC. Hence, monitoring of disease progression and emergence of resistance, as well as frequent analysis of the expression profile of the tumor is mandatory. However, for a long time, the only option to obtain tumor cells was by a punch or core needle biopsy from either the primary tumor or distant metastases, as from lung or bone which might be associated with increased adverse events [50]. Although tissue biopsies remain an important tool in breast cancer management [77] , liquid biopsy provides a new, nearly non-invasive methodology to monitor disease.

1.3 Epithelial to mesenchymal transition and metastasis

Interestingly, some studies show an association of CDK4/6i resistance with epithelial-mesenchymal transition (EMT) [67,68]. EMT describes the shift of rather immobile epithelial cells to more motile mesenchymal cells. This reversible process is essential during embryogenesis but also is likely to facilitate cancer progression and metastasis. The reverse process is called mesenchymal-epithelial transition (MET). Orchestrated by a set of specific transcription factors and microRNAs, epithelial cells lose their apico-basal orientation and cell-to-cell contacts during EMT, enabling tumor cells to migrate and reorganize. The transcription factors Snail1/2, Twist, ZEB, GRHL2, OVOL1/2, PRRX1 as well as the miR-200 family and miR-34 are core factors driving EMT signaling and regulation. Since EMT is associated with morphological changes of tumor cells, structural proteins, and cell surface proteins promoting cell adhesion and cell to cell contacts such as E-cadherin, N-cadherin, fibronectin, vimentin, or integrins are commonly used markers of EMT. Moreover, in adulthood, EMT is still relevant for wound healing [78].

Yet, EMT is also considered pertinent for metastasis in cancer. It forces tumor cells to detach from the primary tumor tissue, enables them to migrate through the connective tissue, and invade blood vessels. Tumor cells detectable in the blood circulation are being then referred to as circulating tumor cells (CTCs). Several factors such as hypoxia, growth factors like the epidermal growth factor (EGF), fibroblast growth factor (FGF) or insulin growth factor (IGF), cytokines, and inflammatory signals can trigger EMT initiation [79]. Analysis of CTCs has revealed, that these cells are not only either epithelial or mesenchymal but that they also may exist in intermediate states and that most CTCs share epithelial and mesenchymal features [80,81]. CTCs must resist the dangers of death induced by loss of cell-cell contacts, called anoikis, have to undergo fundamental structural changes and have gained a degree of plasticity, increased motility, and can hide from immune cells, and survive shear stress [82]. Thus, colonization is an inefficient process and only a small proportion of CTCs forms metastases eventually [83]. Even though most CTCs circulate as single cells, some form

clusters. Homogenous clusters are more likely to form a metastasis [84] and the inclusion of blood cells like platelets, or neutrophils improve the survival of CTCs in circulation and shield them from immune attacks [83]. Once they are stuck in a capillary or adhere to a vessel, they may extravasate into a pre-metastatic niche of the target tissue and form distant metastases [85]. In theory, CTCs could extravasate into any distant organ but stinkingly, all tumor entities form metastasis in specific organs more frequently than in others. The organ tropism is thought to be guided by the interaction of the pre-metastatic niche and the CTCs. Primary tumors may even prepare distant sites for colonization [85], since it has been shown that secreted factors or exosomes might promote vascular leakiness [86], stimulate reorganization of the extracellular matrix (ECM) of a niche [87] or recruit supportive stromal cells [85]. Breast cancer mainly metastasizes into bone, liver, and lung [88]. Interestingly, one group took ctDNA and CTCs into account to model sites of metastasis by machine learning. This new approach of integrating liquid biopsy into disease monitoring could improve patient care [89].

1.4 Liquid biopsy

Generally, liquid biopsy describes the analysis of analytes from body fluids, such as urine, saliva, liquor, whole blood, and plasma. In oncology, analysis of CTCs, ctDNA, cfRNA, extracellular vesicles (EVs), and tumor educated platelets (TEPs) from peripheral blood and plasma or serum is of great interest [77,90]. Due to their minimal to non-invasive nature, liquid biopsies can be taken sequentially, facilitating longitudinal monitoring of disease and therapy response. Thus, liquid biopsy might represent a convenient tool for the management of cancer, could help to detect early-stage cancer, predict therapy response, guide targeted therapies, or predict relapse after therapy [90–92]. Minimal residual disease (MRD) and residual micrometastatic disease remain a problem in breast cancer since they cannot be detected with conventional imaging [93,94]. However, detection of cfDNA from liquid biopsies either by digital droplet PCR (ddPCR) or next-generation sequencing provides an opportunity to detect MRD and makes early therapeutic intervention guided by liquid biopsies feasible [95].

Another difficulty in cancer management is the heterogeneity of most tumors. Spatial heterogeneity refers to the presence of several cellular subclones within a tumor. Thus, a needle biopsy might not contain all subclones. Furthermore, tumors acquire mutations over time. Subclones that provide advantages in dissemination or survival and therapeutic pressure can become more dominant, for example, seen in breast cancer patients with HR+/HER2- primary tumors, but HER2 CTCs and metastases. This change of mutational or expression landscape is referred to as temporal heterogeneity. Liquid biopsy with its multitude of available analytes that can either be derived from the primary lesion or metastases and the possibility for sequential sampling and analysis might mirror the tumoral heterogeneity better than a needle or other tumor biopsies.

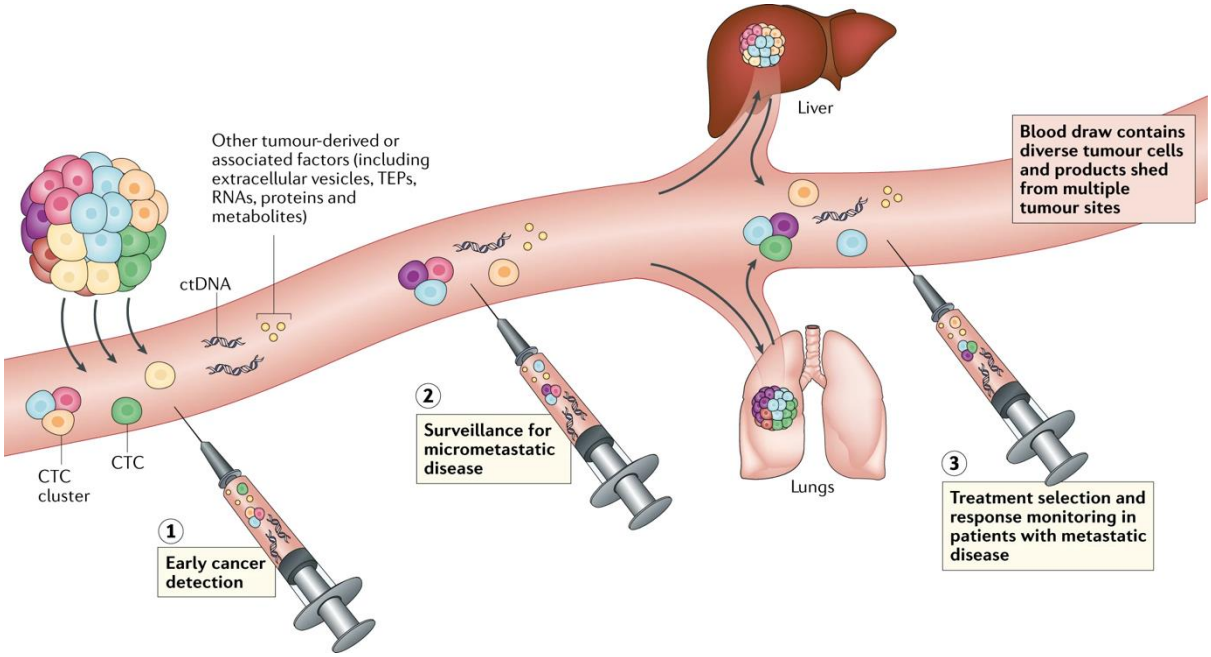

Figure 2: Overview of analytes of liquid biopsy and possible applications of liquid biopsy in cancer management [90]**.** The most relevant analytes from blood used in cancer are CTCs, CTC clusters, ctDNA, ctmiRNAs, secreted proteins, and blood cells that the CTCs may cluster and travel with such as tumor educated platelets. After being detached or secreted from the primary tumor, all these factors promote and facilitate distant metastasis. Therefore, their analysis can be beneficial for the early detection of cancer and metastasis and disease monitoring. Furthermore, some analysis, such as CTC phenotyping for example can even be included in therapy selection.

1.4.1 CTCs for monitoring of progression and prediction of response and resistance to therapies in breast cancer

Already 20 – 30 years ago, first disseminated tumor cells (DTCs) in the bone marrow and then CTCs were detected and associated with poor PFS and OS [96,97]. In 2004, the presence of ≥5 CTCs per 7.5 mL of blood, detected by the CellSearch® System, was determined as a predictive marker for worse PFS and OS in mBC [98]. Ever since, a plethora of clinical studies, considering CTCs, has been conducted [99]. Importantly, the opportunity to report CTCs or DTCs detected in liquid biopsies from peripheral blood, lymph nodes, or bone marrow has been incorporated now in the cancer staging manual as clinical tumor stage cM0(i+) [16]. Advanced techniques nowadays provide the possibility of a molecular in-depth analysis of CTCs, such as detection of copy number alterations (CNA) and mutations or gene amplification, and transcriptomic and proteomic analysis. Furthermore, methylation profiling can be useful in the functional analysis of tumor suppressors or oncogenes [100], thereby supporting treatment decisions [101].

Other studies focus on the expression of certain genes and proteins on CTCs such as IGF-1R [102], androgen receptor (AR) [103,104] or HER2 [105], since the expression of these markers can be useful for the prediction of patient outcome [102] or of the site of metastasis [106,107] and might be an additional rationale for the selection of targeted therapies. This can be further supported by CNA and mutation analysis that may provide information about druggable genetic alterations promoting cancer progression [108,109]. However, additionally to preexisting mutations, some mutations or alterations can emerge under therapeutic pressure and promote therapy resistance. Common

genomic aberrations frequently emerging under endocrine therapy include *ESR1*, *PI3KCA*, *ERBB2,* or *FGFR1* mutations or amplifications [110]. In addition to inter-patient heterogeneity, one study demonstrated inter-CTC heterogeneity on a cohort of 48 patients with advanced breast cancer that were pre-treated with endocrine therapy including AI. Comparison of genomic aberrations of CTCs by single-cell sequencing at baseline and under therapy revealed *ESR1* mutation dynamics as well as the emergence of druggable driver mutations such as mutations in *FGFR2*, *PI3KCA,* or *CDH1*, providing additional therapeutic options [111,112]. Furthermore, molecular CTC analysis has also been proven useful for monitoring chemotherapeutic responsiveness, in the case of triple-negative mBC patients or HR+ mBC patients with triple-negative metastases. The levels of 53BP1, a protein associated with DNA double-strand breaks was increased in patients with HR+ metastases and low genomic integrity, undergoing chemotherapy with eribulin. While 53BP1 levels at baseline did not correlate with PFS, an increase of the protein level over the course of therapy, correlated with improved PFS and might indicate a good response to the therapeutic agent [113].

1.4.2 CTC derived cell lines

As mentioned previously, CTCs remain a rare event and their enrichment requires highly advanced techniques. Hence, short-term *ex vivo* culture of CTCs or CTC-derived cell lines provide a higher cell number and facilitates molecular in-depth analysis.

The usefulness of CTC phenotyping was demonstrated in a study, where RNA-sequencing was performed on CTCs cultured *ex vivo*. All CTC lines were derived from HR+ mBC patients and carried various mutations in *ESR1*, *KRAS*, *FGFR2,* or *TP53*, amongst those in other genes. The sensitivity of these CTC cell lines to assorted therapeutics was tested. This analysis demonstrated the individual response of each CTC-derived cell line to different treatments in dependency to their respective mutational profile, supporting the relevance of molecular phenotyping for therapy decision and individualized treatment [114].

In general, the cultivation and establishment of CTC-derived cell lines remain technically challenging and are rarely successful. Nonetheless, stable CTC-derives cell lines have been established, for example from metastatic colon cancer patients [115], non-small cell lung cancer (NSCLC) [116], or castration-resistant prostate cancer (CRPC) [117]. Another CTC-derived cell line was established in our institute. CTCs were obtained from a heavily treated ER-positive, HER2 negative mBC patient who had received multiple lines of chemotherapy and ET. The cell line shares functionally, tumor-relevant mutations with both primary tumors and the vaginal metastasis, including a mutation in the *CDKN1A* gene, encoding $p21^{CIP1}$ and additionally carries an exclusive *TP53* mutation. Despite reduced sensitivity to estrogen depletion due to E2 independent ERα activity, the cell line was susceptible to CDK4/6 inhibition, implying that the patient would have benefited from a respective inhibitor therapy the patient did not receive at this timepoint [118]. This cell line was also utilized in other studies for further characterization and evaluation of resistance mechanisms. Knockdown experiments revealed a switch from ERα dependent growth to HER2-dependent growth under fulvestrant treatment. HER2+ levels, and concordantly FOXM1 levels, were increased upon fulvestrant treatment in an NFκB dependent manner. Reducing FOXM1

levels in these cells resulted in increased apoptosis. Hence, targeting either FOXM1 directly or by NFκB might be a therapeutic approach to circumvent endocrine resistance [119].

Summarized, molecular analysis of CTCs for early detection of emerging resistance might be handy since it allows for early therapeutic intervention. Regardless of the advantage molecular analysis of CTCs might bring for monitoring responsiveness to therapy and resistance establishment, the number of respective studies and publications remains limited.

1.4.3 Cell-free tumor DNA (CtDNA)

Albeit CTCs represent an important and reliable source of information in liquid biopsy in cancer, their enrichment is technically challenging, laborious, and hindered by their great biological heterogeneity. Generally, cell-free DNA (cfDNA) either can be released by any apoptotic or necrotic cell in the bloodstream or be actively secreted. The tumor-derived fraction (ctDNA) of this DNA has gained increasing interest during the previous years since it is an easily accessible analyte for cancer management and can be used for the detection of point mutations, for methylome profiling, or analyses of copy number alterations [120]. Hence, the number of respective studies, either stratifying patients by the presence of specific mutations in ctDNA to improve individualized treatment [121], detecting MRD and early relapse [93], or monitoring therapy response [122] is increasing rapidly.

Similar to mutations found in CTCs from HR+ mBC, mutant *PI3KCA*, *ESR1,* and *TP53* ctDNA is detected most frequently. Overall, mutant allele frequency (MAF) and the number of detectable alterations correlate with the number of metastases, implying ctDNA as a surrogate marker for tumor burden [123].

ESR1 mutations on the ctDNA level are assessed in a multitude of studies since they are rarely detected in primary tumors but emerge frequently under endocrine therapy. Therefore, tracking the frequency of *ESR1* mutations might be a tool for surveillance of therapy response [122]. One study demonstrated that the number of ET lines positively correlates with the number of patients with detectable *ESR1* mutations in ctDNA [124]. Although CDK4/6 inhibitors are part of the standard-of-care therapy for mBC patients, fewer studies assessing ctDNA levels from blood and concordant mutations have been conducted. Exome sequencing from patients enrolled in the PALOMA-3 study, comparing palbociclib + fulvestrant treatment versus fulvestrant alone, revealed no significant differences in mutational patterns between both treatment arms, implying the emergence of for example *PI3KCA* mutations related to the treatment with fulvestrant but not palbociclib. However, CDK4/6 inhibitor resistance is strongly driven by copy number alterations (CNA) of driver genes leading for example to increased cyclin D1 levels of Rb loss, which are difficult to evaluate on the ctDNA level [1]. Therefore, another study evaluating samples from the PALOMA-3 study, focused on those with ≥ 10% of tumor DNA fraction (n=156) to analyze CNA. Indeed, in the arm with palbociclib, gains of *CCNE1*, *MYC,* or *CDK4* copy numbers were associated with worse PFS, whereas in the placebo + fulvestrant group *ESR1* and *TP53* mutations, as well as gain of FGFR1 and MCL1 copy numbers, were associated with worse PFS. Nonetheless, no marker alteration was of significant predictive relevance, perhaps due to their low prevalence [125]. So far, only the ctDNA dynamics are correlated with PFS for patients treated with palbociclib

and fulvestrant, as was shown on a small patient cohort of 61 HR+ HER2- mBC patients. A decrease of ctDNA levels 30 days after therapy initiation was associated with improved PFS [126].

In summary, these observations suggest a combination of CTC profiling with ctDNA analysis to obtain as much information as possible. This is further supported by a study comparing *ESR1* mutations on CTCs and ctDNA of patients at baseline of first-line endocrine therapy (n=43) or at progression on any kind of endocrine therapy (n=40). Interestingly, mutations exclusive in CTCs or cfDNA were detected, albeit the number of mutations exclusively found on ctDNA (n=9 mutations) was high compared to the single mutation found exclusively in CTCs of one patient [127].

1.5 MicroRNAs

MicroRNAs (miRNAs) are a class of single-stranded, non-coding RNAs of approximately 22nt length. The primary-miRNA (pri-miRNA) transcript is cleaved into a precursor miRNA (pre-miRNA) of ~70 nt length by the RNase III DROSHA. Subsequently, this pre-miRNA is transported to the cytoplasm for further cleavage to the final miRNA by another RNase III named Dicer. Finally, the more unstable miRNA* strand is degraded, and the mature single strand is bound to the argonaut 2 protein, forming the RNA-induced silencing complex (RISC). In this biologically active form, miRNAs negatively regulate gene expression mainly posttranscriptionally by binding to the 3´ untranslated region (UTR) of their respective target gene. Target specificity is determined by the seed region, a sequence of 6 – 8 nucleotides with which miRNAs bind to their target mRNA. By either inhibiting the mRNA translation or even degrading bound mRNAs, they play a regulatory role in various biological processes such as proliferation, apoptosis, and differentiation [128,129].

The mode of action of miRNAs is dependent on the degree of complementarity of their seeding region to their target mRNA. In the case of near to 100% complementarity, the mRNA bound to the miRISC complex is degraded, a process mainly found in plants. In mammals, imperfect complementarity of miRNA and target 3´UTR is predominant, resulting in inhibition of protein translation, even though also imperfect binding can lead to degradation of the mRNA target. Which mode of action is active in a certain situation has not been unrevealed so far [129]. For the reasons stated above, one single miRNA can have up to a hundred targets, and one target can be regulated by multiple different miRNAs, resulting in complex regulatory miRNA-mRNA networks [129].

1.5.1 MicroRNAs in breast cancer

Obviously, miRNAs also are of great interest in the context of cancer and were first linked to it in 2002 [130]. Prominent examples of extensively studied miRNAs in breast cancer are miR-10b-5p and miR-21-5p. MiR-10b-5p has been shown to induce EMT by regulating various key proteins. MiR-21-5p promotes proliferation by the inhibition of several tumor suppressors. Causative for miRNA dysregulation is often genomic instability. According to a study by Calin et al., about 50% of all annotated miRNA genes are located in fragile sites in the genome [130]. Besides being regulatory key players in cancer, the utility of miRNAs as druggable targets or even as therapeutics for different diseases is of pivotal importance. Currently, 11 non-coding RNA (ncRNA)-based drugs for the treatment of multiple diseases have been approved by the FDA, demonstrating the feasibility of

this therapeutic approach. However, ncRNAs are not yet FDA-approved or applied in clinical trials as therapeutics for cancer [131].

MiRNAs have also been described in connection with therapy resistance in breast cancer. In a cell line model, using luminal breast cancer cell lines and their palbociclib-resistant derivates, exosomal miR-432-5p was conferring CDK4/6i resistance by increasing CDK6 levels via induction of the TGF-β pathway. Increased levels of miR-432-5p and CDK6 could also be confirmed in a biopsy taken after palbociclib treatment in comparison to the baseline tissue [132]. Another cell line model exploited the improved efficacy of not only ribociclib but also an AURORA A/B and a PI3KCA inhibitor by additive miR-126 administration [133]. Additionally, in vitro experiments revealed the involvement of miR-223 in response to treatment with palbociclib. Downregulation and in vivo knockout (KO) experiments confirmed that miR-223 levels correlate positively with palbociclib sensitivity, whereas low miR-223 levels were associated with higher resistance towards the CDK4/6 inhibition. Analysis of primary biopsies further showed, that decrease of miR-223 levels is an early event in breast cancer and can already be detected in DCIS [134]. Furthermore, also miR-23b-3p was positively linked to sensitivity to CDK4/6i by downregulation of CDK6. This miRNA is higher expressed in palbociclib-responsive cell lines than in resistant ones and treatment of naively resistant cell lines with respective miRNA mimics could sensitize these cell lines to the treatment. Since the expression of miR-23-3p negatively correlated with the expression of c-MYC in this study, the authors suggested induction of CDK6 expression by decreased miR-23b-3p expression due to high c-MYC levels [135]. Other miRNAs relevant for CDK4/6i response have been described in other cancer entities such as miR-193b in prostate cancer, miR-200a in metastatic melanoma as well and let-7a and miR-21 in thymic T-cell acute lymphoblastic leukemia/lymphoma [136].

Despite these very interesting and promising results, so far monitoring clinical response to anti-CDK4/6 therapy does not include any miRNAs. Generally, in most clinical studies miRNAs were investigated from blood plasma, serum, or exosomal vesicles and only very few studies focus on miRNAs from CTCs [137]. Heterogenous expression of miR-10b on CTCs of breast cancer, prostate, and colorectal cancer patients has been shown by *in situ* hybridization [138]. Likewise, miR-21 was detected on CTCs of breast cancer patients in another publication [139]. Utilizing qPCR, a multitude of miRNAs was detected from blood samples enriched for PBMCs and CTCs [140–142]. Another approach was chosen by a group analyzing the promoter methylation status of genes encoding miRNA 200 family by bisulfate sequencing after enrichment by CellSearch® [143].

That incorporation of miRNAs into phenotyping of CTCs might be beneficial has been exemplified by one study, showing, that the analysis of miR-106b levels additional to detection of E-cadherin and vimentin by qPCR improved the prognostic power for OS [144].

1.5.2 Circulating RNAs

When speaking about circulating RNAs, mostly miRNAs are referred to. They can either circulate as cell-free miRNAs or be cargo of EVs, such as exosomes, and be isolated from any kind of biofluid [145]. However, most commonly, plasma or serum for the detection of blood-based circulating miRNA analysis is used. As they are protected from endogenous RNase activity, circulating miRNAs (ctmiRNAs) are stable markers for breast cancer diagnosis [146,147], detection of

metastases [148] and are even investigated as markers for prognosis and therapy efficacy. A multitude of clinical trials investigates the utility of circulating miRNAs as biomarkers in breast cancer [149]. Yet, circulating or exosomal miRNAs associated with resistance to Cdk 4/6 have not been found so far.

1.5.3 Long non-coding RNAs

Next to miRNAs, long non-coding RNAs (lncRNAs) represent another class of regulatory RNAs. As implied by the name, lncRNAs are characterized by a length of >200 nt and a lack of an open reading frame and thereby lack of protein-coding potential. They are roughly classified due to their genomic localization. When localized between two genes, they are categorized as intergenic, as intragenic or intronic, when they are localized in an intron of a gene or antisense [150]. Unlike miRNAs, lncRNAs can not only regulate negatively but feature diverse modes of action [151]. Due to their length, they can form secondary structures and interact with RNA, DNA, and proteins [150]. For example, they can bind to DNA-binding proteins, such as transcription factors, and thereby prevent interaction or, by binding more than one protein, initiate interaction by providing proximity of the two binding partners. LncRNAs have also been described to bind proteins and guide them to a specific position on the chromatin, either by directly binding to the DNA or adaptor proteins. Such interaction can also be induced by loop formation, resulting in enhanced transcription of a peripheral gene. Thus, lncRNAs can either enhance or suppress the transcription of their respective target. They exert their function either in *cis* or *trans*, meaning that they either interact with their direct genomic neighbors (*cis*) or leave their site of transcription and interact with peripheral chromatin (*trans*) [152]. Hence, they are also involved in regulatory processes in cancer, such as metastasis, EMT, and invasion. Prominent examples of lncRNAs deregulated in cancer are HOTAIR and MALT1, both involved in EMT and metastasis [153]. LncRNAs have also been investigates in the context of CDK4/6i resistance. ERINA is an estrogen responsive lncRNA which promotes cell proliferation by interacting with the E2F/Rb pathway [154]. Depleting the lncRNA ERCL1 in breast cancer cell line cells improved sensitivity to treatment with Fulvestrant and palbociclib whereas overexpression reduced the treatment efficacy. Overexpression of the lncRNA ERCL1 impaired the efficacy of fulvestrant and palbociclib treatment of breast cancer cell line cells whereas its depletion increased sensitivity of tamoxifen resistant cells to the respective treatment [155]. Another rather prominent lncRNA, TROJAN, was demonstrated to promote CDK4/6 inhibition by palbociclib by enhancing transcription of CDK2. Positive correlation of TROJAN levels and CDK2 and KI67 levels has been demonstrated on a cohort of 108 patient samples [156].

1.6 DETECT-studies

The Detect study is a prospective multicenter study with more than 100 participating sites across Germany, enrolling mBC patients. Patients with a HER2 negative primary tumor and CTCs are included in study arms III and IV and further stratified by the HER2 status of their CTCs. In DETECT III patients with HER2+ CTCs were randomized 1:1 and either treated with standard therapy or additional lapatinib administration. In Detect IV patients with HER2- CTCs are enrolled

but treatment decision is then based on the HR status of the primary tumor (Figure 3). HR+ positive, postmenopausal mBC patients receive endocrine therapy and represent the Detect IVa study. Initially, they received concordant therapy with the mTOR inhibitor everolimus, which was replaced with ribociclib in 2018, when CDK4/6i became the standard treatment option in combination with endocrine agents in Germany. The Detect IVb study arm includes HR+ patients with indication for chemotherapy and triple-negative breast cancer (TNBC) patients who receive chemotherapy with eribulin. Patients with HER2+ primary tumors were included in the Detect V study, irrespectively of the HER2 status of their CTCs. After 1:1 randomization they either receive antibody based anti-HER2 therapy combined with chemotherapy and afterward anti-HER2 antibodies combined with ribociclib and endocrine therapy, whereas the other group only receives the latter therapy. Taking the presence of CTCs and their HER2+ expression into account for decision making, the DETECT study program is the first treatment intervention breast cancer study conducted in Germany and the internationally largest therapeutic intervention study on mBC [157].

CTCs obtained during the study will be used for translational research. The Detect IVa study, which this thesis is focused on, analyses DNA damage and repair, detection of several biomarkers such as PI3KCA or ERα, and the measurement of circulating miRNAs and CTCs.

Therapeutic intervention studies based on CTC enumeration and molecular phenotyping such as the DETECT program, taking liquid biopsies into account for cancer management are important to evaluate whether treatment decisions and individualized treatment can be improved by liquid biopsies. Similar studies are conducted for example in France. The STIC trial enrolls HR+ mBC patients who are randomized to an arm receiving therapy based on a clinician's choice or treatment based on CTC enumeration. Patients with less than 5 CTCs/7.5 mL blood receive endocrine therapy whereas patients with ≥ 5 CTCs/7.5 mL of blood receive chemotherapy. The CTCs count is equally reliable for first-line treatment decision as to the clinician´s choice [158]. The CirCé01 trial evaluated, whether mBC patients on their 3rd line of chemotherapy would benefit from a switch of chemotherapy if their CTC count did not decrease after one cycle of chemotherapy but failed to prove so [159]. Evaluation of CTC clusters on OS, elicited by the SWOG S0500 trial showed, that OS was independent of the presence of CTC doublets and clusters and solely dependent on the CTC number per 7.5 mL of blood, as has been demonstrated prior [160]. Phenotyping of CTCs facilitated therapy response for patients of the COMETI Phase 2 trial. By scoring ER, HER2, Ki67, and BCL2 expression, a CTC-Endocrine Therapy Index (CTC-ETI) was determined. A high CTC-ETI (high CTC count and/or low ER and BCL2 and high HER2 KI67) predicted poor outcome as these patients did not benefit from endocrine therapy [161]. While the DETECT IV study is still ongoing, DETECT III is already terminated and first results of this study have already been presented on the San Antonio breast cancer symposium 2020. Importantly, additional treatment with lapatinib versus standard chemotherapy alone was associated with better overall survival [162].

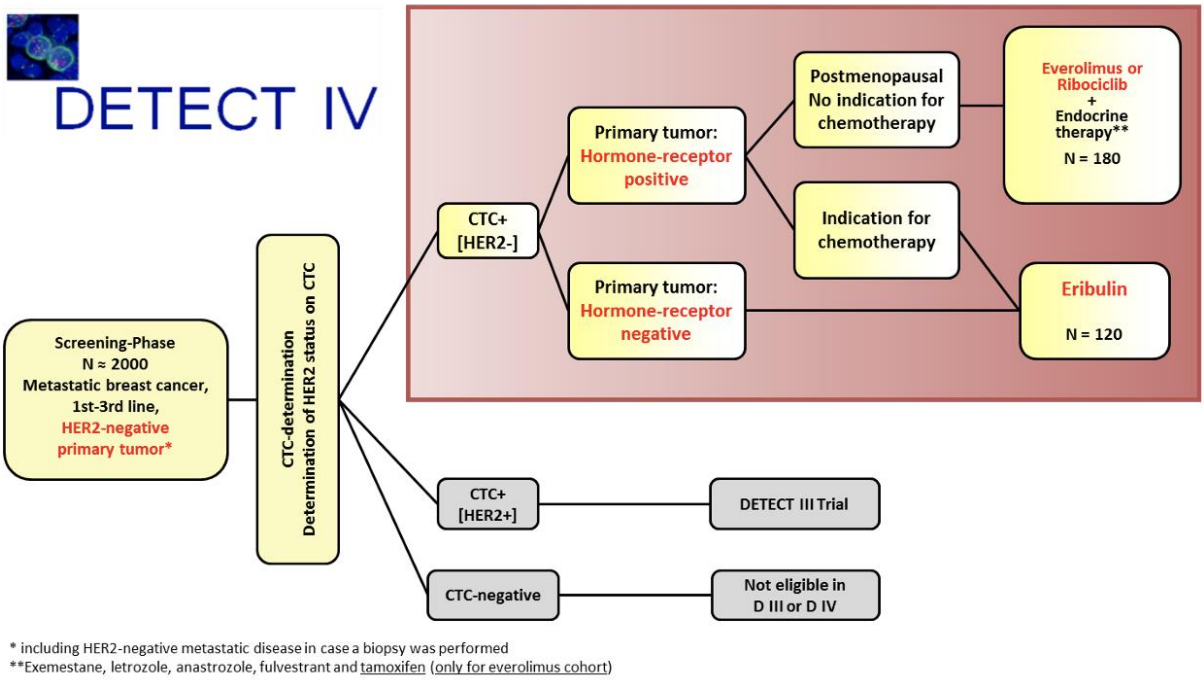

Figure 3: Treatment scheme of the DETECT IVa study [163].

1.7 Aims of this study

Despite a multitude of known drivers of CDK4/6 targeting therapies to date, established markers for CDK4/6 inhibitor resistance do not exist [125,126]. CDK4/6 inhibitors have become standard-of-care therapy for HR+ mBC patients, however, resistance to this therapy is virtually inevitable. Hence, finding markers for early detection of resistance and loss of susceptibility is of utmost importance.

Therefore, this thesis aimed at a) unraveling mechanisms contributing to CDK4/6i resistance, b) finding markers that can be used for early detection of emerging resistance, c) investigating the involvement of miRNAs in the development of resistance and d) testing marker proteins and miRNAs on samples from patients with HR+ mBC treated with CdK4/6 inhibitors.

a) To facilitate the analysis of resistance mechanisms, the luminal A BC cell line MCF7 and a luminal B cell line, derived from CTCs (CTC-ITB-01) and established in our lab should be used to generate ribociclib-resistant cell lines. Since this thesis was embedded in the translational part of the DETECT program, ribociclib was chosen as it is the CDK4/6 inhibitor used in the study. Resistance should be validatedusing cell cycle analysis, functional assays, and determination of deregulated mRNA and proteins by qPCR, Western blot analysis and immunofluorescence, respectively.

b) After confirmation of resistance to ribociclib, the parental cell lines and their respective ribociclib-resistant counterparts should be analyzed by RNA-sequencing (RNA-seq), to find deregulated mRNAs, miRNAs. Newly found deregulated mRNA targets were validated by qPCR and Western Blot and miRNAs by qPCR and *in situ* hybridization. Pathway and network analyses should be performed.

c) Due to the very short length of miRNAs, their detection is technically challenging. Therefore, an *in situ*-based assay should be established. Since the assay should not only be used for *in vitro* experiments but ideally also for detection of miRNAs on CTCs later, the assay should be established not only on pure cell culture samples but also on MCF7 and CTC-ITB-01 cell line cells spiked into blood collected from healthy donors to test different CTC enrichment methods for their compatibility with the assay. Additionally, miRNA *in situ* hybridization (MISH) should be assessed in CellSearch® (CS) cartridges, as most breast cancer samples are by CS, and transfer of the cartridges usually is associated with significant cell loss.

d) To test therapeutic options beyond CDK4/6 inhibitors, the influence of treatment with fulvestrant and alpelisib on the growth and viability of parental and ribociclib-resistant MCF7 and CTC-ITB-01 cells should be examined.

e) In the translational research part of this study, samples of HR+ mBC patients should be collected from patients enrolled in the DETECT study as well as from other patients treated with Cd4/6 inhibitors throughout the time of this thesis after enrichment and detection of CTCs by CellSearch® and other approaches. Here, potential markers for the prediction of CDK4/6 inhibitor resistance established in this thesis should be tested. Results of these experiments should be associated with clinic-pathological and outcome data of the patients.

2 Material and Methods

2.1 Material

2.1.1 Laboratory devices

Table 2: Laboratory devices used for this study

Device	Manufacturer	Company Headquarters
Analytical scale BP610	Sartorius	Göttingen, DE
Analytical scale CP224S-OCE	Sartorius	Göttingen, DE
Automatic Sarpette	Sarstedt	Nümbrecht, DE
ApoTome 2.0	Carl Zeiss	Jena, DE
Axio Observer	Carl Zeiss	Jena, DE
BD FACSCanto flow cytometer	BD Biosciences	Franklin Lakes, NJ, US
BioPhotometer with Thermal Printer DPU-414	Eppendorf	Hamburg, DE
Centrifuge 5417R	Eppendorf	Hamburg, DE
Centrifuge Multifuge 3 S-R	Hereaus Holding	Hanau, DE
Centrifuge Rotofix 32A	Hettich	Tuttlingen, DE
DNA Engine PTC-200	MJ Research	Waltham, MA, US
GloMax Discover Microplate Reader	Promega	Madison, WI, US
Incubator Hera Cell 150	Thermo Fisher Scientific	Waltham, MA, US
Laminar flow cabinet HerasafeTM KS 12	Heraeus Kendro	Langselbold, DE
Magnetic stirring hotplate MR 3001 K	Heidolph	Schwabach, DE
Microscope slide drying oven TDO Sahara	Medite Medical GmbH	Burgdorf, DE
Multipette M4	Eppendorf	Hamburg, DE
Mini Trans-Blot Electrophoretic Transfer Cell	Bio-Rad Laboratories	Hercules, CA, US
Mini-Protean System Casting Stand	Bio-Rad Laboratories	Hercules, CA, US
Mini-Protean Tetra Cell	Bio-Rad Laboratories	Hercules, CA, US
Nanodrop ND100 spectrometer	peqLab	Erlangen, DE
neoLab-Rotator 2-1175	neoLab	Heidelberg, DE
Neubauer counting chamber	Paul Marienfeld GmbH & Co. KG	Lauda-Königshofen, DE
Pipette (2.5 µL, 10 µL, 100 µL, 200 µL, 1000 µL, 5 ml)	Eppendorf	Hamburg, DE
Pipetus	Hirschmann	Eberstadt, DE
Power Pac Basic	Bio-Rad Laboratories	Hercules, CA, US
Power Pac HC	Bio-Rad Laboratories	Hercules, CA, US
NovoCyte Quanteon Flow Cytometer	Agilent Technologies	Santa Clara, CA, US
Stuart Scientific roller mixer SRT5	Bibby Scientific	Staffordshire, UK
ThermoBrite - 110/120 VAC	StatSpin Inc	Westwood, MA, US

Thermocycler C1000 Touch CFX96	Bio-Rad Laboratories	Hercules, CA, US
Tilt/Roll RS-TR 5	Phoenix Instrument	Garbsen, DE
Vortex Genie 2	Scientific Industries	New York, NY, US
Water bath GFL 1002	GFL	Burgwedel, DE
X-ray film processor Curix 60	Agfa	Mortsel, BE

2.1.2 Antibodies

2.1.2.1 Unconjugated antibodies

Table 3: Unconjugated antibodies used for Western Blot analysis in this study.

Antigen	Clone	Dilution	Species	Manufacturer	Company Headquarters	Cat #
α-Tubulin	Poly-clonal	1:20.000	rabbit	Cell Signaling	Danvers, MA, US	2144
BCL2	124	1:1000	mouse	Cell Signaling	Danvers, MA, US	15071
CDK6	DCS83	1:250	mouse	Cell Signaling	Danvers, MA, US	3136S
CDK6	D4S8S	1:250	rabbit	Cell Signaling	Danvers, MA, US	13331
CDK14	C-3	1:1000	mouse	Santa Cruz Biotechnology	Dallas, TX, US	Sc-376366
cyclin D1	E3P5S	1:1000	rabbit	Cell Signaling	Danvers, MA, US	55506
cyclin D3	DCS22	1:2000	mouse	Cell Signaling	Danvers, MA, US	2936
HSC70	B-6	1:10.000	mouse	Santa Cruz	Dallas, TX, US	7298
p21	12D1	1:1000	rabbit	Cell Signaling	Danvers, MA, US	2947
p27	D69C12	1:1000	rabbit	Cell Signaling	Danvers, MA, US	3686
pRB (Ser780)	D59B7	1:1000	rabbit	Cell Signaling	Danvers, MA, US	8180
pRB (Ser795)	Poly-clonal	1:1000	rabbit	Cell Signaling	Danvers, MA, US	9301
RB	4H1	1:1000	rabbit	Cell Signaling	Danvers, MA, US	9309
SOX9	Poly-clonal	1:1000	goat	R&D Systems	Minneapolis, MN, US	AF3075

Table 4: Unconjugated antibodies used for immunofluorescent staining in this study.

Antigen	Clone	Dilution	Species	Manufacturer	Company Headquarters	Cat #
CDK6	D5S8S	1:50	rabbit	Cell Signaling	Danvers, MA, US	13331
Cdk14	C-3	1:50	mouse	Santa Cruz Biotechnology	Dallas, TX, US	Sc-376366
E-Cadherin	36/E	1:200	mouse	BD Transduction Laboratories	Franklin Lakes, NJ, US	610182

Heparan sulfate	10E4	1:400	mouse	AMS Biotechnology	Frankfurt, DE	370255
SOX9	Poly-clonal	1:100	goat	R&D Systems	Minneapolis, MN, US	AF3075

2.1.2.2. Conjugated antibodies

Table 5: Conjugated antibodies used for immunofluorescence in this study.

Antigen	Clone	Conjugate	Dilution	Species	Manu-facturer	Company Head-quarters	Cat #
CD45	HI30	APC	1:150	mouse	Biolegend	San Diego, CA, US	304002
CD45	REA 747	AF647	1:150	recombi-nant	Miltenyi Biotec	Bergisch Gladbach, DE	130-110-633
Pan-Keratin	AE1/ AE3	AF488	1:150-1:300	mouse	Thermo Fisher Scientific	Waltham, MA, US	53-9003-82
Pan-Keratin	AE1/ AE3	eFluor570	1:150-1:300	mouse	Thermo Fisher Scientific	Waltham, MA, US	41-9003-82
Pan-Keratin	AE1/ AE3	PerCP	1:150	mouse	Biotinum	Fremont, CA, US	BNCP 0371-250
Pan-Keratin	C11	AF555	1:200	mouse	Cell Signaling	Danvers, MA, US	3478S

Table 6: Conjugated secondary antibodies used for immunofluorescence staining in this study.

Antigen	Clone	Conjugate	Species	Manu-facturer	Company Head-quarters	Cat #
Mouse IgG	Polyclonal	AF488	rabbit	Thermo Fisher Scientific	Waltham, MA, US	A11059
Rabbit IgG	Polyclonal	AF488	goat	Thermo Fisher Scientific	Waltham, MA, US	A11008
Goat IgG	Polyclonal	AF488	donkey	Thermo Fisher Scientific	Waltham, MA, US	A11005

2.1.3 ISH probes

Table 7: viewRNA DNA probes used for MISH

Target	Type	Detection Label	Manufacturer	Company Headquarters	Assay-ID
miR-16-5p	1	AF546	Thermo Fisher Scientific	Waltham, MA, US	VM1-10232-VCP
miR-21-5p	1	AF546	Thermo Fisher Scientific	Waltham, MA, US	VM1-10236-06
miR-21-5p	4	AF488	Thermo Fisher Scientific	Waltham, MA, US	customized
miR-146a-5p	4	AF488	Thermo Fisher Scientific	Waltham, MA, US	customized
miR-205-5p	4	AF488	Thermo Fisher Scientific	Waltham, MA, US	customized
miR-432-5p	4	AF488	Thermo Fisher Scientific	Waltham, MA, US	customized
CDK6	6	AF647	Thermo Fisher Scientific	Waltham, MA, US	VA6-3169253-VCP
Homo sapiens Check	1	AF546	Thermo Fisher Scientific	Waltham, MA, US	VA1-15726-02

2.1.4 qPCR primer

Table 8: qPCR primer used in this study

Name	Target	Sequence (5' → 3')
β-Actin forward	*ACTB*	CCAACCGCGAGAAGATGA
β-Actin reverse		CCAGAGGCGTACAGGGATAG
ALDH1A1 forward	*ALDH1A1*	GTTAGCTGATGCCGACTTGGA
ALDH1A1 reverse		TCCTGGATGCGGCTATACAAC
BCL2 forward	*BCL2*	CAGGATAACGGAGGCTGGGATG
BCL2 reverse		TTCACTTGTGGCCCAGATAGG
CDK6 forward	*CDK6*	TGACCAGCAGCGGACAAATA
CDK6 reverse		CAAGACTTCGGGTGCTCTGT
CDK14 forward	*CDK14*	CACCAAATGAGGACACATGGC
CDK14 reverse		TGTACAGGGTAAAGCGTTCTGG
CCND1 forward	*CCND1*	GCCCTCGGTGTCCTACTTCA
CCND1 reverse		CTCCTCGCACTTCTGTTCCT
CCND3 forward	*CCND3*	TGGCCCTCTGTGCTACAGATTA
CCND3 reverse		CCTGAGTGCAGCTTCGATCT
CCNE1 forward	*CCNE1*	TTGCTGCTTCGGCCTTGTAT
CCNE1 reverse		CGCACCACTGATACCCTGAAA
CCNE2 forward	*CCNE2*	GAATACTGACTGCTGCTGCCT
CCNE2 reverse		ACTGTCCCACTCCAAACCTGA
CLND1 forward	*CLDN1*	CCAGTCAATGCCAGGTACGAAT

CLND1 reverse		GGCCTTGGTGTTGGGTAAGA
DCS2 forward	*DSC2*	CTTGGAAAGTGGGCCATCCT
DCS2 reverse		CCAGCGTAAACAGGATGCAA
ESR1 forward	*ESR1*	GCTACGAAGTGGGAATGATGAA
ESR1 reverse		TTGGCAGCTCTCATGTCTCC
FN1 forward	*FN1*	CACCATCCAACCTGCGTTTC
FN1 reverse		AGTTGGGGAAGCTCGTCTGT
GRHL2 forward	*GRHL2*	GCCACCAAATCTCTCCGTCA
GRHL2 reverse		CCACCATCACCACACTCCTG
KRT23 forward	*KRT23*	ACTGGAGCGGCAGAACAATG
KRT23 reverse		TTTGATTCTTCCCGTGTCCCTT
LGALS1 forward	*LGALS1*	CTGGAAGTGTTGCAGAGGTGT
LGALS1 reverse		CCGTCAGCTGCCATGTAGTT
MUC13 forward	*MUC13*	GCTGTAACCAGACTGCGGAT
MUC13 reverse		TTGAGACTGGAAGCAACGCA
p16 forward	*CDN2A*	ATCGCGATGTCGCACGGTA
p16 reverse		AATCGGGGATGTCTGAGGGA
p21 forward	*CDN1A*	GCAGACCAGCATGACAGATTTC
p21 reverse		ATGTAGAGCGGGCCTTTGAG
p27 forward	*CDKN1B*	GCTAACTCTGAGGACACGCAT
p27 reverse		TGTTTTGAGTAGAAGAATCGTCGG
PTEN forward	*PTEN*	AAGGCACAAGAGGCCCTAGA
PTEN reverse		GATTGCAAGTTCCGCCACTG
Slug forward	*SLUG/SNAI2*	CAGACCCCCATGCCATTGAA
Slug reverse		TTCTCCCCCGTGTGAGTTCTA
Snail forward	*SNAI1*	GGTTCTTCTGCGCTACTGCT
Snail reverse		TGCTGGAAGGTAAACTCTGGAT
RB forward	*RB1*	TGGTATGTAACAGCGACCGT
RB reverse		CTCCTGGGAGATGTTTACTTCCA
TGFBR1 forward	*TGFBR 1*	TGGGAAATTGCTCGACGATG
TGFBR1 reverse		GCCATTACTCTCAAGGCTTCAC
TGFBR2 forward	*TGFBR2*	TAACAGTGGGCAGGTGGGAAC
TGFBR2 reverse		AGACATCGGTCTGCTTGAAGG
Twist forward	*TWIST*	ATTCAGACCCTCAAGCTGGC
Twist reverse		TTCTCTGGAAACAATGACATCTAGG
Vimentin forward	*VIM*	AGGCGAGGAGAGCAGGATT
Vimentin reverse		AGTGGGTATCAACCAGAGGGA
ZEB1 forward	*ZEB1*	TTACCAGGGAGGAGCAGTGA
ZEB1 reverse		CCTTCCTTTCCTGTGTCATCCT

2.1.5 Commercial kits

Table 9: Commercial kits used in this study

Kit	Manufacturer	Company Headquarters
First Strand cDNA Synthesis Kit	Thermo Fisher Scientific	Waltham, MA, US
magMax™ *mir*Vana™ Total RNA Isolation Kit	Thermo Fisher Scientific	Waltham, MA, US
Maxima SYBR Green/ROX qPCR Mastermix (2x)	Thermo Fisher Scientific	Waltham, MA, US
NucleoSpin RNA	Macherey-Nagel	Düren, DE
Pierce BCA Protein Assay Kit	Thermo Fisher Scientific	Waltham, MA, US
Senescence β-Galactosidase Staining Kit	Cell Signaling Technology	Danvers, MA, US
ViewRNA Cell Plus Assay Kit	Thermo Fisher Scientific	Waltham, MA, US
ViewRNA Cell Plus Cytospin Module Kit	Thermo Fisher Scientific	Waltham, MA, US

2.1.6 Consumables

Table 10: Consumables used in this study

Item	Manufacturer	Company Headquarters
4 chamber Polystyrene Vessel Tissue Culture Treated Glass Slide	Corning	New York, US
6 well plate	Sarstedt	Nümbrecht, DE
12 well plate	Sarstedt	Nümbrecht, DE
96 well plate	Sarstedt	Nümbrecht, DE
Sterile cell strainer, 40 µM	Labsolute® / Th. Geyer	Renningen, DE
Hard-Shell® Low-Profile, Thin-Wall, Skirted 96-Well PCR Plates, White Shell/Clear Well	Bio-Rad Laboratories	Hercules, CA, US
Leucosep™ tubes	Greiner Bio One	Kremsmünster, AT
Microseal 'B' PCR Plate Sealing Film	Bio-Rad Laboratories	Hercules, CA, US
Parafilm	Bemis	Neenah, WI, US
Pipette tips	Sarstedt	Nümbrecht, DE
Serological pipettes	Sarstedt	Nümbrecht, DE
Super RX films	Fujifilm	Minato, JP
T25 flask	Sarstedt	Nümbrecht, DE
T75 flask	Sarstedt	Nümbrecht, DE

2.1.7 Chemicals and reagents

Table 11: Chemicals and reagents used in this study

Chemical	Manufacturer	Company Headquarters
β-Mercaptoethanol	Merck	Darmstadt, DE
Absolute Ethanol	Merck	Darmstadt, DE
Acrylamide	Serva	Heidelberg, DE
Ammoniumpersulfate (APS)	AppliChem	Darmstadt, DE
Bromphenol blue	Merck	Darmstadt, DE
BSA Fraction V	Biomol	Hamburg, DE
CCK-8 (Cell-Counting Kit 8)	Dojindo	Mashiki, JP
Cholera Toxin from *Vibrio cholerae*	Sigma-Aldrich	St. Louis, MO, US
Crystal violet	Sigma-Aldrich	St. Louis, MO, US
Dako real ™ Antibody Diluent	Agilent	Santa Clara, CA US
Antibody Diluent with Background Reducing Components	Agilent	Santa Clara, CA US
DAPI (4‘,6-Diamidin-2-phenylindol)	Carl Roth	Karlsruhe, DE
Denatured Ethanol	Chemsolute / TH Geyer	Renningen, DE
DMSO (Dimethylsulfoxid)	Serva	Heidelberg, DE
DMF (Dimethylformamide)	Cell Signaling Technology	Danvers, MA, US
DTT (Dithiothreitol)	Sigma-Aldrich	St. Louis, MO, US
Ficoll-Paque Plus™	Amersham Bioscience	Buckinghamshire, UK
Glycine	Carl Roth	Karlruhe, DE
Hydrochloric acid (1N)	Carl Roth	Karlsruhe, DE
Hydrocortison	Sigma-Aldrich	St. Louis, MO, US
Hydrogen Peroxide	Fluka (Thermo Fisher)	Waltham, MA, US
Isopropanol	Carl Roth	Karlsruhe, DE
L-Glutamine	PAA Laboratories	Pasching, A
Luminol	Sigma-Aldrich	St. Louis, MO, US
Methanol	J.T. Baker	Deventer, NL
Non-fat dry milk powder	Carl Roth	Karlsruhe, DE
Nonidet P40 (NP40)	Roche Diagnostics	Mannheim, DE
Nuclease free water	Qiagen	Hilden, DE
p-Coumaric acid	Sigma-Aldrich	St. Louis, MO, US
Page Ruler Prestained Protein Ladder 10-180 kDa	Thermo Fisher	Waltham, MA, US
Paraformaldehyde (PFA)	Merck	Darmstadt, DE
ProLonG™ Gold Glass Antifade Mountant	Thermo Fisher	Waltham, MA, US
Propidiumiodide 95%	J&K Scientific	Beijing, CN
Protease Inhibitor Cocktail (100X)	New England BioLabs	Ipswich, MA, US
RNase A	Biozym	Hessisch Olendorf, DE

SDS Solution 20% (Sodium Dodecylsulfate)	AppliChem	Darmstadt, DE
Sodium Chloride	Carl Roth	Karlsruhe, DE
Sodium Deoxycholate	Sigma-Aldrich	St. Louis, MO, US
TEMED (Tetramethylethylenediamine)	Merck	Darmstadt, DE
Tris-EDTA (1x TE), pH 8.0	Sigma-Aldrich	St. Louis, MO, US
Trizma-Base	Sigma-Aldrich	St. Louis, MO, US
Trizma-HCl	Sigma-Aldrich	St. Louis, MO, US
Trypan Blue	Sigma-Aldrich	St. Louis, MO, US
Trypsin-EDTA solution 0.25% (w/v)	Gibco	Eggenstein, DE
Tween-20	Sigma-Aldrich	St. Louis, MO, US

2.1.8 Therapeutic agents

Table 12: Therapeutic agents used in this study

Reagent (trade name)	Chemical name	Function	Manufacturer	Headquarter
alpelisib	BYL719	PIK3CA Inhibitor	Cayman Chemical	Ann Arbor, MI, US
fulvestrant	ICI-182780	SERD	Selleckchem	Houston, TX, US
palbociclib	PD0332991	Cdk 4/6 Inhibitor	Cayman Chemical	Ann Arbor, MI, US
ribociclib	LEE011	Cdk 4/6 Inhibitor	Cayman Chemical	Ann Arbor, MI, US

2.1.9 Cell culture media

Table: Cell culture media composition

Media	Composition
DMEM	450 mL DMEM 50 mL FCS 2 mM L-Glutamine
RPMI 1640 complete	450mL RPMI 1640 50 mL FCS 2 mM L-Glutamine 1x Transferrin, Insulin, Selen 50 ng/mL EGF 10 ng/mL FGF

2.1.10 Buffer

Table 13: Buffer used in this study

Buffer	Composition
10 x Laemmli buffer	25 mM Tris-HCl 192 mM Glycin 0.1% (w/v) SDS
10 x Transfer buffer	48 mM Tris-HCl 39 mM Glycin 0.015% (w/v) SDS 10% (v/v) denatured Ethanol (99%)
3x SDS Sample buffer	180 mM Tris-HCl pH 6.8 30% (w/v) Glycerol 3% (w/v) SDS
ECL (1:1 of solution 1 and 2)	*Solution 1:* 100 mM Tris/HCl, pH 8.5 2.5 mM Luminol 0.4 mM p-Coumaric acid *Solution 2:* 100 mM Tris/HCl, pH 8.5 0.018% H_2O_2
TBS-T pH 7.6	20 mM Tris-HCl 150 mM NaCl 0.05% (v/v) Tween-20

2.1.11 Software

Table 14: Software used for data analysis in this study.

Software	Application	Source
Bio-Rad CFX Manager 3.1	qRT-PCR analysis	Bio-Rad Laboratories, Hercules, CA, US
ImageJ	CFA analysis	*https://imagej.nih.gov/ij/download.html*
GIMP	Image processing	*https://www.gimp24.de/*
GraphPad Prism 9.1.2	Graphics and statistical analysis	Graphpad Software Inc.
In-Silico Online	Statistical Analysis of VIM-detection on CTCs	*http://in-silico.online/*
NCBI Primer Blast	qRT-PCR Primer design	*https://www.ncbi.nlm.nih.gov/tools/primer-blast/*
Zen 2.6 (blue edition)	Microscopical analysis	Carl Zeiss

2.2 Methods

2.2.1 Cell culture methods

2.2.1.1 Cell lines

The cell lines mainly used in this thesis are MCF7 as a well-established luminal A BC cell line and the CTC-ITB-01 which is a luminal B BC cell line derived from CTCs. This cell line is characterized by its sensitivity to estrogen treatment despite constitutive ER signaling and lack of *ERBB2*+ amplification. Molecularly, it shares mutations with the primary tumors as well as the vaginal metastasis (*MAP3K1:* c.2782delT; p.S928Lfs*9 (41%), *MAP3K6:* c.2837C>T; p.P946L (30%), *NF1:* c.4528_4529insG; p.L1510Rfs*20 (90%), *PIK3CA:* c.1252G>A; p.E418K (26%), c.3140A>G; p.H1047R (74%), *TP53:* c.853G>A; p.E285K (92%)). An in-depth characterization of the cell line has been published [118]. Furthermore, ZR-75-1, T47D and CAMA were used as comparable luminal cell lines and MDA 468 and MDA 231 served as exemplary cell lines of TNBC. All cell lines were kindly provided by the Institute of Tumor Biology and were regularly tested negative for mycoplasma.

The MCF7 cell line was successfully authenticated with 100% identity in August 2019.

2.2.1.2 Cell culture

Cells were cultured under sterile conditions at 37 °C and 5 % or 10 % CO_2. Dependent on their growth rates they were split once to twice a week. After rinsing cells with PBS, they were detached by 0.05 % Trypsin which was subsequently inactivated by the addition of FCS containing cell culture media. Following three-minute centrifugation at 244 x g cells were re-seeded in appropriate density or a specific cell number for various experiments. All steps were conducted under a laminar flow hood. All cell lines used were regularly checked for mycoplasma contamination with the Venor GeM Classic Mycoplasma Detection.

2.2.1.3 Cryopreservation of cell culture cells

For long time storage, cells were cryopreserved. After harvest, 1 mL aliquots were frozen in cell culture media with the addition of 10 % DMSO at -80 °C. For re-culture, cryotubes were quickly thawed in a 37 °C water bath and resuspended in 5 mL of pre-warmed cell culture media. After centrifugation at 244 x g for 3 minutes to remove the DMSO-containing media, the cells were reseeded.

2.2.1.4 Generation of ribociclib-resistant derivates

Nearly all patients treated with Cdk 4/6 inhibitors (Cdk 4/6i), eventually develop resistance against these therapeutics. To analyze the molecular mechanisms behind this development, resistant derivates of MCF7 and the CTC-ITB-01 cell line were established. Over a course of 1.5 years, cells were treated with increasing concentrations from 0.2 μM ribociclib up to 1.2 μM for the MCF7 and 1.5 μM for the CTC-ITB-01 cell line. Resistance was confirmed by analysis of cell cycle profiles,

marker expression on mRNA level by qPCR and on protein level by Western Blot. Additionally, CCK-8 assays were performed to identify IC_{50} values.

2.2.1.5 Assessment of cell cycle profiles

The assessment of cell cycle profiles is an important assay to verify established resistance in the respective cell lines since CDK4/6 inhibition should not influence the cell cycle profile of the resistant derivates. Therefore, cells were seeded in T75 flasks so that they would reach approximately 70 % confluency on the day of harvest. Parental cell lines and their resistant derivates were incubated for 3 days (MCF7) or 6 days (CTC-ITB-01), subsequently harvested by short trypsinization of approximately 3 minutes and washed in PBS + 1 % BSA. After counting $1x10^6$ cells per 0.5 mL were fixed by dropwise addition of ice-cold 70 % ethanol and stored at -20 °C until staining. To remove the ethanol, the samples were washed twice by centrifugation at 500 x g for 10 minutes and secondly for 5 minutes at 400 x g. The supernatant was removed carefully, and the pellet vigorously resuspended in washing buffer. Finally, the cells were stained with 20 µg/mL propidium iodide (PI) + 100 µg RNase A in PBS + 0.1 % Tween-20 overnight. The cell cycle profiles were measured at a NovoCyte Quanteon Flow Cytometer and analyzed with the internal software of the device.

2.2.2 Functional assays

2.2.2.1 CCK-8 based proliferation assay

The sensitivity of the cell lines and their respective resistant derivates towards different CDK4/6 inhibitors and other therapeutic agents, was determined by CCK-8 assay. This assay is based on the reduction of a water-soluble tetrazolium salt by dehydrogenases. The colorimetric assay is used to evaluate the metabolic activity of cells which is a proportional parameter for cell viability and can therefore be used to analyze relative cell numbers. Amongst other similar assays like the MTT, XTT, or WST assays, the CCK-8 assay is supposed to be the most sensitive and least cytotoxic one.

Cells were seeded at a density of 3 x 10^3 cells/well (MCF7) or 1.5 x 10^3 cells/well (CTC-ITB-01) in a volume of 100 µL in 96 well plates. The wells at the edges of the plate were filled with PBS to minimize evaporation and ensure equal volume distribution within the plate. After 24 h the cells were treated in triplicate with increasing concentrations between 0.01 – 10 µM of either alpelisib, palbociclib, or ribociclib. After 72 h of incubation for MCF7 and 6 days for the CTC-ITB-01 cells, 10 µL of pre-warmed CCK-8 reagent were added per well and incubated for additional 4 h at 37 °C. Subsequently, the absorbance was measured at 460 nm and background absorbance was determined at 600 nm. The reference absorbance was subtracted from the measured values at 460 nm and then the blank was subtracted from all values. Following calculation of the mean, all samples were analyzed using regression-analysis with the GraphPad Prism software.

2.2.2.2 Colony formation assay

To assess the clonogenic growth of the cell lines chosen for the establishment of ribociclib-resistant derivates, Colony Formation assays (CFA) were performed. MCF7 cells were seeded at a density of 250 cells / well in a 6 well plate, the CTC-ITB-01 cell line at 500 cells / well. Following a resting time of 5 – 6 h, allowing the cells to attach to the plate, the cells were treated with increasing concentrations of either palbociclib or ribociclib. When colonies, defined as the assembly of ≥ 50 cells, had formed the cells were fixed with 70 % Ethanol for 10 minutes. This was the case after 8 days for the MCF7 cells and after 21 days for CTC-ITB-01 cells. Afterwards, staining was performed with 0.1 % of crystal violet solution for 5 minutes. Finally, the plates were thoroughly rinsed with ddH_2O and scanned after air-drying.

The clonogenic growth capacity was furtherly evaluated by analyzing the covered area with the Colony Area Plugin at ImageJ. Values were then normalized to the DMSO control and IC_{50} values were determined with the GraphPad Prism.

2.2.2.3 Senescence β-Galactosidase staining kit

The impact of different treatments on the induction of senescence on different cell lines was analyzed by measurement of the β-Galactosidase activity after treatment. Prior to the staining, MCF7 and CTC-ITB-01 were treated with either 1.2 μM (MCF7) or 1.5 μM (CTC-ITB-01) ribociclib or 1 μM fulvestrant or alpelisib or a combination of 1 μM ribociclib and 0.01 μM of either fulvestrant or alpelisib. All cells were incubated for 72 h except for CTC-ITB-01 cells that were only treated with 1.5 μM ribociclib. Due to their slower replication time, the latter cells had to be incubated for 6 days to allow ribociclib to develop complete effectiveness. The β-Galactosidase staining was conducted following the manufacturer's instructions and eventually analyzed on an Axio Observer Zeiss microscope on brightfield at 200 x total magnification.

2.2.2.4 Microfluidic experiments to investigate adhesive behavior

In collaboration with Yuanyuan Wang and Christian Gorzelanny (Department of Dermatology and Venereology, University Medical Center Hamburg-Eppendorf (UKE)), microfluidic experiments were performed to investigate the capacity of breast cancer cell line cells to adhere to endothelial cells. Primary human umbilical vein endothelial cells (HUVECs) were seeded into the capillaries of the microfluidic device. When confluency was reached, the cells were stimulated with 10 ng/mL TNFα, 4 h before the experiment. Breast cancer cell lines were harvested as described before and resuspended in PBS. Staining was done with CellTrace™ Calcein red or green dye at a dilution of 1:1000 at RT for 10 minutes. After 2 washing steps with PBS at 244 x g for 3 minutes, cells were counted and adjusted to a concentration of 2 x 10^6/mL in CO_2-independent cell culture media. With an air pressure pump system, cells were then perfused with a force of 2 dyne/cm^2 by the BioFlux 200 system. The cells were observed by fluorescent and brightfield microscopy, using an Observer z.1 by Zeiss at 100 x total magnification [164].

Additionally, the level of cell surface heparan sulfate was assessed by FACS. For that purpose, cells were grown to a confluency of approximately 70% and harvested as described previously. After

resuspension of the cell pellet in PBS, the cells were incubated with an anti-heparan sulfate antibody (clone 10E4) diluted 1:400 for 30 minutes on ices. After a washing step with PBS, the cells were incubated with an AF488-labeled anti-mouse IgG antibody diluted 1:1000 for 30 minutes on ICE. Following another washing step with PBS, heparan sulfate levels were assessed by flow cytometry at a BD FACSCanto flow cytometer.

2.2.3 Molecular biological methods

2.2.3.1 RNA isolation

Prior to the isolation, the cell monolayer was washed thrice with PBS, scraped off with 1 mL of PBS, and centrifuged at 750 x g for 3 minutes. Subsequently, the NucleoSpin™ RNA Kit was used, and isolation was performed according to the manufacturer's manual. The RNA was eluted in 40 – 60 µL of nuclease-free water. The concentration and quality of the RNA were determined at a Nanodrop ND100 spectrometer. 260/280 ratios ≥ 2.0 were considered acceptable. The RNA was then stored at -80°C and used for cDNA synthesis or send for RNA-sequencing.

2.2.3.2 Synthesis of cDNA

Total RNA from cell lines was used as a template in qPCR and thus had to be reversely transcribed into cDNA, using the First Strand cDNA Synthesis Kit. Therefore, 500 ng of RNA were transcribed using the random hexamer primers and the M-MuLV Reverse Transcriptase, following the manufacturer's instructions. The program used on the "DNA Engine PTC-200 Thermocycler" was as follows (Table 15):

Table 15: Cycler program for cDNA synthesis

Step	Temperature [°C]	Duration [min]
Annealing	25	5
Reverse Transcription	37	60
Inactivation of Transcriptase	70	5

Finally, the cDNA was diluted 1:10 with nuclease-free water resulting in a concentration of 2.5 ng/µL, assuming a 1:1 transcription and stored at -20 °C.

2.2.3.3 Quantitative polymerase chain reaction (qPCR)

Quantitative-PCR was performed to quantify differential mRNA expression. Beforehand, respective primers were designed utilizing the Primer Blast tool on NCBI. Complementary DNA (cDNA) synthesized from total RNA was then amplified using the Maxima SYBR Green/ROX qPCR Mastermix (2x) and reaction mixes were set up according to the manufacturer´s instructions, summarized in Table 16.

Table 16: Mastermix for qCR

Reagent	Volume [µL]

Maxima SYBR Green/ROX qPCR Mastermix (2x) (Maxima Hot Start Taq DNA Polymerase, dNTPs, SYBR Green)	5
Forward primer (10 µM)	0.3
Reverse primer (10 µM)	0.3
Nuclease-free H_2O	3.4
cDNA (1:10 diluted)	1

Samples were analyzed in triplicates on a 96 well plate in a Thermocycler C1000 Touch CFX96. The program used is summarized in Table 17.

Table 17: Cycler program for mRNA qPCR

Step	Temperature [°C]	Duration	Cycles
Initial denaturation	95	10 min	1
Denaturation	95	15 sec	41
Annealing	60	30 sec	
Elongation	72	30 sec	
Melting curve	65 – 95 (0.5 °C steps)	5 sec (each)	

Fluorescence is measured after each cycle. Since SYBR Green is intercalating only into double-stranded DNA, the fluorescence intensity is increasing with the present cDNA copies and therefore being a proportional parameter. Once reaching an exponential phase the fluorescent signal is reaching a threshold, differentiating a real signal from the background. The cycle, in which this threshold is intersected is called the quantification cycle (Cq) which is used for further analysis. Expression changes or differences were furtherly calculated using the Delta-Delta-Cq method. This method is based on the assumption of a consistently expressed housekeeping gene that can therefore be used for normalization which confirms biological causes of change and not technical issues. In this study, ß-Actin was chosen as a reference gene. Relative fold changes were calculated by the following equation.

1) $\Delta Cq = Cq_{\text{gene of interest}} - Cq_{\text{reference gene}}$
2) $\Delta\Delta Cq = \Delta Cq_{\text{treated}} - \Delta Cq_{\text{untreated}}$
3) Fold change expression = $2^{-\Delta\Delta Cq}$

2.2.3.4 Total RNA isolation for miRNA qPCR

To guarantee the high purity required to reliably perform miRNA qPCR, total RNA was isolated with a bead-based assay. The magMAX™ *mir*Vana™ Total RNA Isolation Kit utilizes magnetic beads for total RNA isolation, including highly efficient miRNA isolation. The manufacturers' protocol was adapted to a 1.5 mL Eppendorf tube format. Prior to the isolation, cel-miR-39 was spiked as a technical control in a concentration of 5 pM. All mixing steps were performed in a Thermoblock at RT and 1000 rpm. Samples were eluted in 50 µL of elution buffer and stored at -80 °C until cDNA synthesis.

2.2.3.5 Synthesis of cDNA from miRNAs

Total RNA isolated by the magMAX™ *mir*Vana™ Total RNA Isolation Kit was reversely transcribed into cDNA by a multi-step assay. The TaqMan™ Advanced miRNA cDNA Synthesis Kit reversely transcribes all present miRNAs in a sample, independently of specific primers. Therefore, all miRNAs are elongated on their 3´-end by polyadenylation and an adaptor is ligated to the 5´-end. Subsequently, these adaptors are recognized by universal primers. To ensure the detection of low abundant miRNAs, the samples are pre-amplified with universal primers. The assay was performed following the manufacturer's protocol.

2.2.3.6 Assessment of miRNA levels by qPCR

For miRNA detection, by qPCR, the TaqMan™ Fast Advanced Master Mix was used due to the manufacturer's instructions, but the volume was bisected to 10 µL. The pre-amplified miRNA cDNA was diluted 1:10 before use and 1 µL was used for each reaction.

Samples were analyzed in triplicates on a 96 well plate in a Thermocycler C1000 Touch CFX96. The program used was as follows (Table 18):

Table 18: Cycler program for miRNA qPCR

Step	Temperature [°C]	Duration	Cycles
UNG incubation	50	2 min	1
Polymerase activation	95	20 sec	1
Denature	95	3 sec	40
Anneal/extend	60	30 sec	

Identically to mRNA qPCR, fluorescence generated by the released TaqMan probed is measured after each replication cycle and the assay evaluated based on the determined Cq-values. Fold-changes were calculated by using the ΔΔCq method. For normalization, miR-484 was chosen, as it was the most homogenously expressed of the tested housekeeping miRNA in the cell lines used in this study.

2.2.3.7 RNA-sequencing

To identify all potential drivers of resistance, cells were sent to Novogene for whole transcriptome RNA-sequencing (RNA-seq). Parental and resistant cell lines were seeded in T75 flasks without any treatment and harvested after 3 days at a confluency of approximately 70%. Total RNA was isolated as described previously (2.2.3.4). The quality of the isolated RNA was controlled for all samples and mRNA, lncRNA, and circRNA were sequenced by paired-end 150 bp sequencing on Illumina NovaSeq platforms. Small RNAs were sequenced with single-end 50bp read length. Albeit all results were evaluated by Novogene, main bioinformatical analysis was done by Dr. Malik Alawi (Bioinformatics Core Facility, UKE).

2.2.4 Protein biochemical methods

2.2.4.1 Production of cellular protein lysate

For Western Blot analyses, protein lysates from cell lines were generated. For that, cells were rinsed with PBS thrice and incubated on ice for 5 minutes with 100-300 µL of 1x SDS lysis buffer that was added phosphatase inhibitor cocktail and 1 mM PMSF before each use. Subsequently, the cells were scraped off and transferred into a 1.5 mL Eppendorf tube. To ensure complete lysis also of the nuclei, the samples were sonicated twice at cycle 0.5 and amplitude 80 % for 15 seconds. To prevent sample heating, the lysates were kept on ice in between sonication steps. After taking an aliquot for the determination of the protein concentration, DTT was added to a final concentration of ~42 µM and saturated bromophenol blue solution was added in a dilution of 1:100. For storage, the samples were kept at -20 °C.

2.2.4.2 Bicinchoninic acid assay for determination of protein concentration of cellular protein lysates

Protein concentrations of whole-cell lysates was assessed by bicinchoninic acid (BCA) test. This assay is based on the reduction of Cu^{2+} to Cu^{1+} by proteins and the colorimetric change of a bicinchoninic acid in the presence of Cu^{1+} due to chelation. From each sample, an aliquot of 2.5 µL was diluted in ddH_2O and the enclosed BSA solution (2 mg/mL) was used to create a standard curve of 0, 100, 200, 400, 600, and 1000 µg/ml. Additionally, 2.5 µL of the 1 x SDS lysis buffer was added to each sample of the standard curve and 500 µL of working reagent was added to all samples, consisting of solution A and B in a ratio of 50:1. Following thoroughly mixing, the samples were heated in a water bath at 55 °C for 2 minutes and immediately stored on ice to prevent saturated color development. The respective absorbances were measured at 562 nm on a photometer.

2.2.4.3 SDS-PAGE

Proteins were separated by SDS – Polyacrylamide Protein Electrophoresis (SDS-PAGE). Since proteins disulfide bridges are reduced by DTT in the lysis buffer and SDS induces a linearization

of the proteins, in addition to conveying negative charge to them, proteins are separated in dependency of their respective molecular weights.

Gels were cast manually, using the "Mini Protean System Casting Stand" (for composition check Table 19). Before loading, the samples were heated at 95 °C for 5 minutes, and briefly spun down to dispose of any residual debris. 1x Laemmli buffer was used as a running buffer. Proteins were separated at 75 V for 20 minutes. After entering the separation gel, the conditions were changed to 120 V for additional 70 – 75 minutes. PreStained PageRuler™ protein ladder and a biotinylated ladder were used for size reference.

Table 19: Composition of SDS-PAGE gels

Component	Separation gel (10%, 5 mL) [mL]	Stacking gel (2 mL) [mL]
H_2O	2.0	1.4
30% Acrylamide	1.7	0.33
1.5 M Tris/HCl (pH 8.8)	1.3	0.25
10% SDS	0.05	0.2
10% APS	0.05	0.2
TEMED	0.02	0.02

2.2.4.4 Protein transfer

Wet transfer was the chosen method for blotting of the proteins to polyvinylidendifluoride (PVDF) membranes. In preparation for the protein transfer, a 0.45 µM PVDF membrane was primed in 100% methanol for 45 minutes to decrease its hydrophobicity. The membrane was then furtherly equilibrated in ddH_2O for 5 minutes and finally equilibrated in transfer buffer for at least 5 minutes. Likewise, sponges and filter paper were soaked in transfer buffer before ethe sandwich assembly. Then, the transfer sandwich, consisting of a sponge, three filter papers, the gel, the membrane, three additional filter papers and another sponge was assembled. The transfer was performed at 100 V, 350 mA for 1 h under cooling conditions. Subsequently, the membrane was briefly rinsed in TBS-T and blocked with 5 % (w/v) dry-milk powder in TBS-T at room temperature (RT) for 1 h. Primary antibodies were either diluted in 5 % (w/v) dry-milk powder in TBS-T or 5 % BSA (w/v) solved in TBS-T according to the antibody datasheets and incubated overnight at 4 °C. After 3 washing steps with TBS-T for 5 minutes each, the membrane was incubated with the respective secondary antibody, diluted in 5 % (w/v) dry-milk powder in TBS-T, for 1 h at RT, followed by 3 additional washing steps. For detection, the membrane was finally incubated for 1 minute in freshly-prepared ECL solution and exposed 1 – 10 minutes to an X-ray film. The homogenously expressed protein Hsc70 served as a loading control.

2.2.5 *In-situ* hybridization and immunological staining

2.2.5.1 Detection of miRNA *in situ* hybridization

Due to their size, the detection of miRNAs remains challenging. Amongst other available methods, miRNA *in situ* hybridization (MISH) represents a fast and highly sensitive one with single-molecule resolution. The "viewRNA cell plus assay kit" was used to detect miRNAs and mRNAs in combination with protein immunofluorescence on adherently grown cell culture cells, cells immobilized on slides by centrifugation (cytospins) of spiked healthy donor samples, and patient samples processed by CellSearch®. Deviating from the manufacturer's protocol, all samples were fixed with 4% paraform aldehyde (PFA) for 15 minutes before the first fixation step of the protocol. Furthermore, the immunostaining was performed after the completed hybridization, not before as specified in the manual. Keratin was stained in dependency of the detected miRNA or mRNA and the fluorescent labels of the respective probes. A pan-keratin antibody cocktail (clone AE1/AE3), either labelled with eFluor570, eFluor450 or PerCP was used in a dilution of 1:150 and CD45 was detected by an APC labeled antibody (clone REA747) also diluted 1:150 and stained for 45 minutes in the dark. All other steps were performed as indicated by the manufacturer. Hybridization was performed in a ThemoBrite in humid conditions to minimize evaporation of the reagents and cytospins were additionally covered with parafilm for that cause. Finally, samples were mounted using the ProLong Glass Antifade mounting medium and miRNA-specific signals were detected by microscopic analysis.

2.2.5.2 Assessment of miRNA-specific signals generated by MISH by fluorescent microscopy

Since miRNAs are localized throughout the cytoplasm, detecting all signals by a single focus plane picture is not possible. Despite the strong signal amplification achieved by the viewRNA Assay, scattered light can hamper reliable detection of distinct miRNA-specific signals. Thus, Z-Stack pictures of 25-40 single frames were taken with an ApoTome 2.0, to picture all miRNA molecules within the cell. The ApoTome provides an improved signal–to–noise ratio by reducing the out–of–focus light. For processing, phase errors were corrected, and a weak Fourier filter option was selected. After creating an ApoTome picture, the z-stacks were merged by using the Maximum Projection option in the Extended Depth of Focus menu. Final pictures were optimized by reducing the background to a reference staining, using the range indicator.

2.2.5.3 Immunofluorescent staining

The localization and abundance of certain proteins in this study was investigated by immunofluorescent staining. Mostly, immunofluorescence (IF) was performed on cell culture cells grown on chamber slides. Furthermore, IF was used to detect CTCs on patient samples by the detection of distinct ex- and inclusion markers.

All samples were fixed with 4% PFA for 15 minutes and washed with PBS for 3 minutes, followed by permeabilization of the cellular membrane with 0.2 % (v/v) Tween-20 in PBS for 15 minutes and a 3-minute washing step with PBS. All primary antibodies were diluted in DAKO GREEN?

As follows: CDK6 – 1:50, CDK14 – 1:50 (final concentration: 4 µg/mL), SOX9 – 1:100 (final concentration: 5 µg/mL) and incubated for 1 (CDK6, CDK14) to 2 h (SOX9). Subsequently, samples were washed thrice with PBS for 3 minutes, followed by incubation with the secondary antibodies, which were diluted 1:200 in DAKO WHITE?? For 45 minutes. Again, the samples were washed thrice with PBS for 3 minutes. Optionally, additional staining of keratin was performed by incubation of the cells with a directly labeled pan-keratin antibody cocktail, consisting of clones C11 and AE1/AE3, being diluted 1:200 and 1:100 in PBS, respectively, for 45 minutes. Nuclei were counterstained with DAPI, diluted 1:500 ins PBS. Before mounting the samples with Fluoromount-G, they were washed thrice with PBS for 3 minutes. All steps were conducted at RT.

2.2.6 Enrichment of circulating tumor cells from patient samples

2.2.6.1 Patient samples

Blood samples from patients with metastatic breast cancer were collected at the Departments of Gynecology and Obstetrics, University Hospital Heidelberg and University Medical Center Hamburg-Eppendorf for the detection of circulating tumor cells with the CellSearch® system at the Institute of Tumor Biology, University Medical Center Hamburg-Eppendorf. From all patients written informed consent was obtained. Analyses were conformed to the principles set out in the WMA Declaration of Helsinki and the Department of Health and Human Services Belmont Report. Blood samples were drawn into standard 7.5 mL ethylenediaminetetraacetic acid (EDTA) vacutainers or in CellSave preservation tubes (Menarini-Silicon Biosystems).

Additionally, peripheral blood from healthy donors was collected by the Institute of Transfusion Medicine (University Medical Center in Hamburg, Germany). All donors provided general written informed consent for their blood samples to be used in scientific studies.

Etical approval was obtained from the Ethics Committee of the "Hamburger Ärztekammer, number PV5392.

2.2.6.2 Enrichment of CTCs by Ficoll-paque™-based density gradient centrifugation

Various enrichment methods for CTCs exist, all based on different mechanisms. Density gradient centrifugation separates components of a sample based on their specific density, in contrast to marker-based enrichment for example used by the CellSearch® system or size-based enrichment as performed by the Parsortix® system. Density gradient centrifugation using Ficoll™-Paque is commonly used method for the enrichment of CTCs and separation of mononuclear cells from other blood components. For that purpose, whole blood from EDTA tubes is diluted with PBS to a total volume of 30 mL and carefully layered on 20 ml of Ficoll-Paque™. After 30 minutes of centrifugation at 400 x g for 30 minutes with soft deceleration the supernatant, including the plasma layer and interphase containing the mononuclear cells, was transferred to a 50 ml Falcon and PBS was added to a final volume of 50 mL. The sample was centrifuged at 400 x g for 10 minutes and the supernatant discarded. After lysis of erythrocytes with an appropriate buffer for 5 minutes, the lysis buffer was diluted with 30 mL of PBS, centrifuged at 400 x g for 10 minutes and the pellet resuspended in 5 – 10 mL of PBS.

This process can be simplified by using Leucosep tubes which contain a porous polyethylen separation disc, making the careful layering of the sample on the Ficoll-Paque layer and the transfer of the interphase unnecessary. Instead, the diluted sample is simply transferred to the Leucsep tube and after centrifugation at 800 x g for 12 minutes, the supernatant was transferred into another falcon tube, the inlet was rinsed with a Pasteur pipette and PBS was added to a total volume of 50 mL. All other steps were identical to the normal procedure. Two kinds of cytospins were made, "large" ones with 7.5 x 10^5 cells and "small" ones, containing 5 x 10^5 cells, by centrifugation at 244 x g for 3 minutes. The slides were airdried overnight and stored at -80°C.

2.2.6.3 Enrichment of CTCs by CellSearch®

The enrichment of CTCs by the CellSearch® System is based on the expression on EpCAM that is unique to cells of epithelial origin. 7.5 mL of peripheral blood, drawn into CellSave tubes containing a fixative that stabilizes cells for 96 h, were processed by the CellSearch® Autoprep System. EpCAM expressing cells were enriched immunomagnetically by anti-EpCAM antibody-covered beads. Using the Profile Kit, the process is completed at this step, providing enriched but unlabeled cells. However, two different kits are provided to additionally stain the cells against Keratin as a positive marker. The CTC kit offers an antibody cocktail against Keratins 8, 18 and 19, labeled with PE, whereas the antibodies of the CXC kit are labeled with FITC, providing more flexibility for the choice of an additional marker. CD45 is highly expressed by lymphocytes and labeled with APC in both kits, serving as an exclusion marker. Afterwards, the enriched sample is transferred into a cartridge and after magnetic alignment at the cartridge wall ready to be scanned by the "CellTracks Analyzer". This device scans the complete sample and provides pictures of Keratin positive "events". These are examined by an experienced scientist to detect Keratin positive, CD45 negative cells, likely to be CTCs. The CellSearch® System is the only FDA-approved CTC enrichment method and metastatic breast cancer one out of three cancer entities, amongst colon and prostate cancer, for which an official prognostic value. The presence of ≥ 5 CTCs / 7.5 mL of blood is associated with significantly shorter PFS and OS of metastatic breast cancer patients, for patients with early-stage cancer, the cutoff is already at ≥1 CTC / 7.5 mL of blood.

CTCs of mBC patients were enriched by the CellSearch system and vimentin was detected in the fourth channel of the device by a FITC-labelled antibody in a final concentration of 1 μg/mL.

2.2.7 Data analysis

2.2.7.1 CCK–8 analysis

Preliminary analysis of the CCK-8 assay was performed using Excel by subtracting the reference value, measured at 600 nm from the absorbance assessed at 450 nm. These values were then copied to GraphPad Prism software and the mean value was calculated. After subtraction of the blank value, all values were normalized to their respective DMSO control. The logarithm of the X-values facilitated the use of non-linear regression. The method "log(inhibitor) vs response (three

parameters) was chosen. In the case of a successful non-linear regression analysis, IC_{50} values are given.

2.2.7.2 CFA analysis

Evaluation of the covered area was the chosen method for CFA analysis. This was done with an ImageJ PlugIn named ColonyArea [165]. ColonyArea automatically determines the area of the well covered by colonies. These values were then copied to GraphPad Prism software and normalized to DMSO. X-Values were logarithmized to calculate IC_{50} values by non-linear regression, applying the log(inhibitor) vs response (three parameters) was chosen. In the case of a successful non-linear regression analysis, IC_{50} values are given.

2.2.7.3 Analysis of qPCR results

Quantitative PCR data were evaluated with the Bio-Rad CFX Manager 3.1. If targets measured from one sample were distributed on different plates, all Actin control thresholds were set to relative fluorescent units (RFU) 50 to facilitate comparison between the different runs. Otherwise, thresholds were only changed to an RFU between 40 and 60 if the automated threshold setting obviously failed. Mean values of technical replicates were copied into Excel and the mean of three independent biological replicates was calculated. To assess fold changes by the ΔΔCq method, as described in 2.2.3.3, all samples, including DMSO controls, were normalized to the ΔCq of the DMSO controls. Thereby, variance also of the controls could be analyzed.

For miRNA analysis, miR-484 or miR-16-5p or a combination of both served as controls for normalization. If present, the spike-in control, cel-miR-39 was a control for the technical homogeneity of the RNA isolation and cDNA synthesis efficacy between samples.

Significance between groups was tested with a 2-way ANOVA using Tukeys test for the correction of multiple testing by using ΔCq values, which are proportional to the $2^{-\Delta\Delta}$ values, and normally distributed. A Family Wise alpha threshold of 0.05 was applied.

2.2.7.4 Analysis of RNA-Seq data

Analysis of the RNA-seq raw data was kindly performed by Dr. Malik Alawi from the Bioinformatics Core Facility at the UKE. This included identification of genes and miRNAs with differential expression in resistant versus parental cell lines, variant calling, pathway analysis and prediction of normalized enrichment scores. Differentially expressed genes were characterized by a log2FC of ≥1 and a FDR of ≤0.1. Gained mutations were identified by a frequency of ≥25% in the resistant cells versus a frequency of 5% in the parental ones. Over enrichment analysis was used to identify enriched pathways in the resistant derivates, using the GO and MSigDB databases. The prediction of activated transcription factors was based on the DoRothEA database.

2.2.7.5 Association of vimentin expression of circulating tumor cells and patient characteristics

To test for associations between vimentin expression of circulating tumor cells and patient characteristics, cross tables were constructed and analyzed using the G-test with Williams' correction (http://in silico.online).

3 Results

3.1 Sensitivity of MCF7 and CTC-ITB-01 to CDK4/6 inhibition

3.1.1 Clonogenic capacity of cells treated with CDK4/6 inhibitors

Prior to start of continuous ribociclib treatment, the sensitivity of the CTC-ITB-01 cell lines was tested. This cell line is particularly interesting for research on mBC CTCs since it is a CTC-derived cell line from a metastatic HR+ BC patient and was categorized as a luminal B cell line[118]. Since this cell line was established before CDK4/6 inhibitors were developed and FDA approved, it is naïve for any CDK4/6 inhibitor, making it a well-suited model to analyze development of resistance. For comparison, MCF7 as a model cell line for luminal A cancer was also chosen for discovering development of resistance. The influence of palbociclib, another CDK4/6 inhibitor on the proliferation was already tested, demonstrating the susceptibility of MCF7 as well as CTC-ITB-01 cells to this treatment [118]. This was further validated by analyzing whether palbociclib and ribociclib would suppress the clonogenicity of these cell lines and whether the impact of both inhibitors was comparable.

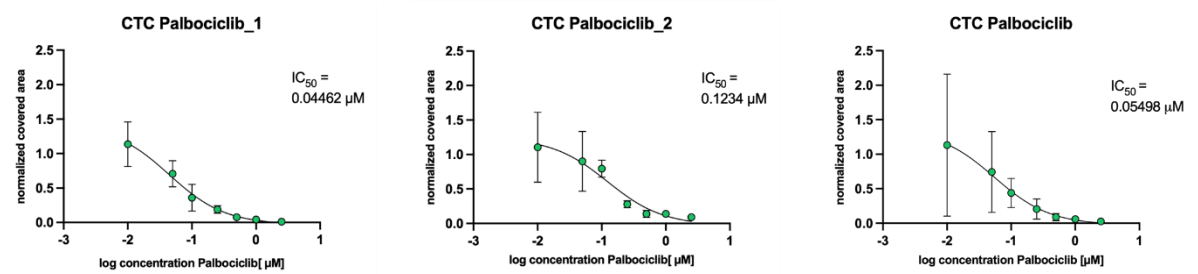

Figure 4: Inhibition of clonogenic growth of CTC-ITB-01 cells by palbociclib. 500 cells were seeded in triplicates in 6 well plates and treated with increasing concentrations of palbociclib between 0.01 µM - 2.5 µM. After 21 days, when colonies had formed, the cells were fixed, stained and the covered areas were evaluated. Two independent biological replicates (n=2) and their summary are depicted. Error bars indicate ±SD.

In concordance with the proliferation data [118], the colony formation assay (CFA) also showed high sensitivity of the CTC-ITB-01 cell line to palbociclib treatment (Figure 4), with an IC_{50} of 0.055 µM, derived from two independent biological replicates. Thereafter, the same experiment was performed with ribociclib.

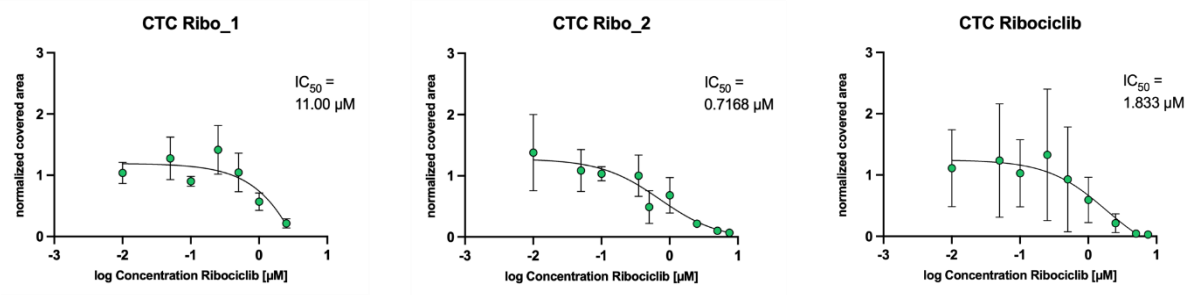

Figure 5: Inhibition of clonogenic growth of CTC-ITB-01 cells by ribociclib. 500 cells were seeded in triplicates in 6 well plates and treated with increasing concentrations of ribociclib between 0.01 µM - 7.5 µM. After 21 days,

when colonies had formed, the cells were fixed, stained and the covered areas were evaluated. Two independent biological replicates (n=2) and their summary are depicted. Error bars indicate ±SD.

As Figure 5 proves, CTC-ITB-01 cells were also susceptible to ribociclib treatment, however, palbociclib exerted a more pronounced inhibition of the clonogenic growth of the cells (Figure 6). However, it should be noted that the highest concentration in the first experiment was 2.5 µM ribociclib, resulting in an IC_{50} value of 11 µM. The values were chosen based on initial experiments performed with palbociclib. After observing the insufficient inhibition of growth by this concentration to model a dose-response-curve and comparison to literature the concentration was increased to 7.5 µM, as the IC_{50} concentration of ribociclib seems to be generally higher [166]. That resulted in an IC_{50} of 0.72 µM, leading to a combined IC_{50} value of 1.807 µM (Figure 5). Overall, complete inhibition of clonogenic growth is already seen at palbociclib concentrations of 0.5 µM, whereas 5 µM of ribociclib was needed for complete growth abrogation (Figure 6).

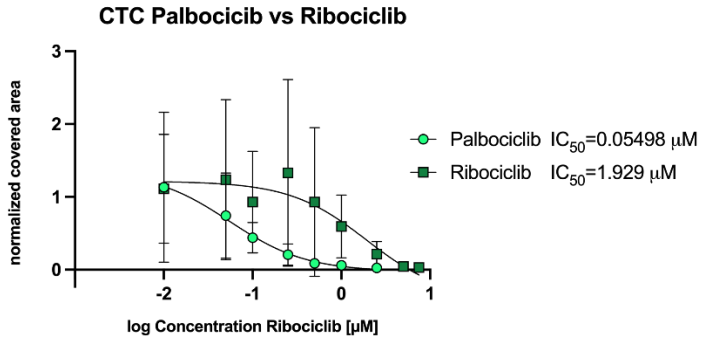

Figure 6: Inhibition of clonogenic growth of CTC-ITB-01 cells by treatment with palbociclib and ribociclib. Comparison of the influence of palbociclib and ribociclib treatment on the clonogenic growth of CTC-ITB-01 cells. 500 cells per well were seeded and colonies were fixed after 21 days. No washout or media exchange was done. Two independent biological experiments were summarized. Error bars indicate ±SD.

Figure 7 compares the response of CTC-ITB-01 and MC7 cells to both inhibitors and demonstrates sensitivity to both CDK4/6 inhibitor treatments as their clonogenic growth capacity was strongly reduced by either inhibitor.

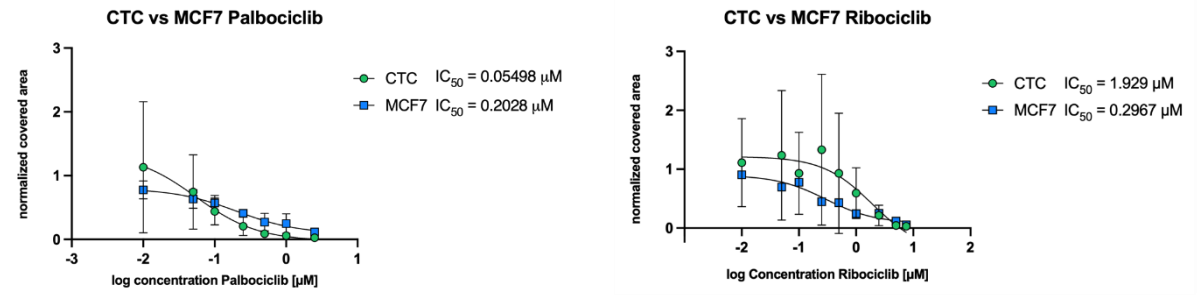

Figure 7: Impact of treatment with CDK4/6 inhibitor on clonogenic growth of CTC-ITB-01 and MCF7 cells. The sensitivity of the clonogenic growth capacity to palbociclib and ribociclib was assessed. 500 CTC-ITB-01 and 250 MCF7 cells were seeded per well and in triplicates. Colonies were fixed after 21 days and 8 days, respectively. No washout or media exchange was done. Two independent biological replicates were summarized, except only one single experiment for MCF7 cells treated with ribociclib. Error bars indicate ±SD.

When treated with palbociclib, the CTC-ITB-01 cells were comparably more sensitive than the MCF7 cells, whereas the latter were more susceptible to ribociclib treatment. Exemplary pictures in Figure 8 of an experiment with ribociclib show the reduction of colony numbers, caused by the CDK4/6 inhibition.

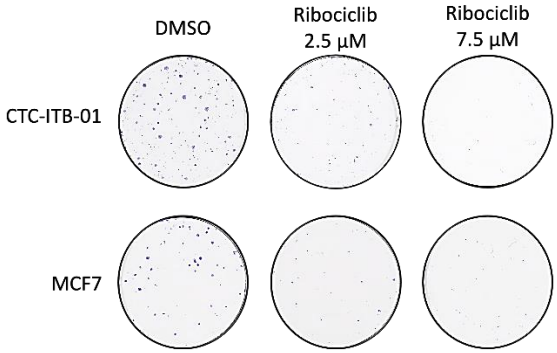

Figure 8: Clonogenic growth inhibition of CTC-ITB-01 and MCF7 cells by ribociclib. Exemplary pictures, taken from one CFA experiment. Ribociclib exerted visible growth inhibition in both cell lines, MCF7 and CTC-ITB-01.

Both inhibitors were effective with an IC_{50} value in a physiologically reasonable range, being in a range of concentration that is also predicted to be found in patients´ blood after drug uptake, making them both suitable candidates for further experiments. Since this thesis is included in the translational part of the Detect IVa study, ribociclib was the inhibitor of choice, as it is part of the therapy regime in the study.

3.2 Establishment of ribociclib-resistant cell lines

One possibility to unravel mechanisms of resistance to CDK4/6 inhibition is the creation of cell lines developing resistance to a respective inhibitor. Ribociclib was chosen, as it is the CDK4/6 inhibitor administered to mBC patients in the Detect IVa study. Starting with a concentration of 0.2 µM, MCF7 and CTC-ITB-01 cells were constantly grown with ribociclib. The concentration was increased when morphological changes were no longer induced by the addition of ribociclib to the growth media. Due to the literature, most luminal A breast cancer cell lines were deemed resistant when the doubling time was comparable to the parental cell line at 1 µM of ribociclib. Yet, preliminary experiments demonstrated insufficient resistance in the CTC-ITB-01 cell line at that concentration (data not shown). Therefore, the concentration was increased to 1.5 µM. Similarly, for MCF7 cells, the final concentration was increased to 1.2 µM to obtain more pronounced effects. A timeline of the establishment of the resistant sublines is presented in Figure 9. MCF7 and CTC-ITB-01 cells were cultivated in parallel without ribociclib over the entire period of time and are referred to as parental cells.

Figure 9: Timeline of the establishment of ribociclib-resistant MCF7 and CTC-ITB-01 (CTC) cell lines. Cells were cultured with continuous ribociclib treatment. The concentration was increased stepwise by 0.2 µM as soon as the cells were morphologically identical to their parental counterparts.

3.2.1 Impact of ribociclib treatment on the cell cycle

Cell cycle profiles were assessed at a continuous growth with 1.2 µM ribociclib for MCF7 cells and 1.5 µM for CTC-ITB-01 cells, the latter generally having a higher G1 fraction compared to the faster-proliferating MCF7 cell line. Summarized cell cycle profiles from three independent biological replicates are shown in Figure 10.

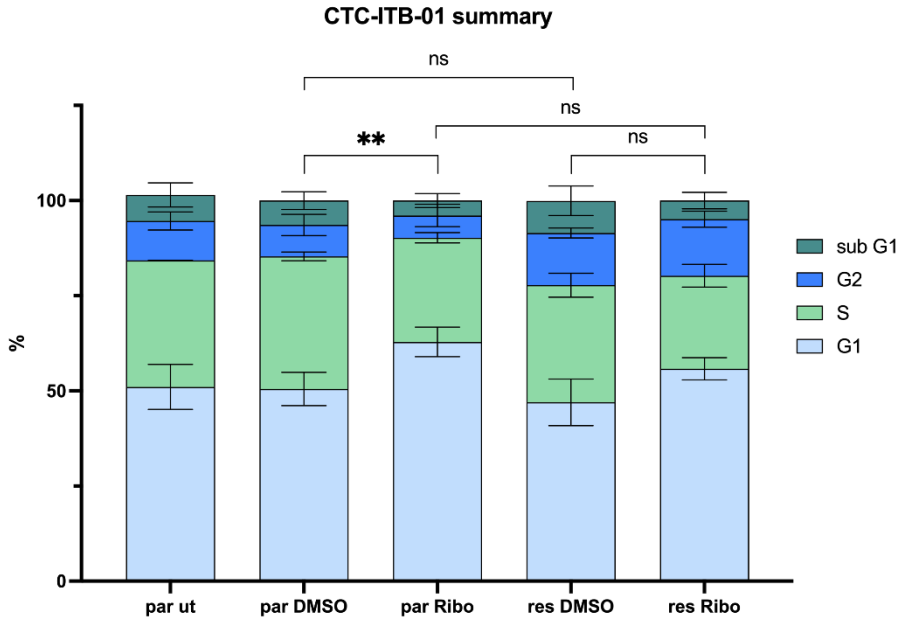

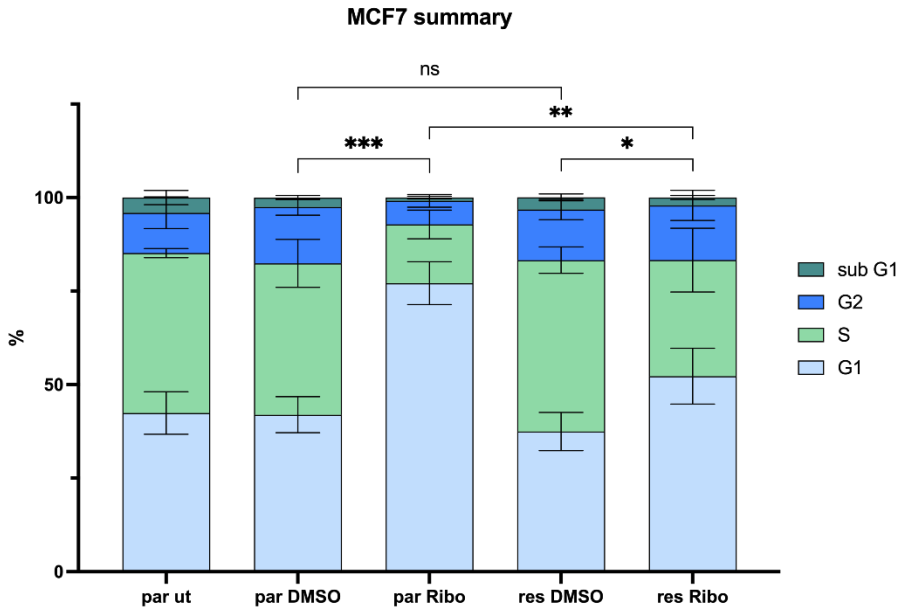

Figure 10: Cell cycle profiles of CTC-ITB-01 and MCF7 cells. Parental and resistant cells were treated with the concentration of ribociclib the resistant derivates were cultivated at. Cell cycle profiles were assessed by propidium iodide staining. The graphs show fractions of cells in different cell cycle phases as measured by FACS of three independent biological replicates. Mean frequencies and ±SD are shown. Significance of G1 changes was calculated by one-way ANOVA using Tukey multiple comparison test ($p > 0.05$ = ns, ≤ 0.05 = *, ≤ 0.01 = **, ≤ 0.001 = ***, ≤ 0.0001 = ****).

Untreated cells were analyzed to rule out any impact of DMSO on the cell cycle. Treatment with 1.2 µM ribociclib arrested a great fraction of parental MCF7 cells in G1. In MCF7, the fraction of cells in G1 increased from 42% to 77%. This increase of the G1 fraction upon treatment was significant as calculated by one-way ANOVA (p=0.0002). DMSO had no impact on the cell cycle in either cell line. In the resistant MCF7 cells, the G1 fraction increased from 38% in the DMSO control to 52% in the ribociclib treated parental cells. Compared to the increase in G1 induction in the parental cell lines of 35%, the increase of 14% in the resistant derivates was comparatively small, yet significant (p=0.0264). The G1 fractions of DMSO treated parental and resistant MCF7 cells did not differ from each other. However, the difference of the G1-fraction induced by ribociclib treatment in parental versus resistant MCF7 cells, was highly significant (p=0.0079).

A similar effect was observed upon treatment with 1.5 µM ribociclib in the parental CTC-ITB-01 cell line. The G1 fraction significantly increased from 50% to 63% (p=0.002) and in the resistant derivates from 47% up to 56% (p=0.1877, ns). Thus, the increase in the parental cell line is higher with 13% compared to only 9% increase of G1 cells induced in the resistant cell line. However, overall, the responsiveness of the CTC-ITB-01 to ribociclib treatment is lower than in MCF7 cells. Again, the G1 fraction of DMSO-treated parental and resistant derivates were comparable. In contrast to the results obtained for MCF7 cells, also the G1 fraction of ribociclib-treated parental and resistant CTC-ITB-01 did not differ significantly.

Another proof for G1 arrest is given by the percentage of cells in S-phase. Figure 11 shows a significant decrease of parental S-phase cells upon treatment with ribociclib (p=0.0001 and p=0.0125 for CTC-ITB-01 and MCF7, respectively), whereas the decrease of S-phase cells in the resistant derivates was not significant (p=0.0537 and p=0.1108 for CTC-ITB-01 and MCF7, respectively).

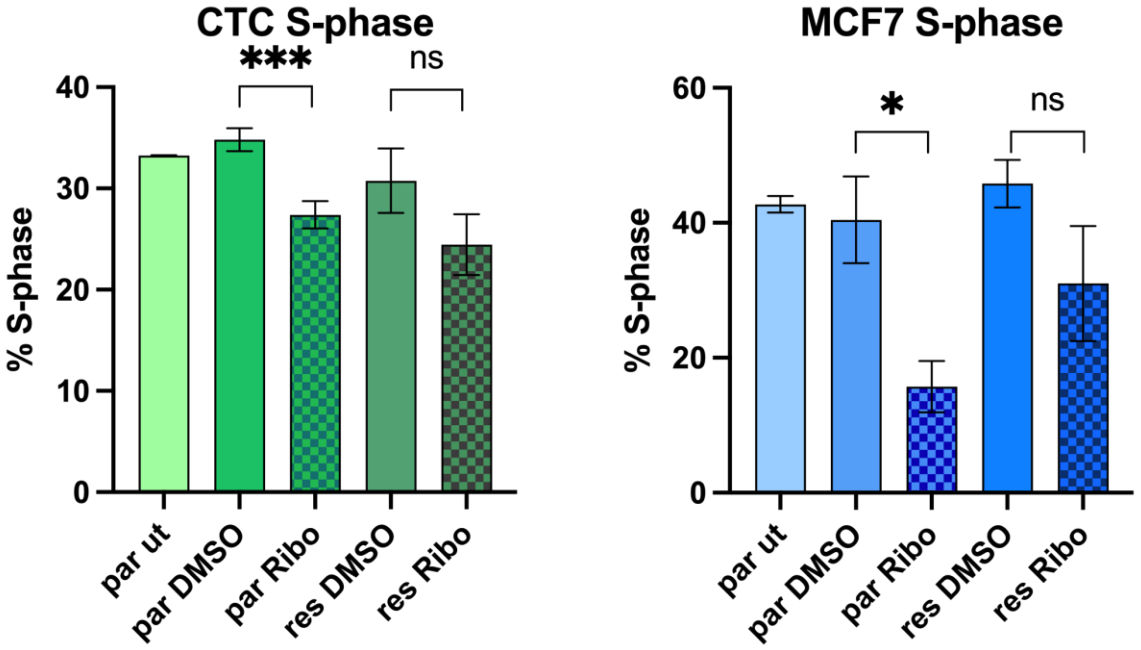

Figure 11: Fraction of cells in S-phase. The graphs show cells in the S-phase as measured by FACS of three independent biological replicates. Mean frequencies and ±SD are shown. Significance of changes of S-phase cells was calculated by one-way ANOVA using Tukey multiple comparison test ($p > 0.05$ = ns, ≤ 0.05 = *, ≤ 0.01 = **, ≤ 0.001 = ***, ≤ 0.0001 = ****).

Summarized, the cell cycle profile analysis provided evidence for established resistance in the CTC-ITB-01 and MCF7 derivates.

3.2.2 Impact of ribociclib treatment on cell viability of parental and resistant derivates

For further validation of established resistance, the impact of ribociclib treatment on the viability of parental and resistant cell lines was compared. CCK-8 assays revealed that resistant CTC-ITB-01 cells indeed show decreased sensitivity to inhibition by ribociclib compared to the parental cell line (Figure 12). The IC_{50} derived from three independent biological replicates was 1.89 µM for the parental cell line whereas the IC_{50} of the resistant cell line was approximately 3.5-fold higher at 6.75 µM.

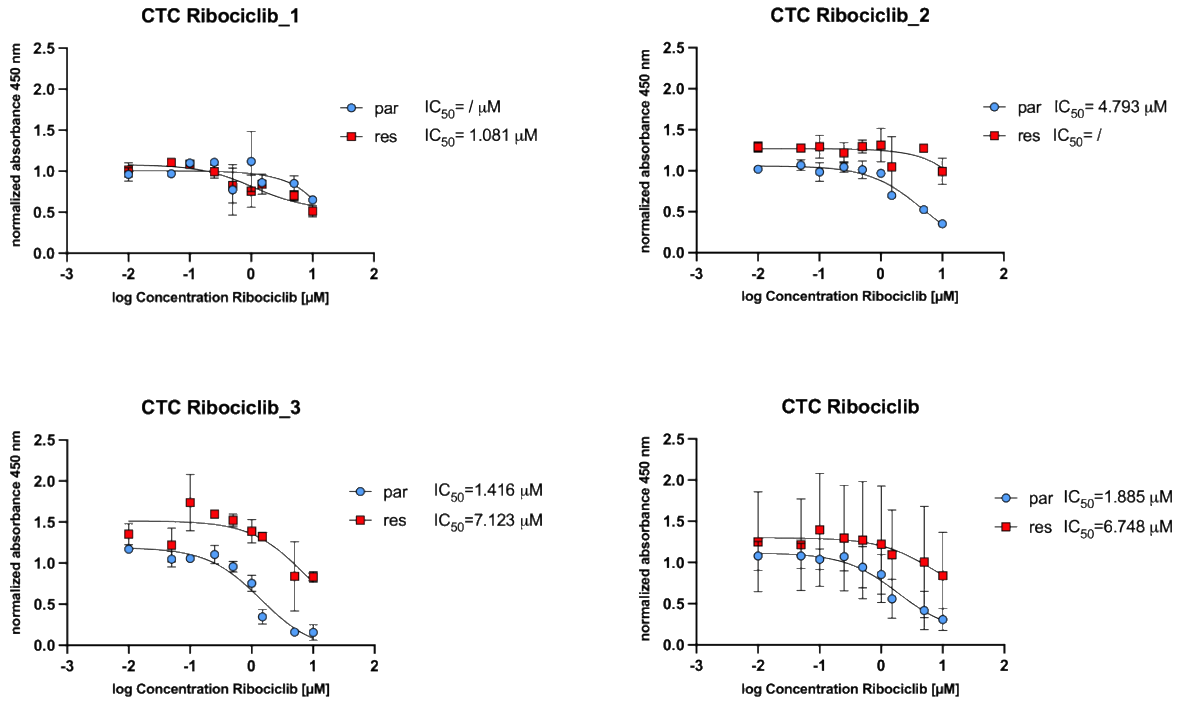

Figure 12: Analysis of the impact of treatment with ribociclib on the viability of parental and resistant CTC-ITB-01 cells. Three independent biological replicates demonstrate decreased sensitivity of the resistant cell line compared to the parental one. 1.5 x10^3 cells per well were seeded in a 96 well plate and treated with increasing concentrations of ribociclib from 0.01 – 10 µM and the absorbance of CCK-8 product was measured after 4 h of incubation at 450 nm. All experiments were assessed in technical triplicates and results were normalized to the DMSO control.

Similar experiments with the MCF7 cells resulted in even more pronounced differences (Figure 13).

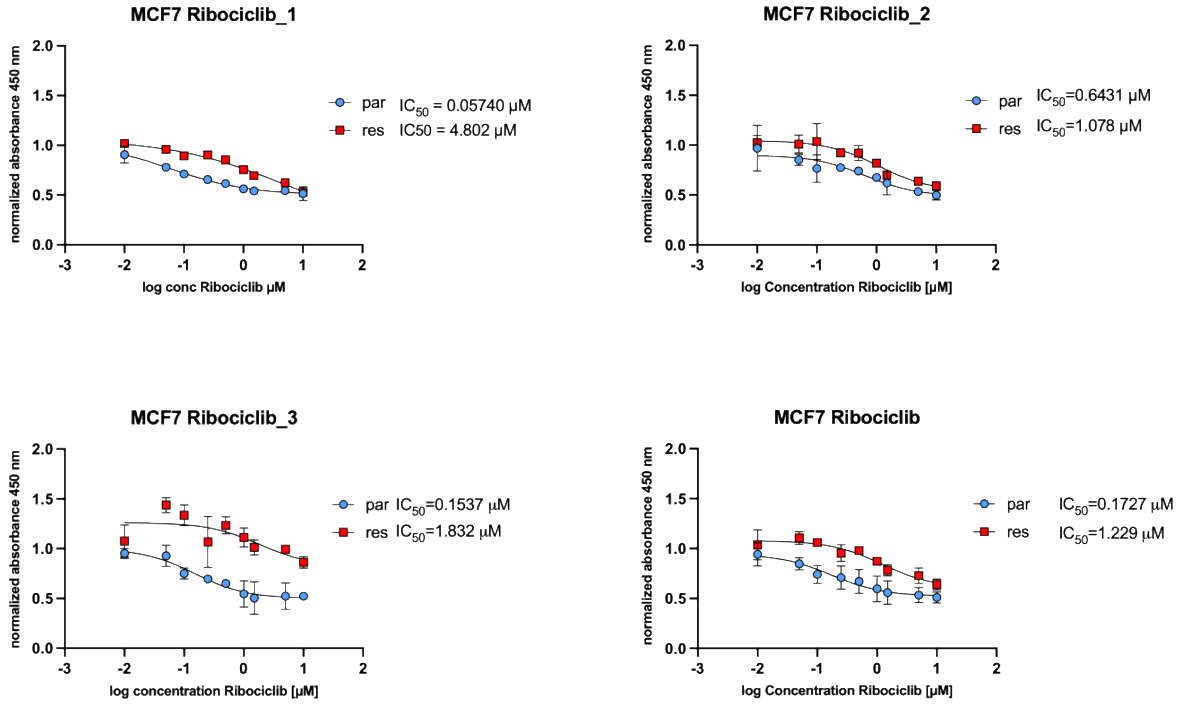

Figure 13: Analysis of the impact of ribociclib on the viability of parental and resistant MCF7 cells. Three independent biological replicates demonstrate decreased sensitivity of the resistant cell line compared to the parental one. $3x10^3$ cells per well were seeded in a 96 well plate and treated with increasing concentrations of ribociclib from 0.01 – 10 µM and the absorbance of the CCK-8 product was measured after 4 h of incubation at 450 nm. All experiments were assessed in technical triplicates and normalized to the DMSO control. Error bars indicate ±SD.

As shown for the CTC-ITB-01 cells, also the resistant MCF7 cell line was less sensitive to ribociclib treatment than the parental counterpart. The determined IC_{50} value of resistant MCF7 cells was 1.23 µM and thus approximately 7-fold higher than that of the parental MCF7 cells, for which IC_{50} was 0.17 µM, confirming successful establishment of resistant sub cell lines.

Resistance was also validated by comparing the inhibition of clonogenic growth in the parental and resistant cell lines, induced by ribociclib. Similarly, CFA demonstrated strongly reduced susceptibility of the resistant cell lines compared to their ribociclib-sensitive counterparts, as shown in Figure 14.

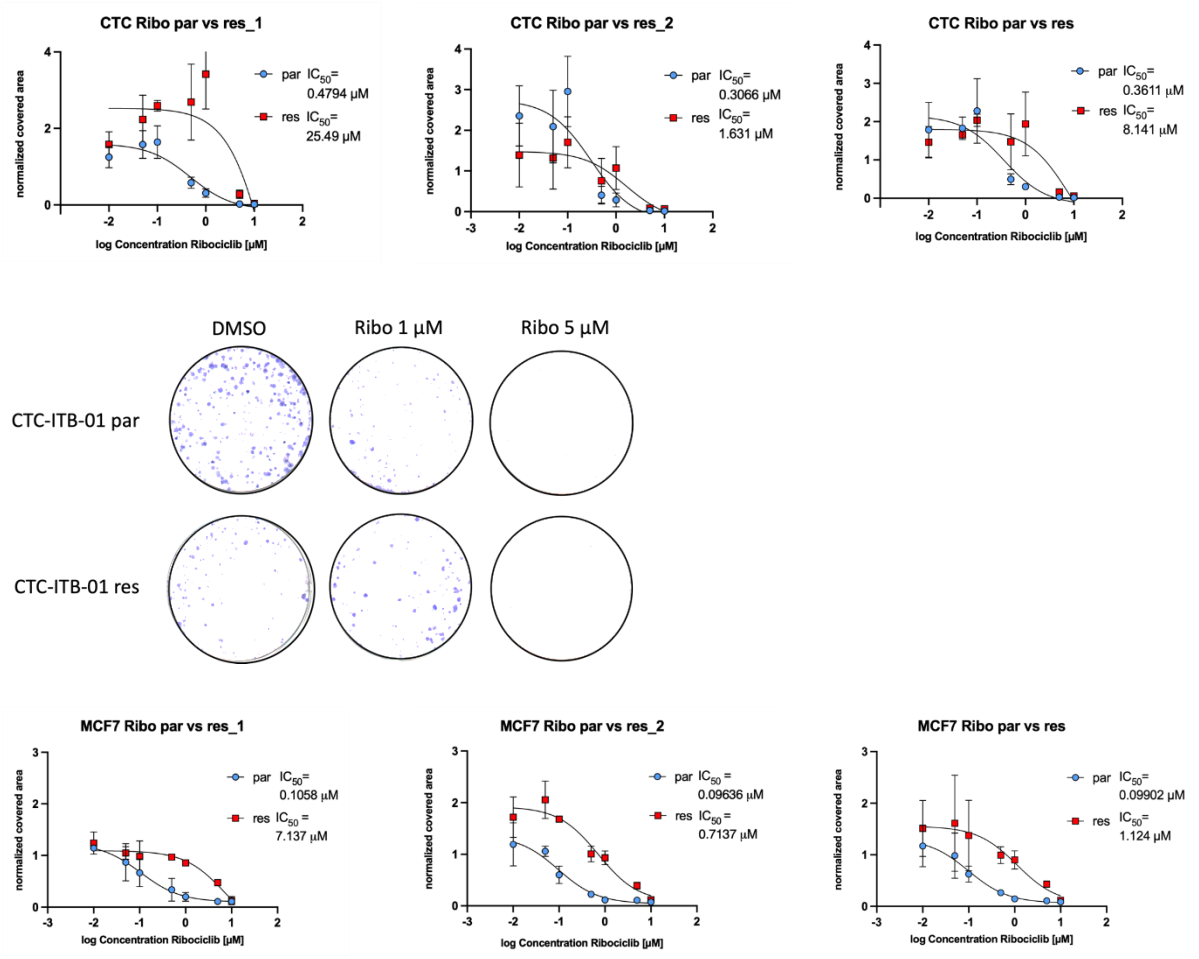

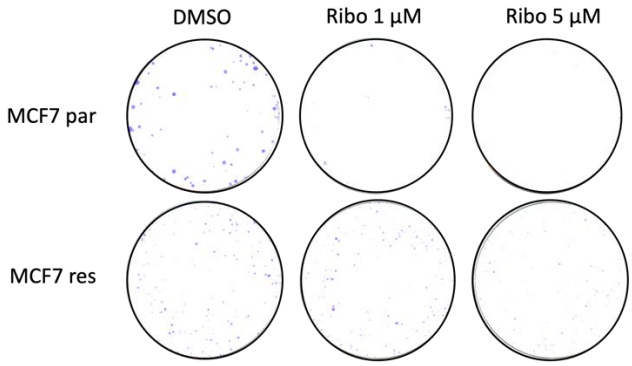

Figure 14: Analysis of the impact of ribociclib on the clonogenic growth of parental and resistant cell lines. 500 CTC-ITB-01 and 250 MCF7 cells were seeded in triplicates in 6 well plates and treated with increasing concentrations between 0.01 µM - 10 µM of ribociclib. After 21 or 8 days, respectively, when colonies had formed, the cells were fixed, stained and the covered area was evaluated. Two independent biological replicates and their summary are shown. Error bars indicate ±SD.

Despite overall stronger impact of ribociclib on the clonogenic growth of all cell lines compared to their viability, the resistance of CTC-ITB-01 and MCF7 cells could be demonstrated in this assay as well. The IC_{50} values of both cell lines were more than 10-fold higher than in the parental ones with 8.14 µM vs 0.36 µM for the CTC-ITB-01 cells and 1.12 µM vs 0.01 µM of the MCF7 cells. In line with the preliminary experiments, CTC-ITB-01 cells were less sensitive to the treatment than the MCF7 cells, however, for both cell lines the IC_{50} values dropped compared to previous experiments (Figure 7) where an IC_{50} value of 1.93 µM was calculated for CTC-ITB-01 cells and 0.3 µM for MCF7 cells. It is important to point out, that the experiments were not performed at the same time. While the results from Figure 7 were performed before the establishment of resistant cells, the ones from Figure 14 were conducted with cells culture parallel to the chronically exposed cells.

3.2.3 Ribociclib induced senescence

Overall, using CFAs a stronger impact of ribociclib on the clonogenic growth of both cell lines and their resistant derivates could be observed than on the viability, assessed in the CCK-8 assay. Since ribociclib by itself is not a cytotoxic but rather a cytostatic drug, inducing senescence [167], this was not unexpected. To prove this hypothesis, β-galactosidase activity in all four cell lines was measured as this enzyme is induced by senescence [168] (Figure 15).

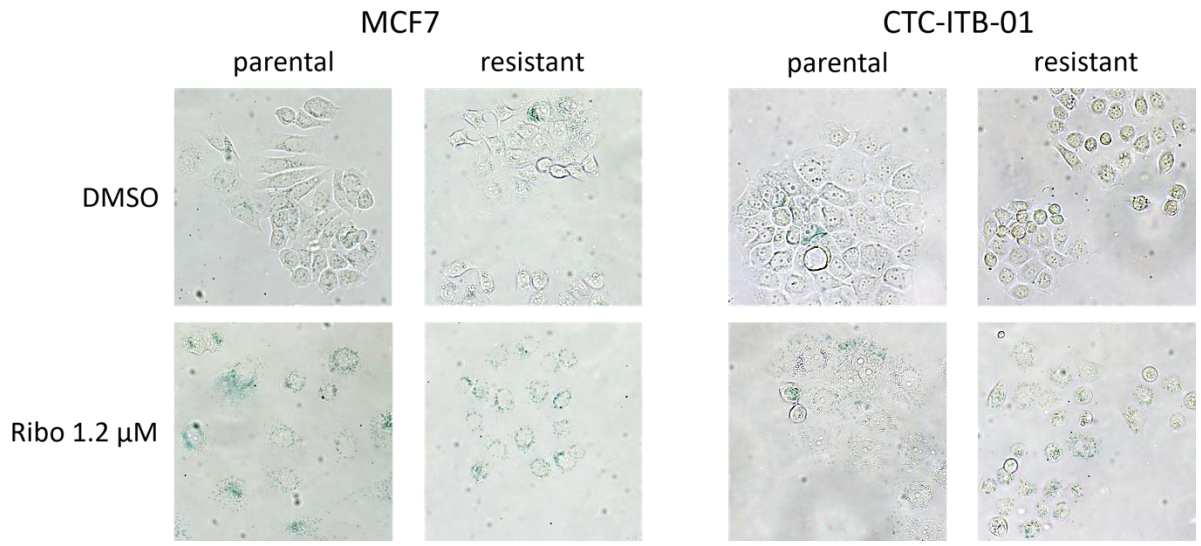

Figure 15: Detection of senescence-induced β-galactosidase activity in ribociclib treated cells. Cells were incubated with ribociclib for 3 days (MCF7) to 6 days (CTC-ITB-01). The staining was developed overnight in an incubator without CO_2-supply and assessed on a Brightfield microscope at 10x magnification.

Despite the flattened and enlarged morphology observed upon ribociclib treatment, the senescence-induced β-galactosidase assay did not clearly show increased senescence in the ribociclib-treated cells. Only in the sample of parental MCF7 cells, a ribociclib-induced increase of blue-stained cells was observed. Still, this might partly explain the differences between results from CFA and CCK-8 assays, since senescent cells might still be metabolically active, while being unable to proliferate. Furthermore, the lack of senescence induction in CTC-ITB-01 cells was in line with the slightly weaker response of this luminal B cell line to CDK4/6i compared to that of the luminal A cell line MCF7.

3.3 Identification of cell-cycle related genes/proteins contributing to the establishment of resistance

When the cell lines were deemed resistant, qPCR and Western blot analyses were performed to identify transcripts/proteins that are potentially involved in the development of resistance to the CdK4/6 inhibitor ribociclib. Changes on mRNA levels induced by continuous ribociclib treatment were analyzed by qPCR.

Based on literature data, several transcripts encoding cell cycle-related proteins involved in the regulation of the G1-phase and G1/G2 transition were analyzed by qPCR and the significance of changes in the expression levels between DMSO-treated control samples and ribociclib-treated samples, respectively, were assessed, using a 2-way ANOVA (Figure 16 A, B).

A

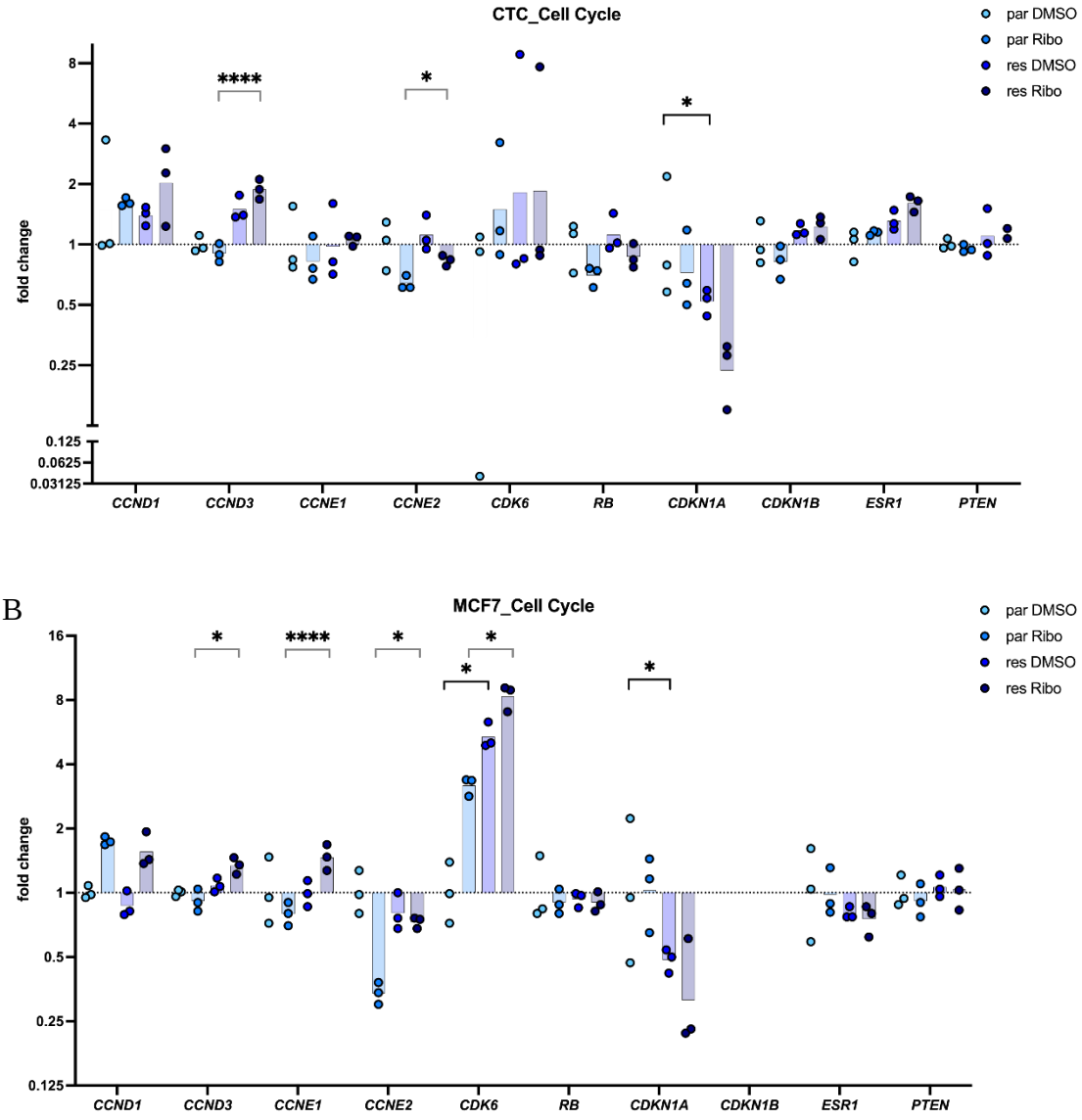

Figure 16: qPCR analysis of transcripts encoding cell cycle-related proteins. $2^{-\Delta\Delta}$ values that represent fold changes of three independent biological experiments are shown. All values were normalized to the respective parental DMSO-treated samples. All transcripts were normalized to *ACTB* transcript levels, which served as a housekeeping gene. Significance was tested with the 2-way ANOVA Tukey test, correcting for multiple comparison. ($p > 0.05$ = ns, ≤ 0.05 = *, ≤ 0.01 = **, ≤ 0.001 = ***, ≤ 0.0001 = ****). Black bars represent comparison of DMSO-treated samples, grey bars ribociclib-treated samples. A: CTC cell line, B: MCF7

To differentiate between immediate changes induced by ribociclib and changes that potentially contribute to resistance, parental and resistant cell lines were equally treated with ribociclib or the solvent DMSO. Ribociclib treatment significantly induced *CCND3* expression in the resistant vs the parental CTC-ITB-01 cells by almost 2-fold (ad. p= <0.0001), whereas the 1.5-fold increase if *CCND3* expression in the DMSO-treated resistant cells compared to the parental was not statistically significant (ad. p=0.0922). Furthermore, *CCNE2* levels were significantly stronger

reduced in ribociclib-treated parental cells than in ribociclib-treated resistant ones (ad. p=0.0296). The only significant change detected between both DMSO-treated cell lines, serving as a control, was the approximately 0.5-fold decrease of *CDKN1A* expression (ad. p=0.0437). No significant changes were observed in *CCND1*, *CCNE1*, *RB*, *CDKN1B*, *ESR1* and *PTEN* transcript levels, neither between the DMSO- nor the ribociclib-treated samples.

In parental MCF7 cells, the altered impact of ribociclib treatment on resistant as compared to parental cells was more obvious. In the resistant cells, *CCND3*, *CCNE1* and *CDK6* levels were significantly increased compared to ribociclib-treated parental cells (ad. p=0.0104, ad. p=<0.0001, ad. p=0.0408 respectively), whereas *CCNE2* levels were decreased, but to a significantly lesser extent than in the treated parental cells (ad. p=0.0104). Comparison of the DMSO treated cell line samples revealed a significant, 5.4-fold increase of *CDK6* expression and a 0.5-fold decrease of *CDKN1A* levels in the resistant cells compared to the parental counterparts (ad. p=0.0056, ad. p=0.022).

Neither in the parental nor in the resistant MCF7 cells, *CDKN2A* (encoding p16) transcripts were detectable and changes of *CCND1*, *RB*, *ESR1* and *PTEN* were not significant. Generally, significant changes of less than ≤ 2-fold or 0.5-fold are marked in the figures, but their biological relevance was hard to estimate and for that reason these genes were not in the focus of the following experiments.

Changes in the expression of cell cycle-regulating proteins considered pivotal for the establishment of resistance to ribociclib were evaluated by Western blot analysis. Protein levels are not necessarily concordant with the respective mRNA levels due to e.g. post transcriptional regulations for example by miRNAs or alterations in translation rates, protein half-lives, protein synthesis and decay or protein transport [169,170].

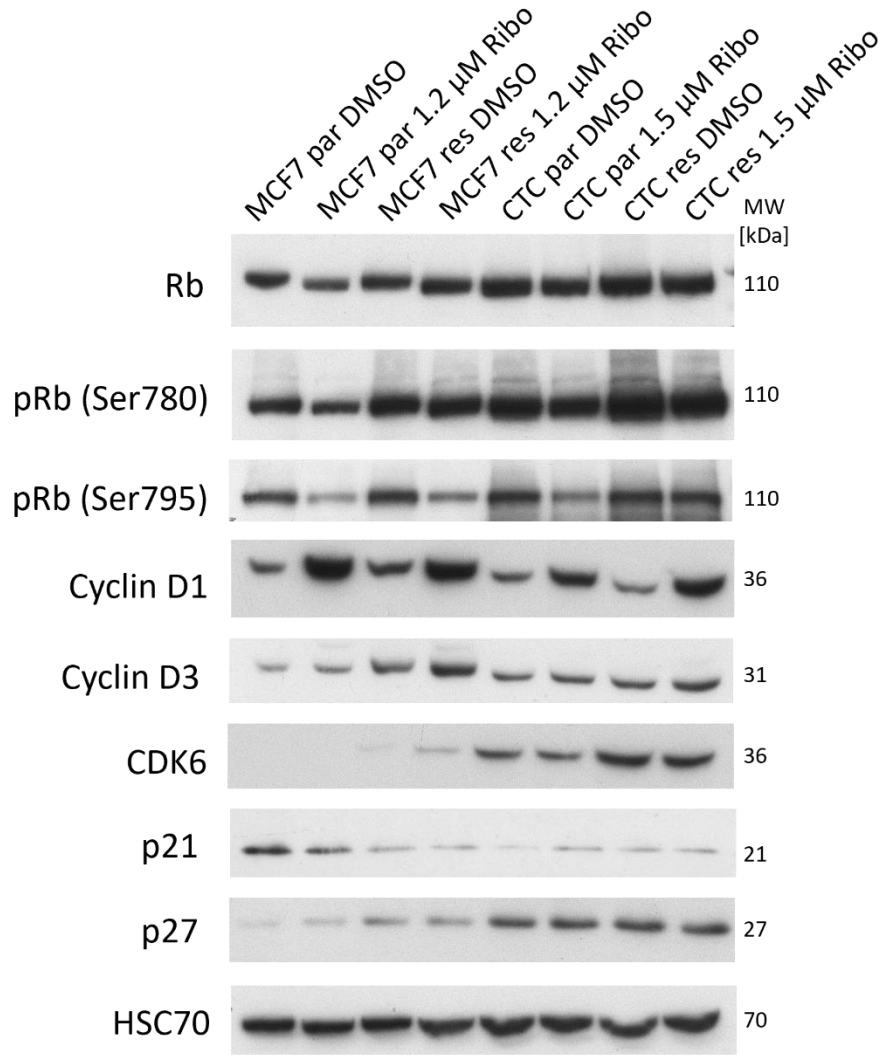

Figure 17: Expression of selected cell cycle-related proteins. Cells were treated with ribociclib for 3 days (MCF7, 1.2 µM) or 6 days (CTC-ITB-01, 1.5 µM). Protein levels of Rb, pRB (Ser780), pRB (Ser795), cyclin D1, cyclin D3, CDK6, p21, and p27 were analyzed by Western blot analysis. Antibody dilutions are described in the material and methods section. The figure shows results from three individual experiments. HSC70 served as a loading control and was determined for each individual experiment.

While both the total level of RB protein as well as levels of Ser780 and Ser795 phosphorylated Rb proteins decreased in parental MCF7 cells treated with ribociclib, in the resistant cells the level of Ser780 phosphorylated Rb was no longer influenced by ribociclib. In contrast, no differences in pRB (795) levels were observed between parental and resistant MCF7 cells. For CTC-ITB-01 cells both pRB (780) as well as pRB (795) levels were higher in the resistant compared to the parental cells treated with ribociclib.

Cyclin D1 levels were markedly increased in MCF7 and CTC-ITB-01 parental and resistant cells when treated with ribociclib.

Levels of cyclin D3 were elevated in resistant MCF7 cells compared to those of the parental cells independently of the treatment. This effect was not evident in the resistant CTC-ITB-01 cells.

Furthermore, for resistant versus parental MCF7 cells Western blot analysis demonstrated an increase in CDK6 protein expression along with an increased mRNA expression as showed by

qPCR (Figure 16). In contrast, in resistant CTC-ITB-01 cells *CDK6* mRNA expression was not significantly changed, whereas CDK6 protein levels were increased in the resistant subline implying a higher stability of CDK6 in the resistant versus the parental cell line. Yet, the strong differences in the CDK6 protein amounts between CTC-ITB-01 and MCF7 mirror the measurement by qPCR (Cq_{par} MCF7: 27, Cq_{par} CTC: ~23, equals a fold change of 2^4= 16-fold).

A reduction of p21 levels in the resistant cell line could be detected in MCF7 cells by Western Blot analysis, but not in the CTC-ITB-01 cell line, despite a significant decrease of *CDKN1A* transcripts in both resistant cell lines (Figure 16). P27 protein expression was not altered in the resistant compared to the parental CTC-ITB-01 cell lines, but surprisingly this protein was stronger expressed in resistant versus parental MCF7 cells.

Summarized, evaluation of mRNA and protein levels deemed relevant for progression from G1 to S phase, supported the assumption of an established resistance to ribociclib in MCF7 and CTC-ITB-01 cells.

3.4 Identification of genes/proteins related to EMT

The induction of the EMT program is a crucial step for cancer progression and metastasis. Increased expression of EMT-related proteins like fibronectin and vimentin as well as transcription factors like ZEB1 have been found in palbociclib-resistant breast cancer cell culture models [67]. EMT is a complex process, orchestrated by multiple transcription factors that either induce or suppress signaling pathways, leading to a more mesenchymal phenotype [171]. Thus, the expression of core transcription factors, known to modulate EMT programming and markers of epithelial and mesenchymal phenotypes were investigated to analyze, whether CDK4/6i resistance is accompanied by EMT induction in this cell culture model. The level of transcripts encoding the master transcription factors ZEB1, Twist1, Snail, and Slug, all positively regulating EMT and GRHL2, a transcription factor counteracting ZEB1 signaling and maintaining the epithelial state were analyzed. Furthermore, the expression of genes encoding markers of an epithelial phenotype (E-cadherin, EPCAM) and mesenchymal markers (N-cadherin, fibronectin and vimentin) was investigated to unravel potential induction of the EMT program (Figure 17).

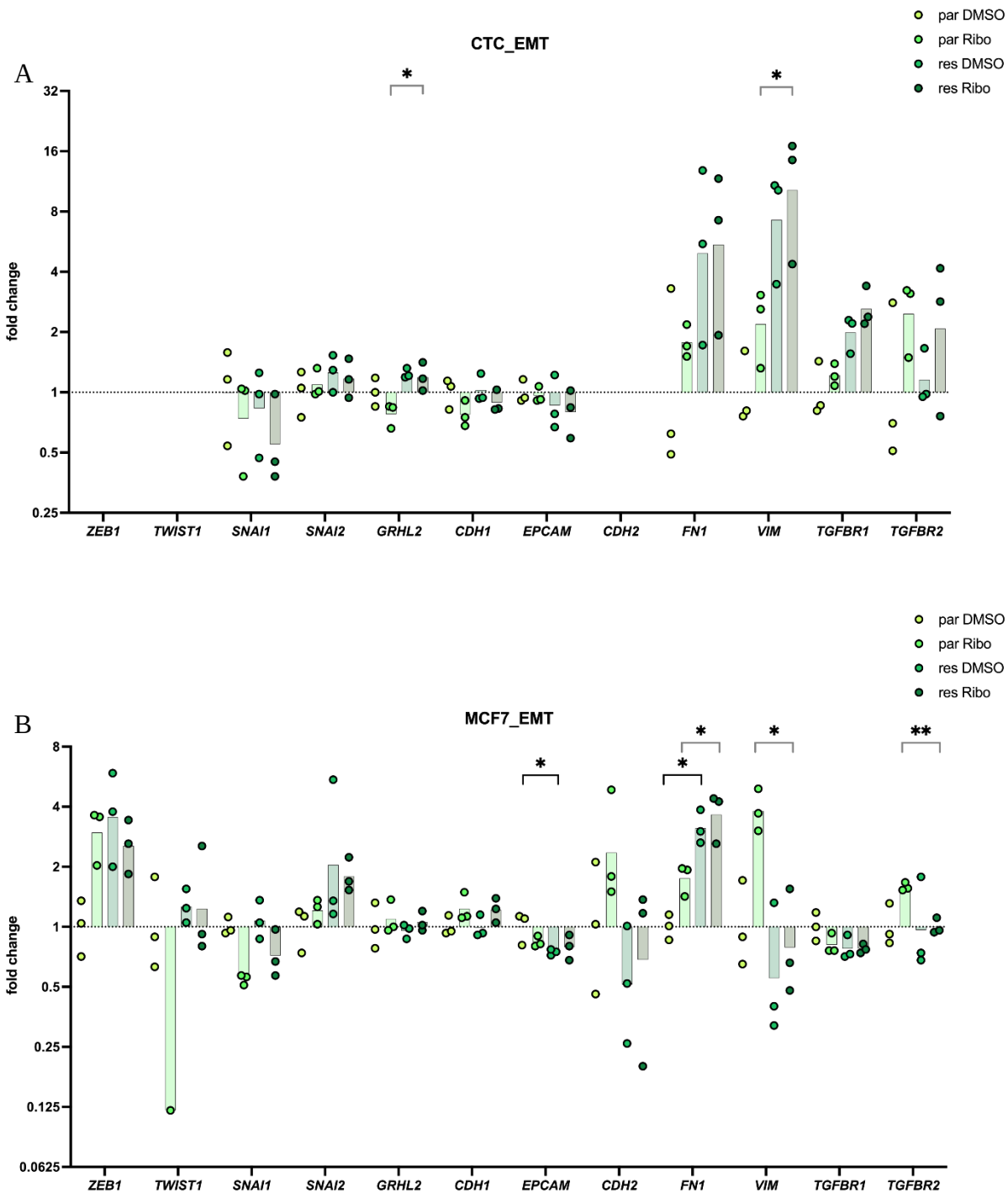

Figure 18: qPCR analysis of EMT-related transcripts. $2^{-\Delta\Delta}$ values that represent fold changes of three independent biological experiments are shown. All values were normalized to the respective parental DMSO-treated sample. All transcripts are normalized to *ACTB* transcript levels, which served as a housekeeping gene. Significance was tested with the 2-way ANOVA Tukey test, correcting for multiple comparison. ($p > 0.05$ = ns, ≤ 0.05 = *, ≤ 0.01 = **, ≤ 0.001 = ***, ≤ 0.0001 = ****). Black bars representing comparison of DMSO-treated samples, grey bars ribociclib-treated samples A: CTC-ITB-01 B: MCF7

Treatment with ribociclib resulted in significantly higher *VIM,* but surprisingly also higher *GRHL2* levels in the resistant CTC-ITB-01 cells than in the treated parental cells (ad. p=0.0342, ad. p=0.0391, respectively). Despite a marked increase of more than 7-fold of *VIM* expression in DMSO-treated resistant cells compared to the parental control, this increase was not significant

(ad. p=0.0806). Likewise, the changes observed in the expression of the EMT-associated genes *SNAI1*, *SNAI2*, *FN1, TGFBR1* and *TGFBR2* and the epithelial markers *CDH1* and *EPCAM,* were not significant. *ZEB1*, *TWIST1* and *CDH2* remained undetectable in both CTC-ITB-01 derivates.

In MCF7 cells, significant changes were also identified. Ribociclib treatment resulted in significantly lower *VIM* and *TGFBR2* levels in the resistant MCF7 cells compared to the parental ones (ad. p=0.0427, ad. p=0.0085, respectively) not supporting the immediate induction of EMT in these cells. On the other hand, the expression of *FN1* was significantly increased in the resistant MCF7 cells versus the parental cells not only upon treatment with ribociclib (ad. p=0.0175), but F*N1* levels were also 3-fold higher in the DMSO-treated resistant MCF7s cells versus the parental ones (ad. p=0.0244). In addition, *EPCAM* levels were significantly decreased by 0.75-fold in DMSO-treated resistant MCF7 cells compared to the parental counterpart. All changes observed at the expression levels of *ZEB1*, *TWIST1*, *SNAI1*, *SNAI2*, *CDH2* and *TGFBR1* as well as of the gene of the epithelial transcription factor *GRHL2*, were not significant. Significant changes of less than ≤ 2-fold for upregulation and less than ≤0.5-fold for downregulated transcripts are shown in the figures, but their biological relevance was considered questionable which is why they were not in the focus of the following experiments.

However, in summary the marked increase of *VIM* expression in the CTC-ITB-01 cells and the significant increase of *FN1* transcripts in the resistant MCF7 cells suggested induction of a more mesenchymal phenotype in both resistant cell lines, albeit perhaps not promoted by the key transcription factors, tested in these experiments.

In summary, due to the results obtained by cell cycle profile analysis and qPCR, supported by the different response to ribociclib treatment of the cells, chronically exposed to ribociclib, the cells were deemed resistant to ribociclib treatment and are hereafter referred by as "resistant" cells.

3.5 Whole transcriptome RNA-sequencing

After confirmation of resistance to ribociclib in the MCF7 and CTC-ITB-01 derivates, total RNA was isolated from three independent biological replicates and sent to Novogene for RNA sequencing. Thereby, novel transcripts not described in the context of resistance to CdK4/6 inhibitors hitherto, but potentially contributing to the occurrence of ribociclib resistance, should be identified. Deregulated mRNA and miRNA transcripts represented the focus of this analysis. Moreover, also long non-coding (lncRNAs), circular RNAs (circRNAs) and genetic variants were evaluated within the framework of this sequencing analysis.

3.5.1 Sequencing of mRNA

Various bioinformatical quality control steps confirmed the sufficient quality of the data for further analysis. A Sample-to-Sample matrix confirmed little variance between biological replicates of one group (Figure 19 A) and the Principal Component Analysis (PCA) (Figure 19 B) revealed less variance between parental and resistant derivates but a higher variance between CTC-ITB-01 and

MCF7 cells. The variance between samples from the parental and resistant cell lines was higher in the MCF7 than the CTC-ITB-01 cell line.

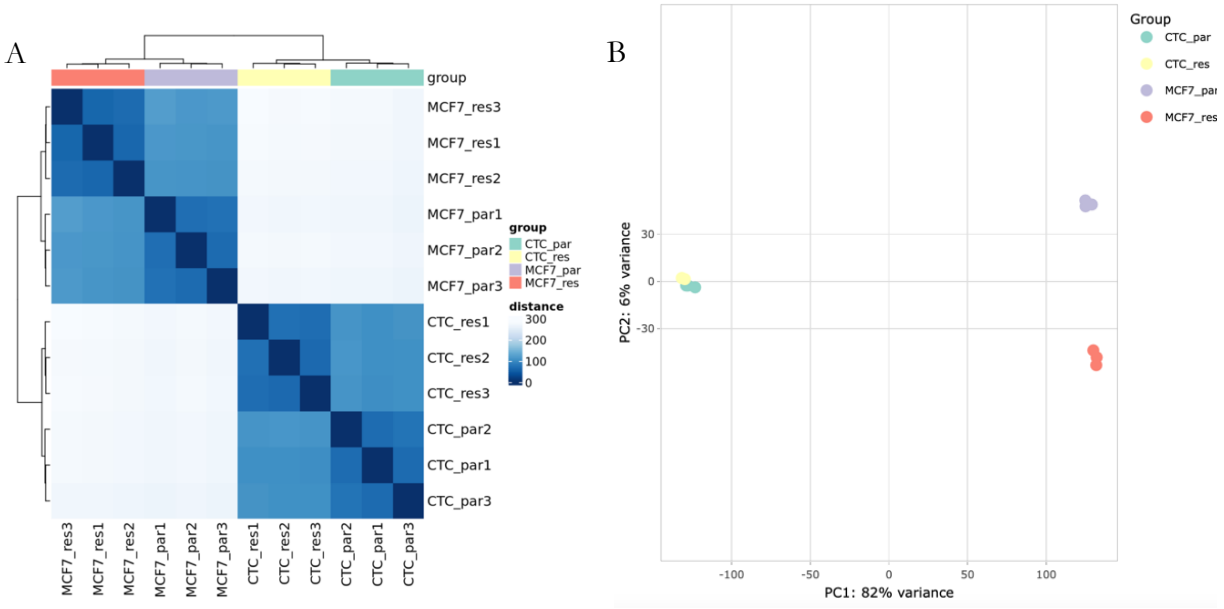

Figure 19: Bioinformatic quality control of data obtained from mRNA-sequencing. A) Biological replicates from the same cell line clustered, confirming relatively homogenous replicates. B) The principal component analysis (PCA) showed less variance between parental and resistant derivates but stronger differences between MCF7 and CTC-ITB-01 cells. (Both figures were created by Dr. Malik Alawi).

Subsequently, differential expression between parental and resistant cell lines was assessed. Transcripts with a log2-fold change (log2FC) ≥1 and a False Discovery Rate (FDR) of ≤0.1 were considered to be changed significantly. Volcano plots of both sub-cell lines of MCF7 and CTC-ITB-01 gave a first impression of the differentially expressed genes in both groups (Figure 20).

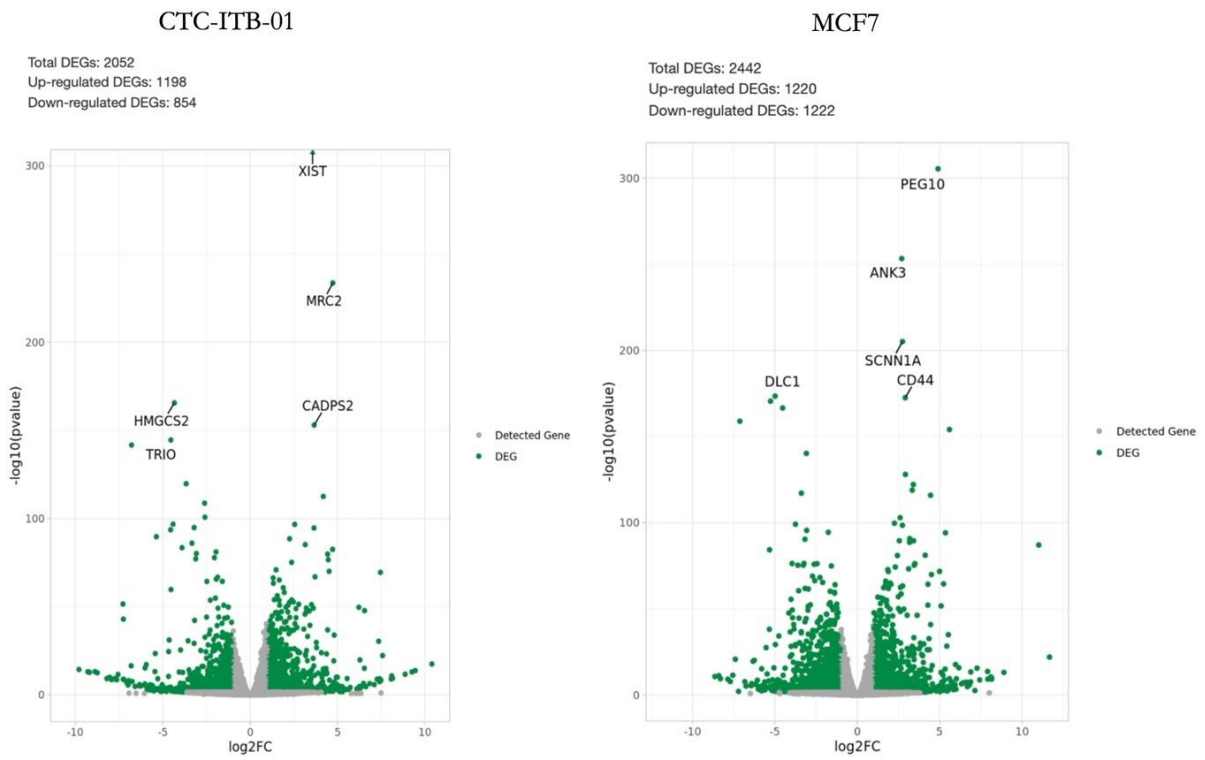

Figure 20: Volcano plots of differentially expressed genes (DEGs) identified by mRNA-sequencing. All transcripts matching the (FDR ≤ 0.1 and |log2FC|≥ 1) criteria, are shown in green. All presented transcripts are deregulated in the resistant cell lines compared to the parental counterpart. The 5 most significantly DEGs are marked in each graph. (Both figures were created by Dr. Malik Alawi).

All five most significantly differentially expressed genes (DEGs) in both resistant cell lines coded for proteins which have already been described in the context of cancer in general. Many of them have also been linked to pathways that might be relevant for resistance development such as proliferation (*DLC1* [172], *SCNN1A* [173]) and invasion (*XIST1* [174], *PEG10* [175]). *CD44*, upregulated in the resistant MCF7 cells, encoding a so-called "cancer-stemness" marker that has been detected on cancer stem cells [176] and is considered relevant in the context of many pathological processes in cancer. On the other hand, the expression of *DLC1*, encoding a tumor-suppressor protein which inhibits tumor cell growth and tumorigenicity in breast cancer was significantly downregulated in resistant versus parental MCF7 cells [172].

In the resistant CTC-ITB-01 cells, in total, 2052 genes were found differently expressed than in the parental cells, 1198 of them upregulated and 854 downregulated. Comparing the resistant MCF7 cells with the parental ones, in total 2442 genes were differentially expressed, 1220 upregulated and 1222 downregulated. After removal of pseudogenes and lncRNAs, the expression of 864 and 602 genes was up- or downregulated, respectively, in the resistant versus parental CTC-ITB-01 cells. Likewise, in the resistant MCF7 compared to parental ones, 875 genes were up-and 902 were downregulated.

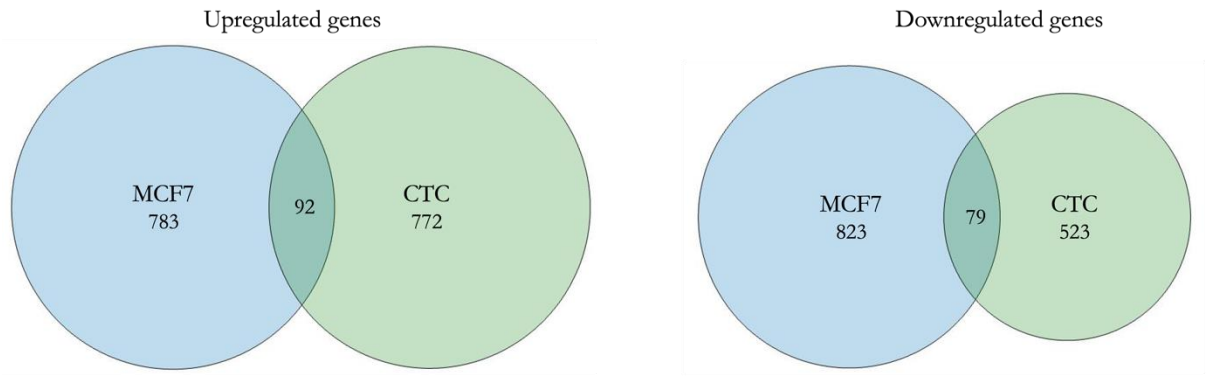

Figure 21: Venn diagrams visualizing DEGs unique to each resistant cell line and shared ones. Venn diagrams are quantitative as the size of a circle is relative to the number of DEGs it represents (only accountable for relative numbers of intra-figure comparisons).

Of these protein-coding upregulated DEGs, 92 were upregulated in both resistant cell lines, whereas 783 and 772 were exclusively upregulated in MCF7 or CTC-ITB-01 cells, respectively. Of the downregulated DEGs, 79 were found in both resistant cell lines, while 823 were exclusively detected in resistant MCF7 cells and 523 in resistant CTC-ITB-01 cells. The whole list of DEGs for each cell line is provided in Supplementary Table S 2 to Supplementary Table S 5.

In order to select DEGs potentially driving resistance from the more than 2000 DEGs of each cell lines, pathway analyses were performed to get an overview of relevant pathways and respective proteins associated with ribociclib resistance.

3.5.2 Pathway analysis of DEGs

Over Representation Analysis (ORA) was performed to identify enriched pathways or biological processes which might me deregulated in the resistant cell lines compared to their parental counterparts. Unlike other methods such as Gene Set Enrichment analysis, the chosen approach only takes DEGs into consideration. The Gene Ontology (GO) knowledgebase, as the biggest database for gene functions was chosen. Enriched pathways of resistant CTC-ITB-01 and MCF7 cells are shown in Figure 22.

A

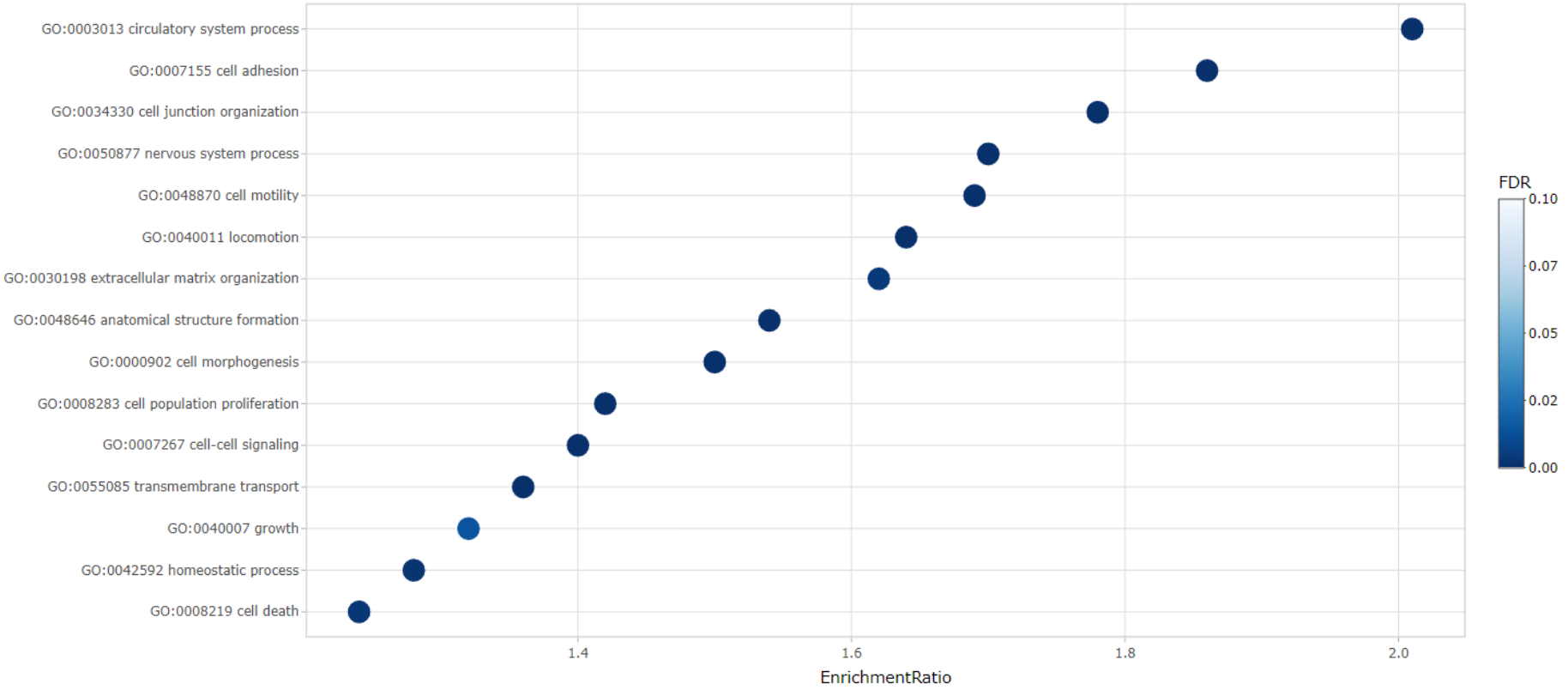
GO:0003013 circulatory system process
GO:0007155 cell adhesion
GO:0034330 cell junction organization
GO:0050877 nervous system process
GO:0048870 cell motility
GO:0040011 locomotion
GO:0030198 extracellular matrix organization
GO:0048646 anatomical structure formation
GO:0000902 cell morphogenesis
GO:0008283 cell population proliferation
GO:0007267 cell-cell signaling
GO:0055085 transmembrane transport
GO:0040007 growth
GO:0042592 homeostatic process
GO:0008219 cell death
1.4
1.6
1.8
2.0
EnrichmentRatio
FDR
0.10
0.07
0.05
0.02
0.00

B

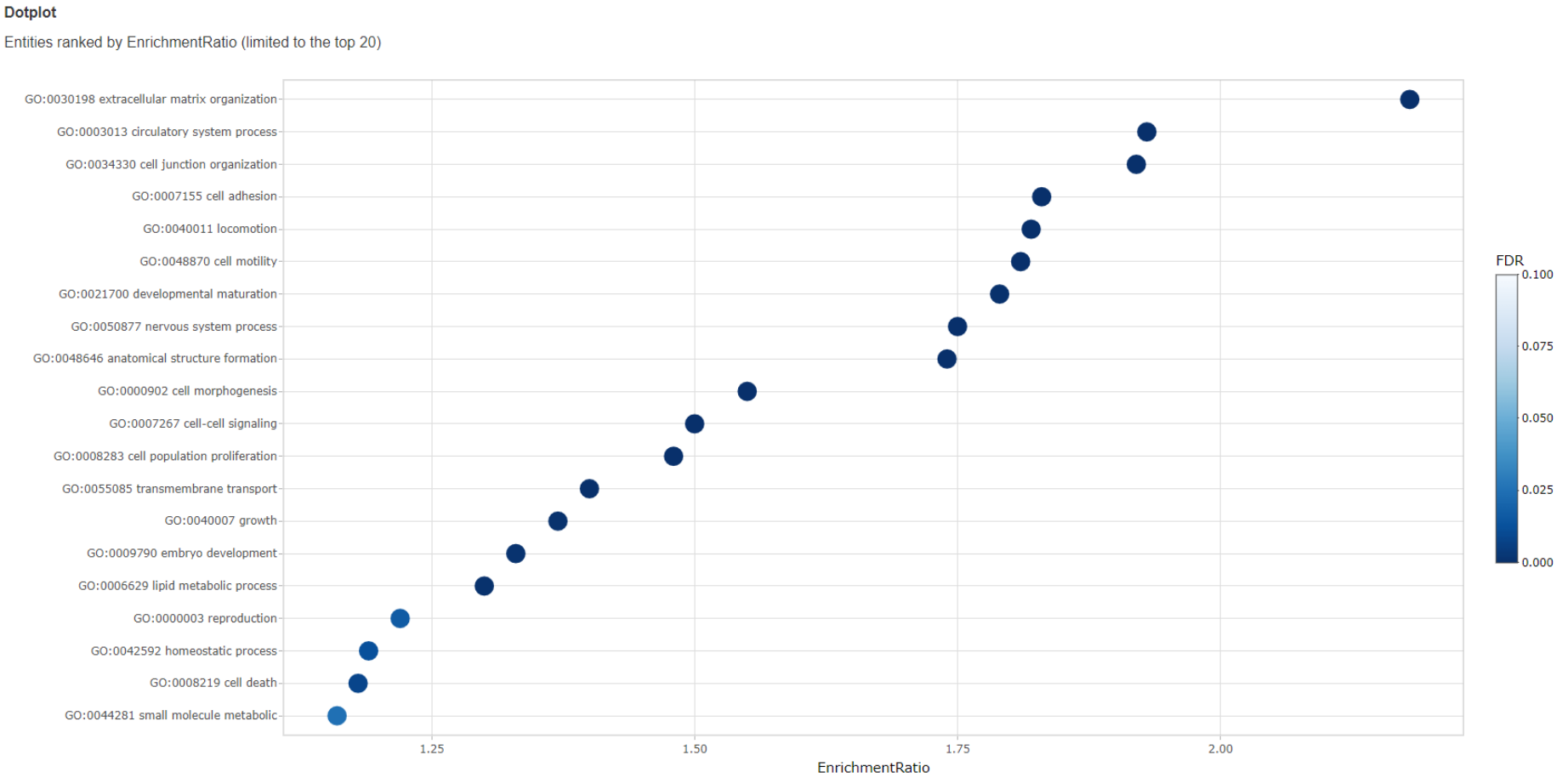

Figure 22: Over representation analysis, GO database. The most significantly deregulated pathways identified by GO are shown for CTC-ITB-01 (A) and MCF7 (B) cells. (Both figures were created by Dr. Malik Alawi).

In both resistant derivates, pathways related to cell adhesion, cell junction organization and cell-cell signaling, cell motility and related pathways like ECM organization, locomotion and anatomical structure formation, circulatory system process and proliferation were enriched. Furthermore, alterations in processes regulating cell death, the nervous system, and homeostasis were enriched in both resistant cell lines.

Surprisingly, cell cycle as a pathway was not enriched in either resistant cell line using this approach and the GO database, albeit several transcripts encoding proteins regulating the cell cycle were differently expressed in the resistant cell lines and were found in the pathway of "cell population proliferation".

Furthermore, ORA was also performed using the Molecular Signatures database (MSigDB), summarizing well-defined biological states and processes. Results are presented in Figure 23.

A

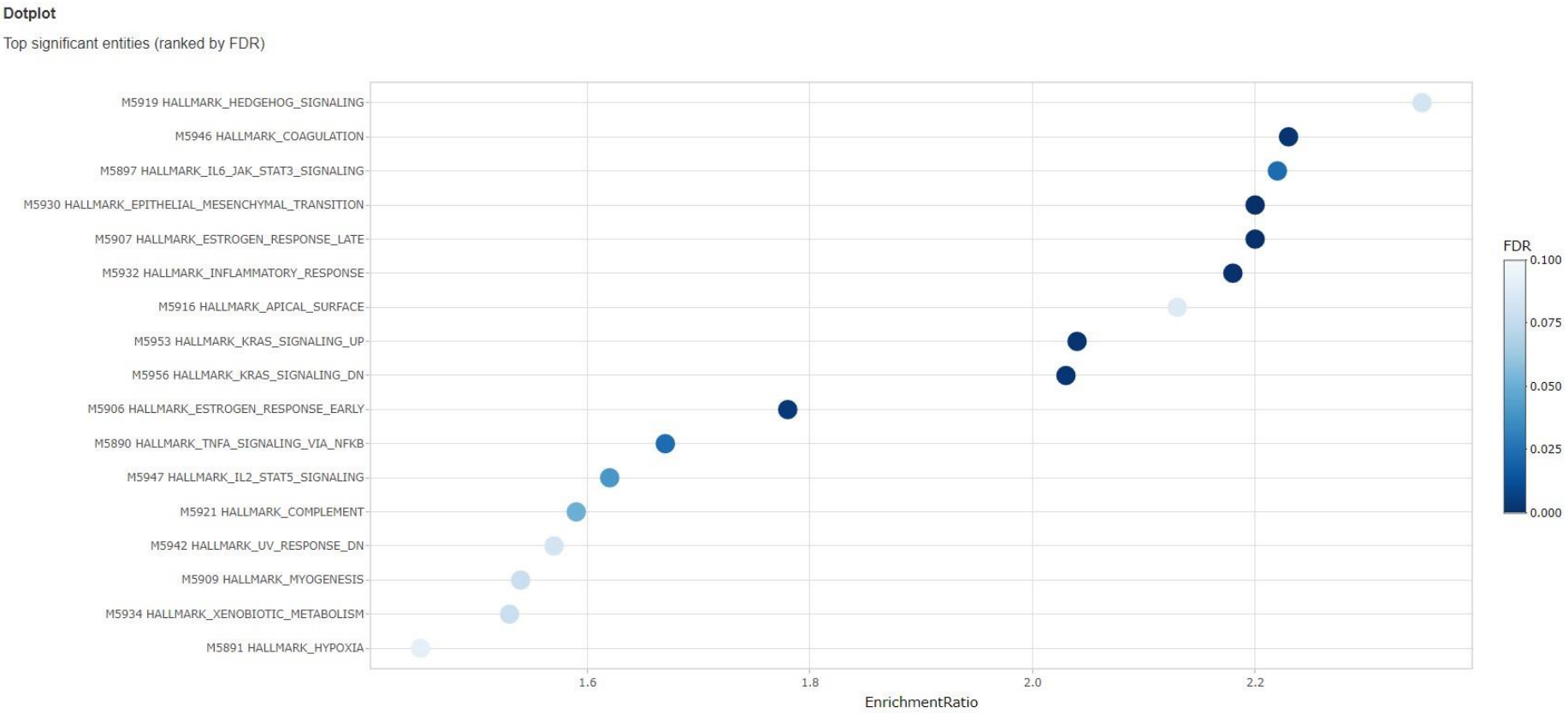
Dotplot
Top significant entities (ranked by FDR)
M5919 HALLMARK_HEDGEHOG_SIGNALING
M5946 HALLMARK_COAGULATION
M5897 HALLMARK_IL6_JAK_STAT3_SIGNALING
M5930 HALLMARK_EPITHELIAL_MESENCHYMAL_TRANSITION
M5907 HALLMARK_ESTROGEN_RESPONSE_LATE
M5932 HALLMARK_INFLAMMATORY_RESPONSE
M5916 HALLMARK_APICAL_SURFACE
M5953 HALLMARK_KRAS_SIGNALING_UP
M5956 HALLMARK_KRAS_SIGNALING_DN
M5906 HALLMARK_ESTROGEN_RESPONSE_EARLY
M5890 HALLMARK_TNFA_SIGNALING_VIA_NFKB
M5947 HALLMARK_IL2_STAT5_SIGNALING
M5921 HALLMARK_COMPLEMENT
M5942 HALLMARK_UV_RESPONSE_DN
M5909 HALLMARK_MYOGENESIS
M5934 HALLMARK_XENOBIOTIC_METABOLISM
M5891 HALLMARK_HYPOXIA
1.6
1.8
2.0
2.2
EnrichmentRatio
FDR
0.100
0.075
0.050
0.025
0.000

B

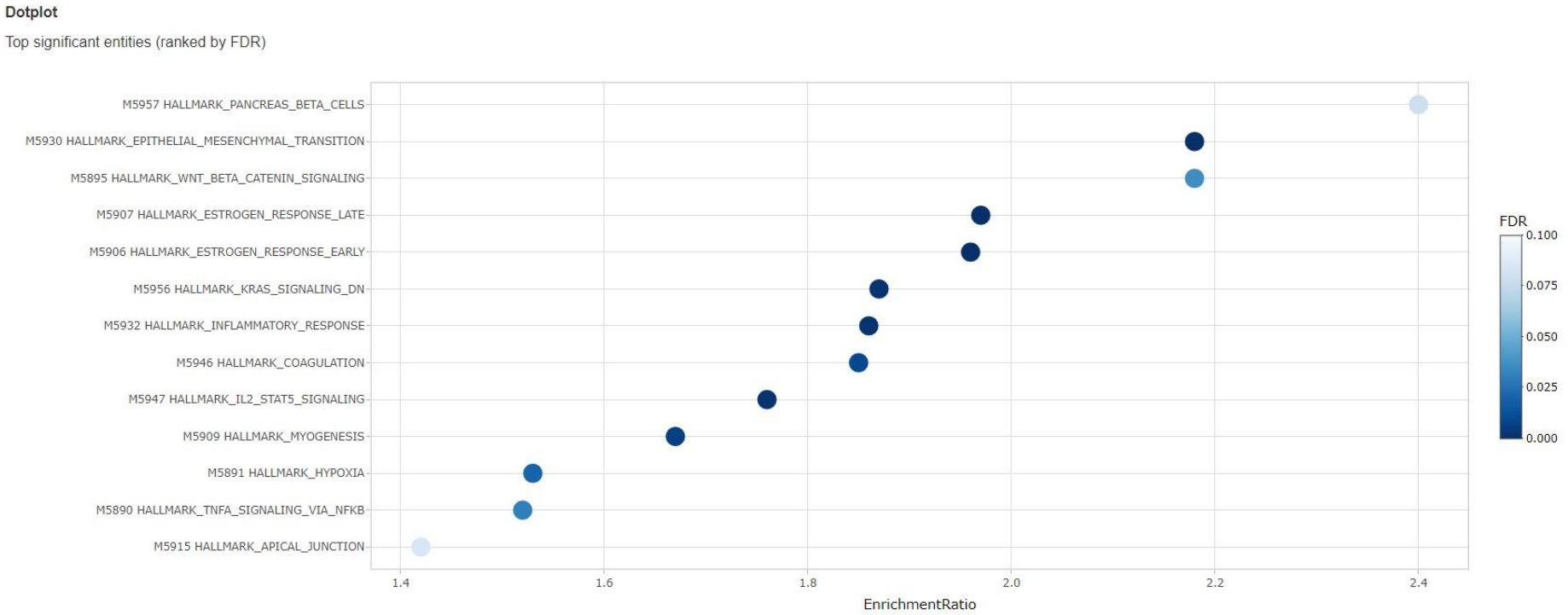

Figure 23: Over representation analysis using the MSigDB. The most significantly deregulated pathways identified from the MSigDB are shown for CTC-ITB-01 (A) and MCF7 (B) cells. (Both figures were created by Dr. Malik Alawi).

Over representation analysis using the MSigDB revealed enrichment of several pathways in both resistant cell lines, like early and late estrogen response, KRAS signaling, coagulation or hypoxia. Interestingly, also the pathway associated with the hallmark of EMT was enriched with high significance in both resistant cell lines.

Out of the multitude of pathways and cancer hallmarks enriched in resistant CTC-ITB-01 and MCF7 cells, cell adhesion and EMT and stemness were chosen for further in-depth analysis, as they were considered to be of particular interest in the context of CDK4/6i resistance. Additionally, also DEGs associated to cell cycle regulation and proliferation were chosen.

Thus, DEGs identified by RNA-seq and encoding proteins according to ORA assigned to either cell adhesion, EMT and cancer-stemness, closely linked to EMT [177], as well as proliferation and cell cycle regulation were selected. Figure 24. exemplifies the log2FC of these selected DEGs in the resistant cells compared to their parental controls. These DEGs were chosen either, because they are well described proteins in the context of their category, were highly differentially expressed, found in several categories or were identified in both resistant cell lines and thus deemed potentially relevant for driving ribociclib resistance.

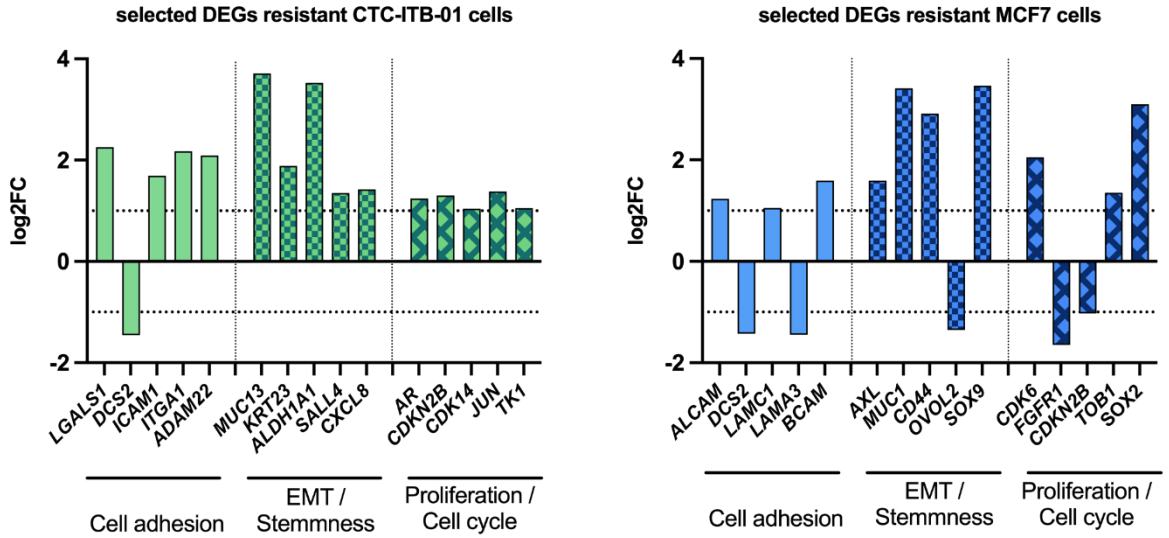

Figure 24: Log2FC of selected DEGs of resistant versus parental cells. Dashed lines represent log2FC thresholds of ±1 (fold change ≥2).

For providing an overview, only five DEGs were chosen in Figure 24, which does not represent all DEGs found in each category. Notably, a relevant proportion of genes cannot only be assigned to only one category or process. Particularly, numerous transcripts coding for proteins related to EMT and cancer-stemness were found, since also many adhesion proteins are linked to EMT, as loss of cell-cell contacts is a crucial step of EMT. Hence, further analysis of the expression of such genes in the resistant derivates of this study was performed.

3.5.3 Increase of EMT and cancer-stemness traits in resistant cell lines

EMT was identified as a highly significantly enriched hallmark in resistant CTC-ITB-01 and MCF7 cells by performing ORA using the MSig databases (Figure 23). However, the datasets of each hallmark in this database are rather small, e.g., the EMT datasets consist of only 48 genes. Therefore, a comparison of DEGs and genes listed in the EMTome [178] database, a pan-cancer database for EMT associated proteins, lncRNA and miRNAs was performed to identify more EMT-associated transcripts that are differentially expressed in resistant CTC-ITB-01 and MCF7 cells.

Notably, induction of EMT often correlates with cells of a cancer-stem cell (CSC) phenotype [177]. These cells are characterized by a specific subset of markers, low proliferation rate and high therapeutic resistance [179]. Since EMT and CSC phenotypes share many characteristics and are commonly activated pathways, they were investigated together.

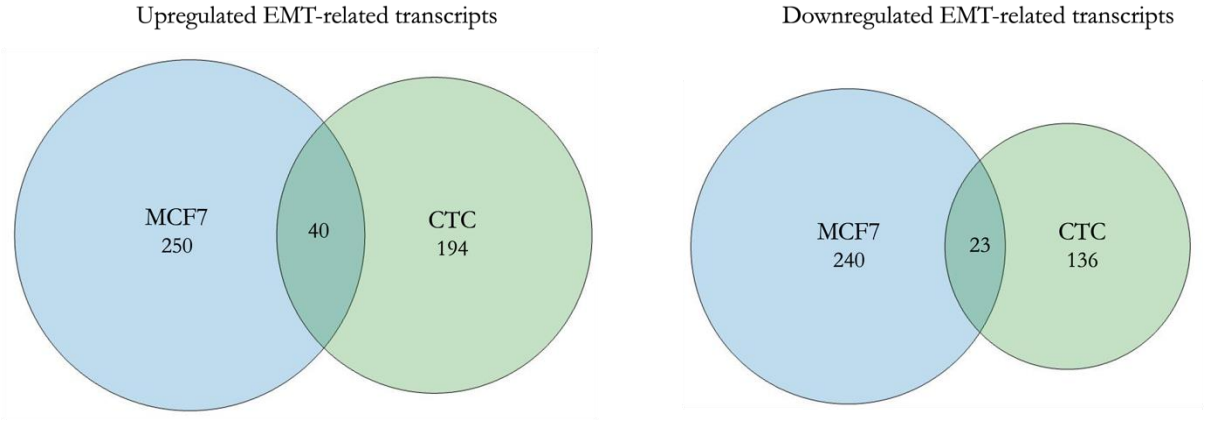

Figure 25: Venn diagrams visualizing DEGs encoding protein associated with EMT unique to each resistant cell line and shared ones. Venn diagrams are quantitative as the size of a circle is relative to the number of DEGs it represents (only accountable for relative numbers of intra-figure comparisons).

Figure 26 depicts the number of transcripts, including lncRNAs that were differentially expressed in the resistant cell lines of this study and registered in the EMTome database. Of the 290 genes, upregulated in resistant MCF7 cells and registered in the EMTome, 40 were also found in the resistant CTC-ITB-01 cells. 250 and 194 transcripts were unique to each cell line respectively. Of the genes downregulated in resistant MCF7, in total 263 were also registered in the EMTome database and 23 of these also downregulated in CTC-ITB-01, where 136 additional exclusive EMT-related transcripts were found. All genes encoding EMT- and stemness-related genes with differential expression are listed in Supplementary Table S 6 to Supplementary Table S 9.

Of these EMT-related genes, the five most up- and downregulated ones, in addition to selected known for their association with the cancer stem cell phenotype, were visualized in Figure 26 and Figure 27.

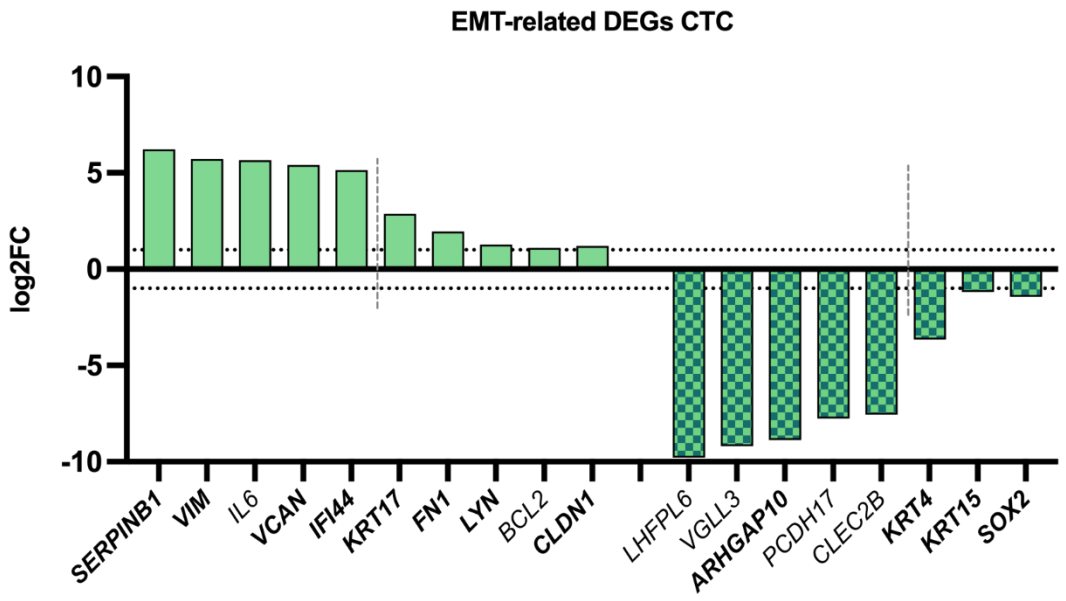

Figure 26: EMT-related genes expressed differentially by resistant CTC-ITB-01 cells. Dashed black lines indicate log2FC thresholds of ±1. Grey dashed lines separate the five most up- or downregulated genes from the selected transcripts, whose encoded proteins are well described in the context of EMT or cancer-stemness or were mentioned previously in this study. Transcripts in bold font were found in BC datasets on the EMTome [178].

In resistant CTC-ITB-01 cells, four out of the five transcripts with the highest log2FC have been published by at least one breast cancer dataset in the EMTome database. Interestingly, vimentin, is amongst the five genes with the highest fold change in resistant CTC-ITB-01, next to *SERPINB1*, *IL6*, *VCAN* and *IFI44*, all being approximately 2^5-fold upregulated. Not as strongly upregulated but still considered pivotal was the increased expression of *FN1*, *AR*, *LYN*, *ALDH1A1*, *BCL2*, *TK1, CDK14* and *CLDN1* transcripts which were listed in the EMTome. Additionally, *MUC13*, *KRT23*, *SALL4* and *CXCL8* were identified as DEGs encoding proteins associated with EMT but were not listed in the EMTome database.(Figure 24 and Figure 26). Fibronectin, like vimentin, is a marker of mesenchymal cells [180]. The Lyn kinase was identified as a part of an EMT signature and mediator of EMT, defined by a panel of epithelial and mesenchymal breast cancer cell lines[181]. ALDH1 is commonly considered as a marker of cancer-cancer-stemness [176]. Also, CDK14 and TK1 have been mentioned in the context of breast cancer stemness [182,183]. The association of EMT with the expression of *BCL2*, *TK1* and *CDK14* has not been described for yet for breast cancer but might be also important because of described functions, such as driving proliferation (AR [184], CDK14 [185]), inhibiting apoptosis (BCL2 [186]) or participating in CDK4/6i response [187] (TK1). KRT23 was identified as a promoter of EMT in ovarian cancer [188]. SALL4 and CXCL8 were both shown to positively regulate EMT in breast cancer [189,190]. The role of MUC13 and CLDN1 in the context of EMT will be discussed in chapter 3.6.

The genes with the highest decrease of expression were *LHFPL6*, *VGLL3*, *ARHGAP10* and *CLEC2B*. Intriguingly, *PCDH17* is described as a tumor suppressor gene, as the respective protein negatively regulates WNT/β-catenin signaling and thereby EMT, suppresses proliferation in breast cancer cell lines and is found downregulated in breast cancer tissue compared to normal breast tissue [191]. SOX2 was shown to maintain cancer-stemness in cancer stem cells (CSCs) and positively regulate WNT signaling [192]. Since EMT includes morphological changes of the cells, changes of proteins of the cytoskeleton are of great importance. Thus, the significant increase of *KRT17*

encoding a protein expression that was shown to induce EMT in oesophageal squamous cell carcinoma [193] and the decreased levels of *KRT4* and *KRT15* could indicate EMT induction in resistant CTC-ITB-01 cells albeit a functional characterization of the respective proteins in this context is lacking so far.

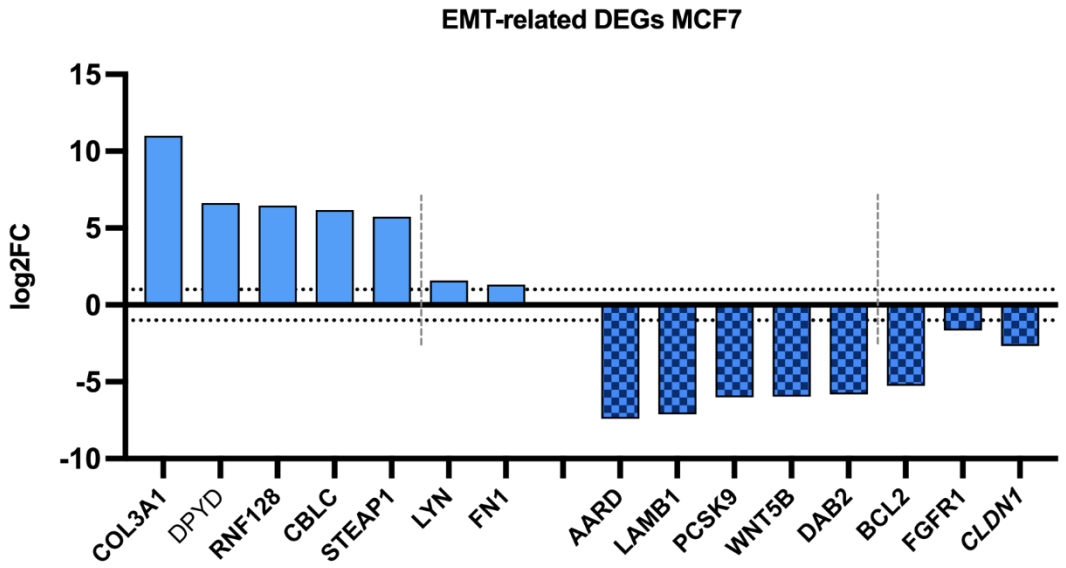

Figure 27: EMT-related genes expressed differentially by resistant MCF7 cells. Dashed black lines indicate log2FC thresholds of ±1. Grey dashed lines separate the five most up- or downregulated genes from the selected transcripts, whose encoded proteins are well described in the context of EMT or cancer-stemness or were mentioned previously in this study. Transcripts in bold font were found in BC datasets on the EMTome [178].

In the resistant MCF7 cells, the genes with highest fold change compared to the parental cells were *COL3A1*, *DPYD*, *RNF128*, *CBLC* and *STEAP1*. Collagen type III α1 is positively linked to metastasis in TNBC [194] while DPYD was identified as an important metabolic enzyme of an EMT-specific signature [195]. Moreover, DEGs that could be of particular interest in the frame of this study were chosen for depiction (Figure 24 and Figure 27). SOX9, in interaction with SOX2 maintains cancer-stemness and induces WNT signaling [192]. CD44 is commonly accepted as a marker of cancer-stemness [176]. Both tyrosine kinases AXL and LYN as well as MUC1 were linked to EMT in breast cancer [181,196,197]. Resistance to ribociclib led to the strongest decrease of the expression of *AARD*, *LAMB1*, *PCSK9*, *WNT5B* and *DAB2*. Surprisingly, in contrary to resistant CTC-ITB-01 cells, the antiapoptotic protein BCL2 was downregulated in resistant MCF7 cells as was *FGFR1*. However, a decrease of the expression of *DSC2* was observed in both resistant cell lines compared to the respective parental counterpart. Furthermore, the expression of the transcription factor *OVOL2*, inducing an epithelial phenotype [171], and *CLDN1* encoding a tight junction protein [198] were significantly reduced in resistant MCF7 cells, further supporting the induction of an EMT-phenotype in these cells. Notably, some DEGs were found in both resistant cells, albeit differentially expressed in different directions, indicating dual function of the respective encoded proteins. The expression of *KRT17* for instance, was increased in resistant CTC-ITB-01 cells whereas it was decreased in resistant MCF7 cells. Keratin 17 has been positively linked to EMT [193] as well as negatively [199] in different tumor entities, suggesting different functions of keratin 17 in the regulation of EMT. Likewise, the expression of *BCL2* and *CLDN1* was increased in resistant

CTC-ITB-01 cells but decreased in resistant MCF7 cells. Up- and downregulation of Claudin 1 has been described in breast cancer [200] and overexpression of BCL2 has been identified as favorable and adverse prognostic factor in breast cancer, depending on the molecular subtype [201,202]. On the contrary, the expression of *KRT4* was downregulated in resistant CTC-ITB-01 cells whereas an increase of its expression was found in resistant MCF7 cells.

Genes of each category were chosen for a validation by qPCR, to test, whether the results obtained by RNA-seq were reproducible. From the DEGs found in the CTC-ITB-01 cell line, CDK14 was chosen, as it was one of the identified genes coding for a protein that is known to drive cell cycle progression but has not yet been described in the context of CDK4/6i. Likewise, SOX9 was chosen for validation from the resistant MCF7 cells sine it is known to promote proliferation and cancer-stemness in various cancers and has been shown to also promote G1-S transition in TNBC cell lines [203]. *ALDH1* was chosen as a transcript coding for a marker of cancer-stemness found upregulated in the resistant CTC-ITB-01 cells. Claudin 1 represents a protein important for the structural integrity of cells and its expression was strongly increased in resistant CTC-ITB-01 cells. Additionally, BCL2 was selected as it was found deregulated in both resistant cell lines, albeit in different directions.

First, the expression of these selected genes was validated by qPCR as depicted in Figure 28.

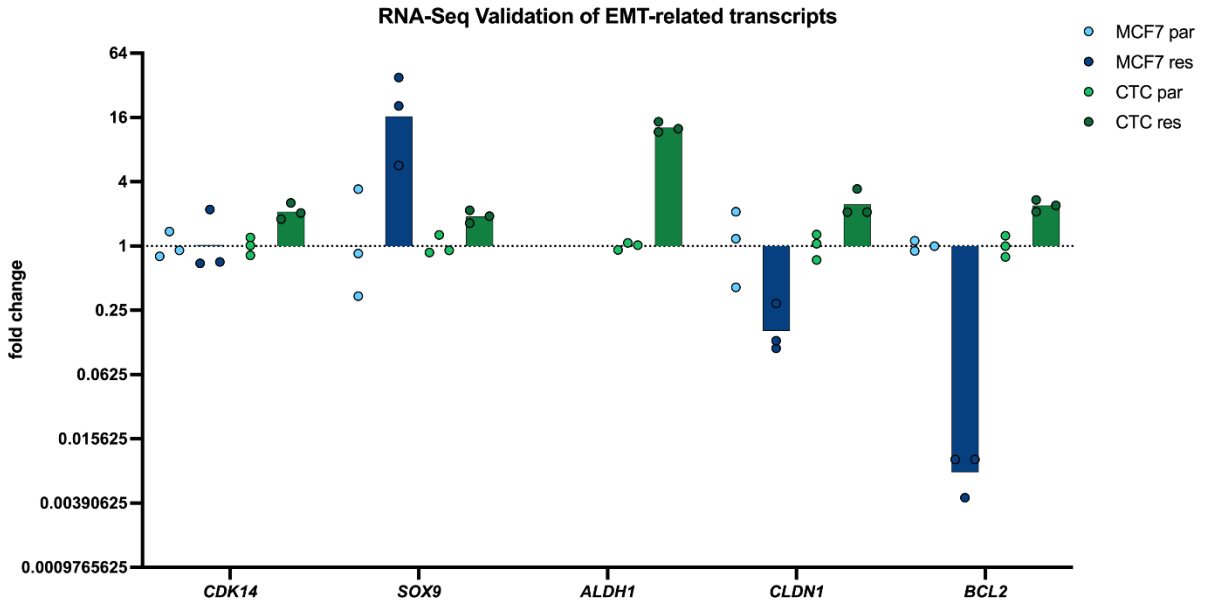

Figure 28: Overview of validation of selected DEGs encoding EMT-related proteins by qPCR. $2^{-\Delta\Delta}$ values that represent fold changes of three independent biological experiments are shown. All values were normalized to the respective DMSO-treated parental sample. All transcripts were normalized to *ACTB*, which served as a housekeeping gene.

The RNA-seq data could be validated and confirmed by qPCR analysis. Thus, to test whether the differential expression of these genes translates also to the protein level, Western Blot analyses for three respective proteins were performed (Figure 29).

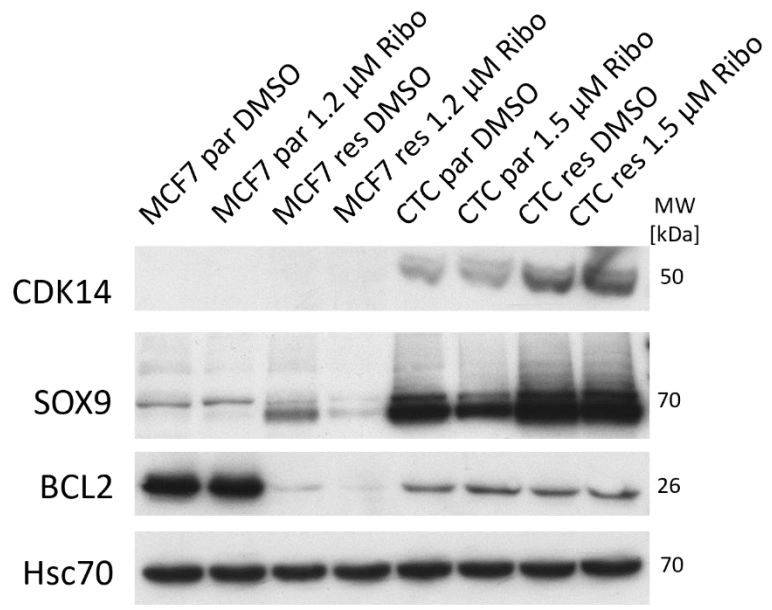

Figure 29: Validation of DEGs on protein level by Western Blot analysis. Cells were treated with ribociclib for 3 days (MCF7, 1.2 µM) or 6 days (CTC-ITB-01, 1.5 µM). Protein levels of CDK14, SOX9 and BCL2 were analyzed by Western blot analysis. HSC70 served as a loading control.

As Figure 29 demonstrates also protein levels were altered according to the findings of RNA-seq and qPCR. While CDK14 was undetectable in MCF7 cells an increase of CDK14 protein level could be detected the resistant compared to parental CTC-ITB-01 cells. Noteworthy, ribociclib treatment did not exert any impact on CDK14 level in neither cell line. SOX9 on the contrary, was detectable in all four cell lines. Notably, SOX9 showed up as a doublet band, perhaps due to post-translational modifications, e.g. phosphorylation [204]. In parental MCF7 cells, ribociclib did not alter the protein level of SOX9, but it strongly reduced SOX9 levels in resistant MCF7 cells. Overall, SOX9 protein levels were markedly higher in DMSO-treated resistant MCF7 cells. However, in parental cells only the upper protein band was detectable whereas in resistant MCF7 cells, mainly the lower band was detected, indicating a switch from phosphorylated to unphosphorylated SOX9. In comparison to MCF7 cells, SOX9 protein levels were markedly higher in all CTC-ITB-01 cells. Ribociclib treatment reduced SOX9 levels in the parental CTC-ITB-01 cells but not in the resistant ones. Furthermore, the levels of SOX9 were upregulated in the samples of the resistant cells compared to parental cells. In samples from CTC-ITB-01 cells, both SOX9 bands were detected, but the lower one was comparably strong, suggesting a high ratio of unphosphorylated to phosphorylated SOX9. BCL2 levels were strongly decreased in the resistant versus parental MCF7 cells. Ribociclib treatment did not influence the BCL2 level of the parental MCF7 cells but reduced them furtherly in the resistant derivates. In contrast to on the 2-fold increase of *BCL2* transcript level, in the resistant CTC-ITB-01 vs the parental cells, an increase of the protein level could not be observed.

Since RNA-seq data did not show differentially expression of the genes encoding the master EMT transcription factors Slug, Snail, Twist, ZEB1 and GRHL2, the expression of additional genes coding for EMT-regulating TFs was analyzed. The results are summarized in Table 20.

Table 20: Genes encoding transcription factors regulating EMT [171] with differential expression in resistant CTC-ITB-01 and MCF7 cells.

EMT TF	Log2FC MCF7	Log2FC CTC-ITB-01	Function
KLF8		-1.32	Inducer
SOX9	3.46	0.79 (FDR=0.04)	Inducer
SOX11	3.2		Inducer
RUNX2	1.49		Inducer (not linked to BC)
GATA4	1.88		Inducer (not linked to BC)
SIX1		2.84	Inducer
OVOL2	-1.35		Suppressor

The summary of differentially expressed genes encoding EMT-regulating TFs demonstrates the upregulating of *SOX9*, *SOX11*, *RUNX2* and *GATA4* in the resistant MCF7 cells. All of the indicated TFs are positive regulators of EMT. Concomitant decrease of *OVOL2* expression, a TF stabilizing an epithelial phenotype, further supports the induction of EMT in resistant MCF7 cells. In the resistant CTC-ITB-01 cells, only the expression of *SIX1* was increased, encoding a TF inducing EMT, whereas the expression of *KLF8*, also encoding a TF positively regulating EMT, was decreased [171].

EMT is often associated with a more spindle-like morphological phenotype and disrupted cell-cell contacts.

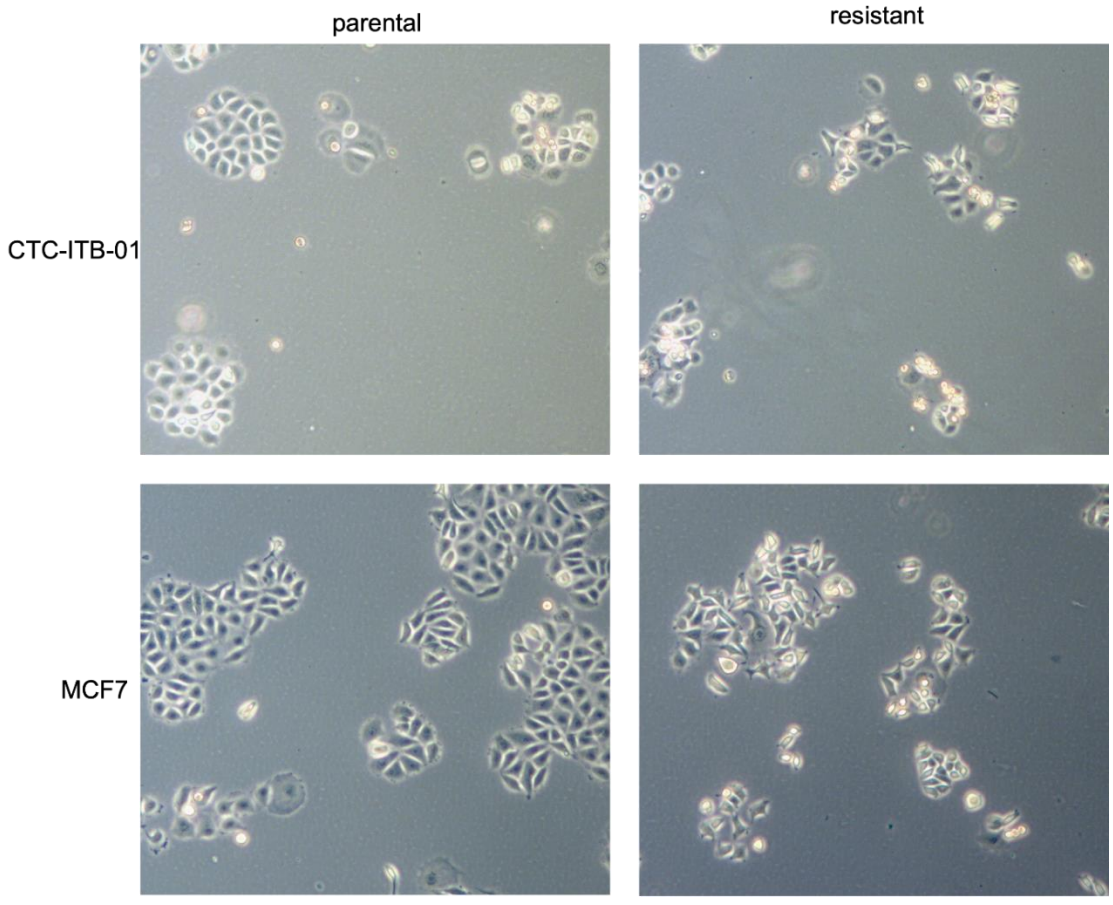

Figure 30: Morphological differences between parental and resistant cell lines. Pictures were taken on a brightfield microscope at 20x magnification.

In cell culture flasks the resistant MCF7 cell line showed loss of cell-cell contacts and a higher number of cells, without the typical cobblestone morphology of MCF7 cells but a more spindle-like shape. In the resistant CTC-ITB-01 cell line, similar observations were made, but overall, the changes were not as pronounced as in MCF7 cells. Still, the growth pattern of adherent cells of both resistant cell lines appeared to be less organized than those of their parental counterparts (Figure 30).

Long non-coding RNAs involved in EMT regulation [205] were not in the focus of this analysis but notably, *XIST* is amongst the most significantly increased transcripts in resistant CTC-ITB-01 cells. XIST was shown to positively modulate EMT in other cancer entities such as colorectal cancer [206], pancreatic cancer [207] and NSCLC [208]. Yet. In breast cancer, a negative regulation of EMT by XIST was shown [209]. In resistant MCF7, increased levels of *HOTAIR* transcripts were identified. This lncRNA is described as an EMT-inducer in various cancers and was also shown to indirectly promote EMT in breast cancer cell line cells and breast cancer stem cells (BCSCs) via regulation of miR-7 levels [210]. Furthermore, the expression of lncRNA SNHG18 was increased in resistant CTC-ITB-01 cells. SNHG18 promoted EMT and increased cell motility in glioma cell line cells [211]. Data on lncRNAs in breast cancer involved in either EMT or CDK4/6i resistance in particular, is limited.

3.6 Adhesive capacity of breast cancer cell line cells

Over Representation Analysis of enriched pathways in the resistant cell lines identified "cell adhesion" as a pathway significantly deregulated in CTC-ITB-01 and MCF7 cells alike. This finding went along with significant changes of the expression of genes (Figure 24), coding for proteins forming cell-cell junctions (*DSC2*, *CLDN1*), cell-surface proteins mediating binding to other cells (*ICAM1, ALCAM, BCAM*), or modulating cell-matrix interactions (*LGALS1*, *MUC13, LAMB1, LAMA3, LAMC1, ADAM22*) [212].

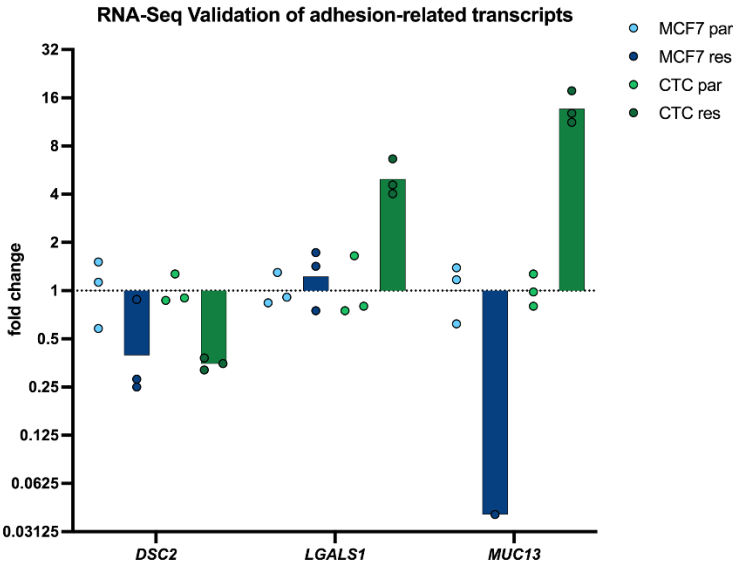

Figure 31: Overview of validation of selected DEGs encoding adhesion-related proteins by qPCR. $2^{-\Delta\Delta}$ values that represent fold changes of three independent biological experiments are shown. All values were normalized to the respective par DMSO sample. All transcripts were normalized to *ACTB*, which served as a housekeeping gene.

As depicted in Figure 24, multiple transcripts related to adhesion were identified as differentially expressed by RNA-seq. *DSC2*, *LGALS1* and *MUC13* expression was validated by qPCR, as they were strongly differentially expressed and served as control for the results obtained by RNA-seq (Figure 31). The different expression levels could be confirmed by qPCR. Desmocollin 2, is a protein crucial for maintaining cell-cell contacts, and its loss is associated with a more mesenchymal cell morphology, enhanced EMT and increased cell migration [213]. Strikingly, *DSC2* expression was strongly decreased in both resistant cell lines. Galectin 1 interacts with proteins of the extracellular matrix (ECM), thereby regulating adhesion to other cells or the ECM. Hence, alterations of its expression level may influence cell invasion and metastasis [214]. In concordance with the RNA-seq data, *LGALS1* expression was strongly increased in resistant CTC-ITB-01 cells compared to the parental ones. Mucin 13 expression is not well-studied for breast cancer, but overexpression of this glycoprotein was reported for gastric and ovarian cancers [215]. In line with the RNA-seq data, *MUC13* transcript levels in MCF7 cells were close to the detection limit of the qPCR, whereas a strong increase of *MUC13* transcripts was observed in resistant versus parental CTC-ITB-01 cells.

Due to these observations, the adhesive capacity of parental and resistant CTC-ITB-01 cells was investigated in a microfluidic system. The BioFlux system provides the possibility to test the adhesion of cells to endothelial, in this case HUVEC cells (HUVECs). Treatment with TNFα induces VCAM-1 expression on the cell surfaces, providing the possibility to evaluate adhesion by this adhesion receptor and its interaction partners such as ICAM-1.

First experiments were conducted, comparing the adhesion of CTC-ITB-01 cells as well as MCF7 cells and MDA-MB-231 cells to non-stimulated and stimulated HUVECs. Thereby, the adhesive capacity of CTC-ITB-01 cells could be compared to a luminal A BC cell line (MCF7) and a TNBC cell line (MDA-MB-231), representing a highly aggressive breast cancer subtype. At lower passages, the CTC-ITB-01 cell line grows mainly adherently, but also contains a small fraction of cells in suspension. Representative pictures of the experiment are shown in Figure 32.

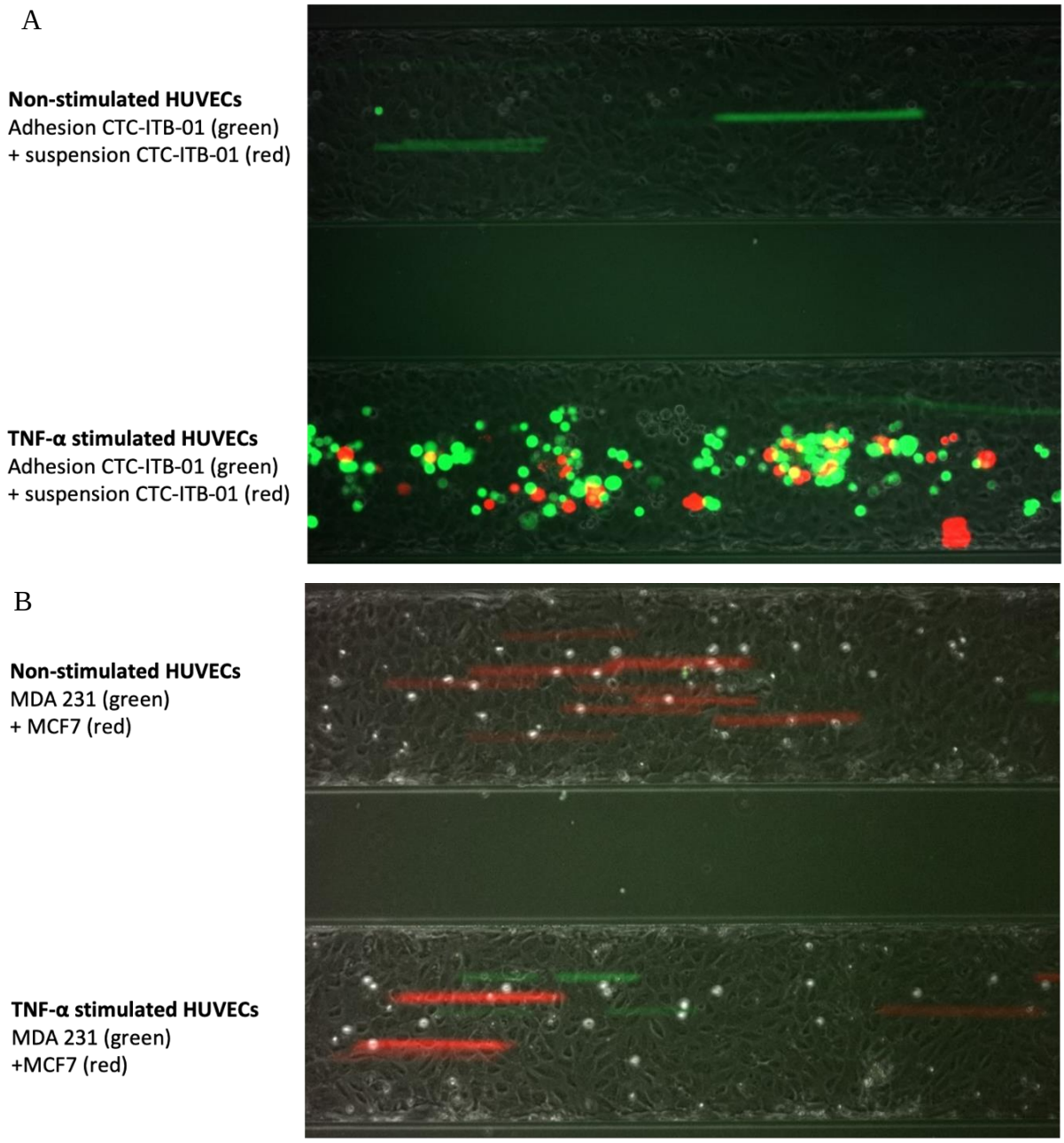

Figure 32: Representative pictures of microfluidic experiments comparing BC cell lines regarding their adhesion to HUVECs. HUVECs were stimulated with TNFα prior to the experiment and the BC cells were stained with CellTrace™ calcein dyes. Cells were perfused at 2 dyne/cm² and pictures were taken at 10x magnification.

As depicted in Figure 32, CTC-ITB-01 cells showed an extraordinarily high adhesive capacity to HUVECs, stimulated with TNFα, in comparison to the two other breast cancer cell lines used in this experiment (MCF7 and MDA-MB-231 cells. While cells of both CTC-ITB-01 fractions were strongly adhesive (Figure 32 A), more cells growing adherently attached to the HUVEC cells than suspension cells. Interestingly, adhesion was only observed to HUVECs activated by TNFα, indicating the importance of an interaction with VCAM-1. One reasonable explanation for this observation of the exceptional adhesion of the CTC-ITB-01 cells, could be provided by the level of cell surface heparan sulfate whose abundance was measured by flow cytometry (Figure 33).

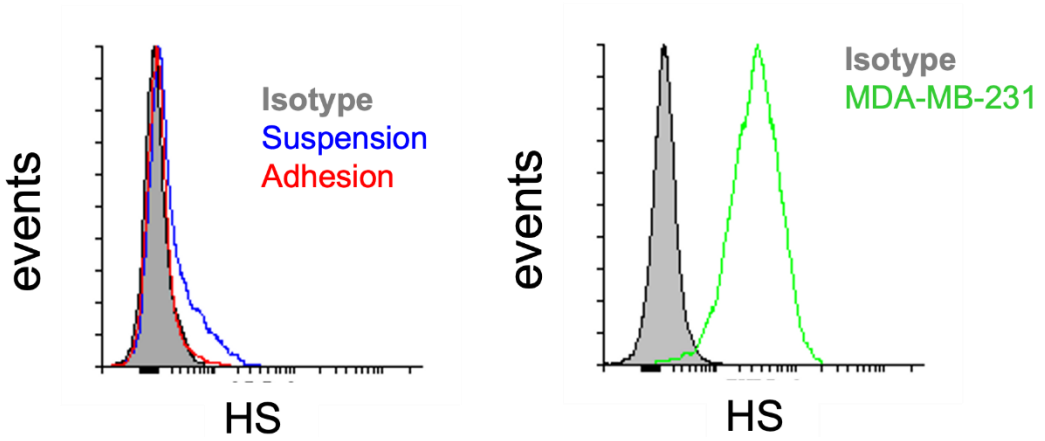

Figure 33: Detection of cell surface heparan sulfate on CTC-ITB-01 cells and MDA 231 cells by flow cytometry. Isotype treated samples served as negative controls.

Figure 33 demonstrates that cells of the adherent and suspension fraction of the CTC-ITB-01 cell line were characterized by a lack of cell-surface heparan sulfate. In contrast, MDA-MB-231 cells, a highly aggressive TNBC cell line, featured higher heparan sulfate levels. This could be an explanation for the strong adhesion of CTC-ITB-01 cells to HUVECs.

Subsequently, parental and resistant cells of both cell lines were compared regarding their adhesive capacity to HUVEC cells, since the enrichment of cell adhesion pathways implied altered adhesion properties.

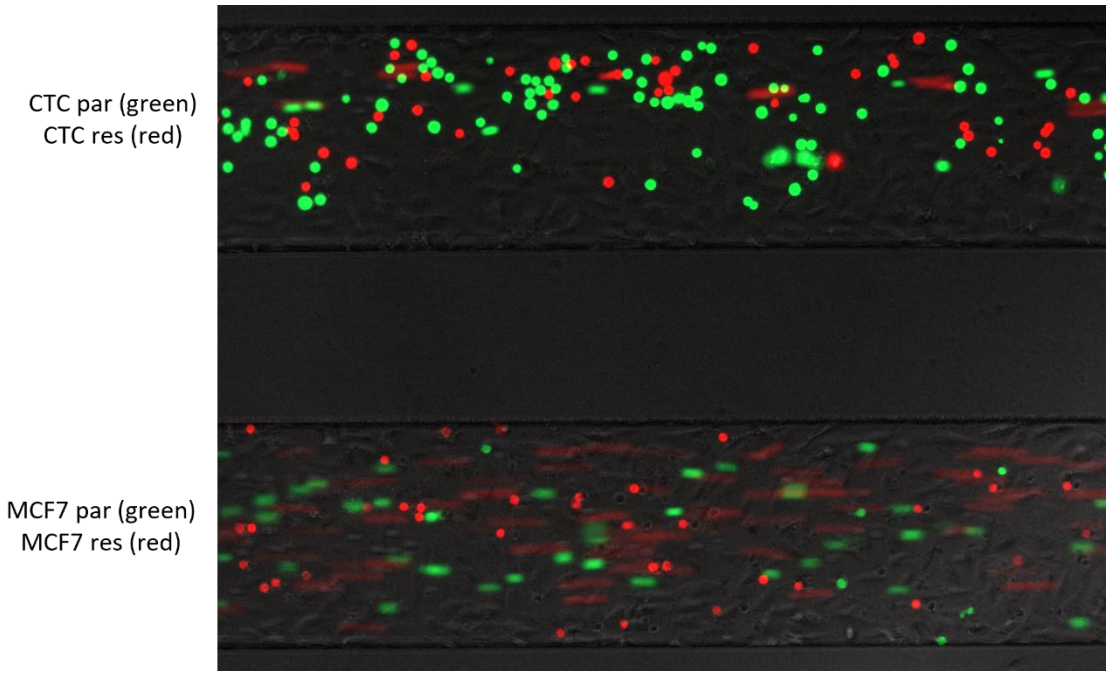

Figure 34: BioFlux experiments comparing the adhesion of parental and resistant CTC-ITB-01 cells and MCF7 cells to TNFα stimulated HUVECs. HUVECs were stimulated with TNFα prior to the experiment and the breast cancer cells were stained with CellTrace™ calcein dyes. Parental cells are stained in green, the respective resistant counterparts in red. Cells were perfused at 2 dyne/cm² and pictures were taken at 10x magnification.

Parental cells, stained in green and resistant cells, stained in red, were combined in a 1:1 ratio, facilitating direct comparison of the number of cells, adhering to the stimulated HUVEC cells.

Surprisingly, despite an increase of *ICAM1*, *PECAM1, ITGA1* and *LAMC2* transcripts in resistant CTC-ITB-01 cells, potentially conveying intercellular interactions with endothelial cells, a decrease of the number of resistant CTC-ITB-01 cells adhering to the HUVECs was observed. On the contrary, as demonstrated by previous experiments, parental MCF7 cells did not adhere to the HUVECs, however, a considerable percentage of resistant MCF7 cells adhered to the endothelial surface.

3.7 Detection of miRNAs by *in situ* hybridization

High levels of sensitivity and specificity are required to reliably quantify the expression of specific microRNAs. Due to their short length, high homology, particularly when belonging to the same family, large differences in the levels of expression as well as the lack of appropriate controls for normalization, detection and quantification of miRNAs remain technically challenging. MicroRNA analysis by bulk qPCR may be biased by several factors, such as inefficient RNA isolation, cDNA synthesis or varying qPCR efficacy. Moreover, heterogeneity of miRNA expression at single cell level cannot be reflected by qPCR. Thus, miRNA *in situ* hybridization (MISH) represents an additional option to detect and quantify levels of miRNAs and to mirror their spatial heterogeneous expression in different cell types with single cell resolution. In the present study, MISH has been established first for miR-21-5p, a miRNA which is known to be highly abundant in MCF7 cells [216]. In addition, an assay should be developed to simultaneously detect microRNAs and mRNAs by *in situ* hybridization as well as proteins by immunofluorescence to comprehensively characterize tumor cells. Finally, this assay should be applied for the detection of circulating tumor cells (CTCs) in blood collected from patients with mBC. Moreover, the potential of this assay to detect mRNAs/proteins and microRNAs resulting from the present study as indicators of resistance to ribociclib should be examined.

An overview of the establishment and integration of the assay starting from cell culture experiments to the analysis of patient samples is given in Figure 40.

3.7.1 Variant calling of resistant cell lines

Mutations in genes encoding proteins or non-coding RNAs might also contribute to the development of resistance to ribociclib and may thus represent druggable targets. They can e.g., be causative for altered signaling or for a complete loss of protein functions. Hence, mutations with a variant allelic frequency of 25% in all 3 samples of resistant cells and not higher than 5% in all 3 samples of parental cells are listed in Table 21.

Table 21: Gained mutations of the resistant CTC-ITB-01 cells. Mutations found in all three replicates of the resistant CTC-ITB-01 but not the parental ones are given.

Gene	Consequence	Protein position	Amino acids	Impact
ACAT1	missense variant	400	R/S	moderate
SORL1	missense variant, splice region variant	254	G/E	moderate
UHRF1BP1L	missense variant	859	C/Y	moderate
CHMP4A	missense variant	153	G/R	moderate
C16orf87	missense variant	150	Q/E	moderate
NF1	missense variant	2450	R/Q	moderate
PLEKHH3	missense variant	255	A/V	moderate
HOXB-AS1	splice acceptor variant, non-coding transcript variant	-	-	high
PRR11	missense variant	65	N/T	moderate
ZNF654	missense variant	841	I/T	moderate
MAP3K5	missense variant	517	T/K	moderate
VWDE	missense variant	1256	Q/K	moderate

Apart from genes rather related to metabolic processes and thus not in our immediate focus of attention in the context of ribociclib resistance, *NF1* [217], *PRR11* [218], *MAP3K5* [219] and *VWDE* [220] genes are all coding for proteins the relevance of which has been described in cancer before. Mutations in the *VWDE* gene were even described as driver oncogenic mutations[220]. The Q1256K mutation detected here, has already been detected in breast cancer (COSMIC or TCGA-A7-A3J0).

Interestingly, CTC-ITB-01 cells already harbor an *NF1* mutation (4528_4529insG; p.L1510Rfs*20) and gained an additional missense mutation (R2450Q) during resistance development, that has not been functionally described yet but was detected in glioblastoma and bladder cancer before according to the Catalogue Of Somatic Mutations (COSMIC). The N65T mutation in *PRR11* and the *MAP3K* T517K mutations are not listed in the COSMIC database, nor have they been described hitherto. Most mentioned mutations lead to missense variants, predicted to have a moderate impact on the integrity of the protein [221].

The mutation in the gene encoding the lncRNA HOXB-AS1 which has already been discussed in the context of cancer cell cancer-stemness in a cell culture model using glioma cells [222] is predicted to cause a splice acceptor variant. Another missense variant leading to an alternative splicing region was detected for *SORL1*.

Table 22: Gained mutations of the resistant MCF7 cells. Mutations found in all three replicates of the resistant MCF7 but not the parental ones are given.

Gene	Consequence	Protein position	Amino acids	Impact
SAMD11	missense variant	443	A/T	moderate
TIMM17A	missense variant	5	A/T	moderate
CEP170	missense variant	1409	D/G	moderate
ARFIP2	missense variant	338	V/L	moderate
TUBA1A	missense variant	221	L/P	moderate
HNRNPA1	missense variant	283	G/V	moderate
ATP6V0A2	missense variant	659	S/C	moderate
TLNRD1	stop gained	311	Q/*	high
DNAH3	missense variant	1782	S/L	moderate
ME2	missense variant, NMD transcript variant	474	P/L	moderate
NOTCH3	missense variant	1340	A/V	moderate
ZNF671	missense variant	149	A/V	moderate
MICALL1	missense variant	309	S/A	moderate
GUF1	missense variant	19	A/V	moderate
PLK4	missense variant	713	I/N	moderate
PJA2	missense variant	666	Q/P	moderate
ZSCAN31	inframe deletion	327	V/-	moderate
ZSCAN31	missense variant	326	K/N	moderate
MT-ND5	missense variant	603	T/M	moderate
HNRNPH2	missense variant	333	V/I	moderate

Resistant MCF7 and CTC-ITB-01 cells did not have any gained mutation in common. Some of the mutations found in resistant MCF7 cells have already been described in the context of breast cancer. *TLNRD1*, e.g., according to UniProt, codes for an actin-binding protein involved in cell proliferation, migration and invasion. The nonsense mutation Q311* is not listed in the COSMIC database but is predicted to have a high impact on the encoded protein.

Likewise, the *NOTCH3* A1340V mutation is not listed there, but Notch3 has been described to promote breast cancer progression. The missense mutation A149V in the *ZNF671* gene, described as a favorable marker for breast cancer by the Human Protein Atlas, is listed as a SNP in the COSMIC database. *PLK4* expression is associated with metastasis in breast cancer, but the detected mutation, I713N is not listed in the COSMIC database. The gene *ZSCAN31* encoding a member of the SCAN domain containing z-finger family harbors two mutations in the resistant MCF7 cells. Importance of ZSCAN31 has been described for hepatocellular carcinomas [223] but other members

have been linked to cell migration, invasion and angiogenesis in breast cancer and other tumors [224]. Neither of the detected mutations is registered in the COSMIC database. Another variant in a transcript that is a target of nonsense-mediated mRNA decay in the *ME2* gene, a stop codon in *TLNRD1*, and an in-frame deletion in *ZSCAN31* were detected.

Strikingly, many genes harboring mutations gained exclusively by the resistant cell lines are related to mitochondrial metabolism, such as *MT-ND5*, *TIMM17A* and *ACAT1* implying also metabolic alterations associated with ribociclib resistance, an observation that has been published on a pancreatic cancer cell culture model [225].

3.7.2 Sequencing of miRNAs

Establishment of resistance to CDK4/6 inhibitors is a complex process and not only driven by proteins, but also by non-coding RNAs. Hence, also miRNAs as important regulatory molecules, may contribute to the development of resistance. Importantly, in contrast to mainly cell cycle-related proteins, less is known about a causal association of miRNAs and the development of resistance to CDK4/6 inhibitors. Therefore miRNA-sequencing was performed to identify miRNAs potentially involved in this process.

First, the miRNA-sequencing data were also subjected to bioinformatical quality control, and the results are presented in Figure 35.

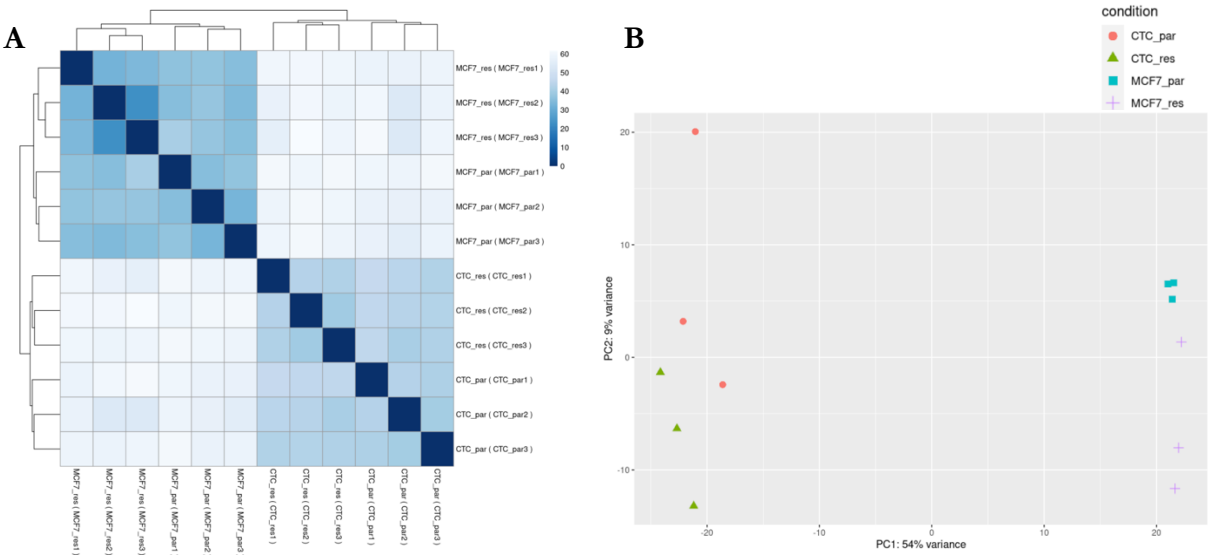

Figure 35: Bioinformatic quality control of miRNA-seq data. A) Biological replicates from the same cell line cluster, confirming homogenous replicates. B) Principal component analysis shows that the variance between CTC-ITB-01 and MCF7 cells was higher than between the respective parental and resistant derivates. (Both figures were created by Dr. Malik Alawi).

Analysis of sample-to-sample distance demonstrates clustering of samples from either MCF7 or CTC-ITB-01 cells (Figure 35). In concordance with that, PCA demonstrates higher variance between CTC-ITB-01 and MCF7 cells and lower variance for the respective comparison of parental and resistant derivates.

The volcano plots in Figure 36 provide an overview of differentially expressed miRNAs of the resistant cell lines compared to their parental counterparts. The criteria for identifying significantly

deregulated miRNAs were the same as used for mRNA analysis, namely a logFC≥1 and an FDR of ≤0.1.

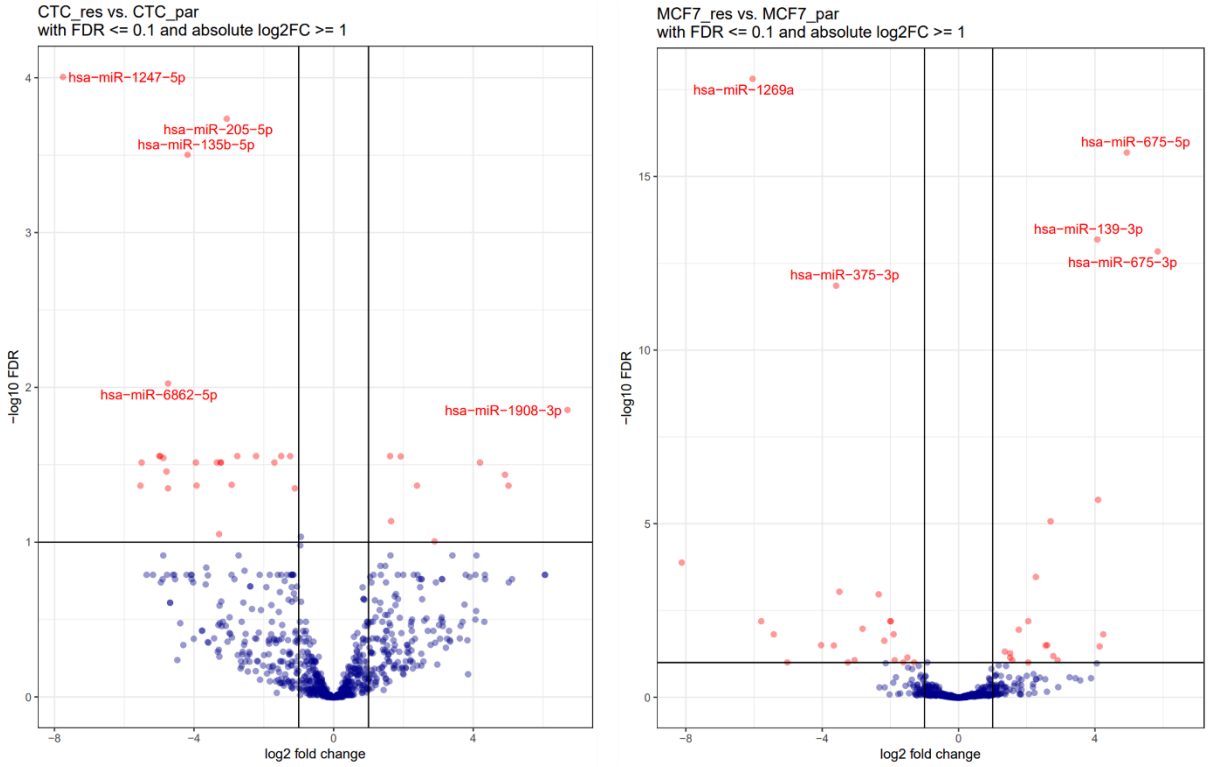

Figure 36: Volcano plots of deregulated miRNAs identified by small RNA-sequencing. All miRNA transcripts matching the (FDR ≤ 0.1 and |log2FC| ≥ 1) criteria, are shown in red and are deregulated in the resistant cell lines compared to the parental counterpart. The 5 most significantly deregulated miRNAs are marked in each graph. (Both figures were created by Dr. Malik Alawi).

Compared to mRNAs a lower number of miRNAs was significantly deregulated in ribociclib-resistant versus parental MCF7 and CTC-ITB-01 cells. Namely, in the resistant CTC-ITB-01 cells, 9 miRNAs were significantly upregulated and 24 downregulated whereas in the resistant MFC7, 29 miRNAs were found significantly upregulated and 21 downregulated, compared to their respective parental counterparts. Notably, miR-200c-5p was down-regulated in ribociclib-resistant CTC-ITB-01 cells. This miRNA belonging to the miR-200 family is well known for its role in EMT suppression [226]. Furthermore, member of this miRNA-family also exert pleiotropic regulatory roles on different adhesion molecules belonging to the adhesion machinery [227]. However, due to its low abundance and to the failure of family subtype-specific MISH probes this miRNA was not further analyzed in this study.

Interestingly, miR-146a-5p was upregulated in both resistant cell lines (not marked in Figure 36). Despite very contradictory publications on the role of miR-146a-5p in breast cancer, this microRNA was chosen for further validation and *in situ* experiments, as it was the only miRNA the level of which was significantly changed in both resistant cell lines.

Additionally, miR-205-5p was chosen as another miRNA of interest and for further validation as it has already been reported to be a tumor-suppressive miRNA, negatively modulating EMT and cancer-stemness [228]. Despite several potentially relevant miRNAs, miR-146a-5p and miR-205-5p

were chosen for future experiments since they were already described in the context of cancer and detected by miRNA-seq with high abundance.

3.7.3 Validation of miR-146a-5p and miR-205-5p expression by qPCR

For validation of miR-146a-5p levels, the same RNA preparations as used for RNA-sequencing were tested by qPCR. MiR-484 served as a housekeeping miRNA, used for normalization in the samples of parental and resistant CTC-ITB-01 cells.

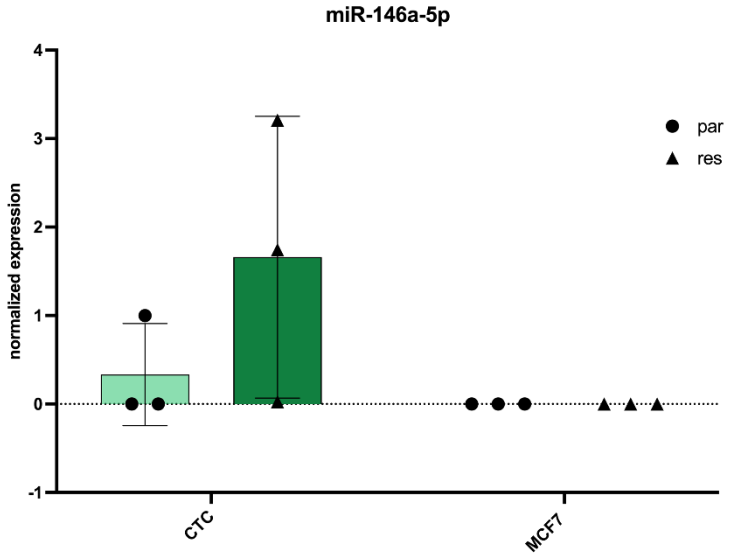

Figure 37: Relative expression of miR-146a-5p measured by qPCR for parental and resistant derivates. The same RNA that was used for sequencing was reversely transcribed and measured by qPCR. The graph shows values derived from three independently isolated RNAs. MiR-484 was used for normalization. Error bars represent SD.

The increased expression of miR-146a-5p in ribociclib-resistant compared to parental CTC-ITB-01 cells could be confirmed for 2 out of 3 biological replicates (Figure 37) which is concordant with the RNA-seq results. Read counts derived from RNA-seq for this miRNA in MCF7 cells were about 100-fold lower than that measured for CTC-ITB-01 cells (Figure 38). Thus, qPCR was not sufficiently sensitive to detect miR-146a-5p in any MCF7 sample.

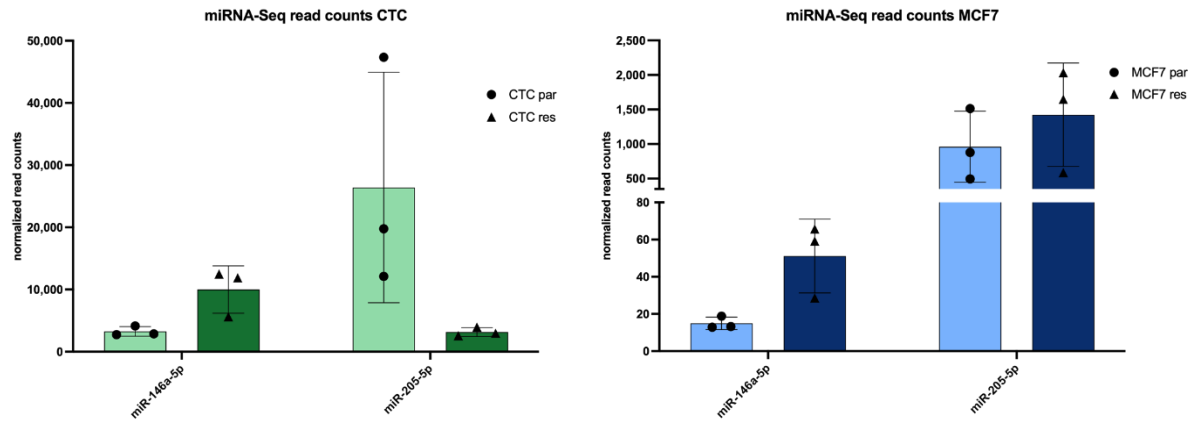

Figure 38: Normalized read counts of miR-146a-5p and miR-205-5p for the parental and resistant CTC-ITB-01 and MCF7 cell lines. Attention must be directed to the different scales of both y-axes.

The expression of miR-146a-5p expression was additionally tested by miRNA *in situ* hybridization (MISH) (chapter 3.7, Figure 39).

Since obtaining reliable MISH results for miR-146a-5p failed, we next focused on miR-205-5p, a tumor-suppressive miRNA the expression of which was decreased in resistant compared to parental CTC-ITB-01 cells according to RNA-seq (Figure 38). First, validation of miRNA levels by qPCR was performed.

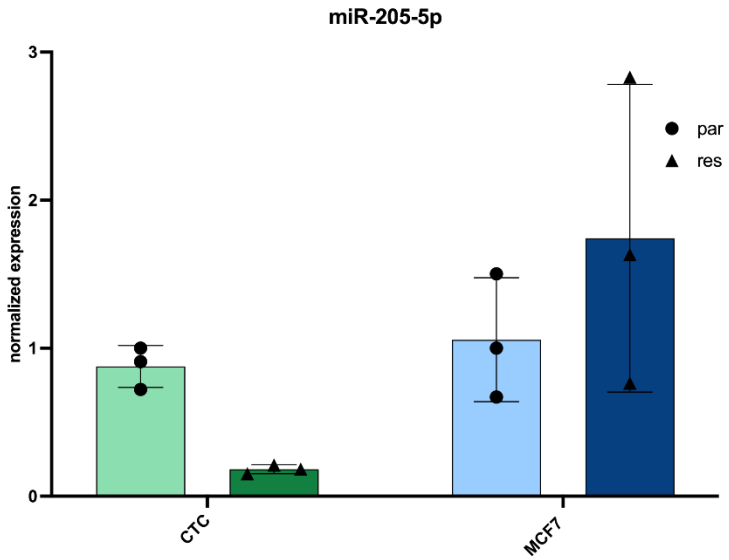

Figure 39: Validation of miR-205-5p expression in parental and resistant CTC-ITB-01 and MCF7 cells. Results of three independent biological replicates, also used for RNA-seq are shown. MiR-484 was used for normalization. Error bars indicate ±SD.

The significant decrease of miR-205-5p expression could be confirmed for all three replicates of resistant compared to parental CTC-ITB-01 cells. While the miR-205-5p level dropped by approximately 80%, no significant changes in miR-205-5p expression were observed between parental and resistant MCF7 cells. Notably, Figure 39 shows the relative expression of both resistant derivates to their respective parental cell line cells, but not a quantitative estimation of the expression of miR-205-5p between CTC-ITB-01 cells and MCF7 cells. As depicted in Figure 38, miR-205-5p levels were markedly lower in MCF7 cells than in CTC-ITB-01 cells.

The decrease of the miR-205-5p-level in the resistant versus parental CTC-ITB-01 cells and the strong differences in its expression between CTC-ITB-01 and MCF7 cells were also validated by MISH (chapter 3.7, Figure 51).

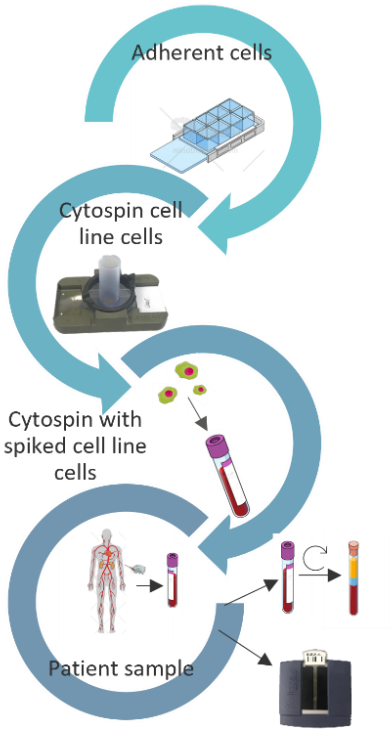

Figure 40: Overview of the workflow of MISH implementation into characterization of circulating tumor cells. Starting from adherent cell culture cells to cells enriched from patient samples by various methods, the assay was established, using mainly miR-21-5p as a highly abundant miRNA in MCF7 cells. The figure was created using mindthegraph.com.

The assay was established on cell culture cells, starting on cells grown adherently on chamber slides, followed by cells immobilized on slides by centrifugation (cytospins). After successful testing, patient samples were mimicked by spiking of MCF7 cells into healthy donor blood. The blood was enriched by commonly used methods. Ficoll-based gradient centrifugation was used for marker- and size-independent enrichment. CellSearch® enrichment was tested as well, as it represents an enrichment method commonly used for breast cancer, since it is FDA-approved and the number of breast cancer CTCs enriched by this method possess prognostic power [98]. Furthermore, the compatibility of this assay with an additional enrichment method and blood tubes mostly used for samples enriched by this method was investigated. The Parsortix® system enriches CTCs marker-independently but size- and plasticity-based and represents an alternative to the CellSearch® system for the enrichment of CTCs with low or lacking EpCAM expression. EpCAM expression may be reduced during EMT, hampering the detection of more mesenchymal-like CTCs by the CellSearch® system. Furthermore, the number of EpCAM positive CTCs varies between different cancer entities [229]. Both enrichment systems require specific blood tubes, containing fixatives, preserving CTCs for several days. It was thus tested whether these fixatives could impair the integrity of miRNA and mRNA, hampering successful detection of these RNAs by *in situ* hybridization (ISH).

3.7.4 MISH on cell culture cells

Initially, MISH was tested on adherent MCF7 cells grown on chamber slides. As identification of CTCs by keratin and further characterization by an additional marker detected by immunostaining is mandatory, concurrent keratin immunofluorescent (IF) staining using a pan-anti-keratin antibody cocktail was tested (Figure 41).

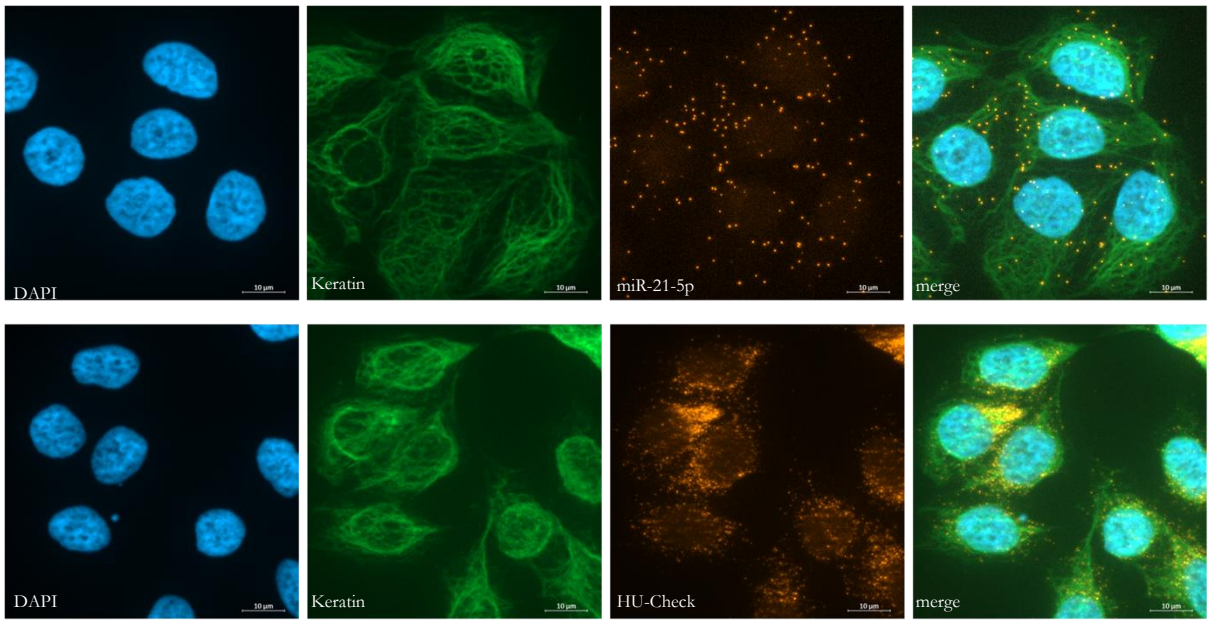

Figure 41: MISH performed on adherent MCF7 cells cultivated on chamber slides. MiR-21-5p (AF 546) was detected as a highly abundant miRNA in MCF7 cells (top). HU Check probe cocktail (AF546 bottom) served as a test probe for the detection of mRNA by ISH. Visualization of keratins was achieved by immunofluorescence staining with a pan-anti-keratin antibody cocktail (clone AE1/AE3, FITC, 1:150). Nuclei were counterstained with DAPI. The picture was taken at 63x magnification with oil and a z-stack was acquired using an ApoTome 2.0. Scale bar represents 10 µM.

Figure 41 demonstrates the feasibility of combined MISH or mRNA ISH and IF staining, providing the possibility to detect mRNA and microRNA on tumor cells, making this technique a promising tool to detect and characterize circulating tumor cells (CTCs). Furthermore, the picture shows the potential of the assay to visualize single target miRNA molecules.

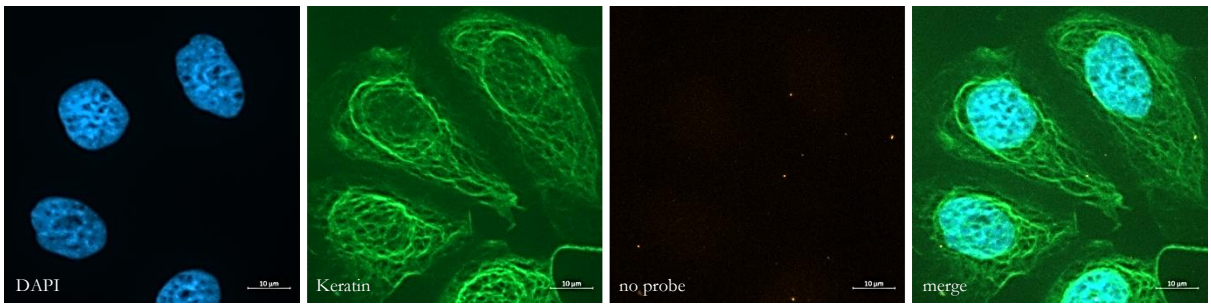

Figure 42: Negative control of MISH performed on adherent MCF7 cells cultivated on chamber slides. No probe was used for hybridization. Visualization of keratins was achieved by immunofluorescence staining with a pan-anti-keratin antibody cocktail (clone AE1/AE3, FITC, 1:150). Nuclei were counterstained with DAPI. The picture was taken at 63x magnification with oil and a z-stack was acquired using an ApoTome 2.0. Scale bar represents 10 µM.

The negative control (Figure 42), performed without using a probe but with all the reagents from the amplification steps shows very low background signals.

To screen blood cell preparations (e.g., peripheral blood mononuclear cells enriched by Ficoll density gradient centrifugation) for the presence of CTCs, cytospins are used frequently. Therefore, the MISH procedure was next applied to MCF7 cells on cytospins. MicroRNA probes are generally only provided with an AF546 label by ThermoFisher since it yields the brightest signals. However, the assay should also be implemented for CellSearch® samples that are by default fluorescently stained with a phycoerythrin-labeled anti-keratin antibody detected in the same channel as AF546-labeled antibodies are detected. Thus, a customized miR-21-5p probe, labeled with AF488 was tested.

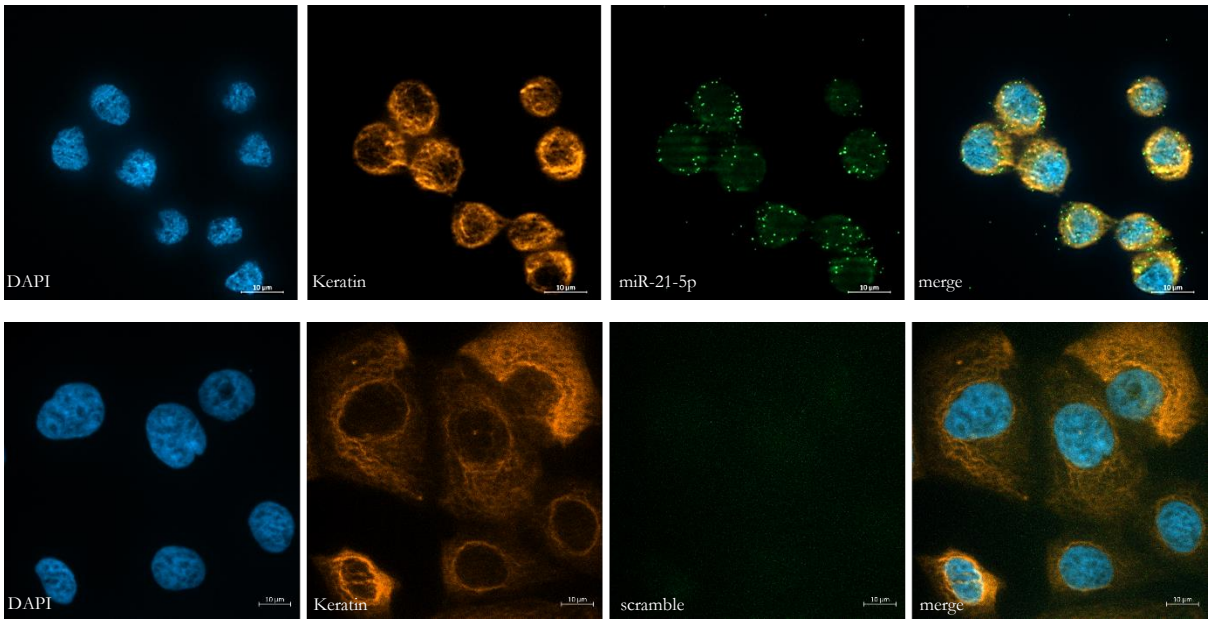

Figure 43: miR-21-5p detection by MISH on MCF7 cells on a cytospin. Keratin expression was detected using a pan-keratin antibody (clone AE1/AE3, PE, 1:300) and miR-21-5p by an AF488 labeled probe. In the control sample, a scramble probe was used. Nuclei were counterstained with DAPI. The pictures were taken at 63x magnification with oil and a z-stack was acquired using an ApoTome 2.0. Scale bar represents 10 μM.

First, this experiment could confirm that also the usage of AF488 labeled miRNA probes prompts signals sufficiently intense to be detected with a common fluorescence microscope. The scramble control, using a probe with a random sequence not complementary to any known human miRNA, demonstrates again the high target-specificity of the assay. Second, detection of miRNAs by MISH is also applicable for cells on cytospins. The compression of the cytoplasm by spinning down the cells did not impair the detection of the target molecules.

To test the specificity of the assay, miR-21-5p expression was tested on four different breast cancer cell lines, namely MCF7, T47D, ZR-75-1 and MDA 468, by MISH and qPCR, as shown in Figure 44.

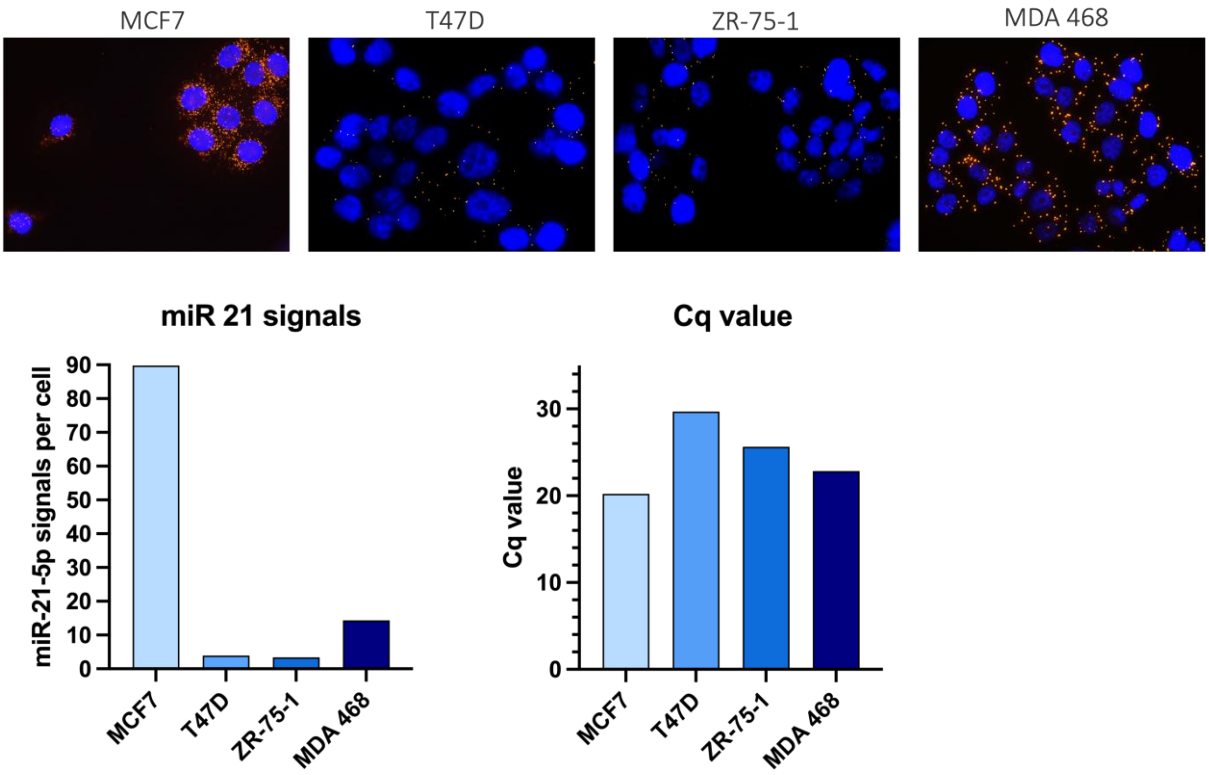

Figure 44: Comparison of miR-21-5p levels assessed by MISH and qPCR. The number of miR-21-5p signals per cell was assessed from ≥ 30 cells by ImageJ particle counter. The shown Cq values are derived from a single experiment.

The number of miR-21-5p signals per cell was measured by the "particle measure tool" in ImageJ and compared to the Cq values of miR-21-5p in the same cell lines measured by qPCR. Since the Cq values correlate inversely to the number of template molecules, the qPCR results matched the miR-21-5p levels detected by MISH. MCF7 cells showed by far the highest signal number of miR-21-5p-specific signals and the lowest Cq value. The abundance of this miRNA was intermediate in the MDA-MB-468 cells, as confirmed by both methods and the lowest levels of miR-21-5p were detected in T47D and ZR-75-1 cells, confirming the specificity of the MISH assay.

3.7.5 Detection of RNAs by MISH on spiked MCF7 cells enriched by density gradient centrifugation

In the next step, MCF7 cells were spiked into blood samples collected from healthy donors and enriched by density gradient centrifugation using Leucosep tubes. Cytospins generated from the enriched MCF7 cells were used for the detection of miR-21-5p by MISH. In addition to miR-21-5p detected in green, the compatibility of mRNA detection with this kind of sample was assessed using the mRNA HU Check probe mix, consisting of probes for the detection of *GAPDH*, *ACTB* and *PPIB* (encoding peptidylprolyl isomerase B), in orange. Keratin was detected with an antibody cocktail labeled with PerCP and the common leukocyte antigen CD45, serving as an exclusion marker for CTCs, was stained with an APC labeled antibody.

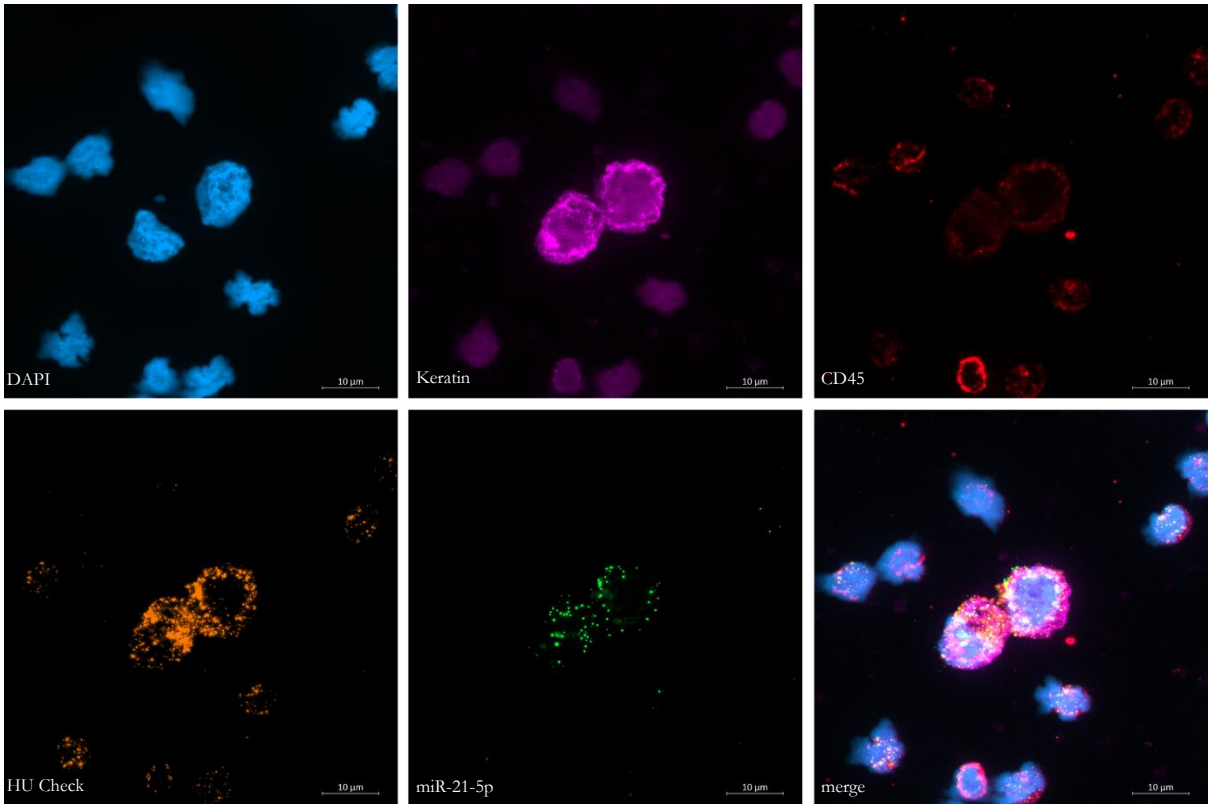

Figure 45: Detection of miR-21-5p and mRNA HU Check probe mix by MISH and mRNA ISH on spiked MCF7 cells enriched by density gradient centrifugation using Ficoll-Paque™. Keratin was detected using a pan-keratin antibody (clone AE1/AE3, PerCP, diluted 1:150). CD45 was detected with a monoclonal antibody (clone REA747, APC, diluted 1:150). For the ISH, a miR-21-5p- specific AF488 labeled probe, and the HU Check probe mix labeled with AF546 were used. Nuclei were counterstained with DAPI. The picture was taken at 63x magnification with oil and a z-stack was acquired using an ApoTome 2.0. Scale bar represents 10 µM.

Detection of two different proteins, keratin, and CD45, was successfully combined with the detection of miR-21-5p and the control mRNAs (mRNA HU Check mix) (Figure 45). The Ficoll based enrichment of MCF7 cells from healthy donor blood did not impair the detection of any target. Moreover, Figure 45 demonstrates that the parallel use of PerCP labeled antibodies and APC labeled antibodies was feasible, despite their close emission peaks (PerCP 678 nm, APC 660 nm), due to their distinct excitation wavelength (PerCP 477 nm, APC 651 nm). As the ISH probes are only available in 4 different labels (AF488, AF546, AF647, AF750), it is important to find a reasonable combination of antibodies to detect the proteins of interest. MiR-21-5p was only detected in MCF7 cells and not in the surrounding leukocytes. In contrast, the control mRNAs were also expressed in leukocytes (Figure 45, bottom left).

For all experiments described hitherto, blood was collected in EDTA tubes. However, for certain applications special tubes, containing fixatives, stabilizing the cells for a longer period and transport are required. Blood for Parsortix® enrichment often is collected in TransFix tubes whereas samples for the CellSearch® system are drawn into CellSave tubes. Thus, MCF7 cells were spiked into healthy donor blood, stored for 24h in the respective tubes and were enriched by these two enrichment methods and furtherly used for MISH and mRNA ISH.

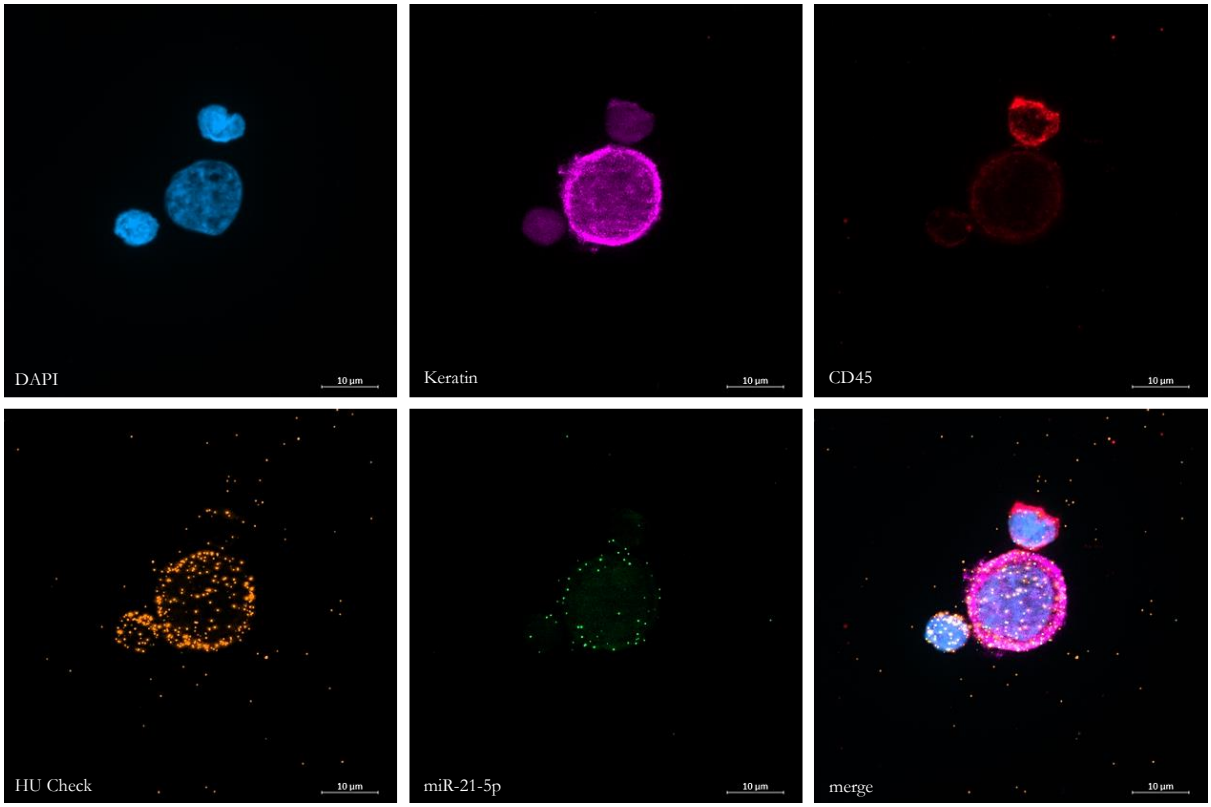

Figure 46*:* Detection of miR-21-5p and mRNA HU Check probe mix by MISH and mRNA ISH on spiked MCF7 cells enriched by Parsortix®. Keratin was detected using a pan-keratin antibody (clone AE1/AE3, PerCP, diluted 1:150). CD45 was detected with a monoclonal antibody (clone HI30, APC, diluted 1:150). For the ISH, a miR-21-5p- specific AF488 labeled probe, and the HU Check probe mix labeled with AF546 were used. Nuclei were counterstained with DAPI. The picture was taken at 63x magnification with oil and a z-stack was acquired using an ApoTome 2.0. Scale bar represents 10 µM.

Figure 46 demonstrates the suitability of the combined MISH/IF method for MCF7 cells enriched by Parsortix®. Strikingly, the fixative of the TransFix tubes seemingly did not degrade mRNA or miRNA. Yet, the background of unspecific signals, particularly in the orange channel, was slightly increased compared to the Leucosep-enriched sample. In contrary to that, the sample enriched by CellSearch® showed less background in the orange channel but a higher number of background signals in the far red one. Additionally, while the number of miRNA signals slightly changed, a strong decrease of mRNA signals could be detected as opposed to the two other enrichment methods, implying a partial degradation of mainly mRNA by the CellSave fixative (Figure 47).

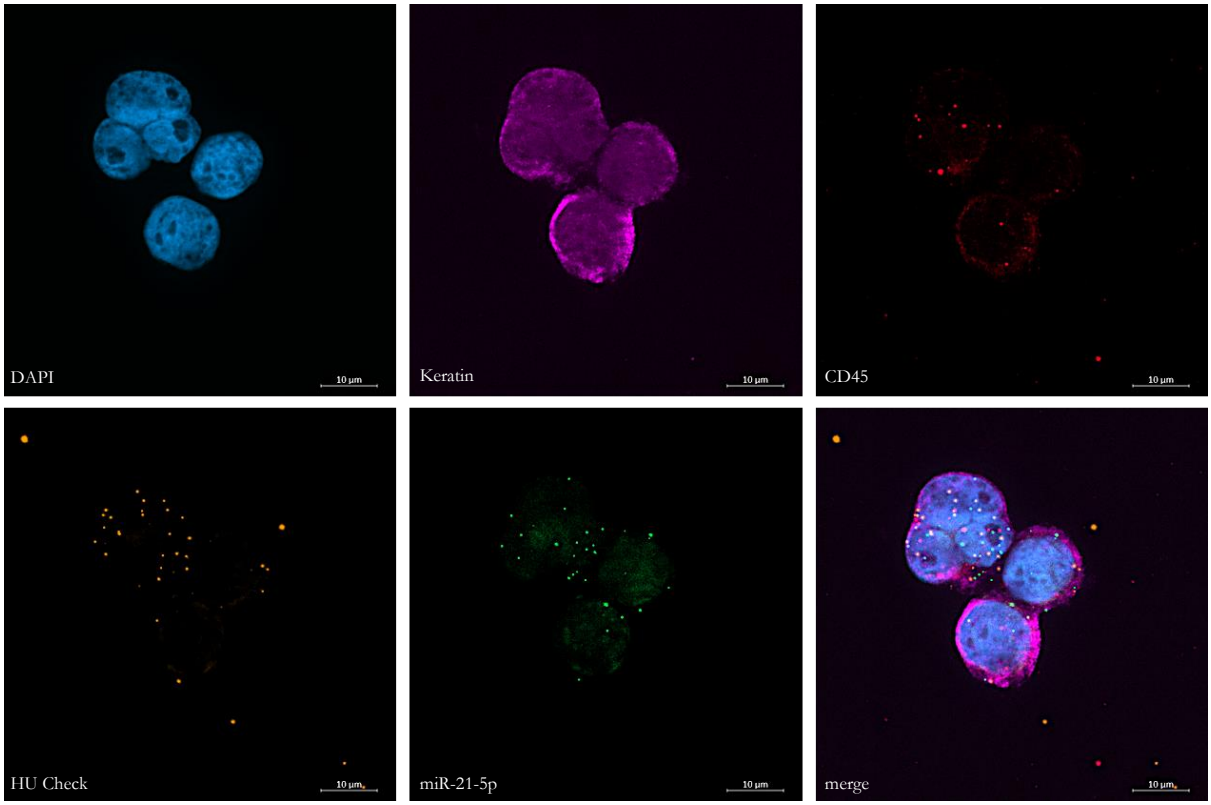

Figure 47: Detection of miR-21-5p and mRNA HU Check probe mix by MISH and mRNA ISH on spiked MCF7 cells enriched by the CellSearch® device. Keratin was detected using a pan-keratin antibody (clone AE1/AE3, PerCP, diluted 1:150). CD45 was detected with a monoclonal antibody (clone HI30, APC, diluted 1:150). For the ISH, a miR-21-5p- specific AF488 labeled probe, and the HU Check probe mix labeled with AF546 were used. Nuclei were counterstained with DAPI. The picture was taken at 63x magnification with oil and a z-stack was acquired using an ApoTome 2.0. Scale bar represents 10 µM.

Hence, a new tube (CellRescue, The Menarini Group) was tested, as it is supposed to contain a fixative that prevents RNA degradation However, the obtained results did not provide an improvement to the results obtained from blood samples collected in CellSave tubes. Thus, while miRNA detection is feasible on samples from a CellSave tube, reliable mRNA detection is not guaranteed due to potential mRNA degradation induced by the fixative.

One of the bottlenecks of performing MISH on CellSearch® samples is the transfer of the cells from the cartridge to a microscope slide, as it is associated with a significant loss of cells for unknown reasons. Therefore, MISH was directly performed in the cartridges and analyzed on a specialized Cell Tracks Analyzer (Janssen Diagnostics, LLC). This device is an adaption from the Cell Tracks Analyzer used to read the CellSearch® cartridges, optimized to identify ISH signals of various fluorescence colors. MiR-21-5p and *CCND1* mRNA were detected on MCF7 cells, spiked into healthy donor blood, and enriched by the CellSearch® Profile kit. This kit provides the same enrichment process as the CTC kit, however, the cells remain unstained as the procedure is stopped before the IF staining. Thus, the staining of the cells in the cartridge can be flexibly adapted to a specific experiment. This provided the possibility to test MISH in the cartridge by the detection of an AF546-labeled miR-21-5p probe and additional testing of mRNA ISH, detecting *CCND1* mRNA with an AF647-labeled probe. Due to the strong keratin staining, the size and morphology, MCF7 wells could be identified unequivocally, albeit the far-red channel was occupied by the *CCND1* probe and the exclusion marker CD45 could not be detected (Figure 48).

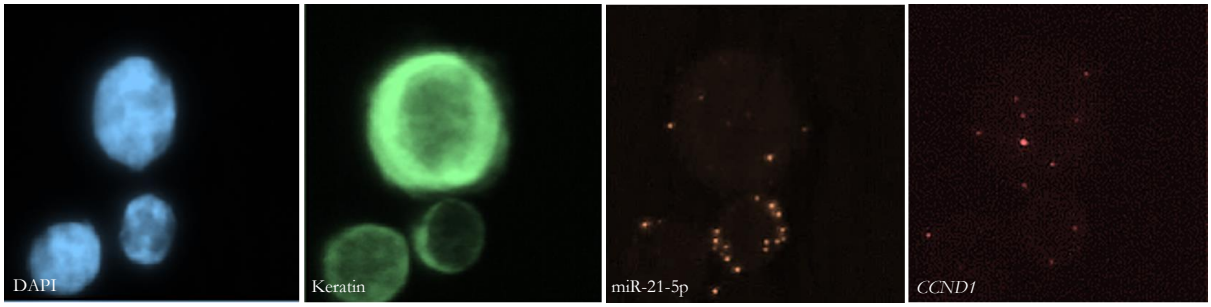

Figure 48: MISH and mRNA ISH performed on spiked MCF7 cells in a CellSearch® cartridge. MiR-21-5p was detected with an AF546-labeled probe and *CCND1* mRNA by an AF647-labeled probe. Keratin was stained with a pan-keratin antibody cocktail (AE1/AE3, FITC, 1:300) and nuclei were counterstained with DAPI. The picture was taken at 20x magnification and a z-stack.

As Figure 48 demonstrates, performing the MISH and mRNA ISH directly in the cartridge is feasible, however, usually the far-red channel is occupied by staining of CD45, and either the green or orange channel is used for the detection of keratin, limiting the number of RNA targets that can be detected simultaneously to keratin, to currently one. Whether probes labeled with AF750 could be detected with this device, remains to be evaluated. However, for the detection of one specific target of interest an in-cartridge MISH or mRNA ISH might be taken into consideration, to avoid loss of CTCs.

For a proof-of-principle experiment, testing the MISH on patient samples, miR-16-5p was chosen, as it is rather abundant in many breast cancer samples and even considered a housekeeping miRNA [230], also often suggested for normalization of miRNA qPCR. Some exemplary pictures of CTCs from two different patient samples are presented in Figure 49.

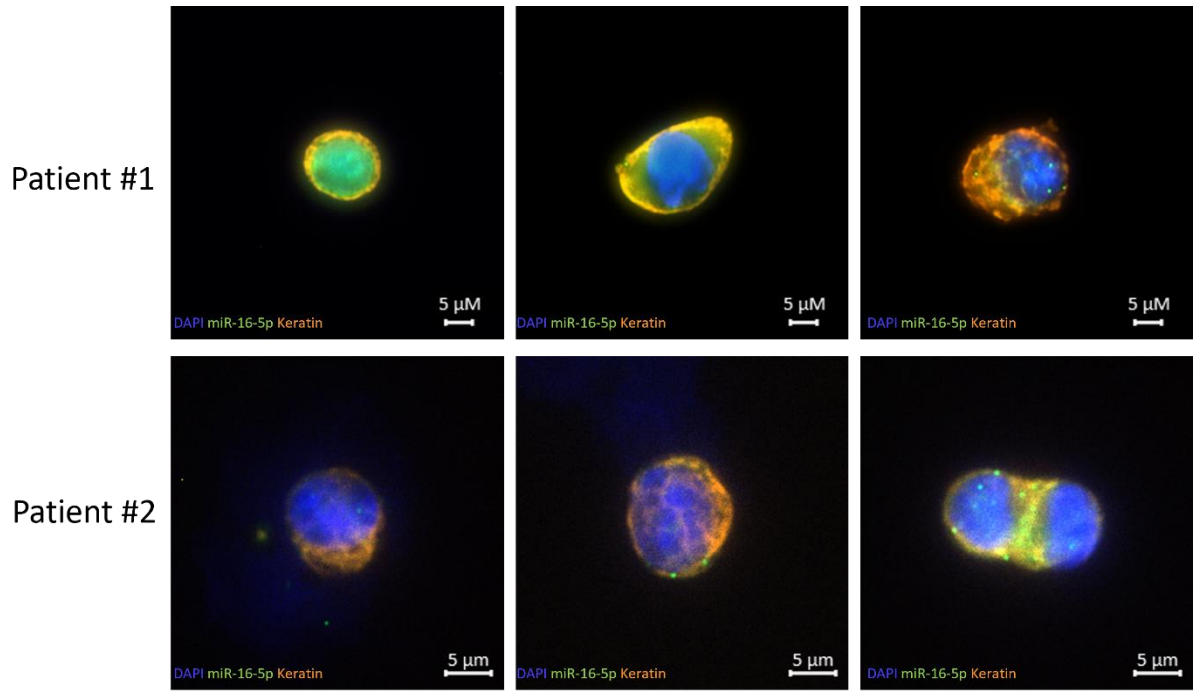

Figure 49. Detection of miR-16-5p on CTCs enriched by CellSearch® from blood samples of HR+ mBC patients using MISH. The samples were processed using the CTC kit. MiR-16-5p was detected using a AF488-labeled probe. The picture was taken at 40x magnification and with a z-stack.

Figure 49 depicts miR-16-5p expression in CTCs. CTCs from patient #1 show a range from no copy to several ones, similar to patient #2, having CTCs with only a few up to 20 copies per cell. This stresses the importance of single-cell resolution when analyzing miRNA expression. Despite being considered homogenously expressed and even suggested to be a housekeeping miRNA in mBC, a substantial heterogeneity of the number of miR-16-5p signals was observed. Also, this analysis is only possible with an assay providing single target molecule resolution. Thus, MISH appears to be an appropriate tool to assess miRNA expression on the single-cell level.

Hence, the assay was used to validate the abundance of miR-146a-5p and miR-205-5p. RNA-seq data identified miR-146a-5p as a miRNA upregulated in resistant CTC-ITB-01 cells as well as resistant MCF7 cells. However, qPCR analysis failed to detect miR-146a-5p in MCF7 cells, perhaps due to its low abundance (Figure 37). Therefore, the RNA-seq data was validated with MISH, detecting miR-146a-5p.

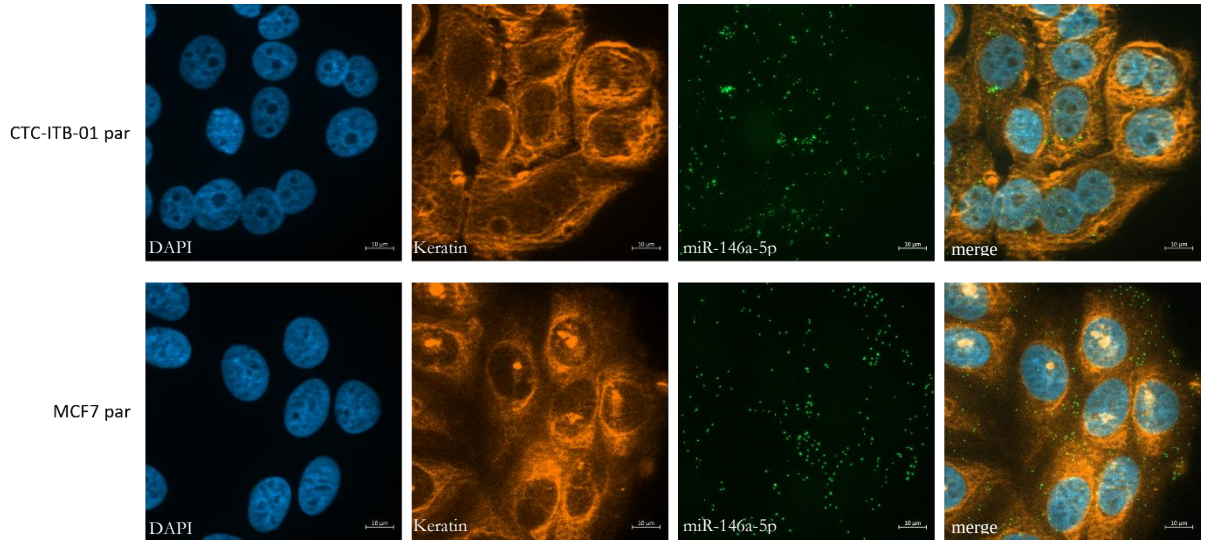

Figure 50: Comparison of miR-146a-5p levels detected by MISH. Keratin was detected using a PE-labeled pan-keratin antibody (clone AE1/AE3, diluted 1:150) and miR-205-5p was visualized by an AF488-labeled probe. The nuclei were counterstained with DAPI. The picture was taken at 63x with oil and a z-stack was acquired using an ApoTome 2.0. Pictures were taken at 63x magnification.

Representative pictures in Figure 50 from the MISH assay demonstrate, that the results were not concordant with neither qPCR results nor RNA-seq data. Based on these experiments, miR-146a-5p levels should have been lower in MCF7 cells than in CTC-ITB-01 cells. Instead, higher numbers of signals were detected in MCF7 cells, likely due to an unspecific probe Therefore, this miRNA was not chosen for further MISH assays, aiming to investigate miRNA expression on CTCs. Instead, miR-205-5p was selected due to the significant decrease of miR-205-5p levels in resistant versus parental CTC-ITB-01 cells and its high abundance. The results obtained by RNA-seq could successfully be confirmed by qPCR analysis (Figure 39) and was additionally validated using the MISH assay.

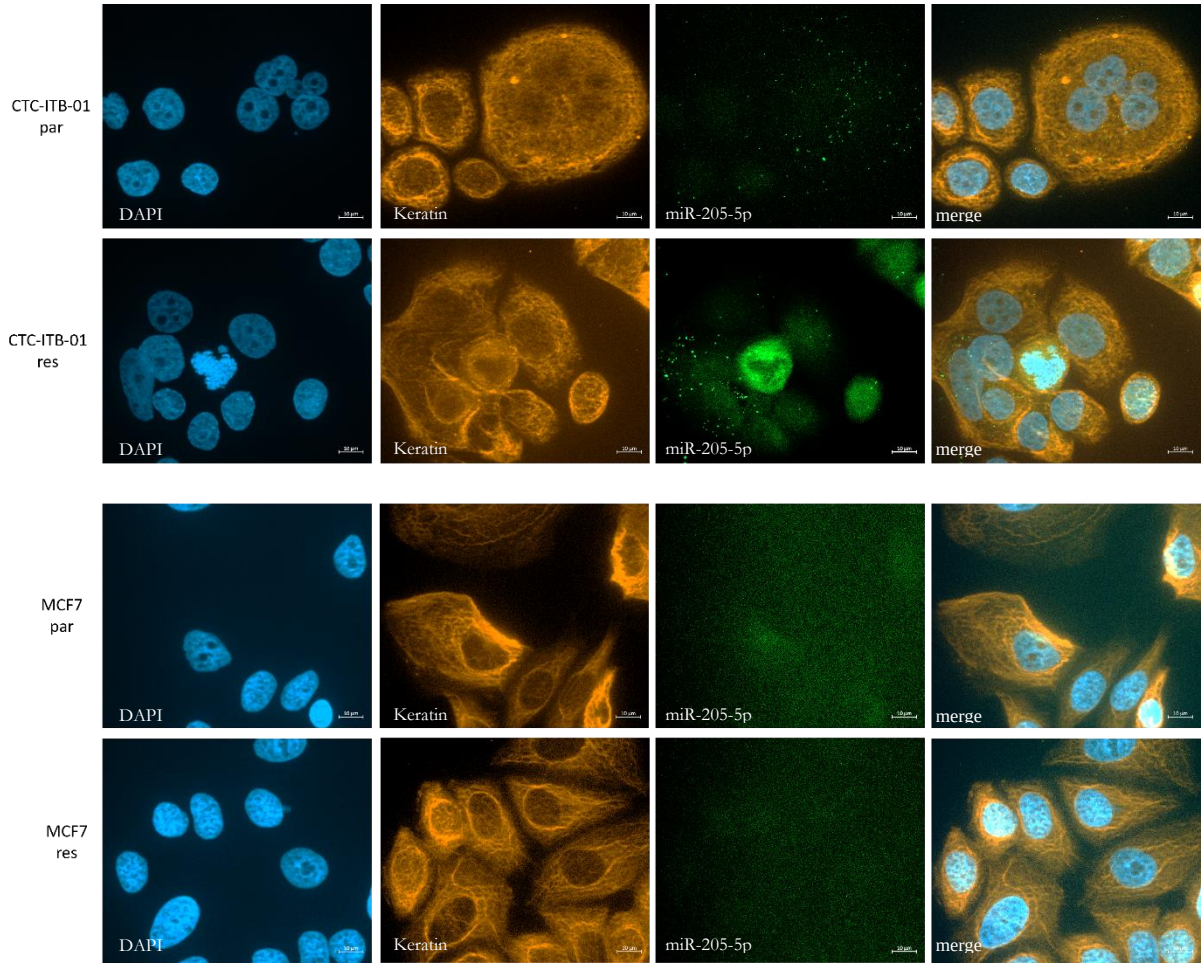

Figure 51: Detection of miR-205-5p by MISH in parental and resistant CTC-ITB-01 and MCF7 cells. Keratin was detected using a PE-labeled pan-keratin antibody (clone AE1/AE3, diluted 1:150) and miR-205-5p was visualized by an AF488-labeled probe. The nuclei were counterstained with DAPI. The picture was taken at 63x with oil and a z-stack was acquired using an ApoTome 2.0. Scale bar represents 10 µM.

Using MISH, detecting miR-205-5p in CTC-ITB-01 and MCF7 derivates, the differences of miR-205-5p expression between the two cell lines could be confirmed (Figure 51). While in parental and resistant CTC-ITB-01 cells distinct green miR-205-5p-specific signals were detected, in MCF7 cells, almost no signals were visible. Yet, the strong decrease of this miRNA, identified by RNA-seq and validated by qPCR, could not be confirmed by this assay. However, the heterogeneous distribution of miRNA signals among different morphological subtypes of cells the CTC-ITB-01 cell line requires further investigation of a higher number of single cells.

Nonetheless, the assay was used to detect miR-205-5p, a tumor-suppressive miRNA downregulated in resistant CTC-ITB-01, in a small number of patient samples (n=2), to test whether this miRNA is a suitable marker for the detection of CDK4/6i-resistant CTCs.

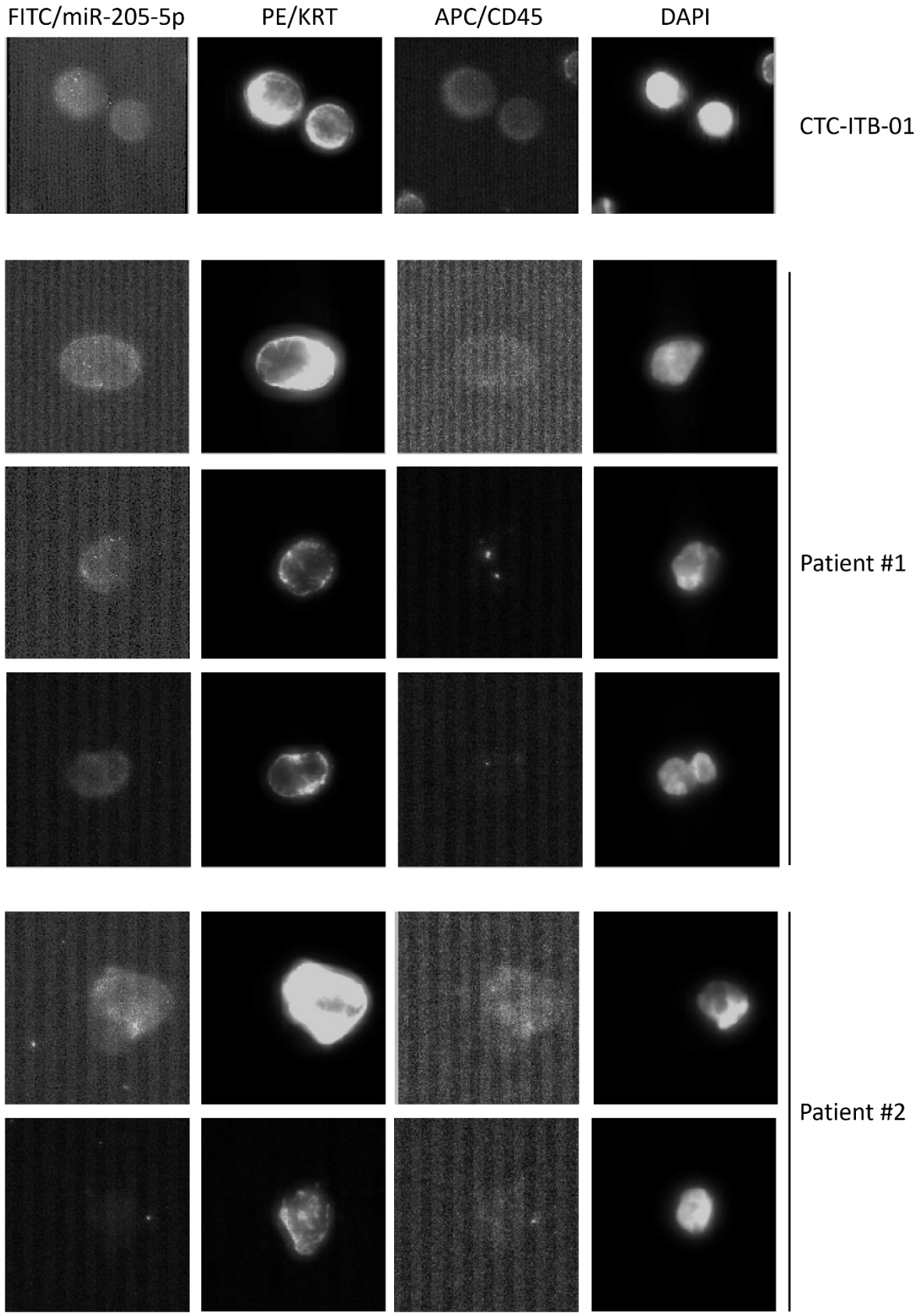

Figure 52: Detection of miR-205-5p by MISH on samples of HR+ mBC patients. MISH was performed in CellSearch® cartridges. The samples were enriched using the CTC kit. MiR-205-5p was detected using an AF488-labeled probe. The picture was taken at 40x magnification and with a z-stack.

Using MISH, miR-205-5p was detected on CTCs from samples of patients with HR+ mBC processed by the CellSearch® system. Parental CTC-ITB-01 cells were used as a positive control, as they had the highest miR-205-5p expression of the cell lines used in this study. However, while the signals using the AF488 labelled probe were sufficiently intense to detect them with 63x oil objective (Figure 51), the resolution achieved with the 40x objective of the Cell Tracks Analyzer, was not sufficient for reliable detection. Thus, analysis of miR-205-5p on CTCs enriched from patient samples was difficult, but in patient #1, some CTCs with potential signals were found (top two rows) as well as CTCs completely negative for miR-205-5p (bottom row). All CTCs detected from patient #2 were negative for miR-205-5p

Summarized, RNA ISH represents an approach, to detect and visualize different RNA species in a variety of sample enriched for CTCs by different enrichment methods. In this study, RNA ISH was used to detect and semi-quantify expression levels of selected miRNAs and mRNAs in resistant and parental CTC-ITB-01 and MCF7 cells. Furthermore, it was also tested on patient samples, enriched for CTCs by the CellSearch® system.

3.8 Therapy options after established resistance to the CDK4/6i ribociclib

As mentioned before, the clinical emergence of resistance to CDK4/6 inhibitors is almost inevitable, and the presented results demonstrate the multitude of involved proteins and altered signaling pathways in this process. Hence, finding therapeutic agents for the treatment of mBC patients resistant to CDK4/6 inhibitor resistant patients is of utmost importance.

3.8.1 Combined endocrine and CDK4/6i treatment

The patient, the CTC-ITB-01 cell line was established from had received several lines of therapy including chemotherapy and treatment with denusomab (monoclonal antibody against RANKL). The aromatase inhibitor letrozole was given additionally in second line and the estrogen receptor antagonist tamoxifen in third line treatment. Finally, the patient died under chemotherapy and denosumab treatment. Fulvestrant, a selective ER degrader is another ER antagonist that in contrast to tamoxifen does not exert any agonist activity and leads to the degradation of ER and PR [231], was not administered to this patient. The CTC-ITB-01 cell line seems to be resistant to sole fulvestrant treatment [119], however a combination of treatment with fulvestrant and ribociclib has not been tested yet.

First, it was examined whether dual inhibition of CDK4/6 and ERα signaling would result in enhanced reduction of viability and clonogenic growth.

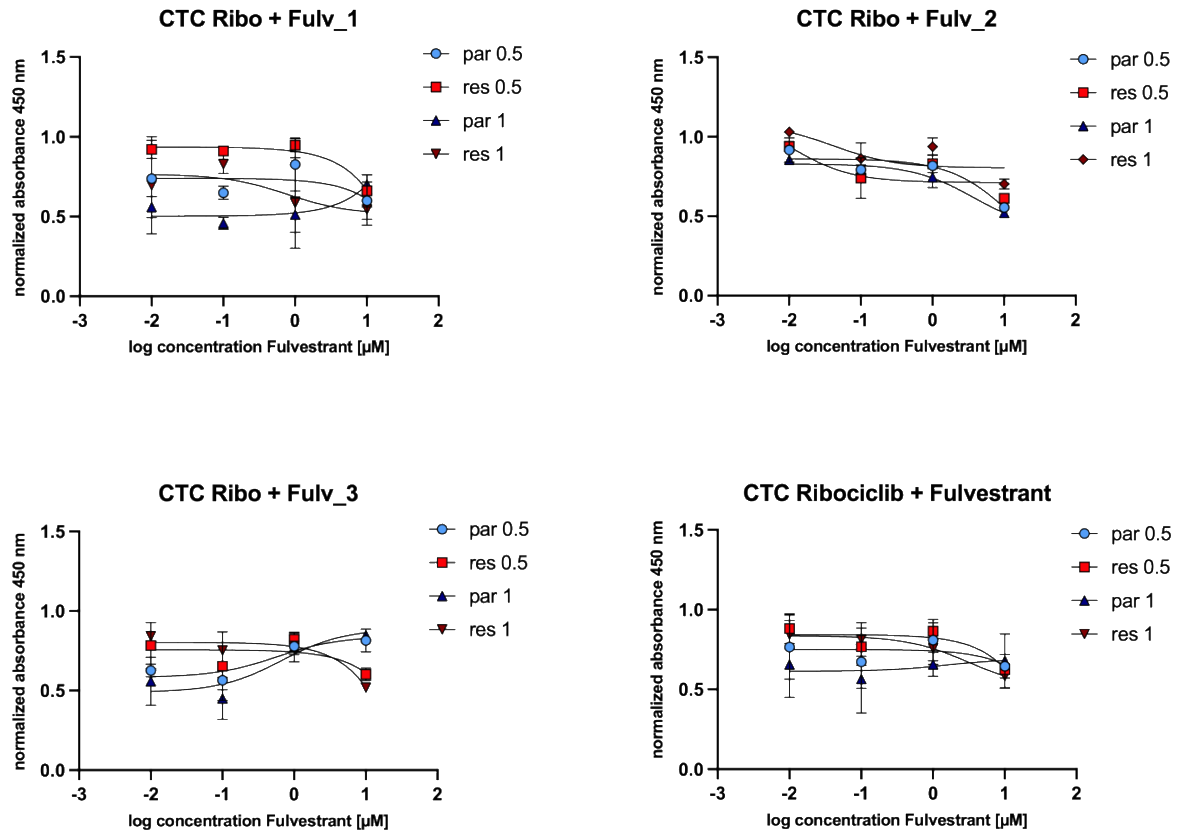

Figure 53: Impact of dual inhibition by fulvestrant and ribociclib on the viability of CTC-ITB-01 cells. Three biologically independent experiments were performed. $3x10^3$ cells per well were seeded in a 96 well plate and treated with either 0.5 µM or 1 µM ribociclib and increasing fulvestrant concentrations (0.01 – 10 µM). The absorbance of the CCK-8 product was measured at 450 nm after 4 h of incubation. All experiments were assessed in technical triplicates and the results were normalized to the respective DMSO control. Error bars indicate ±SD.

Figure 53 demonstrates that the addition of 0.01 – 10 µM fulvestrant to ribociclib had hardly any impact on the viability of neither the parental nor the resistant cell line at the tested concentrations which were derived from literature [119]. When treated with ribociclib only, at 1 µM no reduction of the absorbance in the resistant CTC-ITB-01 cells, (1.2-fold compared to DMSO control) and only a minor reduction of 15% (0.85-fold compared to DMSO control) in the parental cells was observed (Figure **12**). The addition of 1 µM fulvestrant to 1 µM ribociclib led to a 0.76-fold reduction of absorbance in the resistant and a 0.66-fold reduction in parental CTC-ITB-01 cells compared to the respective DMSO controls (Figure 53). The absorbance barely changed with increasing concentrations of fulvestrant suggesting that these cells were resistant to fulvestrant independently of being resistant to exclusive ribociclib treatment or not.

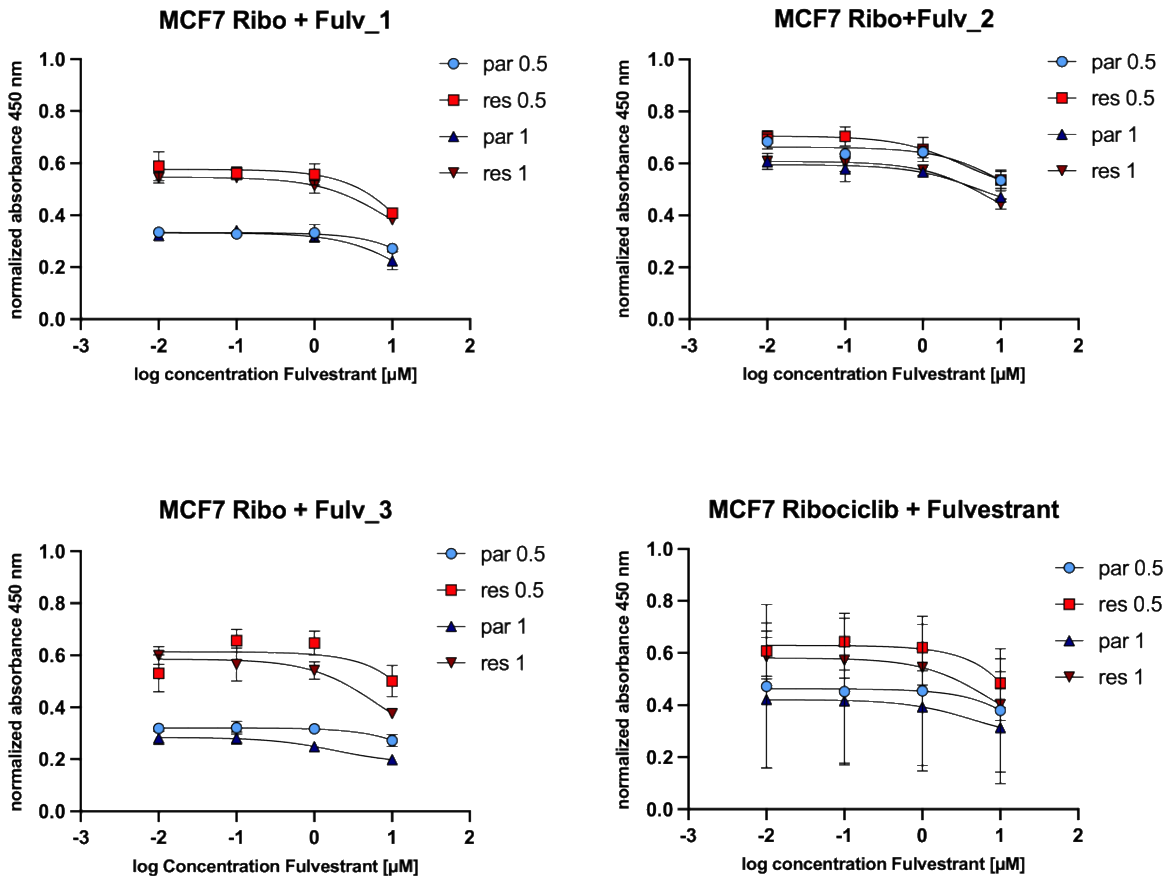

Figure 54: Impact of dual inhibition by fulvestrant and ribociclib on the viability of MCF7 cells. Three biologically independent experiments were performed. $3x10^3$ cells per well were seeded in a 96 well plate and treated with either 0.5 µM or 1 µM ribociclib and increasing fulvestrant concentrations (0.01 – 10 µM). The absorbance of the CCK-8 product was measured at 450 nm after 4 h of incubation. All experiments were assessed in technical triplicates and the results were normalized to the respective DMSO-treated controls. Error bars indicate ±SD.

The addition of fulvestrant had a stronger effect on the viability of MCF7 cells than on that of the CTC-ITB-01 cells, as the viable fraction of parental cells dropped to approximately 40 – 45% at a concentration of 0.01 µM fulvestrant (compared to ~60% at ribociclib only), independently of the ribociclib concentration. Ribociclib-resistant MCF7 cells were slightly less susceptible to the concordant treatment as their viability dropped to 55 – 60%, compared to ~80% of viability with sole ribociclib treatment, (Figure 13). Neither in the resistant nor in the parental MCF7 cells, increasing concentrations of fulvestrant correlated with a significant decrease of viability, as was already observed for the CTC-ITB-01 cell line, indicating again that higher concentrations of ribociclib would be beneficial to induce a stronger response, as increasing concentrations of fulvestrant had no additional effect on the viability.

However, the inhibitory effect of additional fulvestrant treatment on the clonogenic growth of CTC-ITB-01 cells was strong. Compared to the DMSO-treated control, the covered area dropped to 4% and 20% in parental and resistant CTC-ITB-01 cells respectively at 1 µM fulvestrant and to under 5% in both cell lines at a concentration of 10 µM fulvestrant. Likewise, the sensitivity of MCF7 cells in this assay was even higher than in the CCK-8 assay. The addition of fulvestrant,

already at a concentration of 0.01 µM, induced a complete growth inhibition of the parental MCF7 cells. Even the growth of resistant MCF7 cells was inhibited strongly, indicated by the drop of the normalized covered area to under 15% at concentrations of 0.01 µM fulvestrant and 1 µM ribociclib. Increasing the fulvestrant concentration to 10 µM resulted in a normalized covered area of less than 5% for both MCF7 sub-cell lines. Conclusively, this dual treatment was more effective in suppressing clonogenic growth than ribociclib alone. Interestingly, the susceptibility of CTC-ITB-01 and MCF7 cells to this dual inhibition on the clonogenic growth was similar (Figure 55).

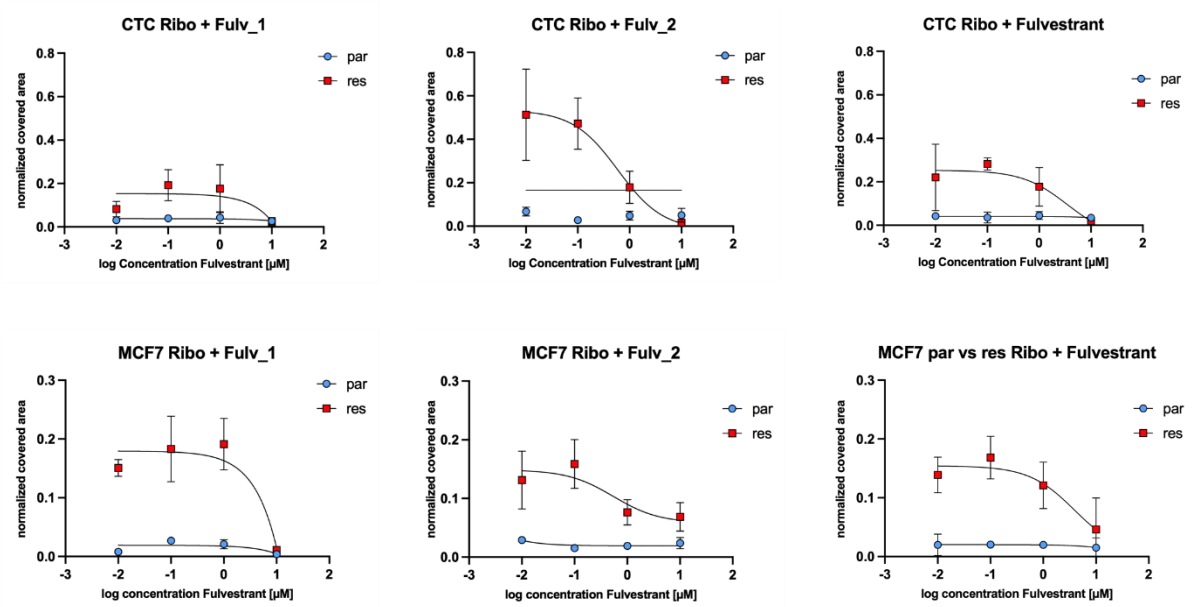

Figure 55: Inhibition of clonogenic growth of CTC-ITB-01 and MCF7 cells by combined treatment with ribociclib and fulvestrant. 500 CTC-ITB-01 cells and 250 MCF7 cells were seeded in triplicates in 6 well plates and treated with increasing concentrations between 0.01 µM - 10 µM of fulvestrant and 1 µM ribociclib. After 21 (CTC-ITB-01) or 8 days (MCF7), when colonies had formed, the cells were fixed, stained and the covered area was evaluated, and the results normalized to the respective DMSO-treated controls. Two independent biological replicates and their summary are shown. Error bars indicate ±SD.

To find out if the discrepancy between the impact of the dual treatment described above on viability and clonogenic growth can be explained by differences in triggering cellular senescence the β-galactosidase activity upon treatment with fulvestrant and ribociclib was evaluated (Figure 56).

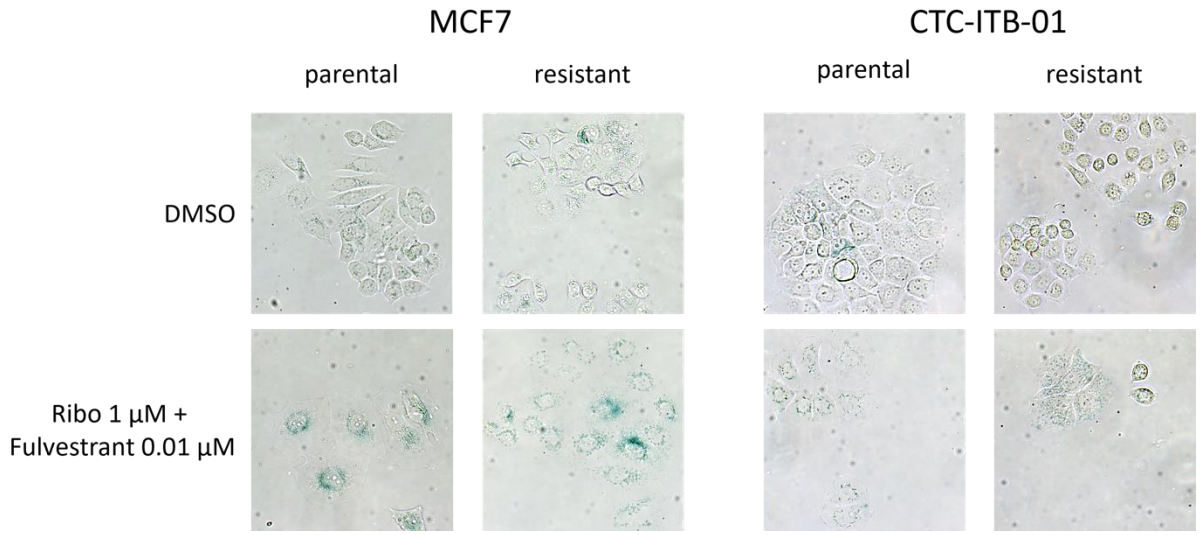

Figure 56: Senescence-induced β-Galactosidase activity in cells treated with ribociclib and fulvestrant. Cells were incubated with 1 µM ribociclib and 0.01 µM fulvestrant for 3 days. The staining was developed overnight in an incubator without CO_2-supply and assessed on a brightfield microscope at 20x magnification.

Indeed, in parental and resistant MCF7 cells treated with ribociclib and fulvestrant an increased intensity of the blue staining, compared to the DMSO treated cells, indicating increased β-galactosidase activity as surrogate for senescent cells, was observed. Comparison to Figure 15 reveals, that the induction of senescence was even stronger in cells treated with both drugs than in ribociclib-treated cells, particularly pronounced in the ribociclib-resistant MCF7 cells. This is in line with the stronger inhibition of clonogenic growth as evidenced by results of the colony formation assay compared to the reduction of cell viability, measured by the CCK-8 assay.

On the contrary, despite their change towards a more flattened and enlarged morphology, β-galactosidase activity was not increased in CTC-ITB-01 cells upon treatment.

3.8.2 Inhibition of PI3Kα by alpelisib in parental and ribociclib-resistant cells

It has been shown previously that the PI3K/mTOR pathway remains activated in CDK4/6i resistant HR-positive breast cancer cells [232]. Moreover, CDK4/6 inhibitors and PI3K inhibitors might inhibit growth of breast cancer cells resistant to endocrine therapy synergistically [233]. *PI3KCA* mutations are common in breast cancer and respective inhibitors are currently investigated as subsequent therapeutic options as described in 1.2.2 [234]. *PIK3CA* mutations, leading to an elevated activity of the p110α subunit of PI3K are a precondition for the clinical application of alpelisib, a PIK3Cα-specific inhibitor [235].

To assess whether ribociclib resistance can be overcome by targeting the PI3K/mTOR pathway, functional assays were performed, investigating the susceptibility of parental and resistant cell lines to PI3K inhibition using alpelisib. Importantly, the MCF7 cell line harbors a *PI3KCA* hotspot mutation (c.1633G>Ap. E545K), and the CTC-ITB-01 cell line is characterized by another hot spot mutation (c.3140A, p.H1047R) and additionally by a less common one (c.1252G>Ap. E418K), making both cell lines suitable models for the analysis of PIK3α inhibition by alpelisib.

The cytotoxicity of alpelisib treatment was assessed by performing CCK-8 assays. First, the impact of treatment with only alpelisib on the viability of parental and resistant cells was tested.

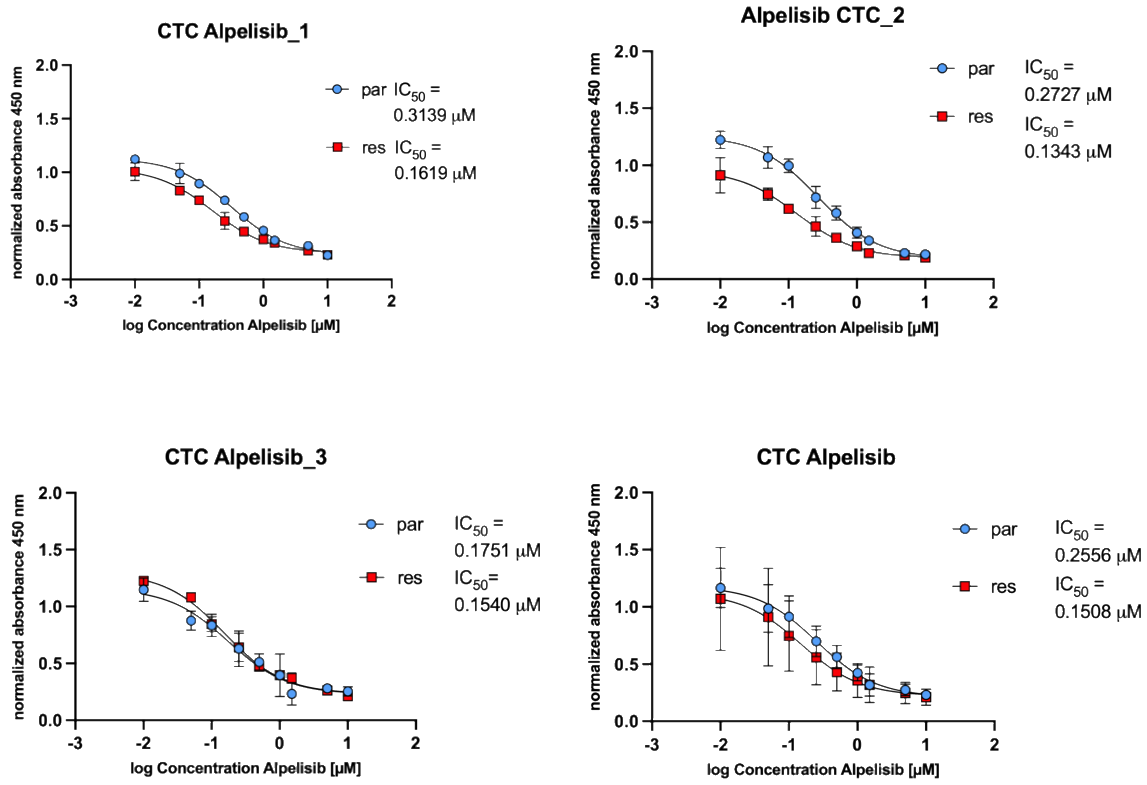

Figure 57: Analysis of the impact of PI3Kα inhibition by alpelisib on the viability of parental and resistant CTC-ITB-01 cells. Three biologically independent experiments were performed. $3x10^3$ cells per well were seeded in a 96 well plate and treated with increasing concentrations of alpelisib (0.01 – 10 µM) for 3 days. The absorbance of the CCK-8 product was measured at 450 nm after 4 h of incubation. All experiments were assessed in technical triplicates and the results normalized to the DMSO-treated control. The independent experiments and the summary are shown, error bars indicate ±SD.

Alpelisib led to a strong reduction of cell viability. At a concentration of 1 µM alpelisib, the viability dropped to 40% in both cell lines (Figure 57, summarized data). Importantly, established ribociclib resistance seemingly did not affect the efficacy of PI3Kα inhibition. There was even a tendency of resistant CTC-ITB-01 cells to be slightly more sensitive to the inhibition, indicated by the IC_{50} value of 0.15 µM compared to 0.26 µm, calculated for the parental CTC-ITB-01 cells.

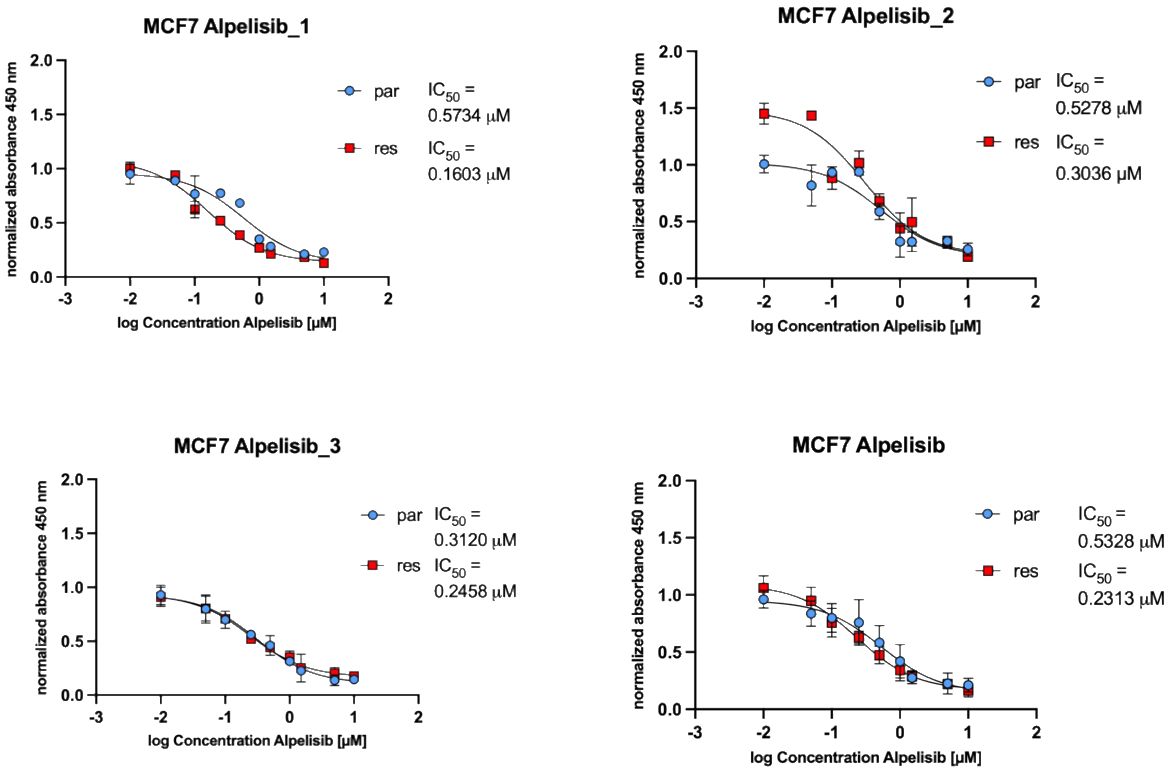

Figure 58: Analysis of the impact of PI3Kα inhibition by alpelisib on the viability of parental and resistant MCF7 cells. Three biologically independent experiments were performed. 1.5x10^3 cells per well were seeded in a 96 well plate and treated with increasing concentrations of alpelisib (0.01 – 10 µM) for 3 days. The absorbanceof the CCK-8 product was measured at 450 nm after 4 h of incubation. All experiments were assessed in technical triplicates and the results were normalized to the DMSO-treated control. The independent experiments and the summary are shown, error bars indicate ±SD.

The response of MCF7 cells to treatment with alpelisib was comparable to that of CTC-ITB-01 cells irrespective of being resistant to ribociclib or not.

Likewise, the viability of MCF7 cells was strongly reduced by 30 – 40% by PI3Kα inhibition at an alpelisib concentration of 1 µM (Figure 58). Again, the resistant MCF7 sub-cell line was slightly more sensitive towards the treatment than the parental one, also proven by the IC_{50} of 0.23 µM compared to the IC_{50} of 0.53 µM of the parental cell line. Strikingly, CTC-ITB-01 cells seem to be characterized by a slightly higher sensitivity than MCF7 cells to the treatment with alpelisib.

3.8.3 Impact of contemporaneous inhibition of CDK4/6 and PI3Kα on parental and resistant CTC-ITB-01 and MCF7 cells

Next, it was investigated whether dual inhibition of PI3Kα by alpelisib and CDK4/6 by ribociclib would have a synergistic or additive impact on the reduction of cell viability of parental and resistant CTC-ITB-01 and MCF7 cells. Again, the CCK-8 assay was utilized to test this hypothesis. The results are depicted in (Figure 59).

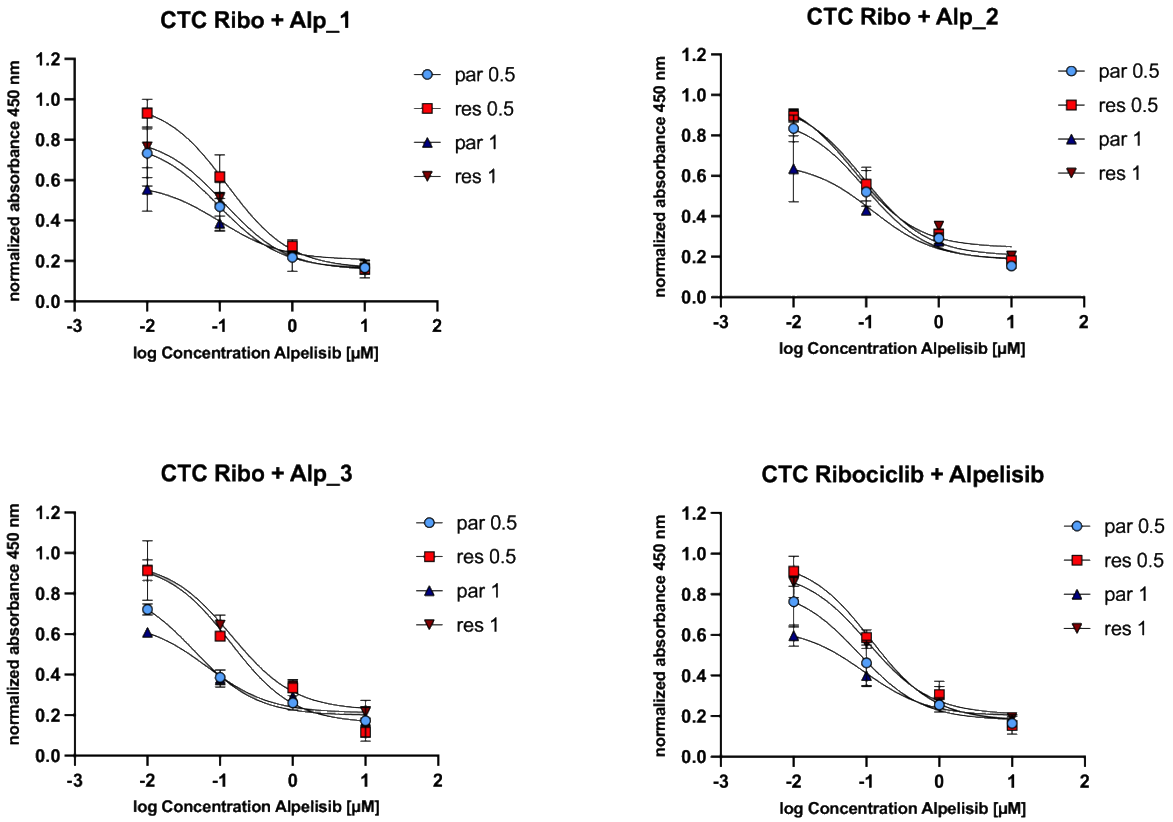

Figure 59: Impact of dual inhibition by alpelisib and ribociclib on the viability of CTC-ITB-01 cells. Three biologically independent experiments were performed. $3x10^3$ cells per well were seeded in a 96 well plate and treated with either 0.5 µM or 1 µM ribociclib and increasing alpelisib concentrations (0.01 – 10 µM) for 3 days. The absorbance of the CCK-8 product was measured at 450 nm after 4 h of incubation. All experiments were assessed in technical triplicates and the results were normalized to the respective DMSO-treated controls. Error bars indicate ±SD.

At lower alpelisib concentrations (0.01 – 0.1 µM), a less pronounced reduction of cell viability was observed in the resistant CTC-ITB-01 cells compared to parental cells. This difference, however, was abolished at higher concentrations of alpelisib. The impact of ribociclib treatment was measurable at low alpelisib concentrations of 0.01 – 0.1 µM, as parental CTC-ITB-01 cells treated with 1 µM ribociclib showed a lower absorbance (~60%) than those treated with 0.5 µM (~76%) at 0.01 µM alpelisib, indicating lower cell viability. The response of the resistant CTC-ITB-01 cells to alpelisib treatment was independent of the ribociclib concentrations used. Overall, the addition of ribociclib to the experiment only had a minor additional effect on the outcome. At a concentration of 1 µM mere alpelisib treatment, the viability had dropped to ~40% in parental and resistant CTC-ITB-01 cells (Figure 57). Addition of ribociclib led to decrease of the normalized absorbance to 25 – 30% independent of the concentrations of ribociclib used in these experiments. However, comparing these results to ribociclib treatment alone (Figure 12), dual inhibition was more effective and addition of alpelisib resulted in a synergistic effect.

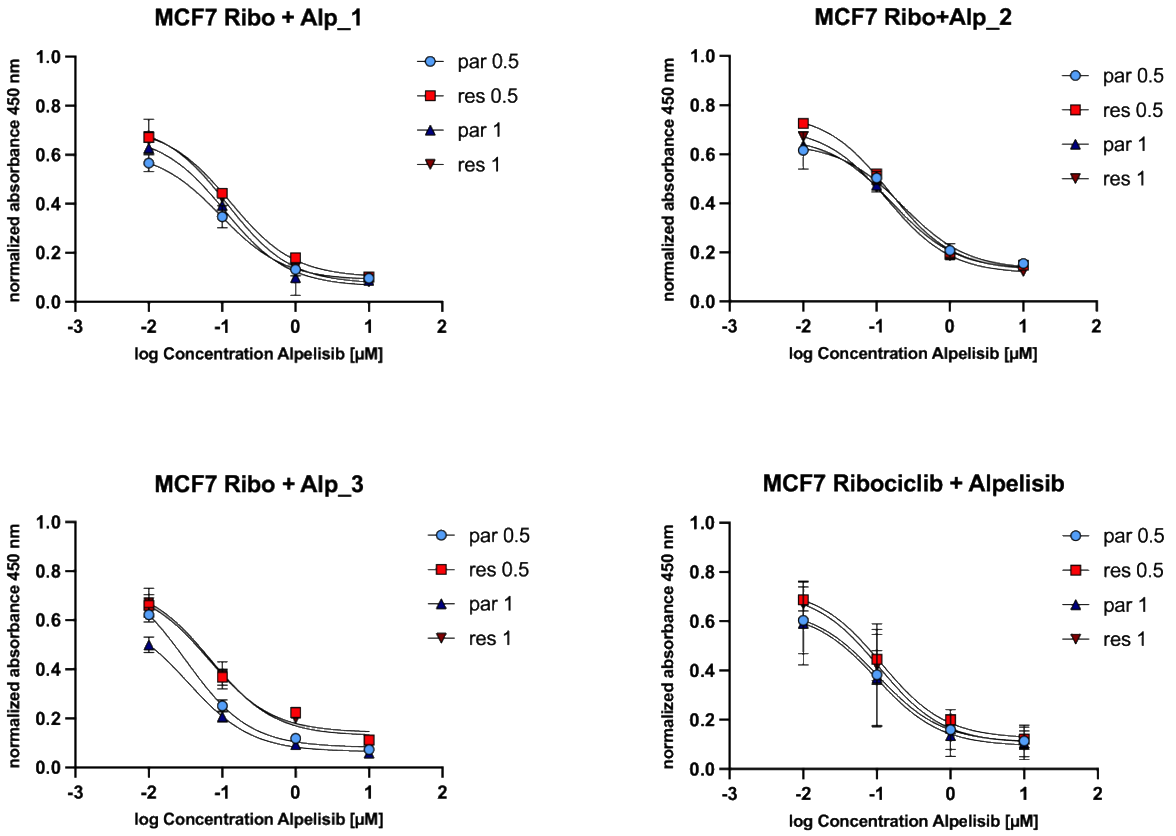

Figure 60: Impact of dual inhibition by alpelisib and ribociclib on the viability of MCF7 cells. Three biologically independent experiments were performed. $3x10^3$ cells per well were seeded in a 96 well plate and treated with either 0.5 µM or 1 µM ribociclib and increasing alpelisib concentrations (0.01 – 10 µM) for 3 days. The absorbance of the CCK-8 product was measured at 450 nm after 4h of incubation. All experiments were assessed in technical triplicates and the results were normalized to the DMSO control.

Parental and resistant MCF7 cells were similarly susceptible to the treatment with both inhibitors. Independent of the ribociclib concentration, the viability of MCF7 cells was reduced stronger upon treatment with both inhibitors than with alpelisib alone (Figure 58). At an alpelisib concentration of 1 µM, normalized absorbance decreased to less than 20% for parental and resistant MCF7 cells, independently of the ribociclib concentration, as compared to a normalized absorbance of around 30-40% when treated with alpelisib only. The concordant inhibition of PI3Kα and CDK4/6 to reduce cell viability was slightly more effective in the MCF7 than in the CTC-ITB-01 cells, but equally effective in parental and resistant sub-cells lines, irrespectively of the ribociclib concentration tested. Again, addition of alpelisib to ribociclib treatment resulted in a synergistic effect as indicated by the strongly reduced cell viability.

Furthermore, the efficacy of combined treatment of ribociclib with alpelisib to inhibit clonogenic growth was assessed (Figure 61).

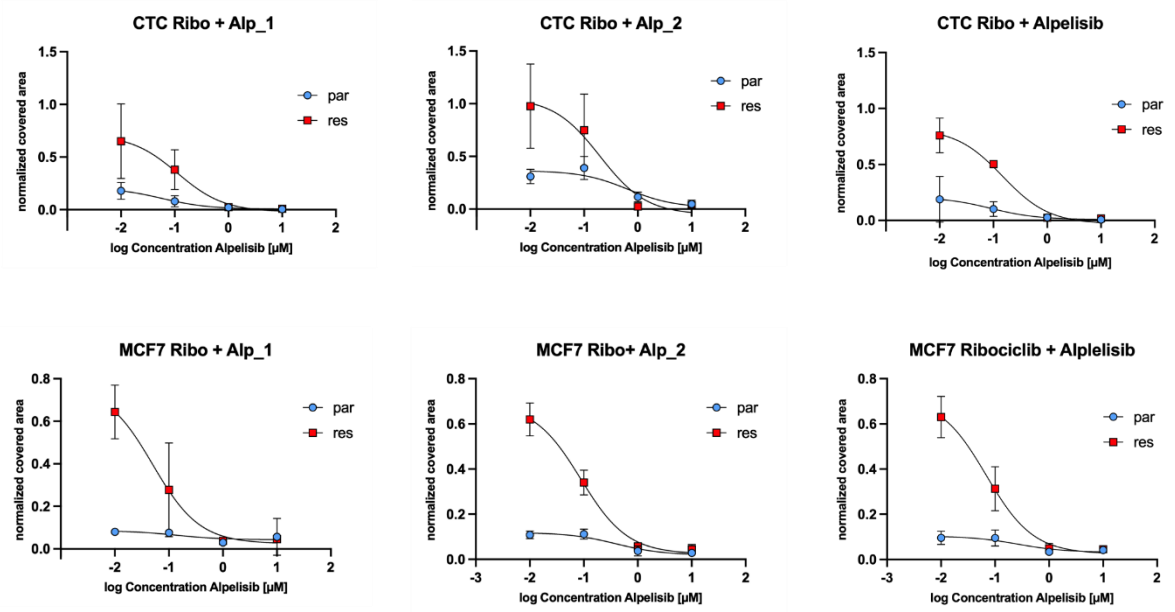

Figure 61: Inhibition of clonogenic growth of CTC-ITB-01 and MCF7 cells by combined treatment with ribociclib and alpelisib. 500 CTC-ITB-01 cells and 250 MCF7 cells were seeded in triplicates in 6 well plates and treated with increasing concentrations between 0.01 µM - 10 µM of alpelisib and 1 µM ribociclib. After 21 (CTC-ITB-01) and 8 days (MCF7), when colonies had formed, the cells were fixed, stained and the covered area was evaluated. Two independent biological replicates and their summary are shown. Error bars indicate ±SD.

Both resistant cell lines were less sensitive to low concentrations (0.01 – 0.1 µM) of alpelisib and simultaneous ribociclib treatment at a concentration of 1 µM compared to their parental counterparts. The normalized covered area of parental CTC-ITB-01 cells was reduced by 80% at a concentration of 0.01 µM alpelisib and was further decreased to <5% at a concentration of 10 µM of alpelisib. Similarly, the clonogenic growth of parental MCF7 cells was strongly reduced to <10% of the normalized covered area at 0.01 µM alpelisib and a concordant concentration of 1 µM ribociclib. On the contrary, while 1 µM alpelisib was sufficient to also reduce the normalized covered areas of the resistant cell lines to <10%, these cells were less sensitive to lower concentrations of alpelisib, with a reduction of the normalized covered area by 24% (CTC-ITB-01) to 40% (MCF7) at a concentration of 0.01 µM alpelisib. Interestingly, in comparison to the combination of ribociclib and fulvestrant, which was more effective in inhibiting the clonogenic growth than in reducing the viability of parental and resistant cells, alpelisib exerted a strong inhibition of clonogenic growth and cell viability. The reduction of clonogenic growth of the parental cell lines by dual treatment with ribociclib and fulvestrant was comparable to that with ribociclib and alpelisib. However, the addition of fulvestrant was superior to alpelisib regarding the inhibition of clonogenic growth of the resistant derivates at lower concentrations (0.01-0.1 µM). On the other hand, the addition of alpelisib exerted a stronger inhibitory impact on the cell viability of all cell lines than fulvestrant addition. In this context, alpelisib and ribociclib work synergistically.

To unravel potential differences in the mode of action of alpelisib compared to fulvestrant (chapter 3.8.1), the β-galactosidase activity was tested (Figure 62).

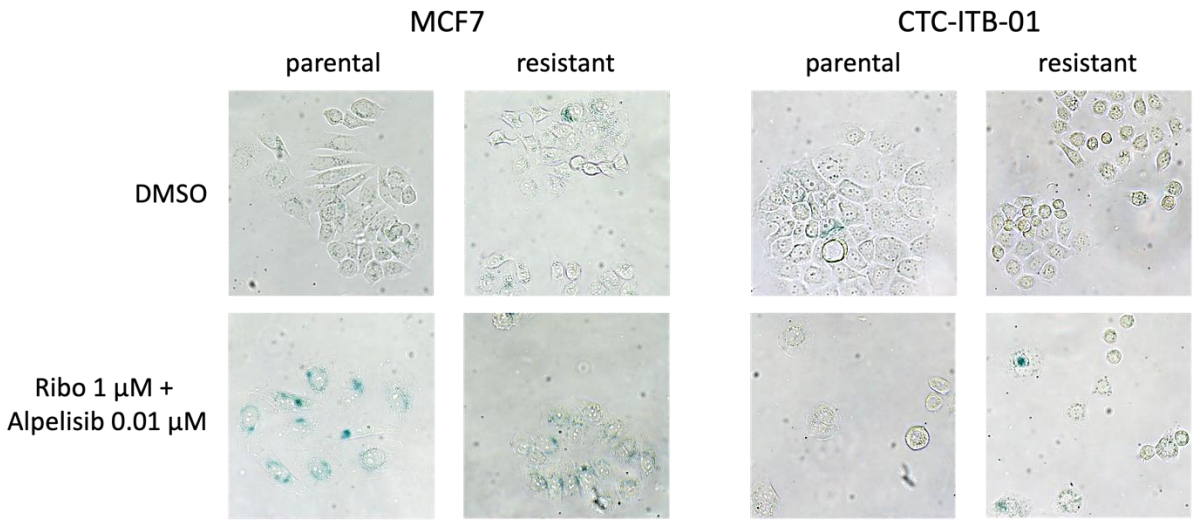

Figure 62: Senescence-induced β-Galactosidase activity in cells treated with ribociclib and alpelisib. Cells were incubated with 1 µM ribociclib and 0.01 µM alpelisib for 3 days. The staining was developed overnight in an incubator without CO_2-supply and assessed on a brightfield microscope at 20x magnification.

Treatment of MCF7 sub-cell lines with 1 µM ribociclib and 0.01 µM alpelisib resulted in increased blue staining, more pronounced in the parental cells but also visibly in the resistant ones, indicating increased β-galactosidase activity. In the CTC-ITB-01 cells, however, there was no increase in neither the number of stained cells nor the staining intensity. Differently from fulvestrant, which induced enlarged and flattened morphology, alpelisib led to an increased number of rounded, perhaps apoptotic cells of all treated cell lines. Higher cytotoxicity of alpelisib would be in line with the demonstrated higher reduction of cell viability by this drug shown by the results of the CCK-8 assay, compared to fulvestrant. Overall, no treatment tested in this study induced senescence in CTC-ITB-01 cells.

3.9 Identification of genes encoding potentially druggable targets by analysis of RNA-seq data

Apart from testing drugs already in clinical use to treat patients with HR+ mBC cancer such as fulvestrant or drugs that are under clinical investigation for the treatment of patients who developed CDK4/6i resistance, like alpelisib, the RNA-seq data were screened for more transcripts encoding potentially druggable targets. An important class of proteins that can be targeted, as they are regulating a plethora of biological processes, are kinases. They can be inhibited by small molecule inhibitors, such as the CDK4/6 inhibitors. Since 2001, when an inhibitor for the fusion product of the Abelson kinase (ABL) and the breakpoint cluster region protein (BCR), a oncogene commonly expressed by chronic myeloid leukemia was approved by the FDA, more than 70 new small molecule inhibitor targeting kinases were approved [236]. Hence, finding kinases that are higher expressed in ribociclib-resistant than in parental cells, could provide novel therapeutic options. Searching transcripts up-regulated in ribociclib-resistant versus parental MCF7 and CTC-ITB-01 cells for those encoding kinases was performed with the help of the Human Kinome-kinase.com database [237]. The Venn diagram in Figure 63 depicts genes encoding kinase with increased expression in resistant CTC-ITB-01 and MCF7 cells compared to their parental counterparts.

Different groups of kinases (protein kinases, lipid kinases, carbohydrate kinases and others) are represented.

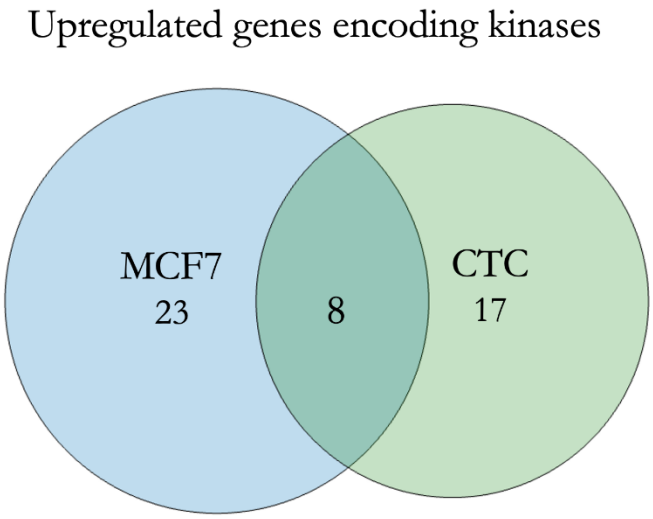

Figure 63: Venn diagram visualizing genes encoding kinases with increased expression in resistant CTC-ITB-01 and MCF7 cells. Venn diagrams are quantitative as the size of a circle is relative to the number of DEGs it represents.

At least 23 kinase-encoding genes were only upregulated in resistant MCF7 cells compared to parental ones, whereas the expression of 17 kinase encoding genes was exclusively increased in resistant versus parental CTC-ITB-01 cells. The expression of *BMPR1B*, *PIK3C2G*, *DCLK1*, *LRRK2*, *LYN*, *NIM1K*, *GASK1B* and *BRSK1* was increased in both resistant cell lines. Notably, two out of these eight kinases, are associated with EMT. Apart from LYN, mentioned earlier in this study, also DCLK1 was linked to EMT, as it reportedly induces EMT by stimulating the WNT/β-catenin pathway [238]. An overview of all upregulated genes encoding kinases is provided in Supplementary Table S 10 and Supplementary Table S 11.

3.10 Analysis of transcription factors with increased activity in resistant CTC-ITB-01 and MCF7 cells

Furthermore, transcription factors could be targeted therapeutically, albeit not as easily as inhibiting kinase activity [239]. This becomes evident in the low number of TFs that are potentially druggable. A pan-cancer analysis, identifying potentially druggable genes (PDGs) in the human genome found that only 40 out of 1396 TFs (0.7%) are druggable [240]. One prominent example of TF-targeted therapy are SERDs and SERMs for the treatment of patients with breast cancer. Both drugs reduce the transcription of ER target genes. Another approach is to degrade TFs with proteolysis targeting chimeara (PROTACs). This describes a molecule with dual function, as it covalently binds to target protein and drives its ubiquitylation with the attached E3 ligase, thereby promoting proteasome-mediated degradation of the target protein. An ER-targeting PROTEAC drug is under current investigation in a clinical phase I study [241]. Alternatively, new drugs should be designed that e.g. directly interfere with protein–DNA interactions of transcription factors contributing to cancer progression [239].

To predict, which key transcription factors were potentially involved in the development of ribociclib resistance, independently of altered expression of the transcription factors themselves, normalized enrichment scores (NES) for the activity of transcription factors were calculated. This analysis took the changes of mRNA levels of transcriptional downstream targets identified by RNA-seq into account and was based on the Discriminant Regulon Expression Analysis (DoRothEA), a gene set resource containing information about transcription factors and their interactions. with transcriptional targets, referred to as regulons [242]. As shown in Figure 64 and Figure 66, several regulons controlled by the indicated transcription factors were predicted to be altered according to this bioinformatic analysis.

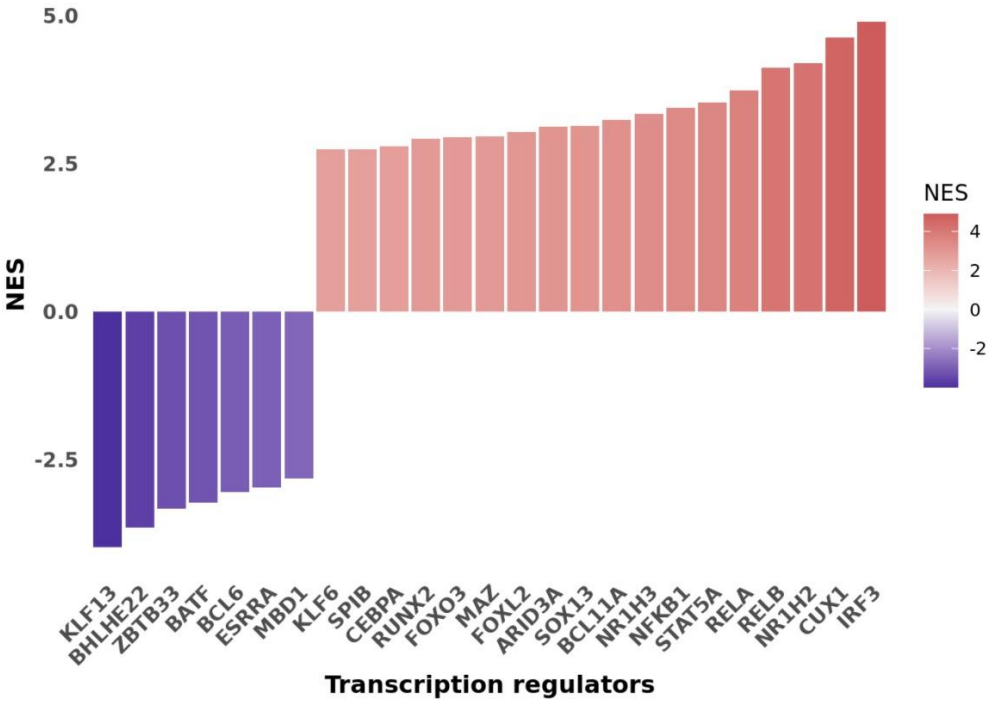

Figure 64: Results of NES calculation of the activity of transcription factors in resistant CTC-ITB-01 cells using DoRothEA. Here the 25 most enriched transcription factors significantly associated with regulons are represented. If enrichment was higher in the resistant or parental cells, positive or negative scores are indicated, respectively. (The figure weas created by Dr. Malik Alawi).

Using the Harmonizome database comprising data about functional associations between genes/proteins and their attributes [243] interactions of biological processes involved in the development of ribociclib resistance could be postulated and data-driven hypotheses be made.

Strikingly, multiple TFs whose expression was not significantly deregulated in resistant CTC-ITB-01 cells were predicted to be activated. Some of these, such as RUNX2 and FOXO3, were also described as EMT transcription factors [171], further supporting the hypothesis of EMT induction in resistant CTC-ITB-01 cells. Among genes co-occuring with the biological term RUNX2 in literature-supported statements describing functions of genes from the GeneRIF Biological Term Annotations datasets are some of those upregulated in ribociclib-resistant CTC-ITB-01 cells according to RNA-seq such as *AR*, *CDKN1A*, *DCLK1*, *miR-146a*, or *SOX9*.

Furthermore, NFκB seemed to be highly activated in resistant CTC-ITB-01 cells, since three proteins of this family (NFκB1, RELA, RELB) were calculated to be more active than in the parental CTC-ITB-01 cells. In breast cancer, NFκB was shown to induce the transcription of *CCND1* and overexpression of *RelA*. Moreover, increased transcriptional activity of NFκB correlated with reduced sensitivity of MCF7 cells to tamoxifen treatment [244]. Several of the genes whose transcription is regulated by NFκB, were also differentially expressed in resistant versus parental CTC-ITB-01 cells, as depicted in Figure 65.

Figure 65: DEGs found in resistant versus parental CTC-ITB-01 cells the expression of which is regulated by NFκB according to DoRothEA. (The figure weas created by Dr. Malik Alawi).

As shown in Figure 65, several genes that were in the focus of this study as they were deemed of potential importance in the context of CDK4/6i resistance are among the genes the transcription of which is regulated by NFκB, such as *AR*, *ICAM1*, *BCL2*, *FN1* and *VIM*. This further supports the hypothesis that the transcriptional activity of NFκB could be essential for promoting ribociclib resistance in the CTC-ITB-01 cells.

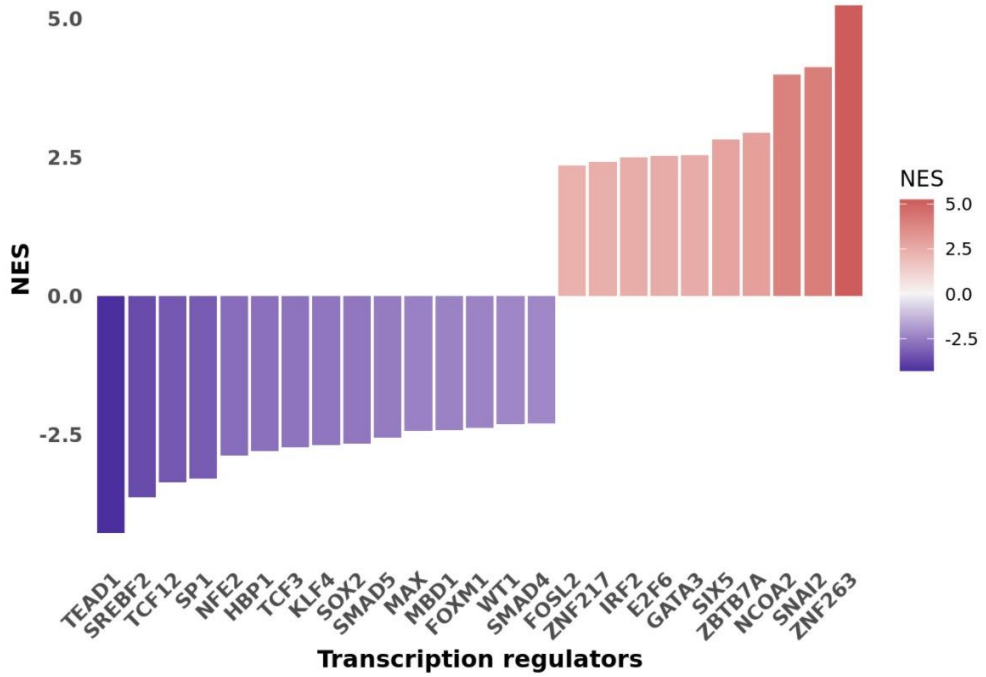

Figure 66: Results of NES calculation of the activity of transcription factors in resistant MCF7 cells using DoRothEA. Here the 25 most enriched transcription factors significantly associated with regulons are represented. If enrichment was higher in the resistant or parental cells, positive or negative scores are indicated, respectively. (The figure weas created by Dr. Malik Alawi).

Likewise, also in MCF7 cells transcription factors were identified to be more active in resistant versus parental cells, whose expression was not necessarily altered in these cells (Figure 66). Interestingly, the EMT-master transcription factor Slug (*SNAI2*) [171], was calculated to be more active in resistant than parental MCF7 cells, which is in line with the analysis of DEGs, further promoting the hypothesis of EMT induction in the resistant MCF7 cells. Surprisingly, despite increased expression of *SOX2* in resistant versus parental MCF7 cells, its transcriptional activity seemed to be lower than in parental MCF7 cells.

Searching the above mentioned Harmonize database, already functional interactions between Slug and the cancer-stemness marker CD44, the expression of which was increased in resistant MCF7 cells, have been described. Yet, using the DoRothEA database, SNAI2 was predicted to up-regulate the transcription of only three genes with differential expression in resistant versus parental MCF7 cells (*VDR*, *JAG1*, *CXCR4*) as shown in Figure 67.

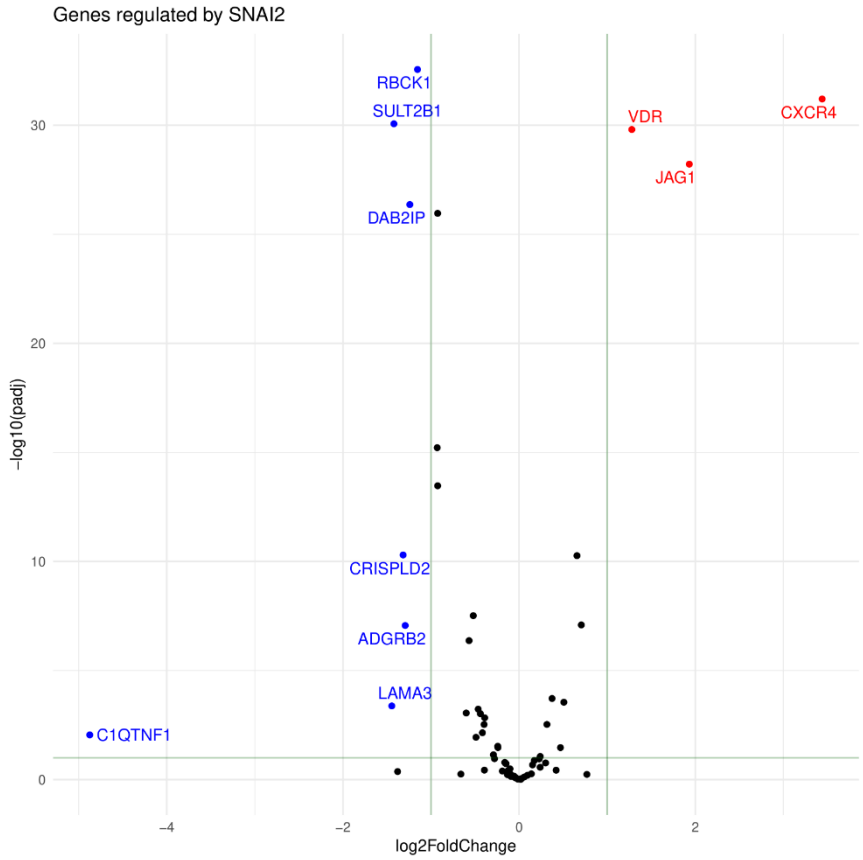

Figure 67: DEGs found in resistant versus parental MCF7 cells the expression of which is regulated by SNAI2 according to DoRothEA. (The figure weas created by Dr. Malik Alawi).

3.11 Testing the detection of potential markers of ribociclib resistance on resistant versus parental CTC-ITB-01 and MCF7 cells

Technically important for the utility as a potential liquid biopsy biomarker expressed by CTCs is the feasibility of fluorescent staining and detection during CellSearch® enrichment and unambiguously discrimination of positive and negative cells. Therefore, CDK6, SOX9 and CDK14 immunofluorescence staining were first tested on cell culture cells to assess the quality of the staining itself and the possibility to discriminate between the differential protein levels in parental and resistant cells. In this study, CDK6 and SOX9 were significantly upregulated in ribociclib-resistant MCF7 cells and CDK14 in resistant CTC-ITB-01 cells. The changes of expression could be validated by qPCR on the mRNA level and transferred to the protein level. All three proteins positively regulate cell cycle progression, making them promising candidates as drivers of ribociclib resistance, as it has already been demonstrated for CDK6 [132]. Exemplary pictures of the IF staining are shown in Figure 69, Figure 70 and Figure 71.

First, mRNA ISH was used to confirm the significant increase of *CDK6* transcripts in the resistant MCF7 cells, demonstrated by RNA-seq and qPCR analysis. Furthermore, the feasibility of *CDK6* mRNA detection as a biomarker for ribociclib resistance at single cell level was evaluated. (Figure 68).

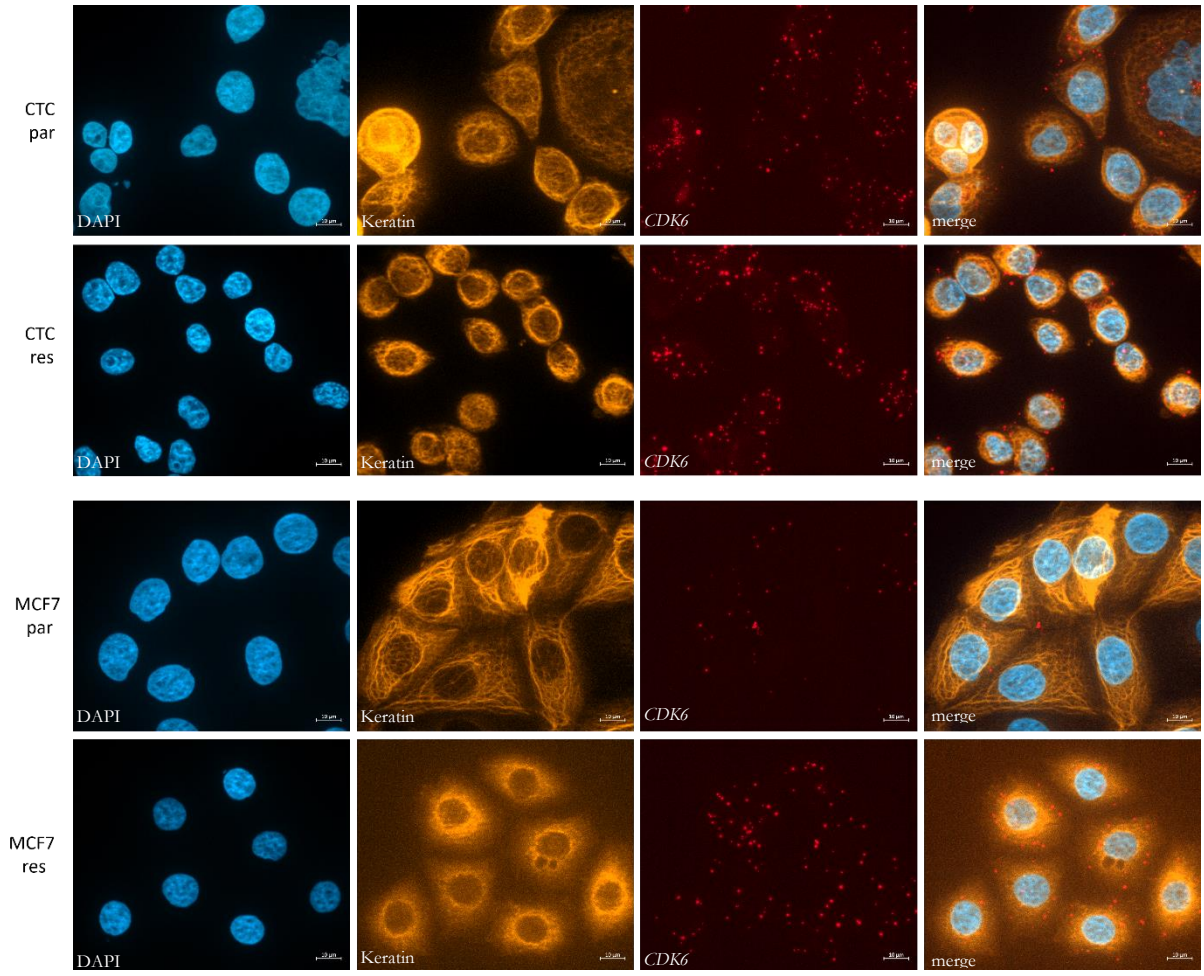

Figure 68: *CDK6* mRNA levels detected by mRNA ISH in parental and resistant CTC-ITB-01 and MCF7 cultivated on chamber slides. All cells were cultivated on chamber slide for 3 days. Pan-keratin was stained using an antibody cocktail (clone AE1/AE3, PE, 1:150 dilution) whereas *CDK6* was detected using a AF647-labeled specific probe. Nuclei were counterstained with DAPI**.** Pictures were taken at 63x magnification with oil and z-stacks were acquired using the ApoTome 2.0. Scale bars represent 10 µM.

Figure 68 demonstrates increased levels of *CDK6* transcripts in resistant compared to parental MCF7 cells. Moreover, mRNA ISH visualizes the intrinsically higher *CDK6* levels of the CTC-ITB-01 cells compared to MCF7 cells, confirming results from RNA-seq and qPCR data. Since Western blot analysis showed that these differences also translate into altered protein levels (Figure 17) and due to these differences of mRNA levels, detected by mRNA ISH, this assay may represent an alternative to IF staining for the analysis of *CDK6* levels on non-fixed cells.

Subsequently, detection of CDK6 protein levels by IF staining was tested.

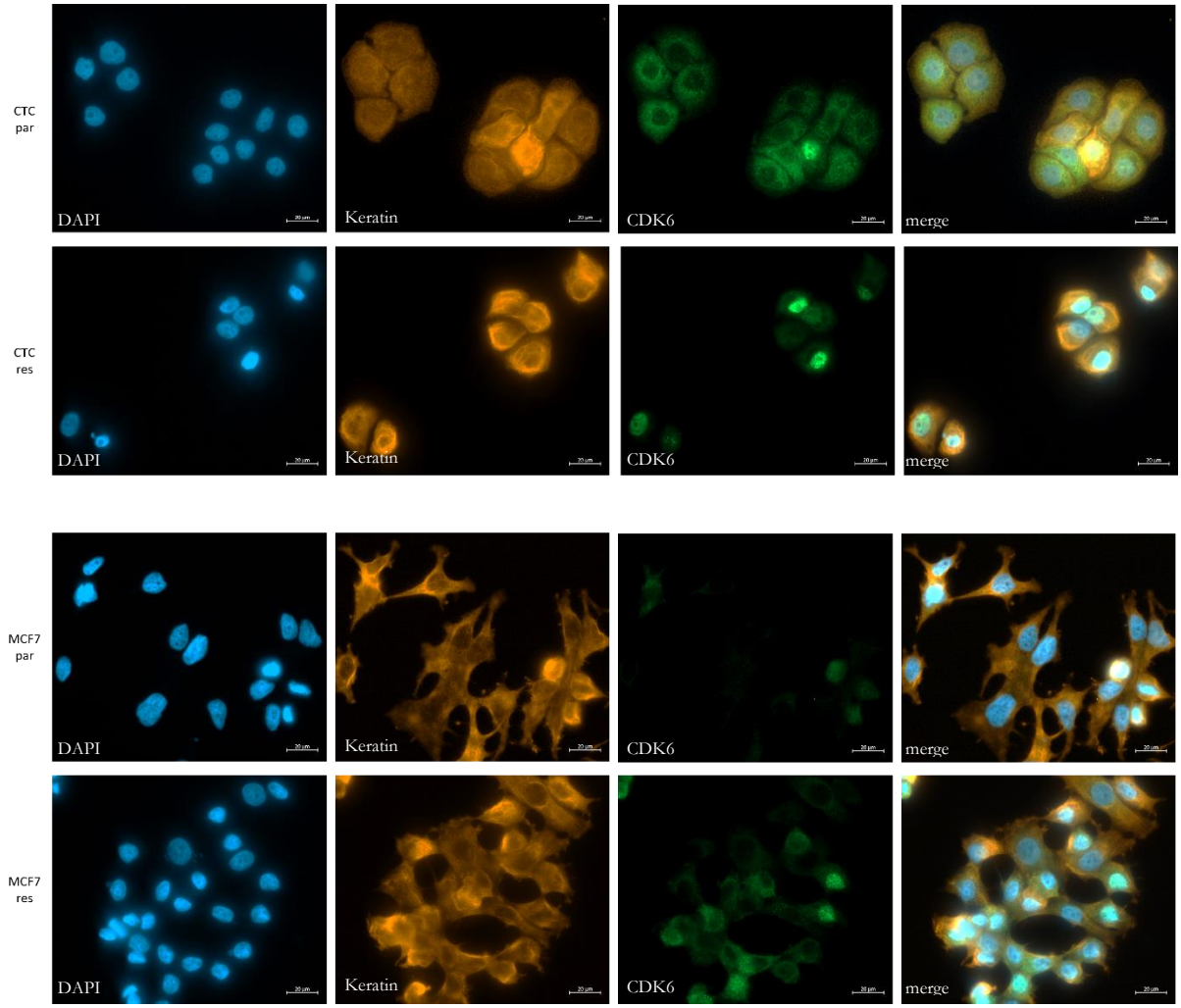

Figure 69: Immunofluorescent staining to detect CDK6 in parental and resistant CTC-ITB-01 and MCF7 cells cultured on chamber slides. CDK6 was detected using a monoclonal antibody (clone D4S8S, 1:50 dilution). Keratin was detected using a pan-keratin antibody cocktail (clone AE1/AE3, 1:100 dilution and C11, 1:200 dilution). Nuclei were counterstained with DAPI. All images were acquired at a Zeiss-Axio Observer, at 40x magnification. Scale bars represent 20 µM.

Figure 69 demonstrates that the results of RNA-seq, qPCR analysis, Western blot analysis, and mRNA ISH could also be confirmed by IF staining. The increase of nuclear CDK6 protein is visualized for the resistant compared to parental MCF7 cells. In general, a higher intensity of CDK6 immunofluorescence was observed in CTC-ITB-01 cells than in MCF7 cells. Additionally, perinuclear CDK6 immunostaining could be observed in parental CTC-ITB-01 and in ribociclib-resistant MCF7 cells. Whether there is any association between the localization of this protein and its activity remains to be investigated.

Moreover, parental and resistant MCF7 were spiked into healthy donor blood and enriched by CellSearch® to test, whether implementation of the staining into the enrichment by the system and detecting differences of CDK6 level between parental and resistant cells is feasible. However, preliminary tests failed. Therefore, CDK6 detection was not tested on patient samples yet.

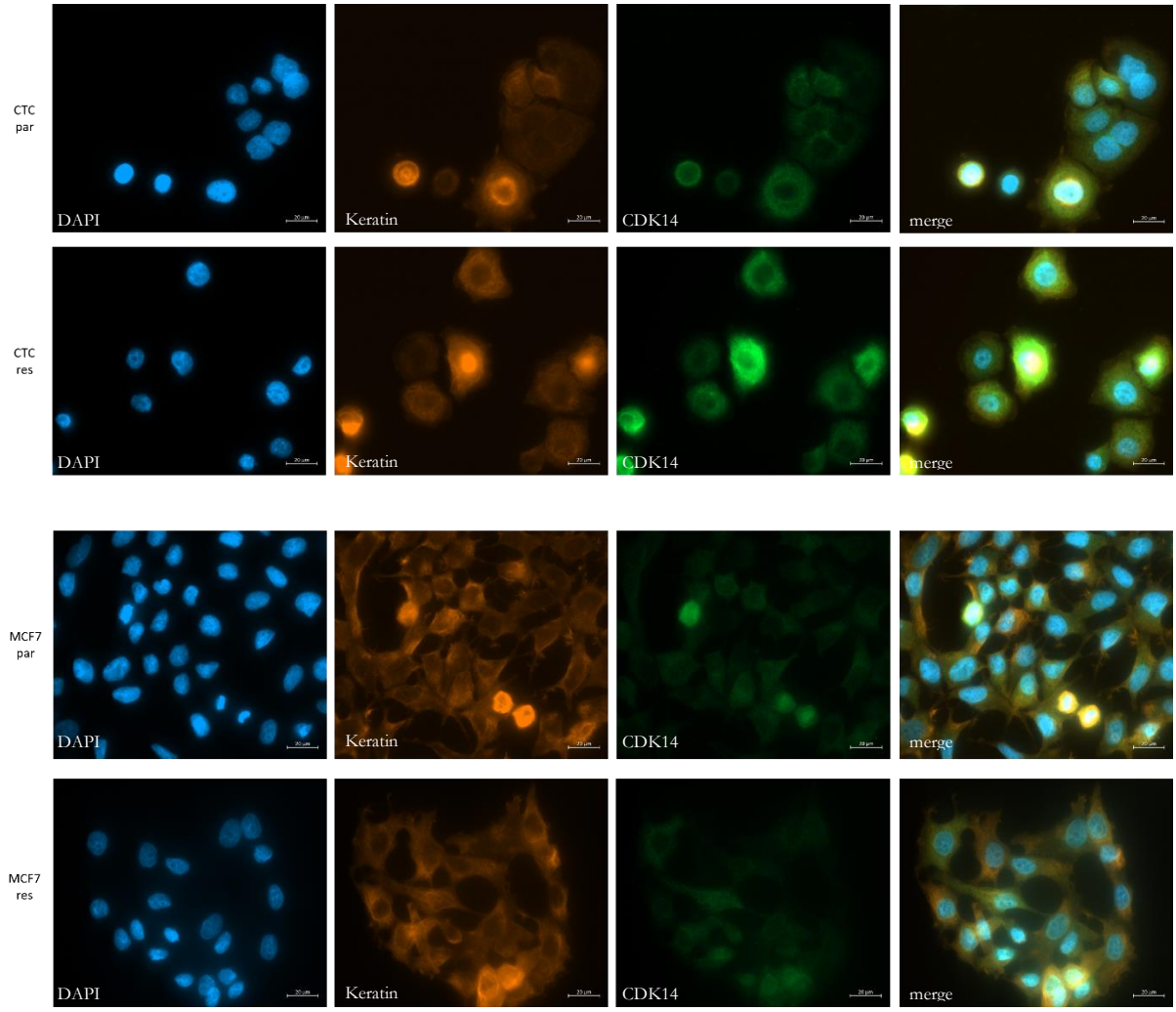

Figure 70: Immunofluorescent staining to detect CDK14 in parental and resistant CTC-ITB-01 and MCF7 cells cultivated on chamber slide. CDK14 was detected using a monoclonal antibody (clone sc-376366, 1:50 dilution). Keratin was detected using a pan-keratin antibody cocktail (clone AE1/AE3, 1:100 dilution and C11, 1:200 dilution). Nuclei were counterstained with DAPI. All images were acquired at a Zeiss-Axio Observer, at 40x magnification. Scale bars represent 20 µM.

As indicated by previous experiments (Figure 29), the expression of CDK14 was low in MCF7 cells, and not altered in resistant MCF7 cells, whereas in comparison, both CTC-ITB-01 derivates expressed this kinase at a higher level (Figure 70). In the resistant but not the parental CTC-ITB-01 cell line cells, cells with a very strong CDK14 immunofluorescent staining were found. This staining did not show a nuclear localization of CDK14 but rather a cytoplasmic and perinuclear one. In all cell lines, the highest CDK14 staining intensity was observed in cells with the strongest keratin staining.

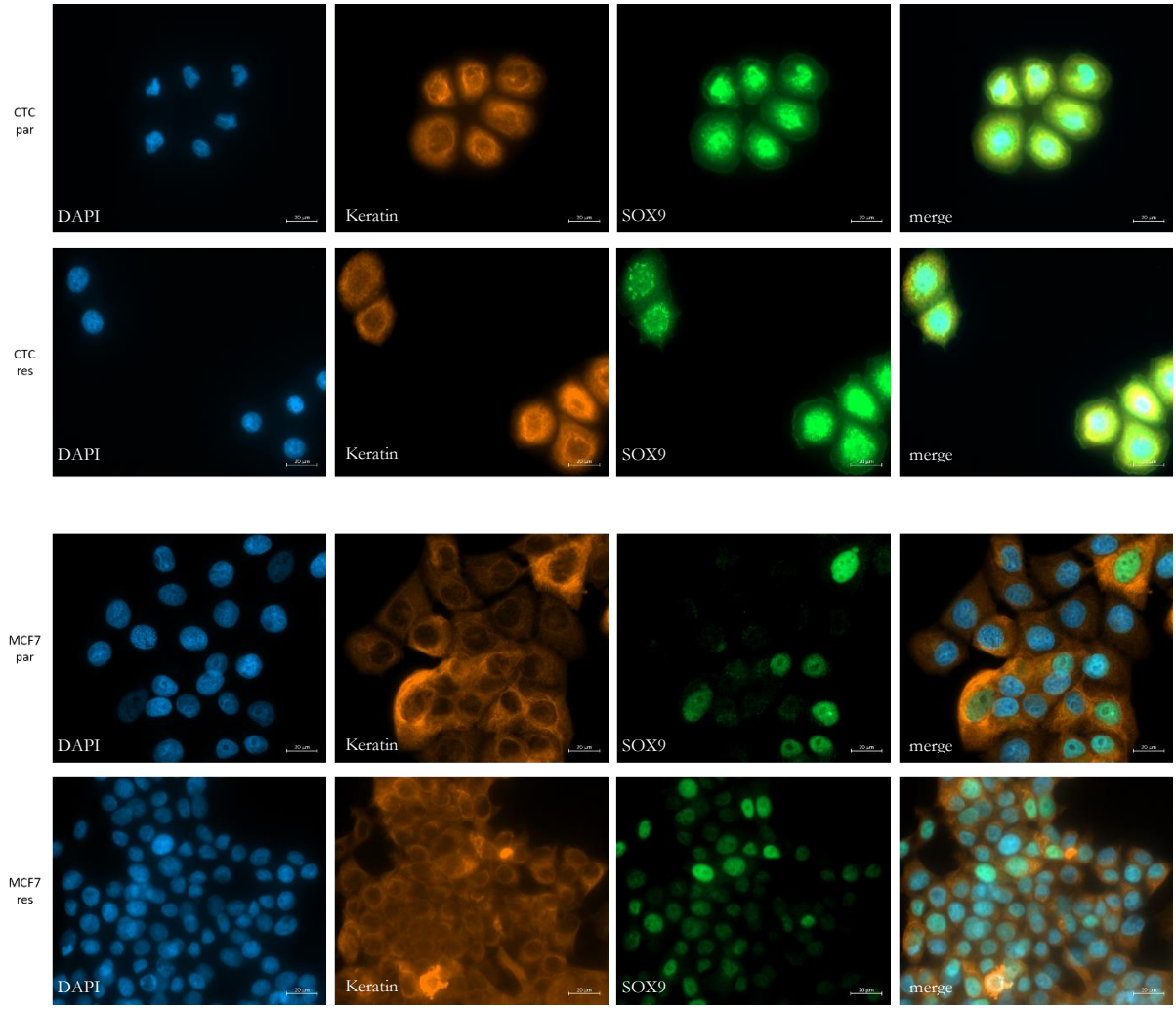

Figure 71: Immunofluorescent staining to detect SOX9 in parental and resistant CTC-ITB-01 and MCF7 cells cultivated on chamber slide. SOX9 was detected using a polyclonal antibody in a 1:100 dilution. Keratin was detected using a pan-keratin antibody cocktail (clone AE1/AE3, 1:100 dilution and clone C11, 1:200 dilution). Nuclei were counterstained with DAPI. All images were acquired at a Zeiss-Axio Observer, at 40x magnification. Scale bars represent 20 µM.

In concordance with the results obtained by RNA-seq, qPCR and Western blot analysis, also the intensity of the IF staining of SOX9 was markedly higher in CTC-ITB-01 cells than in MCF7 cells (Figure 71). However, the increase of SOX9 expression in resistant versus parental CTC-ITB-01 cells, demonstrated on mRNA level (1.8-fold by RNA-seq and 1.9-fold by qPCR) and was also implied by Western blot analysis, could not be visualized by IF staining. In contrast, comparison of SOX9 expression in resistant versus parental MCF7 cells confirmed the significant increase of *SOX9* mRNA level detected by RNA-seq. The intensity of the SOX9 IF staining did not change, but only a low number of parental MCF7 cells was SOX9-positve whereas a higher number of resistant MCF7 cells were positive for SOX9. In all cell lines, nuclear localization of the protein SOX9 IF was observed (Figure 71).

Thus, in addition to testing the quality of immunofluorescent staining of these three potential markers of ribociclib resistance, their protein level was detected on a panel of breast cancer cell lines by Western Blot analysis. MCF7, ZR-75-1 and T47D cells represent the luminal A, MDA 361, BT474 and the CTC-ITB-01 luminal B BC subtypes, SKBR3 is a HER2+ BC cell line and MDA-

MB-231 and MDA-MB-468 are both categorized as TNBC cell lines [245]. An overview of this analysis is provided in Figure 72.

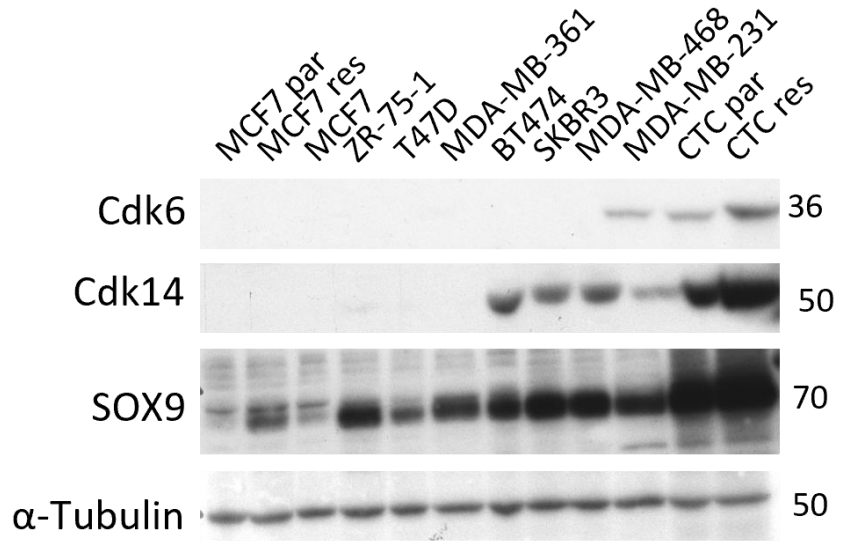

Figure 72: Western blot analysis of the expression of CDK6, CDK14 and SOX9 in a panel of selected BC cell lines. All antibodies were diluted as described in the materials and methods sections.

Indeed, Figure 72 depicts huge variance for the expression of CDK6 and CDK14. CDK6 was only detectable in the resistant CTC-ITB-01 cell line, chosen as positive control for all three proteins, and the TNBC cell line MDA-MB-231. The highest levels of CDK14 were also observed in resistant CTC-ITB-01 cells. No CDK14-specific bands were detected in MCF7, T47D, ZR-75-1 and MDA-MB-361 cells. SOX9 was most strongly expressed in the CTC-ITB-01 cells but also in several other cell lines. Lowest SOX9 expression was detected in parental MCF7 cells.

Overall, no correlation between the amount of CDK6, CDK14 and SOX9 protein and the molecular subtype of the breast cancer cell lines was determined. Even between luminal breast cancer cell lines representing the breast cancer subtype that is commonly treated by CDK4/6 inhibitors, differences in the expression of these proteins were observed.

3.12 Analysis of potential biomarkers associated with ribociclib resistance in CTCs using the CellSearch® system

The CellSearch® system is the only standardized approach to detect and characterize CTCs from carcinoma patients. Although enrichment and detection are based on epithelial features of CTCs, the fourth channel of this system offers the possibility to introduce an additional fluorescently-labeled antibody to further characterize the CTCs also for mesenchymal-like properties. In the present study, a plethora of candidate biomarkers with potential relevance to indicate resistance to CDK4/6 inhibitors were identified. However, for application in the CellSearch® system, suitable antibodies, fluorescence dyes and appropriate concentrations and exposition time have to be tested before clinical application is feasible.

Unfortunately, a FITC-labeled anti-CDK6 antibody chosen for CellSearch® testing was not sensitive enough to demonstrate and confirm the differences of CDK6 protein levels, shown by Western blot analysis and IF staining.

Furthermore, a FITC-labeled anti-SOX9 antibody was chosen for CellSearch® application. For MCF7 as well as CTC-ITB-01 cells nuclear staining of this transcription factor was observed in IF staining, but the strong differences between the cell lines as well as parental versus ribociclib-resistant cells expected from Western blot experiments and immunofluorescence staining could not be convincingly demonstrated (Figure 73).

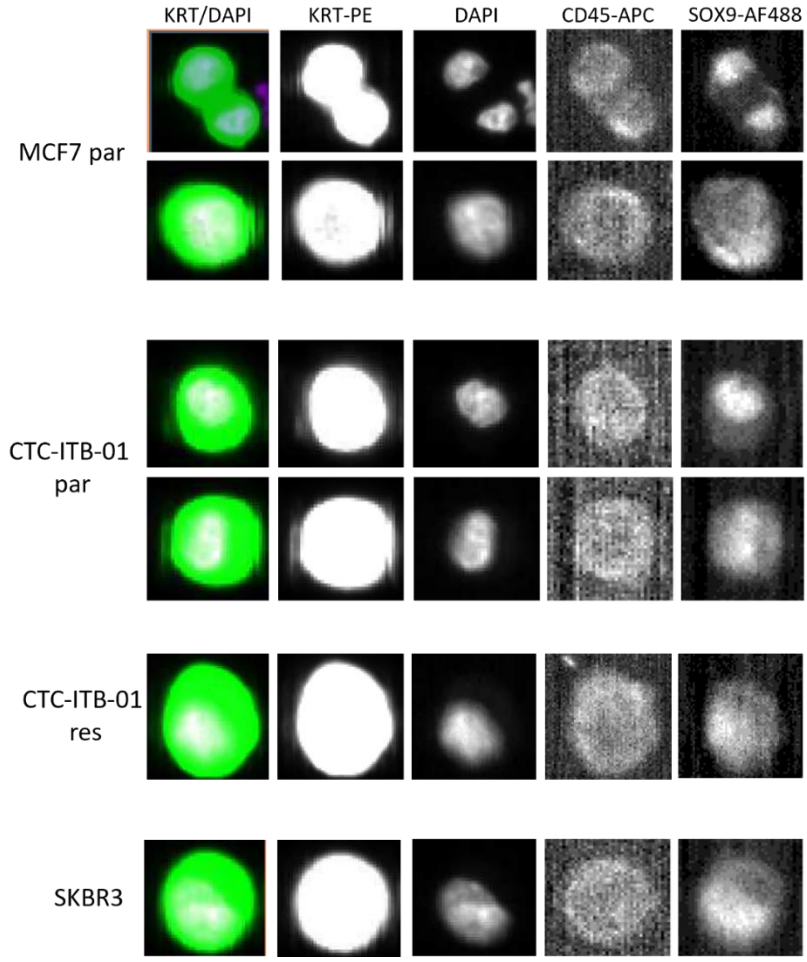

Figure 73: Representative pictures of SOX9 expression on MCF7 cells, CTC-ITB-01 and SKBR3 spiked into blood of healthy donors and enriched by CellSearch®. Cancer cells were identified by DAPI- and keratin positivity and lack of CD45 expression. SOX9 was detected using the AF488 labeled polyclonal antibody a 1:50 dilution (final concentration 2.5 µg/ml). The exposure time was 0.8 seconds. For comparison purposes, $SOX9^{high}$ CTC, $SOX9^{high}$ SKBR3 and $SOX9^{low}$ MCF7 are depicted.

The results of this thesis support the assumption that resistance to CDK4/6 inhibitors is associated with changes that can be attributed to EMT [67], including increased *VIM* expression in resistant versus parental CTC-ITB-01 cells as shown by RNA-seq and qPCR [246,247]. So far, there is a lack of studies in breast cancer patients to detect epithelial-mesenchymal hybrid cells, supposed to be associated with high aggressiveness of breast cancer [248].

Therefore, it was investigated whether vimentin is expressed in CTCs detected during treatment of mBC patients. To this end, vimentin-specific immunofluorescence was analyzed in the fourth channel of the CellSearch® system. Detection of vimentin expression by CellSearch® was already described [2] and reliability for breast cancer was tested by spiking different breast cancer cell lines with known vimentin status into blood from healthy donors. As expected, strong vimentin expression could be demonstrated for MDA-MB-231 cells, whereas MCF7 cells did not show any vimentin-specific immunofluorescence (Figure 74).

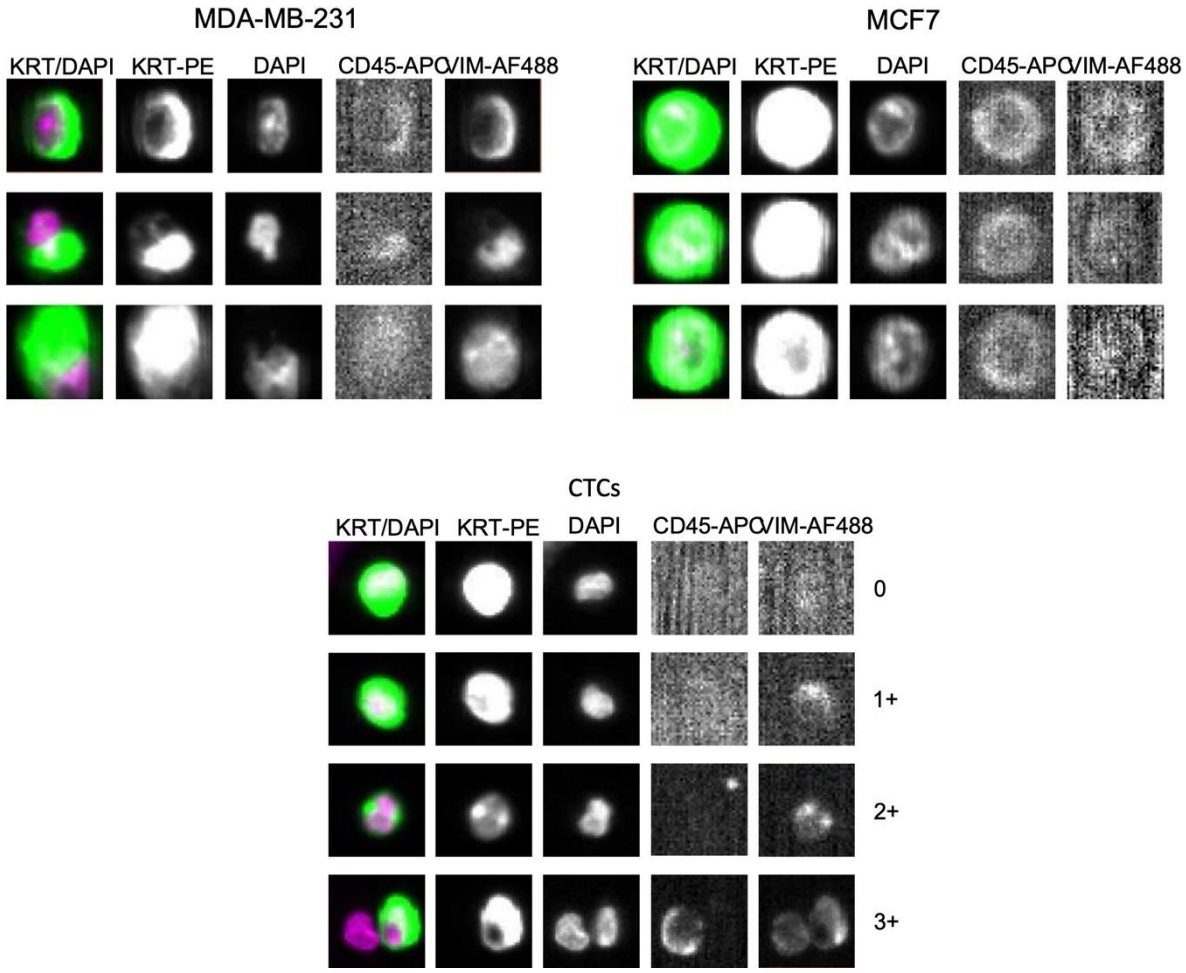

Figure 74: Exemplary pictures of vimentin expression on MDA231 cells, MCF7 cells and CTCs of HR+ mBC sample enriched by CellSearch®. CTCs were identified by DAPI- and keratin positivity and lack of CD45 expression. Vimentin was detected using the AF488 labeled clone V9 in a 1:50 dilution. The exposure time was 0.8 seconds. For comparison purposes, the vimentin-high MDA-MB-231 cells and vimentin -low MCF7 cells are depicted.

Next, this approach was applied to a heterogeneous cohort of 201 mBC patients and vimentin expression of CTCs was determined. Vimentin-positive CTCs (Figure 74) were found in blood samples from 67 patients (33.3%), while 134 patients (66.7%) had only VIM-negative CTCs. The percentage of VIM-positive CTCs was higher in blood samples with higher CTC counts (≥5 versus <5 CTCs/7.5 mL, p=<0.0001, Table 23). However, the intensity of VIM expression was similarly distributed in cases with <5 (1-4) and ≥5 CTCs (Table 23). There were no cases with exclusively moderately or strongly VIM-positive CTCs except one case with only one moderately VIM-positive CTCs.

Table 23: Overview of VIM-positive CTCs in samples of mBC patients. Samples were categorized by low number of CTCs (< 5 (1-4) CTCs/7.5mL of blood) and high number of CTCs (≥ 5 CTCs/7.5 mL of blood).

CTCs/7.5 mL	Number of cases with VIM-negative CTCs	Number of cases with VIM-positive CTCs	Number of cases with 1+ VIM CTCs	Number of cases with CTCs 2+ VIM at highest	Including CTCs with strong VIM expression
<5 (1-4)	52 (38.8%)	8 (11.9%)	4 (50%)	1 (12.5%)	3 (37.5%)
≥5	82 (61.2%)	59 (88.1%)	38 (64.4%)	8 (13.6%)	13 (22%)

Table 24 summarizes molecular subtype of the primary tumor of all 201 mBC patients of whom CTCs were enriched and vimentin expression analyzed.

Table 24: Molecular breast cancer subtype (primary tumor) of patients with vimentin-positive and -negative CTCs and therapies before blood collection.

BC subtype (primary tumor)	Number of cases with ≥ 5 CTCs/7.5 mL	Number of cases with VIM-positive CTCs (n=67)	Number of cases with Vim-negative CTCs (n=134)
HR+	111 (71.6%)	45 (29%)	110 (71%)
HER2+	3 (42.9%)	3 (42.9%)	4 (57.1%)
TNBC	24 (75%)	18 (56.3%)	14 (43.8 %)
No information	3 (42.8%)	1 (14.3%)	6 (85.7%)

Vimentin-positive CTCs were more frequently detected in patients with TNBC and HER2-positive primary tumors than in patients with HR+-positive metastatic breast cancer (p=0.0167, Table 24). However, numbers of patients with <5 (1-4) versus ≥5CTCs/7.5 mL did not differ significantly between HR+, HER2+ and TNBC (p=0.2813, Table 24).

Prior to CTC analyses the mBC patients received several lines of different therapies but data regarding therapies were only available for patients with VIM-positive CTCs. CDK4/6 inhibitors were administered in 12 cases for patients with HR-positive tumors before first blood collection and CTC analysis. All but one of these patients were measured with ≥5 CTCs/7.5 mL blood. However, CTCs with moderate or strong intensity of VIM immunostaining were only found in three cases.

In total, from 23 patients, vimentin expression was determined at least at two different time points during treatment and the dynamics of vimentin expression on CTCs are depicted in Figure 75

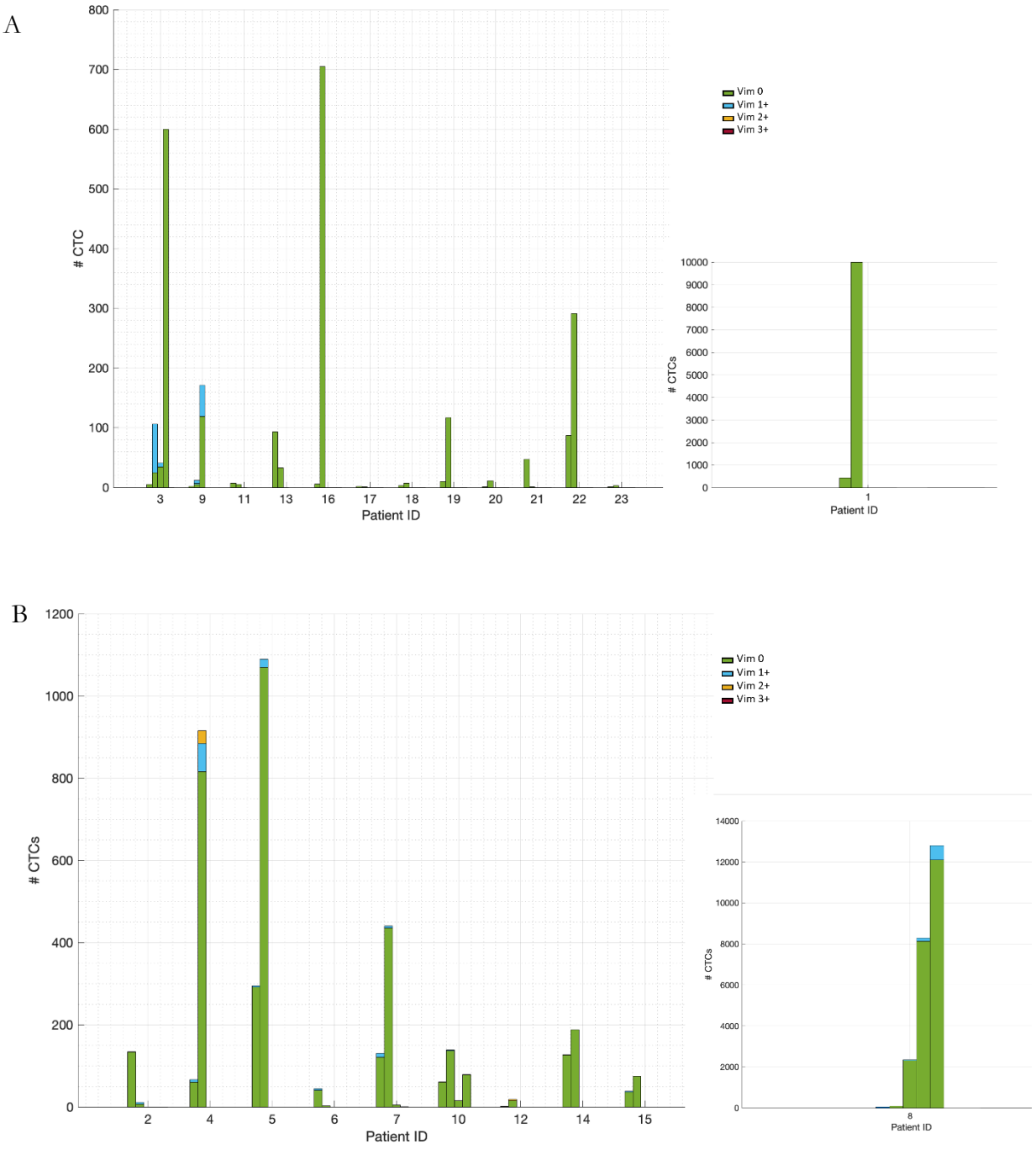

Figure 75: Visualization of the dynamics of vimentin expression on CTCs on a cohort of 23 mBC patients. A: patients with vimentin-negative CTCs at first analysis. B: patients with vimentin-positive CTCs at first analysis. One patient of each cohort is presented separately, since their high CTC count would impede proper visualization of the other patients.

Out of the 13 patients only having vimentin-negative CTCs at their first visit, 2 had vimentin positive CTCs at follow-up visits (patient 3 and 9). Interestingly, patient 9 was the only one who had also strongly vimentin-positive CTCs at one visit. Seven patients out of the 10 with vimentin-positive CTCs at first analysis, also had vimentin-positive CTCs on at least one further visit, whereas three patients had only vimentin-negative CTCs at follow-up visits. Overall, the dynamics

of vimentin-positivity did not differ strongly between the two groups and only one patient with only vimentin-negative CTCs at the first visit had VIM 2+ and VIM 3+ CTCs at follow up, whereas two with vimentin-positive CTCs at first visit had vimentin 2+ CTCs at a later visit. Overall, most CTCs of patients of both groups were vimentin-negative, regardless of whether vimentin-positive CTCs were detected at the first visit. Complete patient data are provided in Supplementary Table S 1.

Due to the multitude of various therapies the patients analyzed in this cohort received, a correlation with vimentin positivity of CTCs and the dynamics of vimentin-positivity during follow up was difficult. Thus, more patients must be followed from first line therapy under comparable therapeutic regimens by CTC analyses.

4 Discussion

Inhibitors of CDK4/6 have become part of the standard-of-care therapy for HR+ mBC patients. Despite initial benefit for the majority of patients, acquisition of resistance is almost inevitable. As mentioned previously, no predictive marker for CDK4/6 inhibitor therapy currently exists. Promising candidates like cyclin D1 and p16 failed in clinical studies [249]. Yet, thymidine-kinase 1 (TK1) recently gained interest as a prognostic marker. High levels of this proliferation marker after therapy initiation or at the time of progression were associated with worse prognosis. The utility of *TK1* levels as a marker of CDK4/6i response was investigated in a retrospective clinical study on patients with luminal mBC., enrolled in the TREnd trial [250]. Likewise, high expression of polo-like kinase 1 (PLK1) correlated with worse median PFS of patients treated with palbociclib in a phase III clinical study (PEARL) [251]. Other promising markers under investigation are amplification of *IGFR1*, *RAD51C* and loss of PTEN protein [252] but the search for predictive markers is ongoing [187]. Thus, this thesis aimed to identify potential new transcripts, proteins and miRNAs, involved in treatment resistance, and to establish reliable detection so that they could potentially serve as new biomarkers for acquired resistance to CDK4/6i.

4.1 Resistance to ribociclib in CTC-ITB-01 and MCF7 cells

Preliminary experiments were performed to test the impact of palbociclib and ribociclib on the viability and clonogenic growth of both cell lines and to compare the impact of both CDK4/6 inhibitors on these cell lines. Indeed, both cell lines were sensitive to CDK4/6i by any of the two inhibitors, confirming literature that shows susceptibility of both cell lines to palbociclib treatment [118,132]. Yet in line with literature, higher concentrations of ribociclib were needed to achieve the same impact as with palbociclib, resulting in markedly higher IC_{50} values determined by the CFA and CCK-8 assays [166,253]. Naturally, a multitude of comparable studies using MCF7 cell have been conducted. However, also the biological mechanisms leasing to ribociclib resistance are manifold and can even differ in resistant sub-clones derived from a common parental cell line [54]. Furthermore, the CTC-ITB-01 cell line is a particularly interesting model in this context, as it mirrors CTCs properties better than a cell line which is not derived from CTCs and is a valuable tool for the identification of liquid biopsy markers.

To facilitate in-depth analysis of resistance mechanisms, ribociclib-resistant cell lines were generated by long-term culture with continuously increasing ribociclib concentrations, and their resistance was confirmed by multiple experiments. First, cell cycle profiles were assessed to evaluate the impact of ribociclib on the fraction of cells arrested in the G1-phase of the cell cycle upon treatment. While ribociclib treatment induced significant G1 arrest in both parental cell lines, also an effect on the resistant derivates was observed, albeit to a lesser extent. The comparison of cells in S-phase further supported these results, as the reduction of S-phase fractions was only significant in the parental cell lines, but not in the resistant ones. That susceptibility to CDK4/6i is not completely lost, also in resistant cell lines as also observed in comparable cell culture models [66,67] and does not exclude established resistance. Hence, functional assays were performed to further confirm the resistance. Ribociclib treatment only had a moderate impact on the viability of all tested cells, while the parental derivates were comparably susceptible to the treatment, indicated by

marked lower IC_{50} values than those of the respective resistant derivates. The reduction of clonogenic growth induced by ribociclib treatment was stronger than the impact of ribociclib on the viability of treated cells, while still demonstrating the established resistance of the respective cell lines, confirming the rather cytostatic and less cytotoxic effect of ribociclib treatment.

Overall, the resulting IC_{50} values for MCF7 cells were comparable with published data [132], whereas such a comparison for the CTC-ITB-01 is lacking, since most published experiments were performed using luminal A BC cell lines such as T47D and MCF7. Yet, all effects introduced by ribociclib treatment were less pronounced in the CTC-ITB-01 cell line, implying a higher intrinsic resistance to CDK4/6i compared to MCF7 cells. Despite overall higher IC_{50} values for the CTC-ITB-01 cell line, they were still in range of concentrations that were used in comparable published studies for the treatment of breast cancer cell lines [66,253,254]. In general, repeated experiments using the parental and resistant CTC-ITB-01 cell lines resulted in rather high variances of outcomes. A reason for that could be the noticeable heterogeneity of single cells from this cell line, growing with different morphological properties and either adherently or in suspension [118]. During continuous culture, an increased percentage of the adherently growing cells was observed, whereas less cells were growing in suspension. Together with the frequent occurrence of multinucleated cells this causes great variance of results from biologically independent functional assays. Furthermore, this cell line does tolerate growing on limited space, for example in wells of a 96 well format, to a lesser extent than MCF7 cells.

Since ribociclib prevents phosphorylation of the retinoblastoma protein (RB) by the CDK4/6/cyclin D1 complex and thereby release of E2F transcription factors, phosphorylation of RB at Ser780 and Ser795 was evaluated by Western blot analysis. The levels of both phosphorylated proteins decreased under ribociclib treatment in the parental cell lines, whereas in resistant CTC-ITB-01 cells no changes in the amount of pRB Ser780 and 795 were induced by ribociclib. This was also true for pRB Ser780 in resistant MCF7 cells, but not for pRB Ser795.

Similar effects have been reported for the phosphorylation site Ser807/811 in a cell culture model analyzing palbociclib treated MCF7 cells. After 24h of treatment, the phosphorylation was strongly reduced whereas after 72h, the amount of phosphorylated RB returned to the baseline level [64]. It is to be assumed, that the chosen incubation time of three days for MCF7 and even 6 days for the CTC-ITB-01 cells was sufficient to enable the cells to circumvent CDK4/6 inhibition and phosphorylate RB by other than the CDK4/6/cyclin D1 complexes. CDK2 was proposed as a binding partner of cyclin D1, promoting G1-S transition [64] and thereby compensating for the inhibition of CDK4/6. Notably, the efficacy of a small inhibitor molecule targeting CDK2, CDK4, and CDK6 for its ability to overcome resistance to CDK4/6 inhibition is currently investigated in a clinical phase 1 study [255]. Other studies performed on luminal A BC cell lines demonstrated a complete lack of phosphorylated RB Ser780 also after 72h [66], furtherly demonstrating the heterogeneity of response and adaption to CDK4/6i. However, treatment times referring to at least 3 doubling times per cell cline are usually chosen to assess full effects of inhibition of CDK4/6 activity and experiments using MCF7 cells are often conducted for 48-96 h of CDK4/6i treatment [64,66,132]. The incubation time was prolonged for the experiments with CTC-ITB-01 cells, due to their longer doubling time compared to that of MCF7 cells.

Differences regarding the induction of senescence measured by β-galactosidase activity could provide a possible explanation for the differences between reduced viability and growth inhibition.

While ribociclib treatment induced β-galactosidase activity stronger in parental than in resistant MCF7 cells, this difference was not observed in parental versus resistant CTC-ITB-01 cells. At a concentration of 1.5 μM ribociclib, no β-galactosidase induction could be detected, indicating that higher concentrations would have been needed to induce senescence. This supports the weaker response of CTC-ITB-01 cells to ribociclib treatment observed in the CCK-8 and CFA assays, indicating an intrinsic partial resistance of this cell line to CDK4/6i treatment.

4.2 Identification of potential drivers of resistance to ribociclib

Analysis of deregulated proteins and mRNAs associated with cell cycle progression further confirmed the established resistance. A plethora of proteins deregulated in either appropriate cell culture models or in clinical samples of patients progressing on CDK4/6i therapy has been published. Based on that, a panel of potential driver genes and proteins was chosen to confirm the resistance of CTC-ITB-01 and MCF7 cells chronically exposed to ribociclib. Indeed, this analysis revealed a significant increase of *CDK6* mRNA expression and elevated CDK6 protein levels in resistant compared to parental MCF7 cells, known as a potential driver of resistance [53,132,256]. Increased CDK6 levels can be triggered by loss of the tumor suppressor FAT-atypical cadherin 1 (FAT1) and consequent Hippo pathway suppression [257]. However, the RNA-seq data did not provide evidence for an up-regulation of *CDK6* expression via this pathway. Interestingly, *CDK6* mRNA and protein levels were inheritably higher in CTC-ITB-01 cells than in MCF7 cells, thus partially explaining the slightly weaker sensitivity to ribociclib treatment observed in the functional assays. In spite of missing up-regulation of *CDK6* transcription, Western blot analysis displayed an elevated protein level in resistant CTC-ITB-01 cells, indicating a potential impact of CDK6 on ribociclib resistance also in this cell line.

In resistant CTC-ITB-01 cells a significant decrease of *CDKN1A* mRNA, coding for the CDK/6 inhibitor $p21^{CIP1}$ tumor suppressor protein was detected. In another study, also ribociclib-resistant MCF7 cells were generated and $p21^{CIP1}$ levels were even proposed as a monitoring marker for the efficacy of CDK4/6 inhibitor therapy [258]. Reduced levels of the endogenous CDK4/6 inhibitor could compensate for CDK4/6 inhibition by ribociclib. However, the strong decrease of *CDKN1A* mRNA could not be confirmed on the protein level by Western blot analysis. For that reason, the importance of decreased *CDKN1A* expression in this resistant cell line for $p21^{CIP1}$ activity requires further experimental elucidation. In contrast to CTC-ITB-01 cells, resistant MCF7 cells exhibited lower *CDKN1A* and $p21^{CIP1}$ levels than their parental counterparts

Interestingly, levels of the CDK6 complex partner cyclin D1 were not increased in the DMSO-treated cell lines but upon ribociclib treatment in both parental and resistant cell lines. Hence, in both models, increased cyclin D1 levels may represent an immediate mechanism of adaptation to CDK4/6 inhibition but do not support stable resistance. Similar observations were made in a study on palbociclib-resistant MCF7 cells. Here, silencing of cyclin D1 could reinforce the palbociclib-induced G1 arrest and inhibition of RB phosphorylation, confirming the relevance of accumulated cyclin D1 for early adaptation to CDK4/6i [64]. Loss of RB has been described to promote CDK4/6i

resistance in cell culture models [259] and in patients alike [260]. Moreover, the ratio of *CCNE1* (cyclin E1 encoding mRNA) and *RB1* expression has even been proposed as an adverse prognostic factor in the NeoPalAna trial to discriminate between patients benefiting of palbociclib treatment or not [63].

However, neither changes of *RB* mRNA nor alterations of protein levels were observed in the resistant cells of the present study. Furthermore, variant calling did not reveal any *RB1* mutation that could contribute to ribociclib resistance in any of the resistant cell lines. Mutations in the *RB* gene may be a very effective way to circumvent CDK4/6 inhibition, but clinically they account only for a small proportion of resistant patients, as only about 5% of patients who received CDK4/6i therapy harbored those mutations [1]. Plenty of other alterations of cell-cycle related proteins have been described in the context of CDK4/6i resistance, such as the amplification of *CDKN2A*, *CCNE1/2*, *CDK4*, *CDK2*, and E2F family member-encoding genes [261,262] as well as losses of the genes coding for cyclin-dependent kinase inhibitors such as $p27^{KIP1}$, going along with altered protein levels. However, alterations of mRNA expression of these genes were not observed in ribociclib-resistant cells established in this study.

It is important to mention, that also proteins not related to cell cycle progression were shown to mediate resistance to CDK4/6 inhibitors. Since the induction of EMT by a TGF-β-dependent pathway as a consequence of CDK4/6i resistance has been discussed before [67,261], genes encoding EMT-related transcription factors and commonly used EMT-indicating markers were also chosen for initial validation of ribociclib resistance in this study. Despite missing alterations in the expression of genes encoding the key transcription factors ZEB1, Snail, Slug and Twist, the expression of several genes related to EMT was changed in resistant compared to parental CTC-ITB-01 and MCF7 cells.

Moreover, additional, and hitherto in the context of resistance to CDK4/6i novel, deregulated genes could be unraveled by RNA-seq in the present study. Apart from proteins related to cell adhesion or EMT, to be discussed later, multiple mRNAs encoding proteins, potentially regulating the cell cycle were found differentially expressed. The upregulation of *CDK6* in resistant MCF7 cells was confirmed by RNA-seq and interestingly, the gene with the most significant differential expression found in these cells was *PEG10*. This gene is located on the same amplicon on chromosome 7q21 as *CDK6* and *CDK14* and has been found to be co-amplified in hepatocellular carcinoma (HCC) cell lines [263]. PEG10 is not a well-described protein, but experimental and clinical data indicate, that it promotes G1/S transition and is associated with increased proliferation and metastasis in breast cancer [264]. Neither *PEG10* nor *CDK6* were upregulated in resistant CTC-ITB-01 cells, but the read counts of both mRNAs were significantly higher in CTC-ITB-01 cells than in MCF7 cells (*PEG10* log2FC=5.55, *CDK6* log2FC=4.32), indicating again a higher intrinsic resistance of the CTC-ITB-01 cell line to CDK4/6 inhibition. Published copy number profiles also depict gain of chromosome 7 [118], likely explaining the high levels of all three transcripts found in this amplicon in comparison to MCF7 cells. However, despite the intrinsically high levels compared to parental MCF7 cells (log2FC=7.16), *CDK14* transcripts were increased in resistant CTC-ITB-01 cells. The encoded kinase, also known as PFTK1 or PFTAIRE, was shown to promote cell cycle progression and proliferation of MDA-MB-231 cells in vitro. CDK14 has a TAIRE binding site, typically found in G2/M cyclins and cyclin Y [265]. Yet, by complexing with cyclin D3, stabilized by

p21^{CIP1} [266,267] CDK14 acts in a similar manner as CDK4/6 and phosphorylates RB at Ser608 and Ser780 [265], thereby promoting G1-S transition. Furthermore, *CDK14* was higher expressed in tumor tissue compared to matched adjacent normal tissue of breast cancer patients with various molecular subtypes and its expression positively correlated with KI67-levels [266]. Thus, we hypothesized that increased CDK14 activity can compensate inhibited CDK4/6 phosphorylation of RB, albeit this needs to be proven in future experiments. The recently developed covalent inhibitor CDK14 FMF-04-159-R [265] is a promising candidate to prove involvement of CDK14 in ribociclib resistance in CTC-ITB-01 cells. Interestingly, *CDK14* is found as a predicted target of miR-205-5p and the increase of *CDK14* in the resistant CTC-ITB-01 cells is accompanied by a significant decrease of miR-205-5p (log2FC=-3.06) in these cells. To ascertain whether *CDK14* levels are regulated by miR-205-5p in this cell line, however, requires experimental testing by using miR-205-5p inhibitors and mimics.

The role of the most significantly DEG identified in resistant CTC-ITB-01 cells, *XIST*, a lncRNA involved in X-chromosome silencing, is discussed controversially in breast cancer. Numerous publications show tumor-suppressive capacity whereas others report oncogenic functions [174]. However, since altered expression of lncRNAs was not a focus of this study, the role of XIST in the context of ribociclib resistance was not further investigated yet.

Another potential driver not yet described in the context of ribociclib resistance is SOX9, an embryonic TF associated with cancer stem cell features [192]. The expression of *SOX9* was significantly upregulated in both resistant cell lines, albeit only reaching the required fold change of ≥2 in resistant MCF7 cells, while the increase was 1.8-fold in resistant versus parental CTC-ITB-01 cells. This transcription factor exerts important functions in various tumor-related processes such as acquisition of cancer-stemness, EMT and also in the development of drug resistance [192,268]. Interestingly, Western blot analysis demonstrated extraordinarily high amounts of SOX9 protein in CTC-ITB-01 cells, the importance of which has to be elucidated in further experimental work.

The increase of *SOX9* expression was sufficient to induce tamoxifen resistance in *in vitro* experiments using MCF7 cells [269]. Mechanistically, SOX9 can contribute to endocrine resistance by increasing ALDH1 activity and expression as well as by induction of the WNT signaling pathway [192], thereby inducing a more cancer stem cell and EMT-like phenotype. ALDH1 activity was not measured in this project but the expression of *ALDH1A1* was increased in resistant CTC-ITB-01 cells and *ALDH2* and *ALDH3* were upregulated in resistant MCF7 cells. Since the *ALDH1A3* mRNA level and ALDH1 activity positively correlated in a respective cell culture model using MCF7 cells, it is likely that ALDH1 activity could be also increased in the resistant cell lines of this project, promoting cancer-stemness and drug resistance. Moreover, SOX9 inhibition was shown to reduce the expression of *AXIN2* and *FZD4*, both encoding key players in the WNT/β-catenin pathway, suggesting a positive correlation of the expression levels of all three proteins. This is in line with the RNA-seq data of the resistant MCF7 cell line, displaying also significant increases of *AXIN2* and *FZD4* expression in addition to the significant increase of *SOX9* transcript levels. In resistant compared to parental CTC-ITB-01 cells, only *AXIN2* levels were significantly increased. In a published cell culture model *SOX9* knockdown led to a delay of G1-S-phase transition, implicating a positive support of cell cycle progression by this transcription factor [269]. Another

interesting aspect of SOX9 activity is its ability to positively regulate expression of the androgen receptor (AR), as demonstrated *in vitro* on prostate cancer cells[204]. Expression of the *AR* gene was also increased in resistant CTC-ITB-01 cells in the present study. Since AR also can promote cell cycle progression its upregulation might also contribute to ribociclib resistance. Indeed, a pre-clinical study showed that AR inhibition could restore sensitivity to palbociclib of resistant MCF7 cells. Notably, enzalutamide, a FDA-approved AR antagonist and palbociclib exerted synergistic effects on palbociclib-resistant cells *in vivo* [184]. Summarized, these *in vitro* results suggest that SOX9 might be involved in the emergence of resistance to ribociclib.

Furthermore, the anti-apoptotic protein BCL2 was significantly deregulated in both resistant cell lines, yet in different directions. While in resistant MCF7 cells, *BCL2* expression was strongly reduced (log2FC=-5.26), it was increased in resistant CTC-ITB-01 cells (log2FC=1.12). Elevated BCL2 levels are not unexpected for a cell line that developed resistance to a therapeutic agent, however, ribociclib did not induce apoptosis to a noticeable extend. The proportion of apoptotic cells upon ribociclib treatment, the morphology of the cultured cells as well as the moderate effect ribociclib treatment on cell viability suggest, that ribociclib is not highly cytotoxic at concentrations used for the experiments in this study. On the contrary, BCL2 revealed to be a favorable prognostic marker in HR+ HER2- breast cancer patients and is associated with improved OS in these patients [270]. In contrast to that, in TNBC patients, high *BCL2* levels were associated with worse patient outcome [271], suggesting different roles of BCL2 in HR+ HER2- and TNBC tumors. Positivity for BCL2 correlates with ER-positivity, HER2 negativity, and low KI67 levels, indicating also anti-proliferative effects of BCL2 [202,270]. Thus, the contradictory findings of *BCL2* expression in both resistant cell lines may be due to different molecular functions in these two cell lines, which would require further elucidation.

Clinical data show that CDK4/6i resistance is not only driven by changes at the transcriptional level but also by gene mutations. Almost one third of patients gained new driver mutations during the course of therapy with fulvestrant and palbociclib in the PALMOA-3 study [1]. For that reason, mutations, exclusively detectable in the resistant cell lines were reviewed. None of the detected mutations has been described to drive CDK4/6 resistance before. The CTC-ITB-01 cell line already harbors a mutation in the *NF1* gene, coding for a tumor suppressor which is frequently mutated (7% in a cohort of 629 mBC patients) in HR+/HER2- metastatic breast cancer. Respective mutations, often acquired after endocrine therapy, are associated with poor outcome [217,272]. During emergence of ribociclib resistance, CTC-ITB-01 cells gained an additional mutation in the *NF1* gene. Likewise, overexpression of the proline rich 11 protein (PRR11) promoted resistance to endocrine therapy in a cohort of 58 patients with ER+ breast cancer [218] by increasing PI3K signaling. However, mutations in the *PRR11* gene as seen in this study have not been described hitherto. Mutations in the *MAP3K5* gene are not yet described in breast cancer but were detected by exome sequencing in 8 out of 85 sequenced melanoma cell lines and in 1 out of 8 melanoma patient samples [219]. However, the mutation detected in resistant CTC-ITB-01 cells, T517K, was not described in this dataset. In breast cancer, MAP3K5, together with c-jun-N-terminal kinase (JUN) and p38, is involved in the induction of apoptosis upon environmental stress [273]. Somatic mutations abrogated this pro-apoptotic function of MAP3K5 in melanoma cell line cells [274]. According to a comparison of NGS data and a gene chip database, creating a "transcriptomic fingerprint", *VWDE* has a mutation prevalence of higher than 5% [220]. However,

the mutation detected in the resistant CTC-ITB-01 cells, has been identified in breast cancer samples before, but was not functionally characterized. Similar to these mutations, also the mutations in oncogenes, found in resistant MCF7 cells, such as the one in *NOTCH3* and in genes related to migration (*TLNRD1* [275], *ZSCAN31* [224]) and metastasis (*PLK4* [276]) are neither registered in the COSMIC database nor were they functionally investigated. Therefore, their impact on the establishment of resistance to CDK4/6i remains elusive and requires further investigation. Intriguingly, whole exome sequencing was performed on biopsies of 68 patients with HR+ mBC and mutations, that were found with higher frequency in patients with either intrinsic or acquired resistance to CDK4/6 inhibitors were identified [277]. Yet, none of these mutations were found in the resistant cells of this study, nor were other mutations detected in the respective genes.

Notably, several mutations were found in genes encoding proteins involved in mitochondrial metabolism. Interestingly, results from *in vitro* experiments demonstrated a correlation of inhibition of CDK4/6 and an increase of the number of mitochondria and thus increased glycolic and oxidative metabolism [225]. These changes in metabolism could be exploited therapeutically, for example by treating cells simultaneously with a BCL2 inhibitor and CDK4/6 inhibitors. Addition of such a drug to a treatment regime of fulvestrant and palbociclib strongly inhibited clonogenic growth of BC cell culture cells, patient-derived organoids and PDX models [186].

In the present study, not only mRNAs potentially associated with ribociclib resistance, but also miRNAs were investigated by small RNA-seq. The potential of miRNAs to convey resistance to CDK4/6i has been demonstrated in a pre-clinical study [132]. Indeed, according to RNA-seq data, several miRNAs were differentially expressed by the resistant cell lines compared to their parental counterparts. MiRNA 1247-5p was most significantly down-regulated in resistant versus parental CTC-ITB-01 cells, but the respective expression levels were extremely low, making their detection technically challenging. Therefore, despite being in line with the results of a clinical study, showing that low miR-1247-5p expression in tissue samples correlated with shorter PFS and OS [278], this miRNA was not chosen for further experiments. Similarly, miR-135-5p, also strongly downregulated in resistant CTC-ITB-01 cells and described as a suppressor of metastasis [279], was very lowly abundant, hindering reliable validation. The only miRNA upregulated out of the five most significantly deregulated miRNAs in the resistant CTC-ITB-01, miR-1908-3p, is higher expressed in breast cancer patients than healthy donors and induced cell proliferation, migration, and invasion in *in vitro* experiments [280]. Yet, due to low abundance, it was not chosen for further experiments.

MiR-1269a was described as a miRNA promoting resistance to hypoxia in breast cancer [281], but its expression was strongly decreased in resistant MCF7 cells. MiRNA-375-3p, also downregulated in the resistant MCF7 cells, is a negative regulator of *CD44*, a cancer-stemness marker strongly increased in resistant MCF7 cells and supposedly preventing tamoxifen resistance by downregulation of HOXB3 [282]. Indeed, re-expression of miR-375 did resensitize tamoxifen resistant MCF7 cells to endocrine treatment [283], confirming the importance of miR-375-3p regulation in the context of endocrine resistance and perhaps also CDK4/6i resistance. Amongst the upregulated miRNAs, miR-139-3p was the only one, described as a tumor suppressor miRNA and to inhibit cell proliferation, migration and invasion [284]. The other two, miR-675-3p and miR-675-5p, were shown to increase colony growth and positively regulate cancer-stemness, thereby

promoting an aggressive phenotype [285]. Summarized, small RNA-seq revealed several miRNAs that potentially are involved in the development of resistance to ribociclib and require further experimental validation.

The most promising candidate miR-146a-5p which was upregulated in both resistant cell lines, and miR-205-5p potentially involved in the emergence of ribociclib resistance will be discussed in chapter 4.3.

The search for new biomarkers in this study mainly relied on RNA-seq data, analyzing differences between parental and ribociclib-resistant cell lines. However, this approach also bears some limitations. First, only two resistant cell lines were analyzed, limiting the number of resistance drivers that can potentially be found, as the diversity of resistance mechanisms is very high [54]. However, results obtained using the CTC-ITB-01 cell line are particularly interesting since it was established directly from cultivated CTCs and might mirror a liquid biopsy from a patient more precisely as for example the MCF7 cell line, which was derived from a pleural effusion. The multitude of various published resistance mechanisms, sometimes even within one cell culture model using the same parental cell lines [54], demonstrate that it is hardly possible to standardize mechanisms resulting in ribociclib or CDK4/6i resistance in general. Thus, the definition of resistance mechanisms induced by only one altered protein or miRNA remains difficult. Moreover, several options for setting significance thresholds for the analysis of RNA-seq data exist. The chosen approach, of log2FC≥1 and FDR≤ 0.1 is similar to the threshold of the 2-fold change and p-value <0.05, chosen for qPCR analysis. Thereby, only DEGs with a rather high fold change were considered, also if their change is not within the highly rigid significance FDR threshold of ≤0.05. Setting the log2FC lower, for example to ≥0.59 and decreasing the FDR to ≤0.05 may detect minor changes with even higher significance. However, this approach was not chosen since the impact of minor fold changes is hard to evaluate and the chosen settings resulted in more robust results. Furthermore, while RNA-seq provides the possibility of transcriptome-wide changes and mutational analysis, changes on the protein level are not assessed. However, due to diverse post-translational modifications, mRNA-levels not necessarily have to correlate with protein levels [169]. Altered protein levels, albeit of great importance, are not detected by the approach of this study and may require other experimental set-ups such as for example proteome analysis by mass spectrometry.

4.3 Increase of EMT traits in ribociclib-resistant CTC-ITB-01 and MCF7 cells

That CDK4/6 inhibition can stimulate the induction of EMT and that CDK4/6 inhibitor resistance is linked with EMT has already been published [67,286]. However, whether CDK4/6 resistance induces EMT or is a consequence of the EMT program, needs to be elucidated. EMT is a crucial process in tumorigenesis, as it is linked to major changes of adhesion molecules inducing loss of cell-cell contacts and a more motile phenotype, allowing cells to migrate and invade adjacent vasculature [78]. Furthermore, EMT is associated with the emergence of cells with stem cell properties [177]. Because ORA, using the MSigDB revealed EMT induction in both resistant cell lines, the EMTome database was chosen to identify DEGs that are associated with EMT as the datasets of

the MSigDB database are rather small. The EMTome is a pan-cancer database providing an overview of EMT signatures, EMT-related genes and EMT interactomes [178]. The comparison of the DEGs from the resistant cell lines derived from RNA-seq data and all EMT-related genes, registered in the EMTome database, revealed high overlap of both datasets, supporting the initial findings of upregulated EMT markers in the resistant cell lines.

Furthermore, the analysis of the five most up- and downregulated genes coding for EMT-related proteins of each resistant cell lines, revealed interesting candidates. Vimentin was within the top five upregulated EMT transcripts in resistant CTC-ITB-01 cells, supporting the hypothesis of induced EMT in these cells. Interleukin 6 (IL6) is a pro-inflammatory cytokine, which can induce EMT and CSC-phenotype via phosphorylation of its downstream target STAT3 [153,287]. However, the expression of *IL6* was very low even in resistant CTC-ITB-01 cells and hence probably not contributing significantly to the induction of the EMT-phenotype in this cell line. Keratin 17 is associated with the basal-like breast cancer subtype and its expression was predictive for poor OS in a pan-cancer analysis[288,289]. A pre-clinical study on pancreatic cell line cells demonstrated that keratin 17 supports proliferation, migration and invasion by stimulating mTOR/S6k1 signaling [290]. Thus, as mTOR is a downstream target of PI3Kα, it might be interesting to detect keratin 17 levels in cells treated with alpelisib. Interestingly, *KRT17* expression was decreased in resistant MCF7 cells. Amongst the top five downregulated transcripts were two genes encoding tumor suppressors of particular interest. Downregulation of ARHGAP10 is related to advanced stages in breast cancer and a high KI67 index [291] whereas PCDH17 can disrupt WNT-signaling and negatively regulate vimentin expression and cancer cell motility [191]. Functional characterization of the encoded protein in breast cancer is lacking hitherto, but low *KRT15* expression correlated with worse OS of patients with invasive breast cancer as assessed on TCGA data [292]. The altered expression of the other genes found by the comparison of DEGs with the EMTome database did not bear any additional information due to either very low abundance of their transcripts or the lack of informative publications. Of the EMT-related genes with increased expression in resistant MCF7 cells, *COL3A1* mRNA displayed the highest fold change. Pre-clinical experiments demonstrated reduced migratory, invasive and adhesive potential of MDA-MB-231 and MDA-MB-468 cells after *COL3A1* knock-down [194]. This is of particular interest, since higher adhesive capacity of resistant MFC7 cells to HUVECs was observed in BioFlux experiments performed in this study. The increased expression of *COL3A1* in resistant MCF7 cells could provide an additional explanation for the elevated adhesion to HUVECs. Therefore, it should be investigated whether translation of the increased *COL3A1* mRNA levels into protein can also be shown. The level of dihydropyrimidine dehydrogenase (DPYD) determined by immunohistochemistry, revealed to be a poor prognostic factor in breast cancer [293]. The *DPYD* gene was identified as part of a metabolic signature of EMT cells, generated by the comparison of datasets containing either epithelial or mesenchymal cancer cell line cells. DPYD was demonstrated to positively regulate the transcriptional activity of Twist. Moreover, it was identified as an essential driver of EMT since the accumulation of DPYD products, dihydrouracil and dihydrothymine is a requirement to induce EMT-reprogramming in cell line cells [195]. However, the abundance of *DPYD* transcripts in resistant MCF7 cells was still low, just as the level of *RNF128* encoding a protein that was negatively linked to the gain of EMT and cancer-stemness in melanoma cells [294]. Hence, the meaning of this finding is questionable. Overexpression of *STEAP1* inhibited proliferation, migration and invasion in

MCF7 cells [295]. DAB2 is commonly downregulated in breast cancer and its loss is associated with the induction of a stable EMT phenotype in MCF10A1 cells, by activating the MAPK pathway [296]. Surprisingly, *FGFR1* expression was reduced in resistant MCF7 cells, since *FGFR1* overexpression was part of a described mechanism of CDK4/6i resistance and the analysis of ctDNA from 34 patients enrolled in the MONALEESA-2 trial, progressing on therapy with ribociclib and fulvestrant revealed *FGFR1* amplification in 41% of patients [76]. In summary, this comparison of DEGs identified in this study with the EMTome partially supports the hypothesis of induction of EMT and cancer-stemness in the resistant cells, but not all findings are in line with published data. Moreover, not all changes at the transcriptional level necessarily translate into respective changes on the protein level, and the analysis of the changes of single transcripts, does not indicate activation or inactivation of the pathway it is involved in.

Interestingly, *CDK14* was also listed as an EMT-related gene in the EMTome database. Multiple cell culture models, using NSCLC [297], pancreatic cancer [298] and colon cancer cell lines [299] have demonstrated a positive correlation of *CDK14* expression and expression of genes coding for markers of a more mesenchymal phenotype like vimentin and N-cadherin, whereas the expression of the epithelial marker E-cadherin correlated negatively. Moreover, CDK14 positively regulated actin stress fiber formation by caldesmon phosphorylation. In hepatocellular carcinoma (HCC) higher *CALD1* expression in tumor tissue than in adjacent normal tissue was observed. Furthermore, the phosphorylation status of caldesmon 1 correlated positively with the detection of peripheral metastases [300]. In breast cancer *CALD*1 expression was found to be associated with resistance to tamoxifen [301]. Interestingly, *CALD1* levels were also elevated in resistant compared to parental CTC-ITB-01 cells, however, the levels of the encoded protein and its phosphorylation status were not assessed. Actin-reorganization is a crucial step of the EMT program, leading to higher motility and increased migration and invasion of tumor cells [298,299,302]. Cell motility indeed was a GO BP pathway found to be enriched in both resistant cell lines by RNA-seq.

As mentioned before, SOX9 is involved in a multitude of tumorigenic processes and is also known to be involved in induction of EMT [303,304]. Being a transcription factor, it stimulates the expression of various EMT-related proteins like vimentin, ZEB1, claudin1 or β-catenin by binding directly to the promotor region of the respective genes, while E-cadherin expression correlates negatively with SOX9 expression [268]. Furthermore, as described previously, SOX9 can stimulate WNT-signaling, which also can initiate EMT [305]. Strikingly, induction of the SOX2-SOX9 axis reportedly maintains breast cancer stem cells, and the expression of both transcriptions factors was significantly upregulated in resistant MCF7 cells compared to parental. Furthermore, a significant increase of *CD44* expression was detected, indicating the induction of stem cell-like properties in resistant MCF7 cells [176]. Interestingly, Western blot analysis revealed a doublet band for SOX9, implying differently phosphorylated forms this protein. Experiments on a murine model of HER2+ breast cancer indicate increased stability and higher transcriptional activity of SOX9 upon phosphorylation [306].

While CDK14 and SOX9 were hypothetically involved in driving ribociclib resistance and EMT, other transcripts identified as EMT-related DEGs in this thesis were more likely deregulated in consequence of resistance and EMT initiation. The *CLDN1* gene was differentially expressed in both resistant cell lines but downregulated in resistant MCF7 cells and upregulated in resistant

CTC-ITB-01 cells. Claudin 1 is crucial for the formation of tight junctions and thus for the maintenance of an epithelial phenotype, functioning as a tumor-suppressor. Thus, its loss in the resistant MCF7 was reasonable, as it facilitates motility and claudin 1^{low} tumors are usually more aggressive, invasive, and correlate with a metastatic phenotype [198]. Contradictory to that claudin 1 expression was also shown to promote migration in MCF7 cells [307] whereas the knockdown of *CLDN1* in a TNBC line suppressed migration and the expression of EMT related proteins, amongst them caldesmon 1 [308], whose coding gene was higher expressed in resistant versus parental CTC-ITB-01 cells. Furthermore, higher claudin 1 levels correlated clinically with the highly aggressive basal-like molecular subtype [309]. In summary, the results regarding claudin 1 expression in breast cancer are quite contradictory, implying either different functions of claudin 1 or its involvement in various pathways. Thus, unraveling the role of *CLDN1* expression in the ribociclib-resistant cell lines would require further investigation. Assessing the localization of claudin 1 could already provide insight in the function of claudin 1, as it is normally localized at the plasma membrane, but immunostainings of tumor tissue revealed, that during tumorigenesis, claudin 1 can also be localized in the cytoplasm. Cytoplasmatic, opposed to membrane-bound claudin 1, was shown to be associated with increased invasiveness of various cancer entities [308]. Hence, it is very important to analyze the cellular localization of claudin 1 in both resistant cell lines. Despite its important role in either maintenance of an epithelial phenotype or driving EMT, claudin 1 expression did not have an impact on OS or PFS in ER+ and ER- breast cancer patients, demonstrated on a cohort of 189 patients [309].

The EMT marker fibronectin, the expression of which was upregulated in both resistant cell lines and vimentin, upregulated in the resistant CTC-ITB-01 cells are commonly used to detect cells of a mesenchymal phenotype. Overexpression of fibronectin, an extracellular matrix glycoprotein can induce an EMT phenotype in MCF7 cells [180] and was associated with tamoxifen resistance in patients with luminal A breast cancer [310]. Likewise, the intermediate filament protein vimentin positively regulates migration and thereby facilitates invasion and metastasis. Increased vimentin levels correlate with an elevated risk of failure of endocrine therapy in patients with advanced breast cancer [246,247]. Finding these markers indicative of EMT increased in both resistant cell lines, yet at rather low abundance, supports the association of ribociclib resistance and induction of EMT.

MicroRNAs are important post-transcriptional regulators of gene expression and a multitude of miRNAs involved in the regulation of genes contributing to EMT induction and the establishment of drug resistance have been described. Well-described miRNAs involved in EMT regulation and listed in the EMTome database are miR-34a and miR-200c-5p. The latter is known as an inhibitor of formation of a cancer-stem cell phenotype and EMT in breast cancer. Members of the miR-200 family create a negative feedback regulation loop with the transcription factor ZEB1, resulting in decreased expression of vimentin and reduced migration and invasion [311,312]. Low expression of miR-200c-5p was detected in parental CTC-ITB-01 cells, whereas this miRNA was not detected in resistant CTC-ITB-01 cells which was in line with the identification of DEGs related to EMT. However, prediction of altered TF activity in resistant versus parental CTC-ITB-01 cells did not reveal altered transcriptional activity of ZEB1 nor were its mRNA levels changed. Strikingly, despite not being listed in the EMTome database, miR-146a-5p, the only miRNA upregulated in both resistant cell lines according to the RNA-seq data, was shown to stimulate invasion and metastasis of breast cancer cell lines. As exosomal cargo, it could activate cancer-associated

fibroblasts in breast cancer mouse models [313]. Moreover, miR-146a-5p was enriched in stem cells of primary breast cancer tumors and was identified as an important factor for the maintenance of the stem cell character of the respective cells [314]. Nonetheless, due to very heterogeneous expression in the CTC-ITB-01 cell lines, very low abundance in MCF7 cells and the lack of a specific MISH probe, this miRNA was not further investigated within this study. Instead, miR-205-5p which is listed in the EMTome database and described as a suppressor of ZEB1 translation, thus inhibiting EMT [228], was chosen for further experiments. The decreased expression of miR-205-5p in resistant CTC-ITB-01 cells identified by RNA-seq could be confirmed by qPCR and MISH. Therefore, the presence of miR-205-5p in CTCs in two samples of patients with HR+ mBC enriched by CellSearch® was analyzed and both, miR-205-5p-positive as well as -negative CTCs were detected. Whether miR-205-5p detection in CTCs has clinical relevance, has to be investigated on a larger patient cohort. Furthermore, a small clinical study demonstrated that circulating cell-free miR-205-5p was less abundant in plasma samples obtained from CTC-positive patients with breast cancer than in samples from CTC-negative patients [315]. Therefore, this miRNA is an interesting potential candidate biomarker for monitoring CDK4/6i response or resistance in HR+ mBC patients. Likewise, miR-375-5p was demonstrated to correlate positively with EMT-properties in tamoxifen-resistant MCF7 cells[283] and was also found strongly downregulated in resistant compared to parental MCF7 cells. MiR-432-5p was demonstrated to convey palbociclib resistance to luminal A breast cancer cell lines, when palbociclib-sensitive cells were incubated with exosomes of palbociclib-resistant cells[132]. This miRNA was also tested on parental and resistant cell lines in the present study but neither RNA-seq nor MISH showed differential expression of miR-432-5p between parental and resistant CTC-ITB-01 and MCF7 cells (Supplementary Figure S 1).

Induced EMT transcriptional programs correspond to a more motile phenotype and thus to increased migration. To test whether the induced EMT phenotype changes the motility of the resistant cell lines, migration and invasion assays would need to be performed.

Overall, RNA-seq data and their validation by qPCR and Western blot analysis suggest induction of EMT-like alterations in the context of ribociclib resistance, albeit both cell lines still maintain their epithelial character, indicated for example by E-cadherin and EPCAM positivity. This implies that resistance to ribociclib is probably associated with a higher grade of plasticity in CTC-ITB-01 and MCF7 cells. Furthermore, the comparison of DEGs with the EMTome revealed a relevant overlap and EMT seems to be relevant for CDK4/6i resistance. However, whether EMT is a consequence of resistance or contributes to the resistance development needs to be examined. Experiments on PDAC cell lines cells have demonstrated, that palbociclib treatment caused induction of a mesenchymal phenotype by stimulating TGFβ signaling, evidenced by the upregulation of for example *VIM* expression and development of a spindle-shape morphology. Although E-cadherin levels were not affected by the induction of EMT, the protein was translocated from the membrane to the cytoplasm[286]. Likewise, no changes in *CDH1* expression were observed in the resistant cell lines of the present study but E-cadherin IF staining did not reveal any differences of the protein localization between parental and resistant derivates. Yet, while in both MCF7 cell lines the typical staining at cell-cell contacts was observed, weaker and diffuse cytoplasmatic staining was detected in both CTC-ITB-01 cell lines (Supplementary Figure S 2).

It has to be mentioned that transcriptional up- or downregulation of canonical EMT transcription factors such as *ZEB1*, *GRHL2*, *TWIST*, *SNAI1* or *SNAI2* was not observed in ribociclib-resistant compared to the parental CTC-ITB-01 or MCF7 cells. However, in resistant versus parental MCF7 cells *SOX9*, *SOX11*, *RUNX2* and *GATA4* transcripts were up- and *OVOL2* transcripts, encoding other EMT transcription factors [171] were down-regulated. In resistant CTC-ITB-01 cells levels of *SIX1* transcripts [171] were higher than in the parental cells. Moreover, based on the DEGs identified by RNA-seq, bioinformatical DoRothEA [242] analysis predicted altered activity of several transcription factors without transcriptional deregulation of the encoding gene itself. In resistant CTC-ITB-01 cells for example the activity of transcription factors NFκB, RELA, RELB were predicted to be increased. Inhibition of members of this transcription factor family were demonstrated to correlate with reduced cell migration and decreased levels of SLUG, TWIST and N-cadherin. In silico analysis revealed binding sites of Slug and Twist for NFκB that were confirmed experimentally [316]. Since no expressional changes of any of these transcription factors was identified in resistant CTC-ITB-01 cells, it remains to be elucidated which genes are transcriptionally stimulated by NFκB in the context of ribociclib resistance. Transcriptional targets of NFκB include e.g. *SOX9* [317], *FN1* [318] and *ICAM1* [319]. The analysis of DEGs the transcription of which could be regulated by NFκB according to the DoRothEA database revealed several genes encoding EMT-related proteins. However, experimental investigation of the role of NFκB transcriptional activity in the resistant CTC-ITB-01 cell line is still required to elucidate its role in supporting ribociclib resistance.

Furthermore, also RUNX2 was identified to be higher transcriptionally active in resistant versus parental CTC-ITB-01 cells. Involvement of RUNX2 in the regulation of EMT was shown in various cancer entities [171]. The induction of EMT in resistant CTC-ITB-01 cells was also indicated by multiple changes of EMT markers, miRNAs and CAMs as well as altered transcriptional activity of transcription factors stimulating EMT. The decrease of miR-205-5p levels and the putative concomitant increase of the level of *CDK14* mRNA, which is predicted to be a direct target of miR-205-5p, could be relevant for stimulating EMT. Also notably, the expression of the *SALL4* gene encoding the Sal-like protein 4 (SALL4), a transcription factor which was shown to stimulate EMT and cancer stem cell properties in breast cancer cell line cells [190], was increased in resistant CTC-ITB-01 cells. In addition, expression of LYN coding for the LYN kinase, known as a positive regulator of EMT, cell motility and invasion in breast cancer, was upregulated in both resistant derivates of this study [181].

Importantly, in resistant MCF7 cells, the activity of the key transcription factor Slug (SNAI2) was predicted to be higher in resistant than in parental cells. Surprisingly, among the genes upregulated by SNAI2 according to the DoRothEA database, were only three genes with differential expression in resistant versus parental MCF7 cells. Interestingly, in our study one of these genes, *CXCR4,* encoding the breast cancer stemness-related C-X-C motif chemokine receptor [320] was significantly upregulated in resistant versus parental MCF-7 cells. However, other transcriptional targets that might not be listed in the DoRothEA database, might still be of importance. This is in line e.g. with increased expression of *RUNX2* in these cells, since experiments using MCF7 cells demonstrated induction of WNT- and TGFβ-dependent EMT via the RUNX2/SLUG-axis [321]. An alternative could be the cooperation of SLUG with SOX9 and SOX2. SOX9 was not only demonstrated to cooperate with SOX2 in inducing cancer-stemness and WNT-dependent EMT in breast cancer

cell line cells [192], but orchestration with SLUG also induced cancer stemness in differentiated breast cancer cells [322]. Therefore, SOX9 activity might be crucial for the induction EMT and cancer-stemness in the resistant MCF7 cells. Furthermore, SLUG was shown to positively regulate *SOX2* expression [323]. SOX2 in turn positively regulates *SOX9* expression [192], implying a functional axis of Slug/SOX2/SOX9 that could be WNT-dependent.

Induction of EMT might be closely linked to therapeutic resistance since EMT-programming is not only associated with deregulation of the expression of adhesion molecules and cytoskeleton proteins, but also of proteins influencing therapeutic efficacy [324]. WNT signaling can lead to increased transcription of genes encoding ATP-binding cassette (ABC) transporter, channeling therapeutic agents out of the cells. Indeed, several *ABCA*, *ABCB*, *ABCC* and *ABCG* transcripts were deregulated in the ribociclib-resistant cell lines, yet in resistant CTC-ITB-01 cells 4 out of 5 dysregulated *ABC* genes were upregulated whereas in resistant MCF7 cells 6 out of 8 were downregulated, suggesting differences regarding the resistance development between both cell lines. Increased expression of ABC transporters is also a typical feature of cancer stem cells (CSCs) [325], characterized further by a slow proliferation rate, high level of plasticity and expression of high *CD44*, *ALDH1*, *VIM*, *FN1*, and *CDH2* and low expression of *CD24* and *CDH1* [326,327].

The approach chosen in this study is limited by basing the classification of "EMT-related" genes and respective proteins by comparing the RNA-seq data with the EMTome database. Despite the size and pan-cancer scope of this database, some DEGs that are not listed in the database, may still be relevant for EMT and cancer-stemness. For example, the expression of *KRT23* and *KRT6A* was increased in the resistant CTC-ITB-01 cells but the encoded proteins were not listed in the EMTome database. Both genes were demonstrated to promote EMT in ovarian cancer and lung adenocarcinoma, respectively [188,328]. Moreover, some EMT-associated genes/proteins described in the literature can act both as EMT inducers or suppressors dependent of the biological context even in the same tumor entity [171,198,200].

In conclusion, EMT and gain of mesenchymal and/or CSC features are usually associated with worse patient outcome [246,310]. Thus, unraveling the specific mechanisms or signaling pathways inducing or suppressing EMT is crucial to identify druggable targets to prevent or reverse this momentous biological program. A potentially druggable target is the tyrosine receptor kinase AXL [329], whose expression was upregulated in resistant MCF7 cells, as it promotes EMT and CSCs phenotypes [330]. There are even kinase inhibitors targeting AXL and LYN in combination, thereby blocking migration of triple negative breast cancer cells [331]. Both in ribociclib-resistant CTC-ITB-01 and MCF7 cells mRNA expression of *LYN* was higher than in the sensitive parental cells, whereas *AXL* expression was exclusively increased in resistant MCF7 cells.

Targeting EMT-specific metabolic changes represents another therapeutic approach that is under clinical investigation [332]. Furthermore, targeting transcription factors also is a potential therapeutic approach, but only a small proportion (0.7%) of the human TFs is druggable [240]. For none of the TFs with calculated increased activity, a drug exists so far [239,241]. However, despite not being therapeutically targetable currently, the identification and analysis of these TF-regulons may unravel mechanisms conveying CDK4/6i resistance

4.4 Changes of adhesive capacity of ribociclib-resistant cells

GO enriched pathways related to cell adhesion and cell-junction organization were found in both resistant cell lines, suggesting a correlation of ribociclib resistance and these pathways. This is of particular interest for the characterization of cancer cells, since alterations of the expression of their adhesion molecules can influence their potential to form metastasis. Here, a distinction must be made between proteins that convey epithelial cell-cell interactions and those that convey binding of epithelial to endothelial cells. Cell adhesion molecules (CAMs) are divided into subgroups, namely the immunoglobulin like superfamily, including mucins, cadherins, selectins and integrins. The latter type of proteins mainly regulates interactions of cells with the extracellular matrix (ECM) whereas the others are involved in cell-cell adhesion [333]. Loss of epithelial cell-cell junctions in the primary tumor is an important step within the metastatic cascade, to allow cells to migrate [334]. Often, suppression of E-cadherin and thus loss of adherens junctions is a consequence of EMT-induction. Loss of adherens junctions is frequently accompanied by disappearance of the other two epithelial junctions, tight junctions and desmosomes [335]. Simultaneously, cells must gain the ability to interact and adhere to endothelial cells, in order to bind to the vascular wall and extravasate into peripheral tissue [336]. Strong adhesion to endothelial cells could therefore imply a high potential to metastasize. E-cadherin is not differentially expressed by neither cell line according to RNA-seq data. However, *CLDN1* encoding claudin1, an important component of tight junctions, was upregulated in resistant CTC-ITB-01 cells and downregulated in resistant MCF7 cells. Both alterations have been reported for different tumor entities and were associated with worse prognosis [200]. Expression of *DSC2*, coding for the desmosome protein desmocollin 2, was strongly reduced in both resistant cell lines established in this study. Desmocollin 2 is not well-studied in breast cancer yet, but the failure to detect it was shown to correlate with shorter OS of patients with pancreatic cancer [337] and could stimulate increased cell motility in esophageal cancer cells [338]. Notably, *in vitro* experiments demonstrated a negative regulation of *DCS2* expression by the androgen receptor (AR) [213], a transcription factor that is significantly higher expressed in resistant than parental CTC-ITB-01 cells at the transcriptional level, implying the presence of a potential regulatory network. Galectin 1, a S-type lectin, was shown to indirectly bind E-selectin, a protein often expressed by endothelial cells [339], and its expression was increased in resistant CTC-ITB-01 cells. On the other hand, galectin 9, significantly suppressed in resistant MCF7 cells, bears anti-metastatic potential due to reducing adhesion of cells to the ECM, as demonstrated on an *in vitro* model [340]. Furthermore, *MUC13* mRNA was significantly higher expressed by resistant than parental CTC-ITB-01 cells. As mentioned previously, mucin 13 is not a well-studied CAM in breast cancer, but mucins in general are overexpressed by a variety of cancer entities and are involved in a multitude of biological functions. Mucins can also interact with ICAM-1, thereby conveying adhesion to VCAM-expressing cells [341]. In the present study, resistant MCF7 cells, *MUC1* mRNA was significantly upregulated (log2FC=3.41). The encoded protein is overexpressed by more than 90% of breast tumors and can stimulate PI3K- and WNT-signaling and was even shown to disrupt adherens junctions [342,343]. Furthermore, transmembranous mucins, mucin 13 belongs to, can also trigger EMT-induction by stimulating WNT-signaling [342]. In addition, transcripts coding for CAMs like integrin α1 and α2b, integrin β8, ICAM-1 and -4, L1CAM, and PECAM1 were found increased or decreased, amongst others, in resistant CTC-ITB-01 cells. In resistant MCF7 cells, the expression of genes coding for ALCAM1 as well as claudin 9 and 11 was deregulated. In summary,

these alterations suggest a change of the adhesion capacity of these cells, losing epithelial cell-cell contacts but gaining the ability to interact with e.g. endothelial cells.

The adhesion of cancer cells to HUVECs was tested in a BioFlux system, facilitating the visualization of adhesion of the epithelial cancer cell line cells to the endothelial HUVECs. Strikingly, CTC-ITB-01 cells were exceptionally adhesive to the endothelial cells (Wang et al. under revision) compared to MCF7 and MDA-MB-231 cells, suggesting potentially high metastatic capacity. The capacity of this cell line to form metastases was demonstrated previously in a mouse xenograft model [118]. Due to the alterations of a multitude of adhesion-related proteins, the adhesion of parental versus resistant CTC-ITB-01 and MCF7 cells was tested. Unexpectedly, the number of resistant CTC-ITB-01 cells able to adhere to HUVECs was lower than that of the parental cells, but the number of resistant versus parental adherent MCF7 cells increased. As the staining of heparan sulfate provided an explanation for the strong adhesion of the parental CTC-ITB-01 cells, this experiments now need to be repeated to investigate potential changes of cell-surface heparan sulfate proteoglycans. Biosynthesis of heparan sulfate is a multi-step process, and several proteins involved in this process, are dysregulated in both resistant cell lines, potentially resulting in altered heparan sulfate abundance [344]. In resistant CTC-ITB-01 cells, a significant reduction of GLCE expression, encoding glucoronyl C5 epimerase, was observed. This enzyme catalyzes a key step in the heparan sulfate biosynthesis, regulating structure and function of heparan sulfate [345]. Altered heparan sulfate modification might also compensate for the significant increase of *HS6ST3* expression, found in both resistant cell lines by RNA-seq. This gene encodes a sulfotransferase, also regulating modifications of heparan sulfate. Furthermore, changes in the expression of core proteins of heparan sulfate proteoglycans were found in resistant CTC-ITB-01 cells. While *GPC4* levels, encoding glypican 4 were significantly increased, *COL18A1* levels, encoding collagen 18 A1, were significantly decreased. However, also in the resistant MCF7 cells, *COL18A1* expression was significantly downregulated, but *GPC6* (glypican 6) expression was significantly increased. Additionally, three 3-O-sulfotransferase isoforms were higher expressed resistant versus parental MCF7 cells. Overall, these changes led us to suggest that heparan sulfate abundance but also modifications may be different in resistant and parental cell lines which needs to be confirmed by further investigation. Alterations of heparan sulfate modifications have already been demonstrated to have major impact on cell signaling and tumorigenesis [344]. Moreover, to unravel specific CAMs conveying the adhesion of the tumor cells to HUVECs, the experiment will be repeated, adding antibodies specific for CAMs, to prevent intervention with HUVEC cells. This might support unraveling potential intervention therapies [333].

4.5 Impact of ribociclib resistance on sensitivity to endocrine therapy and PI3Kα inhibition

After progression on CDK4/6i therapy due to emerging resistance, other therapy options have to be found. Thus, it was first investigated whether ribociclib resistance could impair susceptibility to endocrine therapy and whether the addition of fulvestrant could enhance the inhibitory efficacy of ribociclib. Fulvestrant in combination with riboiciclib did not affect the viability of neither the parental nor the resistant CTC-ITB-01 cells and barely enhanced the effect of sole ribociclib treatment, whereas this drug combination moderately reduced the viability of parental and resistant

MCF7 cells. This is completely concordant with results of a published study, demonstrating that the CTC-ITB-01 cell line is refractory to fulvestrant treatment [119]. In the present study the formation of colonies, however, could be strongly suppressed by the combination of fulvestrant and ribociclib. Yet, ribociclib-resistant CTC-ITB-01 and MCF7 cells were slightly less susceptible to the dual inhibition at lower concentrations of fulvestrant. Differences between resistant and parental derivates were only diminished at the highest concentration of fulvestrant that was tested in these experiments.

Although the metastatic breast cancer patient the cell line is derived from, was not treated with fulvestrant, she received therapy with letrozole and tamoxifen, probably resulting in high endocrine resistance at this time point [118]. However, still ERα-dependent growth was shown by two different studies [118,119].

Therefore, the overall strong reduction of clonogenic growth of the parental CTC-ITB-01 cells, resistant to endocrine treatment and the ribociclib-resistant cell line in particular, was not expected.

Evaluation of the β-galactosidase activity upon combined fulvestrant and ribociclib treatment did not results in differences compared to the DMSO control in neither parental nor resistant CTC-ITB-01 cells. Thus, it is possible that despite transcriptional changes, alterations of protein level and gain of specific mutations induced by long-term exposure to 1.5 μM ribociclib, a higher concentration has to be chosen for functional assays to achieve a stronger response of the cells.

Notably, induction of senescence by CDK4/6 inhibition is deemed a relevant event for the therapeutic efficacy in treated cells [167] but was not observed in the CTC-ITB-01 cells upon any treatment tested in this study. Senescence describes the irreversible arrest in the G1-phase, opposed to quiescence, which is reversible. However, other factors may influence the induction of senescence in cancer cells. For example, reduction of murine double minute 2 (MDM2) and HRAS levels was shown to be a requirement for inducing senescence in cells treated with an CDK4/6 inhibitor, but not quiescence in liposarcoma cell lines [346]. Since ribociclib treatment inhibited cell cycle progression in the parental CTC-ITB-01 cells but did not result in any detectable β-galactosidase activity, CTC-ITB-01 cells likely induce the more unstable quiescent state, a characteristic property of stem cells, upon CDK4/6 inhibition instead of the senescent one, which was observed in resistant MCF7 cells, indicated by increased X-gal staining. Intriguingly, fulvestrant increases the turnover rate of the MDM2 protein and thereby reduces its cellular levels [347], which should result in increased induction of senescence upon dual inhibition of the CTC-ITB-01 cells. But also the concomitant treatment of ribociclib with fulvestrant did not induce noticeable senescence. CDK4/6i-induced senescence could be further exploited therapeutically by specifically targeting senescent cells with so-called senolytics, for example inhibitors of the BCL2 family [167].

In MCF7 cells, the addition of fulvestrant to ribociclib cooperated additively in inhibiting cell viability of parental and resistant cells. Interestingly, in two out of three experiments the response of the resistant and parental cells differed slightly, independently of the ribociclib concentration, showing slightly lower efficacy of this treatment scheme on resistant MCF7 at the tested concentrations. This observation could be explained by decreased dependency on ER signaling of the ribociclib-resistant MCF7 cells, as demonstrated on abemaciclib and ribociclib-resistant MCF7 cells [256]. The same effect was observed in the colony formation assay. Although dual inhibition completely abrogated colony formation already at lowest concentrations, the efficacy was slightly

lower in resistant MCF7 cells. Summarized, these results imply a weak, yet notable cross-resistance to ribociclib and endocrine therapy. Nonetheless, ribociclib and simultaneous fulvestrant treatment was not suitable to reduce viability of ribociclib-resistant CTC-ITB-01 and MCF7 cells sufficiently. However, this drug combination represents a highly efficient treatment combination to inhibit clonogenic growth of luminal A and B cancer cells, also in cells that have developed resistance to ribociclib and/or endocrine treatment (CTC-ITB-01 cells). Clinical trials testing this treatment combination on cohorts of HR+ mBC patients progressing on various CDK4/6 based therapies are ongoing [348].

Inhibitors of the kinase PI3Kα have also been proposed to be promising for the treatment of CDK4/6i-resistant patients and are currently under investigation in a phase II clinical study [234,348]. Cell culture models had confirmed the efficacy of PI3Kα inhibition in abemaciclib and ribociclib-resistant breast cancer cells [232,256]. Strikingly, ribociclib was shown to re-sensitize PI3K inhibitor-resistant cells to alpelisib [72], whereas PI3K inhibition failed to re-sensitize CDK4/6i-resistant cells to a respective inhibitor [64]. In contrast to that, inhibition of PDK1 upstream of PI3K could re-sensitize ribociclib-resistant luminal A breast cancer cell lines to CDK4/6i treatment [66]. All cell lines, parental and resistant ones were nearly equally sensitive to the treatment with alpelisib. In line with that, combined treatment with alpelisib and ribociclib, synergistically reduced viability. Additionally, differences between parental and resistant cells, observed in experiments using only ribociclib, were abolished, indeed confirming that also in our cell culture model inhibition of PI3K activity helped to partially overcome ribociclib resistance.

Other therapeutic approaches to overcome CDK4/6i resistance that have been tested successfully in experimental studies were targeting CDK2 [67], aberrant FGFR signaling [349] and application of degraders of the CDK6/Ink-protein complex [350]. These are also very important approaches that can be applied to ribociclib-resistant CTC-ITB-01 and MCF7 cells in future experiments. CTC-ITB-01 cells generally have higher CDK6 levels than MCF7 cells. $P15^{INK4C}$, encoded by the *CDKN2B* gene, associates specifically with CDK6 but not CDK4, and was identified to mediate resistance to CDK4/6 inhibitors, perhaps by preventing binding of CDK4/6 inhibitors to the kinase complex. Levels of *CDKN2B* mRNA were even increased in resistant versus parental CTC-ITB-01 cells, representing a potential resistance mechanism. Furthermore, the expression of several kinase encoding genes was increased in both resistant cell lines. If protein levels and activities of these kinases are also associated with resistance to ribociclib, they might represent potentially druggable targets.

Summarized, the multitude of changes on protein levels, miRNAs, transcription factors and signaling pathways introduced by chronic exposure to a CDK4/6 inhibitor represents also a multitude of potentially druggable targets. However, whether these approaches are clinically relevant, needs to be elucidated within the next years.

4.6 Detection of potential drivers of ribociclib resistance by Western blot analysis and immunofluorescent staining

Levels of CDK6 protein are frequently increased in breast cancer cell lines resistant to CDK4/6 inhibitors [132]. Amplification of the *CDK6* gene leading to aberrant expression is discussed as

mechanism of resistance [53] and was therefore tested in clinical studies [351]. However, in the PALMOA-3 study that enrolled 521 patients with advanced HR+ breast cancer, the prognostic power of *CDK6* mRNA detection was limited to a subpopulation with bone-only metastasis [352]. Other studies were not successful, perhaps due to large variation in absolute CDK6 levels in different breast cancer subtypes, albeit induction in resistant cells [252,353], which might also be the case for SOX9 and CDK14. Therefore, the levels of CDK6, CDK14 and SOX9 were assessed by Western blot analysis in a panel of breast cancer cell lines of different molecular subtypes. This experiment confirmed very heterogeneous abundance of all three proteins in the selected cell lines but protein levels did not correlate with the molecular subytpes. Nonetheless, the detection of these proteins by IF staining was tested next.

Indeed, IF staining demonstrated clear differentiation between SOX9^{high} CTC-ITB-01 cells and SOX9^{low} MCF7 cells and showed the expected increase of SOX9 levels in the resistant versus parental CTC-ITB-01 and MCF7 cells. As the analysis of SOX9 expression in the resistant and parental cell lines provided encouraging results in both cell lines, first attempts were made to detect SOX9 on cells enriched by the CellSearch® system.

Likewise, CDK14 was detected by IF staining which visualized the difference of CDK14^{high} CTC-ITB-01 cells and CDK14^{low} MCF7 as well as the increase of CDK14 levels in the resistant compared to parental CTC-ITB-01 cells. Yet, the immunostaining will have to be improved to guarantee reliable distinguishment of CDK14^{low} versus CDK14^{high} levels. So far, little is known about the putative function of CDK14 in the context of CDK4/6i resistance, thus being an interesting candidate for further research.

Additionally, changes of miRNA profiles in ribociclib-resistant cell lines were identified in this study. Due to successful implementation of the MISH assay that allows reliable detection of miRNAs on cell culture cells but also on CTCs of patient samples, enriched by various methods, also miRNAs can be investigated as potential biomarker of CDK4/6i resistance. Since this assay also facilitates the detection of other RNA species, also lncRNAs and mRNAs could be discovered.

Detection of CDK6 by IF staining could be used to discriminate between CDK6^{low} MCF7 and CDK6^{high} CTC-ITB-01 cells and could even visualize the increase of CDK6 levels in resistant versus parental MCF7 cell. Yet, first attempts to detect CDK6 on cells enriched by the CellSearch® system failed.

4.7 Ongoing search for liquid biopsy markers indicating CDK4/6i resistance in patients with hormone receptor-positive metastatic breast cancer

Due to the inevitability of the emergence of CDK4/6i resistance and the complexity of resistance mechanisms, finding surrogate markers to monitor response to CDK4/6i therapy is of great importance. The diverse changes of the expression profiles of resistant cells identified in this study, as well as related signaling pathways, do not only pave the way to search for potentially novel druggable targets but could also be used to identify potential biomarkers indicating resistance development in patients. EMT was a major pathway found to be induced in both resistant cell lines of this study and vimentin is a commonly used marker indicating EMT-like changes in cancer cells.

To find out whether characterization of CTCs from mBC patients enriched by the CellSearch® system might help to identify patients who had developed resistance to CDK4/6i therapy, CTCs were analyzed for vimentin expression. Vimentin expression determined on tissue biopsies was suggested as a biomarker to predict endocrine treatment outcome [354]. Despite that, only a low number of studies reporting vimentin expression in breast cancer CTCs is published. For patients with metastatic castration-resistant prostate cancer, vimentin-positive CTCs detected by the CellSearch® system were associated with a poorer outcome than vimentin-negative CTCs [2].

Indeed, vimentin expression was detected in CTCs from 67 patients (33.3%) while 134 patients (66.7%) had only vimentin-negative CTCs. Not unexpectedly, vimentin-positive CTCs were more frequently found in TNBC patients than in patients with HR-positive tumors. Prior to CTC analyses, the mBC patients received several lines of different therapies, including also HR+ mBC patients who were treated with CDK4/6 inhibitors. However, there was no association of including this particular treatment or not and the percentage of vimentin-positive CTCs in HR+ mBC patients. For future studies, detection of vimentin expression of CTCs should be included in clinical studies under comparable therapeutic regimens.

5 Conclusion and Outlook

Despite the high percentage of patients developing resistant to CDK4/6i therapy, suitable and powerful biomarkers for the monitoring of disease response are still lacking. The search for such biomarkers is hampered by the lack of knowledge about the molecular background of resistance to certain drugs observed clinically [252]. Therefore, this thesis aimed to unravel new potential mechanisms driving ribociclib resistance.

RNA-seq of resistant versus parental CTC-ITB-01 and MCF7 cells was used to identify changes regarding the expression of mRNAs and miRNAs induced by long-time exposure to the CDK4/6 inhibitor ribociclib. Except for finding differentially expressed genes encoding proteins regulating the cell cycle, such as *CDK6* in the resistant MCF7 cells and *CDK14* and *CDKN2B* in the resistant CTC-ITB-01 cells, also changes in the expression of genes coding for EMT-related proteins were identified. Furthermore, we observed several changes in the mRNA and miRNA profile of the cells, indicating gains of EMT and stemness traits in the resistant cell lines. In resistant MCF7 cells, *SOX9* out of several SOX-genes with increased expression, was the one with the highest fold change, and was hypothesized to cooperate with *SOX2*, also increased at the transcriptional level and the EMT-transcription factor SLUG. For SLUG, an increased transcriptional activity was predicted based on the differentially expressed genes between resistant and parental MCF7 cells. Increased expression of genes encoding EMT- and stemness-related genes was also observed in resistant CTC-ITB-01 cells, e.g. strong upregulation of *ALDH1* and a marked decrease of the level of miR-205-5p, known to negatively regulate EMT [327]. CDK14 has been functionally associated with the canonical WNT-signaling and was shown to phosphorylate the actin-binding protein caldesmon 1, thereby influencing cell cytoskeleton composition and cell migration. As it is also predicted to be a direct target of miR-205-5p, *CDK14* expression level and activity could not only influence cell cycle progression but also the EMT-program in resistant CTC-ITB-01 cells. Therefore, the relevance of increased *SOX9* expression in resistant MCF7 cells and elevated *CDK14* expression in resistant CTC-ITB-01 will be the main objective of further research. The hypotheses that these proteins contribute to ribociclib resistance will have to be proven experimentally by either knock down/out experiments or treatment of the cells with respective inhibitors. Beyond that, resistant cells are currently cultured without ribociclib to investigate the reversibility of the observed changes. The induction of an EMT phenotype and increased cancer-stemness will likewise have to be confirmed experimentally. Activation of the EMT program usually is accompanied by increased cell motility. Thus, migration and invasion assays will be performed. Moreover, it would be important to target EMT, for example by targeting the WNT-signaling pathway in resistant MCF7 cells, to test whether this would resensitize these cells to treatment with ribociclib, demonstrating whether EMT is contributing to ribociclib resistance or a consequence of unhindered growth and addiction to ribociclib.

In this study, eight kinase encoding genes were found to be deregulated in both MCF7 and CTC-ITB-01 cells resistant to ribociclib compared to the respective parental cell lines, among them DCLK1 and LYN, known to be associated with EMT [181,238] . Thus, experiments to influence and target the activity of these kinases are planned in order to overcome the CDK4/6i resistance and to eventually potentiate therapeutic efficacy of combined treatments.

RNA-seq analysis revealed higher expression of microRNA-146a-5p in both ribociclib-resistant than in the parental cell lines. Thus, from the spectrum of deregulated miRNAs in the context of ribociclib resistance, this miRNA and miRNA-205-5p mentioned above were selected for further experiments using miRNA mimics and inhibitors to study the effects on sensitivity to CDK4/6i, EMT, stemness and adhesion.

The changes of the expression profiles of cell adhesion molecules that were observed in both resistant cell lines also warrant further research. BioFlux experiments demonstrated altered adhesive capacity of the resistant cell lines in comparison to that of their respective parental counterparts. While ribociclib resistance reduced the adhesion of CTC-ITB-01 cells to HUVECs, in MCF7 cells adhesion was increased. The functional explanation for this observation is missing hitherto. First, CAMs, conveying the adhesion of the cancer cells to HUVECs must be identified by specific blockage of CAMs with specific antibodies during these experiments, e.g., ICAM in CTC-ITB-01 cells and ALCAM in MCF7 cells Furthermore, it would be interesting to evaluate, whether the changes in motility and adhesion, induced by ribociclib resistance, influence the metastatic capacity and behavior of these cells in a murine model.

Moreover, IF staining for the detection of SOX9 and CDK14 needs to be optimized and the utility of implementation into the CellSearch® based characterization of CTCs will be tested. The possibility to detect potential markers of resistance by liquid biopsy bears great advantage over examination of only tissue samples, which are less accessible and available. Furthermore, other miRNAs, as well as lncRNAs and circRNAs that were differentially expressed in the resistant cells will be further investigated and their utility as biomarker of resistant CTCs will be evaluated by analyzing clinical liquid biopsy samples collected from breast cancer patients.

References

1. B. O'Leary, R.J. Cutts, Y. Liu, et al. The genetic landscape and clonal evolution of breast cancer resistance to palbociclib plus fulvestrant in the PALOMA-3 trial. *Cancer Discov.* **2018**, 8 (11), 1390–1403.
2. C.R. Lindsay, S. Le Moulec, F. Billiot, et al. Vimentin and Ki67 expression in circulating tumour cells derived from castrate-resistant prostate cancer. *BMC Cancer* **2016**, 16, 168.
3. GLOBOCAN 2020: New Global Cancer Data | UICC https://www.uicc.org/news/globocan-2020-new-global-cancer-data (accessed Aug 4, 2021).
4. Cancer of the Breast (Female) - Cancer Stat Facts https://seer.cancer.gov/statfacts/html/breast.html (accessed Aug 4, 2021).
5. BRCA Gene Mutations: Cancer Risk and Genetic Testing Fact Sheet - National Cancer Institute https://www.cancer.gov/about-cancer/causes-prevention/genetics/brca-fact-sheet (accessed Aug 4, 2021).
6. Invasive Breast Cancer (IDC/ILC) | Types of Invasive Breast Carcinoma https://www.cancer.org/cancer/breast-cancer/about/types-of-breast-cancer/invasive-breast-cancer.html (accessed Aug 4, 2021).
7. H.J.G. Bloom, W.W. Richardson. Histological Grading and Prognosis in Breast Cancer. *Br. J. Cancer* **1957**, 11 (3), 359–377.
8. C.M. Perou, T. Sørlie, M.B. Eisen, et al. Molecular portraits of human breast tumours. *Nature* **2000**, 406 (6797), 747–752.
9. T. Sørlie, C.M. Perou, R. Tibshirani, et al. Gene expression patterns of breast carcinomas distinguish tumor subclasses with clinical implications. *Proc. Natl. Acad. Sci.* **2001**, 98 (19), 10869–10874.
10. P. Wirapati, C. Sotiriou, S. Kunkel, et al. Meta-analysis of gene expression profiles in breast cancer: toward a unified understanding of breast cancer subtyping and prognosis signatures. *Breast Cancer Res.* **2008**, 10 (4), R65.
11. T. Sørlie, R. Tibshirani, J. Parker, et al. Repeated observation of breast tumor subtypes in independent gene expression data sets. *Proc. Natl. Acad. Sci.* **2003**, 100 (14), 8418–8423.
12. C. Fougner, H. Bergholtz, J.H. Norum, T. Sørlie. Re-definition of claudin-low as a breast cancer phenotype. *Nat. Commun.* **2020**, 11 (1), 1787.
13. N. Harbeck, M. Gnant. Breast cancer. *The Lancet* **2017**, 389 (10074), 1134–1150.
14. D.C. Koboldt, R.S. Fulton, M.D. McLellan, et al. Comprehensive molecular portraits of human breast tumours. *Nature* **2012**, 490 (7418), 61–70.
15. X. Dai, T. Li, Z. Bai, et al. Breast cancer intrinsic subtype classification, clinical use and future trends. *Am. J. Cancer Res.* **2015**, 5 (10), 2929–2943.
16. G.N. Hortobagyi, J.L. Connolly, C.J. D'Orsi, et al. Breast. In *AJCC Cancer Staging Manual*; Amin, M. B., Edge, S. B., Greene, F. L., Byrd, D. R., Brookland, R. K., Washington, M. K., Gershenwald, J. E., Compton, C. C., Hess, K. R., Sullivan, D. C., et al., Eds.; Springer International Publishing, Cham, **2017**; pp 589–636.
17. J. Koh, M.J. Kim. Introduction of a New Staging System of Breast Cancer for Radiologists: An Emphasis on the Prognostic Stage. *Korean J. Radiol.* **2019**, 20 (1), 69–82.
18. Y. Feng, M. Spezia, S. Huang, et al. Breast cancer development and progression: Risk factors, cancer stem cells, signaling pathways, genomics, and molecular pathogenesis. *Genes Dis.* **2018**, 5 (2), 77–106.
19. M.C.U. Cheang, S.K. Chia, D. Voduc, et al. Ki67 Index, HER2 Status, and Prognosis of Patients With Luminal B Breast Cancer. *JNCI J. Natl. Cancer Inst.* **2009**, 101 (10), 736–750.
20. V. Zelli, C. Compagnoni, R. Capelli, et al. Circulating MicroRNAs as Prognostic and Therapeutic Biomarkers in Breast Cancer Molecular Subtypes. *J. Pers. Med.* **2020**, 10 (3), 98.
21. A.G. Waks, E.P. Winer. Breast Cancer Treatment: A Review. *JAMA* **2019**, 321 (3), 288–300.
22. N. Howlader, S.F. Altekruse, C.I. Li, et al. US Incidence of Breast Cancer Subtypes Defined by Joint Hormone Receptor and HER2 Status. *JNCI J. Natl. Cancer Inst.* **2014**, 106 (5).

23. M.J. Piccart-Gebhart, M. Procter, B. Leyland-Jones, et al. Trastuzumab after Adjuvant Chemotherapy in HER2-Positive Breast Cancer https://www.nejm.org/doi/10.1056/NEJMoa052306 (accessed Aug 17, 2021).
24. S.M. Swain, J. Baselga, S.-B. Kim, et al. Pertuzumab, Trastuzumab, and Docetaxel in HER2-Positive Metastatic Breast Cancer. *N. Engl. J. Med.* **2015**, 372 (8), 724–734.
25. W.D. Foulkes, I.E. Smith, J.S. Reis-Filho. Triple-Negative Breast Cancer https://www.nejm.org/doi/10.1056/NEJMra1001389 (accessed Aug 17, 2021).
26. K.E. McCann, S.A. Hurvitz, N. McAndrew. Advances in Targeted Therapies for Triple-Negative Breast Cancer. *Drugs* **2019**, 79 (11), 1217–1230.
27. H. Joshi, M.F. Press. 22 - Molecular Oncology of Breast Cancer. In *The Breast (Fifth Edition)*; Bland, K. I., Copeland, E. M., Klimberg, V. S., Gradishar, W. J., Eds.; Elsevier, **2018**; pp 282-307.e5.
28. W.-J. Welboren, F.C.G.J. Sweep, P.N. Span, H.G. Stunnenberg. Genomic actions of estrogen receptor α: what are the targets and how are they regulated? *Endocr. Relat. Cancer* **2009**, 16 (4), 1073–1089.
29. Early Breast Cancer Trialists' Collaborative Group (EBCTCG). Relevance of breast cancer hormone receptors and other factors to the efficacy of adjuvant tamoxifen: patient-level meta-analysis of randomised trials. *The Lancet* **2011**, 378 (9793), 771–784.
30. Y. Hong, R. Rashid, S. Chen. Binding features of steroidal and nonsteroidal inhibitors. *Steroids* **2011**, 76 (8), 802–806.
31. C. Criscitiello, D. Fumagalli, K.S. Saini, S. Loi. Tamoxifen in early-stage estrogen receptor-positive breast cancer: overview of clinical use and molecular biomarkers for patient selection. *OncoTargets Ther.* **2010**, 4, 1–11.
32. J. Anampa, D. Makower, J.A. Sparano. Progress in adjuvant chemotherapy for breast cancer: an overview. *BMC Med.* **2015**, 13, 195.
33. H. Pan, R. Gray, J. Braybrooke, et al. 20-Year Risks of Breast-Cancer Recurrence after Stopping Endocrine Therapy at 5 Years https://www.nejm.org/doi/10.1056/NEJMoa1701830 (accessed Aug 9, 2021).
34. F.A. Fisusi, E.O. Akala. Drug Combinations in Breast Cancer Therapy. *Pharm. Nanotechnol.* **2019**, 7 (3), 3–23.
35. E. Ciruelos, T. Pascual, M.L. Arroyo Vozmediano, et al. The therapeutic role of fulvestrant in the management of patients with hormone receptor-positive breast cancer. *The Breast* **2014**, 23 (3), 201–208.
36. A.B. Hanker, D.R. Sudhan, C.L. Arteaga. Overcoming Endocrine Resistance in Breast Cancer. *Cancer Cell* **2020**, 37 (4), 496–513.
37. M. Piezzo, P. Chiodini, M. Riemma, et al. Progression-Free Survival and Overall Survival of CDK 4/6 Inhibitors Plus Endocrine Therapy in Metastatic Breast Cancer: A Systematic Review and Meta-Analysis. *Int. J. Mol. Sci.* **2020**, 21 (17), 6400.
38. L.M. Spring, S.A. Wander, M. Zangardi, A. Bardia. CDK 4/6 Inhibitors in Breast Cancer: Current Controversies and Future Directions. *Curr. Oncol. Rep.* **2019**, 21 (3), 25.
39. D. Kwapisz. Cyclin-dependent kinase 4/6 inhibitors in breast cancer: palbociclib, ribociclib, and abemaciclib. *Breast Cancer Res. Treat.* **2017**, 166 (1), 41–54.
40. J.J. Gao, J. Cheng, E. Bloomquist, et al. CDK4/6 inhibitor treatment for patients with hormone receptor-positive, HER2-negative, advanced or metastatic breast cancer: a US Food and Drug Administration pooled analysis. *Lancet Oncol.* **2020**, 21 (2), 250–260.
41. J.C. Sachdev, A.C. Sandoval, M. Jahanzeb. Update on Precision Medicine in Breast Cancer. In *Precision Medicine in Cancer Therapy*; Von Hoff, D. D., Han, H., Eds.; Cancer Treatment and Research; Springer International Publishing, Cham, **2019**; pp 45–80.
42. U. Asghar, A.K. Witkiewicz, N.C. Turner, E.S. Knudsen. The history and future of targeting cyclin-dependent kinases in cancer therapy. *Nat. Rev. Drug Discov.* **2015**, 14 (2), 130–146.

43. J.L. Dean, C. Thangavel, A.K. McClendon, C.A. Reed, E.S. Knudsen. Therapeutic CDK4/6 inhibition in breast cancer: key mechanisms of response and failure. *Oncogene* **2010**, 29 (28), 4018–4032.
44. S.P. Gampenrieder, G. Rinnerthaler, R. Greil. CDK4/6 inhibition in luminal breast cancer. *Memo - Mag. Eur. Med. Oncol.* **2016**, 9 (2), 76–81.
45. D.K. Dimova, N.J. Dyson. The E2F transcriptional network: old acquaintances with new faces. *Oncogene* **2005**, 24 (17), 2810–2826.
46. R.S. Finn, J. Dering, D. Conklin, et al. PD 0332991, a selective cyclin D kinase 4/6 inhibitor, preferentially inhibits proliferation of luminal estrogen receptor-positive human breast cancer cell lines in vitro. *Breast Cancer Res.* **2009**, 11 (5), R77.
47. Y. Ishii, S. Waxman, D. Germain. Tamoxifen Stimulates the Growth of Cyclin D1–Overexpressing Breast Cancer Cells by Promoting the Activation of Signal Transducer and Activator of Transcription 3. *Cancer Res.* **2008**, 68 (3), 852–860.
48. R. Hui, G.L. Finney, J.S. Carroll, et al. Constitutive Overexpression of Cyclin D1 but not Cyclin E Confers Acute Resistance to Antiestrogens in T-47D Breast Cancer Cells. *Cancer Res.* **2002**, 62 (23), 6916–6923.
49. K. Jirström, M. Stendahl, L. Rydén, et al. Adverse Effect of Adjuvant Tamoxifen in Premenopausal Breast Cancer with Cyclin D1 Gene Amplification. *Cancer Res.* **2005**, 65 (17), 8009–8016.
50. C.K. Osborne, R. Schiff. MECHANISMS OF ENDOCRINE RESISTANCE IN BREAST CANCER. *Annu. Rev. Med.* **2011**, 62, 233–247.
51. R.S. Finn, J.P. Crown, I. Lang, et al. The cyclin-dependent kinase 4/6 inhibitor palbociclib in combination with letrozole versus letrozole alone as first-line treatment of oestrogen receptor-positive, HER2-negative, advanced breast cancer (PALOMA-1/TRIO-18): a randomised phase 2 study. *Lancet Oncol.* **2015**, 16 (1), 25–35.
52. E.S. Knudsen, G.I. Shapiro, K. Keyomarsi. Selective CDK4/6 Inhibitors: Biologic Outcomes, Determinants of Sensitivity, Mechanisms of Resistance, Combinatorial Approaches, and Pharmacodynamic Biomarkers. *Am. Soc. Clin. Oncol. Educ. Book* **2020**, No. 40, 115–126.
53. C. Yang, Z. Li, T. Bhatt, et al. Acquired CDK6 amplification promotes breast cancer resistance to CDK4/6 inhibitors and loss of ER signaling and dependence. *Oncogene* **2017**, 36 (16), 2255–2264.
54. M. Ono, T. Oba, T. Shibata, K. Ito. The mechanisms involved in the resistance of estrogen receptor-positive breast cancer cells to palbociclib are multiple and change over time. *J. Cancer Res. Clin. Oncol.* **2021**.
55. N. Portman, S. Alexandrou, E. Carson, et al. Overcoming CDK4/6 inhibitor resistance in ER-positive breast cancer. *Endocr. Relat. Cancer* **2019**, 26 (1), R15–R30.
56. J. Wade Harper, G.R. Adami, N. Wei, K. Keyomarsi, S.J. Elledge. The p21 Cdk-interacting protein Cip1 is a potent inhibitor of G1 cyclin-dependent kinases. *Cell* **1993**, 75 (4), 805–816.
57. H. Toyoshima, T. Hunter. p27, a novel inhibitor of G1 cyclin-Cdk protein kinase activity, is related to p21. *Cell* **1994**, 78 (1), 67–74.
58. A.K. Witkiewicz, K.E. Knudsen, A.P. Dicker, E.S. Knudsen. The meaning of p16ink4a expression in tumors. *Cell Cycle* **2011**, 10 (15), 2497–2503.
59. G.E. Konecny, B. Winterhoff, T. Kolarova, et al. Expression of p16 and Retinoblastoma Determines Response to CDK4/6 Inhibition in Ovarian Cancer. *Clin. Cancer Res. Off. J. Am. Assoc. Cancer Res.* **2011**, 17 (6), 1591–1602.
60. A. DeMichele, A.S. Clark, K.S. Tan, et al. CDK 4/6 Inhibitor Palbociclib (PD0332991) in Rb+ Advanced Breast Cancer: Phase II Activity, Safety, and Predictive Biomarker Assessment. *Clin. Cancer Res.* **2015**, 21 (5), 995–1001.
61. R. Finn, Y. Jiang, H. Rugo, et al. LBA15 - Biomarker analyses from the phase 3 PALOMA-2 trial of palbociclib (P) with letrozole (L) compared with placebo (PLB) plus L in postmenopausal women with ER + /HER2– advanced breast cancer (ABC). *Ann. Oncol.* **2016**, 27, vi554.

62. K.R. Stengel, C. Thangavel, D.A. Solomon, et al. Retinoblastoma/p107/p130 Pocket Proteins: PROTEIN DYNAMICS AND INTERACTIONS WITH TARGET GENE PROMOTERS. *J. Biol. Chem.* **2009**, 284 (29), 19265–19271.
63. C. Guarducci, M. Bonechi, M. Benelli, et al. Cyclin E1 and Rb modulation as common events at time of resistance to palbociclib in hormone receptor-positive breast cancer. *Npj Breast Cancer* **2018**, 4 (1), 1–10.
64. M.T. Herrera-Abreu, M. Palafox, U. Asghar, et al. Early Adaptation and Acquired Resistance to CDK4/6 Inhibition in Estrogen Receptor–Positive Breast Cancer. *Cancer Res.* **2016**, 76 (8), 2301–2313.
65. L. Wang, J. Wang, B.W. Blaser, et al. Pharmacologic inhibition of CDK4/6: mechanistic evidence for selective activity or acquired resistance in acute myeloid leukemia. *Blood* **2007**, 110 (6), 2075–2083.
66. V.M. Jansen, N.E. Bhola, J.A. Bauer, et al. Kinome-wide RNA interference screen reveals a role for PDK1 in acquired resistance to CDK4/6 inhibition in ER-positive breast cancer. *Cancer Res.* **2017**, 77 (9), 2488–2499.
67. K. Pandey, N. Park, K.-S. Park, et al. Combined CDK2 and CDK4/6 Inhibition Overcomes Palbociclib Resistance in Breast Cancer by Enhancing Senescence. *Cancers* **2020**, 12 (12), 3566.
68. K. Pandey, H. An, S.K. Kim, et al. Molecular mechanisms of resistance to CDK4/6 inhibitors in breast cancer: A review. *Int. J. Cancer* **2019**, 145 (5), 1179–1188.
69. K. Kollmann, G. Heller, C. Schneckenleithner, et al. A Kinase-Independent Function of CDK6 Links the Cell Cycle to Tumor Angiogenesis. *Cancer Cell* **2013**, 24 (2), 167–181.
70. T.W. Miller, J.M. Balko, E.M. Fox, et al. ERα-dependent E2F transcription can mediate resistance to estrogen deprivation in human breast cancer. *Cancer Discov.* **2011**, 1 (4), 338–351.
71. C. Costa, Y. Wang, A. Ly, et al. PTEN Loss Mediates Clinical Cross-Resistance to CDK4/6 and PI3Kα Inhibitors in Breast Cancer. *Cancer Discov.* **2020**, 10 (1), 72–85.
72. S.R. Vora, D. Juric, N. Kim, et al. CDK 4/6 Inhibitors Sensitize PIK3CA Mutant Breast Cancer to PI3K Inhibitors. *Cancer Cell* **2014**, 26 (1), 136–149.
73. C. Michaloglou, C. Crafter, R. Siersbæk, et al. Combined inhibition of mTOR and CDK4/6 is required for optimal blockade of E2F function and long term growth inhibition in estrogen receptor positive breast cancer. *Mol. Cancer Ther.* **2018**, 17 (5), 908–920.
74. J. Xi, C.X. Ma. Sequencing Endocrine Therapy for Metastatic Breast Cancer: What Do We Do After Disease Progression on a CDK4/6 Inhibitor? *Curr. Oncol. Rep.* **2020**, 22 (6), 57.
75. M. Cristofanilli, N.C. Turner, I. Bondarenko, et al. Fulvestrant plus palbociclib versus fulvestrant plus placebo for treatment of hormone-receptor-positive, HER2-negative metastatic breast cancer that progressed on previous endocrine therapy (PALOMA-3): final analysis of the multicentre, double-blind, phase 3 randomised controlled trial. *Lancet Oncol.* **2016**, 17 (4), 425–439.
76. L. Formisano, Y. Lu, A. Servetto, et al. Aberrant FGFR signaling mediates resistance to CDK4/6 inhibitors in ER+ breast cancer. *Nat. Commun.* **2019**, 10, 1373.
77. F. Pesapane, M.B. Suter, A. Rotili, et al. Will traditional biopsy be substituted by radiomics and liquid biopsy for breast cancer diagnosis and characterisation? *Med. Oncol.* **2020**, 37 (4), 29.
78. M.A. Nieto, R.Y.-J. Huang, R.A. Jackson, J.P. Thiery. EMT: 2016. *Cell* **2016**, 166 (1), 21–45.
79. C.L. Chaffer, B.P. San Juan, E. Lim, R.A. Weinberg. EMT, cell plasticity and metastasis. *Cancer Metastasis Rev.* **2016**, 35 (4), 645–654.
80. I. Pastushenko, A. Brisebarre, A. Sifrim, et al. Identification of the tumour transition states occurring during EMT. *Nature* **2018**, 556 (7702), 463–468.
81. M. Yu, A. Bardia, B.S. Wittner, et al. Circulating Breast Tumor Cells Exhibit Dynamic Changes in Epithelial and Mesenchymal Composition. *Science* **2013**, 339 (6119), 580–584.
82. S.A. Joosse, T.M. Gorges, K. Pantel. Biology, detection, and clinical implications of circulating tumor cells. *EMBO Mol. Med.* **2015**, 7 (1), 1–11.
83. J. Fares, M.Y. Fares, H.H. Khachfe, H.A. Salhab, Y. Fares. Molecular principles of metastasis: a hallmark of cancer revisited. *Signal Transduct. Target. Ther.* **2020**, 5 (1), 1–17.

84. N. Aceto, A. Bardia, D.T. Miyamoto, et al. Circulating Tumor Cell Clusters Are Oligoclonal Precursors of Breast Cancer Metastasis. *Cell* **2014**, 158 (5), 1110–1122.
85. J. Massagué, A.C. Obenauf. Metastatic colonization by circulating tumour cells. *Nature* **2016**, 529 (7586), 298–306.
86. A. Hoshino, B. Costa-Silva, T.-L. Shen, et al. Tumour exosome integrins determine organotropic metastasis. *Nature* **2015**, 527 (7578), 329–335.
87. J.D. Hebert, S.A. Myers, A. Naba, et al. Proteomic Profiling of the ECM of Xenograft Breast Cancer Metastases in Different Organs Reveals Distinct Metastatic Niches. *Cancer Res.* **2020**, 80 (7), 1475–1485.
88. X. Lu, Y. Kang. Organotropism of Breast Cancer Metastasis. *J. Mammary Gland Biol. Neoplasia* **2007**, 12 (2), 153.
89. L. Gerratana, A.A. Davis, M. Polano, et al. Understanding the organ tropism of metastatic breast cancer through the combination of liquid biopsy tools. *Eur. J. Cancer* **2021**, 143, 147–157.
90. M. Ignatiadis, G.W. Sledge, S.S. Jeffrey. Liquid biopsy enters the clinic — implementation issues and future challenges. *Nat. Rev. Clin. Oncol.* **2021**, 18 (5), 297–312.
91. L. Cayrefourcq, C. Alix-Panabières. Clinical relevance of liquid biopsy in breast cancer: update in 2020. *Expert Rev. Mol. Diagn.* **2020**, 20 (9), 913–919.
92. C. Alix-Panabières, K. Pantel. Liquid Biopsy: From Discovery to Clinical Application. *Cancer Discov.* **2021**, 11 (4), 858–873.
93. I. Garcia-Murillas, G. Schiavon, B. Weigelt, et al. Mutation tracking in circulating tumor DNA predicts relapse in early breast cancer. *Sci. Transl. Med.* **2015**, 7 (302), 302ra133-302ra133.
94. K. Pantel, C. Alix-Panabières. Liquid biopsy and minimal residual disease — latest advances and implications for cure. *Nat. Rev. Clin. Oncol.* **2019**, 16 (7), 409–424.
95. H.A. Parsons, J. Rhoades, S.C. Reed, et al. Sensitive detection of minimal residual disease in patients treated for early-stage breast cancer. *Clin. Cancer Res. Off. J. Am. Assoc. Cancer Res.* **2020**, 26 (11), 2556–2564.
96. F.-C. Bidard, C. Proudhon, J.-Y. Pierga. Circulating tumor cells in breast cancer. *Mol. Oncol.* **2016**, 10 (3), 418–430.
97. K. Pantel, C. Alix-Panabières, S. Riethdorf. Cancer micrometastases. *Nat. Rev. Clin. Oncol.* **2009**, 6 (6), 339–351.
98. M. Cristofanilli, G.T. Budd, M.J. Ellis, et al. Circulating tumor cells, disease progression, and survival in metastatic breast cancer. *N. Engl. J. Med.* **2004**, 351 (8), 781–791.
99. F. Schochter, T.W.P. Friedl, A. deGregorio, et al. Are Circulating Tumor Cells (CTCs) Ready for Clinical Use in Breast Cancer? An Overview of Completed and Ongoing Trials Using CTCs for Clinical Treatment Decisions. *Cells* **2019**, 8 (11), 1412.
100. M. Chimonidou, A. Strati, A. Tzitzira, et al. DNA Methylation of Tumor Suppressor and Metastasis Suppressor Genes in Circulating Tumor Cells. *Clin. Chem.* **2011**, 57 (8), 1169–1177.
101. S. Mastoraki, A. Strati, E. Tzanikou, et al. ESR1 Methylation: A Liquid Biopsy–Based Epigenetic Assay for the Follow-up of Patients with Metastatic Breast Cancer Receiving Endocrine Treatment. *Clin. Cancer Res.* **2018**, 24 (6), 1500–1510.
102. A. Gennari, F. Foca, R. Zamarchi, et al. Insulin-like growth factor-1 receptor (IGF-1R) expression on circulating tumor cells (CTCs) and metastatic breast cancer outcome: results from the TransMYME trial. *Breast Cancer Res. Treat.* **2020**, 181 (1), 61–68.
103. T. Fujii, J.M. Reuben, L. Huo, et al. Androgen receptor expression on circulating tumor cells in metastatic breast cancer. *PLoS ONE* **2017**, 12 (9), e0185231.
104. N. Krawczyk, M. Neubacher, F. Meier-Stiegen, et al. Determination of the androgen receptor status of circulating tumour cells in metastatic breast cancer patients. *BMC Cancer* **2019**, 19, 1101.
105. N.V. Jordan, A. Bardia, B.S. Wittner, et al. HER2 expression identifies dynamic functional states within circulating breast cancer cells. *Nature* **2016**, 537 (7618), 102–106.
106. N. Aceto, A. Bardia, B.S. Wittner, et al. AR Expression in breast cancer CTCs associates with bone metastases. *Mol. Cancer Res. MCR* **2018**, 16 (4), 720–727.

107. D. Boral, M. Vishnoi, H.N. Liu, et al. Molecular characterization of breast cancer CTCs associated with brain metastasis. *Nat. Commun.* **2017**, 8, 196.
108. B.L. Khoo, S.C. Lee, P. Kumar, et al. Short-term expansion of breast circulating cancer cells predicts response to anti-cancer therapy. *Oncotarget* **2015**, 6 (17), 15578–15593.
109. M.J.M. Magbanua, H.S. Rugo, D.M. Wolf, et al. Expanded genomic profiling of circulating tumor cells in metastatic breast cancer patients to assess biomarker status and biology over time (CALGB 40502 and CALGB 40503, Alliance). *Clin. Cancer Res. Off. J. Am. Assoc. Cancer Res.* **2018**, 24 (6), 1486–1499.
110. C. Paoletti, A.K. Cani, J.M. Larios, et al. Comprehensive mutation and copy number profiling in archived circulating breast cancer tumor cells documents heterogeneous resistance mechanisms. *Cancer Res.* **2018**, 78 (4), 1110–1122.
111. A.K. Cani, E.M. Dolce, E.P. Darga, et al. Serial monitoring of genomic alterations in circulating tumor cells of ER-positive/HER2-negative advanced breast cancer: feasibility of precision oncology biomarker detection. *Mol. Oncol.* n/a (n/a).
112. C. Gasch, T. Oldopp, O. Mauermann, et al. Frequent detection of PIK3CA mutations in single circulating tumor cells of patients suffering from HER2-negative metastatic breast cancer. *Mol. Oncol.* **2016**, 10 (8), 1330–1343.
113. F. Schochter, K. Werner, C. Köstler, et al. 53BP1 Accumulation in Circulating Tumor Cells Identifies Chemotherapy-Responsive Metastatic Breast Cancer Patients. *Cancers* **2020**, 12 (4), 930.
114. M. Yu, A. Bardia, N. Aceto, et al. Ex vivo culture of circulating breast tumor cells for individualized testing of drug susceptibility. *Science* **2014**, 345 (6193), 216–220.
115. A. Soler, L. Cayrefourcq, T. Mazard, et al. Autologous cell lines from circulating colon cancer cells captured from sequential liquid biopsies as model to study therapy-driven tumor changes. *Sci. Rep.* **2018**, 8, 15931.
116. Z. Que, B. Luo, Z. Zhou, et al. Establishment and characterization of a patient-derived circulating lung tumor cell line in vitro and in vivo. *Cancer Cell Int.* **2019**, 19, 21.
117. V. Faugeroux, E. Pailler, M. Oulhen, et al. Genetic characterization of a unique neuroendocrine transdifferentiation prostate circulating tumor cell-derived eXplant model. *Nat. Commun.* **2020**, 11, 1884.
118. C. Koch, A. Kuske, S.A. Joosse, et al. Characterization of circulating breast cancer cells with tumorigenic and metastatic capacity. *EMBO Mol. Med.* **2020**, 12 (9), e11908.
119. S. Roßwag, C.L. Cotarelo, K. Pantel, et al. Functional Characterization of Circulating Tumor Cells (CTCs) from Metastatic ER+/HER2− Breast Cancer Reveals Dependence on HER2 and FOXM1 for Endocrine Therapy Resistance and Tumor Cell Survival: Implications for Treatment of ER+/HER2− Breast Cancer. *Cancers* **2021**, 13 (8), 1810.
120. L. Keller, Y. Belloum, H. Wikman, K. Pantel. Clinical relevance of blood-based ctDNA analysis: mutation detection and beyond. *Br. J. Cancer* **2021**, 124 (2), 345–358.
121. N.C. Turner, B. Kingston, L.S. Kilburn, et al. Circulating tumour DNA analysis to direct therapy in advanced breast cancer (plasmaMATCH): a multicentre, multicohort, phase 2a, platform trial. *Lancet Oncol.* **2020**, 21 (10), 1296–1308.
122. X. Li, J. Lu, L. Zhang, et al. Clinical Implications of Monitoring ESR1 Mutations by Circulating Tumor DNA in Estrogen Receptor Positive Metastatic Breast Cancer: A Pilot Study. *Transl. Oncol.* **2019**, 13 (2), 321–328.
123. A.A. Davis, S. Jacob, L. Gerratana, et al. Landscape of circulating tumour DNA in metastatic breast cancer. *EBioMedicine* **2020**, 58, 102914.
124. T. Takeshita, Y. Yamamoto, M. Yamamoto-Ibusuki, et al. Clinical significance of plasma cell-free DNA mutations in PIK3CA, AKT1, and ESR1 gene according to treatment lines in ER-positive breast cancer. *Mol. Cancer* **2018**, 17 (1), 67.
125. B. O'Leary, R.J. Cutts, X. Huang, et al. Circulating Tumor DNA Markers for Early Progression on Fulvestrant With or Without Palbociclib in ER+ Advanced Breast Cancer. *JNCI J. Natl. Cancer Inst.* **2020**, 113 (3), 309–317.

126. L. Darrigues, J.-Y. Pierga, A. Bernard-Tessier, et al. Circulating tumor DNA as a dynamic biomarker of response to palbociclib and fulvestrant in metastatic breast cancer patients. *Breast Cancer Res. BCR* **2021**, 23, 31.
127. N. Beije, A.M. Sieuwerts, J. Kraan, et al. Estrogen receptor mutations and splice variants determined in liquid biopsies from metastatic breast cancer patients. *Mol. Oncol.* **2018**, 12 (1), 48–57.
128. F. Abdalla, B. Singh, H.K. Bhat. MicroRNAs and gene regulation in breast cancer. *J. Biochem. Mol. Toxicol.* **2020**, 34 (11), e22567.
129. A. Esquela-Kerscher, F.J. Slack. Oncomirs — microRNAs with a role in cancer. *Nat. Rev. Cancer* **2006**, 6 (4), 259–269.
130. G.A. Calin, C.D. Dumitru, M. Shimizu, et al. Frequent deletions and down-regulation of micro-RNA genes miR15 and miR16 at 13q14 in chronic lymphocytic leukemia. *Proc. Natl. Acad. Sci. U. S. A.* **2002**, 99 (24), 15524–15529.
131. M. Winkle, S.M. El-Daly, M. Fabbri, G.A. Calin. Noncoding RNA therapeutics — challenges and potential solutions. *Nat. Rev. Drug Discov.* **2021**, 1–23.
132. L. Cornell, S.A. Wander, T. Visal, N. Wagle, G.I. Shapiro. MicroRNA-Mediated Suppression of the TGF-β Pathway Confers Transmissible and Reversible CDK4/6 Inhibitor Resistance. *Cell Rep.* **2019**, 26 (10), 2667-2680.e7.
133. F. Baldassari, C. Zerbinati, M. Galasso, et al. Screen for MicroRNA and Drug Interactions in Breast Cancer Cell Lines Points to miR-126 as a Modulator of CDK4/6 and PIK3CA Inhibitors. *Front. Genet.* **2018**, 9, 174.
134. F. Citron, I. Segatto, G.L.R. Vinciguerra, et al. Downregulation of miR-223 Expression Is an Early Event during Mammary Transformation and Confers Resistance to CDK4/6 Inhibitors in Luminal Breast Cancer. *Cancer Res.* **2020**, 80 (5), 1064–1077.
135. W. Ji, W. Zhang, X. Wang, et al. c-myc regulates the sensitivity of breast cancer cells to palbociclib via c-myc/miR-29b-3p/CDK6 axis. *Cell Death Dis.* **2020**, 11 (9), 1–13.
136. A. Andrikopoulou, A. Shalit, E. Zografos, et al. MicroRNAs as Potential Predictors of Response to CDK4/6 Inhibitor Treatment. *Cancers* **2021**, 13 (16), 4114.
137. S. Riethdorf. Detection of microRNAs in circulating tumor cells. *Transl. Cancer Res.* **2018**, 7 (2).
138. C. Gasch, P.N. Plummer, L. Jovanovic, et al. Heterogeneity of miR-10b expression in circulating tumor cells. *Sci. Rep.* **2015**, 5 (1), 15980.
139. F.G. Ortega, J.A. Lorente, J.L. Garcia Puche, et al. miRNA in situ hybridization in circulating tumor cells - MishCTC. *Sci. Rep.* **2015**, 5 (1), 9207.
140. A. Markou, M. Zavridou, I. Sourvinou, et al. Direct Comparison of Metastasis-Related miRNAs Expression Levels in Circulating Tumor Cells, Corresponding Plasma, and Primary Tumors of Breast Cancer Patients. *Clin. Chem.* **2016**, 62 (7), 1002–1011.
141. S.M. Leong, K.M.-L. Tan, H.W. Chua, et al. Paper-Based MicroRNA Expression Profiling from Plasma and Circulating Tumor Cells. *Clin. Chem.* **2017**, 63 (3), 731–741.
142. A.M. Sieuwerts, B. Mostert, J.B. Vries, et al. mRNA and microRNA Expression Profiles in Circulating Tumor Cells and Primary Tumors of Metastatic Breast Cancer Patients. *Clin. Cancer Res.* **2011**, 17 (11), 3600–3618.
143. C.F. Pixberg, K. Raba, F. Müller, et al. Analysis of DNA methylation in single circulating tumor cells. *Oncogene* **2017**, 36 (23), 3223–3231.
144. W. Tan, G. Liang, X. Xie, et al. Incorporating MicroRNA into Molecular Phenotypes of Circulating Tumor Cells Enhances the Prognostic Accuracy for Patients with Metastatic Breast Cancer. *The Oncologist* **2019**, 24 (11), e1044–e1054.
145. R. Drula, L.F. Ott, I. Berindan-Neagoe, K. Pantel, G.A. Calin. MicroRNAs from Liquid Biopsy Derived Extracellular Vesicles: Recent Advances in Detection and Characterization Methods. *Cancers* **2020**, 12 (8), 2009.
146. P.S. Mitchell, R.K. Parkin, E.M. Kroh, et al. Circulating microRNAs as stable blood-based markers for cancer detection. *Proc. Natl. Acad. Sci. U. S. A.* **2008**, 105 (30), 10513–10518.

147. Y. Koi, Y. Tsutani, Y. Nishiyama, et al. Predicting the presence of breast cancer using circulating small RNAs, including those in the extracellular vesicles. *Cancer Sci.* **2020**, 111 (6), 2104–2115.
148. A. McGuire, J.A.L. Brown, M.J. Kerin. Metastatic breast cancer: the potential of miRNA for diagnosis and treatment monitoring. *Cancer Metastasis Rev.* **2015**, 34 (1), 145–155.
149. M.G. Davey, M. Davies, A.J. Lowery, N. Miller, M.J. Kerin. The Role of MicroRNA as Clinical Biomarkers for Breast Cancer Surgery and Treatment. *Int. J. Mol. Sci.* **2021**, 22 (15), 8290.
150. T. Hung, H.Y. Chang. Long noncoding RNA in genome regulation. *RNA Biol.* **2010**, 7 (5), 582–585.
151. J.L. Rinn, H.Y. Chang. Genome Regulation by Long Noncoding RNAs. *Annu. Rev. Biochem.* **2012**, 81 (1), 145–166.
152. F. Kopp, J.T. Mendell. Functional classification and experimental dissection of long noncoding RNAs. *Cell* **2018**, 172 (3), 393–407.
153. W.-X. Peng, P. Koirala, Y.-Y. Mo. LncRNA-mediated regulation of cell signaling in cancer. *Oncogene* **2017**, 36 (41), 5661–5667.
154. Z. Fang, Y. Wang, Z. Wang, et al. ERINA is an estrogen-responsive lncRNA that drives breast cancer through the E2F1/RB1 pathway. *Cancer Res.* **2020**, 80 (20), 4399–4413.
155. H. Yuan, L. Yan, M. Wu, et al. Analysis of the estrogen receptor-associated lncRNA landscape identifies a role for ERLC1 in breast cancer progression. *Cancer Res.* **2021**.
156. X. Jin, L.-P. Ge, D.-Q. Li, et al. LncRNA TROJAN promotes proliferation and resistance to CDK4/6 inhibitor via CDK2 transcriptional activation in ER+ breast cancer. *Mol. Cancer* **2020**, 19, 87.
157. A. Schramm, T.W.P. Friedl, F. Schochter, et al. Therapeutic intervention based on circulating tumor cell phenotype in metastatic breast cancer: concept of the DETECT study program. *Arch. Gynecol. Obstet.* **2016**, 293 (2), 271–281.
158. F.-C. Bidard, W. Jacot, N. Kiavue, et al. Efficacy of Circulating Tumor Cell Count–Driven vs Clinician-Driven First-line Therapy Choice in Hormone Receptor–Positive, ERBB2-Negative Metastatic Breast Cancer. *JAMA Oncol.* **2021**, 7 (1), 1–8.
159. L. Cabel, F. Berger, P. Cottu, et al. Clinical utility of circulating tumour cell-based monitoring of late-line chemotherapy for metastatic breast cancer: the randomised CirCe01 trial. *Br. J. Cancer* **2021**, 124 (7), 1207–1213.
160. C. Paoletti, J. Miao, E.M. Dolce, et al. Circulating Tumor Cell Clusters in patients with Metastatic Breast Cancer: a SWOG S0500 Translational Medicine Study. *Clin. Cancer Res. Off. J. Am. Assoc. Cancer Res.* **2019**, 25 (20), 6089–6097.
161. C. Paoletti, M.M. Regan, M.C. Liu, et al. Abstract P1-01-01: Circulating tumor cell number and CTC-endocrine therapy index predict clinical outcomes in ER positive metastatic breast cancer patients: Results of the COMETI Phase 2 trial. *Cancer Res.* **2017**, 77 (4 Supplement), P1-01.
162. Phase 3 DETECT III Study Suggests CTC Count to be Possible Biomarker for HER2-Directed Therapy in MBC https://www.cancernetwork.com/view/phase-3-detect-iii-study-suggests-ctc-count-to-be-possible-biomarker-for-her2-directed-therapy-in-mbc (accessed Dec 29, 2021).
163. DETECT III Studienprotokoll & Synopse http://www.detect-studien.de/d4-protokoll.html (accessed Nov 24, 2021).
164. A. John, C. Günes, C. Bolenz, et al. Bladder cancer-derived interleukin-1 converts the vascular endothelium into a pro-inflammatory and pro-coagulatory surface. *BMC Cancer* **2020**, 20, 1178.
165. C. Guzmán, M. Bagga, A. Kaur, J. Westermarck, D. Abankwa. ColonyArea: An ImageJ Plugin to Automatically Quantify Colony Formation in Clonogenic Assays. *PLoS ONE* **2014**, 9 (3), e92444.
166. S. Kim, R. Tiedt, A. Loo, et al. The potent and selective cyclin-dependent kinases 4 and 6 inhibitor ribociclib (LEE011) is a versatile combination partner in preclinical cancer models. *Oncotarget* **2018**, 9 (81), 35226–35240.
167. V. Wagner, J. Gil. Senescence as a therapeutically relevant response to CDK4/6 inhibitors. *Oncogene* **2020**, 39 (29), 5165–5176.

168. F. Debacq-Chainiaux, J.D. Erusalimsky, J. Campisi, O. Toussaint. Protocols to detect senescence-associated beta-galactosidase (SA-βgal) activity, a biomarker of senescent cells in culture and in vivo. *Nat. Protoc.* **2009**, 4 (12), 1798–1806.
169. T. Maier, M. Güell, L. Serrano. Correlation of mRNA and protein in complex biological samples. *FEBS Lett.* **2009**, 583 (24), 3966–3973.
170. Y. Liu, A. Beyer, R. Aebersold. On the Dependency of Cellular Protein Levels on mRNA Abundance. *Cell* **2016**, 165 (3), 535–550.
171. P. Debnath, R.S. Huirem, P. Dutta, S. Palchaudhuri. Epithelial–mesenchymal transition and its transcription factors. *Biosci. Rep.* **2021**, 42 (1), BSR20211754.
172. B.-Z. Yuan, X. Zhou, M.E. Durkin, et al. DLC-1 gene inhibits human breast cancer cell growth and in vivo tumorigenicity. *Oncogene* **2003**, 22 (3), 445–450.
173. A.W. Ware, J.J. Harris, T.L. Slatter, H.E. Cunliffe, F.J. McDonald. The epithelial sodium channel has a role in breast cancer cell proliferation. *Breast Cancer Res. Treat.* **2021**, 187 (1), 31–43.
174. S. Ghafouri-Fard, S. Dashti, M. Farsi, M. Taheri, S.A. Mousavinejad. X-Inactive-Specific Transcript: Review of Its Functions in the Carcinogenesis. *Front. Cell Dev. Biol.* **2021**, 9.
175. X. Li, R. Xiao, K. Tembo, et al. PEG10 promotes human breast cancer cell proliferation, migration and invasion. *Int. J. Oncol.* **2016**, 48 (5), 1933–1942.
176. W. Li, H. Ma, J. Zhang, et al. Unraveling the roles of CD44/CD24 and ALDH1 as cancer stem cell markers in tumorigenesis and metastasis. *Sci. Rep.* **2017**, 7 (1), 13856.
177. S.A. Mani, W. Guo, M.-J. Liao, et al. The Epithelial-Mesenchymal Transition Generates Cells with Properties of Stem Cells. *Cell* **2008**, 133 (4), 704–715.
178. S.V. Vasaikar, A.P. Deshmukh, P. den Hollander, et al. EMTome: a resource for pan-cancer analysis of epithelial-mesenchymal transition genes and signatures. *Br. J. Cancer* **2021**, 124 (1), 259–269.
179. S. Palomeras, S. Ruiz-Martínez, T. Puig. Targeting Breast Cancer Stem Cells to Overcome Treatment Resistance. *Molecules* **2018**, 23 (9), 2193.
180. C.-L. Li, D. Yang, X. Cao, et al. Fibronectin induces epithelial-mesenchymal transition in human breast cancer MCF-7 cells via activation of calpain. *Oncol. Lett.* **2017**, 13 (5), 3889–3895.
181. Y.-L. Choi, M. Bocanegra, M.J. Kwon, et al. LYN Is a Mediator of Epithelial-Mesenchymal Transition and a Target of Dasatinib in Breast Cancer. *Cancer Res.* **2010**, 70 (6), 2296–2306.
182. Y. Imawari, R. Mimoto, S. Hirooka, et al. Downregulation of dual-specificity tyrosine-regulated kinase 2 promotes tumor cell proliferation and invasion by enhancing cyclin-dependent kinase 14 expression in breast cancer. *Cancer Sci.* **2018**, 109 (2), 363–372.
183. E.G. Weagel, W. Burrup, R. Kovtun, et al. Membrane expression of thymidine kinase 1 and potential clinical relevance in lung, breast, and colorectal malignancies. *Cancer Cell Int.* **2018**, 18 (1), 135.
184. W. Ji, Y. Shi, X. Wang, et al. Combined Androgen receptor blockade overcomes the resistance of breast cancer cells to palbociclib. *Int. J. Biol. Sci.* **2019**, 15 (3), 522–532.
185. J. Zhu, C. Liu, F. Liu, Y. Wang, M. Zhu. Knockdown of PFTAIRE Protein Kinase 1 (PFTK1) Inhibits Proliferation, Invasion, and EMT in Colon Cancer Cells. *Oncol. Res.* **2016**, 24 (3), 137–144.
186. J.R. Whittle, F. Vaillant, E. Surgenor, et al. Dual Targeting of CDK4/6 and BCL2 Pathways Augments Tumor Response in Estrogen Receptor–Positive Breast Cancer. *Clin. Cancer Res.* **2020**, 26 (15), 4120–4134.
187. A. McCartney, L. Malorni. Potential through simplicity: thymidine kinase-1 as a biomarker for CDK4/6 inhibitors. *Br. J. Cancer* **2020**, 123 (2), 176–177.
188. M. Ren, Y. Gao, Q. Chen, et al. The Overexpression of Keratin 23 Promotes Migration of Ovarian Cancer via Epithelial-Mesenchymal Transition. *BioMed Res. Int.* **2020**, 2020, e8218735.
189. J.M. David, C. Dominguez, D.H. Hamilton, C. Palena. The IL-8/IL-8R Axis: A Double Agent in Tumor Immune Resistance. *Vaccines* **2016**, 4 (3), 22.
190. T. Chen, J.Y.S. Tsang, X.-C. Su, et al. SALL4 promotes tumor progression in breast cancer by targeting EMT. *Mol. Carcinog.* **2020**, 59 (10), 1209–1226.

191. X. Yin, T. Xiang, J. Mu, et al. Protocadherin 17 functions as a tumor suppressor suppressing Wnt/β-catenin signaling and cell metastasis and is frequently methylated in breast cancer. *Oncotarget* **2016**, 7 (32), 51720–51732.
192. G. Domenici, I. Aurrekoetxea-Rodríguez, B.M. Simões, et al. A Sox2–Sox9 signalling axis maintains human breast luminal progenitor and breast cancer stem cells. *Oncogene* **2019**, 38 (17), 3151–3169.
193. Z. Liu, S. Yu, S. Ye, et al. Keratin 17 activates AKT signalling and induces epithelial-mesenchymal transition in oesophageal squamous cell carcinoma. *J. Proteomics* **2020**, 211, 103557.
194. Y. Shi, C. Zheng, Y. Jin, et al. Reduced Expression of METTL3 Promotes Metastasis of Triple-Negative Breast Cancer by m6A Methylation-Mediated COL3A1 Up-Regulation. *Front. Oncol.* **2020**, 10.
195. Y.D. Shaul, E. Freinkman, W.C. Comb, et al. Dihydropyrimidine Accumulation Is Required for the Epithelial-Mesenchymal Transition. *Cell* **2014**, 158 (5), 1094–1109.
196. M.-A. Goyette, S. Duhamel, L. Aubert, et al. The Receptor Tyrosine Kinase AXL Is Required at Multiple Steps of the Metastatic Cascade during HER2-Positive Breast Cancer Progression. *Cell Rep.* **2018**, 23 (5), 1476–1490.
197. T. Hata, H. Rajabi, M. Yamamoto, et al. Targeting MUC1-C Inhibits TWIST1 Signaling in Triple-Negative Breast Cancer. *Mol. Cancer Ther.* **2019**, 18 (10), 1744–1754.
198. Y. Myal, E. Leygue, A.A. Blanchard. Claudin 1 in Breast Tumorigenesis: Revelation of a Possible Novel "Claudin High" Subset of Breast Cancers. *J. Biomed. Biotechnol.* **2010**, 2010, 956897.
199. Y. Zeng, M. Zou, Y. Liu, et al. Keratin 17 Suppresses Cell Proliferation and Epithelial-Mesenchymal Transition in Pancreatic Cancer. *Front. Med.* **2020**, 7.
200. B. Zhou, A. Moodie, A.A.A. Blanchard, E. Leygue, Y. Myal. Claudin 1 in Breast Cancer: New Insights. *J. Clin. Med.* **2015**, 4 (12), 1960–1976.
201. K.-T. Hwang, Y.A. Kim, J. Kim, et al. Prognostic influences of BCL1 and BCL2 expression on disease-free survival in breast cancer. *Sci. Rep.* **2021**, 11 (1), 11942.
202. Y.H. Eom, H.S. Kim, A. Lee, B.J. Song, B.J. Chae. BCL2 as a Subtype-Specific Prognostic Marker for Breast Cancer. *J. Breast Cancer* **2016**, 19 (3), 252–260.
203. Y.-F. Wang, H.-F. Dang, X. Luo, et al. Downregulation of SOX9 suppresses breast cancer cell proliferation and migration by regulating apoptosis and cell cycle arrest. *Oncol. Lett.* **2021**, 22 (1), 1–9.
204. H. Wang, N.C. McKnight, T. Zhang, et al. SOX9 Is Expressed in Normal Prostate Basal Cells and Regulates Androgen Receptor Expression in Prostate Cancer Cells. *Cancer Res.* **2007**, 67 (2), 528–536.
205. M. Gugnoni, A. Ciarrocchi. Long Noncoding RNA and Epithelial Mesenchymal Transition in Cancer. *Int. J. Mol. Sci.* **2019**, 20 (8), 1924.
206. D. Chen, L. Chen, Y. Lu, et al. Long noncoding RNA XIST expedites metastasis and modulates epithelial–mesenchymal transition in colorectal cancer. *Cell Death Dis.* **2017**, 8 (8), e3011–e3011.
207. J. Shen, L. Hong, D. Yu, et al. LncRNA XIST promotes pancreatic cancer migration, invasion and EMT by sponging miR-429 to modulate ZEB1 expression. *Int. J. Biochem. Cell Biol.* **2019**, 113, 17–26.
208. C. Li, L. Wan, Z. Liu, et al. Long non-coding RNA XIST promotes TGF-β-induced epithelial-mesenchymal transition by regulating miR-367/141-ZEB2 axis in non-small-cell lung cancer. *Cancer Lett.* **2018**, 418, 185–195.
209. R. Zheng, S. Lin, L. Guan, et al. Long non-coding RNA XIST inhibited breast cancer cell growth, migration, and invasion via miR-155/CDX1 axis. *Biochem. Biophys. Res. Commun.* **2018**, 498 (4), 1002–1008.
210. H. Zhang, K. Cai, J. Wang, et al. MiR-7, Inhibited Indirectly by LincRNA HOTAIR, Directly Inhibits SETDB1 and Reverses the EMT of Breast Cancer Stem Cells by Downregulating the STAT3 Pathway. *Stem Cells* **2014**, 32 (11), 2858–2868.
211. R. Zheng, Q. Yao, X. Li, B. Xu. Long Noncoding Ribonucleic Acid SNHG18 Promotes Glioma Cell Motility via Disruption of α-Enolase Nucleocytoplasmic Transport. *Front. Genet.* **2019**, 10.

212. Home - Gene - NCBI https://www.ncbi.nlm.nih.gov/gene (accessed Feb 10, 2022).
213. M. Ahram, M.S. Abdullah, S.A. Mustafa, D.B. Alsafadi, A.H. Battah. Androgen downregulates desmocollin-2 in association with induction of mesenchymal transition of breast MDA-MB-453 cancer cells. *Cytoskeleton* n/a (n/a).
214. F.-T. Liu, G.A. Rabinovich. Galectins as modulators of tumour progression. *Nat. Rev. Cancer* **2005**, 5 (1), 29–41.
215. D.M. Maher, B.K. Gupta, S. Nagata, M. Jaggi, S.C. Chauhan. Mucin 13: Structure, Function, and Potential Roles in Cancer Pathogenesis. *Mol. Cancer Res.* **2011**, 9 (5), 531–537.
216. M. Riaz, M.T. van Jaarsveld, A. Hollestelle, et al. miRNA expression profiling of 51 human breast cancer cell lines reveals subtype and driver mutation-specific miRNAs. *Breast Cancer Res.* **2013**, 15 (2), R33.
217. P. Razavi, M.T. Chang, G. Xu, et al. The Genomic Landscape of Endocrine-Resistant Advanced Breast Cancers. *Cancer Cell* **2018**, 34 (3), 427-438.e6.
218. K. Lee, A.L. Guerrero-Zotano, A. Servetto, et al. Proline rich 11 (PRR11) overexpression amplifies PI3K signaling and promotes antiestrogen resistance in breast cancer. *Nat. Commun.* **2020**, 11 (1), 5488.
219. M.S. Stark, S.L. Woods, M.G. Gartside, et al. Frequent somatic mutations in MAP3K5 and MAP3K9 in metastatic melanoma identified by exome sequencing. *Nat. Genet.* **2012**, 44 (2), 165–169.
220. L. Pongor, M. Kormos, C. Hatzis, et al. A genome-wide approach to link genotype to clinical outcome by utilizing next generation sequencing and gene chip data of 6,697 breast cancer patients. *Genome Med.* **2015**, 7, 104.
221. Calculated consequences https://m.ensembl.org/info/genome/variation/prediction/predicted_data.html (accessed Feb 17, 2022).
222. W. Shao, Q. Ding, Y. Guo, et al. A Pan-Cancer Landscape of HOX-Related lncRNAs and Their Association With Prognosis and Tumor Microenvironment. *Front. Mol. Biosci.* **2021**, 8.
223. Q. Liu, Z. Shi, X. Liu, H. Xiao. Correlation between the coexpression of zinc finger and SCAN domain-containing protein 31 and transcriptional activator with PDZ-binding motif and prognosis in hepatocellular carcinoma. *Ann. Transl. Med.* **2020**, 8 (20), 1308.
224. M. Huang, Y. Chen, D. Han, Z. Lei, X. Chu. Role of the zinc finger and SCAN domain-containing transcription factors in cancer. *Am. J. Cancer Res.* **2019**, 9 (5), 816–836.
225. J. Franco, U. Balaji, E. Freinkman, A.K. Witkiewicz, E.S. Knudsen. Metabolic Reprogramming of Pancreatic Cancer Mediated by CDK4/6 Inhibition Elicits Unique Vulnerabilities. *Cell Rep.* **2016**, 14 (5), 979–990.
226. D. Drago-García, J. Espinal-Enríquez, E. Hernández-Lemus. Network analysis of EMT and MET micro-RNA regulation in breast cancer. *Sci. Rep.* **2017**, 7 (1), 13534.
227. S. Valastyan, R.A. Weinberg. Tumor Metastasis: Molecular Insights and Evolving Paradigms. *Cell* **2011**, 147 (2), 275–292.
228. I. Plantamura, A. Cataldo, G. Cosentino, M.V. Iorio. miR-205 in Breast Cancer: State of the Art. *Int. J. Mol. Sci.* **2021**, 22 (1), 27.
229. Z. Eslami-S, L.E. Cortés-Hernández, C. Alix-Panabières. Epithelial Cell Adhesion Molecule: An Anchor to Isolate Clinically Relevant Circulating Tumor Cells. *Cells* **2020**, 9 (8), 1836.
230. G. Rinnerthaler, H. Hackl, F. Hamacher, et al. MiR-16 is the most stable-expressed housekeeping microRNA in breast cancer tissues from primary and metastatic sites. *Ann. Oncol.* **2015**, 26, iii10.
231. R.W. Carlson. The History and Mechanism of Action of Fulvestrant. *Clin. Breast Cancer* **2005**, 6, S5–S8.
232. N.A. O'Brien, M.S.J. McDermott, D. Conklin, et al. Targeting activated PI3K/mTOR signaling overcomes acquired resistance to CDK4/6-based therapies in preclinical models of hormone receptor-positive breast cancer. *Breast Cancer Res.* **2020**, 22 (1), 89.

233. A.S. Clark, I. Makhlin, A. DeMichele. Setting the Pick: Can PI3K Inhibitors Circumvent CDK4/6 Inhibitor Resistance? *Clin. Cancer Res.* **2021**, 27 (2), 371–373.
234. H.S. Rugo, F. Lerebours, E. Ciruelos, et al. Alpelisib plus fulvestrant in PIK3CA-mutated, hormone receptor-positive advanced breast cancer after a CDK4/6 inhibitor (BYLieve): one cohort of a phase 2, multicentre, open-label, non-comparative study. *Lancet Oncol.* **2021**, 22 (4), 489–498.
235. D. Juric, F. Janku, J. Rodón, et al. Alpelisib Plus Fulvestrant in PIK3CA-Altered and PIK3CA-Wild-Type Estrogen Receptor–Positive Advanced Breast Cancer: A Phase 1b Clinical Trial. *JAMA Oncol.* **2019**, 5 (2), e184475.
236. P. Cohen, D. Cross, P.A. Jänne. Kinase drug discovery 20 years after imatinib: progress and future directions. *Nat. Rev. Drug Discov.* **2021**, 20 (7), 551–569.
237. G. Manning, D.B. Whyte, R. Martinez, T. Hunter, S. Sudarsanam. The Protein Kinase Complement of the Human Genome. *Science* **2002**, 298 (5600), 1912–1934.
238. Y.-L. Wang, Y. Li, Y.-G. Ma, W.-Y. Wu. DCLK1 promotes malignant progression of breast cancer by regulating Wnt/β-Catenin signaling pathway. *Eur Rev Med Pharmacol Sci* **2019**, 10.
239. M. Radaeva, A.-T. Ton, M. Hsing, F. Ban, A. Cherkasov. Drugging the 'undruggable'. Therapeutic targeting of protein–DNA interactions with the use of computer-aided drug discovery methods. *Drug Discov. Today* **2021**, 26 (11), 2660–2679.
240. J. Jiang, J. Yuan, Z. Hu, et al. Systematic illumination of druggable genes in cancer genomes. *Cell Rep.* **2022**, 38 (8).
241. J.H. Bushweller. Targeting transcription factors in cancer — from undruggable to reality. *Nat. Rev. Cancer* **2019**, 19 (11), 611–624.
242. L. Garcia-Alonso, C.H. Holland, M.M. Ibrahim, D. Turei, J. Saez-Rodriguez. Benchmark and integration of resources for the estimation of human transcription factor activities. *Genome Res.* **2019**, 29 (8), 1363–1375.
243. A.D. Rouillard, G.W. Gundersen, N.F. Fernandez, et al. The harmonizome: a collection of processed datasets gathered to serve and mine knowledge about genes and proteins. *Database* **2016**, 2016, baw100.
244. P. Khongthong, A.K. Roseweir, J. Edwards. The NF-KB pathway and endocrine therapy resistance in breast cancer. *Endocr. Relat. Cancer* **2019**, 26 (6), R369–R380.
245. X. Dai, H. Cheng, Z. Bai, J. Li. Breast Cancer Cell Line Classification and Its Relevance with Breast Tumor Subtyping. *J. Cancer* **2017**, 8 (16), 3131–3141.
246. Z. Chen, Z. Fang, J. Ma. Regulatory mechanisms and clinical significance of vimentin in breast cancer. *Biomed. Pharmacother.* **2021**, 133, 111068.
247. L. McInroy, A. Määttä. Down-regulation of vimentin expression inhibits carcinoma cell migration and adhesion. *Biochem. Biophys. Res. Commun.* **2007**, 360 (1), 109–114.
248. J. Topa, P. Grešner, A.J. Żaczek, A. Markiewicz. Breast cancer circulating tumor cells with mesenchymal features—an unreachable target? *Cell. Mol. Life Sci.* **2022**, 79 (2), 81.
249. A. McCartney, I. Migliaccio, M. Bonechi, et al. Mechanisms of Resistance to CDK4/6 Inhibitors: Potential Implications and Biomarkers for Clinical Practice. *Front. Oncol.* **2019**, 9, 666.
250. A. McCartney, M. Bonechi, F. De Luca, et al. Plasma Thymidine Kinase Activity as a Biomarker in Patients with Luminal Metastatic Breast Cancer Treated with Palbociclib within the TREnd Trial. *Clin. Cancer Res.* **2020**, 26 (9), 2131–2139.
251. A. Guerrero- Zotano, C. Zielinski, M. Gil-Gil, et al. Abstract PS2-01: Plk1 expression & efficacy of palbociclib in advanced hormonal receptor-positive breast cancer patients from PEARL study (GEICAM 2012-03). *Cancer Res.* **2021**, 81 (4_Supplement), PS2-01.
252. U.S. Asghar, R. Kanani, R. Roylance, S. Mittnacht. Systematic Review of Molecular Biomarkers Predictive of Resistance to CDK4/6 Inhibition in Metastatic Breast Cancer. *JCO Precis. Oncol.* **2022**, No. 6, e2100002.
253. M. Yu, A. Bardia, N. Aceto, et al. Ex vivo culture of circulating breast tumor cells for individualized testing of drug susceptibility. *Science* **2014**, 345 (6193), 216–220.

254. I. Mayayo-Peralta, B. Faggion, L. Hoekman, et al. Ribociclib Induces Broad Chemotherapy Resistance and EGFR Dependency in ESR1 Wildtype and Mutant Breast Cancer. *Cancers* **2021**, 13 (24), 6314.
255. K. Freeman-Cook, R.L. Hoffman, N. Miller, et al. Expanding control of the tumor cell cycle with a CDK2/4/6 inhibitor. *Cancer Cell* **2021**, 39 (10), 1404-1421.e11.
256. M. Iida, D. Toyosawa, M. Nakamura, et al. Decreased ER dependency after acquired resistance to CDK4/6 inhibitors. *Breast Cancer* **2020**.
257. Z. Li, P. Razavi, Q. Li, et al. Loss of the FAT1 Tumor Suppressor Promotes Resistance to CDK4/6 Inhibitors via the Hippo Pathway. *Cancer Cell* **2018**, 34 (6), 893-905.e8.
258. M. Iida, M. Nakamura, E. Tokuda, et al. The p21 levels have the potential to be a monitoring marker for ribociclib in breast cancer. *Oncotarget* **2019**, 10 (47), 4907–4918.
259. V. Kumarasamy, P. Vail, R. Nambiar, A.K. Witkiewicz, E.S. Knudsen. Functional Determinants of Cell Cycle Plasticity and Sensitivity to CDK4/6 Inhibition. *Cancer Res.* **2021**, 81 (5), 1347–1360.
260. R. Condorelli, L. Spring, J. O'Shaughnessy, et al. Polyclonal RB1 mutations and acquired resistance to CDK 4/6 inhibitors in patients with metastatic breast cancer. *Ann. Oncol.* **2018**, 29 (3), 640–645.
261. K. Pandey, H. An, S.K. Kim, et al. Molecular mechanisms of resistance to CDK4/6 inhibitors in breast cancer: A review. *Int. J. Cancer* **2019**, 145 (5), 1179–1188.
262. G. Gomatou, I. Trontzas, S. Ioannou, et al. Mechanisms of resistance to cyclin-dependent kinase 4/6 inhibitors. *Mol. Biol. Rep.* **2021**, 48 (1), 915–925.
263. K. Tsuji, K. Yasui, Y. Gen, et al. PEG10 is a probable target for the amplification at 7q21 detected in hepatocellular carcinoma. *Cancer Genet. Cytogenet.* **2010**, 198 (2), 118–125.
264. T. Xie, S. Pan, H. Zheng, et al. PEG10 as an oncogene: expression regulatory mechanisms and role in tumor progression. *Cancer Cell Int.* **2018**, 18 (1), 112.
265. F.M. Ferguson, Z.M. Doctor, S.B. Ficarro, et al. Discovery of Covalent CDK14 Inhibitors with Pan-TAIRE Family Specificity. *Cell Chem. Biol.* **2019**, 26 (6), 804-817.e12.
266. X. Gu, Y. Wang, H. Wang, et al. Upregulated PFTK1 promotes tumor cell proliferation, migration, and invasion in breast cancer. *Med. Oncol.* **2015**, 32 (7), 195.
267. F. Shu, S. Lv, Y. Qin, et al. Functional characterization of human PFTK1 as a cyclin-dependent kinase. *Proc. Natl. Acad. Sci. U. S. A.* **2007**, 104 (22), 9248–9253.
268. M. Panda, S.K. Tripathi, B.K. Biswal. SOX9: An emerging driving factor from cancer progression to drug resistance. *Biochim. Biophys. Acta BBA - Rev. Cancer* **2021**, 1875 (2), 188517.
269. R. Jeselsohn, M. Cornwell, M. Pun, et al. Embryonic transcription factor SOX9 drives breast cancer endocrine resistance. *Proc. Natl. Acad. Sci. U. S. A.* **2017**, 114 (22), E4482–E4491.
270. M.-K. Seong, J.-Y. Lee, J. Byeon, et al. Bcl-2 is a highly significant prognostic marker of hormone-receptor-positive, human epidermal growth factor receptor-2-negative breast cancer. *Breast Cancer Res. Treat.* **2015**, 150 (1), 141–148.
271. T.M.A. Abdel-Fatah, C. Perry, P. Dickinson, et al. Bcl2 is an independent prognostic marker of triple negative breast cancer (TNBC) and predicts response to anthracycline combination (ATC) chemotherapy (CT) in adjuvant and neoadjuvant settings. *Ann. Oncol.* **2013**, 24 (11), 2801–2807.
272. F. Bertucci, C.K.Y. Ng, A. Patsouris, et al. Genomic characterization of metastatic breast cancers. *Nature* **2019**, 569 (7757), 560–564.
273. Y. Guo, D. Lin, M. Zhang, et al. CLDN6-induced apoptosis via regulating ASK1-p38/JNK signaling in breast cancer MCF-7 cells. *Int. J. Oncol.* **2016**, 48 (6), 2435–2444.
274. T.D. Prickett, B. Zerlanko, J.J. Gartner, et al. Somatic mutations in MAP3K5 attenuate its pro-apoptotic function in melanoma through increased binding to Thioredoxin. *J. Invest. Dermatol.* **2014**, 134 (2), 452–460.
275. A.R. Cowell, G. Jacquemet, A.K. Singh, et al. Talin rod domain–containing protein 1 (TLNRD1) is a novel actin-bundling protein which promotes filopodia formation. *J. Cell Biol.* **2021**, 220 (9), e202005214.
276. K. Kazazian, C. Go, H. Wu, et al. Plk4 Promotes Cancer Invasion and Metastasis through Arp2/3 Complex Regulation of the Actin Cytoskeleton. *Cancer Res.* **2017**, 77 (2), 434–447.

277. S.A. Wander, O. Cohen, X. Gong, et al. The Genomic Landscape of Intrinsic and Acquired Resistance to Cyclin-Dependent Kinase 4/6 Inhibitors in Patients with Hormone Receptor–Positive Metastatic Breast Cancer. *Cancer Discov.* **2020**, 10 (8), 1174–1193.
278. P. Zhang, C. Fan, J. Du, X. Mo, Q. Zhao. Association of miR-1247-5p expression with clinicopathological parameters and prognosis in breast cancer. *Int. J. Exp. Pathol.* **2018**, 99 (4), 199–205.
279. W. Yang, W. Feng, F. Wu, et al. MiR-135-5p inhibits TGF-β-induced epithelial-mesenchymal transition and metastasis by targeting SMAD3 in breast cancer. *J. Cancer* **2020**, 11 (21), 6402–6412.
280. Y. Zhu, Q. Wang, Y. Xia, et al. Evaluation of MiR-1908-3p as a novel serum biomarker for breast cancer and analysis its oncogenic function and target genes. *BMC Cancer* **2020**, 20 (1), 644.
281. N.K. Rana, N. Srivastava, B. Koch. Identification of the key miRNA; hsa-miR-1269a targeting TP53, Caspase-9 and FOXO3a in breast cancer cells under hypoxia by integrated bioinformatics analysis. *Gene Rep.* **2021**, 25, 101408.
282. H. Fu, L. Fu, C. Xie, et al. miR-375 inhibits cancer stem cell phenotype and tamoxifen resistance by degrading HOXB3 in human ER-positive breast cancer. *Oncol. Rep.* **2017**, 37 (2), 1093–1099.
283. A. Ward, A. Balwierz, J.D. Zhang, et al. Re-expression of microRNA-375 reverses both tamoxifen resistance and accompanying EMT-like properties in breast cancer. *Oncogene* **2013**, 32 (9), 1173–1182.
284. W. Zhang, J. Xu, K. Wang, X. Tang, J. He. miR-139-3p suppresses the invasion and migration properties of breast cancer cells by targeting RAB1A. *Oncol. Rep.* **2019**, 42 (5), 1699–1708.
285. E. Peperstraete, C. Lecerf, J. Collette, et al. Enhancement of Breast Cancer Cell Aggressiveness by lncRNA H19 and its Mir-675 Derivative: Insight into Shared and Different Actions. *Cancers* **2020**, 12 (7), 1730.
286. F. Liu, M. Korc. Cdk4/6 Inhibition Induces Epithelial–Mesenchymal Transition and Enhances Invasiveness in Pancreatic Cancer Cells. *Mol. Cancer Ther.* **2012**, 11 (10), 2138–2148.
287. J.-W. Miao, L.-J. Liu, J. Huang. Interleukin-6-induced epithelial-mesenchymal transition through signal transducer and activator of transcription 3 in human cervical carcinoma. *Int. J. Oncol.* **2014**, 45 (1), 165–176.
288. C. Li, Y. Teng, J. Wu, et al. A pan-cancer analysis of the oncogenic role of Keratin 17 (KRT17) in human tumors. *Transl. Cancer Res.* **2021**, 10 (10), 4489–4501.
289. E.A. Rakha, J.S. Reis-Filho, I.O. Ellis. Basal-Like Breast Cancer: A Critical Review. *J. Clin. Oncol.* **2008**, 26 (15), 2568–2581.
290. D. Li, X.-F. Ni, H. Tang, et al. KRT17 Functions as a Tumor Promoter and Regulates Proliferation, Migration and Invasion in Pancreatic Cancer via mTOR/S6k1 Pathway. *Cancer Manag. Res.* **2020**, 12, 2087–2095.
291. Y. Li, B. Zeng, Y. Li, C. Zhang, G. Ren. Downregulated expression of ARHGAP10 correlates with advanced stage and high Ki-67 index in breast cancer. *PeerJ* **2019**, 7, e7431.
292. P. Zhong, R. Shu, H. Wu, et al. Low KRT15 expression is associated with poor prognosis in patients with breast invasive carcinoma. *Exp. Ther. Med.* **2021**, 21 (4), 1–1.
293. J. Horiguchi, H. Takei, Y. Koibuchi, et al. Prognostic significance of dihydropyrimidine dehydrogenase expression in breast cancer. *Br. J. Cancer* **2002**, 86 (2), 222–225.
294. C.-Y. Wei, M.-X. Zhu, Y.-W. Yang, et al. Downregulation of RNF128 activates Wnt/β-catenin signaling to induce cellular EMT and stemness via CD44 and CTTN ubiquitination in melanoma. *J. Hematol. Oncol.J Hematol Oncol* **2019**, 12 (1), 21.
295. J. Xie, Y. Yang, J. Sun, et al. STEAP1 Inhibits Breast Cancer Metastasis and Is Associated With Epithelial–Mesenchymal Transition Procession. *Clin. Breast Cancer* **2019**, 19 (1), e195–e207.
296. J.C. Martin, B.-S. Herbert, B.A. Hocevar. Disabled-2 downregulation promotes epithelial-to-mesenchymal transition. *Br. J. Cancer* **2010**, 103 (11), 1716–1723.
297. M. Jiang, Q. Chen, X. Zhao, et al. Downregulation of PFTK1 Inhibits Migration and Invasion of Non-Small Cell Lung Cancer. *OncoTargets Ther.* **2020**, 13, 9281–9289.

298. L. Zheng, Z. Zhou, Z. He. Knockdown of PFTK1 inhibits tumor cell proliferation, invasion and epithelial-to-mesenchymal transition in pancreatic cancer. *Int. J. Clin. Exp. Pathol.* **2015**, 8 (11), 14005–14012.
299. Y. Zhu, C. Zou, J. Zhang, et al. Dynamically Monitoring the Clonal Evolution of Lung Cancer Based on the Molecular Characterization of Circulating Tumor Cells Using Aptamer Cocktail-Modified Nanosubstrates. *ACS Appl. Mater. Interfaces* **2020**, 12 (5), 5671–5679.
300. W.K.C. Leung, A.K.K. Ching, N. Wong. Phosphorylation of Caldesmon by PFTAIRE1 kinase promotes actin binding and formation of stress fibers. *Mol. Cell. Biochem.* **2011**, 350 (1), 201–206.
301. T.D. Marchi, A.M. Timmermans, M. Smid, et al. Annexin-A1 and caldesmon are associated with resistance to tamoxifen in estrogen receptor positive recurrent breast cancer. *Oncotarget* **2015**, 7 (3), 3098–3110.
302. E.Y.-T. Pang, A.H.-C. Bai, K.-F. To, et al. Identification of PFTAIRE protein kinase 1, a novel cell division cycle-2 related gene, in the motile phenotype of hepatocellular carcinoma cells. *Hepatology* **2007**, 46 (2), 436–445.
303. E. Carrasco-Garcia, L. Lopez, V. Moncho-Amor, et al. SOX9 Triggers Different Epithelial to Mesenchymal Transition States to Promote Pancreatic Cancer Progression. *Cancers* **2022**, 14 (4), 916.
304. J.-Q. Huang, F.-K. Wei, X.-L. Xu, et al. SOX9 drives the epithelial–mesenchymal transition in non-small-cell lung cancer through the Wnt/β-catenin pathway. *J. Transl. Med.* **2019**, 17 (1), 143.
305. J. Chen, Z. Huang, H. Li, et al. MicroRNA-520f-3p inhibits proliferation of gastric cancer cells via targeting SOX9 and thereby inactivating Wnt signaling. *Sci. Rep.* **2020**, 10 (1), 1–10.
306. K.N. Al-Zahrani, J. Abou-Hamad, J. Pascoal, et al. AKT-mediated phosphorylation of Sox9 induces Sox10 transcription in a murine model of HER2-positive breast cancer. *Breast Cancer Res.* **2021**, 23 (1), 55.
307. B. Zhou, A. Blanchard, N. Wang, et al. Claudin 1 Promotes Migration and Increases Sensitivity to Tamoxifen and Anticancer Drugs in Luminal-like Human Breast Cancer Cells MCF7. *Cancer Invest.* **2015**, 33 (9), 429–439.
308. A.A. Blanchard, X. Ma, K.J. Dueck, et al. Claudin 1 expression in basal-like breast cancer is related to patient age. *BMC Cancer* **2013**, 13 (1), 268.
309. A.A. Blanchard, G.P. Skliris, P.H. Watson, et al. Claudins 1, 3, and 4 protein expression in ER negative breast cancer correlates with markers of the basal phenotype. *Virchows Arch.* **2009**, 454 (6), 647–656.
310. D. You, S.P. Jung, Y. Jeong, et al. Fibronectin expression is upregulated by PI-3K/Akt activation in tamoxifen-resistant breast cancer cells. *BMB Rep.* **2017**, 50 (12), 615–620.
311. U. Burk, J. Schubert, U. Wellner, et al. A reciprocal repression between ZEB1 and members of the miR-200 family promotes EMT and invasion in cancer cells. *EMBO Rep.* **2008**, 9 (6), 582–589.
312. S. Brabletz, T. Brabletz. The ZEB/miR-200 feedback loop—a motor of cellular plasticity in development and cancer? *EMBO Rep.* **2010**, 11 (9), 670–677.
313. S.-S. Yang, S. Ma, H. Dou, et al. Breast cancer-derived exosomes regulate cell invasion and metastasis in breast cancer via miR-146a to activate cancer associated fibroblasts in tumor microenvironment. *Exp. Cell Res.* **2020**, 391 (2), 111983.
314. C. Tordonato, M.J. Marzi, G. Giangreco, et al. miR-146 connects stem cell identity with metabolism and pharmacological resistance in breast cancer. *J. Cell Biol.* **2021**, 220 (5), e202009053.
315. L. Kalinkova, N. Nikolaieva, B. Smolkova, et al. miR-205-5p Downregulation and ZEB1 Upregulation Characterize the Disseminated Tumor Cells in Patients with Invasive Ductal Breast Cancer. *Int. J. Mol. Sci.* **2022**, 23 (1), 103.
316. B.R.B. Pires, A.L. Mencalha, G.M. Ferreira, et al. NF-kappaB Is Involved in the Regulation of EMT Genes in Breast Cancer Cells. *PLoS ONE* **2017**, 12 (1), e0169622.
317. L. Sun, L.A. Mathews, S.M. Cabarcas, et al. Epigenetic Regulation of SOX9 by the NF-κB Signaling Pathway in Pancreatic Cancer Stem Cells. *Stem Cells Dayt. Ohio* **2013**, 31 (8), 1454–1466.
318. B.-H. Lee, S.-Y. Park, K.-B. Kang, R.-W. Park, I.-S. Kim. NF-κB activates fibronectin gene expression in rat hepatocytes. *Biochem. Biophys. Res. Commun.* **2002**, 297 (5), 1218–1224.

319. K. Bunting, S. Rao, K. Hardy, et al. Genome-Wide Analysis of Gene Expression in T Cells to Identify Targets of the NF-κB Transcription Factor c-Rel. *J. Immunol.* **2007**, 178 (11), 7097–7109.
320. S. Mukherjee, A. Manna, P. Bhattacharjee, et al. Non-migratory tumorigenic intrinsic cancer stem cells ensure breast cancer metastasis by generation of CXCR4+ migrating cancer stem cells. *Oncogene* **2016**, 35 (37), 4937–4948.
321. N.-O. Chimge, S.K. Baniwal, G.H. Little, et al. Regulation of breast cancer metastasis by Runx2 and estrogen signaling: the role of SNAI2. *Breast Cancer Res.* **2011**, 13 (6), R127.
322. W. Guo, Z. Keckesova, J.L. Donaher, et al. Slug and Sox9 Cooperatively Determine the Mammary Stem Cell State. *Cell* **2012**, 148 (5), 1015–1028.
323. C.L. Alves, D. Elias, M.B. Lyng, M. Bak, H.J. Ditzel. SNAI2 upregulation is associated with an aggressive phenotype in fulvestrant-resistant breast cancer cells and is an indicator of poor response to endocrine therapy in estrogen receptor-positive metastatic breast cancer. *Breast Cancer Res.* **2018**, 20 (1), 60.
324. J. Huang, H. Li, G. Ren. Epithelial-mesenchymal transition and drug resistance in breast cancer (Review). *Int. J. Oncol.* **2015**, 47 (3), 840–848.
325. T. Shibue, R.A. Weinberg. EMT, CSCs, and drug resistance: the mechanistic link and clinical implications. *Nat. Rev. Clin. Oncol.* **2017**, 14 (10), 611–629.
326. A.-P. Morel, M. Lièvre, C. Thomas, et al. Generation of Breast Cancer Stem Cells through Epithelial-Mesenchymal Transition. *PLOS ONE* **2008**, 3 (8), e2888.
327. A. Singh, J. Settleman. EMT, cancer stem cells and drug resistance: an emerging axis of evil in the war on cancer. *Oncogene* **2010**, 29 (34), 4741–4751.
328. B. Yang, W. Zhang, M. Zhang, et al. KRT6A Promotes EMT and Cancer Stem Cell Transformation in Lung Adenocarcinoma. *Technol. Cancer Res. Treat.* **2020**, 19, 1533033820921248.
329. M.-A. Goyette, I.E. Elkholi, C. Apcher, et al. Targeting Axl favors an antitumorigenic microenvironment that enhances immunotherapy responses by decreasing Hif-1α levels. *Proc. Natl. Acad. Sci.* **2021**, 118 (29), e2023868118.
330. M.K. Asiedu, F.D. Beauchamp-Perez, J.N. Ingle, et al. AXL induces epithelial-to-mesenchymal transition and regulates the function of breast cancer stem cells. *Oncogene* **2014**, 33 (10), 1316–1324.
331. K. Pénzes, C. Baumann, I. Szabadkai, et al. Combined inhibition of AXL, Lyn and p130Cas kinases block migration of triple negative breast cancer cells. *Cancer Biol. Ther.* **2014**, 15 (11), 1571–1582.
332. V. Ramesh, T. Brabletz, P. Ceppi. Targeting EMT in Cancer with Repurposed Metabolic Inhibitors. *Trends Cancer* **2020**, 6 (11), 942–950.
333. H. Harjunpää, M. Llort Asens, C. Guenther, S.C. Fagerholm. Cell Adhesion Molecules and Their Roles and Regulation in the Immune and Tumor Microenvironment. *Front. Immunol.* **2019**, 10.
334. D. Reher, B. Klink, A. Deutsch, A. Voss-Böhme. Cell adhesion heterogeneity reinforces tumour cell dissemination: novel insights from a mathematical model. *Biol. Direct* **2017**, 12, 18.
335. G.F. Le Bras, K.J. Taubenslag, C.D. Andl. The regulation of cell-cell adhesion during epithelial-mesenchymal transition, motility and tumor progression. *Cell Adhes. Migr.* **2012**, 6 (4), 365–373.
336. P. Gassmann, A. Enns, J. Haier. Role of Tumor Cell Adhesion and Migration in Organ-Specific Metastasis Formation. *Oncol. Res. Treat.* **2004**, 27 (6), 577–582.
337. Z. Hamidov, A. Altendorf-Hofmann, Y. Chen, et al. Reduced expression of desmocollin 2 is an independent prognostic biomarker for shorter patients survival in pancreatic ductal adenocarcinoma. *J. Clin. Pathol.* **2011**, 64 (11), 990–994.
338. W.-K. Fang, L.-D. Liao, L.-Y. Li, et al. Down-regulated desmocollin-2 promotes cell aggressiveness through redistributing adherens junctions and activating beta-catenin signalling in oesophageal squamous cell carcinoma. *J. Pathol.* **2013**, 231 (2), 257–270.
339. N.M. Reynolds, A. Mohammadalipour, C.R. Hall, et al. Galectin-1 Influences Breast Cancer Cell Adhesion to E-selectin Via Ligand Intermediaries. *Cell. Mol. Bioeng.* **2018**, 11 (1), 37–52.
340. A. Irie, A. Yamauchi, K. Kontani, et al. Galectin-9 as a Prognostic Factor with Antimetastatic Potential in Breast Cancer. *Clin. Cancer Res.* **2005**, 11 (8), 2962–2968.

341. R. Bhatia, S.K. Gautam, A. Cannon, et al. Cancer-associated mucins: role in immune modulation and metastasis. *Cancer Metastasis Rev.* **2019**, 38 (1), 223–236.
342. D.W. Kufe. Mucins in cancer: function, prognosis and therapy. *Nat. Rev. Cancer* **2009**, 9 (12), 874–885.
343. D.W. Kufe. MUC1-C oncoprotein as a target in breast cancer: activation of signaling pathways and therapeutic approaches. *Oncogene* **2013**, 32 (9), 1073–1081.
344. C. Marques, C.A. Reis, R.R. Vivès, A. Magalhães. Heparan Sulfate Biosynthesis and Sulfation Profiles as Modulators of Cancer Signalling and Progression. *Front. Oncol.* **2021**, 11.
345. C. Debarnot, Y.R. Monneau, V. Roig-Zamboni, et al. Substrate binding mode and catalytic mechanism of human heparan sulfate d-glucuronyl C5 epimerase. *Proc. Natl. Acad. Sci.* **2019**, 116 (14), 6760–6765.
346. M. Kovatcheva, D.D. Liu, M.A. Dickson, et al. MDM2 turnover and expression of ATRX determine the choice between quiescence and senescence in response to CDK4 inhibition. *Oncotarget* **2015**, 6 (10), 8226–8243.
347. S.C. Dolfi, A.V. Jäger, D.J. Medina, et al. Fulvestrant treatment alters MDM2 protein turnover and sensitivity of human breast carcinoma cells to chemotherapeutic drugs. *Cancer Lett.* **2014**, 350 (1–2), 52–60.
348. J. Xi, C.X. Ma. Sequencing Endocrine Therapy for Metastatic Breast Cancer: What Do We Do After Disease Progression on a CDK4/6 Inhibitor? *Curr. Oncol. Rep.* **2020**, 22 (6), 57.
349. N. Sobhani, A. Fassl, G. Mondani, D. Generali, T. Otto. Targeting Aberrant FGFR Signaling to Overcome CDK4/6 Inhibitor Resistance in Breast Cancer. *Cells* **2021**, 10 (2), 293.
350. Q. Li, B. Jiang, J. Guo, et al. INK4 Tumor Suppressor Proteins Mediate Resistance to CDK4/6 Kinase Inhibitors. *Cancer Discov.* **2022**, 12 (2), 356–371.
351. R.S. Finn, Y. Liu, Z. Zhu, et al. Biomarker Analyses of Response to Cyclin-Dependent Kinase 4/6 Inhibition and Endocrine Therapy in Women with Treatment-Naïve Metastatic Breast Cancer. *Clin. Cancer Res.* **2020**, 26 (1), 110–121.
352. R.S. Finn, M. Cristofanilli, J. Ettl, et al. Treatment effect of palbociclib plus endocrine therapy by prognostic and intrinsic subtype and biomarker analysis in patients with bone-only disease: a joint analysis of PALOMA-2 and PALOMA-3 clinical trials. *Breast Cancer Res. Treat.* **2020**, 184 (1), 23–35.
353. S.F. Schoninger, S.W. Blain. The Ongoing Search for Biomarkers of CDK4/6 Inhibitor Responsiveness in Breast Cancer. *Mol. Cancer Ther.* **2020**, 19 (1), 3–12.
354. T. De Marchi, J.A. Foekens, A. Umar, J.W.M. Martens. Endocrine therapy resistance in estrogen receptor (ER)-positive breast cancer. *Drug Discov. Today* **2016**, 21 (7), 1181–1188.

Supplementary material

Supplementary Table S 1 : Number of CTCs of patients of whom VIM-expression on CTCs was detected at least twice. Patients marked in green received Cdk4/6 inhibitors.

ID	BC subtype_PT	CTCs	*VIM*-neg	VIM-pos	Days after first visit	CTCs	*VIM*-neg	*VIM*-pos	Days after 1st follow-up	CTCs	VIM-neg	*VIM*-pos	Days after 2nd follow-up	CTCs	VIM-neg	VIM-pos
1	ER+PR+	431	431		44	10,000	n.a., mostly negative									
2	ER+PR+	6	6		1176	705	705									
3	ER+PR+	2	2		106	1	1									
4	ER+PR n.a	3	3		498	7	7									
5	ER+PR+	10	10		113	117	117									
6	ER+PR+	1	1		203	11	11									
7	ER+PR+	47	47		30	1	1									
8	TNBC	7	7		198	5	5									
9	ER+PR+	87	87		31	291	291									
10	ER+PR+	1	1		944	3	3									
11	ER+PR-	93	93		391	33	33									
12	ER+PR+	135	133	2 (1+)	117	13	9	4 (1+)								
13	ER+PR+	5	5		97	86	25	61 (1+)	263	600	600					
14	ER+PR-	66	60	6 (1+)	399	916	816	68 (1+) 32 (2+)								
15	ER+PR+	295	292	3 (1+)	95	1,090	1,070	20 (1+)								

16	ER+PR+	45	40	5 (1+)	245	3	3									
17	ER+PR+	130	121	9 (1+)	42	440	435	5 (1+)	221	1	1					
18	n.a.	48	46	2 (1+)	111	95	92	3 (1+)	114	8,280	8,130	150 (1+)	27	13,000	12,300	700 (1+)
19	TNBC	2	2		264	14	5	2 (1+) 5 (2+)								
20	ER+PR+	61	60	1 (1+)	275	138	137	2 (1+)	182	79	78	1 (1+)				
21	TNBC	2	1	1 (1+)	42	18	15	3 (2+)								
22	ER-PR+	127	126	1 (1+)	15	188	188									
23	ER+PR+	38	36	2 (1+)	11	75	75									

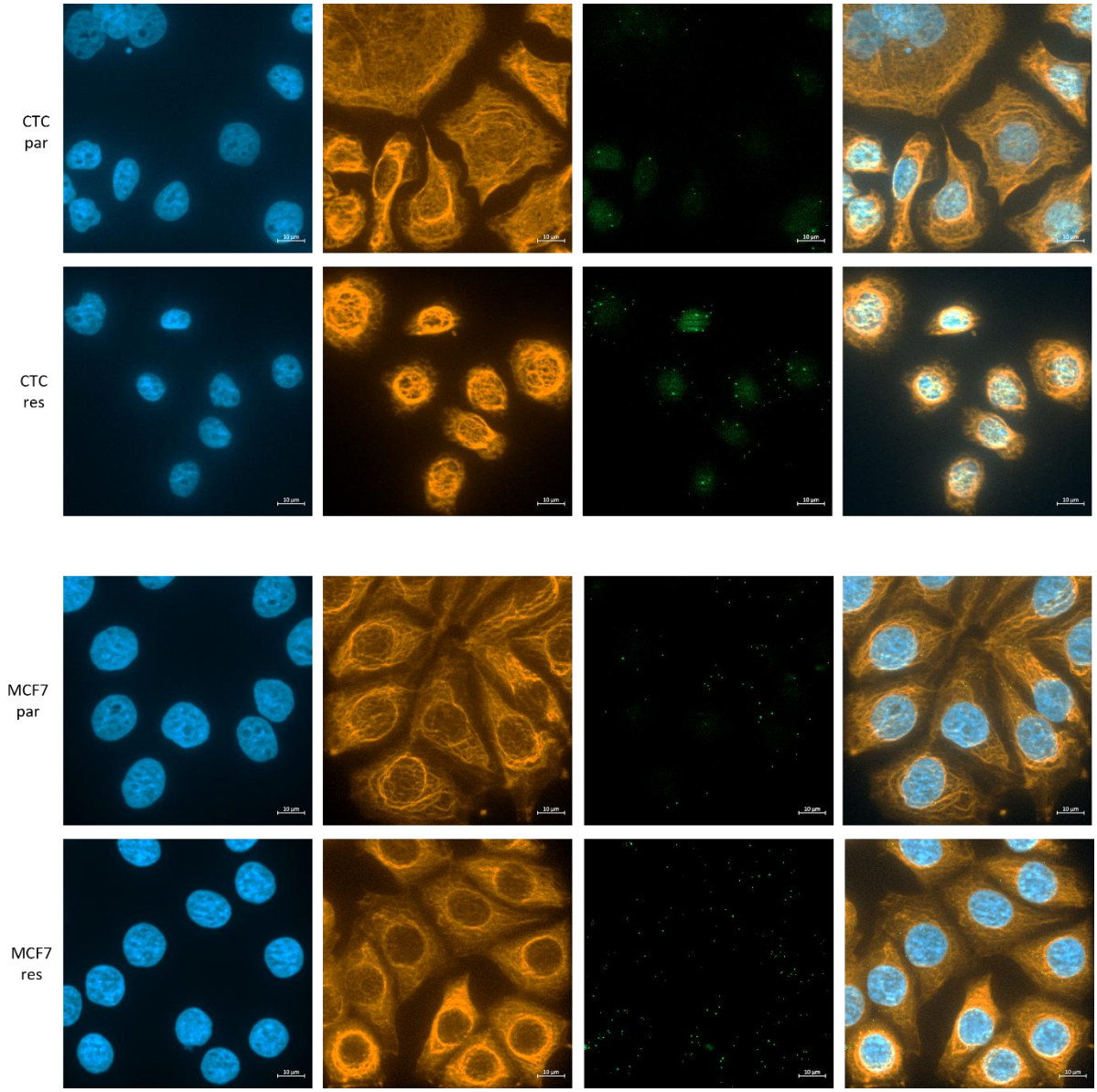

Supplementary Figure S 1: miR-432-5p detection by MISH on parental and resistant CTC-ITB-01 and MCF7 cultivated on chamber slides. Keratin expression was detected using a pan-keratin antibody (clone AE1/AE3, PE, 1:300) and miR-432-5p by an AF488 labeled probe. Nuclei were counterstained with DAPI. The pictures were taken at 63x magnification with oil and a z-stack was acquired using an ApoTome 2.0. Scale bar represents 10 µM.

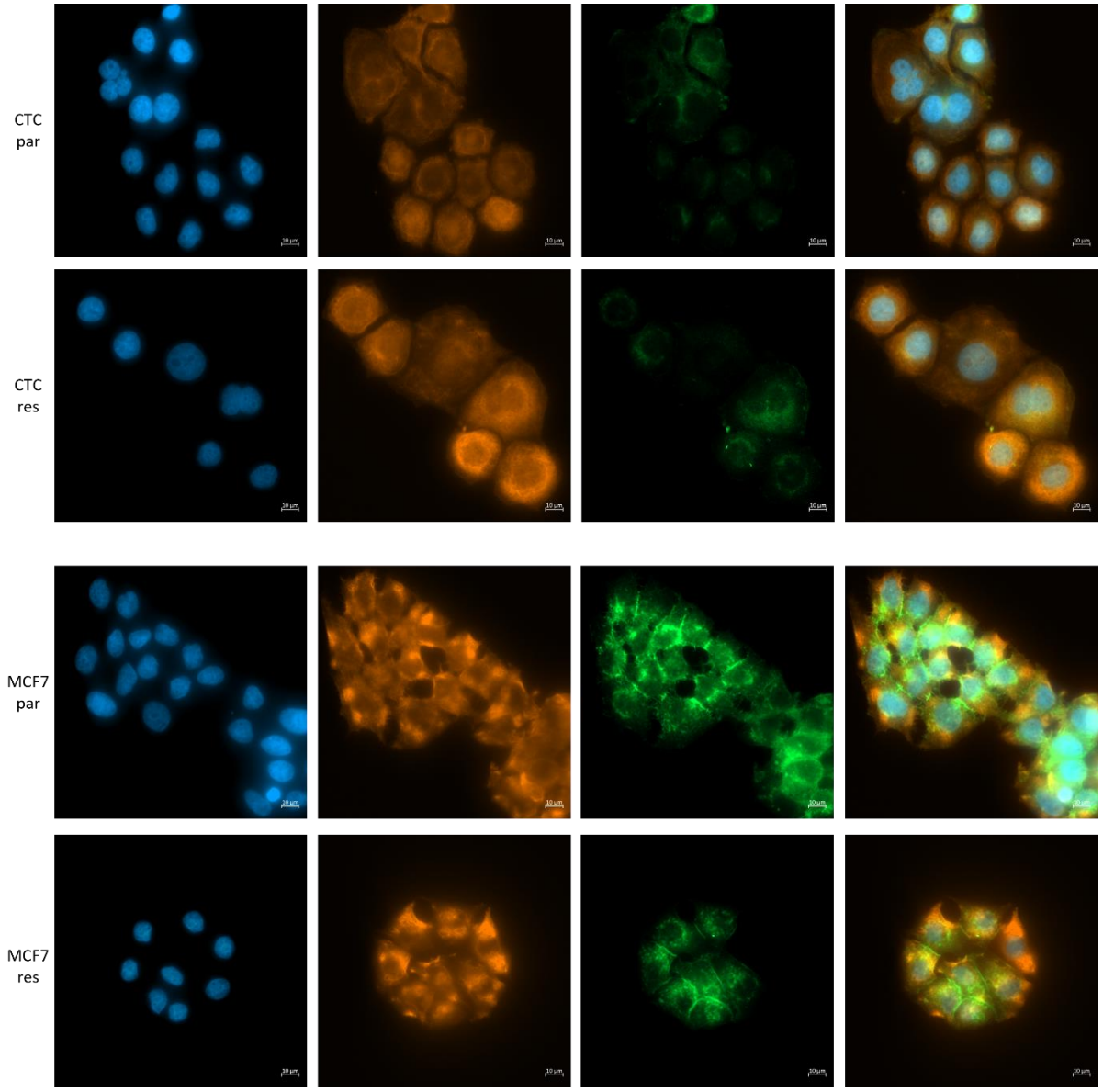

Supplementary Figure S 2: Immunofluorescent staining to detect E-Cadherin in parental and resistant CTC-ITB-01 and MCF7 cells cultivated on chamber slide. E-Cadherin was detected using a monoclonal antibody (clone 36/E, 1:200 dilution). Keratin was detected using a pan-keratin antibody cocktail (clone AE1/AE3, 1:100 dilution and C11, 1:200 dilution). Nuclei were counterstained with DAPI. All images were acquired at a Zeiss-Axio Observer, at 40x magnification. Scale bars represent 20 µM.

Supplementary Table S 2: Genes with increased expression in resistant CTC-ITB-01 cells.

Ensembl	GeneSymbol	gene_biotype	log2FC	FDR
ENSG00000229807	XIST	lncRNA	3,57350584	0
ENSG00000011028	MRC2	protein_coding	4,72829075	3,468E-230
ENSG00000081803	CADPS2	protein_coding	3,66189762	6,856E-150
NSG00000064225	ST3GAL6	protein_coding	4,18291792	9,949E-110
ENSG00000184371	CSF1	protein_coding	2,55009032	4,6281E-94
ENSG00000100170	SLC5A1	protein_coding	3,6516574	4,1537E-92
ENSG00000100097	LGALS1	protein_coding	2,25555311	4,7369E-86
ENSG00000112902	SEMA5A	protein_coding	3,15154848	8,5602E-83
ENSG00000126010	GRPR	protein_coding	4,71563614	3,8106E-80
ENSG00000083720	OXCT1	protein_coding	4,42930487	1,5264E-77
ENSG00000256870	SLC5A8	protein_coding	4,46931006	2,1272E-74
ENSG00000150627	WDR17	protein_coding	2,37050547	6,4546E-73
ENSG00000127954	STEAP4	protein_coding	1,48414552	1,0412E-68
ENSG00000250420	AACSP1	transcribed_unprocessed pseudogene	4,51735407	7,2769E-68
ENSG00000151789	ZNF385D	protein_coding	7,45204765	2,715E-67
ENSG00000173702	MUC13	protein_coding	3,70917439	9,1512E-65
ENSG00000179604	CDC42EP4	protein_coding	1,31476618	3,4775E-64
ENSG00000145685	LHFPL2	protein_coding	1,66580648	5,1299E-63
ENSG00000138696	BMPR1B	protein_coding	1,32737032	3,3608E-61
ENSG00000108244	KRT23	protein_coding	1,89278002	1,0189E-58
ENSG00000112964	GHR	protein_coding	1,95072789	5,0224E-56
ENSG00000096006	CRISP3	protein_coding	1,55296939	3,5059E-54
ENSG00000112977	DAP	protein_coding	1,38041329	6,1823E-52
ENSG00000101974	ATP11C	protein_coding	2,37792121	7,5672E-52
ENSG00000178607	ERN1	protein_coding	1,65915888	1,139E-51
ENSG00000016391	CHDH	protein_coding	2,47221014	1,1214E-50
ENSG00000144868	TMEM108	protein_coding	2,24824206	1,427E-50
ENSG00000159335	PTMS	protein_coding	2,77933339	2,0355E-49
ENSG00000152952	PLOD2	protein_coding	3,5098599	3,1736E-49
ENSG00000213949	ITGA1	protein_coding	2,17510561	5,5065E-49
ENSG00000146242	TPBG	protein_coding	1,68458035	6,0736E-49
ENSG00000145623	OSMR	protein_coding	2,04185896	8,2774E-48
ENSG00000021355	SERPINB1	protein_coding	6,21686314	8,9234E-48
ENSG00000173432	SAA1	protein_coding	3,20997967	2,2236E-47
ENSG00000229314	ORM1	protein_coding	3,61114215	2,7615E-47
ENSG00000119121	TRPM6	protein_coding	2,61811209	5,3006E-47
ENSG00000182798	MAGEB17	protein_coding	6,54554163	6,3098E-46
ENSG00000105419	MEIS3	protein_coding	3,38634992	9,5531E-46
ENSG00000187037	GPR141	protein_coding	1,79653302	2,4409E-45
ENSG00000134339	SAA2	protein_coding	2,14994638	3,2508E-45
ENSG00000125730	C3	protein_coding	3,20914047	4,3351E-45
ENSG00000163697	APBB2	protein_coding	1,55368107	8,1999E-45
ENSG00000140479	PCSK6	protein_coding	1,4437201	8,9141E-45
ENSG00000127249	ATP13A4	protein_coding	3,13691644	6,4208E-44
ENSG00000116711	PLA2G4A	protein_coding	1,60811014	3,8453E-43
ENSG00000198909	MAP3K3	protein_coding	1,24860977	7,7907E-43
ENSG00000143515	ATP8B2	protein_coding	2,2623839	3,6161E-42
ENSG00000184564	SLITRK6	protein_coding	2,62333871	5,3642E-42
ENSG00000173467	AGR3	protein_coding	1,74728631	9,7277E-42
ENSG00000055732	MCOLN3	protein_coding	1,5654878	2,2342E-41
ENSG00000108669	CYTH1	protein_coding	1,14059878	2,8918E-40
ENSG00000137801	THBS1	protein_coding	2,05067483	7,5188E-40
ENSG00000111816	FRK	protein_coding	1,95993895	2,1763E-39
ENSG00000141449	GREB1L	protein_coding	2,56110752	1,2631E-38
ENSG00000214176	PLEKHM1P1	transcribed_unprocessed pseudogene	1,30143173	2,384E-38
ENSG00000144645	OSBPL10	protein_coding	1,22087494	6,1889E-38
ENSG00000099139	PCSK5	protein_coding	3,41901091	9,7363E-38
ENSG00000154305	MIA3	protein_coding	1,11371176	6,369E-37
ENSG00000181458	TMEM45A	protein_coding	2,68065858	1,5943E-36
ENSG00000122176	FMOD	protein_coding	2,11754538	2,1736E-36
ENSG00000197321	SVIL	protein_coding	1,80715688	4,5996E-36
ENSG00000166685	COG1	protein_coding	1,12115623	7,6499E-36
ENSG00000172164	SNTB1	protein_coding	3,06929166	1,1829E-35
ENSG00000185686	PRAME	protein_coding	1,97428888	1,419E-35
ENSG00000057019	DCBLD2	protein_coding	1,33843194	3,3854E-35
ENSG00000258590	NBEAP1	transcribed_unprocessed pseudogene	4,43074679	3,4273E-35
ENSG00000167680	SEMA6B	protein_coding	2,26746962	3,5408E-35
ENSG00000058085	LAMC2	protein_coding	2,49301736	3,5873E-35
ENSG00000134352	IL6ST	protein_coding	1,5040898	8,9667E-35
ENSG00000170745	KCNS3	protein_coding	2,37296493	1,0603E-34
ENSG00000141905	NFIC	protein_coding	1,01285699	2,8801E-34
ENSG00000181744	DIPK2A	protein_coding	1,70068295	1,1149E-33
ENSG00000069974	RAB27A	protein_coding	1,45474729	1,745E-33
ENSG00000184588	PDE4B	protein_coding	1,07348229	3,0007E-33
ENSG00000109466	KLHL2	protein_coding	1,44950504	3,0301E-33
ENSG00000141582	CBX4	protein_coding	1,18375511	3,9742E-33
ENSG00000198929	NOS1AP	protein_coding	2,21032692	4,1257E-33
ENSG00000145545	SRD5A1	protein_coding	1,2703092	5,2781E-33
ENSG00000163597	SNHG16	lncRNA	1,11535152	2,4221E-32
ENSG00000279713		TEC	4,80827632	2,562E-32
ENSG00000167468	GPX4	protein_coding	1,42344868	1,0402E-31
ENSG00000124260	MAGEA10	protein_coding	3,28667024	1,3373E-31
ENSG00000127946	HIP1	protein_coding	1,20000294	3,9727E-31
ENSG00000162627	SNX7	protein_coding	1,78733078	5,3617E-30

ENSG00000150995	ITPR1	protein_coding	1,34635996	8,8144E-30
ENSG00000015133	CCDC88C	protein_coding	1,45793886	1,2588E-29
ENSG00000279864	NCOR1P4	transcribed_processed pseudogene	1,04558284	1,6966E-29
ENSG00000188313	PLSCR1	protein_coding	1,1602003	5,7614E-29
ENSG00000229205	LINC00200	lncRNA	7,3519218	6,5144E-29
ENSG00000145990	GFOD1	protein_coding	1,54476169	7,4286E-29
ENSG00000204237	OXLD1	protein_coding	1,35942217	9,0653E-29
ENSG00000109066	TMEM104	protein_coding	1,0415911	1,1123E-28
ENSG00000155495	MAGEC1	protein_coding	3,78454844	2,9488E-28
ENSG00000174130	TLR6	protein_coding	1,80075627	3,8447E-28
ENSG00000136478	TEX2	protein_coding	1,01096931	5,3518E-28
ENSG00000171867	PRNP	protein_coding	1,74762398	8,5135E-28
ENSG00000078687	TNRC6C	protein_coding	1,07225342	1,3041E-27
ENSG00000185352	HS6ST3	protein_coding	1,66317236	2,8884E-27
ENSG00000078295	ADCY2	protein_coding	2,06211447	6,9457E-27
ENSG00000185359	HGS	protein_coding	1,00002475	8,4243E-27
ENSG00000170962	PDGFD	protein_coding	1,20549008	1,3929E-26
ENSG00000225614	ZNF469	protein_coding	1,41470671	3,4675E-26
ENSG00000206503	HLA-A	protein_coding	1,72374775	4,7734E-26
ENSG00000184792	OSBP2	protein_coding	1,32821727	1,1557E-25
ENSG00000151882	CCL28	protein_coding	3,79911	2,3137E-25
ENSG00000134107	BHLHE40	protein_coding	2,01631167	4,5208E-25
ENSG00000121039	RDH10	protein_coding	1,60063272	4,6221E-25
ENSG00000236283		lncRNA	2,53124502	9,2881E-25
ENSG00000171444	MCC	protein_coding	1,742415	1,0807E-24
ENSG00000198435	NRARP	protein_coding	1,36137683	1,1276E-24
ENSG00000227674	LINC00355	lncRNA	2,29213951	1,5983E-24
ENSG00000078898	BPIFB2	protein_coding	1,18542724	1,6225E-24
ENSG00000160862	AZGP1	protein_coding	1,10962658	1,7983E-24
ENSG00000132334	PTPRE	protein_coding	1,93063978	2,5409E-24
ENSG00000154265	ABCA5	protein_coding	1,24716484	4,2429E-24
ENSG00000169083	AR	protein_coding	1,23954668	5,4211E-24
ENSG00000146530	VWDE	protein_coding	1,68518307	5,8171E-24
ENSG00000105855	ITGB8	protein_coding	3,2222068	8,494E-24
ENSG00000196208	GREB1	protein_coding	2,70307086	1,116E-23
ENSG00000134369	NAV1	protein_coding	1,43854706	1,7235E-23
ENSG00000177738		lncRNA	1,83720522	2,2144E-23
ENSG00000071967	CYBRD1	protein_coding	1,2437644	3,6358E-23
ENSG00000109099	PMP22	protein_coding	2,73177093	6,6579E-23
ENSG00000008277	ADAM22	protein_coding	2,08575982	9,9649E-23
ENSG00000204516	MICB	protein_coding	2,83417988	1,0668E-22
ENSG00000143341	HMCN1	protein_coding	4,07398105	1,2501E-22
ENSG00000168453	HR	protein_coding	1,45718222	1,7924E-22
ENSG00000221869	CEBPD	protein_coding	1,62569053	2,6339E-22
ENSG00000163644	PPM1K	protein_coding	2,08820072	3,2125E-22
ENSG00000135127	BICDL1	protein_coding	1,11170226	3,4672E-22
ENSG00000250510	GPR162	protein_coding	4,37036945	5,2895E-22
ENSG00000179104	TMTC2	protein_coding	1,39531363	6,4071E-22
ENSG00000273654		transcribed_processed pseudogene	3,15794681	1,2507E-21
ENSG00000116991	SIPA1L2	protein_coding	1,60471029	1,631E-21
ENSG00000188906	LRRK2	protein_coding	1,94763577	1,7241E-21
ENSG00000165434	PGM2L1	protein_coding	2,29957033	3,202E-21
ENSG00000239887	C1orf226	protein_coding	2,19674718	3,645E-21
ENSG00000274290	H2BC6	protein_coding	1,30152683	4,0076E-21
ENSG00000080224	EPHA6	protein_coding	3,17134183	4,4019E-21
ENSG00000126890	CTAG2	protein_coding	7,57535995	4,6606E-21
ENSG00000151229	SLC2A13	protein_coding	1,64602267	5,5843E-21
ENSG00000228065	LINC01515	lncRNA	2,15782916	1,1172E-20
ENSG00000070540	WIPI1	protein_coding	1,15415437	1,1543E-20
ENSG00000114423	CBLB	protein_coding	1,48275282	2,2018E-20
ENSG00000167900	TK1	protein_coding	1,05174391	2,2415E-20
ENSG00000136295	TTYH3	protein_coding	1,03558114	2,9965E-20
ENSG00000169604	ANTXR1	protein_coding	1,7206203	2,9965E-20
ENSG00000223969		lncRNA	1,92625748	5,5256E-20
ENSG00000280081	LINC01667	transcribed_processed pseudogene	1,46082127	1,0973E-19
ENSG00000228278	ORM2	protein_coding	3,60133724	1,6357E-19
ENSG00000103021	CCDC113	protein_coding	2,69302024	2,985E-19
ENSG00000114166	KAT2B	protein_coding	1,24406349	4,8373E-19
ENSG00000092964	DPYSL2	protein_coding	1,13325074	7,1323E-19
ENSG00000169814	BTD	protein_coding	1,03508118	1,0317E-18
ENSG00000181788	SIAH2	protein_coding	1,12038638	1,1089E-18
ENSG00000258168		lncRNA	6,2776602	1,1089E-18
ENSG00000134202	GSTM3	protein_coding	1,40610336	2,2557E-18
ENSG00000183010	PYCR1	protein_coding	1,01770095	2,3391E-18
ENSG00000115009	CCL20	protein_coding	1,92061991	2,6802E-18
ENSG00000279041		TEC	3,27476422	3,0087E-18
ENSG00000187231	SESTD1	protein_coding	1,05281744	3,277E-18
ENSG00000178033	CALHM5	protein_coding	4,78491302	3,5866E-18
ENSG00000046774	MAGEC2	protein_coding	2,53238995	4,0775E-18
ENSG00000109089	CDR2L	protein_coding	1,01128904	4,3379E-18
ENSG00000141753	IGFBP4	protein_coding	2,46283986	4,6834E-18
ENSG00000167552	TUBA1A	protein_coding	2,7271855	7,19E-18
ENSG00000114805	PLCH1	protein_coding	1,39634439	7,663E-18
ENSG00000226137	BAIAP2-DT	lncRNA	1,06018795	9,2438E-18
ENSG00000168297	PXK	protein_coding	1,12241029	9,6815E-18
ENSG00000145632	PLK2	protein_coding	1,1851595	1,0204E-17
ENSG00000167861	HID1	protein_coding	1,02173737	1,129E-17

ENSG00000099860	GADD45B	protein_coding	1,44710865	1,3466E-17
ENSG00000184897	H1-10	protein_coding	1,00317663	2,1579E-17
ENSG00000146858	ZC3HAV1L	protein_coding	1,21723004	2,3328E-17
ENSG00000065989	PDE4A	protein_coding	1,74823037	2,8194E-17
ENSG00000183684	ALYREF	protein_coding	1,02125239	2,8705E-17
ENSG00000156475	PPP2R2B	protein_coding	1,19591703	4,6121E-17
ENSG00000185262	UBALD2	protein_coding	1,08525095	5,9981E-17
ENSG00000156804	FBXO32	protein_coding	1,29742174	6,4562E-17
ENSG00000157110	RBPMS	protein_coding	2,52508902	6,5659E-17
ENSG00000284526		protein_coding	1,49645676	6,6064E-17
ENSG00000154153	RETREG1	protein_coding	1,42040784	6,662E-17
ENSG00000111799	COL12A1	protein_coding	2,65709711	7,3084E-17
ENSG00000099250	NRP1	protein_coding	1,34408635	9,1129E-17
ENSG00000131979	GCH1	protein_coding	1,20946187	1,2096E-16
ENSG00000206417	H1-10-AS1	lncRNA	1,36984515	1,228E-16
ENSG00000179083	FAM133A	protein_coding	10,3944723	1,8599E-16
ENSG00000174125	TLR1	protein_coding	2,07802025	2,8559E-16
ENSG00000009694	TENM1	protein_coding	1,36665121	2,9115E-16
ENSG00000260852	FBXL19-AS1	lncRNA	1,06039701	3,6648E-16
ENSG00000109182	CWH43	protein_coding	2,34925942	4,2574E-16
ENSG00000064961	HMG20B	protein_coding	1,03385792	5,0015E-16
ENSG00000143320	CRABP2	protein_coding	1,46650603	5,4123E-16
ENSG00000131746	TNS4	protein_coding	1,48481326	5,7971E-16
ENSG00000130203	APOE	protein_coding	2,2869033	6,5966E-16
ENSG00000174945	AMZ1	protein_coding	1,14277007	9,0593E-16
ENSG00000144366	GULP1	protein_coding	2,34056442	1,093E-15
ENSG00000158163	DZIP1L	protein_coding	1,56818953	1,2484E-15
ENSG00000184454	NCMAP	protein_coding	1,95003918	1,6098E-15
ENSG00000150907	FOXO1	protein_coding	2,05078486	1,7259E-15
ENSG00000169429	CXCL8	protein_coding	1,42157254	1,7814E-15
ENSG00000119698	PPP4R4	protein_coding	3,64205324	2,0823E-15
ENSG00000157796	WDR19	protein_coding	1,24601512	2,9443E-15
ENSG00000265185	SNORD3B-1	snoRNA	1,04926382	3,2232E-15
ENSG00000196517	SLC6A9	protein_coding	1,44873399	4,6257E-15
ENSG00000162896	PIGR	protein_coding	2,52894017	5,8835E-15
ENSG00000075651	PLD1	protein_coding	1,02015972	6,1079E-15
ENSG00000165996	HACD1	protein_coding	2,12461949	7,2227E-15
ENSG00000107438	PDLIM1	protein_coding	1,68946754	1,2469E-14
ENSG00000073849	ST6GAL1	protein_coding	1,06687636	1,8294E-14
ENSG00000132481	TRIM47	protein_coding	1,17186254	2,8387E-14
ENSG00000100077	GRK3	protein_coding	1,01262906	3,2275E-14
ENSG00000282265		lncRNA	6,53411561	3,8519E-14
ENSG00000143512	HHIPL2	protein_coding	1,71248466	5,1842E-14
ENSG00000124343	XG	protein_coding	4,34370877	5,1946E-14
ENSG00000172927	MYEOV	protein_coding	2,69173279	5,2984E-14
ENSG00000197329	PELI1	protein_coding	1,24883781	5,3025E-14
ENSG00000215241	LINC02449	lncRNA	4,2734372	5,7688E-14
ENSG00000249641	HOXC13-AS	lncRNA	1,15754925	8,8697E-14
ENSG00000240032	LNCSRLR	lncRNA	4,17459707	1,2434E-13
ENSG00000183049	CAMK1D	protein_coding	1,74935123	1,436E-13
ENSG00000233930	KRTAP5-AS1	lncRNA	1,7623953	1,5904E-13
ENSG00000165092	ALDH1A1	protein_coding	3,53167873	2,1403E-13
ENSG00000106003	LFNG	protein_coding	1,26659182	2,3193E-13
ENSG00000151575	TEX9	protein_coding	1,24656891	2,6318E-13
ENSG00000085662	AKR1B1	protein_coding	1,54876379	2,6501E-13
ENSG00000182534	MXRA7	protein_coding	1,68257105	2,7005E-13
ENSG00000177728	TMEM94	protein_coding	1,05338898	2,8253E-13
ENSG00000129654	FOXJ1	protein_coding	2,00092411	3,165E-13
ENSG00000283526	PRRT1B	protein_coding	1,49048962	3,8022E-13
ENSG00000226674	TEX41	lncRNA	1,77331968	6,839E-13
ENSG00000285751		lncRNA	9,44573506	6,839E-13
ENSG00000064651	SLC12A2	protein_coding	1,06243041	7,3976E-13
ENSG00000270641	TSIX	lncRNA	3,04586805	8,9564E-13
ENSG00000120306	CYSTM1	protein_coding	1,11458385	1,0373E-12
ENSG00000111058	ACSS3	protein_coding	1,3148733	1,0587E-12
ENSG00000079482	OPHN1	protein_coding	1,01696064	1,1632E-12
ENSG00000140297	GCNT3	protein_coding	2,38544864	1,3571E-12
ENSG00000214313	AZGP1P1	transcribed_unprocessed pseudogene	1,60256402	1,5319E-12
ENSG00000106571	GLI3	protein_coding	1,48358709	1,54E-12
ENSG00000214797		lncRNA	3,46717907	1,6341E-12
ENSG00000139910	NOVA1	protein_coding	1,04590271	2,4111E-12
ENSG00000253125		lncRNA	1,46582504	2,622E-12
ENSG00000135596	MICAL1	protein_coding	1,30985343	2,82E-12
ENSG00000113805	CNTN3	protein_coding	9,25633718	3,5557E-12
ENSG00000147010	SH3KBP1	protein_coding	2,43096382	4,1454E-12
ENSG00000080200	CRYBG3	protein_coding	1,76069733	5,9262E-12
ENSG00000158186	MRAS	protein_coding	1,53746509	6,0235E-12
ENSG00000119655	NPC2	protein_coding	1,06159931	6,7969E-12
ENSG00000139915	MDGA2	protein_coding	3,32828847	7,4746E-12
ENSG00000137462	TLR2	protein_coding	4,38973238	8,3076E-12
ENSG00000232233	LINC02043	lncRNA	1,31306107	8,3971E-12
ENSG00000167191	GPRC5B	protein_coding	1,73532362	8,7292E-12
ENSG00000254290		lncRNA	1,95913652	8,9387E-12
ENSG00000130045	NXNL2	protein_coding	1,57084107	1,0264E-11
ENSG00000136048	DRAM1	protein_coding	1,2644198	1,0748E-11
ENSG00000151632	AKR1C2	protein_coding	1,67164142	1,362E-11
ENSG00000152503	TRIM36	protein_coding	1,67285949	1,3664E-11
ENSG00000166974	MAPRE2	protein_coding	1,25858318	1,5084E-11
ENSG00000276980		lncRNA	3,89339297	1,5307E-11

ENSG00000166750	SLFN5	protein_coding	1,50643336	1,5456E-11
ENSG00000183044	ABAT	protein_coding	1,19775627	1,5947E-11
ENSG00000136531	SCN2A	protein_coding	4,15523436	1,7055E-11
ENSG00000164294	GPX8	protein_coding	1,0538627	1,7867E-11
ENSG00000127561	SYNGR3	protein_coding	1,20487533	2,1751E-11
ENSG00000018236	CNTN1	protein_coding	2,96843245	2,228E-11
ENSG00000109265	CRACD	protein_coding	2,69947729	2,279E-11
ENSG00000122862	SRGN	protein_coding	4,38131575	3,1257E-11
ENSG00000150667	FSIP1	protein_coding	1,73153421	3,1577E-11
ENSG00000197261	C6orf141	protein_coding	3,18300601	4,429E-11
ENSG00000181038	METTL23	protein_coding	1,04483761	5,0626E-11
ENSG00000206192	ANKRD20A9P	unprocessed_pseudogene	1,28451735	5,5127E-11
ENSG00000114790	ARHGEF26	protein_coding	1,9059347	5,8079E-11
ENSG00000147883	CDKN2B	protein_coding	1,29936647	5,8979E-11
ENSG00000116017	ARID3A	protein_coding	1,06095623	5,9785E-11
ENSG00000158639	PAGE5	protein_coding	8,86727874	6,164E-11
ENSG00000180616	SSTR2	protein_coding	2,62307447	7,7726E-11
ENSG00000047457	CP	protein_coding	3,40354582	7,9262E-11
ENSG00000112773	TENT5A	protein_coding	1,24052077	8,0031E-11
ENSG00000154917	RAB6B	protein_coding	1,241663	9,0707E-11
ENSG00000253522	MIR3142HG	lncRNA	1,70033951	1,0129E-10
ENSG00000165259	HDX	protein_coding	4,16857644	1,1146E-10
ENSG00000197860	SGTB	protein_coding	1,1929384	1,2251E-10
ENSG00000076716	GPC4	protein_coding	1,14357889	1,2622E-10
ENSG00000102362	SYTL4	protein_coding	1,0843438	1,2682E-10
ENSG00000050344	NFE2L3	protein_coding	1,08680192	1,3772E-10
ENSG00000145362	ANK2	protein_coding	1,59668724	1,4319E-10
ENSG00000050628	PTGER3	protein_coding	1,8505162	1,8087E-10
ENSG00000161682	FAM171A2	protein_coding	1,60040576	2,0563E-10
ENSG00000261051		lncRNA	3,69189661	2,1874E-10
ENSG00000039560	RAI14	protein_coding	2,07027344	2,3473E-10
ENSG00000132535	DLG4	protein_coding	1,18194671	2,4659E-10
ENSG00000262209	PCDHGB3	protein_coding	1,5164046	2,4971E-10
ENSG00000173852	DPY19L1	protein_coding	1,08811481	2,7157E-10
ENSG00000107242	PIP5K1B	protein_coding	1,25347052	3,3438E-10
ENSG00000141542	RAB40B	protein_coding	1,06837799	3,5365E-10
ENSG00000167355	OR51B5	protein_coding	1,60262945	3,5503E-10
ENSG00000147255	IGSF1	protein_coding	8,09820932	4,6609E-10
ENSG00000148488	ST8SIA6	protein_coding	1,30800922	4,7432E-10
ENSG00000181722	ZBTB20	protein_coding	1,13395227	5,0238E-10
ENSG00000230484	OR51A10P	unitary_pseudogene	2,41141629	5,1228E-10
ENSG00000090339	ICAM1	protein_coding	1,69111998	5,4347E-10
ENSG00000128422	KRT17	protein_coding	2,8728684	5,9993E-10
ENSG00000188039	NWD1	protein_coding	1,60557901	7,452E-10
ENSG00000050438	SLC4A8	protein_coding	1,02049261	7,5645E-10
ENSG00000189171	S100A13	protein_coding	1,23281473	7,638E-10
ENSG00000185046	ANKS1B	protein_coding	1,46552816	7,9114E-10
ENSG00000073150	PANX2	protein_coding	1,41426649	8,172E-10
ENSG00000115257	PCSK4	protein_coding	1,14802073	9,9495E-10
ENSG00000155849	ELMO1	protein_coding	2,03842872	1,2838E-09
ENSG00000144712	CAND2	protein_coding	1,20807374	1,2981E-09
ENSG00000070731	ST6GALNAC2	protein_coding	1,22627498	1,3271E-09
ENSG00000198053	SIRPA	protein_coding	1,18716553	1,3383E-09
ENSG00000275832	ARHGAP23	protein_coding	1,03922666	1,4999E-09
ENSG00000183251	OR51B4	protein_coding	4,1023276	1,6125E-09
ENSG00000286456		lncRNA	1,41278929	1,9297E-09
ENSG00000151746	BICD1	protein_coding	1,13186784	1,995E-09
ENSG00000185761	ADAMTSL5	protein_coding	1,01527001	1,9993E-09
ENSG00000244155	CYP4F34P	unprocessed_pseudogene	1,75089008	2,0761E-09
ENSG00000258883	NBEAP4	unprocessed_pseudogene	4,92841379	2,2344E-09
ENSG00000278626		lncRNA	4,99100188	2,3756E-09
ENSG00000168646	AXIN2	protein_coding	1,72163273	2,4369E-09
ENSG00000138642	HERC6	protein_coding	1,65450354	2,8018E-09
ENSG00000145431	PDGFC	protein_coding	1,56228664	3,3333E-09
ENSG00000004838	ZMYND10	protein_coding	1,86802269	3,4277E-09
ENSG00000141519	CCDC40	protein_coding	1,45181692	3,5314E-09
ENSG00000248424	OR51K1P	unprocessed_pseudogene	3,10011217	3,615E-09
ENSG00000215769	ARHGAP27P1-BPTFP1-KPNA2P3	lncRNA	1,08392091	3,7417E-09
ENSG00000197405	C5AR1	protein_coding	1,73410997	4,0067E-09
ENSG00000125848	FLRT3	protein_coding	1,01604575	4,0524E-09
ENSG00000111859	NEDD9	protein_coding	1,57773383	4,6179E-09
ENSG00000163596	ICA1L	protein_coding	1,53817832	5,5564E-09
ENSG00000185015	CA13	protein_coding	1,57557722	5,985E-09
ENSG00000135842	NIBAN1	protein_coding	1,52608159	6,5411E-09
ENSG00000138722	MMRN1	protein_coding	8,15039999	8,0282E-09
ENSG00000259370		lncRNA	2,2842299	8,254E-09
ENSG00000153714	LURAP1L	protein_coding	1,07545329	9,2845E-09
ENSG00000180801	ARSJ	protein_coding	1,25735967	9,5135E-09
ENSG00000206530	CFAP44	protein_coding	1,21471633	9,9623E-09
ENSG00000135636	DYSF	protein_coding	1,5760579	1,0829E-08
ENSG00000067113	PLPP1	protein_coding	1,1355943	1,2048E-08
ENSG00000114698	PLSCR4	protein_coding	5,54652363	1,2142E-08
ENSG00000167646	DNAAF3	protein_coding	1,1242222	1,3497E-08
ENSG00000205181	LINC00654	lncRNA	1,54879318	1,3884E-08
ENSG00000212916	MAP10	protein_coding	2,83367681	1,4515E-08
ENSG00000109738	GLRB	protein_coding	2,63758881	1,483E-08
ENSG00000251026	LINC02163	lncRNA	3,48587083	1,4954E-08
ENSG00000281706	LINC01012	lncRNA	7,40888937	1,5603E-08

ENSG00000262202		lncRNA	1,34563875	1,769E-08
ENSG00000229131		lncRNA	8,06378076	1,8296E-08
ENSG00000179082	C9orf106	lncRNA	1,33257124	2,1102E-08
ENSG00000276107	THBS1-IT1	lncRNA	2,119077	2,3447E-08
ENSG00000204019	CT83	protein_coding	7,26263106	2,5451E-08
ENSG00000118997	DNAH7	protein_coding	1,96566251	2,6639E-08
ENSG00000065320	NTN1	protein_coding	1,37818814	2,8504E-08
ENSG00000148965	SAA4	protein_coding	2,46281687	2,886E-08
ENSG00000135519	KCNH3	protein_coding	1,66686397	3,0018E-08
ENSG00000228113		lncRNA	1,31310672	3,2645E-08
ENSG00000169750	RAC3	protein_coding	1,01574108	3,44E-08
ENSG00000006638	TBXA2R	protein_coding	1,69657108	3,8241E-08
ENSG00000105613	MAST1	protein_coding	1,48970885	4,1513E-08
ENSG00000177469	CAVIN1	protein_coding	1,07711424	4,3834E-08
ENSG00000113211	PCDHB6	protein_coding	1,5494785	4,5124E-08
ENSG00000254087	LYN	protein_coding	1,2748514	4,674E-08
ENSG00000166250	CLMP	protein_coding	1,63148386	4,8845E-08
ENSG00000230490		lncRNA	1,04341132	5,4046E-08
ENSG00000134955	SLC37A2	protein_coding	2,22623633	5,4268E-08
ENSG00000197249	SERPINA1	protein_coding	1,9829984	5,8232E-08
ENSG00000287460		lncRNA	7,37540768	6,083E-08
ENSG00000170075	GPR37L1	protein_coding	2,06677506	7,0522E-08
ENSG00000163734	CXCL3	protein_coding	4,53627613	8,3173E-08
ENSG00000008311	AASS	protein_coding	1,75811418	9,5211E-08
ENSG00000238178		lncRNA	7,4828087	9,5759E-08
ENSG00000145284	SCD5	protein_coding	1,17075371	1,0742E-07
ENSG00000171791	BCL2	protein_coding	1,11592651	1,2356E-07
ENSG00000161082	CELF5	protein_coding	1,43232784	1,2572E-07
ENSG00000071282	LMCD1	protein_coding	1,01847295	1,4842E-07
ENSG00000232807		lncRNA	1,51284985	1,4842E-07
ENSG00000162366	PDZK1IP1	protein_coding	1,0177488	1,4933E-07
ENSG00000263585		lncRNA	1,07915515	1,494E-07
ENSG00000186481	ANKRD20A5P	transcribed_unprocessed pseudogene	1,77526257	1,5953E-07
ENSG00000182117	NOP10	protein_coding	1,02411439	1,89E-07
ENSG00000101115	SALL4	protein_coding	1,34641562	1,9628E-07
ENSG00000144824	PHLDB2	protein_coding	1,12682879	1,9736E-07
ENSG00000254109	RBPMS-AS1	lncRNA	3,36442603	2,0202E-07
ENSG00000254799	SLC25A47P1	processed_pseudogene	2,41504203	2,0645E-07
ENSG00000168939	SPRY3	protein_coding	1,31153667	2,1677E-07
ENSG00000143502	SUSD4	protein_coding	1,9772095	2,695E-07
ENSG00000133083	DCLK1	protein_coding	2,06167815	2,7898E-07
ENSG00000150687	PRSS23	protein_coding	1,499222	3,2542E-07
ENSG00000174607	UGT8	protein_coding	2,5667141	3,4896E-07
ENSG00000153982	GDPD1	protein_coding	2,36845656	3,5E-07
ENSG00000198774	RASSF9	protein_coding	4,15399335	4,0007E-07
ENSG00000104427	ZC2HC1A	protein_coding	1,43734487	4,1266E-07
ENSG00000278621	THBS1-AS1	lncRNA	2,43914013	4,1398E-07
ENSG00000113248	PCDHB15	protein_coding	2,64180098	4,2833E-07
ENSG00000206535	LNP1	protein_coding	1,46887821	4,3779E-07
ENSG00000088727	KIF9	protein_coding	1,191079	4,5071E-07
ENSG00000106366	SERPINE1	protein_coding	3,44578994	4,6717E-07
ENSG00000167104	BPIFB6	protein_coding	1,30243336	4,8893E-07
ENSG00000286321		lncRNA	7,40600598	4,9476E-07
ENSG00000270344	POC1B-AS1	lncRNA	1,13584453	5,1435E-07
ENSG00000118557	PMFBP1	protein_coding	2,05844857	5,7898E-07
ENSG00000168301	KCTD6	protein_coding	1,04495171	5,8145E-07
ENSG00000214456	PLIN5	protein_coding	1,19295633	6,1906E-07
ENSG00000204642	HLA-F	protein_coding	1,95084114	6,2679E-07
ENSG00000253846	PCDHGA10	protein_coding	1,36783011	6,8219E-07
ENSG00000197599	CCDC154	protein_coding	1,01338457	6,9121E-07
ENSG00000171488	LRRC8C	protein_coding	1,76606002	6,9335E-07
ENSG00000167359	OR51I1	protein_coding	2,5043407	7,0481E-07
ENSG00000235831	BHLHE40-AS1	lncRNA	2,03407238	7,3052E-07
ENSG00000167419	LPO	protein_coding	4,8110051	7,5349E-07
ENSG00000120328	PCDHB12	protein_coding	1,76411708	7,5411E-07
ENSG00000262576	PCDHGA4	protein_coding	1,29260573	8,0467E-07
ENSG00000250786	SNHG18	lncRNA	1,83186244	8,4161E-07
ENSG00000168016	TRANK1	protein_coding	1,1544135	8,8121E-07
ENSG00000253873	PCDHGA11	protein_coding	1,3447781	9,0091E-07
ENSG00000279806		TEC	1,70324306	9,0457E-07
ENSG00000144935	TRPC1	protein_coding	1,0435109	9,0971E-07
ENSG00000253910	PCDHGB2	protein_coding	1,04831771	9,5992E-07
ENSG00000263934	SNORD3A	snoRNA	1,10916054	9,6178E-07
ENSG00000228636	LINC02663	lncRNA	2,40831495	1,0461E-06
ENSG00000165424	ZCCHC24	protein_coding	1,2863481	1,0671E-06
ENSG00000204052	LRRC73	protein_coding	1,08229225	1,0686E-06
ENSG00000163686	ABHD6	protein_coding	1,55382644	1,0719E-06
ENSG00000175155	YPEL2	protein_coding	1,31925677	1,2927E-06
ENSG00000186446	ZNF501	protein_coding	3,45401239	1,3817E-06
ENSG00000003096	KLHL13	protein_coding	1,37296646	1,5265E-06
ENSG00000099256	PRTFDC1	protein_coding	1,62580164	1,6412E-06
ENSG00000227398	KIF9-AS1	lncRNA	1,02447966	1,7818E-06
ENSG00000164764	SBSPON	protein_coding	1,93603225	1,7902E-06
ENSG00000232638		lncRNA	1,4591748	1,7987E-06
ENSG00000167676	PLIN4	protein_coding	1,02792979	2,2729E-06
ENSG00000121552	CSTA	protein_coding	2,88423159	2,2882E-06
ENSG00000287263		lncRNA	2,16686792	2,4293E-06
ENSG00000235631	RNF148	protein_coding	4,07111644	2,7221E-06
ENSG00000003400	CASP10	protein_coding	1,44570148	2,7326E-06

ENSG00000253304	TMEM200B	protein_coding	2,08044564	2,9786E-06
ENSG00000105642	KCNN1	protein_coding	2,92233786	3,0934E-06
ENSG00000138670	RASGEF1B	protein_coding	2,28451294	3,1132E-06
ENSG00000271614	ATP2B1-AS1	lncRNA	1,38834018	3,1322E-06
ENSG00000224383	PRR29	protein_coding	2,40026114	3,2424E-06
ENSG00000239445	ST3GAL6-AS1	lncRNA	4,87524979	3,6894E-06
ENSG00000184557	SOCS3	protein_coding	1,5748684	3,8354E-06
ENSG00000214021	TTLL3	protein_coding	1,24595975	3,9623E-06
ENSG00000233614	DDX11L10	transcribed_unprocessed pseudogene	6,48625003	4,0898E-06
ENSG00000196917	HCAR1	protein_coding	1,38516593	4,6871E-06
ENSG00000188050	RNF133	protein_coding	4,75226618	4,7036E-06
ENSG00000274565		lncRNA	6,84124827	4,7332E-06
ENSG00000124713	GNMT	protein_coding	2,16724155	4,9141E-06
ENSG00000241720		lncRNA	1,6532806	5,4906E-06
ENSG00000269586	CT45A10	protein_coding	1,17138665	5,5092E-06
ENSG00000100842	EFS	protein_coding	1,63889977	5,6574E-06
ENSG00000255622	PCDHB17P	transcribed_unprocessed pseudogene	1,84202912	5,7809E-06
ENSG00000242756	RHOT1P3	processed_pseudogene	1,85667131	6,3646E-06
ENSG00000205420	KRT6A	protein_coding	1,06851336	6,4458E-06
ENSG00000258710	LINC01193	lncRNA	1,00336697	6,6769E-06
ENSG00000165521	EML5	protein_coding	1,16220702	7,394E-06
ENSG00000005379	TSPOAP1	protein_coding	1,22413032	7,4155E-06
ENSG00000166351	POTED	protein_coding	3,2551827	8,2343E-06
ENSG00000063180	CA11	protein_coding	2,27638066	8,4382E-06
ENSG00000274840		lncRNA	1,42058735	8,6259E-06
ENSG00000253731	PCDHGA6	protein_coding	1,16445129	8,8081E-06
ENSG00000169184	MN1	protein_coding	2,03002185	9,0988E-06
ENSG00000262074	SNORD3B-2	snoRNA	1,20679594	9,1152E-06
ENSG00000227568	SNX18P26	processed_pseudogene	1,720773	9,6244E-06
ENSG00000272086	GOLPH3-DT	lncRNA	2,0509729	1,0236E-05
ENSG00000233273	AMMECR1LP1	processed_pseudogene	2,16499555	1,0418E-05
ENSG00000141391	PRELID3A	protein_coding	1,12106762	1,1149E-05
ENSG00000260563		lncRNA	1,52194463	1,2448E-05
ENSG00000258932		transcribed_processed pseudogene	2,03790767	1,263E-05
ENSG00000183186	C2CD4C	protein_coding	1,73823445	1,2858E-05
ENSG00000086288	NME8	protein_coding	1,7295199	1,3163E-05
ENSG00000108797	CNTNAP1	protein_coding	1,16850201	1,5223E-05
ENSG00000271605	MILR1	protein_coding	2,77110782	1,6228E-05
ENSG00000250771		transcribed_unprocessed pseudogene	7,10090426	1,7116E-05
ENSG00000268509		lncRNA	1,6692227	1,7205E-05
ENSG00000262943	ALOX12P2	transcribed_unprocessed pseudogene	1,92526059	1,7646E-05
ENSG00000160469	BRSK1	protein_coding	1,05769753	1,7774E-05
ENSG00000227766		unprocessed_pseudogene	2,03825986	1,8274E-05
ENSG00000133134	BEX2	protein_coding	1,39896052	1,8865E-05
ENSG00000244265	SIAH2-AS1	lncRNA	1,02586857	1,8939E-05
ENSG00000149212	SESN3	protein_coding	1,80954264	1,9358E-05
ENSG00000116774	OLFML3	protein_coding	1,77757394	2,1363E-05
ENSG00000206075	SERPINB5	protein_coding	1,08314938	2,1416E-05
ENSG00000115596	WNT6	protein_coding	1,47843211	2,1829E-05
ENSG00000146001	PCDHB18P	transcribed_unprocessed pseudogene	2,81612061	2,3543E-05
ENSG00000147689	FAM83A	protein_coding	2,06451443	2,3639E-05
ENSG00000176723	ZNF843	protein_coding	2,39149515	2,5166E-05
ENSG00000107249	GLIS3	protein_coding	3,34440564	2,5196E-05
ENSG00000279012	OR51B2	protein_coding	3,29150618	2,6375E-05
ENSG00000235978		lncRNA	1,10480503	2,6562E-05
ENSG00000224728	IMPDH1P8	processed_pseudogene	1,77318189	2,6934E-05
ENSG00000104332	SFRP1	protein_coding	1,96469226	2,7046E-05
ENSG00000261804		lncRNA	1,05223492	2,8742E-05
ENSG00000248909	HMGB1P21	processed_pseudogene	3,23131277	2,8994E-05
ENSG00000198398	TMEM207	protein_coding	5,01649435	3,024E-05
ENSG00000283000	LINC02635	lncRNA	1,52606413	3,5443E-05
ENSG00000101096	NFATC2	protein_coding	1,17644512	3,6193E-05
ENSG00000196565	HBG2	protein_coding	3,28151704	3,7475E-05
ENSG00000118156	ZNF541	protein_coding	3,9845021	4,0734E-05
ENSG00000178538	CA8	protein_coding	1,02872712	4,161E-05
ENSG00000100228	RAB36	protein_coding	3,27361846	4,1851E-05
ENSG00000144045	DQX1	protein_coding	1,04843319	4,2262E-05
ENSG00000089692	LAG3	protein_coding	2,63140344	4,2391E-05
ENSG00000108551	RASD1	protein_coding	1,49148963	4,4166E-05
ENSG00000150594	ADRA2A	protein_coding	1,54548184	4,5138E-05
ENSG00000110031	LPXN	protein_coding	1,03950272	4,8375E-05
ENSG00000266680		lncRNA	1,19103015	5,2099E-05
ENSG00000168916	ZNF608	protein_coding	2,44994377	5,4743E-05
ENSG00000079257	LXN	protein_coding	1,86876535	5,6448E-05
ENSG00000173706	HEG1	protein_coding	1,13168906	6,0188E-05
ENSG00000267283		lncRNA	1,02256941	6,0465E-05
ENSG00000158747	NBL1	protein_coding	1,17659315	6,1674E-05
ENSG00000188211	NCR3LG1	protein_coding	1,20048159	6,7281E-05
ENSG00000286314		lncRNA	1,21065676	6,7291E-05
ENSG00000261371	PECAM1	protein_coding	1,5647902	6,7602E-05
ENSG00000185745	IFIT1	protein_coding	2,03531161	7,4157E-05
ENSG00000206561	COLQ	protein_coding	1,62121776	7,7135E-05
ENSG00000062716	VMP1	protein_coding	1,14599412	7,9562E-05
ENSG00000199568	RNU5A-1	snRNA	1,43346168	8,1017E-05

ENSG00000164938	TP53INP1	protein_coding	1,25855276	8,3263E-05
ENSG00000146038	DCDC2	protein_coding	2,32859812	9,056E-05
ENSG00000185261	KIAA0825	protein_coding	2,15671215	9,0748E-05
ENSG00000150873	C2orf50	protein_coding	1,34369048	9,4507E-05
ENSG00000113763	UNC5A	protein_coding	1,34482018	9,6543E-05
ENSG00000271788		lncRNA	2,79268033	9,6959E-05
ENSG00000197172	MAGEA6	protein_coding	2,63249179	9,76E-05
ENSG00000162068	NTN3	protein_coding	1,47410517	0,00010148
ENSG00000137573	SULF1	protein_coding	4,23448015	0,00010724
ENSG00000248515		lncRNA	1,35545632	0,00010874
ENSG00000108813	DLX4	protein_coding	1,14025692	0,00010915
ENSG00000185736	ADARB2	protein_coding	6,4137792	0,00011015
ENSG00000281091		lncRNA	3,5244014	0,00011121
ENSG00000114654	EFCC1	protein_coding	1,99690561	0,00011688
ENSG00000176532	PRR15	protein_coding	1,01613028	0,00011933
ENSG00000199697	RNU6-446P	snRNA	4,64367618	0,00012069
ENSG00000235823	OLMALINC	lncRNA	1,02691794	0,00012489
ENSG00000148082	SHC3	protein_coding	1,11355656	0,0001267
ENSG00000167105	TMEM92	protein_coding	1,78975405	0,00013034
ENSG00000177606	JUN	protein_coding	1,37990971	0,00013072
ENSG00000235501	CNN3-DT	lncRNA	2,217977	0,0001325
ENSG00000128656	CHN1	protein_coding	1,05903807	0,00013501
ENSG00000136490	LIMD2	protein_coding	1,17445486	0,00014013
ENSG00000172575	RASGRP1	protein_coding	1,86822566	0,0001428
ENSG00000005961	ITGA2B	protein_coding	1,51994864	0,00014292
ENSG00000234602	MCIDAS	protein_coding	1,34592689	0,00014498
ENSG00000184271	POU6F1	protein_coding	3,4436005	0,000145
ENSG00000265458	NARF-AS2	lncRNA	1,66845868	0,0001547
ENSG00000140986	RPL3L	protein_coding	1,80168237	0,00016408
ENSG00000179066		lncRNA	6,25115305	0,00016408
ENSG00000286208		lncRNA	5,25961749	0,00016539
ENSG00000114646	CSPG5	protein_coding	1,1107856	0,00016905
ENSG00000197580	BCO2	protein_coding	1,06308338	0,00017193
ENSG00000242781	LINC02050	lncRNA	3,88929547	0,00018709
ENSG00000165879	FRAT1	protein_coding	1,01508542	0,00018772
ENSG00000095637	SORBS1	protein_coding	1,62462978	0,00018958
ENSG00000237786	GFOD1-AS1	lncRNA	2,17424884	0,00019058
ENSG00000270685	IGHV1OR15-6	IG_V_pseudogene	6,6209681	0,00019078
ENSG00000198959	TGM2	protein_coding	1,91083315	0,00019159
ENSG00000196378	ZNF34	protein_coding	1,21330739	0,00019987
ENSG00000250337	PURPL	lncRNA	1,23221996	0,00020207
ENSG00000262979		lncRNA	1,63612354	0,00020311
ENSG00000234352		lncRNA	1,13721475	0,0002047
ENSG00000260289		lncRNA	1,26394365	0,0002131
ENSG00000102309	PIN4	protein_coding	1,04587001	0,0002176
ENSG00000111728	ST8SIA1	protein_coding	1,41042105	0,00022046
ENSG00000129946	SHC2	protein_coding	4,09783757	0,00022847
ENSG00000197479	PCDHB11	protein_coding	1,01448282	0,00023298
ENSG00000229422		lncRNA	1,03859152	0,00023815
ENSG00000173250	GPR151	protein_coding	3,19554624	0,0002383
ENSG00000242516	LINC00960	lncRNA	2,09017707	0,00024413
ENSG00000170439	METTL7B	protein_coding	5,09065286	0,00026098
ENSG00000142185	TRPM2	protein_coding	1,95311363	0,0002612
ENSG00000164749	HNF4G	protein_coding	1,1202741	0,00026983
ENSG00000261641		lncRNA	1,03378783	0,00027444
ENSG00000227471	AKR1B15	protein_coding	2,17837786	0,00029406
ENSG00000235713		unprocessed_pseudogene	1,52868675	0,00033829
ENSG00000206344	HCG27	lncRNA	1,22724386	0,0003415
ENSG00000262223		lncRNA	1,49986583	0,00035587
ENSG00000265800		lncRNA	1,06344537	0,00036722
ENSG00000254042	SLIT3-AS2	lncRNA	1,60987175	0,00038974
ENSG00000286133		lncRNA	3,9452329	0,00039368
ENSG00000221025	MIR1250	miRNA	2,56918948	0,00041499
ENSG00000166780	BMERB1	protein_coding	1,73979233	0,00046704
ENSG00000279970		TEC	1,89935057	0,00047553
ENSG00000026025	VIM	protein_coding	5,72446525	0,00047828
ENSG00000101695	RNF125	protein_coding	1,04864011	0,00048035
ENSG00000270562		lncRNA	2,26755844	0,00048236
ENSG00000261770		lncRNA	1,25710483	0,00048565
ENSG00000188263	IL17REL	protein_coding	1,33999961	0,00052688
ENSG00000259070	LINC00639	lncRNA	2,03272991	0,00053419
ENSG00000260989		lncRNA	3,06881922	0,00055052
ENSG00000139044	B4GALNT3	protein_coding	1,43680875	0,00055452
ENSG00000119508	NR4A3	protein_coding	1,33872282	0,00055462
ENSG00000177989	ODF3B	protein_coding	1,59633762	0,00055539
ENSG00000166831	RBPMS2	protein_coding	1,24223352	0,00057364
ENSG00000276101		lncRNA	1,01216163	0,00058685
ENSG00000182389	CACNB4	protein_coding	1,35421206	0,00058922
ENSG00000184922	FMNL1	protein_coding	1,01313186	0,00059263
ENSG00000241717	VWFP1	transcribed_unprocessed pseudogene	1,40293512	0,00059452
ENSG00000166349	RAG1	protein_coding	2,00604374	0,00060625
ENSG00000246792		lncRNA	3,19810775	0,00062335
ENSG00000064886	CHI3L2	protein_coding	2,44737485	0,00063802
ENSG00000214274	ANG	protein_coding	1,69587368	0,00064866
ENSG00000175832	ETV4	protein_coding	1,31732998	0,00066639
ENSG00000248498	ASNSP1	transcribed_unprocessed pseudogene	1,31480983	0,00067073
ENSG00000250064		lncRNA	6,31096972	0,00067994
ENSG00000286103		lncRNA	1,22738214	0,00068137

ENSG00000100060	MFNG	protein_coding	1,40422799	0,00068755
ENSG00000152527	PLEKHH2	protein_coding	4,20875396	0,00070593
ENSG00000163347	CLDN1	protein_coding	1,19737738	0,00071244
ENSG00000140564	FURIN	protein_coding	1,50521574	0,00075216
ENSG00000287120		lncRNA	4,91186276	0,00079663
ENSG00000171954	CYP4F22	protein_coding	3,16998919	0,00083383
ENSG00000099260	PALMD	protein_coding	1,11441162	0,00086417
ENSG00000186648	CARMIL3	protein_coding	1,31306974	0,00087489
ENSG00000163536	SERPINI1	protein_coding	1,55732105	0,00088624
ENSG00000091137	SLC26A4	protein_coding	2,67265281	0,00090933
ENSG00000153291	SLC25A27	protein_coding	1,06774615	0,00094058
ENSG00000184058	TBX1	protein_coding	1,36587476	0,00095148
ENSG00000134363	FST	protein_coding	2,00167172	0,00096976
ENSG00000121101	TEX14	protein_coding	1,39689814	0,00097695
ENSG00000258038	LINC02327	lncRNA	1,05480941	0,00099196
ENSG00000150471	ADGRL3	protein_coding	4,74229713	0,00100189
ENSG00000165507	DEPP1	protein_coding	1,72952296	0,00104553
ENSG00000225180	PVALEF	protein_coding	2,07845138	0,00104839
ENSG00000166741	NNMT	protein_coding	1,92177215	0,00106411
ENSG00000177721	ANXA2R	protein_coding	1,03596143	0,00107396
ENSG00000187775	DNAH17	protein_coding	1,38165504	0,00108396
ENSG00000287317		lncRNA	6,29150911	0,00108422
ENSG00000174370	C11orf45	protein_coding	1,05165378	0,00111029
ENSG00000248677	LINC02102	lncRNA	2,69172736	0,0011175
ENSG00000249685		lncRNA	1,38500614	0,0011501
ENSG00000075213	SEMA3A	protein_coding	6,16995756	0,0011951
ENSG00000139117	CPNE8	protein_coding	1,23875008	0,00124341
ENSG00000241935	HOGA1	protein_coding	1,51428241	0,00125409
ENSG00000125744	RTN2	protein_coding	1,1071492	0,00126402
ENSG00000228420	LINC01768	lncRNA	2,23430941	0,00127411
ENSG00000134668	SPOCD1	protein_coding	1,08085967	0,00130584
ENSG00000124102	PI3	protein_coding	2,18881085	0,00131368
ENSG00000188738	FSIP2	protein_coding	1,94424598	0,0013142
ENSG00000243449	C4orf48	protein_coding	1,2762463	0,00132174
ENSG00000175946	KLHL38	protein_coding	2,77178802	0,00134756
ENSG00000237849	NFYAP1	processed_pseudogene	5,1160847	0,00134765
ENSG00000092758	COL9A3	protein_coding	1,09086324	0,0013849
ENSG00000239407		lncRNA	1,05946464	0,00140659
ENSG00000138650	PCDH10	protein_coding	3,71801634	0,00141175
ENSG00000169122	FAM110B	protein_coding	1,79542837	0,00146476
ENSG00000157765	SLC34A2	protein_coding	3,06669759	0,00157814
ENSG00000105122	RASAL3	protein_coding	3,5181337	0,00158795
ENSG00000232400	RAD17P1	processed_pseudogene	1,57970452	0,00160006
ENSG00000118596	SLC16A7	protein_coding	4,48586091	0,00165969
ENSG00000105717	PBX4	protein_coding	1,43074277	0,0016674
ENSG00000284500		lncRNA	3,30453499	0,00169753
ENSG00000268615		lncRNA	1,69177504	0,00176764
ENSG00000036530	CYP46A1	protein_coding	1,88999775	0,00181137
ENSG00000159403	C1R	protein_coding	1,00725957	0,00184512
ENSG00000254122	PCDHGB7	protein_coding	1,05292757	0,0018487
ENSG00000187994	RINL	protein_coding	1,05129864	0,00191457
ENSG00000129682	FGF13	protein_coding	1,19645198	0,00194358
ENSG00000171944	OR52A5	protein_coding	6,17934417	0,00194909
ENSG00000172602	RND1	protein_coding	1,02483739	0,0019749
ENSG00000253159	PCDHGA12	protein_coding	1,08236162	0,0019879
ENSG00000263563	UBBP4	transcribed_unprocessed pseudogene	4,74455644	0,00199758
ENSG00000284834		unprocessed_pseudogene	2,14029655	0,00202645
ENSG00000120324	PCDHB10	protein_coding	1,02255929	0,00204935
ENSG00000267078		lncRNA	1,47987353	0,0020797
ENSG00000130487	KLHDC7B	protein_coding	2,46783833	0,0021059
ENSG00000188856	RPSAP47	processed_pseudogene	1,04295658	0,00210952
ENSG00000279255		TEC	1,79835958	0,00219749
ENSG00000228314	CYP4F29P	transcribed_unprocessed pseudogene	1,24111912	0,00222244
ENSG00000137628	DDX60	protein_coding	1,17127178	0,00225003
ENSG00000270194	GOLGA4-AS1	lncRNA	1,02324829	0,00225464
ENSG00000153132	CLGN	protein_coding	2,57343081	0,00225725
ENSG00000130052	STARD8	protein_coding	2,24237882	0,00225873
ENSG00000161031	PGLYRP2	protein_coding	3,41300078	0,00225873
ENSG00000160182	TFF1	protein_coding	1,24695763	0,00228775
ENSG00000223518	CSNK1A1P1	transcribed_processed pseudogene	1,13867875	0,00232258
ENSG00000240972	MIF	protein_coding	1,70071946	0,00235342
ENSG00000226930	GTF2IP2	unprocessed_pseudogene	4,34154698	0,00237124
ENSG00000141655	TNFRSF11A	protein_coding	4,50899072	0,00245502
ENSG00000286912		lncRNA	1,42237622	0,00257924
ENSG00000124249	KCNK15	protein_coding	1,2332977	0,00259597
ENSG00000170006	TMEM154	protein_coding	1,07608531	0,00263756
ENSG00000128965	CHAC1	protein_coding	1,11958442	0,00269851
ENSG00000038427	VCAN	protein_coding	5,41172434	0,00275653
ENSG00000113946	CLDN16	protein_coding	2,03927612	0,00278558
ENSG00000259435	OR4N3P	transcribed_unprocessed pseudogene	6,09796525	0,00279131
ENSG00000175985	PLEKHD1	protein_coding	1,12674908	0,00285991
ENSG00000249855	EEF1A1P19	processed_pseudogene	1,54475092	0,00291997
ENSG00000185527	PDE6G	protein_coding	2,23944137	0,00298481
ENSG00000270513		processed_pseudogene	3,0696141	0,00299421
ENSG00000167600	CYP2S1	protein_coding	1,601892	0,00301443
ENSG00000261652	C15orf65	protein_coding	5,12369703	0,00301911

ENSG00000163376	KBTBD8	protein_coding	1,0359121	0,00302568
ENSG00000152689	RASGRP3	protein_coding	3,59984241	0,00303151
ENSG00000184194	GPR173	protein_coding	1,31985771	0,00303344
ENSG00000258875		lncRNA	1,73896542	0,00308287
ENSG00000172458	IL17D	protein_coding	1,19060755	0,00310856
ENSG00000248668	OXCT1-AS1	lncRNA	5,36957879	0,00311789
ENSG00000279660		TEC	4,59453488	0,00320941
ENSG00000115414	FN1	protein_coding	1,95444168	0,00324322
ENSG00000025708	TYMP	protein_coding	1,32063393	0,00325586
ENSG00000214319	CXADRP1	processed_pseudogene	3,57179366	0,00328193
ENSG00000159387	IRX6	protein_coding	2,98425054	0,00332438
ENSG00000285128		lncRNA	1,26548115	0,00337868
ENSG00000227619		lncRNA	1,85002127	0,003382
ENSG00000253363		lncRNA	1,32746879	0,003382
ENSG00000250038		lncRNA	1,43672146	0,00354881
ENSG00000073712	FERMT2	protein_coding	1,15070218	0,00359344
ENSG00000208037	MIR320A	miRNA	5,12745854	0,00360069
ENSG00000223584	TVP23CP1	processed_pseudogene	1,30219738	0,00360868
ENSG00000286447		lncRNA	2,53120684	0,00363983
ENSG00000254987		lncRNA	2,09053925	0,00368395
ENSG00000188779	SKOR1	protein_coding	1,46418251	0,00375082
ENSG00000258927		lncRNA	1,08612057	0,00383992
ENSG00000274751		lncRNA	1,4448334	0,00394087
ENSG00000183784	DOCK8-AS1	lncRNA	1,16701623	0,00398406
ENSG00000058404	CAMK2B	protein_coding	1,51174808	0,00400546
ENSG00000161681	SHANK1	protein_coding	4,5170942	0,0040743
ENSG00000122786	CALD1	protein_coding	1,36697883	0,00419016
ENSG00000132563	REEP2	protein_coding	1,30583502	0,00426919
ENSG00000136244	IL6	protein_coding	5,65550724	0,0042769
ENSG00000188343	CIBAR1	protein_coding	1,46297531	0,00441715
ENSG00000267280	TBX2-AS1	lncRNA	1,33158949	0,00446752
ENSG00000287190		lncRNA	1,36655493	0,00447341
ENSG00000236359	OR51B8P	unprocessed_pseudogene	2,39293372	0,0044807
ENSG00000232815	DUX4L50	unprocessed_pseudogene	1,28369686	0,00458849
ENSG00000107796	ACTA2	protein_coding	1,46328091	0,00469604
ENSG00000113070	HBEGF	protein_coding	1,32022162	0,00470396
ENSG00000272142	LYRM4-AS1	lncRNA	1,29561352	0,00475759
ENSG00000164128	NPY1R	protein_coding	1,44620178	0,00481088
ENSG00000157064	NMNAT2	protein_coding	2,28683073	0,00491755
ENSG00000135835	KIAA1614	protein_coding	1,05429823	0,0049568
ENSG00000167895	TMC8	protein_coding	1,1764084	0,00501374
ENSG00000176399	DMRTA1	protein_coding	1,86668835	0,00502415
ENSG00000199032	MIR425	miRNA	2,36565665	0,0050293
ENSG00000226891	LINC01359	lncRNA	2,85664051	0,00509525
ENSG00000279753		TEC	1,34290901	0,00518552
ENSG00000229124	VIM-AS1	lncRNA	5,49290825	0,00521705
ENSG00000231466		processed_pseudogene	1,24173114	0,00525751
ENSG00000239899	RN7SL674P	misc_RNA	3,60664068	0,00540152
ENSG00000286329		lncRNA	3,85760431	0,00547829
ENSG00000136931	NR5A1	protein_coding	1,17150619	0,00590638
ENSG00000274765		lncRNA	5,27331533	0,00592621
ENSG00000213386		processed_pseudogene	5,28104059	0,00596927
ENSG00000225768	LINC02620	lncRNA	4,39884497	0,00607507
ENSG00000130477	UNC13A	protein_coding	2,00474331	0,00608099
ENSG00000249740	OSMR-AS1	lncRNA	1,34308822	0,0062226
ENSG00000212195	U3	snoRNA	1,45438604	0,00623677
ENSG00000125735	TNFSF14	protein_coding	3,6989333	0,00624733
ENSG00000254535	PABPC4L	protein_coding	1,89191554	0,00628261
ENSG00000251209	LINC00923	lncRNA	2,47982581	0,00633076
ENSG00000138311	ZNF365	protein_coding	1,85683167	0,00642547
ENSG00000231566	LINC02595	lncRNA	1,21434011	0,00643477
ENSG00000175471	MCTP1	protein_coding	1,87345851	0,00656251
ENSG00000197506	SLC28A3	protein_coding	4,48012402	0,00664342
ENSG00000105928	GSDME	protein_coding	1,52872845	0,00669111
ENSG00000229544	NKX1-2	protein_coding	1,33113287	0,00683096
ENSG00000168772	CXXC4	protein_coding	2,52590178	0,00687105
ENSG00000149599	DUSP15	protein_coding	3,98290225	0,00688319
ENSG00000230847	OCLNP1	unprocessed_pseudogene	1,10916655	0,00706518
ENSG00000260392		lncRNA	3,09751375	0,00715853
ENSG00000101336	HCK	protein_coding	4,52651435	0,00719576
ENSG00000139269	INHBE	protein_coding	4,09966076	0,0073373
ENSG00000275202		lncRNA	1,34934699	0,00737803
ENSG00000226377		lncRNA	1,33992181	0,00740001
ENSG00000117407	ARTN	protein_coding	2,64930423	0,00740079
ENSG00000165730	STOX1	protein_coding	1,30345089	0,00745915
ENSG00000143552	NUP210L	protein_coding	1,42861007	0,0075267
ENSG00000182326	C1S	protein_coding	1,1205625	0,00760624
ENSG00000223735	OR51B3P	unprocessed_pseudogene	2,56387701	0,00778615
ENSG00000105479	ODAD1	protein_coding	1,47961753	0,00787217
ENSG00000128203	ASPHD2	protein_coding	1,31544921	0,0079296
ENSG00000226238		lncRNA	2,61014242	0,00794866
ENSG00000228450	NLRP7P1	processed_pseudogene	5,1657535	0,00795838
ENSG00000278022		lncRNA	1,20316201	0,00808015
ENSG00000085514	PILRA	protein_coding	1,00905179	0,0080813
ENSG00000228201		lncRNA	1,88795262	0,00824748
ENSG00000114378	HYAL1	protein_coding	1,27581586	0,00829878
ENSG00000105219	CCNP	protein_coding	1,43088716	0,00835154
ENSG00000273448		lncRNA	1,18274021	0,00836898
ENSG00000180543	TSPYL5	protein_coding	2,60552544	0,00837402
ENSG00000138356	AOX1	protein_coding	1,21334962	0,00864007

ENSG00000043591	ADRB1	protein_coding	1,02173264	0,00867553
ENSG00000093134	VNN3	protein_coding	3,39863123	0,00880389
ENSG00000225689		lncRNA	1,48937977	0,00881666
ENSG00000276115		lncRNA	1,98260874	0,00881666
ENSG00000082482	KCNK2	protein_coding	1,75450633	0,0090287
ENSG00000118515	SGK1	protein_coding	1,31537077	0,00905619
ENSG00000258922		lncRNA	1,62981912	0,00935551
ENSG00000175544	CABP4	protein_coding	4,04409242	0,00936876
ENSG00000235500	SNX19P2	processed_pseudogene	1,05064978	0,00946942
ENSG00000174123	TLR10	protein_coding	2,58767285	0,0096
ENSG00000257242	LINC01619	lncRNA	1,42807796	0,00967323
ENSG00000176894	PXMP2	protein_coding	1,02055203	0,00968511
ENSG00000177238	TRIM72	protein_coding	2,24308608	0,00987824
ENSG00000168675	LDLRAD4	protein_coding	2,1062517	0,00988354
ENSG00000198691	ABCA4	protein_coding	1,38985072	0,00991089
ENSG00000183153	GJD3	protein_coding	1,23870035	0,01003186
ENSG00000227908	FLJ31104	lncRNA	2,07211256	0,01010953
ENSG00000207633	MIR505	miRNA	5,01719207	0,01024454
ENSG00000139626	ITGB7	protein_coding	1,17936893	0,01031847
ENSG00000267385		protein_coding	1,36595691	0,01039699
ENSG00000139144	PIK3C2G	protein_coding	2,6859474	0,01050201
ENSG00000274026	FAM27E3	lncRNA	1,39728488	0,01061433
ENSG00000278266		lncRNA	1,00610879	0,0107186
ENSG00000079215	SLC1A3	protein_coding	1,10973037	0,01073527
ENSG00000233901	LINC01503	lncRNA	1,18296622	0,01081113
ENSG00000262172		lncRNA	1,12793816	0,01097403
ENSG00000260992	DOCK9-DT	lncRNA	1,83688206	0,01103094
ENSG00000287299		lncRNA	1,12786348	0,01103094
ENSG00000200651	Y_RNA	misc_RNA	1,13641515	0,01134078
ENSG00000285646		lncRNA	1,20788103	0,01148392
ENSG00000207864	MIR27B	miRNA	1,18557829	0,01175798
ENSG00000287345		lncRNA	1,5527348	0,01185353
ENSG00000106327	TFR2	protein_coding	3,35808203	0,0118661
ENSG00000151883	PARP8	protein_coding	3,97813928	0,01204175
ENSG00000157227	MMP14	protein_coding	1,7217442	0,01216917
ENSG00000151689	INPP1	protein_coding	1,1422918	0,01226177
ENSG00000217733	CCT7P1	processed_pseudogene	1,80240481	0,01228774
ENSG00000185567	AHNAK2	protein_coding	1,1644613	0,01234595
ENSG00000259803	SLC22A31	protein_coding	1,1545954	0,0125383
ENSG00000278630	LINC02335	lncRNA	1,38640198	0,01258598
ENSG00000231574	LINC02015	lncRNA	1,68145767	0,01295615
ENSG00000240057		lncRNA	1,95216638	0,01297343
ENSG00000168306	ACOX2	protein_coding	2,42533714	0,01302374
ENSG00000223813		lncRNA	1,07232947	0,01334284
ENSG00000169064	ZBBX	protein_coding	2,98974815	0,01335571
ENSG00000016402	IL20RA	protein_coding	1,41037091	0,01337342
ENSG00000269961	ERBIN-DT	lncRNA	3,52188998	0,01337903
ENSG00000132357	CARD6	protein_coding	1,6764448	0,01338355
ENSG00000258872	FDPSP3	transcribed_processed pseudogene	1,78289378	0,01350755
ENSG00000267416	HEATR6-DT	lncRNA	1,34484855	0,01353155
ENSG00000106829	TLE4	protein_coding	2,12284499	0,01359998
ENSG00000263883	EEF1DP7	transcribed_processed pseudogene	2,46006692	0,01359998
ENSG00000267121	FMNL1-DT	lncRNA	2,43011022	0,0136334
ENSG00000155254	MARVELD1	protein_coding	1,17794344	0,01367931
ENSG00000224669		processed_pseudogene	2,23215508	0,01376832
ENSG00000250329	KDELC1P1	processed_pseudogene	1,67307571	0,01380846
ENSG00000259087		lncRNA	3,95851854	0,01380846
ENSG00000172780	RAB43	protein_coding	1,02599993	0,01395203
ENSG00000138772	ANXA3	protein_coding	1,1212862	0,01403023
ENSG00000148604	RGR	protein_coding	4,42801094	0,01426758
ENSG00000111186	WNT5B	protein_coding	2,68021865	0,01438049
ENSG00000269807		lncRNA	1,21989191	0,01438058
ENSG00000234618	RPSAP9	processed_pseudogene	1,77255536	0,01442195
ENSG00000134321	RSAD2	protein_coding	2,1073575	0,01445236
ENSG00000145198	VWA5B2	protein_coding	1,18374818	0,01469356
ENSG00000254251		lncRNA	1,38550096	0,01499218
ENSG00000260209		lncRNA	1,55144111	0,01503445
ENSG00000110811	P3H3	protein_coding	4,32189966	0,01505414
ENSG00000180044	C3orf80	protein_coding	4,06401871	0,01558755
ENSG00000070808	CAMK2A	protein_coding	2,07766186	0,01560568
ENSG00000128342	LIF	protein_coding	1,12777832	0,01599026
ENSG00000104267	CA2	protein_coding	3,80579195	0,01616126
ENSG00000181585	TMIE	protein_coding	1,59418587	0,01652244
ENSG00000232081	LARGE-IT1	lncRNA	3,84040745	0,01654592
ENSG00000152910	CNTNAP4	protein_coding	2,86389553	0,01654943
ENSG00000286791		lncRNA	1,35689463	0,01655158
ENSG00000212747	RTL8B	protein_coding	3,80847793	0,01661401
ENSG00000163879	DNALI1	protein_coding	2,6884963	0,01672623
ENSG00000144218	AFF3	protein_coding	3,8044539	0,0167305
ENSG00000196159	FAT4	protein_coding	3,80675571	0,01677189
ENSG00000268104	SLC6A14	protein_coding	1,05345263	0,01696487
ENSG00000154310	TNIK	protein_coding	2,05820768	0,01703658
ENSG00000271133	ITGB8-AS1	lncRNA	4,49846541	0,01703658
ENSG00000000971	CFH	protein_coding	2,6091828	0,01709537
ENSG00000253361		lncRNA	1,44278089	0,01710634
ENSG00000261845		lncRNA	1,08837073	0,01719642
ENSG00000220008	LINGO3	protein_coding	2,66301726	0,01758725
ENSG00000066230	SLC9A3	protein_coding	1,02922697	0,01782855

ENSG00000262652		lncRNA	1,2570984	0,01797144
ENSG00000242715	CCDC169	protein_coding	1,13682084	0,01838978
ENSG00000242419	PCDHGC4	protein_coding	1,26037937	0,01843748
ENSG00000058091	CDK14	protein_coding	1,04173125	0,0184941
ENSG00000273212		lncRNA	1,41633839	0,01857796
ENSG00000278936		lncRNA	1,75143897	0,01866161
ENSG00000183813	CCR4	protein_coding	1,0546876	0,01884899
ENSG00000270714	MICOS10P2	processed_pseudogene	2,28039169	0,01893033
ENSG00000283563		protein_coding	1,36383673	0,01919949
ENSG00000115165	CYTIP	protein_coding	4,28532306	0,01950576
ENSG00000146674	IGFBP3	protein_coding	1,33453268	0,01954691
ENSG00000265692	LINC01970	lncRNA	1,03119481	0,01966638
ENSG00000126970	ZC4H2	protein_coding	3,96466351	0,02007359
ENSG00000230107		lncRNA	3,01865861	0,02011144
ENSG00000124749	COL21A1	protein_coding	1,46605589	0,02014579
ENSG00000107719	PALD1	protein_coding	1,15469139	0,02069649
ENSG00000168356	SCN11A	protein_coding	1,80770551	0,02106537
ENSG00000259295	CSPG4P12	transcribed_unprocessed pseudogene	1,24899945	0,02125165
ENSG00000248712	CCDC153	protein_coding	1,14735749	0,02142924
ENSG00000140798	ABCC12	protein_coding	1,03023429	0,02158487
ENSG00000286846		lncRNA	1,15799044	0,0218372
ENSG00000006071	ABCC8	protein_coding	1,24048672	0,02192373
ENSG00000274225		lncRNA	1,24853474	0,02220119
ENSG00000154645	CHODL	protein_coding	4,49262735	0,02233515
ENSG00000266668	MIR5692C2	miRNA	1,04065795	0,0225851
ENSG00000138641	HERC3	protein_coding	2,30259233	0,0228233
ENSG00000216035	MIR938	miRNA	4,52218895	0,02320719
ENSG00000253366	GUSBP16	unprocessed_pseudogene	2,12647073	0,02333363
ENSG00000259709		lncRNA	1,51118272	0,02368926
ENSG00000267430		processed_pseudogene	2,43833386	0,02378661
ENSG00000254208		lncRNA	2,55029411	0,02391162
ENSG00000254016	ALG1L10P	unprocessed_pseudogene	4,11825352	0,02415359
ENSG00000116014	KISS1R	protein_coding	4,31202083	0,02433906
ENSG00000123700	KCNJ2	protein_coding	2,13015866	0,02433906
ENSG00000123360	PDE1B	protein_coding	4,09924338	0,02457755
ENSG00000244558	KCNK15-AS1	lncRNA	1,15922657	0,02458549
ENSG00000279369		TEC	2,40977973	0,02480517
ENSG00000248489	LINC02062	lncRNA	2,37947999	0,02487312
ENSG00000081853	PCDHGA2	protein_coding	1,24493902	0,02527446
ENSG00000205693	MANSC4	protein_coding	3,74302824	0,02545601
ENSG00000278771	RN7SL3	misc_RNA	1,05540422	0,02555425
ENSG00000267036		processed_pseudogene	3,81973508	0,02556947
ENSG00000242828		lncRNA	3,74638636	0,02667545
ENSG00000273472		lncRNA	1,51123038	0,02760103
ENSG00000203647		processed_pseudogene	1,10211136	0,02767734
ENSG00000259802		lncRNA	1,19061074	0,02805001
ENSG00000184451	CCR10	protein_coding	1,51086536	0,02861712
ENSG00000225546	LINC02476	lncRNA	3,22117378	0,02861712
ENSG00000248697	TOX4P1	processed_pseudogene	2,25996727	0,02862348
ENSG00000276223		lncRNA	1,36100174	0,02863611
ENSG00000286689		lncRNA	1,83001093	0,0288504
ENSG00000198108	CHSY3	protein_coding	2,81434011	0,02943735
ENSG00000272221		lncRNA	1,12787188	0,02951436
ENSG00000135338	LCA5	protein_coding	1,23054422	0,02975276
ENSG00000170909	OSCAR	protein_coding	3,50544165	0,03002877
ENSG00000277563		misc_RNA	1,77778726	0,03002877
ENSG00000277969		lncRNA	1,08297773	0,03003952
ENSG00000224843	LINC00240	lncRNA	1,33351803	0,03023256
ENSG00000012223	LTF	protein_coding	1,79399059	0,03038024
ENSG00000279286		TEC	1,29742246	0,03039478
ENSG00000257829		lncRNA	1,00283637	0,03043635
ENSG00000266405	CBX3P2	transcribed_processed pseudogene	2,33635375	0,03044586
ENSG00000228727	SAPCD1	protein_coding	2,23487959	0,03047879
ENSG00000282815	TEX13C	protein_coding	3,23328369	0,03061
ENSG00000102313	ITIH6	protein_coding	1,30049618	0,03075897
ENSG00000006042	TMEM98	protein_coding	1,01390172	0,03083527
ENSG00000119630	PGF	protein_coding	3,56384323	0,03095956
ENSG00000111052	LIN7A	protein_coding	1,98354855	0,03100371
ENSG00000196183	RPS2P4	processed_pseudogene	3,37678455	0,03155399
ENSG00000227145	IL21-AS1	lncRNA	3,55645854	0,03190647
ENSG00000279600		TEC	1,2431527	0,0319341
ENSG00000184659	FOXD4L4	protein_coding	1,24095395	0,03211554
ENSG00000272750		lncRNA	1,00365076	0,03245468
ENSG00000256001		lncRNA	2,94304634	0,03255177
ENSG00000123119	NECAB1	protein_coding	1,16625324	0,03263575
ENSG00000183484	GPR132	protein_coding	1,83512838	0,03264458
ENSG00000132821	VSTM2L	protein_coding	2,51979412	0,03271988
ENSG00000137441	FGFBP2	protein_coding	2,73924968	0,03312748
ENSG00000286579		lncRNA	1,05551724	0,03329695
ENSG00000143344	RGL1	protein_coding	1,22445766	0,03342098
ENSG00000274964		lncRNA	1,13191296	0,03356037
ENSG00000276545	PCDHGB9P	unprocessed_pseudogene	1,15262063	0,03423997
ENSG00000276533		lncRNA	1,72161958	0,03433157
ENSG00000185479	KRT6B	protein_coding	1,15720933	0,03450578
ENSG00000172031	EPHX4	protein_coding	1,25997804	0,03547887
ENSG00000281501	SEPSECS-AS1	lncRNA	1,20096011	0,03581563
ENSG00000258824		lncRNA	1,03787984	0,03595672
ENSG00000269886		lncRNA	2,67052407	0,03610991

ENSG00000007933	FMO3	protein_coding	4,73622264	0,03627994
ENSG00000279107		TEC	1,16097517	0,03650933
ENSG00000267201	LINC01775	lncRNA	1,02764785	0,03666814
ENSG00000266145	RHOT1P1	processed_pseudogene	3,32782857	0,03709368
ENSG00000249850	KRT18P31	processed_pseudogene	1,04099081	0,0374413
ENSG00000133048	CHI3L1	protein_coding	4,56822407	0,03744992
ENSG00000243762		lncRNA	1,19156616	0,03770889
ENSG00000248803		processed_pseudogene	2,61692584	0,03775747
ENSG00000166432	ZMAT1	protein_coding	1,41898698	0,03784161
ENSG00000275765		lncRNA	1,07794356	0,03853434
ENSG00000145506	NKD2	protein_coding	1,79846959	0,03872606
ENSG00000286369		lncRNA	4,14565445	0,0392915
ENSG00000187959	CPSF4L	protein_coding	1,40271536	0,03936954
ENSG00000175336	APOF	protein_coding	2,50687011	0,03942648
ENSG00000269371		lncRNA	1,01360833	0,03956904
ENSG00000255727	LINC01489	lncRNA	2,19032767	0,03958187
ENSG00000115355	CCDC88A	protein_coding	1,13393862	0,0396458
ENSG00000162989	KCNJ3	protein_coding	2,86247111	0,03977124
ENSG00000269954		lncRNA	1,47883041	0,04007297
ENSG00000139219	COL2A1	protein_coding	3,93074436	0,0401645
ENSG00000172232	AZU1	protein_coding	2,17182263	0,04019325
ENSG00000263718	SEPTIN9-DT	lncRNA	1,2498644	0,04093444
ENSG00000169682	SPNS1	protein_coding	1,05804139	0,04104723
ENSG00000118160	SLC8A2	protein_coding	1,95260223	0,04120774
ENSG00000013619	MAMLD1	protein_coding	2,86577233	0,04124812
ENSG00000200783	RN7SKP180	misc_RNA	2,97663966	0,04199232
ENSG00000260018		lncRNA	1,2670334	0,04224424
ENSG00000228328	PGK1P1	processed_pseudogene	1,58896848	0,04238168
ENSG00000123838	C4BPA	protein_coding	1,21913885	0,04251971
ENSG00000139352	ASCL1	protein_coding	2,1288457	0,04266803
ENSG00000166268	MYRFL	protein_coding	2,40750675	0,0427481
ENSG00000259240	MIR4713HG	lncRNA	3,30124253	0,04285966
ENSG00000164125	GASK1B	protein_coding	1,1077671	0,04304875
ENSG00000274712		transcribed_unprocessed pseudogene	2,43522652	0,04314524
ENSG00000258997	NF1P2	unprocessed_pseudogene	1,80379907	0,04328694
ENSG00000249492		lncRNA	1,06887326	0,04336711
ENSG00000216490	IFI30	protein_coding	1,402783	0,0434305
ENSG00000216906		processed_pseudogene	1,16653135	0,04355335
ENSG00000133640	LRRIQ1	protein_coding	1,29499642	0,04384689
ENSG00000279703		TEC	4,00740808	0,04416329
ENSG00000156689	GLYATL2	protein_coding	3,51460978	0,04433238
ENSG00000259345		lncRNA	2,00865479	0,0445167
ENSG00000243649	CFB	protein_coding	1,09052392	0,04568334
ENSG00000116741	RGS2	protein_coding	1,36733036	0,04599111
ENSG00000224578	HNRNPA1P48	protein_coding	1,03450922	0,04649411
ENSG00000274849		lncRNA	1,05418192	0,04703724
ENSG00000238279		lncRNA	1,45440118	0,04726505
ENSG00000165512	ZNF22	protein_coding	2,33821351	0,04733093
ENSG00000234719	NPIPB2	protein_coding	3,16615281	0,04754534
ENSG00000177453	NIM1K	protein_coding	1,14885529	0,04796172
ENSG00000270022		lncRNA	1,36813614	0,04840124
ENSG00000159527	PGLYRP3	protein_coding	3,92125034	0,04874872
ENSG00000259611	LINC01582	lncRNA	2,08406441	0,04874982
ENSG00000280007		lncRNA	1,16337897	0,04902781
ENSG00000213023	SYT3	protein_coding	3,38758431	0,04905751
ENSG00000127863	TNFRSF19	protein_coding	3,99333226	0,04912724
ENSG00000250001		lncRNA	3,65585616	0,04954319
ENSG00000196136	SERPINA3	protein_coding	2,69117562	0,04979396
ENSG00000235947	EGOT	lncRNA	1,66976367	0,04984932
ENSG00000100626	GALNT16	protein_coding	1,01182651	0,05032234
ENSG00000260509		lncRNA	3,99237336	0,05097837
ENSG00000185477	GPRIN3	protein_coding	3,80361152	0,05135274
ENSG00000250234		lncRNA	1,85837974	0,05178528
ENSG00000215244	LINC02649	lncRNA	1,06668284	0,051901
ENSG00000245552		lncRNA	1,94891956	0,0520996
ENSG00000272137		lncRNA	3,97887359	0,05224882
ENSG00000280278	FLJ30679	TEC	3,4532579	0,05245623
ENSG00000234753	FOXP4-AS1	lncRNA	1,18746199	0,05271527
ENSG00000179899	PHC1P1	processed_pseudogene	1,44530496	0,05281122
ENSG00000188257	PLA2G2A	protein_coding	1,26554235	0,05343326
ENSG00000277728		lncRNA	1,02829012	0,05343326
ENSG00000249345	LINC02405	lncRNA	1,17421346	0,05369464
ENSG00000261889		lncRNA	1,28707144	0,05392461
ENSG00000137965	IFI44	protein_coding	5,13787209	0,05439719
ENSG00000259498	TPM1-AS	lncRNA	1,12256065	0,05452468
ENSG00000186377	CYP4X1	protein_coding	1,47660552	0,05532887
ENSG00000260284	TPSP2	unprocessed_pseudogene	3,16053446	0,05532887
ENSG00000077935	SMC1B	protein_coding	3,60804252	0,05567594
ENSG00000273447		lncRNA	3,92052452	0,05568774
ENSG00000170819	BFSP2	protein_coding	3,01004895	0,05571267
ENSG00000285571		lncRNA	4,08253791	0,05585394
ENSG00000215930	MIR942	miRNA	1,78001013	0,05592387
ENSG00000180447	GAS1	protein_coding	2,051559	0,05601025
ENSG00000278873	PRO1804	TEC	3,97044335	0,05643288
ENSG00000266959		processed_pseudogene	2,72528025	0,0566204
ENSG00000126709	IFI6	protein_coding	1,74145957	0,05662626
ENSG00000224397	PELATON	lncRNA	1,95488709	0,05669377
ENSG00000225094	SETP20	processed_pseudogene	3,83753841	0,05726239
ENSG00000118407	FILIP1	protein_coding	1,3270561	0,05727446

ENSG00000201616	RNU1-91P	snRNA	1,0620906	0,05778213
ENSG00000225857	LINC02816	lncRNA	1,87574559	0,05797226
ENSG00000275160		processed_pseudogene	3,1645914	0,05833879
ENSG00000266144	MIR4654	miRNA	2,38696838	0,05844136
ENSG00000175267	VWA3A	protein_coding	1,82848832	0,05865855
ENSG00000286416		lncRNA	1,18181461	0,05918045
ENSG00000285943		protein_coding	1,08827127	0,0594544
ENSG00000267308	LINC01764	lncRNA	2,80977562	0,05968844
ENSG00000249069	LINC01033	lncRNA	3,6108805	0,06006105
ENSG00000139174	PRICKLE1	protein_coding	1,78679366	0,06061472
ENSG00000283444	GPR141BP	unitary_pseudogene	1,4727805	0,06085855
ENSG00000229356	LRRC3-DT	lncRNA	1,18424342	0,06127364
ENSG00000171847	FAM90A1	protein_coding	5,28395732	0,06185609
ENSG00000146013	GFRA3	protein_coding	2,2419278	0,06204161
ENSG00000183171		processed_pseudogene	3,48290366	0,0622811
ENSG00000188013	MEIS3P2	processed_pseudogene	1,08759174	0,06240566
ENSG00000179967	PPP1R14BP3	processed_pseudogene	1,79560679	0,06267488
ENSG00000227076		lncRNA	1,67798883	0,06354669
ENSG00000256625		unprocessed_pseudogene	3,97954002	0,06358937
ENSG00000281347	NF1P9	transcribed_unprocessed_pseudogene	1,12661412	0,06443083
ENSG00000235838	HSP90AB7P	processed_pseudogene	2,23691544	0,06523492
ENSG00000278662	GOLGA6L10	protein_coding	1,03317752	0,06538473
ENSG00000163380	LMOD3	protein_coding	1,03628597	0,06630456
ENSG00000206113	CFAP99	protein_coding	2,09665799	0,06630456
ENSG00000279246		TEC	1,19882032	0,06634538
ENSG00000286895		lncRNA	2,00510779	0,06653357
ENSG00000158458	NRG2	protein_coding	1,31184929	0,06653537
ENSG00000254180		lncRNA	1,31931229	0,06678154
ENSG00000287780		lncRNA	1,39512696	0,06700621
ENSG00000242614	RN7SL164P	misc_RNA	1,17642002	0,06737124
ENSG00000253878		lncRNA	1,02665865	0,06737124
ENSG00000267637		lncRNA	1,47661114	0,06781716
ENSG00000266473	HELZ-AS1	lncRNA	1,94649962	0,06785367
ENSG00000214919		lncRNA	1,07682207	0,06814053
ENSG00000182575	NXPH3	protein_coding	1,05830313	0,06817402
ENSG00000254505	CHMP4A	protein_coding	1,01327976	0,06834312
ENSG00000234807	LINC01135	lncRNA	1,50072956	0,06853278
ENSG00000233297	RASA4DP	unprocessed_pseudogene	2,06282952	0,06889983
ENSG00000242391		lncRNA	3,79168947	0,0690513
ENSG00000221953	C1orf229	lncRNA	2,96707033	0,06983703
ENSG00000196092	PAX5	protein_coding	1,1497962	0,06987484
ENSG00000230316	FEZF1-AS1	lncRNA	3,12450884	0,06997554
ENSG00000260009	LINC02130	lncRNA	2,22965349	0,07008178
ENSG00000183690	EFHC2	protein_coding	1,2602663	0,0704633
ENSG00000260702		unprocessed_pseudogene	3,77579879	0,07085735
ENSG00000265948		lncRNA	3,60044282	0,07127116
ENSG00000105641	SLC5A5	protein_coding	1,47703554	0,07209574
ENSG00000239607	RN7SL573P	misc_RNA	2,65595831	0,07227561
ENSG00000105371	ICAM4	protein_coding	2,60101385	0,07239314
ENSG00000206341	HLA-H	unprocessed_pseudogene	1,84220427	0,07249109
ENSG00000213025	COX20P1	processed_pseudogene	2,12846041	0,07249602
ENSG00000177519	RPRM	protein_coding	1,23319242	0,0725864
ENSG00000244668	SNRPCP3	processed_pseudogene	2,34076151	0,07275592
ENSG00000104889	RNASEH2A	protein_coding	1,10391478	0,07299935
ENSG00000272763		lncRNA	2,80288105	0,07309583
ENSG00000279020	C18orf15	TEC	1,92736298	0,07348689
ENSG00000273141		lncRNA	3,41641368	0,07419627
ENSG00000236529		lncRNA	1,09291576	0,07423001
ENSG00000175463	TBC1D10C	protein_coding	1,47306565	0,07426558
ENSG00000257842	LINC02588	lncRNA	3,17633737	0,07436182
ENSG00000166428	PLD4	protein_coding	2,84756071	0,07445751
ENSG00000229852		lncRNA	1,54554383	0,07477701
ENSG00000120262	CCDC170	protein_coding	3,12842956	0,07485836
ENSG00000223725		lncRNA	1,85642059	0,07502477
ENSG00000252242	RNU7-115P	snRNA	1,96789306	0,07507462
ENSG00000258813		lncRNA	1,45367946	0,07511941
ENSG00000196844	PATE2	protein_coding	3,38593484	0,07541785
ENSG00000031081	ARHGAP31	protein_coding	1,24012208	0,07549159
ENSG00000277342		lncRNA	1,43536524	0,07637168
ENSG00000267751	BSG-AS1	lncRNA	1,0908859	0,07651444
ENSG00000160539	PLPP7	protein_coding	1,92652088	0,07676537
ENSG00000240583	AQP1	protein_coding	1,35874718	0,07688713
ENSG00000131044	TTLL9	protein_coding	2,87874676	0,07836907
ENSG00000145832	SLC25A48	protein_coding	3,00830632	0,07912937
ENSG00000224216		lncRNA	1,45919525	0,0792235
ENSG00000096088	PGC	protein_coding	2,32750401	0,07945197
ENSG00000263155	MYZAP	protein_coding	1,70812814	0,07989218
ENSG00000241269		lncRNA	1,53859336	0,08018852
ENSG00000237738	RNF216-IT1	lncRNA	1,33007984	0,08022627
ENSG00000244607	CCDC13	protein_coding	1,50870221	0,08043158
ENSG00000287975		lncRNA	1,42791918	0,08044581
ENSG00000233108	GLCCI1-DT	lncRNA	1,19914137	0,0810663
ENSG00000091986	CCDC80	protein_coding	1,30182061	0,08180967
ENSG00000146090	RASGEF1C	protein_coding	3,40994387	0,08220189
ENSG00000272906		lncRNA	1,00514326	0,08250834
ENSG00000095596	CYP26A1	protein_coding	2,39227414	0,08252266
ENSG00000240964	RN7SL751P	misc_RNA	1,44104043	0,08260714
ENSG00000255508		protein_coding	1,34800631	0,08292835
ENSG00000255992		lncRNA	1,19111374	0,08294923

ENSG00000240531	RPL21P123	transcribed_processed pseudogene	3,82734766	0,08298259
ENSG00000221883	ARIH2OS	lncRNA	1,25607131	0,08316537
ENSG00000234841		processed_pseudogene	2,39383445	0,08347746
ENSG00000250906		lncRNA	1,59195568	0,08431571
ENSG00000240668	KRT8P36	processed_pseudogene	1,94702741	0,08450005
ENSG00000095370	SH2D3C	protein_coding	3,09778205	0,08459933
ENSG00000152672	CLEC4F	protein_coding	2,84919968	0,08480281
ENSG00000102935	ZNF423	protein_coding	3,35175227	0,08492456
ENSG00000225864		unprocessed_pseudogene	1,953798	0,08518027
ENSG00000135929	CYP27A1	protein_coding	1,3359854	0,08522304
ENSG00000228873		lncRNA	3,50215295	0,08533948
ENSG00000273320		lncRNA	1,74203542	0,08653022
ENSG00000214067		processed_pseudogene	2,21294647	0,08684423
ENSG00000261766		lncRNA	1,1160904	0,08708088
ENSG00000286607		lncRNA	3,40867369	0,08737087
ENSG00000261386		lncRNA	1,29640794	0,08753696
ENSG00000254273		processed_pseudogene	1,87095015	0,08846
ENSG00000271737		lncRNA	1,37716786	0,089259
ENSG00000140511	HAPLN3	protein_coding	1,90251835	0,08956685
ENSG00000250254	PTTG2	protein_coding	2,46281577	0,08985359
ENSG00000112837	TBX18	protein_coding	2,15436539	0,08998208
ENSG00000185467	KPNA7	protein_coding	2,01099196	0,09031561
ENSG00000139351	SYCP3	protein_coding	1,43960215	0,09049427
ENSG00000159307	SCUBE1	protein_coding	2,78376772	0,09115877
ENSG00000113721	PDGFRB	protein_coding	2,21074835	0,09153175
ENSG00000242318		processed_pseudogene	2,2359413	0,09206288
ENSG00000125869	LAMP5	protein_coding	2,25335917	0,09226528
ENSG00000148483	TMEM236	protein_coding	2,0266275	0,09229398
ENSG00000150281	CTF1	protein_coding	3,13639308	0,09234357
ENSG00000205189	ZBTB10	protein_coding	2,18447732	0,09234357
ENSG00000157335	CLEC18C	protein_coding	1,52067998	0,09250043
ENSG00000285938		protein_coding	2,13153301	0,09284937
ENSG00000255837	TAS2R20	protein_coding	1,06257636	0,09304054
ENSG00000101638	ST8SIA5	protein_coding	1,29303726	0,09423672
ENSG00000170577	SIX2	protein_coding	2,19273038	0,09426691
ENSG00000277597		lncRNA	1,31215109	0,09459931
ENSG00000278642		lncRNA	2,40210672	0,09483616
ENSG00000265113		lncRNA	2,160127	0,09514161
ENSG00000228124		lncRNA	3,20811631	0,09554419
ENSG00000288552		lncRNA	3,95344061	0,09554419
ENSG00000183778	B3GALT5	protein_coding	1,32870791	0,09565944
ENSG00000164106	SCRG1	protein_coding	3,53212761	0,09569225
ENSG00000126778	SIX1	protein_coding	2,84276153	0,09573153
ENSG00000176788	BASP1	protein_coding	2,84800737	0,09587288
ENSG00000223802	CERS1	protein_coding	1,94491332	0,09623522
ENSG00000171502	COL24A1	protein_coding	1,93554764	0,09628695
ENSG00000270426		lncRNA	1,1321659	0,09658298
ENSG00000240219		lncRNA	2,24148597	0,09661191
ENSG00000288046		lncRNA	3,32506877	0,09681424
ENSG00000174640	SLCO2A1	protein_coding	1,81539242	0,09693619
ENSG00000159763	PIP	protein_coding	2,77821488	0,09725256
ENSG00000179978	NAIPP2	unprocessed_pseudogene	1,62585904	0,09749537
ENSG00000251363	LINC02315	lncRNA	1,14024635	0,09777258
ENSG00000118514	ALDH8A1	protein_coding	1,58489788	0,09803856
ENSG00000260996		lncRNA	1,66565359	0,09835758
ENSG00000239440	LINC02008	lncRNA	4,27659371	0,09852861
ENSG00000183615	FAM167B	protein_coding	2,07895779	0,09892553
ENSG00000183833	CFAP91	protein_coding	2,64847916	0,09909729
ENSG00000142449	FBN3	protein_coding	1,19623139	0,09950013

Supplementary Table S 3: Genes with decreased expression in resistant CTC-ITB-01 cells.

Ensembl	GeneSymbol	gene_biotype	log2FC	FDR
ENSG00000134240	HMGCS2	protein_coding	-4,33367146	2,452E-162
ENSG00000038382	TRIO	protein_coding	-4,53510489	1,538E-141
ENSG00000198947	DMD	protein_coding	-6,78525897	8,995E-139
ENSG00000170477	KRT4	protein_coding	-3,66321142	6,673E-117
ENSG00000073464	CLCN4	protein_coding	-2,608849	5,428E-106
ENSG00000156113	KCNMA1	protein_coding	-2,58717891	4,523E-98
ENSG00000213401	MAGEA12	protein_coding	-4,41013969	3,7114E-94
ENSG00000184828	ZBTB7C	protein_coding	-3,20649823	2,6713E-92
ENSG00000152127	MGAT5	protein_coding	-4,55083707	4,3192E-91
ENSG00000170921	TANC2	protein_coding	-5,36621394	3,2429E-87
ENSG00000177932	ZNF354C	protein_coding	-3,33017794	1,3149E-83
ENSG00000281406	BLACAT1	protein_coding	-3,89865339	4,3165E-81
ENSG00000101871	MID1	protein_coding	-1,95417835	9,5655E-79
ENSG00000242779	ZNF702P	transcribed_processed pseudogene	-3,0782399	7,7661E-78
ENSG00000153292	ADGRF1	protein_coding	-2,04487017	1,53E-75
ENSG00000103381	CPPED1	protein_coding	-3,11455422	7,05E-75
ENSG00000186767	SPIN4	protein_coding	-1,86310199	1,6099E-64
ENSG00000137460	FHDC1	protein_coding	-1,94163807	1,6446E-63
ENSG00000134531	EMP1	protein_coding	-1,59306871	2,975E-62
ENSG00000147041	SYTL5	protein_coding	-2,47734543	3,2341E-62
ENSG00000261115	TMEM178B	protein_coding	-4,52906634	1,079E-57
ENSG00000112655	PTK7	protein_coding	-1,98902786	8,4167E-53
ENSG00000149260	CAPN5	protein_coding	-2,28128663	1,0599E-51
ENSG00000139973	SYT16	protein_coding	-7,27698117	1,4431E-49

ENSG00000168672	LRATD2	protein_coding	-1,50858961	6,9425E-49
ENSG00000101868	POLA1	protein_coding	-1,24577852	7,6336E-48
ENSG00000005020	SKAP2	protein_coding	-1,84040539	2,7006E-47
ENSG00000104783	KCNN4	protein_coding	-1,80175489	2,6547E-42
ENSG00000105971	CAV2	protein_coding	-2,49424184	2,7209E-42
ENSG00000139793	MBNL2	protein_coding	-1,29967946	4,267E-42
ENSG00000182871	COL18A1	protein_coding	-1,46424734	1,1833E-41
ENSG00000137177	KIF13A	protein_coding	-7,25431622	3,4034E-41
ENSG00000062282	DGAT2	protein_coding	-3,17887125	1,7001E-40
ENSG00000089177	KIF16B	protein_coding	-1,0627202	1,9913E-39
ENSG00000147394	ZNF185	protein_coding	-1,60840228	8,1132E-39
ENSG00000268119		lncRNA	-1,8927853	1,415E-37
ENSG00000155761	SPAG17	protein_coding	-2,29160102	4,4999E-35
ENSG00000181544	FANCB	protein_coding	-1,58149658	8,721E-34
ENSG00000132164	SLC6A11	protein_coding	-2,34240014	7,79E-33
ENSG00000196743	GM2A	protein_coding	-1,34237884	1,167E-32
ENSG00000116688	MFN2	protein_coding	-1,10044724	2,479E-32
ENSG00000163430	FSTL1	protein_coding	-1,89270013	5,753E-32
ENSG00000102243	VGLL1	protein_coding	-1,96388642	8,7556E-32
ENSG00000166025	AMOTL1	protein_coding	-1,61837353	2,6417E-31
ENSG00000198689	SLC9A6	protein_coding	-2,58513238	3,7716E-31
ENSG00000151729	SLC25A4	protein_coding	-1,49921344	4,2358E-31
ENSG00000187017	ESPN	protein_coding	-1,30072012	4,428E-30
ENSG00000198624	CCDC69	protein_coding	-2,0902295	8,444E-30
ENSG00000022267	FHL1	protein_coding	-4,63432826	1,2669E-29
ENSG00000138604	GLCE	protein_coding	-1,28161407	2,0757E-29
ENSG00000189339	SLC35E2B	protein_coding	-1,12377362	2,4751E-29
ENSG00000255571	MIR9-3HG	lncRNA	-3,55222687	3,6136E-29
ENSG00000079308	TNS1	protein_coding	-1,30330129	1,9253E-28
ENSG00000142156	COL6A1	protein_coding	-3,20776256	9,1176E-28
ENSG00000138399	FASTKD1	protein_coding	-1,24292858	2,1077E-27
ENSG00000218739	CEBPZOS	protein_coding	-1,05041481	2,3234E-27
ENSG00000235437	LINC01278	lncRNA	-1,80049005	2,9624E-27
ENSG00000125879	OTOR	protein_coding	-2,40498024	6,7552E-27
ENSG00000138029	HADHB	protein_coding	-1,09388722	8,1355E-27
ENSG00000082512	TRAF5	protein_coding	-2,07148736	8,9499E-27
ENSG00000243566	UPK3B	protein_coding	-1,40028698	9,3264E-27
ENSG00000166816	LDHD	protein_coding	-2,12796117	4,2498E-26
ENSG00000255690	TRIL	protein_coding	-1,73665715	5,3974E-26
ENSG00000102174	PHEX	protein_coding	-1,89901813	7,798E-26
ENSG00000106348	IMPDH1	protein_coding	-1,37031438	3,4614E-25
ENSG00000179913	B3GNT3	protein_coding	-1,268857	4,0653E-25
ENSG00000163485	ADORA1	protein_coding	-2,03044202	4,4251E-25
ENSG00000048052	HDAC9	protein_coding	-1,70895656	1,2029E-24
ENSG00000234284	ZNF879	protein_coding	-3,9822905	4,2429E-24
ENSG00000186104	CYP2R1	protein_coding	-2,01638867	5,0155E-24
ENSG00000213967	ZNF726	protein_coding	-1,15056375	6,2002E-24
ENSG00000269825		protein_coding	-1,11727636	6,2056E-24
ENSG00000265107	GJA5	protein_coding	-2,82572776	7,9821E-24
ENSG00000134324	LPIN1	protein_coding	-1,07521198	9,4929E-24
ENSG00000068078	FGFR3	protein_coding	-1,56662437	1,943E-23
ENSG00000152766	ANKRD22	protein_coding	-2,14182531	2,1082E-23
ENSG00000132359	RAP1GAP2	protein_coding	-1,08572831	2,5602E-23
ENSG00000258077		lncRNA	-4,6640651	3,0884E-23
ENSG00000071242	RPS6KA2	protein_coding	-2,52700335	3,6438E-23
ENSG00000165548	TMEM63C	protein_coding	-1,28823151	9,7693E-23
ENSG00000166387	PPFIBP2	protein_coding	-1,04603569	1,1765E-22
ENSG00000137642	SORL1	protein_coding	-1,333785	1,4096E-22
ENSG00000267886		lncRNA	-5,43187165	3,3145E-22
ENSG00000126016	AMOT	protein_coding	-1,52200859	3,9213E-22
ENSG00000158715	SLC45A3	protein_coding	-1,07100689	5,5299E-22
ENSG00000155380	SLC16A1	protein_coding	-1,36216447	1,2507E-21
ENSG00000182749	PAQR7	protein_coding	-1,35116886	4,9362E-21
ENSG00000162441	LZIC	protein_coding	-1,1670313	5,2146E-21
ENSG00000255346	NOX5	protein_coding	-2,27510799	7,4437E-21
ENSG00000204272	NBDY	protein_coding	-1,66672146	1,688E-20
ENSG00000104549	SQLE	protein_coding	-1,05406468	1,8526E-20
ENSG00000187608	ISG15	protein_coding	-1,44548305	2,7257E-20
ENSG00000058668	ATP2B4	protein_coding	-1,37080935	5,5551E-20
ENSG00000030419	IKZF2	protein_coding	-1,18438022	8,0743E-20
ENSG00000176171	BNIP3	protein_coding	-1,08714732	1,207E-19
ENSG00000176771	NCKAP5	protein_coding	-2,49975884	1,3032E-19
ENSG00000136193	SCRN1	protein_coding	-1,16946321	2,9403E-19
ENSG00000040933	INPP4A	protein_coding	-1,03653381	4,5172E-19
ENSG00000172478	MAB21L4	protein_coding	-1,08009341	8,1643E-19
ENSG00000144354	CDCA7	protein_coding	-1,04947141	1,0218E-18
ENSG00000147100	SLC16A2	protein_coding	-1,93874198	1,4093E-18
ENSG00000277639		protein_coding	-1,8788966	2,1567E-18
ENSG00000130150	MOSPD2	protein_coding	-1,25950333	2,8303E-18
ENSG00000102886	GDPD3	protein_coding	-1,55753693	4,7171E-18
ENSG00000197779	ZNF81	protein_coding	-1,04683754	4,8108E-18
ENSG00000100767	PAPLN	protein_coding	-1,24717432	7,0343E-18
ENSG00000147251	DOCK11	protein_coding	-2,14183709	7,634E-18
ENSG00000001084	GCLC	protein_coding	-1,00971604	9,2027E-18
ENSG00000162545	CAMK2N1	protein_coding	-1,39693201	1,3332E-17
ENSG00000115041	KCNIP3	protein_coding	-1,21920175	1,4592E-17
ENSG00000188130	MAPK12	protein_coding	-1,27116127	2,3001E-17
ENSG00000080854	IGSF9B	protein_coding	-1,58627622	2,9471E-17
ENSG00000260220	CCDC187	protein_coding	-1,65253063	3,3437E-17
ENSG00000198948	MFAP3L	protein_coding	-1,74769813	4,484E-17

ENSG00000006025	OSBPL7	protein_coding	-1,39303491	4,6528E-17
ENSG00000230937	MIR205HG	lncRNA	-2,32450497	5,1858E-17
ENSG00000101187	SLCO4A1	protein_coding	-1,03351128	6,8042E-17
ENSG00000142632	ARHGEF19	protein_coding	-1,03792522	8,8798E-17
ENSG00000055163	CYFIP2	protein_coding	-1,20282168	1,9083E-16
ENSG00000161905	ALOX15	protein_coding	-1,51210372	2,0902E-16
ENSG00000163590	PPM1L	protein_coding	-1,09633471	2,1156E-16
ENSG00000174307	PHLDA3	protein_coding	-1,6776648	3,3406E-16
ENSG00000064655	EYA2	protein_coding	-5,94589657	4,0728E-16
ENSG00000106605	BLVRA	protein_coding	-1,00737005	4,0939E-16
ENSG00000196636	SDHAF3	protein_coding	-1,64829091	4,1802E-16
ENSG00000099219	ERMP1	protein_coding	-1,03203107	7,8543E-16
ENSG00000185247	MAGEA11	protein_coding	-6,80873728	1,7522E-15
ENSG00000134755	DSC2	protein_coding	-1,46052293	1,7836E-15
ENSG00000124006	OBSL1	protein_coding	-1,22318466	2,209E-15
ENSG00000134986	NREP	protein_coding	-1,10916712	3,0325E-15
ENSG00000181444	ZNF467	protein_coding	-1,05067836	3,4252E-15
ENSG00000112414	ADGRG6	protein_coding	-2,75462082	3,695E-15
ENSG00000117114	ADGRL2	protein_coding	-2,34200799	3,9739E-15
ENSG00000251095		lncRNA	-2,68186579	4,05E-15
ENSG00000106772	PRUNE2	protein_coding	-2,23155864	5,1577E-15
ENSG00000124243	BCAS4	protein_coding	-1,35478029	6,4877E-15
ENSG00000095203	EPB41L4B	protein_coding	-1,07287555	1,2093E-14
ENSG00000196172	ZNF681	protein_coding	-1,12406479	1,456E-14
ENSG00000169047	IRS1	protein_coding	-1,59560261	2,176E-14
ENSG00000237515	SHISA9	protein_coding	-6,01671405	2,9E-14
ENSG00000088340	FER1L4	transcribed_unitary pseudogene	-1,67846413	3,7639E-14
ENSG00000143333	RGS16	protein_coding	-1,29619724	3,8586E-14
ENSG00000156299	TIAM1	protein_coding	-2,04117292	4,2732E-14
ENSG00000165757	JCAD	protein_coding	-1,87026152	4,6594E-14
ENSG00000110484	SCGB2A2	protein_coding	-1,69573164	8,5027E-14
ENSG00000103310	ZP2	protein_coding	-3,01505719	8,7026E-14
ENSG00000069812	HES2	protein_coding	-2,08103869	1,3285E-13
ENSG00000183722	LHFPL6	protein_coding	-9,79467557	1,8026E-13
ENSG00000102349	KLF8	protein_coding	-1,32440286	2,5287E-13
ENSG00000135824	RGS8	protein_coding	-3,50346357	2,9914E-13
ENSG00000245848	CEBPA	protein_coding	-1,01054813	3,4338E-13
ENSG00000115616	SLC9A2	protein_coding	-2,08497238	4,0826E-13
ENSG00000054392	HHAT	protein_coding	-1,9537086	4,8727E-13
ENSG00000186204	CYP4F12	protein_coding	-2,95182329	5,4306E-13
ENSG00000071909	MYO3B	protein_coding	-2,43371954	6,7188E-13
ENSG00000226124	FTCDNL1	protein_coding	-1,99816962	7,0822E-13
ENSG00000127129	EDN2	protein_coding	-2,1396142	8,5965E-13
ENSG00000142627	EPHA2	protein_coding	-1,19123549	1,0358E-12
ENSG00000116771	AGMAT	protein_coding	-1,03068362	1,1475E-12
ENSG00000112319	EYA4	protein_coding	-1,65974689	1,731E-12
ENSG00000197134	ZNF257	protein_coding	-1,16660818	2,0342E-12
ENSG00000135374	ELF5	protein_coding	-5,44861282	2,4172E-12
ENSG00000071205	ARHGAP10	protein_coding	-8,88107439	2,4867E-12
ENSG00000185386	MAPK11	protein_coding	-1,13267013	2,6235E-12
ENSG00000235538		lncRNA	-9,28902474	3,0093E-12
ENSG00000113389	NPR3	protein_coding	-2,05553488	3,9054E-12
ENSG00000179023	KLHDC7A	protein_coding	-1,40861043	4,0559E-12
ENSG00000106066	CPVL	protein_coding	-4,0632789	4,1058E-12
ENSG00000212978		lncRNA	-1,34151649	4,839E-12
ENSG00000183943	PRKX	protein_coding	-1,12716135	4,9626E-12
ENSG00000206538	VGLL3	protein_coding	-9,19553641	5,5406E-12
ENSG00000128268	MGAT3	protein_coding	-2,3922477	5,9523E-12
ENSG00000153404	PLEKHG4B	protein_coding	-2,02236547	5,9523E-12
ENSG00000006210	CX3CL1	protein_coding	-3,85987572	6,5184E-12
ENSG00000169071	ROR2	protein_coding	-3,19597225	6,5317E-12
ENSG00000138678	GPAT3	protein_coding	-1,3225683	7,0421E-12
ENSG00000170381	SEMA3E	protein_coding	-1,18184985	7,2655E-12
ENSG00000186806	VSIG10L	protein_coding	-1,30618269	7,7341E-12
ENSG00000149596	JPH2	protein_coding	-1,00083174	8,1101E-12
ENSG00000116663	FBXO6	protein_coding	-1,3703627	8,7308E-12
ENSG00000228630	HOTAIR	lncRNA	-8,74243813	9,8823E-12
ENSG00000169740	ZNF32	protein_coding	-1,07435278	1,0835E-11
ENSG00000139998	RAB15	protein_coding	-1,00604368	1,1748E-11
ENSG00000167767	KRT80	protein_coding	-1,01868972	1,6537E-11
ENSG00000169403	PTAFR	protein_coding	-1,04908426	1,6537E-11
ENSG00000157873	TNFRSF14	protein_coding	-1,46772836	1,7571E-11
ENSG00000162999	DUSP19	protein_coding	-1,42664269	1,9047E-11
ENSG00000205426	KRT81	protein_coding	-1,1661336	2,2978E-11
ENSG00000140505	CYP1A2	protein_coding	-3,45047668	2,6456E-11
ENSG00000171401	KRT13	protein_coding	-1,89542616	3,2716E-11
ENSG00000187210	GCNT1	protein_coding	-1,35025772	3,6307E-11
ENSG00000288649	ACTL10	protein_coding	-1,68055557	3,8176E-11
ENSG00000271936		lncRNA	-1,10015923	4,1271E-11
ENSG00000227038	GTF2IP7	transcribed_unprocessed pseudogene	-1,17990834	4,3753E-11
ENSG00000155850	SLC26A2	protein_coding	-1,82874851	6,9625E-11
ENSG00000110852	CLEC2B	protein_coding	-7,55679911	8,2489E-11
ENSG00000284485	MIR205	miRNA	-2,4323668	8,86E-11
ENSG00000162407	PLPP3	protein_coding	-1,03976074	1,043E-10
ENSG00000173320	STOX2	protein_coding	-2,89840603	1,978E-10
ENSG00000134548	SPX	protein_coding	-2,99450306	2,0702E-10
ENSG00000142606	MMEL1	protein_coding	-1,43951752	2,7448E-10
ENSG00000088726	TMEM40	protein_coding	-2,25862569	2,7918E-10

ENSG00000163235	TGFA	protein_coding	-1,03614753	3,6183E-10
ENSG00000116141	MARK1	protein_coding	-1,57686734	3,6186E-10
ENSG00000168032	ENTPD3	protein_coding	-1,55227361	3,7911E-10
ENSG00000170873	MTSS1	protein_coding	-1,30650568	4,3263E-10
ENSG00000182379	NXPH4	protein_coding	-1,1977526	4,7826E-10
ENSG00000182585	EPGN	protein_coding	-1,19634065	4,7826E-10
ENSG00000259977		lncRNA	-3,29869331	6,4572E-10
ENSG00000269516	CYP4F23P	transcribed_unprocessed pseudogene	-2,84146568	6,8077E-10
ENSG00000133466	C1QTNF6	protein_coding	-1,14448428	7,5645E-10
ENSG00000196793	ZNF239	protein_coding	-1,03318522	8,3702E-10
ENSG00000136928	GABBR2	protein_coding	-4,67094254	8,5397E-10
ENSG00000149527	PLCH2	protein_coding	-1,49957274	9,8484E-10
ENSG00000253438	PCAT1	lncRNA	-1,29197577	1,0522E-09
ENSG00000265763	ZNF488	protein_coding	-1,08715568	1,2395E-09
ENSG00000178585	CTNNBIP1	protein_coding	-1,08819565	1,4004E-09
ENSG00000169550	MUC15	protein_coding	-1,95277187	1,5529E-09
ENSG00000173267	SNCG	protein_coding	-1,59893587	1,9188E-09
ENSG00000103316	CRYM	protein_coding	-1,185587	2,3252E-09
ENSG00000069122	ADGRF5	protein_coding	-3,19692819	2,3749E-09
ENSG00000136866	ZFP37	protein_coding	-1,85315782	2,3837E-09
ENSG00000225882	LINC01456	lncRNA	-8,03931699	2,5078E-09
ENSG00000142973	CYP4B1	protein_coding	-1,93309434	3,1961E-09
ENSG00000156284	CLDN8	protein_coding	-1,40469808	3,4939E-09
ENSG00000072840	EVC	protein_coding	-1,63357137	4,1003E-09
ENSG00000247134		lncRNA	-3,42971344	4,7158E-09
ENSG00000172889	EGFL7	protein_coding	-1,21296573	4,7723E-09
ENSG00000176896	TCEANC	protein_coding	-1,32950898	4,8679E-09
ENSG00000242732	RTL5	protein_coding	-2,27707409	5,9985E-09
ENSG00000173175	ADCY5	protein_coding	-2,00953955	7,2897E-09
ENSG00000105974	CAV1	protein_coding	-1,83699181	9,2245E-09
ENSG00000182890	GLUD2	protein_coding	-1,13087476	1,0626E-08
ENSG00000161642	ZNF385A	protein_coding	-1,18113613	1,1255E-08
ENSG00000141040	ZNF287	protein_coding	-1,86073268	1,1256E-08
ENSG00000253552	HOXA-AS2	lncRNA	-8,20212451	1,1815E-08
ENSG00000236008	LINC01814	lncRNA	-2,61008044	1,2474E-08
ENSG00000118946	PCDH17	protein_coding	-7,75781229	1,2997E-08
ENSG00000100292	HMOX1	protein_coding	-1,2950089	1,33E-08
ENSG00000173391	OLR1	protein_coding	-5,28508751	1,409E-08
ENSG00000114349	GNAT1	protein_coding	-1,48738605	1,6941E-08
ENSG00000138735	PDE5A	protein_coding	-1,48102305	2,239E-08
ENSG00000184185	KCNJ12	protein_coding	-3,14922996	2,2783E-08
ENSG00000183850	ZNF730	protein_coding	-7,26483128	2,996E-08
ENSG00000100342	APOL1	protein_coding	-1,69632944	3,0877E-08
ENSG00000172403	SYNPO2	protein_coding	-3,56541216	3,2436E-08
ENSG00000244405	ETV5	protein_coding	-7,21717009	3,839E-08
ENSG00000101441	CST4	protein_coding	-7,92971623	4,052E-08
ENSG00000223773	CD99P1	transcribed_unprocessed pseudogene	-1,21269828	4,1982E-08
ENSG00000227487	NCAM1-AS1	lncRNA	-3,05943675	4,5829E-08
ENSG00000261754		lncRNA	-7,63147026	4,8944E-08
ENSG00000157827	FMNL2	protein_coding	-1,93276352	7,5576E-08
ENSG00000145349	CAMK2D	protein_coding	-1,1221384	8,7031E-08
ENSG00000042493	CAPG	protein_coding	-1,50795122	9,9341E-08
ENSG00000175556	LONRF3	protein_coding	-2,97868334	1,1058E-07
ENSG00000144452	ABCA12	protein_coding	-2,45765595	1,2327E-07
ENSG00000107282	APBA1	protein_coding	-1,74139855	1,2647E-07
ENSG00000137501	SYTL2	protein_coding	-1,04808961	1,2959E-07
ENSG00000171608	PIK3CD	protein_coding	-1,57299401	1,4914E-07
ENSG00000178726	THBD	protein_coding	-6,94061159	1,5632E-07
ENSG00000136235	GPNMB	protein_coding	-2,55219496	1,6018E-07
ENSG00000172379	ARNT2	protein_coding	-1,55356534	1,7046E-07
ENSG00000149582	TMEM25	protein_coding	-1,01547809	1,7304E-07
ENSG00000145246	ATP10D	protein_coding	-1,4367642	1,8432E-07
ENSG00000153208	MERTK	protein_coding	-2,64532222	1,9945E-07
ENSG00000134256	CD101	protein_coding	-1,04574596	2,2629E-07
ENSG00000130635	COL5A1	protein_coding	-1,41811624	2,3816E-07
ENSG00000215788	TNFRSF25	protein_coding	-1,27562705	2,5475E-07
ENSG00000175318	GRAMD2A	protein_coding	-1,70816385	2,7706E-07
ENSG00000060138	YBX3	protein_coding	-2,71105537	2,9847E-07
ENSG00000140450	ARRDC4	protein_coding	-1,33595505	3,1554E-07
ENSG00000196781	TLE1	protein_coding	-2,2686588	3,6261E-07
ENSG00000166823	MESP1	protein_coding	-1,57588591	3,7288E-07
ENSG00000155265	GOLGA7B	protein_coding	-1,60784398	3,8885E-07
ENSG00000188042	ARL4C	protein_coding	-6,74612837	4,0072E-07
ENSG00000115112	TFCP2L1	protein_coding	-2,23551523	4,4243E-07
ENSG00000213801	ZNF321P	transcribed_processed pseudogene	-1,01903205	4,4504E-07
ENSG00000130038	CRACR2A	protein_coding	-1,24557048	4,9568E-07
ENSG00000138134	STAMBPL1	protein_coding	-2,06284533	5,0316E-07
ENSG00000183036	PCP4	protein_coding	-1,73967459	5,5889E-07
ENSG00000138193	PLCE1	protein_coding	-3,00454124	5,7516E-07
ENSG00000261599	HERC2P8	transcribed_unprocessed pseudogene	-1,6548931	6,1672E-07
ENSG00000154342	WNT3A	protein_coding	-2,45298236	6,8127E-07
ENSG00000006747	SCIN	protein_coding	-1,63286301	7,0009E-07
ENSG00000124615	MOCS1	protein_coding	-1,24571379	8,0594E-07
ENSG00000268658	LINC00664	lncRNA	-1,62962031	8,2585E-07
ENSG00000166582	CENPV	protein_coding	-1,55164486	9,0275E-07
ENSG00000250423	KIAA1210	protein_coding	-3,32995597	9,6901E-07

ENSG00000182648	LINC01006	lncRNA	-1,09058303	1,0478E-06
ENSG00000198835	GJC2	protein_coding	-1,56938633	1,1349E-06
ENSG00000077063	CTTNBP2	protein_coding	-3,13200897	1,2306E-06
ENSG00000110492	MDK	protein_coding	-1,22000807	1,2636E-06
ENSG00000162949	CAPN13	protein_coding	-2,55577902	1,377E-06
ENSG00000171903	CYP4F11	protein_coding	-1,23011047	1,3944E-06
ENSG00000103196	CRISPLD2	protein_coding	-1,25373863	1,5265E-06
ENSG00000002587	HS3ST1	protein_coding	-7,04870053	1,9795E-06
ENSG00000165591	FAAH2	protein_coding	-1,16917284	2,383E-06
ENSG00000225606		lncRNA	-2,61695597	2,3966E-06
ENSG00000138798	EGF	protein_coding	-1,39443999	2,6445E-06
ENSG00000197165	SULT1A2	protein_coding	-1,52829732	2,9711E-06
ENSG00000198223	CSF2RA	protein_coding	-1,01643426	3,1475E-06
ENSG00000167723	TRPV3	protein_coding	-1,37452533	3,2143E-06
ENSG00000235590	GNAS-AS1	lncRNA	-3,97112431	3,6115E-06
ENSG00000149294	NCAM1	protein_coding	-3,99977927	3,7682E-06
ENSG00000064763	FAR2	protein_coding	-1,41246517	3,822E-06
ENSG00000117148	ACTL8	protein_coding	-2,68780823	3,834E-06
ENSG00000224975	INE1	lncRNA	-1,12529339	4,5984E-06
ENSG00000198788	MUC2	protein_coding	-2,16610771	4,8296E-06
ENSG00000255666	LINC02700	lncRNA	-3,79880538	5,0064E-06
ENSG00000198910	L1CAM	protein_coding	-2,5882524	5,0985E-06
ENSG00000112782	CLIC5	protein_coding	-3,30222765	5,3186E-06
ENSG00000197497	ZNF665	protein_coding	-1,8305557	5,4525E-06
ENSG00000105997	HOXA3	protein_coding	-3,27921736	5,4566E-06
ENSG00000147234	FRMPD3	protein_coding	-1,92004884	6,363E-06
ENSG00000261713	SSTR5-AS1	lncRNA	-2,54627145	6,7266E-06
ENSG00000257335	MGAM	protein_coding	-1,24261727	6,8462E-06
ENSG00000259692		lncRNA	-1,83061481	6,8509E-06
ENSG00000158104	HPD	protein_coding	-1,25524806	7,1273E-06
ENSG00000204860	FAM201A	lncRNA	-6,02122798	7,5232E-06
ENSG00000230882		processed_pseudogene	-1,06024696	8,0531E-06
ENSG00000118004	COLEC11	protein_coding	-1,94615942	8,4849E-06
ENSG00000174599	TRAM1L1	protein_coding	-1,38218987	8,5486E-06
ENSG00000227486		lncRNA	-1,10987344	8,8633E-06
ENSG00000122735	DNAI1	protein_coding	-1,79728943	9,2826E-06
ENSG00000230699		lncRNA	-1,10605329	9,6079E-06
ENSG00000261068		lncRNA	-1,04881049	9,8858E-06
ENSG00000198535	C2CD4A	protein_coding	-3,15720544	1,0231E-05
ENSG00000243069	ARHGEF26-AS1	lncRNA	-2,67645485	1,0317E-05
ENSG00000173269	MMRN2	protein_coding	-1,36433373	1,0408E-05
ENSG00000198930	CSAG1	protein_coding	-2,6594653	1,0639E-05
ENSG00000170324	FRMPD2	protein_coding	-3,88010287	1,0683E-05
ENSG00000178597	PSAPL1	protein_coding	-1,39108514	1,1866E-05
ENSG00000154198	CYP4Z2P	transcribed_unprocessed pseudogene	-1,44465089	1,2964E-05
ENSG00000215834	FMO9P	transcribed_unprocessed pseudogene	-1,94577071	1,2964E-05
ENSG00000142875	PRKACB	protein_coding	-1,0053412	1,3005E-05
ENSG00000256971	LINC00508	lncRNA	-6,9713685	1,3736E-05
ENSG00000203727	SAMD5	protein_coding	-1,01332369	1,4087E-05
ENSG00000171303	KCNK3	protein_coding	-6,32954053	1,6139E-05
ENSG00000203867	RBM20	protein_coding	-1,35521448	1,7666E-05
ENSG00000091428	RAPGEF4	protein_coding	-1,15579672	1,7729E-05
ENSG00000115526	CHST10	protein_coding	-5,03142151	1,9197E-05
ENSG00000102024	PLS3	protein_coding	-5,71792604	2,1003E-05
ENSG00000136689	IL1RN	protein_coding	-3,9831322	2,1491E-05
ENSG00000255173		lncRNA	-1,07748649	2,4186E-05
ENSG00000198739	LRRTM3	protein_coding	-2,34729952	2,6848E-05
ENSG00000204161	TMEM273	protein_coding	-2,92812844	2,692E-05
ENSG00000260027	HOXB7	protein_coding	-1,11778936	2,7581E-05
ENSG00000199059	MIR135B	miRNA	-6,9888566	2,7582E-05
ENSG00000143942	CHAC2	protein_coding	-1,11388169	2,7629E-05
ENSG00000184898	RBM43	protein_coding	-1,12002113	2,8519E-05
ENSG00000223573	TINCR	protein_coding	-1,02053566	3,057E-05
ENSG00000154930	ACSS1	protein_coding	-1,69985636	3,4258E-05
ENSG00000158445	KCNB1	protein_coding	-1,50415196	3,5223E-05
ENSG00000235169	SMIM1	protein_coding	-1,61310263	3,6277E-05
ENSG00000188732	FAM221A	protein_coding	-2,60413088	3,6942E-05
ENSG00000269397		lncRNA	-1,03548441	3,7475E-05
ENSG00000068650	ATP11A	protein_coding	-5,71386098	3,9255E-05
ENSG00000204287	HLA-DRA	protein_coding	-2,32053681	3,9342E-05
ENSG00000268105		processed_pseudogene	-6,01683832	4,385E-05
ENSG00000103154	NECAB2	protein_coding	-1,51673891	4,5641E-05
ENSG00000197872	CYRIA	protein_coding	-3,17972776	4,9257E-05
ENSG00000229676	ZNF492	protein_coding	-5,60157936	5,1018E-05
ENSG00000169783	LINGO1	protein_coding	-5,64851588	5,1321E-05
ENSG00000183888	SRARP	protein_coding	-1,00120184	5,1321E-05
ENSG00000240875	LINC00886	lncRNA	-1,16333835	5,1337E-05
ENSG00000165025	SYK	protein_coding	-5,59392607	5,3822E-05
ENSG00000170954	ZNF415	protein_coding	-4,01670039	5,9155E-05
ENSG00000171174	RBKS	protein_coding	-1,16134116	6,3447E-05
ENSG00000044459	CNTLN	protein_coding	-1,89718828	6,4989E-05
ENSG00000173567	ADGRF3	protein_coding	-1,55590836	6,5233E-05
ENSG00000047597	XK	protein_coding	-1,13188614	7,02E-05
ENSG00000237926		unprocessed_pseudogene	-6,34778424	7,3912E-05
ENSG00000163207	IVL	protein_coding	-1,91359836	7,5345E-05
ENSG00000172123	SLFN12	protein_coding	-6,26042542	7,9495E-05
ENSG00000137819	PAQR5	protein_coding	-2,08725099	8,9452E-05

ENSG00000154127	UBASH3B	protein_coding	-1,70812992	9,8271E-05
ENSG00000272281	TPTE2P2	transcribed_unprocessed pseudogene	-2,837576	9,9889E-05
ENSG00000182518	FAM104B	protein_coding	-1,04306192	0,00010308
ENSG00000111961	SASH1	protein_coding	-1,07370153	0,00010745
ENSG00000101144	BMP7	protein_coding	-5,6633827	0,00011114
ENSG00000184471	C1QTNF8	protein_coding	-3,12663823	0,00011509
ENSG00000165731	RET	protein_coding	-1,70466608	0,00012384
ENSG00000166535	A2ML1	protein_coding	-2,41711002	0,0001286
ENSG00000162639	HENMT1	protein_coding	-1,07087188	0,00013996
ENSG00000287169		lncRNA	-6,586328	0,00014819
ENSG00000176387	HSD11B2	protein_coding	-1,04370339	0,00014864
ENSG00000255129		lncRNA	-1,99104056	0,00016455
ENSG00000154654	NCAM2	protein_coding	-2,51585216	0,00016534
ENSG00000273983	H3C8	protein_coding	-1,46461123	0,00017017
ENSG00000287362		lncRNA	-2,90538478	0,00017121
ENSG00000189149	CRYM-AS1	transcribed_unitary pseudogene	-1,01088692	0,00018102
ENSG00000253978	CTB-178M22.2	lncRNA	-2,14828823	0,00018177
ENSG00000196167	COLCA1	lncRNA	-2,83338257	0,00018848
ENSG00000075673	ATP12A	protein_coding	-2,90928246	0,0001947
ENSG00000256196		lncRNA	-1,58998786	0,00021152
ENSG00000228623	ZNF883	transcribed_unprocessed pseudogene	-2,77239019	0,00021463
ENSG00000144648	ACKR2	protein_coding	-1,15150643	0,00021933
ENSG00000146122	DAAM2	protein_coding	-2,59619214	0,00022501
ENSG00000162009	SSTR5	protein_coding	-1,70230635	0,00022628
ENSG00000136274	NACAD	protein_coding	-1,77914677	0,00024952
ENSG00000108830	RND2	protein_coding	-2,31837666	0,00025489
ENSG00000160408	ST6GALNAC6	protein_coding	-1,33912745	0,00025763
ENSG00000172461	FUT9	protein_coding	-1,35526316	0,00027514
ENSG00000186891	TNFRSF18	protein_coding	-1,04717636	0,00027524
ENSG00000228613		lncRNA	-1,4300652	0,00027721
ENSG00000204624	DISP3	protein_coding	-1,16531984	0,00028856
ENSG00000268416		lncRNA	-3,56480947	0,00029827
ENSG00000114923	SLC4A3	protein_coding	-1,09312726	0,0003163
ENSG00000158352	SHROOM4	protein_coding	-4,5654729	0,00031819
ENSG00000134627	PIWIL4	protein_coding	-2,45356577	0,00032924
ENSG00000231868		lncRNA	-1,41017455	0,00034281
ENSG00000115919	KYNU	protein_coding	-1,27590992	0,00035591
ENSG00000283945	LINC00032	transcribed_unprocessed pseudogene	-1,38424043	0,00035922
ENSG00000130720	FIBCD1	protein_coding	-1,20057798	0,00037946
ENSG00000152137	HSPB8	protein_coding	-1,01601904	0,00039218
ENSG00000138411	HECW2	protein_coding	-1,46953548	0,00042946
ENSG00000212719	LINC02693	lncRNA	-1,08646336	0,0004369
ENSG00000114405	C3orf14	protein_coding	-4,98144978	0,0004496
ENSG00000285679		lncRNA	-1,0937091	0,00045611
ENSG00000253706		lncRNA	-3,83155038	0,00045815
ENSG00000184612	RPL7P26	processed_pseudogene	-3,8036552	0,00047422
ENSG00000175928	LRRN1	protein_coding	-1,61363803	0,00047683
ENSG00000171346	KRT15	protein_coding	-1,19272837	0,00048488
ENSG00000226445		lncRNA	-3,15999675	0,00064422
ENSG00000267767	LINC01801	lncRNA	-5,13916851	0,00071567
ENSG00000159239		protein_coding	-2,48798739	0,00072902
ENSG00000128340	RAC2	protein_coding	-5,71038023	0,00073059
ENSG00000132170	PPARG	protein_coding	-1,48560345	0,00073959
ENSG00000204941	PSG5	protein_coding	-2,75892453	0,00075376
ENSG00000275481		lncRNA	-1,07934512	0,00075683
ENSG00000186529	CYP4F3	protein_coding	-2,68741632	0,00082231
ENSG00000134765	DSC1	protein_coding	-5,52675511	0,00087654
ENSG00000163873	GRIK3	protein_coding	-1,73492954	0,00089328
ENSG00000100505	TRIM9	protein_coding	-1,43398833	0,00091546
ENSG00000248206		lncRNA	-3,47796301	0,00092531
ENSG00000256347	OR8R1P	unprocessed_pseudogene	-1,14966683	0,00093143
ENSG00000229393		lncRNA	-1,44377661	0,00093807
ENSG00000086289	EPDR1	protein_coding	-4,69088002	0,00098806
ENSG00000204710	SPDYC	protein_coding	-1,57369833	0,00104008
ENSG00000205669	ACOT6	protein_coding	-1,50493287	0,00104049
ENSG00000259882		unprocessed_pseudogene	-5,84045491	0,00105587
ENSG00000287778		lncRNA	-5,67326622	0,00111871
ENSG00000137648	TMPRSS4	protein_coding	-2,73150809	0,00112244
ENSG00000167653	PSCA	protein_coding	-1,20547856	0,00112244
ENSG00000106689	LHX2	protein_coding	-1,07876531	0,00112711
ENSG00000180251	SLC9A4	protein_coding	-2,83365503	0,00117249
ENSG00000188859	FAM78B	protein_coding	-4,81787349	0,00119081
ENSG00000205978	NYNRIN	protein_coding	-1,35906933	0,00120874
ENSG00000232023	LINC01807	lncRNA	-5,07780087	0,00125493
ENSG00000186564	FOXD2	protein_coding	-1,06145477	0,0013075
ENSG00000284633		lncRNA	-2,31653633	0,00134765
ENSG00000237125	HAND2-AS1	lncRNA	-4,66907936	0,00134779
ENSG00000259485	LINC02253	lncRNA	-4,22508239	0,00136065
ENSG00000042062	RIPOR3	protein_coding	-1,72629489	0,00140004
ENSG00000265972	TXNIP	protein_coding	-1,58042617	0,00141195
ENSG00000187642	PERM1	protein_coding	-1,04156501	0,00151557
ENSG00000179859	RNF227	protein_coding	-1,32132882	0,00153805
ENSG00000258245	RPL10P13	processed_pseudogene	-5,59898693	0,00155079
ENSG00000158220	ESYT3	protein_coding	-2,48612406	0,00158785
ENSG00000107159	CA9	protein_coding	-1,61021043	0,00163458
ENSG00000259723		lncRNA	-4,83687119	0,00165825

ENSG00000180066	LINC02870	lncRNA	-1,85327682	0,0016674
ENSG00000198183	BPIFA1	protein_coding	-1,69327805	0,00168395
ENSG00000012124	CD22	protein_coding	-1,32065882	0,00176245
ENSG00000121797	CCRL2	protein_coding	-5,35087906	0,00186823
ENSG00000285789		lncRNA	-5,66275689	0,00195649
ENSG00000259148	YWHAZP1	processed_pseudogene	-2,59754253	0,00199171
ENSG00000269190	FBXO17	protein_coding	-1,1201412	0,00208491
ENSG00000249602		lncRNA	-2,27964799	0,00227546
ENSG00000286662		lncRNA	-1,84502802	0,00228021
ENSG00000133019	CHRM3	protein_coding	-4,58439935	0,00228657
ENSG00000150630	VEGFC	protein_coding	-4,61024718	0,00231129
ENSG00000189229		lncRNA	-3,324247	0,0023843
ENSG00000157111	TMEM171	protein_coding	-3,24288585	0,00249639
ENSG00000157554	ERG	protein_coding	-4,72728694	0,00262724
ENSG00000240541	TM4SF1-AS1	lncRNA	-1,65311615	0,0027922
ENSG00000237276	ANO7L1	transcribed_unprocessed pseudogene	-1,01392396	0,00281978
ENSG00000156564	LRFN2	protein_coding	-2,34467766	0,00285418
ENSG00000177599	ZNF491	protein_coding	-1,04847781	0,0028597
ENSG00000169026	SLC49A3	protein_coding	-1,12747964	0,00287769
ENSG00000233820		transcribed_processed pseudogene	-2,63395762	0,00290947
ENSG00000233757		protein_coding	-1,47975571	0,00293037
ENSG00000253958	CLDN23	protein_coding	-1,06282167	0,00320235
ENSG00000228933		lncRNA	-4,41909695	0,00322112
ENSG00000120833	SOCS2	protein_coding	-3,10804929	0,00335013
ENSG00000224093	BCAR3-AS1	lncRNA	-1,07557974	0,00343356
ENSG00000140379	BCL2A1	protein_coding	-2,01056645	0,00349731
ENSG00000204131	NHSL2	protein_coding	-1,28279687	0,00367355
ENSG00000261126	RBFADN	lncRNA	-1,42893845	0,00367668
ENSG00000167755	KLK6	protein_coding	-4,91093276	0,00374905
ENSG00000120329	SLC25A2	protein_coding	-4,81610456	0,00389076
ENSG00000088881	EBF4	protein_coding	-1,37124348	0,004006
ENSG00000269994	LINC02893	lncRNA	-1,19412405	0,00403972
ENSG00000174827	PDZK1	protein_coding	-1,2890623	0,00418701
ENSG00000116106	EPHA4	protein_coding	-4,17836676	0,00433619
ENSG00000287581		lncRNA	-4,53096297	0,0046699
ENSG00000228421		lncRNA	-1,86363743	0,0047213
ENSG00000228150		lncRNA	-1,74817116	0,00484244
ENSG00000256417		lncRNA	-1,89784165	0,00495502
ENSG00000260644	HERC2P5	transcribed_unprocessed pseudogene	-1,14400547	0,00503888
ENSG00000231542	TAB3-AS1	lncRNA	-2,35379426	0,00509525
ENSG00000238090		processed_pseudogene	-5,51644073	0,00513672
ENSG00000232044	SILC1	lncRNA	-1,46360925	0,00519902
ENSG00000166828	SCNN1G	protein_coding	-4,18969657	0,00522538
ENSG00000131018	SYNE1	protein_coding	-1,0016652	0,00523158
ENSG00000198729	PPP1R14C	protein_coding	-2,39059117	0,00528131
ENSG00000225548	LINC01980	lncRNA	-1,09415389	0,00529307
ENSG00000170915	PAQR8	protein_coding	-4,13366411	0,00566219
ENSG00000197083	ZNF300P1	transcribed_unprocessed_pseudogene	-1,41504272	0,00572605
ENSG00000153993	SEMA3D	protein_coding	-5,34793039	0,00580063
ENSG00000224875	EML4-AS1	lncRNA	-1,69686225	0,00581406
ENSG00000254550	OMP	protein_coding	-2,22745193	0,00585343
ENSG00000230896		lncRNA	-1,10854673	0,00590484
ENSG00000215859	PDZK1P1	transcribed_unprocessed pseudogene	-2,16155718	0,00592621
ENSG00000120708	TGFBI	protein_coding	-1,2938814	0,00593024
ENSG00000235726		lncRNA	-1,29101822	0,00599991
ENSG00000263818	RDM1P5	transcribed_processed pseudogene	-2,15201279	0,00602042
ENSG00000203697	CAPN8	protein_coding	-1,09713753	0,00604874
ENSG00000271789		lncRNA	-1,19874079	0,0060807
ENSG00000278896		TEC	-2,5314864	0,00610219
ENSG00000170927	PKHD1	protein_coding	-1,13153747	0,00623934
ENSG00000185272	RBM11	protein_coding	-1,56149829	0,00639527
ENSG00000248599	FLJ42969	lncRNA	-1,93807738	0,00646146
ENSG00000234311		lncRNA	-4,95373412	0,00653307
ENSG00000187689	AMTN	protein_coding	-5,29179308	0,00681182
ENSG00000117600	PLPPR4	protein_coding	-1,72316687	0,00687105
ENSG00000148053	NTRK2	protein_coding	-2,12523178	0,00688406
ENSG00000122592	HOXA7	protein_coding	-1,30296416	0,00691313
ENSG00000158482	SNX29P1	unprocessed_pseudogene	-1,34664258	0,00694686
ENSG00000270802		processed_pseudogene	-1,15530882	0,00701486
ENSG00000212939		lncRNA	-5,33444366	0,00704476
ENSG00000184599	TAFA3	protein_coding	-1,75070217	0,00705569
ENSG00000151388	ADAMTS12	protein_coding	-3,95417878	0,0073042
ENSG00000198542	ITGBL1	protein_coding	-5,80927294	0,00733904
ENSG00000203801	LINC00222	lncRNA	-3,00996203	0,00748428
ENSG00000225075		lncRNA	-1,33383494	0,00751796
ENSG00000223368		processed_pseudogene	-5,89639956	0,00774987
ENSG00000226476	LINC01748	lncRNA	-4,23623603	0,00778203
ENSG00000237940	LINC01238	lncRNA	-1,01214436	0,00822815
ENSG00000189051	RNF222	protein_coding	-1,75138243	0,00830458
ENSG00000196196	HRCT1	protein_coding	-2,8371949	0,0084937
ENSG00000233728		lncRNA	-1,06278049	0,00873855
ENSG00000280106		TEC	-1,34404282	0,00879736
ENSG00000258969	LINC02307	lncRNA	-1,9045148	0,00915583
ENSG00000136231	IGF2BP3	protein_coding	-2,06848091	0,00915632

ENSG00000246596		transcribed_unprocessed_pseudogene	-3,51608613	0,00958356
ENSG00000236528		lncRNA	-1,67564722	0,01000397
ENSG00000186369	LINC00643	transcribed_unitary_pseudogene	-5,67179031	0,01033906
ENSG00000171759	PAH	protein_coding	-1,95268084	0,01034153
ENSG00000248740	LINC02428	lncRNA	-3,09891235	0,01034703
ENSG00000260368		lncRNA	-1,27053846	0,01041792
ENSG00000253554	LINC01414	lncRNA	-2,98045792	0,01078479
ENSG00000256146		lncRNA	-2,42761182	0,01096827
ENSG00000275371		lncRNA	-2,04078451	0,01096937
ENSG00000149328	GLB1L2	protein_coding	-2,77793331	0,01102638
ENSG00000260177		lncRNA	-1,60543369	0,01104713
ENSG00000267056		processed_pseudogene	-1,18446929	0,01142195
ENSG00000153721	CNKSR3	protein_coding	-1,13714637	0,01148234
ENSG00000011201	ANOS1	protein_coding	-1,05502539	0,01161928
ENSG00000228705	LINC00659	lncRNA	-1,07418221	0,01165369
ENSG00000164690	SHH	protein_coding	-2,1057906	0,01180562
ENSG00000215146		transcribed_unprocessed pseudogene	-2,28123874	0,01222736
ENSG00000237301		lncRNA	-3,0333094	0,01229919
ENSG00000261759		lncRNA	-1,24749904	0,01243068
ENSG00000215915	ATAD3C	protein_coding	-1,46752904	0,01258047
ENSG00000236204	LINC01376	lncRNA	-1,29300762	0,01262686
ENSG00000267053		lncRNA	-3,32521433	0,01288681
ENSG00000236467	KCNMA1-AS1	lncRNA	-2,93573772	0,01293517
ENSG00000224189	HAGLR	lncRNA	-2,01582774	0,01297343
ENSG00000287080	H3C3	protein_coding	-3,89554513	0,01310971
ENSG00000254963		lncRNA	-1,08904108	0,01310987
ENSG00000256469		lncRNA	-1,51594453	0,01311628
ENSG00000249379		lncRNA	-1,41702397	0,0131169
ENSG00000129167	TPH1	protein_coding	-2,02755201	0,01359998
ENSG00000070601	FRMPD1	protein_coding	-2,07764744	0,01371103
ENSG00000285825	CCDC15-DT	lncRNA	-2,06477953	0,01381474
ENSG00000255200	PGAM1P8	transcribed_processed pseudogene	-1,04795843	0,0138804
ENSG00000272438		lncRNA	-1,50574817	0,01391745
ENSG00000105991	HOXA1	protein_coding	-4,73570635	0,01395703
ENSG00000180071	ANKRD18A	protein_coding	-3,90562807	0,01399659
ENSG00000138792	ENPEP	protein_coding	-3,89559402	0,01399863
ENSG00000182938	OTOP3	protein_coding	-1,71712231	0,01413112
ENSG00000197444	OGDHL	protein_coding	-3,88900576	0,0142188
ENSG00000162873	KLHDC8A	protein_coding	-2,46609178	0,01432546
ENSG00000057468	MSH4	protein_coding	-1,04056929	0,01443471
ENSG00000146192	FGD2	protein_coding	-2,61952562	0,01448051
ENSG00000138271	GPR87	protein_coding	-1,86945604	0,01471935
ENSG00000224940	PRRT4	protein_coding	-1,24406331	0,01496234
ENSG00000273090		lncRNA	-1,03991365	0,01499218
ENSG00000287782		lncRNA	-1,60465706	0,01499218
ENSG00000055118	KCNH2	protein_coding	-1,60477915	0,01512408
ENSG00000286145		lncRNA	-3,2317064	0,01541703
ENSG00000285103		lncRNA	-1,10139058	0,01636095
ENSG00000260093		lncRNA	-4,11304486	0,01725756
ENSG00000178773	CPNE7	protein_coding	-1,37255747	0,01735411
ENSG00000179935	LINC00652	lncRNA	-2,52632461	0,01749419
ENSG00000100985	MMP9	protein_coding	-3,88575207	0,01808749
ENSG00000132122	SPATA6	protein_coding	-1,07859183	0,01835926
ENSG00000286989		lncRNA	-1,58728032	0,01884899
ENSG00000167080	B4GALNT2	protein_coding	-1,84577494	0,01921815
ENSG00000184163	C1QTNF12	protein_coding	-1,02426791	0,01937814
ENSG00000181126	HLA-V	transcribed_unprocessed pseudogene	-4,97631277	0,0197219
ENSG00000287592		lncRNA	-2,62936133	0,02022911
ENSG00000226508	LINC01918	lncRNA	-4,36822161	0,02050769
ENSG00000189409	MMP23B	protein_coding	-1,53516133	0,02052893
ENSG00000271109		lncRNA	-2,98818868	0,02063462
ENSG00000226944	RNF207-AS1	lncRNA	-1,57261376	0,02109436
ENSG00000278472		lncRNA	-1,68640522	0,02126412
ENSG00000267606		lncRNA	-3,39104484	0,02133392
ENSG00000185052	SLC24A3	protein_coding	-1,82011553	0,02152818
ENSG00000118729	CASQ2	protein_coding	-5,06057617	0,02169576
ENSG00000229732		lncRNA	-2,03506711	0,02179608
ENSG00000186188	FFAR4	protein_coding	-1,45792472	0,02192373
ENSG00000267580		lncRNA	-1,40163254	0,0221387
ENSG00000213144		processed_pseudogene	-1,35263501	0,02233515
ENSG00000224848		lncRNA	-2,45989236	0,02240168
ENSG00000287550		lncRNA	-3,86764048	0,02287478
ENSG00000239396	RN7SL414P	misc_RNA	-1,67191779	0,0231867
ENSG00000163283	ALPP	protein_coding	-4,41386182	0,02325984
ENSG00000260465		lncRNA	-1,82630267	0,023672
ENSG00000240216	CPHL1P	transcribed_unitary pseudogene	-1,14512185	0,02370936
ENSG00000041515	MYO16	protein_coding	-3,92021204	0,02372363
ENSG00000137941	TTLL7	protein_coding	-3,72437109	0,0239182
ENSG00000269289		lncRNA	-3,27336808	0,02395942
ENSG00000270135		lncRNA	-1,5988488	0,02433308
ENSG00000207119	U3	snoRNA	-5,50500314	0,02438898
ENSG00000225602	MTOR-AS1	lncRNA	-1,69657131	0,02439634
ENSG00000004848	ARX	protein_coding	-3,75171889	0,02443115
ENSG00000285570		lncRNA	-1,32009527	0,02443115

ENSG00000286707		lncRNA	-1,99192094	0,02463224
ENSG00000207922		miRNA	-1,06898715	0,02470293
ENSG00000242574	HLA-DMB	protein_coding	-1,6547178	0,02484728
ENSG00000069667	RORA	protein_coding	-1,12162412	0,02507389
ENSG00000157703	SVOPL	protein_coding	-1,29786189	0,02511439
ENSG00000207721	MIR186	miRNA	-1,58735662	0,02515565
ENSG00000263595	RN7SL823P	misc_RNA	-4,33923331	0,02531664
ENSG00000074416	MGLL	protein_coding	-1,02241223	0,02533996
ENSG00000227214	HCG15	lncRNA	-1,15469631	0,02595415
ENSG00000263080		lncRNA	-1,36467251	0,02616817
ENSG00000203469		lncRNA	-1,44884642	0,02632816
ENSG00000165323	FAT3	protein_coding	-4,19234027	0,02667118
ENSG00000215808	LINC01139	lncRNA	-2,01354602	0,02668422
ENSG00000255874	PRECSIT	lncRNA	-2,28831104	0,02673154
ENSG00000112139	MDGA1	protein_coding	-1,32494332	0,02707279
ENSG00000183023	SLC8A1	protein_coding	-1,55787249	0,02715511
ENSG00000236397	DDX11L2	unprocessed_pseudogene	-1,6388682	0,02745243
ENSG00000268350	FAM156A	protein_coding	-1,41258188	0,02751691
ENSG00000270147		lncRNA	-2,10876544	0,02791229
ENSG00000219607	PPP1R3G	protein_coding	-3,01686878	0,02819646
ENSG00000132205	EMILIN2	protein_coding	-3,8778282	0,02829337
ENSG00000173809	TDRD12	protein_coding	-1,14335114	0,02861712
ENSG00000130558	OLFM1	protein_coding	-2,2048059	0,02870906
ENSG00000287069		lncRNA	-1,14377491	0,0290459
ENSG00000177191	B3GNT8	protein_coding	-1,35117793	0,02921735
ENSG00000273275		lncRNA	-1,29941444	0,02999807
ENSG00000262801		lncRNA	-3,86043501	0,03002877
ENSG00000131620	ANO1	protein_coding	-1,40579839	0,03017015
ENSG00000176153	GPX2	protein_coding	-1,71799954	0,03024453
ENSG00000149403	GRIK4	protein_coding	-3,75079917	0,03031664
ENSG00000254740		lncRNA	-2,78272159	0,03032983
ENSG00000274928	KRT89P	transcribed_unprocessed pseudogene	-3,13957208	0,03043601
ENSG00000236651	DLX2-DT	lncRNA	-2,25017618	0,03080403
ENSG00000215875	ST13P20	processed_pseudogene	-4,81643997	0,03113542
ENSG00000165887	ANKRD2	protein_coding	-1,37185157	0,03202904
ENSG00000233429	HOTAIRM1	lncRNA	-4,47991482	0,03239859
ENSG00000157884	CIB4	protein_coding	-3,83661039	0,03244586
ENSG00000257524		protein_coding	-1,59386314	0,03315591
ENSG00000267260		lncRNA	-1,99814814	0,03342143
ENSG00000223784	LINP1	lncRNA	-4,04382763	0,03342865
ENSG00000131050	BPIFA2	protein_coding	-1,18347067	0,03353445
ENSG00000133055	MYBPH	protein_coding	-4,10746118	0,03422991
ENSG00000268533		protein_coding	-1,63979934	0,03424397
ENSG00000271774		lncRNA	-4,00564186	0,03424397
ENSG00000237489	C10orf143	protein_coding	-1,08178129	0,03450578
ENSG00000249992	TMEM158	protein_coding	-3,16655907	0,03456269
ENSG00000189223	PAX8-AS1	lncRNA	-1,56656061	0,03484328
ENSG00000064205	CCN5	protein_coding	-1,10903333	0,03502503
ENSG00000262668		lncRNA	-4,29057264	0,03505507
ENSG00000205667	ARSH	protein_coding	-3,51123359	0,03553127
ENSG00000168961	LGALS9	protein_coding	-1,0931098	0,03573227
ENSG00000135902	CHRND	protein_coding	-2,42305956	0,03585579
ENSG00000254826		lncRNA	-3,32479869	0,03675258
ENSG00000158560	DYNC1I1	protein_coding	-2,13191216	0,03695876
ENSG00000286163		lncRNA	-2,42933413	0,03711257
ENSG00000122574	WIPF3	protein_coding	-1,03872795	0,03713615
ENSG00000236527	ARF4P2	processed_pseudogene	-2,28923191	0,03736007
ENSG00000266075	RN7SL574P	misc_RNA	-2,76434795	0,03767247
ENSG00000280109	PLAC4	lncRNA	-1,09434935	0,03769845
ENSG00000273343		lncRNA	-1,21376037	0,03776856
ENSG00000272842		lncRNA	-2,2140733	0,03860748
ENSG00000255404		lncRNA	-1,42306694	0,03868969
ENSG00000279685	MAPT-IT1	lncRNA	-1,02281616	0,03883732
ENSG00000179542	SLITRK4	protein_coding	-3,48716788	0,03888697
ENSG00000234469	CLDN34	protein_coding	-2,24454781	0,03897718
ENSG00000255310		lncRNA	-3,48842234	0,03917753
ENSG00000052850	ALX4	protein_coding	-3,56149446	0,03920212
ENSG00000180861	LINC01559	lncRNA	-3,61747159	0,03947915
ENSG00000039139	DNAH5	protein_coding	-3,47729427	0,03950248
ENSG00000197816	CCDC180	protein_coding	-1,02717636	0,03963283
ENSG00000164604	GPR85	protein_coding	-1,61093116	0,03983299
ENSG00000260941	LINC00622	lncRNA	-2,5152461	0,04005694
ENSG00000231482		lncRNA	-1,7526447	0,04160929
ENSG00000284713	SMIM38	protein_coding	-1,67192213	0,04183072
ENSG00000201470	RNY4P7	misc_RNA	-1,21199818	0,04190458
ENSG00000257403		unprocessed_pseudogene	-2,10963237	0,04196775
ENSG00000283269		transcribed_unprocessed pseudogene	-4,77274332	0,04206252
ENSG00000230550	ERLNC1	lncRNA	-1,55623307	0,04224424
ENSG00000278891		TEC	-4,03558355	0,04251971
ENSG00000183067	IGSF5	protein_coding	-1,46069014	0,0426212
ENSG00000140481	CCDC33	protein_coding	-3,38753075	0,04266803
ENSG00000261186	LINC01238	lncRNA	-1,90177735	0,04266803
ENSG00000260805		lncRNA	-1,07691697	0,04272733
ENSG00000140931	CMTM3	protein_coding	-1,30068251	0,04283596
ENSG00000053524	MCF2L2	protein_coding	-1,81083119	0,04328694
ENSG00000218416		lncRNA	-1,27714702	0,04391272
ENSG00000251893	SNORA70	snoRNA	-4,03749052	0,04399846
ENSG00000181449	SOX2	protein_coding	-1,44989594	0,04424358

ENSG00000087128	TMPRSS11E	protein_coding	-2,56338807	0,04443494
ENSG00000224387		lncRNA	-1,45956365	0,04463237
ENSG00000248144	ADH1C	protein_coding	-1,70934686	0,04499407
ENSG00000233635		lncRNA	-3,74572618	0,04573684
ENSG00000167754	KLK5	protein_coding	-2,46741821	0,04580437
ENSG00000136425	CIB2	protein_coding	-1,08933149	0,04607162
ENSG00000178852	EFCAB13	protein_coding	-1,37142058	0,0461522
ENSG00000271730		lncRNA	-4,33159372	0,04794618
ENSG00000218690	H2AC10P	transcribed_unprocessed pseudogene	-1,38177619	0,04815584
ENSG00000235008		processed_pseudogene	-2,29300297	0,04924178
ENSG00000280202		TEC	-1,072639	0,0493298
ENSG00000274918		lncRNA	-4,05778481	0,04962349
ENSG00000143195	ILDR2	protein_coding	-2,24353498	0,04968504
ENSG00000232006		lncRNA	-2,84932513	0,04974321
ENSG00000109906	ZBTB16	protein_coding	-3,00981491	0,04998698
ENSG00000131183	SLC34A1	protein_coding	-2,1709292	0,05001211
ENSG00000202119	RNU6-302P	snRNA	-4,16278793	0,0505866
ENSG00000149243	KLHL35	protein_coding	-1,02229858	0,05087345
ENSG00000258088		lncRNA	-5,10329676	0,05114935
ENSG00000286057		TEC	-2,59465378	0,05199841
ENSG00000155974	GRIP1	protein_coding	-1,16866294	0,05257314
ENSG00000254027		lncRNA	-2,27284338	0,05302552
ENSG00000273245		lncRNA	-1,13926153	0,05324124
ENSG00000255298	OR8G5	protein_coding	-1,07879975	0,05343326
ENSG00000264529	DNAJB6P8	transcribed_processed pseudogene	-3,99496058	0,05391985
ENSG00000272369		lncRNA	-2,31622704	0,05403678
ENSG00000274528		lncRNA	-1,78279318	0,05410615
ENSG00000204889	KRT40	protein_coding	-1,51318411	0,05416269
ENSG00000124935	SCGB1D2	protein_coding	-2,17930527	0,05432183
ENSG00000281189	GHET1	lncRNA	-1,17068093	0,05434404
ENSG00000207260	RNU6-35P	snRNA	-1,75783299	0,0545843
ENSG00000287630		lncRNA	-3,58550013	0,05544636
ENSG00000169031	COL4A3	protein_coding	-3,75974989	0,0556055
ENSG00000285868		protein_coding	-1,30595312	0,05574693
ENSG00000249898	MCPH1-AS1	lncRNA	-1,33001059	0,05604016
ENSG00000202415	RN7SKP269	misc_RNA	-1,22071295	0,05649046
ENSG00000235961	PNMA6A	protein_coding	-1,34142935	0,05705425
ENSG00000091482	SMPX	protein_coding	-2,47924238	0,05787409
ENSG00000165124	SVEP1	protein_coding	-2,44742508	0,05863757
ENSG00000225439	BOLA3-AS1	lncRNA	-1,2808618	0,0587679
ENSG00000256811		lncRNA	-1,35323363	0,06014627
ENSG00000107518	ATRNL1	protein_coding	-3,32137549	0,06030441
ENSG00000150510	FAM124A	protein_coding	-1,10807339	0,06051362
ENSG00000181690	PLAG1	protein_coding	-3,51298395	0,0607473
ENSG00000204758		lncRNA	-1,47613274	0,06096056
ENSG00000233124	LINC00456	lncRNA	-2,75388187	0,06096056
ENSG00000101605	MYOM1	protein_coding	-1,59014063	0,06181984
ENSG00000204380	PKP4-AS1	lncRNA	-1,120395	0,06206061
ENSG00000168913	ENHO	protein_coding	-1,85448261	0,06247077
ENSG00000183773	AIFM3	protein_coding	-1,2538802	0,06247077
ENSG00000182463	TSHZ2	protein_coding	-3,69784668	0,06300714
ENSG00000227954	TARID	lncRNA	-1,70522647	0,06358937
ENSG00000245466		lncRNA	-1,90048231	0,06377652
ENSG00000141665	FBXO15	protein_coding	-1,81622432	0,0644227
ENSG00000185883	ATP6V0C	protein_coding	-1,19888497	0,06443083
ENSG00000236751	LINC01186	lncRNA	-1,54900259	0,06474392
ENSG00000280193		TEC	-3,03055322	0,06475749
ENSG00000200701	RNU6-674P	snRNA	-2,04611015	0,06524249
ENSG00000169439	SDC2	protein_coding	-3,2193157	0,06587982
ENSG00000266289		lncRNA	-1,35876208	0,06627225
ENSG00000253667		processed_pseudogene	-3,54102636	0,06707199
ENSG00000261898		lncRNA	-1,95314237	0,06762226
ENSG00000236307	EEF1E1P1	processed_pseudogene	-2,23231248	0,06774246
ENSG00000178460	MCMDC2	protein_coding	-1,04206714	0,06806005
ENSG00000233251		lncRNA	-3,22165204	0,06814053
ENSG00000124302	CHST8	protein_coding	-2,63277672	0,06945312
ENSG00000105695	MAG	protein_coding	-3,22409326	0,06964898
ENSG00000265566	RN7SL605P	misc_RNA	-2,0321647	0,0697997
ENSG00000176697	BDNF	protein_coding	-1,87269304	0,06995811
ENSG00000283355		TEC	-3,970022	0,07072082
ENSG00000128262	POM121L9P	transcribed_unprocessed pseudogene	-2,13270195	0,07118219
ENSG00000125430	HS3ST3B1	protein_coding	-3,20258017	0,07127116
ENSG00000233296	TMEM18-DT	lncRNA	-1,22355228	0,07127116
ENSG00000142623	PADI1	protein_coding	-1,25695317	0,07173151
ENSG00000259755		lncRNA	-1,92345355	0,07182025
ENSG00000183775	KCTD16	protein_coding	-2,14512672	0,072484
ENSG00000236393		lncRNA	-2,55318404	0,072484
ENSG00000224789		lncRNA	-1,89428443	0,07292363
ENSG00000224023	EDRF1-DT	lncRNA	-2,43220069	0,07411303
ENSG00000198417	MT1F	protein_coding	-1,35662588	0,07436182
ENSG00000226690		protein_coding	-3,59724599	0,07490545
ENSG00000175868	CALCB	protein_coding	-1,93710186	0,07500538
ENSG00000163803	PLB1	protein_coding	-2,17341824	0,07529085
ENSG00000204118	NAP1L6P	transcribed_processed pseudogene	-3,20861299	0,07552509
ENSG00000234112		processed_pseudogene	-2,41486714	0,07562703
ENSG00000235493	LINC01967	lncRNA	-1,83244059	0,07651796

ENSG00000278811	LINC00624	lncRNA	-1,77256218	0,07688323
ENSG00000235512	TAB3-AS2	lncRNA	-1,74922958	0,07688713
ENSG00000201544	SNORA16B	snoRNA	-1,83351389	0,07764191
ENSG00000155875	SAXO1	protein_coding	-1,91738663	0,07771982
ENSG00000135697	BCO1	protein_coding	-1,68607552	0,07879877
ENSG00000280054		TEC	-1,21743635	0,07895657
ENSG00000201659	RNU12-2P	snRNA	-3,84017786	0,0793308
ENSG00000254420		lncRNA	-2,39188975	0,07943513
ENSG00000164120	HPGD	protein_coding	-3,18797786	0,07945197
ENSG00000254369	HOXA-AS3	lncRNA	-3,14837438	0,08003986
ENSG00000260576	EIF5A2P1	processed_pseudogene	-1,62293186	0,08051744
ENSG00000165685	TMEM52B	protein_coding	-3,8435678	0,08142834
ENSG00000232762		lncRNA	-3,58397883	0,08179764
ENSG00000233571		lncRNA	-2,19654827	0,08358906
ENSG00000286010		lncRNA	-2,17946762	0,08399913
ENSG00000183166	CALN1	protein_coding	-2,48488957	0,08489581
ENSG00000226465		lncRNA	-1,35735626	0,08499449
ENSG00000267992		lncRNA	-3,2532871	0,08500799
ENSG00000207344	SNORA22C	snoRNA	-2,69476558	0,08569236
ENSG00000230483		lncRNA	-2,12522537	0,08620921
ENSG00000249242	TMEM150C	protein_coding	-1,21368384	0,08652561
ENSG00000272463		lncRNA	-3,43643993	0,0868253
ENSG00000168243	GNG4	protein_coding	-3,79369703	0,08730082
ENSG00000257743	MGAM2	protein_coding	-1,39621961	0,08853358
ENSG00000152217	SETBP1	protein_coding	-2,50423088	0,08896678
ENSG00000168447	SCNN1B	protein_coding	-1,95105642	0,09015709
ENSG00000272963	OR7A19P	unprocessed_pseudogene	-2,89173805	0,09022405
ENSG00000138185	ENTPD1	protein_coding	-1,04880557	0,09022722
ENSG00000262362		lncRNA	-1,39347667	0,09042172
ENSG00000130294	KIF1A	protein_coding	-2,5039728	0,09044787
ENSG00000242553		lncRNA	-1,47211977	0,09072145
ENSG00000121898	CPXM2	protein_coding	-2,14219863	0,09155806
ENSG00000222068	RN7SKP154	misc_RNA	-3,61348201	0,09183327
ENSG00000257181		lncRNA	-1,10575523	0,09206288
ENSG00000174912	METTL15P1	processed_pseudogene	-1,12234009	0,09284683
ENSG00000272660		lncRNA	-1,31583668	0,09284683
ENSG00000268628		lncRNA	-1,39332064	0,09318436
ENSG00000260500		lncRNA	-1,20941923	0,09432517
ENSG00000234705	HMGA1P4	lncRNA	-1,00046808	0,09449466
ENSG00000207923	MIR559	miRNA	-1,35441113	0,09493662
ENSG00000197149		processed_pseudogene	-3,53613625	0,09623522
ENSG00000217624	YWHAZP10	processed_pseudogene	-2,97341516	0,09635389
ENSG00000280543	ASAP1-IT2	lncRNA	-1,04913953	0,09694303
ENSG00000253532		lncRNA	-2,02862533	0,09696767
ENSG00000254762		lncRNA	-1,33579205	0,09762818
ENSG00000224891	ARL14EPP1	processed_pseudogene	-1,42303962	0,09768155
ENSG00000248099	INSL3	protein_coding	-1,98398444	0,09775942
ENSG00000224577	LINC01117	lncRNA	-1,17019688	0,09850706
ENSG00000234818		lncRNA	-1,27685969	0,09851179
ENSG00000232645	LINC01431	lncRNA	-1,51564127	0,0986579
ENSG00000143369	ECM1	protein_coding	-1,49011462	0,09909729

Supplementary Table S 4: Genes with increased expression in resistant MCF7 cells.

Ensembl	GeneSymbol	gene_biotype	log2FC	FDR
ENSG00000242265	PEG10	protein_coding	4,90534405	9,792E-302
ENSG00000151150	ANK3	protein_coding	2,7024672	6,722E-250
ENSG00000111319	SCNN1A	protein_coding	2,74779806	6,6E-202
ENSG00000026508	CD44	protein_coding	2,91419103	1,4E-169
ENSG00000275266		misc_RNA	5,59707083	2,211E-151
ENSG00000130021	PUDP	protein_coding	2,92593226	2,06E-125
ENSG00000100234	TIMP3	protein_coding	3,40500203	1,43E-119
ENSG00000100867	DHRS2	protein_coding	3,33977602	2,415E-116
ENSG00000169169	CPT1C	protein_coding	4,45350648	2,002E-113
ENSG00000137393	RNF144B	protein_coding	2,6042724	1,854E-100
ENSG00000033327	GAB2	protein_coding	2,25845295	3,0287E-97
ENSG00000105464	GRIN2D	protein_coding	2,74219721	4,0236E-96
ENSG00000126010	GRPR	protein_coding	5,35486464	8,1567E-92
ENSG00000129038	LOXL1	protein_coding	3,18076495	1,8824E-88
ENSG00000104783	KCNN4	protein_coding	2,55514766	2,8773E-87
ENSG00000147642	SYBU	protein_coding	3,42093932	2,8773E-87
ENSG00000176887	SOX11	protein_coding	3,17749644	2,1832E-86
ENSG00000168542	COL3A1	protein_coding	11,0175849	7,6695E-85
ENSG00000095321	CRAT	protein_coding	4,12717293	6,3667E-79
ENSG00000115457	IGFBP2	protein_coding	2,43903047	9,1536E-79
ENSG00000189221	MAOA	protein_coding	3,49943245	4,2489E-74
ENSG00000187098	MITF	protein_coding	3,45618161	3,0808E-73
ENSG00000243566	UPK3B	protein_coding	2,30896956	3,1052E-72
ENSG00000064787	BCAS1	protein_coding	3,1224511	3,5124E-71
ENSG00000157514	TSC22D3	protein_coding	1,85724149	1,0902E-70
ENSG00000167779	IGFBP6	protein_coding	4,99850055	1,0425E-69
ENSG00000137331	IER3	protein_coding	1,89252015	1,175E-69
ENSG00000127990	SGCE	protein_coding	4,50577004	6,2655E-68
ENSG00000133121	STARD13	protein_coding	1,73019332	4,0793E-64
ENSG00000161267	BDH1	protein_coding	2,00151199	5,5172E-63
ENSG00000173175	ADCY5	protein_coding	5,24193833	1,4345E-62
ENSG00000102401	ARMCX3	protein_coding	1,72354223	2,1717E-62
ENSG00000230836	LINC01293	lncRNA	4,29438287	2,3351E-62
ENSG00000105810	CDK6	protein_coding	2,05033917	2,3674E-62

ENSG00000135074	ADAM19	protein_coding	2,75222039	2,1154E-61
ENSG00000104419	NDRG1	protein_coding	2,62453108	1,4792E-60
ENSG00000139651	ZNF740	protein_coding	1,60516537	2,2254E-60
ENSG00000148841	ITPRIP	protein_coding	1,89689295	5,8107E-60
ENSG00000172461	FUT9	protein_coding	2,6671354	7,7892E-57
ENSG00000183018	SPNS2	protein_coding	2,49624523	2,7773E-55
ENSG00000100219	XBP1	protein_coding	1,25388325	5,4761E-55
ENSG00000057252	SOAT1	protein_coding	1,47881275	1,733E-54
ENSG00000163637	PRICKLE2	protein_coding	1,59963642	7,4408E-54
ENSG00000139631	CSAD	protein_coding	1,78068756	3,2296E-53
ENSG00000169251	NMD3	protein_coding	1,75919784	3,0933E-52
ENSG00000150347	ARID5B	protein_coding	1,40894851	2,436E-51
ENSG00000172296	SPTLC3	protein_coding	4,28987443	2,0944E-50
ENSG00000188404	SELL	protein_coding	5,09087657	5,7008E-50
ENSG00000118369	USP35	protein_coding	1,81845188	5,8761E-50
ENSG00000158321	AUTS2	protein_coding	2,50403757	1,9581E-48
ENSG00000110436	SLC1A2	protein_coding	2,83266151	3,8414E-48
ENSG00000198797	BRINP2	protein_coding	1,98943127	4,3601E-48
ENSG00000082438	COBLL1	protein_coding	1,42395647	1,8074E-47
ENSG00000141232	TOB1	protein_coding	1,35375306	3,4183E-47
ENSG00000198832	SELENOM	protein_coding	2,61456212	7,1515E-47
ENSG00000100393	EP300	protein_coding	1,02148234	5,1629E-46
ENSG00000118985	ELL2	protein_coding	1,52588612	4,198E-45
ENSG00000223523		lncRNA	3,02936444	1,1709E-44
ENSG00000196368	NUDT11	protein_coding	3,63461963	1,2995E-44
ENSG00000129422	MTUS1	protein_coding	1,15407532	1,4502E-44
ENSG00000179862	CITED4	protein_coding	2,15041525	2,7654E-44
ENSG00000079482	OPHN1	protein_coding	1,85680649	5,3533E-44
ENSG00000279207		TEC	1,4102325	6,8489E-44
ENSG00000178053	MLF1	protein_coding	1,86307228	9,4046E-42
ENSG00000264364	DYNLL2	protein_coding	1,07981846	1,0341E-41
ENSG00000235123	DSCAM-AS1	lncRNA	1,44699531	1,5858E-41
ENSG00000150995	ITPR1	protein_coding	1,66277239	2,3908E-41
ENSG00000161671	EMC10	protein_coding	1,36355891	6,412E-41
ENSG00000104447	TRPS1	protein_coding	1,48581544	6,7763E-41
ENSG00000168743	NPNT	protein_coding	1,58779398	2,2953E-40
ENSG00000095739	BAMBI	protein_coding	1,56207679	3,8279E-40
ENSG00000075426	FOSL2	protein_coding	1,38719803	8,201E-40
ENSG00000116016	EPAS1	protein_coding	4,45602038	2,283E-39
ENSG00000184564	SLITRK6	protein_coding	2,14832074	2,981E-39
ENSG00000182986	ZNF320	protein_coding	1,75385637	4,1932E-39
ENSG00000187535	IFT140	protein_coding	1,09004718	1,4396E-38
ENSG00000102393	GLA	protein_coding	1,33643981	1,6448E-38
ENSG00000185442	FAM174B	protein_coding	1,22614701	1,2767E-37
ENSG00000196557	CACNA1H	protein_coding	1,01783027	7,5737E-37
ENSG00000147100	SLC16A2	protein_coding	2,11491007	2,4557E-36
ENSG00000185551	NR2F2	protein_coding	1,2585668	1,3613E-35
ENSG00000172197	MBOAT1	protein_coding	1,51442313	1,4027E-35
ENSG00000187210	GCNT1	protein_coding	2,20242876	3,6764E-35
ENSG00000116667	C1orf21	protein_coding	1,6571907	5,0576E-35
ENSG00000196139	AKR1C3	protein_coding	2,15734073	1,0687E-34
ENSG00000127824	TUBA4A	protein_coding	2,20319623	1,9621E-34
ENSG00000163590	PPM1L	protein_coding	1,62286522	2,8201E-34
ENSG00000135709	KIAA0513	protein_coding	1,10426607	3,0296E-34
ENSG00000166821	PEX11A	protein_coding	1,79729432	6,5108E-34
ENSG00000152558	TMEM123	protein_coding	1,09989733	7,0933E-34
ENSG00000130600	H19	lncRNA	5,53046145	1,4108E-33
ENSG00000185352	HS6ST3	protein_coding	2,24138362	1,5691E-33
ENSG00000121101	TEX14	protein_coding	2,14236567	3,5952E-33
ENSG00000059728	MXD1	protein_coding	1,36374837	1,4036E-32
ENSG00000121966	CXCR4	protein_coding	3,44071003	6,2152E-32
ENSG00000179715	PCED1B	protein_coding	2,04673761	1,189E-31
ENSG00000181467	RAP2B	protein_coding	1,18261526	1,6708E-31
ENSG00000081923	ATP8B1	protein_coding	1,02290469	2,0723E-31
ENSG00000231233	CFAP58-DT	lncRNA	4,35687244	2,1056E-31
ENSG00000157483	MYO1E	protein_coding	1,16647689	3,1077E-31
ENSG00000182287	AP1S2	protein_coding	1,34727843	5,7345E-31
ENSG00000186153	WWOX	protein_coding	1,37890183	5,7873E-31
ENSG00000182890	GLUD2	protein_coding	2,11550204	7,683E-31
ENSG00000144218	AFF3	protein_coding	2,20510624	7,8261E-31
ENSG00000102886	GDPD3	protein_coding	2,2302855	8,8176E-31
ENSG00000111424	VDR	protein_coding	1,27964747	1,566E-30
ENSG00000257337		lncRNA	1,36148663	2,103E-30
ENSG00000143412	ANXA9	protein_coding	1,31848266	2,3385E-30
ENSG00000166582	CENPV	protein_coding	2,43862265	4,9753E-30
ENSG00000106546	AHR	protein_coding	1,72897729	8,4178E-30
ENSG00000067840	PDZD4	protein_coding	2,3010798	1,4592E-29
ENSG00000108963	DPH1	protein_coding	1,18239447	2,5767E-29
ENSG00000170017	ALCAM	protein_coding	1,22790369	4,0894E-29
ENSG00000101384	JAG1	protein_coding	1,93243209	6,0516E-29
ENSG00000156587	UBE2L6	protein_coding	2,2388347	6,0524E-29
ENSG00000135547	HEY2	protein_coding	2,62941366	7,1372E-29
ENSG00000133138	TBC1D8B	protein_coding	1,55494961	7,6126E-29
ENSG00000236886		lncRNA	3,8296336	7,6126E-29
ENSG00000198960	ARMCX6	protein_coding	1,51536682	1,3998E-28
ENSG00000106829	TLE4	protein_coding	4,04286958	2,2745E-28
ENSG00000103260	METRN	protein_coding	1,10288707	2,3843E-28
ENSG00000150054	MPP7	protein_coding	1,02904398	2,3843E-28
ENSG00000104381	GDAP1	protein_coding	1,99965476	4,0251E-28
ENSG00000134215	VAV3	protein_coding	1,29774372	6,2976E-28

ENSG00000159399	HK2	protein_coding	1,63671716	1,0904E-27
ENSG00000164056	SPRY1	protein_coding	3,87086377	1,7994E-27
ENSG00000110080	ST3GAL4	protein_coding	1,45504303	2,2804E-27
ENSG00000211689	TRGC1	TR_C_gene	5,43702025	3,8787E-27
ENSG00000006747	SCIN	protein_coding	3,34057768	4,4956E-27
ENSG00000156804	FBXO32	protein_coding	1,83354585	5,0838E-27
ENSG00000124493	GRM4	protein_coding	2,23534429	6,2356E-27
ENSG00000188997	KCTD21	protein_coding	1,20371845	8,8611E-27
ENSG00000008323	PLEKHG6	protein_coding	1,61264214	1,0741E-26
ENSG00000166816	LDHD	protein_coding	1,86111701	1,7598E-26
ENSG00000109929	SC5D	protein_coding	1,36602443	1,9973E-26
ENSG00000159388	BTG2	protein_coding	1,5863145	2,7603E-26
ENSG00000168398	BDKRB2	protein_coding	1,98697002	3,0034E-26
ENSG00000168077	SCARA3	protein_coding	1,64819848	9,0543E-26
ENSG00000227619		lncRNA	3,03060299	9,0592E-26
ENSG00000196542	SPTSSB	protein_coding	1,20284718	9,5005E-26
ENSG00000198933	TBKBP1	protein_coding	1,43948747	1,1166E-25
ENSG00000182606	TRAK1	protein_coding	1,13909341	1,1403E-25
ENSG00000287064		lncRNA	3,75547975	1,1807E-25
ENSG00000168546	GFRA2	protein_coding	3,26447816	1,1966E-25
ENSG00000134531	EMP1	protein_coding	3,46601748	1,3381E-25
ENSG00000030419	IKZF2	protein_coding	1,45523899	1,733E-25
ENSG00000204991	SPIRE2	protein_coding	1,5607606	2,2573E-25
ENSG00000106541	AGR2	protein_coding	1,13876161	2,4035E-25
ENSG00000103187	COTL1	protein_coding	1,28442347	2,4838E-25
ENSG00000074527	NTN4	protein_coding	2,10724778	2,495E-25
ENSG00000261801	LOXL1-AS1	lncRNA	1,14688606	2,7213E-25
ENSG00000173281	PPP1R3B	protein_coding	1,2813119	2,8529E-25
ENSG00000105641	SLC5A5	protein_coding	4,37530478	3,6732E-25
ENSG00000134369	NAV1	protein_coding	1,64794938	3,6732E-25
ENSG00000138795	LEF1	protein_coding	4,24298598	4,1786E-25
ENSG00000151726	ACSL1	protein_coding	1,17703723	4,4169E-25
ENSG00000166575	TMEM135	protein_coding	1,41105305	4,8385E-25
ENSG00000120262	CCDC170	protein_coding	1,13300837	5,5454E-25
ENSG00000162989	KCNJ3	protein_coding	2,14731877	7,2795E-25
ENSG00000261115	TMEM178B	protein_coding	1,12714446	8,5223E-25
ENSG00000174749	FAM241A	protein_coding	1,36855975	1,6864E-24
ENSG00000107984	DKK1	protein_coding	1,31254307	2,1465E-24
ENSG00000125730	C3	protein_coding	2,69540527	2,799E-24
ENSG00000164649	CDCA7L	protein_coding	1,59149878	4,2845E-24
ENSG00000128011	LRFN1	protein_coding	1,54961647	5,0719E-24
ENSG00000103056	SMPD3	protein_coding	3,16775317	7,907E-24
ENSG00000137936	BCAR3	protein_coding	1,08549781	9,8595E-24
ENSG00000174307	PHLDA3	protein_coding	1,01417871	1,5633E-23
ENSG00000135245	HILPDA	protein_coding	1,07846792	1,7047E-23
ENSG00000196074	SYCP2	protein_coding	1,35467589	1,7863E-23
ENSG00000183098	GPC6	protein_coding	1,21296845	2,223E-23
ENSG00000165905	LARGE2	protein_coding	1,71182822	2,5031E-23
ENSG00000026559	KCNG1	protein_coding	1,30953154	4,022E-23
ENSG00000137648	TMPRSS4	protein_coding	2,24800858	4,6724E-23
ENSG00000120885	CLU	protein_coding	1,4126557	6,5731E-23
ENSG00000125398	SOX9	protein_coding	3,45886078	7,298E-23
ENSG00000125534	PPDPF	protein_coding	1,0712185	1,2345E-22
ENSG00000163898	LIPH	protein_coding	2,29298046	1,456E-22
ENSG00000156453	PCDH1	protein_coding	1,58415992	1,5929E-22
ENSG00000164946	FREM1	protein_coding	3,90748254	1,6087E-22
ENSG00000135862	LAMC1	protein_coding	1,05345903	2,076E-22
ENSG00000278730		lncRNA	1,05748431	2,4253E-22
ENSG00000176641	RNF152	protein_coding	1,57972588	2,484E-22
ENSG00000184384	MAML2	protein_coding	3,41857257	3,8674E-22
ENSG00000224738		lncRNA	1,10577012	4,8341E-22
ENSG00000152284	TCF7L1	protein_coding	2,29737021	5,6074E-22
ENSG00000263753	LINC00667	lncRNA	3,18193957	7,2369E-22
ENSG00000163485	ADORA1	protein_coding	1,59605557	8,4724E-22
ENSG00000129682	FGF13	protein_coding	3,10398227	8,5757E-22
ENSG00000168952	STXBP6	protein_coding	3,97089653	9,2677E-22
ENSG00000186472	PCLO	protein_coding	1,8425462	9,5618E-22
ENSG00000041353	RAB27B	protein_coding	1,19389971	1,3316E-21
ENSG00000157992	KRTCAP3	protein_coding	1,9369288	2,1039E-21
ENSG00000141934	PLPP2	protein_coding	1,113274	2,4321E-21
ENSG00000057593	F7	protein_coding	2,72263086	2,51E-21
ENSG00000166387	PPFIBP2	protein_coding	1,2969057	4,1003E-21
ENSG00000116661	FBXO2	protein_coding	2,08724417	4,8617E-21
ENSG00000166206	GABRB3	protein_coding	11,6717373	5,5067E-21
ENSG00000165272	AQP3	protein_coding	2,31477585	6,3408E-21
ENSG00000102554	KLF5	protein_coding	1,15615834	1,9256E-20
ENSG00000114631	PODXL2	protein_coding	1,33085089	2,3721E-20
ENSG00000111846	GCNT2	protein_coding	1,65557205	2,7397E-20
ENSG00000157303	SUSD3	protein_coding	1,61338921	4,1456E-20
ENSG00000170381	SEMA3E	protein_coding	2,31081843	1,19E-19
ENSG00000163993	S100P	protein_coding	3,45128917	1,3082E-19
ENSG00000000460	C1orf112	protein_coding	1,01703652	1,4883E-19
ENSG00000139211	AMIGO2	protein_coding	1,61925387	2,1676E-19
ENSG00000113916	BCL6	protein_coding	1,17513065	4,1876E-19
ENSG00000144369	FAM171B	protein_coding	1,2332051	5,2658E-19
ENSG00000118596	SLC16A7	protein_coding	1,28510701	8,2795E-19
ENSG00000115267	IFIH1	protein_coding	1,48517716	1,0602E-18
ENSG00000152766	ANKRD22	protein_coding	2,61784333	1,1446E-18
ENSG00000144476	ACKR3	protein_coding	2,16247991	1,2139E-18
ENSG00000176463	SLCO3A1	protein_coding	1,59415262	1,5292E-18

ENSG00000165644	COMTD1	protein_coding	1,14527086	1,6658E-18
ENSG00000249846	LINC02021	lncRNA	2,98736357	1,8679E-18
ENSG00000163435	ELF3	protein_coding	1,16338939	1,9089E-18
ENSG00000238117		lncRNA	2,79916451	2,6748E-18
ENSG00000239389	PCDHA13	protein_coding	1,38752024	2,8773E-18
ENSG00000004799	PDK4	protein_coding	3,10017794	2,963E-18
ENSG00000175984	DENND2C	protein_coding	1,45411264	3,2222E-18
ENSG00000117472	TSPAN1	protein_coding	1,56412148	4,5045E-18
ENSG00000145349	CAMK2D	protein_coding	1,03085064	4,7972E-18
ENSG00000173482	PTPRM	protein_coding	4,01494484	5,8092E-18
ENSG00000179456	ZBTB18	protein_coding	1,88156005	6,0753E-18
ENSG00000008086	CDKL5	protein_coding	1,07720953	6,1031E-18
ENSG00000102409	BEX4	protein_coding	1,43289188	6,2115E-18
ENSG00000196440	ARMCX4	protein_coding	2,57902297	7,4917E-18
ENSG00000228022	HCG20	lncRNA	2,02206259	1,2801E-17
ENSG00000137767	SQOR	protein_coding	1,11602222	1,7269E-17
ENSG00000231584	FAHD2CP	transcribed_unprocessed pseudogene	1,77023965	2,2117E-17
ENSG00000277476		lncRNA	1,15508258	2,3406E-17
ENSG00000050628	PTGER3	protein_coding	2,25179616	2,9836E-17
ENSG00000230490		lncRNA	1,66162836	3,1096E-17
ENSG00000196511	TPK1	protein_coding	2,1665378	4,5489E-17
ENSG00000112902	SEMA5A	protein_coding	1,30552311	5,2934E-17
ENSG00000128791	TWSG1	protein_coding	1,14574121	5,4791E-17
ENSG00000237854	LINC00674	transcribed_unprocessed pseudogene	1,07603877	6,2183E-17
ENSG00000205730	ITPRIPL2	protein_coding	1,21782537	6,434E-17
ENSG00000125430	HS3ST3B1	protein_coding	2,39523584	7,4792E-17
ENSG00000257966	OLA1P3	processed_pseudogene	5,96648469	8,3426E-17
ENSG00000162836	ACP6	protein_coding	1,11526585	1,1448E-16
ENSG00000186642	PDE2A	protein_coding	3,09799325	1,3986E-16
ENSG00000196352	CD55	protein_coding	1,10296041	1,4979E-16
ENSG00000106392	C1GALT1	protein_coding	1,16810607	2,522E-16
ENSG00000157502	PWWP3B	protein_coding	4,55187173	3,0199E-16
ENSG00000124243	BCAS4	protein_coding	1,17953311	3,5443E-16
ENSG00000081665	ZNF506	protein_coding	1,09441168	4,4151E-16
ENSG00000206557	TRIM71	protein_coding	2,56380212	4,4351E-16
ENSG00000184867	ARMCX2	protein_coding	1,35621711	5,9947E-16
ENSG00000100302	RASD2	protein_coding	3,20409313	8,9058E-16
ENSG00000145569	OTULINL	protein_coding	2,26952052	9,0401E-16
ENSG00000007516	BAIAP3	protein_coding	1,430872	1,0312E-15
ENSG00000111961	SASH1	protein_coding	2,10715249	1,0553E-15
ENSG00000103154	NECAB2	protein_coding	2,02367902	1,2316E-15
ENSG00000197321	SVIL	protein_coding	1,12765118	1,286E-15
ENSG00000130813	SHFL	protein_coding	2,02516844	1,3747E-15
ENSG00000079257	LXN	protein_coding	3,44386975	1,4253E-15
ENSG00000179913	B3GNT3	protein_coding	1,18092596	1,5623E-15
ENSG00000134463	ECHDC3	protein_coding	1,36765468	1,5765E-15
ENSG00000241288	LINC02614	lncRNA	1,62085093	1,7171E-15
ENSG00000205413	SAMD9	protein_coding	2,00646139	2,0835E-15
ENSG00000170485	NPAS2	protein_coding	1,20519858	2,2476E-15
ENSG00000076864	RAP1GAP	protein_coding	1,09551923	2,525E-15
ENSG00000142273	CBLC	protein_coding	6,16956772	5,3108E-15
ENSG00000178718	RPP25	protein_coding	1,031536	5,7366E-15
ENSG00000254087	LYN	protein_coding	1,58799098	6,2728E-15
ENSG00000151640	DPYSL4	protein_coding	1,55405925	7,0786E-15
ENSG00000116663	FBXO6	protein_coding	1,42416681	7,1611E-15
ENSG00000272273	IER3-AS1	lncRNA	2,19093291	7,521E-15
ENSG00000090238	YPEL3	protein_coding	1,76452836	8,1879E-15
ENSG00000125999	BPIFB1	protein_coding	7,2722095	9,3554E-15
ENSG00000139679	LPAR6	protein_coding	2,66846676	1,0172E-14
ENSG00000140993	TIGD7	protein_coding	1,02882944	1,4154E-14
ENSG00000187134	AKR1C1	protein_coding	1,48333404	1,632E-14
ENSG00000089486	CDIP1	protein_coding	1,84921367	1,9419E-14
ENSG00000171124	FUT3	protein_coding	2,1737425	2,1964E-14
ENSG00000168032	ENTPD3	protein_coding	3,99102837	2,364E-14
ENSG00000121653	MAPK8IP1	protein_coding	1,17713418	2,6507E-14
ENSG00000171724	VAT1L	protein_coding	5,33334481	2,9654E-14
ENSG00000246174	KCTD21-AS1	lncRNA	1,29356319	3,2285E-14
ENSG00000186603	HPDL	protein_coding	1,64877505	3,2869E-14
ENSG00000168298	H1-4	protein_coding	1,05292762	3,5041E-14
ENSG00000165959	CLMN	protein_coding	1,10845828	3,7524E-14
ENSG00000101400	SNTA1	protein_coding	1,39335193	5,7755E-14
ENSG00000197937	ZNF347	protein_coding	1,3870371	6,0287E-14
ENSG00000228933		lncRNA	4,13404488	6,5016E-14
ENSG00000119714	GPR68	protein_coding	1,15705302	7,4018E-14
ENSG00000103202	NME4	protein_coding	1,08741861	7,5056E-14
ENSG00000173890	GPR160	protein_coding	1,40533692	7,9663E-14
ENSG00000142552	RCN3	protein_coding	3,33359	8,2207E-14
ENSG00000274750	H3C6	protein_coding	1,14000888	8,8817E-14
ENSG00000068903	SIRT2	protein_coding	1,04079073	9,1748E-14
ENSG00000123342	MMP19	protein_coding	4,46023653	9,58E-14
ENSG00000177675	CD163L1	protein_coding	1,5721494	1,062E-13
ENSG00000165171	METTL27	protein_coding	1,55364575	1,2477E-13
ENSG00000009950	MLXIPL	protein_coding	1,63413119	1,5658E-13
ENSG00000166825	ANPEP	protein_coding	3,76199644	1,583E-13
ENSG00000186205	MTARC1	protein_coding	1,09498381	1,8949E-13
ENSG00000169239	CA5B	protein_coding	1,32385571	2,3618E-13
ENSG00000149573	MPZL2	protein_coding	1,10708224	2,6203E-13
ENSG00000005001	PRSS22	protein_coding	1,19286569	2,6398E-13

ENSG00000228630	HOTAIR	lncRNA	1,64171523	2,8723E-13
ENSG00000124302	CHST8	protein_coding	1,53432696	2,9548E-13
ENSG00000181019	NQO1	protein_coding	1,00090991	3,4788E-13
ENSG00000179023	KLHDC7A	protein_coding	3,10434848	4,9102E-13
ENSG00000165300	SLITRK5	protein_coding	1,71951814	5,5127E-13
ENSG00000185090	MANEAL	protein_coding	1,03635382	5,6903E-13
ENSG00000151789	ZNF385D	protein_coding	7,91147198	6,1156E-13
ENSG00000206075	SERPINB5	protein_coding	1,92692289	9,0581E-13
ENSG00000166450	PRTG	protein_coding	1,0756564	9,6862E-13
ENSG00000198049	AVPR1B	protein_coding	6,89342931	1,1185E-12
ENSG00000104892	KLC3	protein_coding	1,40957167	1,1263E-12
ENSG00000099377	HSD3B7	protein_coding	1,01812914	1,2521E-12
ENSG00000089820	ARHGAP4	protein_coding	1,33469557	1,3974E-12
ENSG00000011201	ANOS1	protein_coding	2,58192788	1,4045E-12
ENSG00000088340	FER1L4	transcribed_unitary pseudogene	1,31024149	1,6013E-12
ENSG00000185686	PRAME	protein_coding	1,98843581	1,6507E-12
ENSG00000180535	BHLHA15	protein_coding	1,48261119	1,756E-12
ENSG00000174804	FZD4	protein_coding	1,20956407	1,9094E-12
ENSG00000248587	GDNF-AS1	lncRNA	5,08876086	1,9425E-12
ENSG00000259129	LINC00648	lncRNA	8,90376181	2,051E-12
ENSG00000237515	SHISA9	protein_coding	1,23293276	2,0659E-12
ENSG00000115266	APC2	protein_coding	1,50888939	2,4191E-12
ENSG00000128283	CDC42EP1	protein_coding	1,14791465	3,348E-12
ENSG00000154146	NRGN	protein_coding	1,2237363	3,7556E-12
ENSG00000265763	ZNF488	protein_coding	1,3997983	4,2099E-12
ENSG00000274561		lncRNA	1,09518017	5,1333E-12
ENSG00000177469	CAVIN1	protein_coding	1,29412369	6,2019E-12
ENSG00000131773	KHDRBS3	protein_coding	1,71516672	6,3033E-12
ENSG00000232682		lncRNA	2,98373897	6,8257E-12
ENSG00000118946	PCDH17	protein_coding	3,53319092	7,0581E-12
ENSG00000186891	TNFRSF18	protein_coding	1,72289078	8,034E-12
ENSG00000187994	RINL	protein_coding	2,11671863	8,0872E-12
ENSG00000170379	TCAF2	protein_coding	2,40798268	8,6516E-12
ENSG00000204616	TRIM31	protein_coding	3,88528951	8,8442E-12
ENSG00000153029	MR1	protein_coding	1,28673108	9,1574E-12
ENSG00000282988		protein_coding	1,65665499	9,6009E-12
ENSG00000189120	SP6	protein_coding	1,17848444	1,1623E-11
ENSG00000130203	APOE	protein_coding	2,05344406	1,7597E-11
ENSG00000182472	CAPN12	protein_coding	1,51886015	1,8669E-11
ENSG00000178568	ERBB4	protein_coding	1,97926814	1,98E-11
ENSG00000253250	C8orf88	protein_coding	2,33931958	2,0789E-11
ENSG00000165655	ZNF503	protein_coding	1,33123074	2,3713E-11
ENSG00000262528		lncRNA	1,82941528	2,6752E-11
ENSG00000105877	DNAH11	protein_coding	2,80247932	2,7088E-11
ENSG00000151136	BTBD11	protein_coding	1,79142492	2,7734E-11
ENSG00000264964	TWSG1-DT	lncRNA	2,26982288	3,1086E-11
ENSG00000115255	REEP6	protein_coding	1,30308198	3,2332E-11
ENSG00000131746	TNS4	protein_coding	1,73391938	3,6789E-11
ENSG00000132669	RIN2	protein_coding	1,19437925	3,6807E-11
ENSG00000175175	PPM1E	protein_coding	1,27551365	3,7339E-11
ENSG00000168621	GDNF	protein_coding	5,20519199	5,7146E-11
ENSG00000207422	RNU6-813P	snRNA	1,33522407	5,8433E-11
ENSG00000234678	ELF3-AS1	lncRNA	1,08765156	6,2803E-11
ENSG00000135333	EPHA7	protein_coding	2,66702439	7,0816E-11
ENSG00000100346	CACNA1I	protein_coding	1,45164613	7,3282E-11
ENSG00000269313	MAGIX	protein_coding	1,63396035	8,5341E-11
ENSG00000146411	SLC2A12	protein_coding	4,06841408	8,8377E-11
ENSG00000169783	LINGO1	protein_coding	1,98660742	8,8818E-11
ENSG00000123388	HOXC11	protein_coding	1,04957372	9,7178E-11
ENSG00000165434	PGM2L1	protein_coding	1,39260141	1,0435E-10
ENSG00000137720	C11orf1	protein_coding	1,6683354	1,1248E-10
ENSG00000132535	DLG4	protein_coding	1,22237157	1,1272E-10
ENSG00000204792	LINC01291	lncRNA	3,70741285	1,1547E-10
ENSG00000143320	CRABP2	protein_coding	1,14990464	1,1604E-10
ENSG00000128881	TTBK2	protein_coding	1,03916115	1,2417E-10
ENSG00000154118	JPH3	protein_coding	1,1060555	1,2696E-10
ENSG00000162636	FAM102B	protein_coding	1,48202464	1,4097E-10
ENSG00000107105	ELAVL2	protein_coding	1,92299171	1,4222E-10
ENSG00000162878	PKDCC	protein_coding	1,67033708	1,5371E-10
ENSG00000166819	PLIN1	protein_coding	2,37852166	1,7025E-10
ENSG00000166289	PLEKHF1	protein_coding	1,36180266	1,9171E-10
ENSG00000280079		TEC	2,12774249	1,9538E-10
ENSG00000133639	BTG1	protein_coding	1,01413023	1,9793E-10
ENSG00000158089	GALNT14	protein_coding	1,33377588	2,1792E-10
ENSG00000107099	DOCK8	protein_coding	2,38950887	2,3511E-10
ENSG00000169750	RAC3	protein_coding	1,12385452	2,4813E-10
ENSG00000115594	IL1R1	protein_coding	1,89439989	2,8442E-10
ENSG00000132970	WASF3	protein_coding	1,03950823	2,9119E-10
ENSG00000006757	PNPLA4	protein_coding	1,76965116	3,0087E-10
ENSG00000260337		lncRNA	2,1481378	3,9888E-10
ENSG00000168447	SCNN1B	protein_coding	2,3053571	5,19E-10
ENSG00000138356	AOX1	protein_coding	1,82081911	5,4198E-10
ENSG00000099954	CECR2	protein_coding	2,7911009	5,5215E-10
ENSG00000241717	VWFP1	transcribed_unprocessed pseudogene	8,12203206	6,1642E-10
ENSG00000070759	TESK2	protein_coding	1,50847543	6,4332E-10
ENSG00000132170	PPARG	protein_coding	1,181988	7,3886E-10
ENSG00000144199	FAHD2B	protein_coding	1,68179401	7,4139E-10
ENSG00000171044	XKR6	protein_coding	1,42960416	8,7669E-10

ENSG00000204516	MICB	protein_coding	1,3940498	9,813E-10
ENSG00000196668	LINC00173	lncRNA	2,67250581	1,037E-09
ENSG00000205426	KRT81	protein_coding	2,36623239	1,2481E-09
ENSG00000149256	TENM4	protein_coding	4,37201107	1,3916E-09
ENSG00000173917	HOXB2	protein_coding	3,05308702	1,6067E-09
ENSG00000164845	FAM86FP	transcribed_unprocessed pseudogene	1,69714167	1,9228E-09
ENSG00000242575	TUBAP13	transcribed_processed pseudogene	4,22240671	2,0335E-09
ENSG00000198183	BPIFA1	protein_coding	8,15215271	2,0685E-09
ENSG00000185499	MUC1	protein_coding	3,41149988	2,3525E-09
ENSG00000196684	HSH2D	protein_coding	1,72449916	2,3913E-09
ENSG00000235863	B3GALT4	protein_coding	1,45563651	2,4329E-09
ENSG00000182795	C1orf116	protein_coding	1,97079991	2,6864E-09
ENSG00000136574	GATA4	protein_coding	1,88185294	2,9893E-09
ENSG00000166828	SCNN1G	protein_coding	2,05878078	3,0288E-09
ENSG00000196371	FUT4	protein_coding	1,25179069	3,1155E-09
ENSG00000162949	CAPN13	protein_coding	1,9746307	3,2231E-09
ENSG00000269954		lncRNA	1,87862893	3,269E-09
ENSG00000105852	PON3	protein_coding	2,70318971	4,3414E-09
ENSG00000158486	DNAH3	protein_coding	1,86767272	4,8929E-09
ENSG00000007314	SCN4A	protein_coding	5,59952646	5,0572E-09
ENSG00000099330	OCEL1	protein_coding	1,17053617	5,3174E-09
ENSG00000267383		lncRNA	2,21544423	5,6287E-09
ENSG00000133874	RNF122	protein_coding	1,7310842	5,7473E-09
ENSG00000215148	PRSS41	protein_coding	6,01955962	6,4054E-09
ENSG00000120658	ENOX1	protein_coding	2,60587335	6,6519E-09
ENSG00000268864		transcribed_unprocessed pseudogene	3,14869161	7,2189E-09
ENSG00000175197	DDIT3	protein_coding	1,13596219	7,5052E-09
ENSG00000228830		lncRNA	1,03189699	7,6865E-09
ENSG00000110375	UPK2	protein_coding	1,43018491	7,7434E-09
ENSG00000225606		lncRNA	2,76595505	7,9678E-09
ENSG00000150764	DIXDC1	protein_coding	1,0918497	8,8025E-09
ENSG00000214510	SPINK13	protein_coding	7,92336771	9,5333E-09
ENSG00000170915	PAQR8	protein_coding	1,67680513	1,0649E-08
ENSG00000173093	CCDC63	protein_coding	8,15665346	1,086E-08
ENSG00000170684	ZNF296	protein_coding	1,26790009	1,1434E-08
ENSG00000214274	ANG	protein_coding	3,56920764	1,2831E-08
ENSG00000149212	SESN3	protein_coding	2,27644598	1,6483E-08
ENSG00000140807	NKD1	protein_coding	1,04033866	1,7635E-08
ENSG00000255517		lncRNA	1,18530706	1,9975E-08
ENSG00000129455	KLK8	protein_coding	3,60312408	2,068E-08
ENSG00000109738	GLRB	protein_coding	1,80553072	2,1131E-08
ENSG00000081059	TCF7	protein_coding	2,09558207	2,1927E-08
ENSG00000107957	SH3PXD2A	protein_coding	1,38803962	2,2114E-08
ENSG00000288024		lncRNA	7,43408695	2,5631E-08
ENSG00000006534	ALDH3B1	protein_coding	1,38614514	2,6643E-08
ENSG00000115194	SLC30A3	protein_coding	1,51585973	2,6825E-08
ENSG00000086205	FOLH1	protein_coding	5,30094436	2,7601E-08
ENSG00000167889	MGAT5B	protein_coding	1,70764706	3,038E-08
ENSG00000124370	MCEE	protein_coding	1,03825885	3,0995E-08
ENSG00000084628	NKAIN1	protein_coding	1,54773385	3,3363E-08
ENSG00000178445	GLDC	protein_coding	2,04802462	3,4341E-08
ENSG00000123095	BHLHE41	protein_coding	1,96294829	3,5267E-08
ENSG00000159247	TUBBP5	transcribed_unprocessed pseudogene	1,53131933	3,8685E-08
ENSG00000272512		lncRNA	1,02461586	3,878E-08
ENSG00000167925	GHDC	protein_coding	1,06633125	4,0355E-08
ENSG00000102032	RENBP	protein_coding	2,97773391	4,3557E-08
ENSG00000157927	RADIL	protein_coding	1,63039459	4,4045E-08
ENSG00000170775	GPR37	protein_coding	1,07388701	4,4452E-08
ENSG00000110492	MDK	protein_coding	1,2157258	4,5314E-08
ENSG00000141968	VAV1	protein_coding	1,04128241	4,6408E-08
ENSG00000111879	FAM184A	protein_coding	1,95291065	5,5415E-08
ENSG00000204961	PCDHA9	protein_coding	3,20176816	6,0606E-08
ENSG00000137868	STRA6	protein_coding	1,96243732	6,3391E-08
ENSG00000152527	PLEKHH2	protein_coding	1,47339423	6,6272E-08
ENSG00000197191	CYSRT1	protein_coding	1,63594985	6,938E-08
ENSG00000115461	IGFBP5	protein_coding	3,20941035	7,063E-08
ENSG00000172264	MACROD2	protein_coding	1,16333101	7,2314E-08
ENSG00000005243	COPZ2	protein_coding	2,6030609	7,5174E-08
ENSG00000164619	BMPER	protein_coding	1,40055269	7,6642E-08
ENSG00000188488	SERPINA5	protein_coding	2,76242338	7,7302E-08
ENSG00000070882	OSBPL3	protein_coding	3,9023319	8,0559E-08
ENSG00000149922	TBX6	protein_coding	1,68859059	8,1079E-08
ENSG00000101188	NTSR1	protein_coding	2,32754406	8,3506E-08
ENSG00000228224	NACA4P	transcribed_processed pseudogene	4,1068705	8,4264E-08
ENSG00000130513	GDF15	protein_coding	1,67260299	8,8519E-08
ENSG00000026950	BTN3A1	protein_coding	1,71300102	9,3833E-08
ENSG00000119121	TRPM6	protein_coding	1,80705968	9,5177E-08
ENSG00000268854		lncRNA	1,68931219	9,7574E-08
ENSG00000152454	ZNF256	protein_coding	1,03854185	9,9098E-08
ENSG00000124813	RUNX2	protein_coding	1,49267509	1,0006E-07
ENSG00000168646	AXIN2	protein_coding	1,48219922	1,1377E-07
ENSG00000258092		lncRNA	1,100666	1,1669E-07
ENSG00000172201	ID4	protein_coding	1,28785559	1,2032E-07
ENSG00000047457	CP	protein_coding	2,76316372	1,2085E-07
ENSG00000171126	KCNG3	protein_coding	1,37200234	1,3683E-07

ENSG00000260279		lncRNA	1,15345597	1,698E-07
ENSG00000184454	NCMAP	protein_coding	1,80946114	1,7034E-07
ENSG00000188505	NCCRP1	protein_coding	2,60768806	1,8884E-07
ENSG00000173267	SNCG	protein_coding	2,36442666	1,977E-07
ENSG00000263325		lncRNA	2,79683527	2,1604E-07
ENSG00000061656	SPAG4	protein_coding	1,48676335	2,2157E-07
ENSG00000185477	GPRIN3	protein_coding	5,69727507	2,2979E-07
ENSG00000163364	LINC01116	lncRNA	1,45719617	2,3724E-07
ENSG00000139973	SYT16	protein_coding	1,84811727	2,4901E-07
ENSG00000100003	SEC14L2	protein_coding	1,25169443	2,5495E-07
ENSG00000225768	LINC02620	lncRNA	3,13749338	2,6641E-07
ENSG00000139112	GABARAPL1	protein_coding	1,00722597	2,8561E-07
ENSG00000242615		transcribed_processed pseudogene	6,88058898	3,23E-07
ENSG00000104205	SGK3	protein_coding	1,06592686	3,6412E-07
ENSG00000102048	ASB9	protein_coding	1,68854093	3,7234E-07
ENSG00000107159	CA9	protein_coding	5,12986272	3,7834E-07
ENSG00000204228	HSD17B8	protein_coding	1,01847129	3,8225E-07
ENSG00000112561	TFEB	protein_coding	1,43847875	3,9181E-07
ENSG00000166823	MESP1	protein_coding	1,62120167	4,029E-07
ENSG00000286159		lncRNA	1,03345368	4,0736E-07
ENSG00000118257	NRP2	protein_coding	3,111661	4,1482E-07
ENSG00000288538		lncRNA	1,73376884	4,4249E-07
ENSG00000164647	STEAP1	protein_coding	5,73897022	4,4363E-07
ENSG00000143891	GALM	protein_coding	1,15228861	4,5099E-07
ENSG00000228714		lncRNA	6,64715246	4,5691E-07
ENSG00000280832	GSEC	lncRNA	1,10646612	4,7444E-07
ENSG00000187244	BCAM	protein_coding	1,59328377	5,2391E-07
ENSG00000186026	ZNF284	protein_coding	1,29782645	5,2971E-07
ENSG00000120875	DUSP4	protein_coding	1,51714047	5,3298E-07
ENSG00000198739	LRRTM3	protein_coding	5,2026496	5,8511E-07
ENSG00000260710		lncRNA	2,04264834	5,893E-07
ENSG00000188641	DPYD	protein_coding	6,62552773	5,9443E-07
ENSG00000118137	APOA1	protein_coding	2,63847571	6,0883E-07
ENSG00000035664	DAPK2	protein_coding	1,00289078	6,6346E-07
ENSG00000120708	TGFBI	protein_coding	2,03158135	7,029E-07
ENSG00000270882	H4C14	protein_coding	1,33583567	7,3009E-07
ENSG00000175879	HOXD8	protein_coding	2,75642515	7,3702E-07
ENSG00000185519	FAM131C	protein_coding	2,12298661	7,3866E-07
ENSG00000233237	LINC00472	lncRNA	1,306082	7,4072E-07
ENSG00000133135	RNF128	protein_coding	6,47835194	7,4123E-07
ENSG00000147408	CSGALNACT1	protein_coding	1,42537964	8,0235E-07
ENSG00000183784	DOCK8-AS1	lncRNA	1,8161929	8,9063E-07
ENSG00000232442	MHENCR	lncRNA	1,1224904	9,4425E-07
ENSG00000228412	LNC-LBCS	lncRNA	1,71753746	9,8183E-07
ENSG00000144648	ACKR2	protein_coding	1,85969842	1,0676E-06
ENSG00000119508	NR4A3	protein_coding	1,75073208	1,1111E-06
ENSG00000236699	ARHGEF38	protein_coding	1,90494806	1,1207E-06
ENSG00000235944	ZNF815P	transcribed_unprocessed pseudogene	1,13260013	1,279E-06
ENSG00000180806	HOXC9	protein_coding	1,14124414	1,299E-06
ENSG00000164638	SLC29A4	protein_coding	1,07486864	1,3347E-06
ENSG00000266709		lncRNA	2,40844777	1,4238E-06
ENSG00000267481		lncRNA	1,429223	1,5261E-06
ENSG00000131378	RFTN1	protein_coding	1,89713286	1,6043E-06
ENSG00000181449	SOX2	protein_coding	3,09721162	1,6481E-06
ENSG00000156049	GNA14	protein_coding	1,06511032	1,7231E-06
ENSG00000227038	GTF2IP7	transcribed_unprocessed pseudogene	1,66163264	1,7445E-06
ENSG00000107518	ATRNL1	protein_coding	2,85733924	1,7837E-06
ENSG00000254531	FLJ20021	lncRNA	1,54378485	1,8346E-06
ENSG00000211452	DIO1	protein_coding	4,01131241	2,2186E-06
ENSG00000117226	GBP3	protein_coding	1,67437392	2,3042E-06
ENSG00000134258	VTCN1	protein_coding	2,03741644	2,3896E-06
ENSG00000117115	PADI2	protein_coding	1,32986202	2,4829E-06
ENSG00000169302	STK32A	protein_coding	4,10310085	2,5133E-06
ENSG00000181856	SLC2A4	protein_coding	1,28404411	2,5807E-06
ENSG00000105388	CEACAM5	protein_coding	3,4753362	2,634E-06
ENSG00000186364	NUDT17	protein_coding	1,12856842	2,6377E-06
ENSG00000274080		lncRNA	1,69805178	2,7744E-06
ENSG00000260284	TPSP2	unprocessed_pseudogene	1,28471333	2,8789E-06
ENSG00000125864	BFSP1	protein_coding	1,2133566	2,8793E-06
ENSG00000225595	LINC01623	lncRNA	3,95802102	2,9296E-06
ENSG00000198467	TPM2	protein_coding	1,37385763	3,0085E-06
ENSG00000104369	JPH1	protein_coding	1,3328143	3,1034E-06
ENSG00000223823	LINC01342	lncRNA	3,72424937	3,2032E-06
ENSG00000268379		processed_pseudogene	2,61910696	3,4777E-06
ENSG00000183813	CCR4	protein_coding	6,33279641	3,505E-06
ENSG00000241361	SLC25A24P1	transcribed_unprocessed pseudogene	1,1107044	3,5247E-06
ENSG00000188883	KLRG2	protein_coding	1,01812666	3,5283E-06
ENSG00000255310		lncRNA	1,40914739	3,5895E-06
ENSG00000211695	TRGV9	TR_V_gene	4,56803725	3,8109E-06
ENSG00000143382	ADAMTSL4	protein_coding	2,12153535	3,8959E-06
ENSG00000278704		protein_coding	1,60058542	3,9303E-06
ENSG00000237807		lncRNA	1,53454941	3,9307E-06
ENSG00000162496	DHRS3	protein_coding	1,9041789	3,947E-06
ENSG00000181634	TNFSF15	protein_coding	3,16631853	3,956E-06
ENSG00000095303	PTGS1	protein_coding	1,9591974	4,0486E-06
ENSG00000236829		transcribed_processed	1,18906551	4,39E-06

		pseudogene		
ENSG00000250423	KIAA1210	protein_coding	3,68975857	4,6547E-06
ENSG00000110881	ASIC1	protein_coding	1,01151082	5,4583E-06
ENSG00000279742		TEC	1,55937498	5,7182E-06
ENSG00000257808		lncRNA	2,53908294	6,0784E-06
ENSG00000280160		TEC	1,23203125	6,3442E-06
ENSG00000267265	GP6-AS1	lncRNA	1,55805319	6,37E-06
ENSG00000167653	PSCA	protein_coding	1,7073548	6,9626E-06
ENSG00000228705	LINC00659	lncRNA	1,64439781	7,093E-06
ENSG00000168135	KCNJ4	protein_coding	3,00361255	7,1684E-06
ENSG00000253671		lncRNA	1,3616431	7,1684E-06
ENSG00000153064	BANK1	protein_coding	3,12230528	8,1363E-06
ENSG00000260528	FAM157C	lncRNA	1,00928286	8,4222E-06
ENSG00000279196		TEC	1,13710493	8,4292E-06
ENSG00000196427	NBPF4	protein_coding	1,25618501	8,4428E-06
ENSG00000152377	SPOCK1	protein_coding	2,95514323	8,463E-06
ENSG00000134240	HMGCS2	protein_coding	5,13582842	8,6142E-06
ENSG00000121236	TRIM6	protein_coding	1,29913574	8,8195E-06
ENSG00000145908	ZNF300	protein_coding	5,94090972	9,3992E-06
ENSG00000139178	C1RL	protein_coding	1,28469217	9,9385E-06
ENSG00000133134	BEX2	protein_coding	1,40133292	1,0319E-05
ENSG00000214429	CYCSP6	processed_pseudogene	5,08399884	1,0954E-05
ENSG00000116774	OLFML3	protein_coding	1,75616449	1,1299E-05
ENSG00000144229	THSD7B	protein_coding	6,81439442	1,1319E-05
ENSG00000007908	SELE	protein_coding	5,90993247	1,1561E-05
ENSG00000186326	RGS9BP	protein_coding	1,16393116	1,1718E-05
ENSG00000103888	CEMIP	protein_coding	1,87681995	1,2415E-05
ENSG00000166033	HTRA1	protein_coding	1,15669728	1,3197E-05
ENSG00000151617	EDNRA	protein_coding	3,61283383	1,4451E-05
ENSG00000157833	GAREM2	protein_coding	1,41610466	1,5027E-05
ENSG00000232973	CYP1B1-AS1	lncRNA	1,23472197	1,5633E-05
ENSG00000196353	CPNE4	protein_coding	2,20812359	1,6517E-05
ENSG00000236283		lncRNA	4,20359689	1,6894E-05
ENSG00000187730	GABRD	protein_coding	1,21747575	1,8351E-05
ENSG00000233198	RNF224	protein_coding	1,53012471	1,8356E-05
ENSG00000251151	HOXC-AS3	lncRNA	1,5487002	1,8865E-05
ENSG00000187957	DNER	protein_coding	2,53949799	1,9282E-05
ENSG00000286081		lncRNA	2,78672101	1,9761E-05
ENSG00000006638	TBXA2R	protein_coding	2,0461944	2,1402E-05
ENSG00000139269	INHBE	protein_coding	1,88629758	2,2483E-05
ENSG00000116761	CTH	protein_coding	1,18494524	2,2683E-05
ENSG00000110975	SYT10	protein_coding	1,4747971	2,3462E-05
ENSG00000174514	MFSD4A	protein_coding	1,78937545	2,3952E-05
ENSG00000106025	TSPAN12	protein_coding	5,05866752	2,4708E-05
ENSG00000280219		TEC	3,19123054	2,4924E-05
ENSG00000287900		lncRNA	2,73725284	2,5401E-05
ENSG00000177098	SCN4B	protein_coding	2,71987285	2,5613E-05
ENSG00000230699		lncRNA	1,21665398	2,6043E-05
ENSG00000160469	BRSK1	protein_coding	1,10746607	2,6438E-05
ENSG00000138311	ZNF365	protein_coding	1,64582552	2,7805E-05
ENSG00000125845	BMP2	protein_coding	3,19200568	2,7968E-05
ENSG00000176049	JAKMIP2	protein_coding	1,6735874	2,847E-05
ENSG00000230148	HOXB-AS1	lncRNA	3,60596558	2,984E-05
ENSG00000204257	HLA-DMA	protein_coding	1,03123003	2,9884E-05
ENSG00000117643	MAN1C1	protein_coding	1,35726156	2,99E-05
ENSG00000204044	SLC12A5-AS1	lncRNA	1,49234474	2,9926E-05
ENSG00000164061	BSN	protein_coding	1,02010563	3,0462E-05
ENSG00000170122	FOXD4	protein_coding	1,78368913	3,1172E-05
ENSG00000248787		lncRNA	1,271304	3,4144E-05
ENSG00000186777	ZNF732	protein_coding	1,11559651	3,5507E-05
ENSG00000222019	URAHP	transcribed_unprocessed pseudogene	1,15954467	3,7086E-05
ENSG00000167619	TMEM145	protein_coding	2,27462174	3,7735E-05
ENSG00000185269	NOTUM	protein_coding	3,1421985	3,7773E-05
ENSG00000175556	LONRF3	protein_coding	3,1349778	4,0383E-05
ENSG00000261294		lncRNA	1,10934292	4,1644E-05
ENSG00000287430		lncRNA	2,39553481	4,2289E-05
ENSG00000010310	GIPR	protein_coding	1,56303644	4,4424E-05
ENSG00000245750	DRAIC	lncRNA	1,66108766	4,5381E-05
ENSG00000214575	CPEB1	protein_coding	2,83792522	4,5708E-05
ENSG00000114646	CSPG5	protein_coding	1,24546475	4,8987E-05
ENSG00000198483	ANKRD35	protein_coding	3,09278274	4,94E-05
ENSG00000186470	BTN3A2	protein_coding	1,17779454	4,997E-05
ENSG00000163689	CFAP20DC	protein_coding	1,16059448	5,0685E-05
ENSG00000233622	CYP2T1P	transcribed_unitary pseudogene	1,65587335	5,136E-05
ENSG00000287566		lncRNA	3,23069875	5,193E-05
ENSG00000183566	BPIFA4P	transcribed_unprocessed pseudogene	4,97789852	5,4904E-05
ENSG00000116990	MYCL	protein_coding	1,12723498	6,032E-05
ENSG00000165507	DEPP1	protein_coding	2,58922687	6,6013E-05
ENSG00000142530	FAM71E1	protein_coding	1,27723096	6,6824E-05
ENSG00000138061	CYP1B1	protein_coding	1,26712262	6,7611E-05
ENSG00000100373	UPK3A	protein_coding	1,72522703	7,4049E-05
ENSG00000099365	STX1B	protein_coding	1,12026009	7,4106E-05
ENSG00000226416	MRPL23-AS1	lncRNA	4,10495536	7,9782E-05
ENSG00000287595		lncRNA	3,12878226	8,0877E-05
ENSG00000118495	PLAGL1	protein_coding	1,70085742	8,1839E-05
ENSG00000233080	LINC01399	transcribed_processed pseudogene	1,53272336	8,3335E-05

ENSG00000251364		lncRNA	2,19249979	8,8882E-05
ENSG00000108387	SEPTIN4	protein_coding	1,88464231	8,9539E-05
ENSG00000257268		lncRNA	6,68749602	0,00010184
ENSG00000163884	KLF15	protein_coding	2,12255318	0,00010286
ENSG00000005108	THSD7A	protein_coding	4,90145347	0,00010648
ENSG00000174130	TLR6	protein_coding	1,26753274	0,00010706
ENSG00000285128		lncRNA	5,46513816	0,00011025
ENSG00000068079	IFI35	protein_coding	1,36414429	0,00011157
ENSG00000166473	PKD1L2	polymorphic_pseudogene	1,46468928	0,00011429
ENSG00000068615	REEP1	protein_coding	1,27026614	0,0001173
ENSG00000172828	CES3	protein_coding	1,73229893	0,00011785
ENSG00000119938	PPP1R3C	protein_coding	1,76020224	0,00011927
ENSG00000167992	VWCE	protein_coding	1,44255757	0,00012354
ENSG00000153162	BMP6	protein_coding	1,22641143	0,00012527
ENSG00000166510	CCDC68	protein_coding	1,00370266	0,00012618
ENSG00000225255	PSLNR	lncRNA	2,45127313	0,00012937
ENSG00000257591	ZNF625	protein_coding	5,60458089	0,00013031
ENSG00000267757	EML2-AS1	lncRNA	2,90509994	0,000141
ENSG00000121005	CRISPLD1	protein_coding	2,58416024	0,00017176
ENSG00000134955	SLC37A2	protein_coding	2,06363457	0,00017199
ENSG00000106018	VIPR2	protein_coding	2,86021843	0,00017423
ENSG00000118004	COLEC11	protein_coding	3,88477314	0,00017589
ENSG00000231131	LNCAROD	lncRNA	1,45001556	0,00018745
ENSG00000130270	ATP8B3	protein_coding	1,60437527	0,00019235
ENSG00000224141	MIR548XHG	lncRNA	5,78562432	0,0001937
ENSG00000087589	CASS4	protein_coding	1,33715405	0,00020499
ENSG00000250740		lncRNA	1,72568971	0,00020595
ENSG00000147251	DOCK11	protein_coding	1,78222116	0,00020606
ENSG00000238178		lncRNA	5,41598729	0,00021099
ENSG00000260572		lncRNA	1,74933254	0,00022145
ENSG00000237773		lncRNA	1,33510272	0,00023698
ENSG00000189136	UBE2Q2P1	transcribed_unprocessed pseudogene	1,08312822	0,0002486
ENSG00000156218	ADAMTSL3	protein_coding	1,85942716	0,00026347
ENSG00000281005	LINC00921	lncRNA	1,47213996	0,00026732
ENSG00000162746	FCRLB	protein_coding	1,15730842	0,00027158
ENSG00000259275		lncRNA	1,71164232	0,00028468
ENSG00000086548	CEACAM6	protein_coding	1,10247147	0,00028686
ENSG00000138696	BMPR1B	protein_coding	3,56934613	0,0002923
ENSG00000231439	WASIR2	lncRNA	1,42479027	0,00029705
ENSG00000182326	C1S	protein_coding	1,39280405	0,00030905
ENSG00000131050	BPIFA2	protein_coding	4,58051796	0,00031128
ENSG00000285679		lncRNA	2,01370002	0,00031783
ENSG00000189212	DPY19L2P1	transcribed_unprocessed pseudogene	1,57628648	0,00031794
ENSG00000180336	MEIOC	protein_coding	1,27989804	0,00031952
ENSG00000164125	GASK1B	protein_coding	1,50839252	0,00034333
ENSG00000258932		transcribed_processed pseudogene	5,17941977	0,0003446
ENSG00000186281	GPAT2	protein_coding	4,24877796	0,00035538
ENSG00000108602	ALDH3A1	protein_coding	1,53290761	0,00035899
ENSG00000164411	GJB7	protein_coding	1,03667561	0,0003742
ENSG00000174498	IGDCC3	protein_coding	2,07532957	0,00039247
ENSG00000160862	AZGP1	protein_coding	4,86101917	0,00041818
ENSG00000145431	PDGFC	protein_coding	1,00886327	0,00042676
ENSG00000251287	ALG1L2	protein_coding	3,34649282	0,00043255
ENSG00000128242	GAL3ST1	protein_coding	3,66212909	0,00045136
ENSG00000232586	KIAA1614-AS1	lncRNA	1,12806649	0,00046058
ENSG00000078053	AMPH	protein_coding	2,94268448	0,00046465
ENSG00000249853	HS3ST5	protein_coding	4,84522063	0,00047631
ENSG00000249917	LINC00536	lncRNA	2,30560232	0,00047732
ENSG00000182798	MAGEB17	protein_coding	4,86252219	0,00047859
ENSG00000276007		lncRNA	1,59326211	0,00048079
ENSG00000152433	ZNF547	protein_coding	1,15632216	0,00048176
ENSG00000187045	TMPRSS6	protein_coding	1,88799952	0,00050634
ENSG00000177453	NIM1K	protein_coding	1,811804	0,00051156
ENSG00000224008	LINC01441	lncRNA	3,08535253	0,00051591
ENSG00000161551	ZNF577	protein_coding	1,50754501	0,00053547
ENSG00000240065	PSMB9	protein_coding	1,12607049	0,00053547
ENSG00000267023	LRRC37A16P	transcribed_unprocessed pseudogene	1,17878553	0,0005387
ENSG00000254109	RBPMS-AS1	lncRNA	1,1377588	0,00054314
ENSG00000167711	SERPINF2	protein_coding	3,06996288	0,00056705
ENSG00000261744	ZFPM1-AS1	lncRNA	1,4620547	0,00056968
ENSG00000236039	LINC02889	lncRNA	3,19032678	0,00058046
ENSG00000243323	PTPRVP	unitary_pseudogene	2,47057602	0,00059265
ENSG00000253554	LINC01414	lncRNA	5,45376979	0,00059476
ENSG00000113739	STC2	protein_coding	1,08449181	0,00060961
ENSG00000135218	CD36	protein_coding	1,81156229	0,00060961
ENSG00000006283	CACNA1G	protein_coding	1,81816571	0,00061603
ENSG00000103460	TOX3	protein_coding	4,73674711	0,00064141
ENSG00000153551	CMTM7	protein_coding	1,44441185	0,00064406
ENSG00000228328	PGK1P1	processed_pseudogene	2,24403447	0,00064723
ENSG00000139144	PIK3C2G	protein_coding	2,15798159	0,00064992
ENSG00000249288	SLC25A15P5	unprocessed_pseudogene	5,64356617	0,00067094
ENSG00000100739	BDKRB1	protein_coding	2,13879608	0,00071173
ENSG00000111452	ADGRD1	protein_coding	1,04468293	0,00075014
ENSG00000277010		lncRNA	1,10917702	0,00076476
ENSG00000279330		TEC	2,03825111	0,00079914
ENSG00000123407	HOXC12	protein_coding	1,86191994	0,00081553

ENSG00000278385		lncRNA	1,24640833	0,00082213
ENSG00000197046	SIGLEC15	protein_coding	1,32213883	0,00084472
ENSG00000020181	ADGRA2	protein_coding	1,09369202	0,00084594
ENSG00000227218		lncRNA	1,29078549	0,00087211
ENSG00000227088		lncRNA	4,96989193	0,00089093
ENSG00000185052	SLC24A3	protein_coding	1,72330427	0,00095018
ENSG00000232358		lncRNA	1,7092908	0,00095835
ENSG00000260430		lncRNA	1,43950208	0,0010067
ENSG00000217275		processed_pseudogene	1,31330232	0,00102221
ENSG00000005187	ACSM3	protein_coding	1,42682835	0,00102677
ENSG00000230615		lncRNA	1,65608929	0,00103242
ENSG00000092200	RPGRIP1	protein_coding	1,88900651	0,00104733
ENSG00000140986	RPL3L	protein_coding	2,20902593	0,00105621
ENSG00000153292	ADGRF1	protein_coding	4,65343934	0,00110987
ENSG00000105427	CNFN	protein_coding	2,1457387	0,00111403
ENSG00000141622	RNF165	protein_coding	2,0127366	0,00111474
ENSG00000186086	NBPF6	protein_coding	1,92567853	0,00120116
ENSG00000139445	FOXN4	protein_coding	5,00410124	0,0012277
ENSG00000287553		lncRNA	1,41794386	0,0012363
ENSG00000080031	PTPRH	protein_coding	1,41615524	0,00128038
ENSG00000234996	ACTG1P25	transcribed_processed pseudogene	1,08692612	0,00132008
ENSG00000147231	RADX	protein_coding	2,23904398	0,00132066
ENSG00000128683	GAD1	protein_coding	1,24255034	0,001328
ENSG00000245904		lncRNA	1,67290098	0,00136363
ENSG00000164674	SYTL3	protein_coding	1,33197232	0,00138944
ENSG00000286163		lncRNA	3,06587175	0,00139902
ENSG00000275371		lncRNA	3,00937658	0,0015056
ENSG00000247011		lncRNA	1,79095566	0,00160279
ENSG00000107738	VSIR	protein_coding	2,83960591	0,00160466
ENSG00000127507	ADGRE2	protein_coding	1,22170865	0,00162767
ENSG00000135269	TES	protein_coding	1,81538336	0,00163688
ENSG00000180818	HOXC10	protein_coding	1,1734915	0,00165972
ENSG00000183760	ACP7	protein_coding	1,79180577	0,00167449
ENSG00000168386	FILIP1L	protein_coding	1,38498238	0,00167535
ENSG00000234967		lncRNA	1,08721615	0,00173019
ENSG00000104237	RP1	protein_coding	5,02452128	0,00174345
ENSG00000117407	ARTN	protein_coding	1,04936858	0,0017932
ENSG00000258743	LINC02301	lncRNA	3,34388699	0,0018084
ENSG00000260018		lncRNA	1,18340113	0,0018662
ENSG00000270084	GAS5-AS1	lncRNA	1,03244779	0,00187268
ENSG00000272566		lncRNA	4,7414873	0,00196008
ENSG00000204175	GPRIN2	protein_coding	3,16638007	0,0019898
ENSG00000177455	CD19	protein_coding	4,16841869	0,0020194
ENSG00000136205	TNS3	protein_coding	1,31068989	0,00204011
ENSG00000119771	KLHL29	protein_coding	1,28016682	0,00204678
ENSG00000247809	NR2F2-AS1	lncRNA	1,5003512	0,00205001
ENSG00000104833	TUBB4A	protein_coding	1,55975418	0,00205729
ENSG00000071909	MYO3B	protein_coding	4,55250864	0,00207918
ENSG00000182489	XKRX	protein_coding	1,15398241	0,00208462
ENSG00000176428	VPS37D	protein_coding	1,09259924	0,0021435
ENSG00000270640		lncRNA	1,17521863	0,00214828
ENSG00000286593		lncRNA	4,5814581	0,00218634
ENSG00000129654	FOXJ1	protein_coding	3,8372343	0,00225197
ENSG00000242732	RTL5	protein_coding	1,03808819	0,00227584
ENSG00000226823	SUGT1P1	unprocessed_pseudogene	1,52743977	0,00227986
ENSG00000196866	H2AC7	protein_coding	1,42431094	0,00230011
ENSG00000264672	SEPTIN4-AS1	lncRNA	1,58460488	0,00231589
ENSG00000278840		lncRNA	5,99403884	0,002351
ENSG00000255443	CD44-AS1	lncRNA	5,33076592	0,00235117
ENSG00000258647	LINC00930	lncRNA	2,5180575	0,00236546
ENSG00000159403	C1R	protein_coding	1,1380651	0,00238285
ENSG00000170899	GSTA4	protein_coding	1,07089344	0,00238662
ENSG00000156222	SLC28A1	protein_coding	4,55557112	0,00239586
ENSG00000269495		lncRNA	1,7980201	0,00243171
ENSG00000170458	CD14	protein_coding	2,4379627	0,00245171
ENSG00000210194	MT-TE	Mt_tRNA	1,07092378	0,00245261
ENSG00000204287	HLA-DRA	protein_coding	2,27221191	0,00245886
ENSG00000196932	TMEM26	protein_coding	2,01567334	0,00248015
ENSG00000129951	PLPPR3	protein_coding	1,25116791	0,00251195
ENSG00000197142	ACSL5	protein_coding	4,901367	0,00252796
ENSG00000257298		lncRNA	1,7031806	0,00262117
ENSG00000284395	PERCC1	protein_coding	1,69243893	0,00262293
ENSG00000143473	KCNH1	protein_coding	2,38007239	0,00264512
ENSG00000129595	EPB41L4A	protein_coding	1,17297135	0,00273674
ENSG00000227400		lncRNA	4,78465272	0,0027405
ENSG00000170577	SIX2	protein_coding	1,38220897	0,00275865
ENSG00000267546		lncRNA	1,74402392	0,00275865
ENSG00000204710	SPDYC	protein_coding	1,33957924	0,00279124
ENSG00000186191	BPIFB4	protein_coding	4,84138722	0,00281789
ENSG00000196620	UGT2B15	protein_coding	1,95574683	0,00282383
ENSG00000234899	SOX9-AS1	lncRNA	1,658303	0,00283641
ENSG00000264019		lncRNA	1,05109017	0,00291439
ENSG00000204936	CD177	protein_coding	2,24155564	0,00291993
ENSG00000183688	RFLNB	protein_coding	1,28886551	0,00295822
ENSG00000172575	RASGRP1	protein_coding	1,14915823	0,00307943
ENSG00000078898	BPIFB2	protein_coding	4,2161138	0,0032222
ENSG00000265595	MIR4756	miRNA	2,82850179	0,00330344
ENSG00000197180	CH17-340M24.3	lncRNA	1,35371778	0,00333907
ENSG00000227803		lncRNA	1,90880481	0,00346272

ENSG00000232296		processed_pseudogene	3,7816422	0,00348361
ENSG00000226314	ZNF192P1	transcribed_unprocessed pseudogene	1,77884052	0,0035244
ENSG00000261101		lncRNA	1,62954387	0,00355898
ENSG00000271009		lncRNA	1,12963634	0,00384737
ENSG00000102760	RGCC	protein_coding	3,02610587	0,00387448
ENSG00000152154	TMEM178A	protein_coding	4,54670847	0,00393601
ENSG00000237149	ZNF503-AS2	lncRNA	1,28599096	0,00395337
ENSG00000215218	UBE2QL1	protein_coding	1,44698574	0,00400602
ENSG00000136928	GABBR2	protein_coding	1,7001454	0,00412658
ENSG00000139055	ERP27	protein_coding	1,35797445	0,00417729
ENSG00000226051	ZNF503-AS1	lncRNA	3,01901521	0,00420087
ENSG00000256193	LINC00507	lncRNA	5,84530647	0,00420452
ENSG00000212195	U3	snoRNA	1,05056479	0,00420748
ENSG00000250337	PURPL	lncRNA	1,73131594	0,00437199
ENSG00000185532	PRKG1	protein_coding	2,12077144	0,00452312
ENSG00000273035		lncRNA	1,55708919	0,00473969
ENSG00000214359	RPL18P10	processed_pseudogene	4,36111288	0,00479512
ENSG00000277661		lncRNA	4,09966348	0,00485629
ENSG00000204618	RNF39	protein_coding	1,03187243	0,00487962
ENSG00000235961	PNMA6A	protein_coding	1,96714629	0,00489342
ENSG00000198488	B3GNT6	protein_coding	1,57769778	0,00492739
ENSG00000258603		lncRNA	2,05264865	0,00499229
ENSG00000250786	SNHG18	lncRNA	1,05139843	0,00504914
ENSG00000269019	HOMER3-AS1	lncRNA	1,9055847	0,00507876
ENSG00000253944		lncRNA	2,11519938	0,00509228
ENSG00000224897	POT1-AS1	lncRNA	2,27160363	0,00514142
ENSG00000251689		processed_pseudogene	1,80071519	0,00514766
ENSG00000287550		lncRNA	1,83868089	0,00522077
ENSG00000107551	RASSF4	protein_coding	1,73641966	0,00539348
ENSG00000257696		lncRNA	1,88143818	0,00549729
ENSG00000136378	ADAMTS7	protein_coding	1,01856463	0,00559527
ENSG00000121552	CSTA	protein_coding	2,04369871	0,00576025
ENSG00000235910	APOA1-AS	lncRNA	5,11217196	0,00595815
ENSG00000251095		lncRNA	1,14895827	0,00596179
ENSG00000260394	LINC02867	lncRNA	1,50871347	0,00600168
ENSG00000264278	ZNF236-DT	lncRNA	1,36888311	0,0060638
ENSG00000105639	JAK3	protein_coding	1,13467673	0,00637805
ENSG00000234055		lncRNA	4,21914256	0,00653339
ENSG00000087884	AAMDC	protein_coding	1,11245102	0,00654501
ENSG00000173947	PIFO	protein_coding	1,41289753	0,00664542
ENSG00000170689	HOXB9	protein_coding	4,10933196	0,00678624
ENSG00000268756		lncRNA	4,74032711	0,0068361
ENSG00000227911	LINC02344	lncRNA	1,6520287	0,00685577
ENSG00000168209	DDIT4	protein_coding	1,07945508	0,00693211
ENSG00000188263	IL17REL	protein_coding	1,53254917	0,0070718
ENSG00000169035	KLK7	protein_coding	4,77254668	0,00713682
ENSG00000164342	TLR3	protein_coding	4,11185525	0,00714061
ENSG00000188681	TEKT4P2	transcribed_unprocessed pseudogene	1,81777327	0,00725394
ENSG00000196581	AJAP1	protein_coding	4,09196049	0,00728675
ENSG00000109705	NKX3-2	protein_coding	1,48222762	0,00737199
ENSG00000133083	DCLK1	protein_coding	1,19622412	0,00748357
ENSG00000186280	KDM4D	protein_coding	1,30097951	0,00760206
ENSG00000081853	PCDHGA2	protein_coding	1,14558725	0,00769354
ENSG00000228950		lncRNA	1,43527595	0,00783051
ENSG00000211891	IGHE	IG_C_gene	2,11454962	0,00786956
ENSG00000178695	KCTD12	protein_coding	2,61397731	0,0079901
ENSG00000104967	NOVA2	protein_coding	2,27730022	0,00803082
ENSG00000258451	EGILA	lncRNA	3,89942393	0,00810456
ENSG00000141977	CIB3	protein_coding	2,52050502	0,00813164
ENSG00000116176	TPSG1	protein_coding	1,11533557	0,00814512
ENSG00000101197	BIRC7	protein_coding	2,87259345	0,00846991
ENSG00000204701	OR2J3	protein_coding	4,05254437	0,00851007
ENSG00000125354	SEPTIN6	protein_coding	1,0667324	0,00882385
ENSG00000182742	HOXB4	protein_coding	3,97345544	0,00889366
ENSG00000166046	TCP11L2	protein_coding	1,0035437	0,00898931
ENSG00000154134	ROBO3	protein_coding	1,13711295	0,00905682
ENSG00000079435	LIPE	protein_coding	1,17126029	0,00923771
ENSG00000285935		lncRNA	3,1181248	0,00928397
ENSG00000162039	MEIOB	protein_coding	2,84792411	0,00947014
ENSG00000162981	LRATD1	protein_coding	1,0979631	0,00967998
ENSG00000164076	CAMKV	protein_coding	4,94714491	0,00985733
ENSG00000256196		lncRNA	1,21990912	0,00991767
ENSG00000133055	MYBPH	protein_coding	4,20958955	0,00994225
ENSG00000247228		lncRNA	1,05824369	0,01006472
ENSG00000150281	CTF1	protein_coding	1,48430574	0,01006672
ENSG00000184774	MGAT4EP	transcribed_unitary pseudogene	5,23748934	0,01013463
ENSG00000168811	IL12A	protein_coding	1,86004858	0,01041758
ENSG00000174171		lncRNA	2,66224966	0,01053472
ENSG00000069764	PLA2G10	protein_coding	3,12755181	0,01072727
ENSG00000227252		lncRNA	1,01372399	0,01078107
ENSG00000180834	MAP6D1	protein_coding	1,01865168	0,01110668
ENSG00000187848	P2RX2	protein_coding	2,05474919	0,01118854
ENSG00000223776	LGALS8-AS1	lncRNA	1,4915674	0,01158104
ENSG00000164932	CTHRC1	protein_coding	1,3054692	0,0115987
ENSG00000175877	TMEM270	protein_coding	1,07190204	0,01189276
ENSG00000149972	CNTN5	protein_coding	7,14261476	0,01192273
ENSG00000218281	H2AC9P	unprocessed_pseudogene	2,31109077	0,01220748

ENSG00000279930		TEC	1,67237961	0,01226597
ENSG00000251535		processed_pseudogene	1,89401222	0,01266133
ENSG00000148942	SLC5A12	protein_coding	3,88571523	0,01280508
ENSG00000260213	CENPN-AS1	lncRNA	1,54624153	0,01299145
ENSG00000163209	SPRR3	protein_coding	3,727145	0,01301986
ENSG00000238118	SLC25A24P2	unprocessed_pseudogene	1,36761661	0,01306976
ENSG00000249267	LINC00939	lncRNA	4,9192636	0,01310238
ENSG00000250326		lncRNA	1,97722901	0,01331663
ENSG00000279653		TEC	1,28894396	0,01347079
ENSG00000166313	APBB1	protein_coding	1,19207444	0,01360402
ENSG00000255298	OR8G5	protein_coding	1,11451912	0,01364145
ENSG00000135697	BCO1	protein_coding	2,04612158	0,01386208
ENSG00000138653	NDST4	protein_coding	5,50242738	0,01389154
ENSG00000183036	PCP4	protein_coding	1,29892916	0,01393667
ENSG00000188738	FSIP2	protein_coding	1,58254751	0,01430227
ENSG00000257178		lncRNA	3,1885279	0,01430227
ENSG00000214145	LINC00887	lncRNA	1,47773657	0,01443291
ENSG00000256971	LINC00508	lncRNA	4,37309097	0,0144758
ENSG00000061918	GUCY1B1	protein_coding	1,20488686	0,0146364
ENSG00000251194		lncRNA	2,77581154	0,01464505
ENSG00000287342		lncRNA	4,17240728	0,01536489
ENSG00000079385	CEACAM1	protein_coding	1,79272798	0,01595427
ENSG00000237761		lncRNA	4,2925005	0,01605656
ENSG00000205978	NYNRIN	protein_coding	1,06655138	0,01641223
ENSG00000267259	ERVE-1	lncRNA	1,70502621	0,01659087
ENSG00000086717	PPEF1	protein_coding	1,50142788	0,01666763
ENSG00000261759		lncRNA	1,40805503	0,01671637
ENSG00000255153	TOLLIP-AS1	lncRNA	1,23631549	0,01677469
ENSG00000160963	COL26A1	protein_coding	2,02262692	0,01705958
ENSG00000272989	LINC02012	lncRNA	1,38077651	0,01705958
ENSG00000261812	TUBB8P7	transcribed_unprocessed pseudogene	2,74622058	0,01707639
ENSG00000257839		lncRNA	2,29269512	0,01711956
ENSG00000232756	DDX3ILA1	lncRNA	3,59818141	0,01720103
ENSG00000267352	SH3GL1P3	processed_pseudogene	1,12398823	0,01726087
ENSG00000163283	ALPP	protein_coding	3,34334645	0,01735406
ENSG00000105497	ZNF175	protein_coding	3,59674132	0,0174659
ENSG00000271858	CYB561D2	lncRNA	1,35198585	0,01779663
ENSG00000278915		lncRNA	1,05276152	0,01795627
ENSG00000174145	NWD2	protein_coding	4,12412467	0,01803318
ENSG00000273853		lncRNA	1,96166845	0,01843958
ENSG00000225518	LINC01703	lncRNA	1,39373923	0,01858272
ENSG00000233725	NRAD1	lncRNA	2,34078837	0,01863603
ENSG00000188906	LRRK2	protein_coding	1,05934608	0,01869485
ENSG00000115590	IL1R2	protein_coding	3,83065236	0,01889906
ENSG00000152467	ZSCAN1	protein_coding	4,24487388	0,01893599
ENSG00000226592		processed_pseudogene	5,45001362	0,01907435
ENSG00000189295	ANKRD62P1-PARP4P3	lncRNA	4,48152564	0,01907547
ENSG00000233834		lncRNA	1,61411391	0,01939781
ENSG00000150594	ADRA2A	protein_coding	1,53589994	0,01986322
ENSG00000232624	LINC01517	lncRNA	3,59675877	0,01986836
ENSG00000143178	TBX19	protein_coding	1,14434844	0,01998565
ENSG00000286393		lncRNA	3,97800144	0,02012589
ENSG00000074803	SLC12A1	protein_coding	4,80214298	0,02023132
ENSG00000171303	KCNK3	protein_coding	2,50982233	0,02050841
ENSG00000140481	CCDC33	protein_coding	1,29761116	0,02052005
ENSG00000100033	PRODH	protein_coding	3,65182328	0,02057132
ENSG00000185974	GRK1	protein_coding	2,82378829	0,02103121
ENSG00000146216	TTBK1	protein_coding	1,04337166	0,02149604
ENSG00000265100		lncRNA	1,1351385	0,021507
ENSG00000288025		lncRNA	1,13855867	0,02161839
ENSG00000268658	LINC00664	lncRNA	1,27533683	0,02182508
ENSG00000162944	RFTN2	protein_coding	3,01211133	0,02246256
ENSG00000172061	LRRC15	protein_coding	1,74586138	0,02305095
ENSG00000267905	VSIG10L-AS1	lncRNA	3,50977054	0,02305573
ENSG00000167895	TMC8	protein_coding	1,01259785	0,0231586
ENSG00000188039	NWD1	protein_coding	1,12842732	0,02359484
ENSG00000225285	LINC01770	lncRNA	2,23353704	0,02377842
ENSG00000228288	PCAT6	lncRNA	1,45741336	0,02377842
ENSG00000178297	TMPRSS9	protein_coding	1,05377558	0,02396047
ENSG00000230140	NPAS2-AS1	lncRNA	3,1213097	0,02398686
ENSG00000275805		lncRNA	3,77907455	0,02403706
ENSG00000100053	CRYBB3	protein_coding	1,26240427	0,02430175
ENSG00000270659		lncRNA	1,07383712	0,02444761
ENSG00000229331	GK-IT1	lncRNA	4,46548281	0,02462485
ENSG00000203650	LINC01285	lncRNA	2,73571494	0,02469673
ENSG00000262312		lncRNA	1,12205965	0,02477047
ENSG00000159409	CELF3	protein_coding	1,47855322	0,02509716
ENSG00000287737		lncRNA	1,12542946	0,0253669
ENSG00000163072	NOSTRIN	protein_coding	1,74103356	0,02612266
ENSG00000279660		TEC	1,84306212	0,02617128
ENSG00000231574	LINC02015	lncRNA	1,40642878	0,02634345
ENSG00000102003	SYP	protein_coding	1,1400346	0,02677962
ENSG00000264575	LINC00526	lncRNA	3,42634852	0,02724773
ENSG00000263004	AKAP1-DT	lncRNA	1,53960754	0,0274942
ENSG00000233101	HOXB-AS3	lncRNA	3,39088642	0,02781113
ENSG00000231134	TCF7L1-IT1	lncRNA	2,31354407	0,02781875
ENSG00000102445	RUBCNL	protein_coding	1,48886256	0,0279113
ENSG00000139219	COL2A1	protein_coding	2,5263013	0,0280165

ENSG00000278946		lncRNA	1,64376796	0,0281453
ENSG00000256347	OR8R1P	unprocessed_pseudogene	2,53263369	0,02817975
ENSG00000267892		lncRNA	1,09239865	0,02842266
ENSG00000075073	TACR2	protein_coding	1,48810531	0,02863849
ENSG00000232036		processed_pseudogene	1,87646637	0,02863849
ENSG00000163273	NPPC	protein_coding	1,73708491	0,02870212
ENSG00000006606	CCL26	protein_coding	2,72808616	0,02875087
ENSG00000279836		TEC	2,08158956	0,02900766
ENSG00000260954		lncRNA	1,36533607	0,02918208
ENSG00000277386		lncRNA	1,64456536	0,02937349
ENSG00000231133	HAR1B	lncRNA	3,61498271	0,02956054
ENSG00000154099	DNAAF1	protein_coding	1,02444899	0,02963544
ENSG00000143365	RORC	protein_coding	1,21035226	0,03043622
ENSG00000184497	TMEM255B	protein_coding	1,21906634	0,03057459
ENSG00000158683	PKD1L1	protein_coding	1,58585256	0,03065227
ENSG00000178573	MAF	protein_coding	1,26741885	0,03065227
ENSG00000164398	ACSL6	protein_coding	3,82485552	0,03095682
ENSG00000250412	KLHL2P1	unprocessed_pseudogene	1,23610552	0,03104897
ENSG00000167549	CORO6	protein_coding	1,50710599	0,03128573
ENSG00000231672	DIRC3	lncRNA	1,34944559	0,03159242
ENSG00000287354		lncRNA	2,25863143	0,03171264
ENSG00000286895		lncRNA	2,48541137	0,03171849
ENSG00000141314	RHBDL3	protein_coding	1,98956984	0,03196879
ENSG00000065325	GLP2R	protein_coding	2,31897413	0,03243312
ENSG00000114248	LRRC31	protein_coding	3,45982435	0,03252103
ENSG00000230393		lncRNA	2,48998848	0,03298854
ENSG00000254990		lncRNA	3,9586616	0,03312696
ENSG00000247199		lncRNA	2,45811533	0,03316021
ENSG00000102962	CCL22	protein_coding	3,46094098	0,03345345
ENSG00000179593	ALOX15B	protein_coding	3,46012866	0,03346726
ENSG00000276317		lncRNA	2,37066987	0,03374691
ENSG00000260816		lncRNA	1,03247513	0,03400034
ENSG00000106031	HOXA13	protein_coding	1,87426995	0,03406643
ENSG00000203685	STUM	protein_coding	1,46825212	0,03411651
ENSG00000233593	LINC02609	lncRNA	1,14591533	0,03446107
ENSG00000246526	LINC02481	lncRNA	1,17041123	0,0346784
ENSG00000171408	PDE7B	protein_coding	3,22033788	0,03469083
ENSG00000165029	ABCA1	protein_coding	1,24803268	0,03560646
ENSG00000283000	LINC02635	lncRNA	2,19716846	0,03569761
ENSG00000269815		lncRNA	3,59808264	0,03613998
ENSG00000021645	NRXN3	protein_coding	4,2494332	0,03653936
ENSG00000170615	SLC26A5	protein_coding	4,01399079	0,03699788
ENSG00000239440	LINC02008	lncRNA	5,02578316	0,03708467
ENSG00000198729	PPP1R14C	protein_coding	1,57443702	0,03746993
ENSG00000238311	SNORD13E	snoRNA	4,00384055	0,03852515
ENSG00000271387	C1orf21-DT	lncRNA	1,89208047	0,03855131
ENSG00000258314		lncRNA	2,45904497	0,03861948
ENSG00000102359	SRPX2	protein_coding	2,69529967	0,03892822
ENSG00000212512	Y_RNA	misc_RNA	1,72983543	0,03926045
ENSG00000260464		lncRNA	1,12207912	0,0401247
ENSG00000268583		lncRNA	1,60500057	0,04044129
ENSG00000283537		transcribed_unprocessed pseudogene	2,13187609	0,04128356
ENSG00000224167	LINC01357	lncRNA	3,64251792	0,04175867
ENSG00000273821		lncRNA	1,33903691	0,0418717
ENSG00000147485	PXDNL	protein_coding	1,63915815	0,04222418
ENSG00000272259	LINC01749	lncRNA	2,11524916	0,04270236
ENSG00000212939		lncRNA	4,25650572	0,0429854
ENSG00000275109	MIR6504	miRNA	4,13102597	0,04347149
ENSG00000256139		lncRNA	1,29271798	0,0435317
ENSG00000272438		lncRNA	1,46572661	0,04356463
ENSG00000005844	ITGAL	protein_coding	1,22745482	0,04369985
ENSG00000111348	ARHGDIB	protein_coding	1,08004945	0,04450565
ENSG00000103316	CRYM	protein_coding	1,86715642	0,04451608
ENSG00000278901		lncRNA	1,84735778	0,04477244
ENSG00000264701		lncRNA	1,29184877	0,04485937
ENSG00000170935	NCBP2L	protein_coding	1,06553189	0,04527752
ENSG00000125122	LRRC29	transcribed_unitary pseudogene	1,07935014	0,04544705
ENSG00000227076		lncRNA	1,76713467	0,0455167
ENSG00000282048		lncRNA	3,17306938	0,04597168
ENSG00000167105	TMEM92	protein_coding	3,27177571	0,046553
ENSG00000241362	RPL36AP43	processed_pseudogene	1,19722146	0,04666509
ENSG00000137573	SULF1	protein_coding	1,14371971	0,04695838
ENSG00000088992	TESC	protein_coding	1,8847295	0,04701258
ENSG00000268081		lncRNA	3,06828647	0,04784141
ENSG00000220008	LINGO3	protein_coding	1,90690169	0,04801492
ENSG00000235021		lncRNA	3,65729342	0,04819164
ENSG00000166509	CLEC3A	protein_coding	2,96800854	0,04828983
ENSG00000115414	FN1	protein_coding	1,31988582	0,04954102
ENSG00000246250		lncRNA	2,18462467	0,04957338
ENSG00000179776	CDH5	protein_coding	3,84086507	0,04984043
ENSG00000252859	RNU6-375P	snRNA	3,58022643	0,05008277
ENSG00000104826	LHB	protein_coding	2,54297485	0,05051846
ENSG00000278700	Metazoa_SRP	misc_RNA	1,12129919	0,05064408
ENSG00000229951	FLJ31356	lncRNA	1,53771601	0,05089408
ENSG00000100181	TPTEP1	transcribed_unprocessed pseudogene	3,65324062	0,0509083
ENSG00000255045		lncRNA	1,57379098	0,0509485
ENSG00000121858	TNFSF10	protein_coding	2,70157394	0,05133988

ENSG00000131183	SLC34A1	protein_coding	2,7886798	0,0515283
ENSG00000274560		lncRNA	3,49431402	0,05186299
ENSG00000254528		lncRNA	2,83228906	0,05189587
ENSG00000059377	TBXAS1	protein_coding	1,0020759	0,05247329
ENSG00000266570	MIR5579	miRNA	3,1585352	0,05276152
ENSG00000120075	HOXB5	protein_coding	3,23756936	0,05365196
ENSG00000265168		lncRNA	1,44171414	0,05401098
ENSG00000262429		lncRNA	1,23726658	0,0546705
ENSG00000112559	MDFI	protein_coding	3,23676588	0,05478823
ENSG00000251188		processed_pseudogene	1,05769973	0,05481025
ENSG00000256128	LINC00944	lncRNA	3,81404843	0,05492647
ENSG00000176723	ZNF843	protein_coding	1,21371713	0,05500208
ENSG00000225087		lncRNA	1,48185761	0,05503126
ENSG00000132639	SNAP25	protein_coding	1,81999466	0,05507154
ENSG00000231194	FARP1-AS1	lncRNA	1,16858441	0,0552949
ENSG00000167754	KLK5	protein_coding	2,05885826	0,05547863
ENSG00000225215	SMARCE1P1	processed_pseudogene	2,50840529	0,0557084
ENSG00000125462	MIR9-1HG	lncRNA	1,21042972	0,05639497
ENSG00000183888	SRARP	protein_coding	3,23666708	0,05660986
ENSG00000110693	SOX6	protein_coding	1,68564518	0,05748334
ENSG00000157613	CREB3L1	protein_coding	3,65102911	0,05758344
ENSG00000262823		lncRNA	2,80100623	0,05816128
ENSG00000204128	C2orf72	protein_coding	1,2110427	0,05834059
ENSG00000255366		lncRNA	3,64361348	0,05837106
ENSG00000157703	SVOPL	protein_coding	1,85141062	0,05885927
ENSG00000254340		lncRNA	2,00510175	0,05905744
ENSG00000083814	ZNF671	protein_coding	3,23589191	0,05943631
ENSG00000165028	NIPSNAP3B	protein_coding	1,48542779	0,05944711
ENSG00000260228		lncRNA	1,54899331	0,05944857
ENSG00000268628		lncRNA	1,86340692	0,05947172
ENSG00000173212	MAB21L3	protein_coding	1,30085258	0,05957686
ENSG00000255198	SNHG9	lncRNA	1,685983	0,06003816
ENSG00000152049	KCNE4	protein_coding	3,47041185	0,06005461
ENSG00000176597	B3GNT5	protein_coding	1,03492351	0,06092278
ENSG00000267191	ZNF45-AS1	lncRNA	2,11232935	0,06096157
ENSG00000170324	FRMPD2	protein_coding	1,18049418	0,06128419
ENSG00000167601	AXL	protein_coding	1,59113647	0,06128976
ENSG00000237259	ZNF133-AS1	lncRNA	3,12557954	0,06171133
ENSG00000254964		lncRNA	1,49057626	0,06171133
ENSG00000285094	LINC01488	lncRNA	1,41369196	0,06171133
ENSG00000264175	MIR3189	miRNA	1,39593279	0,06186194
ENSG00000184388	PABPC1L2B	protein_coding	1,30983054	0,06219199
ENSG00000228100	LINC01820	lncRNA	4,1304674	0,06280135
ENSG00000278177		lncRNA	1,73299477	0,06300202
ENSG00000252494	RNU6-126P	snRNA	1,57335268	0,06304273
ENSG00000261114		lncRNA	1,37851061	0,06309328
ENSG00000159860	TCAF2P1	transcribed_unprocessed pseudogene	2,39427207	0,06317151
ENSG00000224899	LINC02830	lncRNA	2,17566691	0,06350875
ENSG00000173213	TUBB8B	protein_coding	2,0325	0,06377151
ENSG00000235795		lncRNA	2,67727836	0,06412491
ENSG00000235343	LINC01665	lncRNA	3,96621554	0,06416402
ENSG00000170477	KRT4	protein_coding	3,01329707	0,06468543
ENSG00000121797	CCRL2	protein_coding	3,64516881	0,06482505
ENSG00000065618	COL17A1	protein_coding	2,04382298	0,0649253
ENSG00000179284	DAND5	protein_coding	2,79518235	0,06565067
ENSG00000189350	TOGARAM2	protein_coding	3,40802139	0,06598649
ENSG00000248121	SMURF2P1	transcribed_unprocessed pseudogene	2,0202639	0,06679118
ENSG00000285570		lncRNA	1,40958843	0,0674664
ENSG00000260989		lncRNA	2,54880258	0,06888383
ENSG00000259402		lncRNA	1,64693392	0,06913697
ENSG00000235996		lncRNA	2,31008958	0,0692979
ENSG00000149403	GRIK4	protein_coding	1,57891606	0,07095648
ENSG00000136573	BLK	protein_coding	1,97518717	0,07260761
ENSG00000227811	INKA2-AS1	lncRNA	1,14643839	0,07284647
ENSG00000096088	PGC	protein_coding	2,77474262	0,07286027
ENSG00000207612	MIR604	miRNA	2,01917554	0,07354317
ENSG00000207617	MIR3074	miRNA	3,66885996	0,07368967
ENSG00000069431	ABCC9	protein_coding	1,90928493	0,0752604
ENSG00000270792		lncRNA	1,46099764	0,07557383
ENSG00000253882		transcribed_unprocessed pseudogene	1,50728099	0,0757161
ENSG00000212597	RNU6-876P	snRNA	3,46626492	0,07581906
ENSG00000087085	ACHE	protein_coding	1,28071386	0,0758615
ENSG00000256150	ITFG2-AS1	lncRNA	1,21528357	0,07589826
ENSG00000126838	PZP	protein_coding	2,44105635	0,07591809
ENSG00000267344		lncRNA	1,10747978	0,07616367
ENSG00000257842	LINC02588	lncRNA	1,37757365	0,07708357
ENSG00000138079	SLC3A1	protein_coding	1,21280824	0,07718438
ENSG00000280339		TEC	1,89266448	0,07728599
ENSG00000236117	LINC01639	lncRNA	2,28081184	0,0775161
ENSG00000243746	EEF1A1P10	processed_pseudogene	3,87943733	0,0775529
ENSG00000272482		lncRNA	2,23259835	0,07841754
ENSG00000002587	HS3ST1	protein_coding	2,26102384	0,07923257
ENSG00000283982		lncRNA	3,01626385	0,07984956
ENSG00000232754		lncRNA	2,72023151	0,08012095
ENSG00000153132	CLGN	protein_coding	1,0669875	0,08123091
ENSG00000204802		lncRNA	1,24064202	0,08140471
ENSG00000279289		TEC	2,12106725	0,08155269

ENSG00000243069	ARHGEF26-AS1	lncRNA	1,01465675	0,08176691
ENSG00000234886	MTND5P26	processed_pseudogene	2,2811758	0,08226022
ENSG00000228404		lncRNA	3,6442694	0,08289515
ENSG00000110324	IL10RA	protein_coding	1,87362102	0,08428377
ENSG00000091482	SMPX	protein_coding	3,45152267	0,08462656
ENSG00000260601		lncRNA	1,67845731	0,08464766
ENSG00000255247	NECTIN1-AS1	lncRNA	3,8384858	0,08502653
ENSG00000103375	AQP8	protein_coding	2,83545286	0,08509507
ENSG00000130528	HRC	protein_coding	3,18642065	0,08524441
ENSG00000258352	IFITM3P6	transcribed_processed pseudogene	1,63257337	0,08554589
ENSG00000260095		lncRNA	2,11475431	0,08569913
ENSG00000166086	JAM3	protein_coding	2,31148674	0,08591142
ENSG00000271447	MMP28	protein_coding	3,45487477	0,0866603
ENSG00000231419	LINC00689	lncRNA	1,87015488	0,08674241
ENSG00000255471		lncRNA	1,74930405	0,08674241
ENSG00000228275	ARMCX3-AS1	lncRNA	1,45887134	0,08721894
ENSG00000287527		lncRNA	3,81313173	0,08745821
ENSG00000278811	LINC00624	lncRNA	1,27659046	0,08753006
ENSG00000226690		protein_coding	2,66689601	0,08775516
ENSG00000063015	SEZ6	protein_coding	2,30966347	0,08840428
ENSG00000242741	LINC02005	lncRNA	1,01007478	0,08855172
ENSG00000169418	NPR1	protein_coding	1,14708959	0,08960412
ENSG00000162444	RBP7	protein_coding	1,45249896	0,0897088
ENSG00000267073		lncRNA	3,73762448	0,09105427
ENSG00000259511	UBE2Q2L	transcribed_unprocessed pseudogene	2,95536751	0,09261398
ENSG00000279516	FAM230C	lncRNA	2,97379904	0,09321873
ENSG00000234775		lncRNA	2,24343025	0,09478551
ENSG00000269918		lncRNA	1,04919195	0,09521085
ENSG00000167755	KLK6	protein_coding	1,59797936	0,09552876
ENSG00000252341	Y_RNA	misc_RNA	3,66490106	0,09552876
ENSG00000229666	MAST4-AS1	lncRNA	1,33739596	0,09586054
ENSG00000279791		TEC	2,36631266	0,09607718
ENSG00000250451	HOXC-AS1	lncRNA	1,29239476	0,09617783
ENSG00000243224		lncRNA	1,11226934	0,09651566
ENSG00000238279		lncRNA	2,61021885	0,09662491
ENSG00000225014	KCTD9P1	transcribed_processed pseudogene	3,32498998	0,09725235
ENSG00000231948	HS1BP3-IT1	lncRNA	3,49561829	0,0976304
ENSG00000228503		lncRNA	1,49742263	0,09767877
ENSG00000207588	MIR593	miRNA	1,12041811	0,09843597
ENSG00000254678		processed_pseudogene	3,2759931	0,09843597
ENSG00000267666		lncRNA	1,41319803	0,09858879
ENSG00000088827	SIGLEC1	protein_coding	2,62877894	0,09862547
ENSG00000256612	CYP2B7P	transcribed_unprocessed pseudogene	1,70005551	0,09886118
ENSG00000280164		lncRNA	2,00676512	0,09891184
ENSG00000268812	LIF-AS2	lncRNA	1,36058185	0,09901084
ENSG00000163520	FBLN2	protein_coding	2,40225413	0,09901493
ENSG00000263033		lncRNA	2,20264323	0,09904917
ENSG00000264982		lncRNA	1,96239255	0,09932275
ENSG00000255753		processed_pseudogene	3,46349397	0,09977915
ENSG00000266602		lncRNA	2,97210846	0,09983573

Supplementary Table S 5: Genes with decreased expression in resistant MCF7 cells.

Ensembl	GeneSymbol	gene_biotype	log2FC	FDR
ENSG00000164741	DLC1	protein_coding	-4,98396746	2,112E-170
ENSG00000171791	BCL2	protein_coding	-5,26014312	1,125E-167
ENSG00000138386	NAB1	protein_coding	-4,52402068	9,659E-164
ENSG00000091136	LAMB1	protein_coding	-7,12197365	3,806E-156
ENSG00000164292	RHOBTB3	protein_coding	-3,0858946	1,349E-137
ENSG00000145860	RNF145	protein_coding	-3,38814404	1,352E-114
ENSG00000167552	TUBA1A	protein_coding	-3,74579634	1,0674E-96
ENSG00000222041	CYTOR	lncRNA	-3,06699565	3,6312E-93
ENSG00000175920	DOK7	protein_coding	-1,75259115	4,1715E-92
ENSG00000106853	PTGR1	protein_coding	-3,17093702	4,2044E-88
ENSG00000128656	CHN1	protein_coding	-5,31769099	4,3696E-82
ENSG00000189334	S100A14	protein_coding	-3,22684478	3,2336E-74
ENSG00000164690	SHH	protein_coding	-3,95439075	3,5717E-74
ENSG00000177189	RPS6KA3	protein_coding	-2,43994611	4,3609E-74
ENSG00000005249	PRKAR2B	protein_coding	-2,61188983	9,0708E-74
ENSG00000133687	TMTC1	protein_coding	-3,27245418	3,0224E-73
ENSG00000082497	SERTAD4	protein_coding	-3,60339016	3,1254E-73
ENSG00000126822	PLEKHG3	protein_coding	-1,57026251	7,7845E-73
ENSG00000166833	NAV2	protein_coding	-2,71041071	5,7684E-67
ENSG00000130707	ASS1	protein_coding	-2,26102176	3,0339E-66
ENSG00000099204	ABLIM1	protein_coding	-2,57756303	2,214E-64
ENSG00000147526	TACC1	protein_coding	-2,09313719	2,2598E-63
ENSG00000101266	CSNK2A1	protein_coding	-1,34175645	4,5035E-62
ENSG00000251348	HSPD1P11	processed_pseudogene	-3,16745597	5,7668E-60
ENSG00000167741	GGT6	protein_coding	-2,96445002	1,0808E-59
ENSG00000065320	NTN1	protein_coding	-3,55046927	1,158E-58
ENSG00000170500	LONRF2	protein_coding	-1,6389451	2,3258E-58
ENSG00000088832	FKBP1A	protein_coding	-1,3719773	9,7727E-58
ENSG00000125818	PSMF1	protein_coding	-1,37099297	2,8507E-57
ENSG00000171631	P2RY6	protein_coding	-4,01556625	9,8103E-54

ENSG00000163697	APBB2	protein_coding	-1,63370528	8,3015E-52
ENSG00000054690	PLEKHH1	protein_coding	-1,23642572	5,1484E-51
ENSG00000164023	SGMS2	protein_coding	-1,70610853	6,3951E-51
ENSG00000172965	MIR4435-2HG	lncRNA	-2,84196447	1,5128E-50
ENSG00000130635	COL5A1	protein_coding	-2,97401704	1,0127E-49
ENSG00000151612	ZNF827	protein_coding	-1,53251005	1,464E-49
ENSG00000100311	PDGFB	protein_coding	-1,23410262	1,0052E-48
ENSG00000136141	LRCH1	protein_coding	-1,46953395	8,4572E-48
ENSG00000155850	SLC26A2	protein_coding	-3,94337527	1,3016E-47
ENSG00000112796	ENPP5	protein_coding	-2,98708438	1,4896E-47
ENSG00000125834	STK35	protein_coding	-1,15375107	3,3471E-46
ENSG00000196604	POTEF	protein_coding	-4,14935034	6,5532E-46
ENSG00000116584	ARHGEF2	protein_coding	-1,23162922	2,5921E-45
ENSG00000188643	S100A16	protein_coding	-1,87004155	2,7677E-45
ENSG00000123094	RASSF8	protein_coding	-1,84939365	3,7933E-45
ENSG00000122042	UBL3	protein_coding	-1,19724382	1,7232E-43
ENSG00000036672	USP2	protein_coding	-2,23005836	1,7708E-43
ENSG00000162892	IL24	protein_coding	-3,92418753	3,0653E-43
ENSG00000125089	SH3TC1	protein_coding	-3,53010284	5,6788E-43
ENSG00000177614	PGBD5	protein_coding	-3,10169942	9,5888E-43
ENSG00000137962	ARHGAP29	protein_coding	-2,2129676	3,4157E-42
ENSG00000164211	STARD4	protein_coding	-2,31772087	1,0091E-41
ENSG00000213468	FIRRE	lncRNA	-1,65840193	1,0341E-41
ENSG00000198807	PAX9	protein_coding	-1,43686428	1,3767E-41
ENSG00000197121	PGAP1	protein_coding	-1,45165159	2,3985E-41
ENSG00000111237	VPS29	protein_coding	-1,35375722	4,1356E-41
ENSG00000198879	SFMBT2	protein_coding	-3,17155647	6,6659E-41
ENSG00000135048	CEMIP2	protein_coding	-1,41217399	7,0875E-41
ENSG00000204740	MALRD1	protein_coding	-2,41915061	1,1269E-40
ENSG00000145632	PLK2	protein_coding	-1,83947971	1,2734E-40
ENSG00000169604	ANTXR1	protein_coding	-2,40553837	1,5597E-40
ENSG00000073464	CLCN4	protein_coding	-3,85390077	2,1779E-39
ENSG00000186298	PPP1CC	protein_coding	-1,38623074	2,1836E-39
ENSG00000116675	DNAJC6	protein_coding	-1,93825518	2,283E-39
ENSG00000177679	SRRM3	protein_coding	-1,67880943	4,3976E-39
ENSG00000169583	CLIC3	protein_coding	-1,94825486	7,5374E-38
ENSG00000154640	BTG3	protein_coding	-2,26370632	8,3411E-38
ENSG00000099284	MACROH2A2	protein_coding	-3,82865098	8,3108E-37
ENSG00000272419	LINC01145	transcribed_unprocessed pseudogene	-5,33146599	1,1819E-36
ENSG00000133477	FAM83F	protein_coding	-2,69575783	5,2003E-36
ENSG00000122863	CHST3	protein_coding	-2,47891447	9,2058E-36
ENSG00000138411	HECW2	protein_coding	-1,5514811	1,1186E-35
ENSG00000188219	POTEE	protein_coding	-3,39293723	2,8272E-35
ENSG00000120594	PLXDC2	protein_coding	-1,72119176	3,4111E-35
ENSG00000070182	SPTB	protein_coding	-4,06625463	3,6764E-35
ENSG00000151376	ME3	protein_coding	-2,0371012	8,8552E-35
ENSG00000250240		lncRNA	-3,39413065	1,2933E-34
ENSG00000164171	ITGA2	protein_coding	-1,921673	1,3044E-34
ENSG00000167703	SLC43A2	protein_coding	-1,30208471	5,9777E-34
ENSG00000070778	PTPN21	protein_coding	-2,96468691	6,5108E-34
ENSG00000140280	LYSMD2	protein_coding	-1,60126076	7,876E-34
ENSG00000164251	F2RL1	protein_coding	-2,19577271	1,396E-33
ENSG00000136944	LMX1B	protein_coding	-1,51389139	1,7695E-33
ENSG00000125875	TBC1D20	protein_coding	-1,27955895	1,8073E-33
ENSG00000187017	ESPN	protein_coding	-1,41526775	2,7016E-33
ENSG00000125826	RBCK1	protein_coding	-1,15351302	2,7602E-33
ENSG00000167723	TRPV3	protein_coding	-2,75679948	3,3794E-33
ENSG00000124942	AHNAK	protein_coding	-1,15994439	5,0194E-33
ENSG00000149043	SYT8	protein_coding	-2,65379139	6,9047E-33
ENSG00000277147	LINC00869	transcribed_unprocessed pseudogene	-4,75215626	7,5483E-33
ENSG00000168907	PLA2G4F	protein_coding	-2,12264743	8,6438E-33
ENSG00000218336	TENM3	protein_coding	-1,76079538	1,0224E-32
ENSG00000198743	SLC5A3	protein_coding	-1,27514906	1,0301E-32
ENSG00000128872	TMOD2	protein_coding	-1,99333573	1,2753E-32
ENSG00000168785	TSPAN5	protein_coding	-1,86860342	2,4215E-32
ENSG00000120149	MSX2	protein_coding	-1,87966306	2,9063E-32
ENSG00000157540	DYRK1A	protein_coding	-1,10274129	3,3588E-32
ENSG00000145730	PAM	protein_coding	-1,33043954	6,5112E-32
ENSG00000141574	SECTM1	protein_coding	-2,74123478	6,9593E-32
ENSG00000119638	NEK9	protein_coding	-1,33175645	1,5776E-31
ENSG00000118513	MYB	protein_coding	-1,96963916	1,7223E-31
ENSG00000275342	PRAG1	protein_coding	-1,63437601	8,1123E-31
ENSG00000088002	SULT2B1	protein_coding	-1,4215135	8,542E-31
ENSG00000108352	RAPGEFL1	protein_coding	-1,01800572	8,8868E-31
ENSG00000120913	PDLIM2	protein_coding	-1,93700025	2,0431E-30
ENSG00000138835	RGS3	protein_coding	-1,15039694	2,7362E-30
ENSG00000159228	CBR1	protein_coding	-1,18567386	3,6668E-30
ENSG00000111799	COL12A1	protein_coding	-3,08050323	5,9021E-30
ENSG00000196850	PPTC7	protein_coding	-1,28719243	6,0299E-30
ENSG00000130449	ZSWIM6	protein_coding	-1,41356541	7,4381E-30
ENSG00000134716	CYP2J2	protein_coding	-2,28619789	9,9177E-30
ENSG00000174437	ATP2A2	protein_coding	-1,37914735	1,1106E-29
ENSG00000177732	SOX12	protein_coding	-1,06580324	2,3168E-29
ENSG00000092969	TGFB2	protein_coding	-3,49709192	4,9249E-29
ENSG00000137261	KIAA0319	protein_coding	-2,81272842	1,0329E-28
ENSG00000196510	ANAPC7	protein_coding	-1,28672308	1,6044E-28
ENSG00000081803	CADPS2	protein_coding	-1,52725802	1,9669E-28
ENSG00000029153	ARNTL2	protein_coding	-2,16102474	2,3281E-28

ENSG00000117114	ADGRL2	protein_coding	-4,96470736	4,9515E-28
ENSG00000075651	PLD1	protein_coding	-3,74711412	5,4877E-28
ENSG00000111331	OAS3	protein_coding	-1,20255351	1,1183E-27
ENSG00000178401	DNAJC22	protein_coding	-3,32415941	1,5196E-27
ENSG00000148700	ADD3	protein_coding	-3,74305081	2,6642E-27
ENSG00000106804	C5	protein_coding	-2,43678801	2,9671E-27
ENSG00000165025	SYK	protein_coding	-2,26085402	3,0191E-27
ENSG00000163293	NIPAL1	protein_coding	-1,46657695	3,1334E-27
ENSG00000088833	NSFL1C	protein_coding	-1,19113685	4,1475E-27
ENSG00000105329	TGFB1	protein_coding	-1,32405475	4,3143E-27
ENSG00000136848	DAB2IP	protein_coding	-1,24059239	4,3143E-27
ENSG00000091409	ITGA6	protein_coding	-4,0118372	4,7743E-27
ENSG00000168350	DEGS2	protein_coding	-3,22368609	5,3849E-27
ENSG00000150938	CRIM1	protein_coding	-1,37623407	1,0193E-26
ENSG00000274020	LINC01138	lncRNA	-5,52954225	2,7502E-26
ENSG00000075275	CELSR1	protein_coding	-1,01859671	2,9366E-26
ENSG00000139684	ESD	protein_coding	-1,21219124	3,7158E-26
ENSG00000174808	BTC	protein_coding	-2,8941071	4,3486E-26
ENSG00000243927	MRPS6	protein_coding	-1,19195177	8,5729E-26
ENSG00000171798	KNDC1	protein_coding	-1,69114267	1,5773E-25
ENSG00000182809	CRIP2	protein_coding	-1,01529379	1,6824E-25
ENSG00000175356	SCUBE2	protein_coding	-3,09999451	1,7015E-25
ENSG00000079819	EPB41L2	protein_coding	-1,90718991	2,2901E-25
ENSG00000145284	SCD5	protein_coding	-2,14213214	2,9089E-25
ENSG00000111058	ACSS3	protein_coding	-1,81163912	4,0125E-25
ENSG00000135549	PKIB	protein_coding	-1,23227918	4,0125E-25
ENSG00000127152	BCL11B	protein_coding	-1,25095094	4,9568E-25
ENSG00000006831	ADIPOR2	protein_coding	-1,1052932	5,7247E-25
ENSG00000159128	IFNGR2	protein_coding	-1,44041955	8,6152E-25
ENSG00000102038	SMARCA1	protein_coding	-3,33717579	1,1118E-24
ENSG00000111229	ARPC3	protein_coding	-1,37853159	1,2163E-24
ENSG00000114993	RTKN	protein_coding	-1,23081692	1,2498E-24
ENSG00000185432	METTL7A	protein_coding	-1,9760744	1,7776E-24
ENSG00000135127	BICDL1	protein_coding	-1,2208223	3,573E-24
ENSG00000157538	VPS26C	protein_coding	-1,10261617	4,0553E-24
ENSG00000143013	LMO4	protein_coding	-1,73644607	7,2304E-24
ENSG00000197702	PARVA	protein_coding	-1,13536607	9,0066E-24
ENSG00000159267	HLCS	protein_coding	-1,24839356	1,4831E-23
ENSG00000101115	SALL4	protein_coding	-2,00994485	3,9673E-23
ENSG00000125898	FAM110A	protein_coding	-1,24951429	6,1378E-23
ENSG00000197892	KIF13B	protein_coding	-1,31140946	6,5731E-23
ENSG00000173706	HEG1	protein_coding	-2,83092211	6,6404E-23
ENSG00000183049	CAMK1D	protein_coding	-2,25755632	7,2885E-23
ENSG00000138131	LOXL4	protein_coding	-2,83094498	8,3931E-23
ENSG00000182871	COL18A1	protein_coding	-1,01459625	8,8847E-23
ENSG00000111012	CYP27B1	protein_coding	-2,93088489	9,7654E-23
ENSG00000001561	ENPP4	protein_coding	-1,8620264	1,4283E-22
ENSG00000237945	LINC00649	lncRNA	-2,67180754	1,552E-22
ENSG00000184500	PROS1	protein_coding	-3,9679299	2,4751E-22
ENSG00000163701	IL17RE	protein_coding	-2,49896315	2,9382E-22
ENSG00000135119	RNFT2	protein_coding	-1,34445402	3,053E-22
ENSG00000064195	DLX3	protein_coding	-1,87090642	3,5437E-22
ENSG00000107819	SFXN3	protein_coding	-1,73201763	4,5193E-22
ENSG00000165983	PTER	protein_coding	-1,48230726	5,02E-22
ENSG00000108679	LGALS3BP	protein_coding	-1,84800576	6,0965E-22
ENSG00000064666	CNN2	protein_coding	-1,03729807	8,1517E-22
ENSG00000138759	FRAS1	protein_coding	-2,98876327	1,0427E-21
ENSG00000136854	STXBP1	protein_coding	-2,3191948	1,9739E-21
ENSG00000182985	CADM1	protein_coding	-1,26769312	2,6715E-21
ENSG00000177096	PHETA2	protein_coding	-4,0633141	3,0512E-21
ENSG00000122970	IFT81	protein_coding	-1,33069028	4,8889E-21
ENSG00000091490	SEL1L3	protein_coding	-1,28751881	5,3398E-21
ENSG00000163545	NUAK2	protein_coding	-1,61459537	6,9323E-21
ENSG00000197043	ANXA6	protein_coding	-1,52823226	7,4051E-21
ENSG00000073060	SCARB1	protein_coding	-1,22385191	1,1472E-20
ENSG00000127129	EDN2	protein_coding	-2,81240943	1,1916E-20
ENSG00000143153	ATP1B1	protein_coding	-1,39191129	1,4191E-20
ENSG00000120896	SORBS3	protein_coding	-1,67148982	1,5151E-20
ENSG00000176788	BASP1	protein_coding	-1,46941004	1,6297E-20
ENSG00000073712	FERMT2	protein_coding	-3,27629886	1,6589E-20
ENSG00000205726	ITSN1	protein_coding	-1,12398299	2,472E-20
ENSG00000106070	GRB10	protein_coding	-1,90561815	4,3251E-20
ENSG00000171236	LRG1	protein_coding	-1,63342716	4,6632E-20
ENSG00000184441		lncRNA	-1,23699956	4,8591E-20
ENSG00000106571	GLI3	protein_coding	-1,94955291	4,9519E-20
ENSG00000205002	AARD	protein_coding	-7,39663858	9,2303E-20
ENSG00000198780	FAM169A	protein_coding	-2,08151389	1,0151E-19
ENSG00000100558	PLEK2	protein_coding	-2,91634285	1,978E-19
ENSG00000125170	DOK4	protein_coding	-1,96524605	2,0582E-19
ENSG00000077782	FGFR1	protein_coding	-1,65160009	2,5485E-19
ENSG00000140044	JDP2	protein_coding	-1,82164494	2,8756E-19
ENSG00000166398	GARRE1	protein_coding	-1,20929334	3,1986E-19
ENSG00000188064	WNT7B	protein_coding	-1,08714051	3,8585E-19
ENSG00000162409	PRKAA2	protein_coding	-6,24357523	3,8994E-19
ENSG00000156711	MAPK13	protein_coding	-1,14198459	5,7548E-19
ENSG00000198133	TMEM229B	protein_coding	-1,63355059	6,015E-19
ENSG00000109265	CRACD	protein_coding	-2,30733979	8,2795E-19
ENSG00000187889	FYB2	protein_coding	-6,32155427	1,2495E-18
ENSG00000166886	NAB2	protein_coding	-1,19041401	1,2689E-18
ENSG00000145675	PIK3R1	protein_coding	-1,02806629	1,4584E-18

ENSG00000233930	KRTAP5-AS1	lncRNA	-1,70417517	1,6693E-18
ENSG00000185920	PTCH1	protein_coding	-1,9746419	1,8679E-18
ENSG00000154553	PDLIM3	protein_coding	-2,87352968	2,0596E-18
ENSG00000164294	GPX8	protein_coding	-1,41176017	3,4107E-18
ENSG00000115596	WNT6	protein_coding	-3,87518144	3,9049E-18
ENSG00000247315	ZCCHC3	protein_coding	-1,18718881	6,6379E-18
ENSG00000165410	CFL2	protein_coding	-2,57332918	8,1517E-18
ENSG00000116574	RHOU	protein_coding	-1,08540735	1,7995E-17
ENSG00000151690	MFSD6	protein_coding	-1,11931591	1,8122E-17
ENSG00000118276	B4GALT6	protein_coding	-3,6076367	2,2117E-17
ENSG00000135063	FAM189A2	protein_coding	-2,42864481	2,5034E-17
ENSG00000151718	WWC2	protein_coding	-1,15432098	3,2233E-17
ENSG00000127954	STEAP4	protein_coding	-2,60600865	3,694E-17
ENSG00000169129	AFAP1L2	protein_coding	-3,38268187	3,9489E-17
ENSG00000134533	RERG	protein_coding	-1,01625281	5,3758E-17
ENSG00000069966	GNB5	protein_coding	-1,06285294	6,3716E-17
ENSG00000058404	CAMK2B	protein_coding	-2,94563167	7,0019E-17
ENSG00000167528	ZNF641	protein_coding	-1,56115757	7,6001E-17
ENSG00000188153	COL4A5	protein_coding	-1,66298889	7,6344E-17
ENSG00000088826	SMOX	protein_coding	-1,39667427	8,2469E-17
ENSG00000272405		lncRNA	-1,32000064	1,22E-16
ENSG00000226777	FAM30A	lncRNA	-2,66029789	1,5787E-16
ENSG00000251129	LINC02506	lncRNA	-3,03996146	1,7204E-16
ENSG00000286058		lncRNA	-1,73011183	2,0261E-16
ENSG00000101255	TRIB3	protein_coding	-1,10087343	2,2228E-16
ENSG00000251493	FOXD1	protein_coding	-2,43836379	2,5742E-16
ENSG00000111231	GPN3	protein_coding	-1,19809915	3,3281E-16
ENSG00000115919	KYNU	protein_coding	-1,13978636	4,0025E-16
ENSG00000182240	BACE2	protein_coding	-2,11056808	4,3055E-16
ENSG00000171992	SYNPO	protein_coding	-2,04934928	5,9174E-16
ENSG00000169926	KLF13	protein_coding	-1,57814174	6,0289E-16
ENSG00000140284	SLC27A2	protein_coding	-1,28982726	6,7297E-16
ENSG00000113532	ST8SIA4	protein_coding	-1,55459977	7,9563E-16
ENSG00000114450	GNB4	protein_coding	-3,11774718	8,0489E-16
ENSG00000125841	NRSN2	protein_coding	-1,03006479	8,1481E-16
ENSG00000214357	NEURL1B	protein_coding	-1,20131474	1,0624E-15
ENSG00000177570	SAMD12	protein_coding	-1,79728435	1,1612E-15
ENSG00000147255	IGSF1	protein_coding	-1,99473416	1,6322E-15
ENSG00000254535	PABPC4L	protein_coding	-3,6497848	2,1149E-15
ENSG00000132481	TRIM47	protein_coding	-1,27103394	2,2544E-15
ENSG00000185917	SETD4	protein_coding	-1,14717142	2,52E-15
ENSG00000197747	S100A10	protein_coding	-1,03649734	3,0959E-15
ENSG00000115380	EFEMP1	protein_coding	-2,13675289	5,0768E-15
ENSG00000163069	SGCB	protein_coding	-1,20157347	5,6633E-15
ENSG00000175894	TSPEAR	protein_coding	-5,05212346	6,3778E-15
ENSG00000118762	PKD2	protein_coding	-1,13919449	6,4227E-15
ENSG00000003400	CASP10	protein_coding	-2,34875085	8,6394E-15
ENSG00000226067	LINC00623	lncRNA	-4,37547828	9,402E-15
ENSG00000171617	ENC1	protein_coding	-1,05165407	9,4675E-15
ENSG00000137462	TLR2	protein_coding	-3,13125182	1,0305E-14
ENSG00000117525	F3	protein_coding	-1,96861729	1,1624E-14
ENSG00000159733	ZFYVE28	protein_coding	-1,34768662	1,2332E-14
ENSG00000144824	PHLDB2	protein_coding	-1,90810281	1,4213E-14
ENSG00000140022	STON2	protein_coding	-1,16208719	1,4835E-14
ENSG00000166426	CRABP1	protein_coding	-2,17175787	1,6187E-14
ENSG00000148180	GSN	protein_coding	-1,07780701	1,889E-14
ENSG00000151322	NPAS3	protein_coding	-5,79750829	2,0298E-14
ENSG00000070404	FSTL3	protein_coding	-1,00554105	2,1508E-14
ENSG00000134755	DSC2	protein_coding	-1,43421778	4,0767E-14
ENSG00000196092	PAX5	protein_coding	-1,76527667	4,9126E-14
ENSG00000147256	ARHGAP36	protein_coding	-2,37695188	5,0931E-14
ENSG00000100767	PAPLN	protein_coding	-1,32719983	6,8575E-14
ENSG00000185305	ARL15	protein_coding	-1,58703412	6,9275E-14
ENSG00000163347	CLDN1	protein_coding	-2,68094747	7,0839E-14
ENSG00000145779	TNFAIP8	protein_coding	-1,2971208	7,5514E-14
ENSG00000109819	PPARGC1A	protein_coding	-2,50497935	9,2587E-14
ENSG00000148677	ANKRD1	protein_coding	-3,84887062	1,0533E-13
ENSG00000235092	ID2-AS1	lncRNA	-2,07754721	1,0647E-13
ENSG00000082781	ITGB5	protein_coding	-1,05210222	1,4546E-13
ENSG00000129675	ARHGEF6	protein_coding	-2,23613454	1,655E-13
ENSG00000196132	MYT1	protein_coding	-3,00367401	1,6727E-13
ENSG00000237356		lncRNA	-1,69379951	1,7814E-13
ENSG00000130598	TNNI2	protein_coding	-3,4638355	1,8446E-13
ENSG00000138678	GPAT3	protein_coding	-1,44612342	2,1179E-13
ENSG00000120910	PPP3CC	protein_coding	-1,30019295	2,1591E-13
ENSG00000162891	IL20	protein_coding	-3,21725431	2,2358E-13
ENSG00000114541	FRMD4B	protein_coding	-1,70076337	2,2503E-13
ENSG00000102098	SCML2	protein_coding	-1,13848953	2,3135E-13
ENSG00000277363	SRCIN1	protein_coding	-1,04337698	2,3733E-13
ENSG00000248515		lncRNA	-3,72711524	2,4756E-13
ENSG00000106123	EPHB6	protein_coding	-2,87094383	2,6452E-13
ENSG00000120322	PCDHB8	protein_coding	-1,03939715	2,6643E-13
ENSG00000124225	PMEPA1	protein_coding	-1,04335552	3,0183E-13
ENSG00000234771	SLC25A25-AS1	lncRNA	-1,29491286	3,4788E-13
ENSG00000064655	EYA2	protein_coding	-2,01506521	3,587E-13
ENSG00000100842	EFS	protein_coding	-2,08059362	3,7044E-13
ENSG00000223960	CHROMR	lncRNA	-1,22111307	3,9256E-13
ENSG00000115902	SLC1A4	protein_coding	-2,18345814	4,1469E-13
ENSG00000104518	GSDMD	protein_coding	-2,97249173	4,2306E-13
ENSG00000144677	CTDSPL	protein_coding	-1,19410072	4,2306E-13

ENSG00000128567	PODXL	protein_coding	-2,02796232	4,6013E-13
ENSG00000137267	TUBB2A	protein_coding	-1,27824603	4,7063E-13
ENSG00000152217	SETBP1	protein_coding	-1,13411972	5,1863E-13
ENSG00000165816	VWA2	protein_coding	-3,38463043	5,2238E-13
ENSG00000092068	SLC7A8	protein_coding	-3,77071656	6,9761E-13
ENSG00000174032	SLC25A30	protein_coding	-1,09514362	7,116E-13
ENSG00000196159	FAT4	protein_coding	-1,60311148	7,3285E-13
ENSG00000078900	TP73	protein_coding	-3,78016347	8,608E-13
ENSG00000116678	LEPR	protein_coding	-2,1988538	9,822E-13
ENSG00000055732	MCOLN3	protein_coding	-2,49028951	1,0295E-12
ENSG00000174827	PDZK1	protein_coding	-2,36519225	1,4334E-12
ENSG00000163291	PAQR3	protein_coding	-1,0159005	1,5823E-12
ENSG00000205189	ZBTB10	protein_coding	-2,72439809	1,7254E-12
ENSG00000135916	ITM2C	protein_coding	-1,1748647	2,1096E-12
ENSG00000123643	SLC36A1	protein_coding	-1,01007073	2,7436E-12
ENSG00000108846	ABCC3	protein_coding	-1,22536235	3,3855E-12
ENSG00000169862	CTNND2	protein_coding	-1,37879436	3,6107E-12
ENSG00000196154	S100A4	protein_coding	-2,11185702	3,7886E-12
ENSG00000173083	HPSE	protein_coding	-1,66344106	4,461E-12
ENSG00000196189	SEMA4A	protein_coding	-1,17971793	4,4619E-12
ENSG00000169504	CLIC4	protein_coding	-2,53783098	4,5373E-12
ENSG00000205517	RGL3	protein_coding	-1,7186292	5,1044E-12
ENSG00000011028	MRC2	protein_coding	-1,14153145	5,4623E-12
ENSG00000073282	TP63	protein_coding	-2,84182129	7,1364E-12
ENSG00000118402	ELOVL4	protein_coding	-1,28447619	1,1655E-11
ENSG00000087494	PTHLH	protein_coding	-5,46621635	1,4083E-11
ENSG00000240891	PLCXD2	protein_coding	-2,63842726	1,5876E-11
ENSG00000285867		lncRNA	-2,41215556	1,8322E-11
ENSG00000246695	RASSF8-AS1	lncRNA	-2,55141191	1,8427E-11
ENSG00000044459	CNTLN	protein_coding	-2,32770853	1,8902E-11
ENSG00000110888	CAPRIN2	protein_coding	-1,30904337	2,3735E-11
ENSG00000156011	PSD3	protein_coding	-1,36016418	2,4956E-11
ENSG00000247828	TMEM161B-AS1	lncRNA	-1,06149919	2,9547E-11
ENSG00000162174	ASRGL1	protein_coding	-1,69529524	2,9741E-11
ENSG00000133401	PDZD2	protein_coding	-1,98898656	3,2154E-11
ENSG00000273706	LHX1	protein_coding	-1,64571563	3,3408E-11
ENSG00000049449	RCN1	protein_coding	-1,17160673	4,6778E-11
ENSG00000103196	CRISPLD2	protein_coding	-1,31679037	5,0127E-11
ENSG00000155621	C9orf85	protein_coding	-1,10422896	6,0519E-11
ENSG00000213937	CLDN9	protein_coding	-1,82041495	6,4127E-11
ENSG00000079215	SLC1A3	protein_coding	-7,54793827	7,4068E-11
ENSG00000169403	PTAFR	protein_coding	-1,56257618	7,4098E-11
ENSG00000138772	ANXA3	protein_coding	-2,38702177	7,628E-11
ENSG00000187955	COL14A1	protein_coding	-4,49653965	8,0101E-11
ENSG00000100077	GRK3	protein_coding	-1,12091167	8,2289E-11
ENSG00000122786	CALD1	protein_coding	-2,88989779	8,8377E-11
ENSG00000058866	DGKG	protein_coding	-1,43215604	9,9308E-11
ENSG00000243701	DUBR	lncRNA	-1,34186242	1,3472E-10
ENSG00000167693	NXN	protein_coding	-1,07857874	1,3931E-10
ENSG00000274265		lncRNA	-8,3942803	1,4415E-10
ENSG00000188818	ZDHHC11	protein_coding	-1,29180912	1,4974E-10
ENSG00000109586	GALNT7	protein_coding	-1,77517382	1,5075E-10
ENSG00000177283	FZD8	protein_coding	-1,23710169	1,5075E-10
ENSG00000136052	SLC41A2	protein_coding	-1,01343788	1,8162E-10
ENSG00000170919	TPT1-AS1	lncRNA	-1,30782928	2,0542E-10
ENSG00000135643	KCNMB4	protein_coding	-3,36636374	2,4871E-10
ENSG00000153404	PLEKHG4B	protein_coding	-2,84384911	2,592E-10
ENSG00000198689	SLC9A6	protein_coding	-1,10556095	2,6822E-10
ENSG00000176399	DMRTA1	protein_coding	-1,04048085	3,3771E-10
ENSG00000249242	TMEM150C	protein_coding	-1,3714784	3,4686E-10
ENSG00000150676	CCDC83	protein_coding	-1,60427755	3,5648E-10
ENSG00000275557		lncRNA	-8,63917553	3,7891E-10
ENSG00000184584	STING1	protein_coding	-2,58043237	4,0541E-10
ENSG00000135439	AGAP2	protein_coding	-1,31535145	4,1641E-10
ENSG00000143845	ETNK2	protein_coding	-2,22507383	4,3668E-10
ENSG00000149269	PAK1	protein_coding	-1,41160473	6,054E-10
ENSG00000188910	GJB3	protein_coding	-2,77607902	6,4524E-10
ENSG00000139044	B4GALNT3	protein_coding	-3,74463557	7,3449E-10
ENSG00000237004	ZNRF2P1	transcribed_processed pseudogene	-1,20943216	7,6578E-10
ENSG00000170293	CMTM8	protein_coding	-1,91786131	8,1393E-10
ENSG00000155961	RAB39B	protein_coding	-1,67902142	8,7074E-10
ENSG00000150456	EEF1AKMT1	protein_coding	-1,15907623	9,4914E-10
ENSG00000108852	MPP2	protein_coding	-1,20128123	1,0583E-09
ENSG00000106733	NMRK1	protein_coding	-1,26126682	1,0763E-09
ENSG00000134595	SOX3	protein_coding	-1,78124766	1,0983E-09
ENSG00000107954	NEURL1	protein_coding	-2,15720742	1,1061E-09
ENSG00000224903	RNF32-AS1	lncRNA	-1,85920189	1,1373E-09
ENSG00000234284	ZNF879	protein_coding	-1,53640045	1,2052E-09
ENSG00000137843	PAK6	protein_coding	-2,14957934	1,2529E-09
ENSG00000229953		lncRNA	-1,22934249	1,3882E-09
ENSG00000135519	KCNH3	protein_coding	-1,55012447	1,422E-09
ENSG00000186951	PPARA	protein_coding	-1,12242809	1,4894E-09
ENSG00000148082	SHC3	protein_coding	-1,81439869	1,7108E-09
ENSG00000143816	WNT9A	protein_coding	-1,68247525	2,3601E-09
ENSG00000138172	CALHM2	protein_coding	-1,22555462	2,8243E-09
ENSG00000253125		lncRNA	-1,20279648	2,8243E-09
ENSG00000146094	DOK3	protein_coding	-1,12918766	3,2082E-09
ENSG00000138639	ARHGAP24	protein_coding	-3,19749999	3,5023E-09

ENSG00000088726	TMEM40	protein_coding	-3,0104973	3,6925E-09
ENSG00000100167	SEPTIN3	protein_coding	-1,36398418	3,9466E-09
ENSG00000172379	ARNT2	protein_coding	-1,58857737	3,9701E-09
ENSG00000172164	SNTB1	protein_coding	-2,58222725	4,5786E-09
ENSG00000169071	ROR2	protein_coding	-2,84279442	4,6352E-09
ENSG00000156103	MMP16	protein_coding	-1,63369335	5,0536E-09
ENSG00000131711	MAP1B	protein_coding	-1,29906262	5,3559E-09
ENSG00000156689	GLYATL2	protein_coding	-8,3019027	5,8577E-09
ENSG00000259953		lncRNA	-1,61456687	5,9539E-09
ENSG00000101871	MID1	protein_coding	-2,42623867	6,3947E-09
ENSG00000167081	PBX3	protein_coding	-1,40094312	6,8762E-09
ENSG00000075886	TUBA3D	protein_coding	-3,2007284	7,4203E-09
ENSG00000198934	MAGEE1	protein_coding	-1,19598114	7,8106E-09
ENSG00000175928	LRRN1	protein_coding	-2,53588327	8,4731E-09
ENSG00000119514	GALNT12	protein_coding	-2,25191657	9,1133E-09
ENSG00000228649	SNHG26	lncRNA	-1,37620318	9,5069E-09
ENSG00000137338	PGBD1	protein_coding	-1,71040679	9,8971E-09
ENSG00000225377	NRSN2-AS1	lncRNA	-1,1335939	1,0847E-08
ENSG00000172716	SLFN11	protein_coding	-7,84879868	1,1231E-08
ENSG00000120693	SMAD9	protein_coding	-2,85657384	1,3646E-08
ENSG00000181418	DDN	protein_coding	-2,45054245	1,6011E-08
ENSG00000080200	CRYBG3	protein_coding	-2,02466791	1,7235E-08
ENSG00000286342		lncRNA	-3,69280768	1,8162E-08
ENSG00000198624	CCDC69	protein_coding	-1,04906615	2,068E-08
ENSG00000101298	SNPH	protein_coding	-4,82658758	2,1028E-08
ENSG00000137821	LRRC49	protein_coding	-1,13026781	2,1585E-08
ENSG00000145757	SPATA9	protein_coding	-5,13616415	2,2599E-08
ENSG00000124749	COL21A1	protein_coding	-3,92042299	2,3818E-08
ENSG00000154734	ADAMTS1	protein_coding	-3,50759073	2,7945E-08
ENSG00000184304	PRKD1	protein_coding	-2,16944729	2,8366E-08
ENSG00000115468	EFHD1	protein_coding	-1,91949886	2,9712E-08
ENSG00000147650	LRP12	protein_coding	-1,02799098	3,0653E-08
ENSG00000077522	ACTN2	protein_coding	-2,60393004	3,0956E-08
ENSG00000104154	SLC30A4	protein_coding	-1,33642964	3,3506E-08
ENSG00000241837	ATP5PO	protein_coding	-1,10075783	4,1354E-08
ENSG00000104755	ADAM2	protein_coding	-6,05747302	4,2224E-08
ENSG00000183145	RIPPLY3	protein_coding	-1,58989146	4,4156E-08
ENSG00000180730	SHISA2	protein_coding	-2,72801646	5,321E-08
ENSG00000092295	TGM1	protein_coding	-1,15539866	5,6981E-08
ENSG00000254827	SLC22A18AS	protein_coding	-2,29170027	5,7444E-08
ENSG00000272068	BCAN-AS1	lncRNA	-1,07697666	6,0589E-08
ENSG00000162782	TDRD5	protein_coding	-1,10582352	6,2685E-08
ENSG00000056558	TRAF1	protein_coding	-2,90940856	6,6456E-08
ENSG00000180269	GPR139	protein_coding	-2,77000019	6,7071E-08
ENSG00000137745	MMP13	protein_coding	-2,54070269	6,8666E-08
ENSG00000176595	KBTBD11	protein_coding	-1,48182075	8,0277E-08
ENSG00000122025	FLT3	protein_coding	-4,70279388	8,4146E-08
ENSG00000121753	ADGRB2	protein_coding	-1,29297126	8,5979E-08
ENSG00000269958		lncRNA	-1,03664106	8,6389E-08
ENSG00000149289	ZC3H12C	protein_coding	-1,20934057	8,6977E-08
ENSG00000132932	ATP8A2	protein_coding	-5,37509141	9,9106E-08
ENSG00000214595	EML6	protein_coding	-1,76663614	1,0615E-07
ENSG00000171759	PAH	protein_coding	-2,6284712	1,1281E-07
ENSG00000277117		protein_coding	-1,38922074	1,1331E-07
ENSG00000184985	SORCS2	protein_coding	-1,59428702	1,2492E-07
ENSG00000004948	CALCR	protein_coding	-3,11284084	1,3389E-07
ENSG00000109321	AREG	protein_coding	-2,36246849	1,3613E-07
ENSG00000184261	KCNK12	protein_coding	-3,01208836	1,3995E-07
ENSG00000250303	LINC02762	lncRNA	-1,17488647	1,4263E-07
ENSG00000125850	OVOL2	protein_coding	-1,3523198	1,4361E-07
ENSG00000118507	AKAP7	protein_coding	-2,05578506	1,7146E-07
ENSG00000172478	MAB21L4	protein_coding	-1,56948663	1,9008E-07
ENSG00000280649		TEC	-7,70149672	1,997E-07
ENSG00000171310	CHST11	protein_coding	-2,38054788	2,02E-07
ENSG00000151320	AKAP6	protein_coding	-2,18084702	2,048E-07
ENSG00000125378	BMP4	protein_coding	-1,37151343	2,2647E-07
ENSG00000106772	PRUNE2	protein_coding	-6,81773058	2,3991E-07
ENSG00000174469	CNTNAP2	protein_coding	-1,96782327	2,4736E-07
ENSG00000259527	LINC00052	lncRNA	-3,03405196	2,6056E-07
ENSG00000126562	WNK4	protein_coding	-1,67306202	2,6345E-07
ENSG00000160145	KALRN	protein_coding	-1,85177045	2,6385E-07
ENSG00000169621	APLF	protein_coding	-2,28465147	2,6523E-07
ENSG00000151883	PARP8	protein_coding	-1,65582699	2,7306E-07
ENSG00000182578	CSF1R	protein_coding	-3,23854133	3,0156E-07
ENSG00000084636	COL16A1	protein_coding	-1,3334633	3,2977E-07
ENSG00000281571		TEC	-5,61136635	3,44E-07
ENSG00000109113	RAB34	protein_coding	-3,87064913	3,4662E-07
ENSG00000185158	LRRC37B	protein_coding	-1,08264866	3,7442E-07
ENSG00000188707	ZBED6CL	protein_coding	-1,0896632	4,2502E-07
ENSG00000144290	SLC4A10	protein_coding	-2,13419434	4,3676E-07
ENSG00000121454	LHX4	protein_coding	-1,22259666	4,4289E-07
ENSG00000159110	IFNAR2	protein_coding	-1,12315578	4,4524E-07
ENSG00000224842		lncRNA	-2,21040806	4,8133E-07
ENSG00000197444	OGDHL	protein_coding	-1,16589539	5,3298E-07
ENSG00000206561	COLQ	protein_coding	-2,75117331	5,5805E-07
ENSG00000172137	CALB2	protein_coding	-4,40632416	6,4212E-07
ENSG00000280287		TEC	-1,23941777	7,3194E-07
ENSG00000278948		TEC	-1,11193711	8,1803E-07
ENSG00000138347	MYPN	protein_coding	-4,49049432	8,7328E-07
ENSG00000152669	CCNO	protein_coding	-2,78256643	9,1204E-07

ENSG00000188549	CCDC9B	protein_coding	-1,08855514	9,5636E-07
ENSG00000173930	SLCO4C1	protein_coding	-2,18089019	9,7047E-07
ENSG00000204856	FAM216A	protein_coding	-1,10222667	1,0796E-06
ENSG00000107614	TRDMT1	protein_coding	-1,11211	1,1736E-06
ENSG00000279662		TEC	-1,77203027	1,1794E-06
ENSG00000170006	TMEM154	protein_coding	-1,52097842	1,189E-06
ENSG00000172403	SYNPO2	protein_coding	-3,08641239	1,3106E-06
ENSG00000174607	UGT8	protein_coding	-1,77252571	1,3798E-06
ENSG00000112183	RBM24	protein_coding	-1,02295156	1,4606E-06
ENSG00000197405	C5AR1	protein_coding	-1,28985766	1,5897E-06
ENSG00000236975	LINC02814	lncRNA	-4,90845694	1,6653E-06
ENSG00000118515	SGK1	protein_coding	-2,04398074	1,6947E-06
ENSG00000225968	ELFN1	protein_coding	-2,20514408	1,7424E-06
ENSG00000136237	RAPGEF5	protein_coding	-1,10742863	1,941E-06
ENSG00000112320	SOBP	protein_coding	-1,99274117	1,9622E-06
ENSG00000120093	HOXB3	protein_coding	-1,50525632	2,1533E-06
ENSG00000138640	FAM13A	protein_coding	-1,33431196	2,4156E-06
ENSG00000140564	FURIN	protein_coding	-1,9063586	2,4352E-06
ENSG00000276850		lncRNA	-3,96219165	2,4528E-06
ENSG00000197415	VEPH1	protein_coding	-1,33410238	2,4889E-06
ENSG00000165730	STOX1	protein_coding	-1,18406268	2,5022E-06
ENSG00000183401	CCDC159	protein_coding	-1,1854288	2,538E-06
ENSG00000164241	C5orf63	protein_coding	-1,0420153	2,5604E-06
ENSG00000043591	ADRB1	protein_coding	-2,36446935	2,6136E-06
ENSG00000143546	S100A8	protein_coding	-3,20618279	2,6355E-06
ENSG00000226945		processed_pseudogene	-3,1669683	2,6736E-06
ENSG00000228672	PROB1	protein_coding	-1,57592267	2,7154E-06
ENSG00000173320	STOX2	protein_coding	-1,33359317	2,7969E-06
ENSG00000236081	ELFN1-AS1	lncRNA	-6,41283076	2,8373E-06
ENSG00000106688	SLC1A1	protein_coding	-2,41046937	2,8849E-06
ENSG00000250802	ZBED3-AS1	lncRNA	-1,08891603	2,961E-06
ENSG00000183092	BEGAIN	protein_coding	-1,07320958	3,044E-06
ENSG00000115844	DLX2	protein_coding	-1,63616617	3,2018E-06
ENSG00000125775	SDCBP2	protein_coding	-1,69978347	3,5793E-06
ENSG00000129646	QRICH2	protein_coding	-1,52637709	3,8261E-06
ENSG00000013619	MAMLD1	protein_coding	-1,14592985	3,8959E-06
ENSG00000124343	XG	protein_coding	-2,69275869	4,3787E-06
ENSG00000258526		lncRNA	-1,16895154	5,4091E-06
ENSG00000147234	FRMPD3	protein_coding	-2,31024359	6,0955E-06
ENSG00000145246	ATP10D	protein_coding	-1,20298047	6,2922E-06
ENSG00000187950	OVCH1	protein_coding	-6,1999338	6,4356E-06
ENSG00000133962	CATSPERB	protein_coding	-1,30304511	6,5129E-06
ENSG00000188959	C9orf152	protein_coding	-1,68887052	6,9168E-06
ENSG00000254416	LINC02732	lncRNA	-2,97533408	7,076E-06
ENSG00000183111	ARHGEF37	protein_coding	-1,15036065	7,1136E-06
ENSG00000286912		lncRNA	-1,57945151	7,4991E-06
ENSG00000100344	PNPLA3	protein_coding	-1,28090513	8,0132E-06
ENSG00000241399	CD302	protein_coding	-1,98730379	8,4199E-06
ENSG00000153294	ADGRF4	protein_coding	-1,27795225	9,351E-06
ENSG00000157470	FAM81A	protein_coding	-1,04426794	9,351E-06
ENSG00000234602	MCIDAS	protein_coding	-2,22290631	9,8172E-06
ENSG00000273760		lncRNA	-4,26077673	9,8746E-06
ENSG00000205018		lncRNA	-1,9560936	1,0655E-05
ENSG00000234869		lncRNA	-1,29347079	1,1701E-05
ENSG00000115935	WIPF1	protein_coding	-2,71314771	1,1845E-05
ENSG00000165474	GJB2	protein_coding	-1,99959008	1,2317E-05
ENSG00000003137	CYP26B1	protein_coding	-1,49242641	1,2777E-05
ENSG00000175697	GPR156	protein_coding	-2,47635407	1,2912E-05
ENSG00000086730	LAT2	protein_coding	-1,43886493	1,3319E-05
ENSG00000162894	FCMR	protein_coding	-1,49410571	1,359E-05
ENSG00000164850	GPER1	protein_coding	-1,89422328	1,4808E-05
ENSG00000143512	HHIPL2	protein_coding	-1,85080682	1,5357E-05
ENSG00000197847	SLC22A20P	transcribed_unitary pseudogene	-1,14736522	1,5564E-05
ENSG00000135824	RGS8	protein_coding	-2,42381479	1,7633E-05
ENSG00000196476	C20orf96	protein_coding	-1,04686234	1,9244E-05
ENSG00000166407	LMO1	protein_coding	-3,39735888	2,0073E-05
ENSG00000144452	ABCA12	protein_coding	-1,90677359	2,063E-05
ENSG00000170439	METTL7B	protein_coding	-1,10709843	2,119E-05
ENSG00000175093	SPSB4	protein_coding	-1,5746301	2,1578E-05
ENSG00000069188	SDK2	protein_coding	-1,685317	2,1591E-05
ENSG00000105549	THEG	protein_coding	-3,5517531	2,3066E-05
ENSG00000227507	LTB	protein_coding	-2,05570218	2,3958E-05
ENSG00000248323	LUCAT1	lncRNA	-4,13112997	2,7253E-05
ENSG00000165188	RNF183	protein_coding	-5,1291759	2,7663E-05
ENSG00000169594	BNC1	protein_coding	-4,69276974	3,057E-05
ENSG00000138587	MNS1	protein_coding	-1,45950199	3,1512E-05
ENSG00000223808		lncRNA	-1,39237841	3,2258E-05
ENSG00000104368	PLAT	protein_coding	-5,74461278	3,2395E-05
ENSG00000261065		lncRNA	-1,97756404	3,3249E-05
ENSG00000189283	FHIT	protein_coding	-1,2428409	3,4228E-05
ENSG00000108813	DLX4	protein_coding	-1,53695282	3,4295E-05
ENSG00000168671	UGT3A2	protein_coding	-6,44060675	3,6555E-05
ENSG00000154310	TNIK	protein_coding	-3,17842891	3,758E-05
ENSG00000111339	ART4	protein_coding	-3,9078627	3,7919E-05
ENSG00000154316	TDH	transcribed_unitary pseudogene	-1,47692623	3,8843E-05
ENSG00000147883	CDKN2B	protein_coding	-1,02987866	4,3559E-05
ENSG00000222035	KIAA2012-AS1	lncRNA	-6,73801469	4,3645E-05
ENSG00000148468	FAM171A1	protein_coding	-1,54176876	4,4424E-05

ENSG00000288658		protein_coding	-2,62282396	4,6338E-05
ENSG00000228340	MIR646HG	lncRNA	-1,13582447	5,0222E-05
ENSG00000227825	SLC9A7P1	transcribed_processed pseudogene	-6,74957666	5,0501E-05
ENSG00000261754		lncRNA	-2,88421227	5,3101E-05
ENSG00000144331	ZNF385B	protein_coding	-5,22276836	5,3865E-05
ENSG00000245213		lncRNA	-1,23895617	5,5924E-05
ENSG00000105784	RUNDC3B	protein_coding	-1,73957364	5,7109E-05
ENSG00000077063	CTTNBP2	protein_coding	-2,9885219	5,7948E-05
ENSG00000215388	ACTG1P3	processed_pseudogene	-3,15238257	5,9882E-05
ENSG00000153208	MERTK	protein_coding	-1,15205731	6,1977E-05
ENSG00000258927		lncRNA	-5,58491678	6,8151E-05
ENSG00000109255	NMU	protein_coding	-2,16400109	6,8569E-05
ENSG00000171033	PKIA	protein_coding	-2,80841209	7,0584E-05
ENSG00000250420	AACSP1	transcribed_unprocessed pseudogene	-2,23444069	7,4537E-05
ENSG00000102271	KLHL4	protein_coding	-3,79982096	8,0211E-05
ENSG00000111186	WNT5B	protein_coding	-5,97709402	8,2201E-05
ENSG00000281404	LINC01176	lncRNA	-1,09164632	8,4966E-05
ENSG00000286733	LINC02348	lncRNA	-2,6217901	8,9539E-05
ENSG00000116329	OPRD1	protein_coding	-2,57709604	9,1232E-05
ENSG00000196405	EVL	protein_coding	-1,59990693	9,2618E-05
ENSG00000280594	BTG3-AS1	lncRNA	-5,59521069	9,8419E-05
ENSG00000128815	WDFY4	protein_coding	-2,73081742	9,97E-05
ENSG00000113083	LOX	protein_coding	-2,90943733	0,0001015
ENSG00000157554	ERG	protein_coding	-2,47957149	0,00010155
ENSG00000132122	SPATA6	protein_coding	-1,66062646	0,0001018
ENSG00000078596	ITM2A	protein_coding	-3,38899695	0,00010626
ENSG00000188886	ASTL	protein_coding	-4,59378465	0,0001063
ENSG00000151164	RAD9B	protein_coding	-2,20595192	0,00010634
ENSG00000178597	PSAPL1	protein_coding	-2,47350988	0,00010917
ENSG00000251867		lncRNA	-2,77329893	0,00011081
ENSG00000056487	PHF21B	protein_coding	-2,02064681	0,00011267
ENSG00000101000	PROCR	protein_coding	-2,05070531	0,00011277
ENSG00000116141	MARK1	protein_coding	-5,31005596	0,0001147
ENSG00000162946	DISC1	protein_coding	-2,06868169	0,00011565
ENSG00000277268	LHX1-DT	lncRNA	-1,80415606	0,00011662
ENSG00000198682	PAPSS2	protein_coding	-1,56990202	0,0001173
ENSG00000125508	SRMS	protein_coding	-1,20033546	0,00012075
ENSG00000163220	S100A9	protein_coding	-1,95994213	0,00012191
ENSG00000267801		lncRNA	-1,16030057	0,00012364
ENSG00000049192	ADAMTS6	protein_coding	-3,89105008	0,00013596
ENSG00000139714	MORN3	protein_coding	-2,60518036	0,00013642
ENSG00000203930	LINC00632	lncRNA	-1,39433168	0,00015589
ENSG00000270115		lncRNA	-1,36506187	0,0001662
ENSG00000136114	THSD1	protein_coding	-2,35885703	0,00016684
ENSG00000182492	BGN	protein_coding	-4,5305288	0,00017199
ENSG00000113211	PCDHB6	protein_coding	-1,4340651	0,00018387
ENSG00000139737	SLAIN1	protein_coding	-2,45950523	0,00018762
ENSG00000133069	TMCC2	protein_coding	-1,56073177	0,00019311
ENSG00000161298	ZNF382	protein_coding	-2,02552366	0,00019326
ENSG00000260317		lncRNA	-3,72987903	0,00021137
ENSG00000146955	RAB19	protein_coding	-2,106323	0,00022171
ENSG00000287979		lncRNA	-1,78366113	0,00024627
ENSG00000115825	PRKD3	protein_coding	-1,15735727	0,00024747
ENSG00000064042	LIMCH1	protein_coding	-1,44479009	0,00025254
ENSG00000164604	GPR85	protein_coding	-5,53217903	0,00028194
ENSG00000134363	FST	protein_coding	-2,6541515	0,0002923
ENSG00000270022		lncRNA	-1,99721498	0,0002923
ENSG00000171488	LRRC8C	protein_coding	-1,33002333	0,00030494
ENSG00000106366	SERPINE1	protein_coding	-2,68672297	0,00030723
ENSG00000139352	ASCL1	protein_coding	-2,78418676	0,00031794
ENSG00000287190		lncRNA	-1,4808116	0,0003276
ENSG00000053524	MCF2L2	protein_coding	-2,34106569	0,00032832
ENSG00000006210	CX3CL1	protein_coding	-2,73952257	0,00033509
ENSG00000240694	PNMA2	protein_coding	-5,31223033	0,00033604
ENSG00000280303	ERICD	lncRNA	-1,7709113	0,00034268
ENSG00000168539	CHRM1	protein_coding	-1,30229351	0,00034924
ENSG00000251410		lncRNA	-4,49690089	0,00035104
ENSG00000253361		lncRNA	-1,94448904	0,00035538
ENSG00000234737	KRT18P15	processed_pseudogene	-2,79351072	0,0003554
ENSG00000106066	CPVL	protein_coding	-5,23139459	0,00035858
ENSG00000005513	SOX8	protein_coding	-2,18204001	0,00039058
ENSG00000134013	LOXL2	protein_coding	-2,15867104	0,00039292
ENSG00000259319		lncRNA	-2,39204436	0,00040558
ENSG00000170271	FAXDC2	protein_coding	-1,55282922	0,00041412
ENSG00000053747	LAMA3	protein_coding	-1,44533633	0,00041835
ENSG00000132915	PDE6A	protein_coding	-5,7576711	0,00043435
ENSG00000197580	BCO2	protein_coding	-3,20480886	0,00044477
ENSG00000165887	ANKRD2	protein_coding	-3,3300688	0,00045163
ENSG00000071967	CYBRD1	protein_coding	-3,11240404	0,00045432
ENSG00000253771	TPTE2P1	transcribed_unprocessed pseudogene	-1,82456453	0,00045835
ENSG00000107242	PIP5K1B	protein_coding	-1,4236242	0,00046018
ENSG00000256546		lncRNA	-1,98998958	0,00046435
ENSG00000254479	SLC25A1P1	processed_pseudogene	-3,14842545	0,00046798
ENSG00000280070		TEC	-5,21196981	0,00048571
ENSG00000168143	FAM83B	protein_coding	-1,88522274	0,00051591
ENSG00000177202	SPACA4	protein_coding	-2,94376828	0,00052487
ENSG00000161031	PGLYRP2	protein_coding	-1,640506	0,00055514

ENSG00000162882	HAAO	protein_coding	-2,16821051	0,00055773
ENSG00000287925		lncRNA	-5,74573905	0,00057776
ENSG00000223749	MIR503HG	lncRNA	-1,13088247	0,00058816
ENSG00000092421	SEMA6A	protein_coding	-3,05164571	0,00059337
ENSG00000168405	CMAHP	transcribed_unitary pseudogene	-1,80453476	0,00060281
ENSG00000185046	ANKS1B	protein_coding	-1,02748812	0,0006211
ENSG00000184058	TBX1	protein_coding	-1,76537668	0,00062471
ENSG00000279878		TEC	-1,02663968	0,00064001
ENSG00000271141		lncRNA	-3,28773342	0,00064583
ENSG00000118777	ABCG2	protein_coding	-1,85773874	0,00065182
ENSG00000183844	FAM3B	protein_coding	-2,79131624	0,00065645
ENSG00000226928	RPS14P4	processed_pseudogene	-3,69099218	0,00070066
ENSG00000157654	PALM2AKAP2	protein_coding	-1,80556917	0,00070564
ENSG00000105825	TFPI2	protein_coding	-1,99582949	0,00071554
ENSG00000205592	MUC19	protein_coding	-1,78706333	0,00072074
ENSG00000198189	HSD17B11	protein_coding	-1,64158575	0,0007463
ENSG00000177108	ZDHHC22	protein_coding	-4,96209154	0,00075784
ENSG00000286381		lncRNA	-1,02672049	0,00077146
ENSG00000102385	DRP2	protein_coding	-1,91356422	0,00078291
ENSG00000168675	LDLRAD4	protein_coding	-2,59818076	0,00078718
ENSG00000153071	DAB2	protein_coding	-5,81530061	0,00078844
ENSG00000063127	SLC6A16	protein_coding	-1,25604602	0,00079914
ENSG00000287603		lncRNA	-1,15892106	0,00081192
ENSG00000099998	GGT5	protein_coding	-4,00498275	0,00085542
ENSG00000279631		TEC	-2,22427	0,0009454
ENSG00000142973	CYP4B1	protein_coding	-1,66948813	0,00105766
ENSG00000112782	CLIC5	protein_coding	-5,08118658	0,00112361
ENSG00000272168	CASC15	lncRNA	-2,00024579	0,00112703
ENSG00000154065	ANKRD29	protein_coding	-1,63467999	0,00116539
ENSG00000187550	SBK2	protein_coding	-2,09642313	0,00121865
ENSG00000169247	SH3TC2	protein_coding	-1,33289965	0,00122246
ENSG00000132692	BCAN	protein_coding	-1,25687027	0,00123602
ENSG00000159433	STARD9	protein_coding	-1,70203225	0,00123658
ENSG00000064763	FAR2	protein_coding	-1,10417884	0,00124095
ENSG00000261485	PAN3-AS1	lncRNA	-1,2851675	0,00124125
ENSG00000260025	CRIM1-DT	lncRNA	-4,87718036	0,00125849
ENSG00000115295	CLIP4	protein_coding	-1,20557795	0,00126608
ENSG00000147689	FAM83A	protein_coding	-1,64755498	0,00127133
ENSG00000241322	CDRT1	protein_coding	-1,31534987	0,00127515
ENSG00000077279	DCX	protein_coding	-4,3349876	0,00135464
ENSG00000251682		processed_pseudogene	-1,42394335	0,00136268
ENSG00000162006	MSLNL	protein_coding	-1,60820591	0,00139063
ENSG00000230550	ERLNC1	lncRNA	-2,18499709	0,00144265
ENSG00000273448		lncRNA	-1,55839835	0,0014799
ENSG00000284052		lncRNA	-5,05315929	0,00149085
ENSG00000251026	LINC02163	lncRNA	-1,21182769	0,00149528
ENSG00000280433		protein_coding	-1,08197192	0,00153928
ENSG00000085514	PILRA	protein_coding	-2,13063112	0,00158759
ENSG00000158270	COLEC12	protein_coding	-2,69261143	0,00159175
ENSG00000073792	IGF2BP2	protein_coding	-3,29459307	0,00167535
ENSG00000091428	RAPGEF4	protein_coding	-1,63114238	0,00168911
ENSG00000203706	SERTAD4-AS1	lncRNA	-3,10164325	0,00181666
ENSG00000106327	TFR2	protein_coding	-1,04606498	0,00187736
ENSG00000234224	TMEM229A	protein_coding	-3,65899128	0,00188289
ENSG00000261026		lncRNA	-1,46116064	0,00197397
ENSG00000272077		lncRNA	-1,0546736	0,0020045
ENSG00000140563	MCTP2	protein_coding	-2,64327855	0,00204505
ENSG00000146013	GFRA3	protein_coding	-4,519374	0,00204505
ENSG00000228873		lncRNA	-4,97367786	0,00210695
ENSG00000198223	CSF2RA	protein_coding	-4,42087883	0,00211001
ENSG00000086570	FAT2	protein_coding	-2,92365484	0,00211166
ENSG00000159640	ACE	protein_coding	-1,24516855	0,00211461
ENSG00000169174	PCSK9	protein_coding	-6,00449199	0,00212871
ENSG00000102057	KCND1	protein_coding	-1,59775546	0,00218008
ENSG00000223760	MED15P9	transcribed_unprocessed pseudogene	-3,26495992	0,00219385
ENSG00000204882	GPR20	protein_coding	-2,83833365	0,00219941
ENSG00000145526	CDH18	protein_coding	-2,53708189	0,00229397
ENSG00000185436	IFNLR1	protein_coding	-1,41735908	0,00231998
ENSG00000090539	CHRD	protein_coding	-1,83906936	0,00235496
ENSG00000136235	GPNMB	protein_coding	-1,38410013	0,00239586
ENSG00000184809	B3GALT5-AS1	lncRNA	-1,76532878	0,00243895
ENSG00000184226	PCDH9	protein_coding	-1,00043742	0,00248015
ENSG00000140839	CLEC18B	protein_coding	-2,07919688	0,00248732
ENSG00000154330	PGM5	protein_coding	-1,67902613	0,00257032
ENSG00000284883		unprocessed_pseudogene	-4,20726133	0,00257032
ENSG00000137441	FGFBP2	protein_coding	-5,22971974	0,00262207
ENSG00000104043	ATP8B4	protein_coding	-1,2103914	0,0026888
ENSG00000279481		TEC	-1,80632619	0,0026953
ENSG00000170049	KCNAB3	protein_coding	-1,09750448	0,00270361
ENSG00000253266		lncRNA	-1,35051342	0,00270693
ENSG00000100604	CHGA	protein_coding	-2,59617568	0,00273674
ENSG00000147573	TRIM55	protein_coding	-3,86582508	0,00275865
ENSG00000175832	ETV4	protein_coding	-1,20478462	0,00276327
ENSG00000133661	SFTPD	protein_coding	-2,72694329	0,00278219
ENSG00000268364	SMC5-DT	lncRNA	-1,05612811	0,00286256
ENSG00000064692	SNCAIP	protein_coding	-3,25030333	0,00289357
ENSG00000254453	NAV2-AS2	lncRNA	-2,96851225	0,00289726
ENSG00000228463		transcribed_processed	-1,55452616	0,00306145

		pseudogene		
ENSG00000136425	CIB2	protein_coding	-2,42216889	0,0030649
ENSG00000281357	ARRDC3-AS1	lncRNA	-1,28551685	0,00311819
ENSG00000168679	SLC16A4	protein_coding	-1,16635054	0,00312003
ENSG00000232124		lncRNA	-2,1782347	0,00312279
ENSG00000274322		protein_coding	-3,95606071	0,00313637
ENSG00000259985		lncRNA	-4,0649624	0,00315624
ENSG00000280035		TEC	-2,18828168	0,00316729
ENSG00000154277	UCHL1	protein_coding	-1,36135274	0,00325634
ENSG00000169668	BCRP2	transcribed_unprocessed pseudogene	-4,63186956	0,00328626
ENSG00000272777		lncRNA	-1,54645501	0,00329034
ENSG00000130818	ZNF426	protein_coding	-1,05213513	0,00334184
ENSG00000184368	MAP7D2	protein_coding	-2,43552698	0,00334746
ENSG00000125046	SSUH2	protein_coding	-1,41188867	0,00341405
ENSG00000281332	LINC00997	lncRNA	-1,02572869	0,00344354
ENSG00000248445	SEMA6A-AS1	lncRNA	-1,74848164	0,00350451
ENSG00000258944		lncRNA	-1,4952679	0,00353519
ENSG00000166106	ADAMTS15	protein_coding	-1,48881046	0,00358776
ENSG00000152086	TUBA3E	protein_coding	-2,62295702	0,00371095
ENSG00000158008	EXTL1	protein_coding	-2,5041562	0,00373503
ENSG00000222724	RNU2-63P	snRNA	-1,42903803	0,00377878
ENSG00000205085	FAM71F2	protein_coding	-1,03889144	0,00378083
ENSG00000270062		lncRNA	-1,93347562	0,00384099
ENSG00000270190		lncRNA	-4,4129672	0,00389729
ENSG00000152380	FAM151B	protein_coding	-1,15263034	0,00391575
ENSG00000163499	CRYBA2	protein_coding	-3,01938161	0,00397473
ENSG00000255252		lncRNA	-1,98556878	0,00406902
ENSG00000279673		TEC	-2,92637963	0,00408909
ENSG00000139344	AMDHD1	protein_coding	-2,53177228	0,00418454
ENSG00000254230		lncRNA	-2,70676944	0,00418821
ENSG00000127249	ATP13A4	protein_coding	-2,47295486	0,00420305
ENSG00000279020	C18orf15	TEC	-2,64484087	0,00439214
ENSG00000160223	ICOSLG	protein_coding	-2,66267115	0,00447244
ENSG00000267056		processed_pseudogene	-1,1078836	0,00456277
ENSG00000188050	RNF133	protein_coding	-3,52613933	0,00465296
ENSG00000170819	BFSP2	protein_coding	-5,13836231	0,00482929
ENSG00000273343		lncRNA	-1,24682302	0,00486544
ENSG00000248238	LINC02438	lncRNA	-3,0234683	0,00487455
ENSG00000167165	UGT1A6	protein_coding	-4,36207097	0,00492023
ENSG00000135318	NT5E	protein_coding	-2,34806287	0,00496792
ENSG00000112139	MDGA1	protein_coding	-1,71568607	0,00504019
ENSG00000185015	CA13	protein_coding	-1,20647689	0,00506659
ENSG00000076706	MCAM	protein_coding	-1,09162357	0,00514924
ENSG00000281501	SEPSECS-AS1	lncRNA	-1,45355394	0,00525459
ENSG00000128655	PDE11A	protein_coding	-5,59280048	0,00530295
ENSG00000144214	LYG1	protein_coding	-2,91485643	0,00540988
ENSG00000228623	ZNF883	transcribed_unprocessed pseudogene	-4,51846565	0,00544064
ENSG00000198691	ABCA4	protein_coding	-3,73087281	0,00546747
ENSG00000278952		TEC	-1,40084864	0,00552157
ENSG00000157064	NMNAT2	protein_coding	-1,39479255	0,00559527
ENSG00000271155		lncRNA	-4,80766125	0,00559527
ENSG00000270038		lncRNA	-4,49363056	0,00568795
ENSG00000243446	RN7SL284P	misc_RNA	-1,70289787	0,00569174
ENSG00000257653		lncRNA	-1,44627863	0,00587266
ENSG00000280721	LINC01943	lncRNA	-2,76935667	0,00587636
ENSG00000227359		lncRNA	-1,70199132	0,00588081
ENSG00000265158	LRRC37A7P	transcribed_processed pseudogene	-4,2352376	0,00590866
ENSG00000126970	ZC4H2	protein_coding	-2,09041016	0,00591482
ENSG00000214954	LRRC69	protein_coding	-1,2221706	0,00595236
ENSG00000232480	TGFB2-AS1	lncRNA	-4,10039091	0,0059596
ENSG00000132563	REEP2	protein_coding	-1,07189855	0,00599415
ENSG00000273489		lncRNA	-1,74447182	0,00610163
ENSG00000128422	KRT17	protein_coding	-1,3173422	0,00610607
ENSG00000255150	EID3	protein_coding	-1,08495739	0,00626622
ENSG00000229321		lncRNA	-1,44963112	0,00635495
ENSG00000241770		lncRNA	-2,16501468	0,00638423
ENSG00000164764	SBSPON	protein_coding	-4,23815522	0,00664325
ENSG00000063180	CA11	protein_coding	-1,00226736	0,00670936
ENSG00000269938		lncRNA	-1,20201555	0,00690956
ENSG00000227456	LINC00310	lncRNA	-1,56011176	0,00716259
ENSG00000177181	RIMKLA	protein_coding	-1,42520177	0,00716313
ENSG00000243986	ENO1P3	processed_pseudogene	-1,53232749	0,00718301
ENSG00000230922		lncRNA	-2,08796642	0,00736002
ENSG00000148680	HTR7	protein_coding	-2,78058823	0,00744274
ENSG00000270571		lncRNA	-2,27647177	0,00754536
ENSG00000260604		lncRNA	-1,39245864	0,00765909
ENSG00000169126	ODAD2	protein_coding	-3,43822485	0,00786956
ENSG00000158050	DUSP2	protein_coding	-1,68578803	0,00788683
ENSG00000185933	CALHM1	protein_coding	-4,50085575	0,00808385
ENSG00000261572		lncRNA	-3,52645617	0,00808605
ENSG00000250057		lncRNA	-2,8288282	0,00810663
ENSG00000101460	MAP1LC3A	protein_coding	-4,66575245	0,00814175
ENSG00000224511	LINC00365	lncRNA	-2,11675134	0,00817968
ENSG00000197576	HOXA4	protein_coding	-2,63827187	0,00822231
ENSG00000233461		lncRNA	-1,13115108	0,00829358
ENSG00000229719	MIR194-2HG	lncRNA	-1,85812945	0,00850902
ENSG00000200718	RN7SKP103	misc_RNA	-4,35450301	0,008583

ENSG00000279568		TEC	-1,49450301	0,00869815
ENSG00000169856	ONECUT1	protein_coding	-1,08368085	0,00879773
ENSG00000181433	SAGE1	protein_coding	-4,05895313	0,00882278
ENSG00000173918	C1QTNF1	protein_coding	-4,8746106	0,0088933
ENSG00000172901	LVRN	protein_coding	-1,56509601	0,00891492
ENSG00000170667	RASA4B	protein_coding	-1,28797291	0,0089461
ENSG00000151388	ADAMTS12	protein_coding	-2,3199437	0,00906259
ENSG00000165168	CYBB	protein_coding	-2,83325526	0,00962478
ENSG00000280042		TEC	-1,16818846	0,00966996
ENSG00000242578		lncRNA	-2,46108108	0,0096776
ENSG00000166535	A2ML1	protein_coding	-1,66861278	0,0098181
ENSG00000227436	FCF1P1	processed_pseudogene	-2,57661309	0,00984001
ENSG00000253598	SLC10A5	protein_coding	-1,37726627	0,00985269
ENSG00000135205	CCDC146	protein_coding	-1,98688939	0,00986473
ENSG00000244620		lncRNA	-5,85080736	0,00986473
ENSG00000013297	CLDN11	protein_coding	-3,38337988	0,00987519
ENSG00000047617	ANO2	protein_coding	-4,70560783	0,01004981
ENSG00000170835	CEL	protein_coding	-1,05713031	0,01029093
ENSG00000111335	OAS2	protein_coding	-1,26265135	0,01066325
ENSG00000273271		lncRNA	-2,48531751	0,01069241
ENSG00000197565	COL4A6	protein_coding	-2,59296417	0,01078107
ENSG00000112599	GUCA1B	protein_coding	-1,7208168	0,01098019
ENSG00000286964		lncRNA	-1,27994653	0,01120318
ENSG00000115738	ID2	protein_coding	-1,17370562	0,01140099
ENSG00000187775	DNAH17	protein_coding	-1,27743371	0,01143227
ENSG00000230928		lncRNA	-1,73896534	0,01151726
ENSG00000285994		lncRNA	-1,75249888	0,01171465
ENSG00000214336	FOXI3	protein_coding	-4,55462955	0,0117559
ENSG00000203697	CAPN8	protein_coding	-1,14388893	0,01188365
ENSG00000110799	VWF	protein_coding	-1,74837569	0,01190741
ENSG00000031081	ARHGAP31	protein_coding	-1,649269	0,01194013
ENSG00000250461		processed_pseudogene	-2,73417048	0,01194013
ENSG00000177822	TENM3-AS1	lncRNA	-1,14826505	0,01198901
ENSG00000213144		processed_pseudogene	-1,31226141	0,01213134
ENSG00000074416	MGLL	protein_coding	-1,03075141	0,0123196
ENSG00000279694		TEC	-2,25421492	0,0125442
ENSG00000062524	LTK	protein_coding	-2,29099272	0,01263794
ENSG00000274954		lncRNA	-1,47216568	0,01279958
ENSG00000137198	GMPR	protein_coding	-1,32606142	0,01284492
ENSG00000100505	TRIM9	protein_coding	-2,01308039	0,01294952
ENSG00000118523	CCN2	protein_coding	-2,13102426	0,01319161
ENSG00000166159	LRTM2	protein_coding	-3,94171195	0,0132323
ENSG00000169181	GSG1L	protein_coding	-2,68179304	0,01347536
ENSG00000197467	COL13A1	protein_coding	-4,84476073	0,01365008
ENSG00000182585	EPGN	protein_coding	-2,20264503	0,0138996
ENSG00000287390		lncRNA	-5,15476681	0,01404494
ENSG00000224388	BACE2-IT1	lncRNA	-2,1168471	0,01416055
ENSG00000138670	RASGEF1B	protein_coding	-1,61359389	0,01456571
ENSG00000180616	SSTR2	protein_coding	-1,95377262	0,01485821
ENSG00000261655		lncRNA	-2,73692316	0,01495315
ENSG00000249685		lncRNA	-1,89078573	0,01501157
ENSG00000234293	BACH1-IT3	lncRNA	-4,32695594	0,0151226
ENSG00000267452	LINC02073	lncRNA	-4,74584591	0,01525977
ENSG00000279821		TEC	-1,31481648	0,01536136
ENSG00000286042	LCAL1	lncRNA	-4,24899661	0,01540068
ENSG00000286274		lncRNA	-1,86438041	0,01545348
ENSG00000228817	BACH1-IT2	lncRNA	-1,4697492	0,01546797
ENSG00000285257		unprocessed_pseudogene	-1,22216431	0,01549618
ENSG00000188833	ENTPD8	protein_coding	-1,02035519	0,01557283
ENSG00000234769	WASH4P	unprocessed_pseudogene	-1,22981064	0,01569477
ENSG00000254574		lncRNA	-1,46390785	0,01569477
ENSG00000233690	EBAG9P1	processed_pseudogene	-4,66855253	0,01583511
ENSG00000010295	IFFO1	protein_coding	-2,17606843	0,01591835
ENSG00000235865	GSN-AS1	lncRNA	-1,43961983	0,01610397
ENSG00000125848	FLRT3	protein_coding	-2,3722138	0,01613108
ENSG00000171401	KRT13	protein_coding	-1,3304703	0,01632833
ENSG00000154198	CYP4Z2P	transcribed_unprocessed_pseudogene	-3,86147239	0,01673045
ENSG00000198939	ZFP2	protein_coding	-1,3489912	0,01714592
ENSG00000234493	RHOXF1P1	transcribed_unprocessed_pseudogene	-5,79250035	0,01722995
ENSG00000240583	AQP1	protein_coding	-2,073273	0,01763257
ENSG00000058335	RASGRF1	protein_coding	-4,81106881	0,01772505
ENSG00000231952	DPY19L1P2	unprocessed_pseudogene	-1,82222577	0,01858272
ENSG00000157510	AFAP1L1	protein_coding	-3,92986505	0,01858503
ENSG00000147378	FATE1	protein_coding	-5,05835126	0,01893555
ENSG00000242182	RN7SL745P	misc_RNA	-1,82841028	0,01900673
ENSG00000089505	CMTM1	protein_coding	-1,30788339	0,01945842
ENSG00000198074	AKR1B10	protein_coding	-1,23431143	0,0198243
ENSG00000154143	PANX3	protein_coding	-4,95460868	0,01983044
ENSG00000258655	ARHGAP5-AS1	lncRNA	-1,07510322	0,01983044
ENSG00000185031	SLC2A3P2	processed_pseudogene	-4,26745771	0,01985505
ENSG00000259556		unprocessed_pseudogene	-1,03781213	0,01995636
ENSG00000249635		lncRNA	-3,5917467	0,01997873
ENSG00000271553		lncRNA	-1,21830621	0,02031905
ENSG00000264483	MIR5008	miRNA	-4,23191031	0,02043824
ENSG00000135362	PRR5L	protein_coding	-1,51130999	0,02053684
ENSG00000286321		lncRNA	-3,91725814	0,02061509
ENSG00000271303	SRXN1	protein_coding	-1,39837966	0,02064723
ENSG00000251003	ZFPM2-AS1	lncRNA	-1,55248714	0,02066983

ENSG00000128805	ARHGAP22	protein_coding	-1,38191219	0,02077506
ENSG00000022556	NLRP2	protein_coding	-3,55713144	0,0209002
ENSG00000285868		protein_coding	-1,83427034	0,02090857
ENSG00000205022	PABPN1L	protein_coding	-1,20828985	0,02098655
ENSG00000243398	RN7SL141P	misc_RNA	-1,51417312	0,02144636
ENSG00000188649	CC2D2B	protein_coding	-1,68142251	0,02161839
ENSG00000250081		lncRNA	-3,66982665	0,02168673
ENSG00000197291	RAMP2-AS1	lncRNA	-3,87390117	0,02175009
ENSG00000113749	HRH2	protein_coding	-1,92275546	0,02180106
ENSG00000161835	TAMALIN	protein_coding	-1,06424305	0,02204419
ENSG00000186409	CCDC30	protein_coding	-1,2069501	0,0222647
ENSG00000184471	C1QTNF8	protein_coding	-2,01237527	0,0225238
ENSG00000269883		lncRNA	-4,22196233	0,0225238
ENSG00000270720		lncRNA	-4,01246412	0,0225238
ENSG00000261713	SSTR5-AS1	lncRNA	-1,52378986	0,02252946
ENSG00000111275	ALDH2	protein_coding	-1,61809657	0,02267573
ENSG00000267078		lncRNA	-1,53732511	0,02272575
ENSG00000255794	RMST	lncRNA	-3,93363978	0,02313414
ENSG00000235631	RNF148	protein_coding	-1,89768971	0,02320978
ENSG00000207092	Y_RNA	misc_RNA	-4,95662374	0,02384416
ENSG00000234323	LINC01505	lncRNA	-4,45369051	0,02426749
ENSG00000187688	TRPV2	protein_coding	-4,70574243	0,02428549
ENSG00000279954		lncRNA	-2,78436215	0,02450723
ENSG00000279013		TEC	-4,89433549	0,02522876
ENSG00000251745	RNU7-124P	snRNA	-1,61338731	0,02525896
ENSG00000070886	EPHA8	protein_coding	-3,61403351	0,02528794
ENSG00000280382		lncRNA	-2,39884089	0,02546696
ENSG00000230426	LINC01036	lncRNA	-3,64571507	0,0255472
ENSG00000286787		lncRNA	-2,01548709	0,02587444
ENSG00000279713		TEC	-1,52454747	0,02640614
ENSG00000230510	PPP5D1	transcribed_unprocessed pseudogene	-1,02754916	0,02662239
ENSG00000213145	CRIP1	protein_coding	-1,39446031	0,02671086
ENSG00000153823	PID1	protein_coding	-3,79064362	0,02677962
ENSG00000199545	RNA5SP195	rRNA_pseudogene	-1,52135742	0,02688463
ENSG00000155962	CLIC2	protein_coding	-1,11833731	0,0268989
ENSG00000225548	LINC01980	lncRNA	-2,60683852	0,0271799
ENSG00000279168		lncRNA	-2,39034384	0,02753114
ENSG00000151623	NR3C2	protein_coding	-1,46785217	0,02781113
ENSG00000224430	MKRN5P	processed_pseudogene	-1,73874777	0,02800445
ENSG00000135919	SERPINE2	protein_coding	-1,46948749	0,02809241
ENSG00000157445	CACNA2D3	protein_coding	-4,24591619	0,02832782
ENSG00000177692	DNAJC28	protein_coding	-1,24875736	0,02837269
ENSG00000170390	DCLK2	protein_coding	-2,462326	0,02950611
ENSG00000047648	ARHGAP6	protein_coding	-1,86793883	0,02979128
ENSG00000137841	PLCB2	protein_coding	-3,8792215	0,03010398
ENSG00000244607	CCDC13	protein_coding	-3,84143206	0,03012661
ENSG00000274372	LINC02804	lncRNA	-1,12628801	0,03012956
ENSG00000167617	CDC42EP5	protein_coding	-1,28834889	0,03019652
ENSG00000198513	ATL1	protein_coding	-1,17431725	0,03020248
ENSG00000129167	TPH1	protein_coding	-3,29461054	0,03046675
ENSG00000259709		lncRNA	-1,1220129	0,03058862
ENSG00000272732		lncRNA	-1,30589328	0,0306202
ENSG00000259092	TRAV30	TR_V_gene	-3,06647203	0,03082286
ENSG00000250259		lncRNA	-1,35499307	0,03083911
ENSG00000018236	CNTN1	protein_coding	-3,64117123	0,03090108
ENSG00000230847	OCLNP1	unprocessed_pseudogene	-1,56435249	0,03106577
ENSG00000259362		lncRNA	-3,39166843	0,03158822
ENSG00000279472		lncRNA	-1,06905333	0,03168193
ENSG00000249916		lncRNA	-7,20038878	0,03168315
ENSG00000152402	GUCY1A2	protein_coding	-4,11524891	0,03170564
ENSG00000205853	RFPL3S	lncRNA	-2,35149397	0,03170564
ENSG00000215493		processed_pseudogene	-4,52559376	0,03170564
ENSG00000229955		lncRNA	-1,3024488	0,03186885
ENSG00000119630	PGF	protein_coding	-1,30575702	0,03234148
ENSG00000154645	CHODL	protein_coding	-3,85321464	0,03255276
ENSG00000271862		lncRNA	-1,17630155	0,03267477
ENSG00000111405	ENDOU	protein_coding	-3,70036695	0,0330151
ENSG00000265871	MIR3174	miRNA	-1,30927347	0,03311725
ENSG00000271714		lncRNA	-4,90139237	0,03339966
ENSG00000272983		lncRNA	-1,9379824	0,03352891
ENSG00000136689	IL1RN	protein_coding	-1,53600237	0,03361156
ENSG00000231466		processed_pseudogene	-1,18085829	0,03395777
ENSG00000245526	LINC00461	lncRNA	-1,13371357	0,03552275
ENSG00000283511		transcribed_unitary pseudogene	-1,72285836	0,03603953
ENSG00000276434		lncRNA	-1,01917399	0,03621697
ENSG00000204314	PRRT1	protein_coding	-1,33329364	0,03738848
ENSG00000175820	CCDC168	protein_coding	-3,00946828	0,03740315
ENSG00000165379	LRFN5	protein_coding	-3,83685195	0,03777387
ENSG00000259495		lncRNA	-2,3839854	0,03781148
ENSG00000258620		lncRNA	-1,50302578	0,03794246
ENSG00000202119	RNU6-302P	snRNA	-4,38638579	0,03851063
ENSG00000198944	SOWAHA	protein_coding	-1,14255859	0,03852515
ENSG00000132967	HMGB1P5	transcribed_processed pseudogene	-1,02883174	0,03862993
ENSG00000215861		transcribed_unprocessed pseudogene	-1,72471369	0,03866905
ENSG00000125851	PCSK2	protein_coding	-2,11828728	0,03909785
ENSG00000238297	U3	snoRNA	-4,07489513	0,03917379

ENSG00000243289	AGAP13P	unprocessed_pseudogene	-2,18311854	0,0391792
ENSG00000225555		lncRNA	-1,22098365	0,03946378
ENSG00000285130		protein_coding	-2,11360905	0,0396731
ENSG00000253931		lncRNA	-3,68716955	0,03984312
ENSG00000165899	OTOGL	protein_coding	-3,43429909	0,0401247
ENSG00000232662	LDHBP1	processed_pseudogene	-4,0933805	0,04039237
ENSG00000100288	CHKB	protein_coding	-2,20113898	0,04046001
ENSG00000124882	EREG	protein_coding	-1,1621843	0,04046001
ENSG00000272638		lncRNA	-1,64344667	0,0405813
ENSG00000226891	LINC01359	lncRNA	-1,87471727	0,04072604
ENSG00000257894		lncRNA	-1,68977137	0,04092186
ENSG00000253307		lncRNA	-2,00927573	0,04132382
ENSG00000170482	SLC23A1	protein_coding	-1,63551629	0,04163304
ENSG00000270343	UNGP3	processed_pseudogene	-3,28889142	0,04191343
ENSG00000132958	TPTE2	protein_coding	-3,53772417	0,04201753
ENSG00000278590	RN7SL113P	misc_RNA	-3,80229183	0,04212647
ENSG00000139971	ARMH4	protein_coding	-2,35323306	0,04248578
ENSG00000171476	HOPX	protein_coding	-3,40775124	0,04255624
ENSG00000260672		lncRNA	-1,67323753	0,04270316
ENSG00000116299	ELAPOR1	protein_coding	-1,21992447	0,04288396
ENSG00000256811		lncRNA	-2,36444956	0,04296913
ENSG00000274421		lncRNA	-1,26396747	0,04296913
ENSG00000265702		lncRNA	-1,92609284	0,04341072
ENSG00000137819	PAQR5	protein_coding	-1,4336829	0,04441075
ENSG00000182511	FES	protein_coding	-1,88489782	0,04485013
ENSG00000138829	FBN2	protein_coding	-1,1651703	0,0448601
ENSG00000223023	Y_RNA	misc_RNA	-2,58366741	0,04523361
ENSG00000108771	DHX58	protein_coding	-1,20215873	0,04533346
ENSG00000101306	MYLK2	protein_coding	-1,283275	0,04538692
ENSG00000205560	CPT1B	protein_coding	-1,15683599	0,04575011
ENSG00000258661		lncRNA	-3,65578216	0,04625922
ENSG00000182782	HCAR2	protein_coding	-1,71176144	0,04667171
ENSG00000257176		lncRNA	-1,63356963	0,04670792
ENSG00000102755	FLT1	protein_coding	-3,50033568	0,04679188
ENSG00000272948		lncRNA	-2,16202298	0,04694593
ENSG00000105131	EPHX3	protein_coding	-1,110284	0,0475778
ENSG00000128298	BAIAP2L2	protein_coding	-1,0928111	0,04785275
ENSG00000179909	ZNF154	protein_coding	-3,43079704	0,04792168
ENSG00000235770	LINC00607	lncRNA	-2,21316012	0,0479956
ENSG00000173261	PLAC8L1	protein_coding	-1,18696095	0,04802604
ENSG00000279665		TEC	-1,56241088	0,0480475
ENSG00000231431	FAR2P4	transcribed_unprocessed pseudogene	-1,08199043	0,04807682
ENSG00000272682		lncRNA	-3,39133691	0,04845319
ENSG00000178852	EFCAB13	protein_coding	-1,45342418	0,04856491
ENSG00000181007	ZFP82	protein_coding	-3,37971239	0,04856884
ENSG00000271452		lncRNA	-1,06442353	0,04866751
ENSG00000228251		lncRNA	-1,36956124	0,04925365
ENSG00000128203	ASPHD2	protein_coding	-1,10772175	0,04938606
ENSG00000275393		lncRNA	-1,06538398	0,0500139
ENSG00000174099	MSRB3	protein_coding	-2,72262967	0,05012778
ENSG00000197776	KLHDC1	protein_coding	-1,44619797	0,05020912
ENSG00000212199	RNU6-127P	snRNA	-3,8530737	0,05034219
ENSG00000145040	UCN2	protein_coding	-2,0599669	0,05085185
ENSG00000146166	LGSN	protein_coding	-4,20106899	0,05107033
ENSG00000115155	OTOF	protein_coding	-2,57760014	0,05172301
ENSG00000239218	RPS20P22	transcribed_processed pseudogene	-1,8977985	0,05229738
ENSG00000198108	CHSY3	protein_coding	-2,32429476	0,05267393
ENSG00000250906		lncRNA	-1,49051511	0,0527555
ENSG00000006837	CDKL3	protein_coding	-1,05805674	0,05289942
ENSG00000234840	LINC01239	lncRNA	-3,38540523	0,05302427
ENSG00000274776		lncRNA	-1,72635634	0,05344612
ENSG00000244641	RPS26P43	processed_pseudogene	-3,79179867	0,05365196
ENSG00000106006	HOXA6	protein_coding	-1,17563355	0,05369634
ENSG00000236449		lncRNA	-1,82647407	0,05379305
ENSG00000177409	SAMD9L	protein_coding	-3,37923659	0,05451586
ENSG00000132357	CARD6	protein_coding	-1,7448487	0,05484835
ENSG00000173762	CD7	protein_coding	-3,39164511	0,0554442
ENSG00000176046	NUPR1	protein_coding	-1,11820549	0,05589136
ENSG00000273210		lncRNA	-1,92919895	0,05619807
ENSG00000213707	HMGB1P10	processed_pseudogene	-1,87549711	0,05629702
ENSG00000235558	GUSBP17	unprocessed_pseudogene	-3,5397887	0,05642387
ENSG00000068366	ACSL4	protein_coding	-1,15353254	0,0579693
ENSG00000254413	CHKB-CPT1B	protein_coding	-2,16980602	0,05853287
ENSG00000135363	LMO2	protein_coding	-1,46376835	0,05857519
ENSG00000106328	FSCN3	protein_coding	-1,96904258	0,05885892
ENSG00000233154	LINC01762	lncRNA	-3,53994509	0,0589934
ENSG00000080573	COL5A3	protein_coding	-3,04417916	0,05943631
ENSG00000228420	LINC01768	lncRNA	-2,89251115	0,05953783
ENSG00000172350	ABCG4	protein_coding	-1,29003656	0,05957686
ENSG00000196482	ESRRG	protein_coding	-1,08693074	0,05961208
ENSG00000212128	TAS2R13	protein_coding	-1,3425144	0,0600484
ENSG00000128262	POM121L9P	transcribed_unprocessed pseudogene	-3,65551252	0,06016368
ENSG00000224413		lncRNA	-3,80978049	0,06076116
ENSG00000258479	LINC00640	lncRNA	-3,65269712	0,06091575
ENSG00000236670	KRT18P5	processed_pseudogene	-1,16101155	0,06092278
ENSG00000109743	BST1	protein_coding	-3,94581519	0,06197898
ENSG00000105808	RASA4	protein_coding	-1,24081673	0,06227162

ENSG00000199627	RNU6-1010P	snRNA	-4,06358446	0,06236239
ENSG00000286681		lncRNA	-1,21032591	0,06296293
ENSG00000228887	EEF1DP1	processed_pseudogene	-1,62589218	0,06308021
ENSG00000271105	SCML2P2	processed_pseudogene	-1,73174988	0,06333192
ENSG00000167588	GPD1	protein_coding	-1,22578375	0,06339216
ENSG00000101194	SLC17A9	protein_coding	-2,04232414	0,06344755
ENSG00000224389	C4B	protein_coding	-1,79125739	0,06350875
ENSG00000259793		lncRNA	-3,88193146	0,06384571
ENSG00000101144	BMP7	protein_coding	-1,06846905	0,06394355
ENSG00000224794		lncRNA	-3,47238739	0,06422792
ENSG00000240770	C21orf91-OT1	lncRNA	-1,65255377	0,06468543
ENSG00000161132		unprocessed_pseudogene	-3,83790076	0,06560763
ENSG00000197099		lncRNA	-2,85445862	0,06574341
ENSG00000205089	CCNI2	protein_coding	-2,03943148	0,06579228
ENSG00000204539	CDSN	protein_coding	-1,61325722	0,06633611
ENSG00000278250	Metazoa_SRP	misc_RNA	-2,0706203	0,06653262
ENSG00000226496	LINC00323	lncRNA	-4,02591315	0,06693482
ENSG00000184956	MUC6	protein_coding	-1,48992031	0,06751296
ENSG00000069667	RORA	protein_coding	-1,27109955	0,06784315
ENSG00000235663	SAPCD1-AS1	lncRNA	-1,33579854	0,06818394
ENSG00000156140	ADAMTS3	protein_coding	-1,86835986	0,0683434
ENSG00000101278	RPS10P5	processed_pseudogene	-3,54236916	0,06879814
ENSG00000273174		lncRNA	-3,66718649	0,06886351
ENSG00000095596	CYP26A1	protein_coding	-1,30333969	0,06934968
ENSG00000221639		snoRNA	-1,6353662	0,06946804
ENSG00000254862	LGR4-AS1	lncRNA	-3,62853934	0,06952934
ENSG00000270557		lncRNA	-1,49253825	0,06970907
ENSG00000246898	LINC00920	lncRNA	-3,62163033	0,06974369
ENSG00000254363		lncRNA	-2,17096551	0,07050002
ENSG00000267414	SETBP1-DT	lncRNA	-1,67502936	0,07072053
ENSG00000278462		lncRNA	-2,17326368	0,07126623
ENSG00000224016		unprocessed_pseudogene	-3,85659825	0,07135452
ENSG00000182533	CAV3	protein_coding	-3,84391705	0,07157081
ENSG00000279753		TEC	-1,08460951	0,07168531
ENSG00000144158	SNRPA1P1	processed_pseudogene	-1,93491724	0,07215109
ENSG00000175985	PLEKHD1	protein_coding	-1,13765013	0,07279806
ENSG00000160179	ABCG1	protein_coding	-1,24253212	0,07294462
ENSG00000249593		lncRNA	-1,00588859	0,07334619
ENSG00000173557	FAM166C	protein_coding	-3,66035481	0,0734877
ENSG00000274191		lncRNA	-1,9335184	0,07372576
ENSG00000260896	ARLNC1	lncRNA	-2,94472653	0,07373483
ENSG00000255126		lncRNA	-2,85178978	0,07377299
ENSG00000214988	RPL7AP26	processed_pseudogene	-2,30156536	0,07449839
ENSG00000204140	CLPSL1	protein_coding	-3,58197987	0,07475595
ENSG00000138100	TRIM54	protein_coding	-2,3760174	0,07487811
ENSG00000280453		TEC	-1,12361465	0,07488062
ENSG00000188525		lncRNA	-3,88277494	0,07495666
ENSG00000241709	RN7SL265P	misc_RNA	-1,5970036	0,07501733
ENSG00000197177	ADGRA1	protein_coding	-3,72572794	0,07502516
ENSG00000204706	MAMDC2-AS1	lncRNA	-2,77879538	0,0752604
ENSG00000196119	OR8A1	protein_coding	-1,21625329	0,07545465
ENSG00000231840	TMEM139-AS1	lncRNA	-1,13558038	0,07581906
ENSG00000135472	FAIM2	protein_coding	-3,2600034	0,07589826
ENSG00000221760	MIR548J	miRNA	-3,68089347	0,07687436
ENSG00000233924	RPSAP13	processed_pseudogene	-1,02730473	0,07736074
ENSG00000166558	SLC38A8	protein_coding	-2,99714868	0,07753442
ENSG00000277911		lncRNA	-2,3261828	0,07763045
ENSG00000236095		lncRNA	-1,59095997	0,07785673
ENSG00000120664	SPART-AS1	lncRNA	-1,65229806	0,077972
ENSG00000285531		processed_pseudogene	-1,1486518	0,07862609
ENSG00000154928	EPHB1	protein_coding	-1,41467873	0,07906627
ENSG00000249057	MAST4-IT1	lncRNA	-1,94185558	0,079644
ENSG00000288045		lncRNA	-3,57270453	0,07971406
ENSG00000264572	MIR4296	miRNA	-1,12673419	0,07993866
ENSG00000286935		lncRNA	-2,70382557	0,08024448
ENSG00000272234		lncRNA	-3,66500534	0,0806511
ENSG00000182732	RGS6	protein_coding	-1,11010661	0,08080295
ENSG00000260971		lncRNA	-2,66455195	0,08094166
ENSG00000231769		lncRNA	-2,11661687	0,0812576
ENSG00000260585		lncRNA	-2,04654451	0,08140471
ENSG00000250413	SLC2A9-AS1	lncRNA	-3,65775733	0,08196137
ENSG00000259687	LINC01220	lncRNA	-1,67302029	0,08246109
ENSG00000233871	DLG5-AS1	lncRNA	-1,05724506	0,08340087
ENSG00000170476	MZB1	protein_coding	-1,54417417	0,0839931
ENSG00000283416	MIR1910	miRNA	-1,23235728	0,08442045
ENSG00000272472		lncRNA	-1,31933591	0,08484808
ENSG00000235903	CPB2-AS1	lncRNA	-1,26933792	0,08497255
ENSG00000185634	SHC4	protein_coding	-1,36199872	0,08538038
ENSG00000233297	RASA4DP	unprocessed_pseudogene	-1,68166898	0,08594391
ENSG00000259744		lncRNA	-4,08565089	0,08607738
ENSG00000237423	LINC01522	lncRNA	-1,48650621	0,0865425
ENSG00000258111		processed_pseudogene	-4,01658876	0,08710819
ENSG00000227695	DNMBP-AS1	lncRNA	-1,70076246	0,08762852
ENSG00000225292		lncRNA	-3,62154949	0,08764605
ENSG00000178809	TRIM73	protein_coding	-1,91240429	0,08817777
ENSG00000272030		lncRNA	-1,06094738	0,08896859
ENSG00000223861		processed_pseudogene	-1,01279819	0,09040639
ENSG00000197245	FAM110D	protein_coding	-3,17835994	0,09054833
ENSG00000183625	CCR3	protein_coding	-1,03514314	0,09061788
ENSG00000184588	PDE4B	protein_coding	-3,06020924	0,09084191

ENSG00000223979	SMCR2	lncRNA	-3,64331906	0,09115668
ENSG00000112981	NME5	protein_coding	-1,76823226	0,09121077
ENSG00000144642	RBMS3	protein_coding	-3,06097834	0,09127729
ENSG00000236311	TLX1NB	lncRNA	-3,814932	0,09127729
ENSG00000082126	MPP4	protein_coding	-3,26546525	0,09128334
ENSG00000286502		lncRNA	-2,24741015	0,09138038
ENSG00000272046		lncRNA	-3,0595275	0,09159587
ENSG00000261040	WFDC21P	transcribed_unitary pseudogene	-2,39744312	0,09164542
ENSG00000226963		lncRNA	-2,36804934	0,09175005
ENSG00000144868	TMEM108	protein_coding	-3,06148022	0,091816
ENSG00000228470		lncRNA	-2,65503868	0,09224381
ENSG00000166979	EVA1C	protein_coding	-3,06071869	0,09261015
ENSG00000270095		lncRNA	-1,42934635	0,09297814
ENSG00000169908	TM4SF1	protein_coding	-1,78743554	0,09305566
ENSG00000239219		lncRNA	-3,23982457	0,09315386
ENSG00000265943		lncRNA	-1,27068331	0,09319157
ENSG00000251199		lncRNA	-3,05866351	0,09355788
ENSG00000230870	FBXW11P1	processed_pseudogene	-2,32598862	0,09372092
ENSG00000113396	SLC27A6	protein_coding	-1,71464301	0,09394385
ENSG00000121318	TAS2R10	protein_coding	-3,65339343	0,09408529
ENSG00000224464	PGAM1P6	processed_pseudogene	-1,17119031	0,09416394
ENSG00000099139	PCSK5	protein_coding	-3,06106112	0,09478981
ENSG00000197816	CCDC180	protein_coding	-1,25727443	0,09498569
ENSG00000260757		lncRNA	-3,26518988	0,09498569
ENSG00000236953	ZDHHC20-IT1	lncRNA	-2,0835382	0,0949868
ENSG00000102290	PCDH11X	protein_coding	-1,81311239	0,09526704
ENSG00000259868		lncRNA	-3,38788284	0,09552876
ENSG00000260641		lncRNA	-1,20534806	0,09552876
ENSG00000226250	LINC00408	lncRNA	-3,0617392	0,09554121
ENSG00000283897		lncRNA	-1,60513259	0,09564865
ENSG00000125820	NKX2-2	protein_coding	-1,83734037	0,09607718
ENSG00000251015	SLC25A30-AS1	lncRNA	-3,41386728	0,09635524
ENSG00000136866	ZFP37	protein_coding	-3,06138628	0,09688027
ENSG00000182308	DCAF4L1	protein_coding	-1,19879788	0,0970468
ENSG00000258279	LINC00592	lncRNA	-2,51953771	0,09820387
ENSG00000178662	CSRNP3	protein_coding	-3,05720926	0,09823287
ENSG00000225882	LINC01456	lncRNA	-1,00081268	0,09823568
ENSG00000145358	DDIT4L	protein_coding	-2,27521459	0,09843597
ENSG00000253586		lncRNA	-2,1284344	0,09843597
ENSG00000253973		lncRNA	-3,3449785	0,09843865
ENSG00000249947	XBP1P1	processed_pseudogene	-1,74107187	0,09893222
ENSG00000227141		processed_pseudogene	-2,32601454	0,09900633
ENSG00000227082	LINC02798	lncRNA	-1,93366971	0,09926324
ENSG00000171954	CYP4F22	protein_coding	-1,45249687	0,09928338
ENSG00000237732	CT75	transcribed_unprocessed pseudogene	-2,03022816	0,09970453
ENSG00000140297	GCNT3	protein_coding	-3,05657856	0,09987169

Supplementary Table S 6: Genes of EMT-related proteins with increased expression in resistant CTC-ITB-01 cells.

Gene ID	Log2FC
SERPINB1	6,21686314
VIM	5,72446525
IL6	5,65550724
VCAN	5,41172434
IFI44	5,13787209
MRC2	4,72829075
CHI3L1	4,56822407
CXCL3	4,53627613
HCK	4,52651435
SLC16A7	4,48586091
TLR2	4,38973238
SRGN	4,38131575
P3H3	4,32189966
SULF1	4,23448015
PLEKHH2	4,20875396
ST3GAL6	4,18291792
INHBE	4,09966076
PDE1B	4,09924338
TNFRSF19	3,99333226
FAT4	3,80675571
CA2	3,80579195
AFF3	3,8044539
SLC5A1	3,6516574
ALDH1A1	3,53167873
PLOD2	3,5098599
SERPINE1	3,44578994
CP	3,40354582
GLIS3	3,34440564
SAA1	3,20997967
SEMA5A	3,15154848
CCDC170	3,12842956
SNTB1	3,06929166
KRT17	2,8728684
BASP1	2,84800737
SCUBE1	2,78376772
PMP22	2,73177093
TUBA1A	2,7271855
TMEM45A	2,68065858
WNT5B	2,68021865
COL12A1	2,65709711
ARTN	2,64930423
CFH	2,6091828
CLGN	2,57343081
CSF1	2,55009032
LAMC2	2,49301736
CHDH	2,47221014
IGFBP4	2,46283986
CHI3L2	2,44737485
SH3KBP1	2,43096382
GCNT3	2,38544864
ATP11C	2,37792121
CWH43	2,34925942
GULP1	2,34056442
HERC3	2,30259233
PGM2L1	2,29957033
RASGEF1B	2,28451294
CA11	2,27638066
ATP8B2	2,2623839
LGALS1	2,25555311
SLC37A2	2,22623633
PDGFRB	2,21074835
NOS1AP	2,21032692
C1orf226	2,19674718
PI3	2,18881085
TLE4	2,12284499
FMOD	2,11754538
PPM1K	2,08820072
FAM167B	2,07895779
RAI14	2,07027344
FAM83A	2,06451443
ADCY2	2,06211447
GAS1	2,051559
FOXO1	2,05078486
THBS1	2,05067483
ELMO1	2,03842872
IFIT1	2,03531161
MN1	2,03002185
BHLHE40	2,01631167
FST	2,00167172
SERPINA1	1,9829984
SFRP1	1,96469226
FRK	1,95993895
FN1	1,95444168
HLA-F	1,95084114
MIR192	1,9240444
NNMT	1,92177215
TGM2	1,91083315
LXN	1,86876535
RASGRP1	1,86822566
ZNF365	1,85683167
SNHG18	1,83186244
SLCO2A1	1,81539242
SESN3	1,80954264
SVIL	1,80715688
NKD2	1,79846959
LTF	1,79399059
PRICKLE1	1,78679366
OLFML3	1,77757394
LRRC8C	1,76606002
KCNK2	1,75450633
AGR3	1,74728631
BMERB1	1,73979233
C5AR1	1,73410997
DEPP1	1,72952296
MMP14	1,7217442
AXIN2	1,72163273
ANTXR1	1,7206203
HHIPL2	1,71248466
TBXA2R	1,69657108
ANG	1,69587368
ICAM1	1,69111998
TPBG	1,68458035
MXRA7	1,68257105
CARD6	1,6764448
AKR1C2	1,67164142
CEBPD	1,62569053
PLA2G4A	1,60811014
CYP2S1	1,601892
RDH10	1,60063272
ANK2	1,59668724
NEDD9	1,57773383
DYSF	1,5760579
SOCS3	1,5748684
PECAM1	1,5647902
PDGFC	1,56228664
APBB2	1,55368107
AKR1B1	1,54876379
MRAS	1,53746509
GSDME	1,52872845
NIBAN1	1,52608159
CAMK2B	1,51174808
FURIN	1,50521574
STEAP4	1,48414552
GLI3	1,48358709
WNT6	1,47843211
CYP4X1	1,47660552
CRABP2	1,46650603
ACTA2	1,46328091
CCDC88C	1,45793886
RAB27A	1,45474729
GADD45B	1,44710865
NAV1	1,43854706
CXCL8	1,42157254
IL20RA	1,41037091
GSTM3	1,40610336
IFI30	1,402783
HCAR1	1,38516593
JUN	1,37990971
RGS2	1,36733036
CALD1	1,36697883
ITPR1	1,34635996
NRP1	1,34408635
DCBLD2	1,33843194
IGFBP3	1,33453268
HBEGF	1,32022162
ETV4	1,31732998
MICAL1	1,30985343
CCDC80	1,30182061
FBXO32	1,29742174
ZCCHC24	1,2863481
LYN	1,2748514
DRAM1	1,2644198
EPHX4	1,25997804
MAPRE2	1,25858318
ARSJ	1,25735967
TFF1	1,24695763
WDR19	1,24601512
TTLL3	1,24595975
KAT2B	1,24406349
CYBRD1	1,2437644
RBPMS2	1,24223352
AR	1,23954668
ST6GALNAC2	1,22627498
RGL1	1,22445766
AOX1	1,21334962
GCH1	1,20946187
PDGFD	1,20549008
HIP1	1,20000294
CLDN1	1,19737738
FGF13	1,19645198
SIRPA	1,18716553
PLK2	1,1851595
MARVELD1	1,17794344
NBL1	1,17659315
DDX60	1,17127178
AHNAK2	1,1644613
PLSCR1	1,1602003
KRT6B	1,15720933
FERMT2	1,15070218
GPC4	1,14357889
CYTH1	1,14059878
CCDC88A	1,13393862
DPYSL2	1,13325074
BICD1	1,13186784
HEG1	1,13168906
LIF	1,12777832
ANXA3	1,1212862
C1S	1,1205625
BCL2	1,11592651
CYSTM1	1,11458385
PALMD	1,11441162
BICDL1	1,11170226
AZGP1	1,10962658
GASK1B	1,1077671
COL9A3	1,09086324
CFB	1,09052392
DPY19L1	1,08811481
SERPINB5	1,08314938
LRRC73	1,08229225
SPOCD1	1,08085967
CAVIN1	1,07711424
KRT6A	1,06851336
RAB40B	1,06837799
SLC25A27	1,06774615
SLC12A2	1,06243041
NPC2	1,06159931
CHN1	1,05903807
GPX8	1,0538627

SLC6A14	1,05345263
TK1	1,05174391
RINL	1,05129864
KCTD6	1,04495171
TRPC1	1,0435109
CDK14	1,04173125
PCDHB10	1,02255929
HID1	1,02173737
ALYREF	1,02125239
LMCD1	1,01847295
PDZK1IP1	1,0177488
PRR15	1,01613028
FLRT3	1,01604575
CDR2L	1,01128904
C1R	1,00725957
HGS	1,00002475

Supplementary Table S 7: Genes of EMT-related proteins with decreased expression in resistant CTC-ITB-01 cells.

Gene ID	Log2FC
LHFPL6	-9,794675571
VGLL3	-9,195536415
ARHGAP10	-8,881074389
PCDH17	-7,757812288
CLEC2B	-7,556799113
KIF13A	-7,254316223
HS3ST1	-7,048700528
THBD	-6,940611594
FAM201A	-6,021227981
ITGBL1	-5,809272945
RAC2	-5,710380233
BMP7	-5,663382699
SYK	-5,59392607
ELF5	-5,44861282
KLK6	-4,910932763
EPDR1	-4,690880024
FHL1	-4,634328262
VEGFC	-4,610247177
TRIO	-4,535104892
FAT3	-4,19234027
MIR200C	-4,178840748
EPHA4	-4,178366758
NCAM1	-3,999779275
IL1RN	-3,983132199
ADAMTS12	-3,954178777
ANKRD18A	-3,905628069
MMP9	-3,885752073
COL4A3	-3,759749893
TTLL7	-3,724371092
KRT4	-3,663211419
MIR9-3HG	-3,552226875
CCDC33	-3,38753075
MAG	-3,224093255
SDC2	-3,219315702
COL6A1	-3,207762564
HS3ST3B1	-3,202580166
HPGD	-3,187977861
TMEM158	-3,166559067
SOCS2	-3,108049287
GLB1L2	-2,777933314
ADGRG6	-2,754620822
TMPRSS4	-2,73150809
YBX3	-2,711055371
MERTK	-2,645322219
FGD2	-2,619525618
L1CAM	-2,588252396
KCNMA1	-2,587178907
SLC9A6	-2,58513238
TMPRSS11E	-2,56338807
CAPN13	-2,555779019
CAV2	-2,494241836
KLK5	-2,467418209
ABCA12	-2,457655951
PPP1R14C	-2,390591168
ADGRL2	-2,342007991
TMEM40	-2,258625691
OLFM1	-2,204805902
ANKRD22	-2,141825311
DYNC1I1	-2,131912157
SHH	-2,105790597
HES2	-2,081038688
IGF2BP3	-2,068480913
NPR3	-2,055534882
ADGRF1	-2,044870172
ADORA1	-2,030442021
BCL2A1	-2,010566451
ADCY5	-2,009539545
VGLL1	-1,963886425
FHDC1	-1,941638073
FMNL2	-1,932763525
FSTL1	-1,892700126
BDNF	-1,872693042
JCAD	-1,870261523
GPR87	-1,869456043
SKAP2	-1,840405389
CAV1	-1,83699181
SLC26A2	-1,828748507
KCNN4	-1,801754894
GPX2	-1,717999542
ADH1C	-1,709346856
HDAC9	-1,708956564
GRAMD2A	-1,708163848
UBASH3B	-1,708129916
RET	-1,704666078
ACSS1	-1,69985636
AMOTL1	-1,618373528
GPR85	-1,610931156
CA9	-1,610210433
ZNF185	-1,608402281
EMP1	-1,593068705
FANCB	-1,581496576
TXNIP	-1,580426174
PIK3CD	-1,572994013
FGFR3	-1,566624372
ARNT2	-1,553565337
LRATD2	-1,508589614
CAPG	-1,507951224
KCNB1	-1,504151962
ECM1	-1,490114624
PPARG	-1,485603455
TNFRSF14	-1,467728358
COL18A1	-1,464247343
DSC2	-1,460522929
SOX2	-1,449895941
ISG15	-1,445483051
TRIM9	-1,433988329
COL5A1	-1,41811624
ANO1	-1,405798394
CAMK2N1	-1,396932008
EGF	-1,394439993
FUT9	-1,355263165
RBM20	-1,355214478
ARRDC4	-1,335955046
SORL1	-1,333785
MDGA1	-1,32494332
GPAT3	-1,322568302
CD22	-1,320658824
TNS1	-1,303301287
CMTM3	-1,300682506
HMOX1	-1,295008899
TGFBI	-1,293881396
PDZK1	-1,289062295
B3GNT3	-1,268857001
PADI1	-1,256953172
CRISPLD2	-1,253738633
CYP4F11	-1,23011047
OBSL1	-1,223184662
PSCA	-1,20547856
CYFIP2	-1,202821677
FIBCD1	-1,200577979
KRT15	-1,192728373
IKZF2	-1,184380221
FAAH2	-1,169172838
KRT81	-1,166133599
C1QTNF6	-1,144484285
CNKSR3	-1,137146374
CAMK2D	-1,122138404
HOXB7	-1,117789363
NREP	-1,109167121
PPM1L	-1,096334706
ZNF488	-1,087155681
BNIP3	-1,08714732
LINC02693	-1,086463363
SASH1	-1,07370153
EPB41L4B	-1,072875553
CLDN23	-1,062821666
PTAFR	-1,049084265
SYTL2	-1,048089614
PPFIBP2	-1,046035688
HSD11B2	-1,043703392
PLPP3	-1,039760736
TGFA	-1,036147533
SLCO4A1	-1,033511278
ZNF239	-1,033185225
ERMP1	-1,032031067
MGLL	-1,022412231
CEBPA	-1,010548133
PRKACB	-1,005341202
SYNE1	-1,001665199

Supplementary Table S 8: Genes of EMT-related proteins with increased expression in resistant MCF7 cells.

Gene ID	Log2FC
COL3A1	11,0175849
DPYD	6,62552773
RNF128	6,47835194
CBLC	6,16956772
STEAP1	5,73897022
ADCY5	5,24193833
CA9	5,12986272
TSPAN12	5,05866752
IGFBP6	4,99850055
PEG10	4,90534405
THSD7A	4,90145347
AZGP1	4,86101917
KLK7	4,77254668
TOX3	4,73674711
ADGRF1	4,65343934
EPAS1	4,45602038
SPTLC3	4,28987443
LEF1	4,24298598
HOXB9	4,10933196
SLC2A12	4,06841408
TLE4	4,04286958
PTPRM	4,01494484
STXBP6	3,97089653
FREM1	3,90748254
OSBPL3	3,9023319
SPRY1	3,87086377
IL1R2	3,83065236
ANPEP	3,76199644
SPRR3	3,727145
PRODH	3,65182328

CREB3L1	3,65102911
NUDT11	3,63461963
EDNRA	3,61283383
KLK8	3,60312408
ANG	3,56920764
PCDH17	3,53319092
MAOA	3,49943245
CEACAM5	3,4753362
EMP1	3,46601748
ALOX15B	3,46012866
SOX9	3,45886078
MITF	3,45618161
S100P	3,45128917
LXN	3,44386975
CXCR4	3,44071003
SYBU	3,42093932
MUC1	3,41149988
TIMP3	3,40500203
DHRS2	3,33977602
RCN3	3,33359
PDE7B	3,22033788
IGFBP5	3,20941035
BMP2	3,19200568
LOXL1	3,18076495
SOX11	3,17749644
NOTUM	3,1421985
PLA2G10	3,12755181
BCAS1	3,1224511
NRP2	3,111661
FGF13	3,10398227
PDK4	3,10017794
SOX2	3,09721162
HOXB2	3,05308702
RGCC	3,02610587
KRT4	3,01329707
SPOCK1	2,95514323
CD44	2,91419103
CPEB1	2,83792522
DNAH11	2,80247932
CP	2,76316372
ADAM19	2,75222039
SCNN1A	2,74779806
ANK3	2,7024672
FUT9	2,6671354
HEY2	2,62941366
NDRG1	2,62453108
ANKRD22	2,61784333
SELENOM	2,61456212
ENOX1	2,60587335
RNF144B	2,6042724
COPZ2	2,6030609
DEPP1	2,58922687
KCNN4	2,55514766
DNER	2,53949799
IGFBP2	2,43903047
FBLN2	2,40225413
HS3ST3B1	2,39523584
KRT81	2,36623239
NTSR1	2,32754406
AQP3	2,31477585
JAM3	2,31148674
LIPH	2,29298046
SESN3	2,27644598
HS3ST1	2,26102384
TMPRSS4	2,24800858
UBE2L6	2,2388347
AFF3	2,20510624
TUBA4A	2,20319623
FUT3	2,1737425
ACKR3	2,16247991
AKR1C3	2,15734073
KLF15	2,12255318
RINL	2,11671863
SASH1	2,10715249
SLC37A2	2,06363457
KLK5	2,05885826
GLDC	2,04802462
PCED1B	2,04673761
TBXA2R	2,0461944
COL17A1	2,04382298
VTCN1	2,03741644
TGFBI	2,03158135
SAMD9	2,00646139
BDKRB2	1,98697002
CAPN13	1,9746307
C1orf116	1,97079991
BHLHE41	1,96294829
STRA6	1,96243732
PTGS1	1,9591974
FAM184A	1,95291065
KRTCAP3	1,9369288
JAG1	1,93243209
SERPINB5	1,92692289
DHRS3	1,9041789
RFTN1	1,89713286
IL1R1	1,89439989
IER3	1,89252015
INHBE	1,88629758
CEMIP	1,87681995
IL10RA	1,87362102
MLF1	1,86307228
FBXO32	1,83354585
AOX1	1,82081911
CD36	1,81156229
CEACAM1	1,79272798
BTBD11	1,79142492
OLFML3	1,75616449
LRRC15	1,74586138
RASSF4	1,73641966
CES3	1,73229893
STARD13	1,73019332
AHR	1,72897729
KHDRBS3	1,71516672
MGAT5B	1,70764706
PSCA	1,7073548
PLAGL1	1,70085742
GBP3	1,67437392
GDF15	1,67260299
PKDCC	1,67033708
ITPR1	1,66277239
HPDL	1,64877505
SCARA3	1,64819848
NAV1	1,64794938
ZNF365	1,64582552
CYSRT1	1,63594985
PPM1L	1,62286522
AMIGO2	1,61925387
PLEKHG6	1,61264214
ATP8B3	1,60437527
PRICKLE2	1,59963642
KLK6	1,59797936
ADORA1	1,59605557
BCAM	1,59328377
CDCA7L	1,59149878
AXL	1,59113647
LYN	1,58799098
NPNT	1,58779398
PCDH1	1,58415992
PPP1R14C	1,57443702
TSPAN1	1,56412148
BAMBI	1,56207679
ALDH3A1	1,53290761
SUGT1P1	1,52743977
SLC30A3	1,51585973
ARMCX6	1,51536682
GASK1B	1,50839252
RUNX2	1,49267509
RUBCNL	1,48886256
IFIH1	1,48517716
AXIN2	1,48219922
SOAT1	1,47881275
PLEKHH2	1,47339423
IKZF2	1,45523899
VWCE	1,44255757
TFEB	1,43847875
ACSM3	1,42682835
CSGALNACT1	1,42537964
COBLL1	1,42395647
PTPRH	1,41615524
CLU	1,4126557
KLC3	1,40957167
ARID5B	1,40894851
ZNF488	1,3997983
SNTA1	1,39335193
C1S	1,39280405
PGM2L1	1,39260141
ALDH3B1	1,38614514
FILIP1L	1,38498238
WWOX	1,37890183
TPM2	1,37385763
IFI35	1,36414429
ERP27	1,35797445
TOB1	1,35375306
AP1S2	1,34727843
ARHGAP4	1,33469557
PADI2	1,32986202
FN1	1,31988582
ANXA9	1,31848266
DKK1	1,31254307
TNS3	1,31068989
KCNG1	1,30953154
SEMA5A	1,30552311
CTHRC1	1,3054692
VAV3	1,29774372
CCDC33	1,29761116
PPFIBP2	1,2969057
CAVIN1	1,29412369
RFLNB	1,28886551
ID4	1,28785559
MR1	1,28673108
SLC16A7	1,28510701
C1RL	1,28469217
COTL1	1,28442347
PPP1R3B	1,2813119
VDR	1,27964747
MAF	1,26741885
CYP1B1	1,26712262
NR2F2	1,2585668
SEC14L2	1,25169443
ABCA1	1,24803268
GAD1	1,24255034
FAM171B	1,2332051
FAM174B	1,22614701
GPC6	1,21296845
FZD4	1,20956407
GUCY1B1	1,20488686
PRSS22	1,19286569
APBB1	1,19207444
PPARG	1,181988
B3GNT3	1,18092596
ACSL1	1,17703723
BCL6	1,17513065
HOXC10	1,1734915
EPB41L4A	1,17297135
ELF3	1,16338939
GPR68	1,15705302
HTRA1	1,15669728
KLF5	1,15615834
MTUS1	1,15407532
GALM	1,15228861
CRABP2	1,14990464
RASGRP1	1,14915823
CDC42EP1	1,14791465
TWSG1	1,14574121
COMTD1	1,14527086

SULF1	1,14371971
TRAK1	1,13909341
AGR2	1,13876161
C1R	1,1380651
CCDC170	1,13300837
SVIL	1,12765118
SQOR	1,11602222
PLPP2	1,113274
CLMN	1,10845828
MPZL2	1,10708224
CEACAM6	1,10247147
LRATD1	1,0979631
RAP1GAP	1,09551923
ADGRA2	1,09369202
DIXDC1	1,0918497
BCAR3	1,08549781
STC2	1,08449181
ARHGDIB	1,08004945
HILPDA	1,07846792
GSTA4	1,07089344
CLGN	1,0669875
SEPTIN6	1,0667324
LAMC1	1,05345903
SNHG18	1,05139843
ARTN	1,04936858
VAV1	1,04128241
MCEE	1,03825885
RNF39	1,03187243
CAMK2D	1,03085064
MPP7	1,02904398
ATP8B1	1,02290469
PDGFC	1,00886327
GABARAPL1	1,00722597
DAPK2	1,00289078
NQO1	1,00090991

Supplementary Table S 9: Genes of EMT-related proteins with decreased expression in resistant MCF7 cells.

Gene ID	Log2FC
AARD	-7,39663858
LAMB1	-7,12197365
PCSK9	-6,00449199
WNT5B	-5,97709402
DAB2	-5,81530061
PLAT	-5,74461278
GPR85	-5,53217903
PTHLH	-5,46621635
CHN1	-5,31769099
PNMA2	-5,31223033
BCL2	-5,26014312
DLC1	-4,98396746
ADGRL2	-4,96470736
COL13A1	-4,84476073
RASGRF1	-4,81106881
TRPV2	-4,70574243
BGN	-4,5305288
COL14A1	-4,49653965
CALB2	-4,40632416
ITGA6	-4,0118372
GGT5	-4,00498275
PROS1	-3,9679299
SHH	-3,95439075
SLC26A2	-3,94337527
IL24	-3,92418753
ADAMTS6	-3,89105008
PLCB2	-3,8792215
WNT6	-3,87518144
ANKRD1	-3,84887062
PID1	-3,79064362
SLC7A8	-3,77071656
TUBA1A	-3,74579634
ENDOU	-3,70036695
ADAMTS1	-3,50759073
FLT1	-3,50033568
TGFB2	-3,49709192
ITM2A	-3,38899695
CLDN11	-3,38337988
AFAP1L2	-3,38268187
SAMD9L	-3,37923659
SMARCA1	-3,33717579
FERMT2	-3,27629886
CSF1R	-3,23854133
S100A14	-3,22684478
S100A8	-3,20618279
PTGR1	-3,17093702
TLR2	-3,13125182
GNB4	-3,11774718
CALCR	-3,11284084
CYBRD1	-3,11240404
RHOBTB3	-3,0858946
COL12A1	-3,08050323
RBMS3	-3,06097834
EVA1C	-3,06071869
GCNT3	-3,05657856
COL5A3	-3,04417916
TMEM40	-3,0104973
ENPP5	-2,98708438
COL5A1	-2,97401704
PTPN21	-2,96468691
CAMK2B	-2,94563167
CYP27B1	-2,93088489
FAT2	-2,92365484
PLEK2	-2,91634285
LOX	-2,90943733
TRAF1	-2,90940856
CALD1	-2,88989779
PDLIM3	-2,87352968
TP63	-2,84182129
LOXL4	-2,83094498
HEG1	-2,83092211
PKIA	-2,80841209
GJB3	-2,77607902
SECTM1	-2,74123478
MSRB3	-2,72262967
WIPF1	-2,71314771
FAM83F	-2,69575783
COLEC12	-2,69261143
SERPINE1	-2,68672297
CLDN1	-2,68094747
FST	-2,6541515
PRKAR2B	-2,61188983
STEAP4	-2,60600865
SNTB1	-2,58222725
ABLIM1	-2,57756303
CFL2	-2,57332918
MMP13	-2,54070269
CLIC4	-2,53783098
IL17RE	-2,49896315
CHST3	-2,47891447
FOXD1	-2,43836379
C5	-2,43678801
ANTXR1	-2,40553837
ANXA3	-2,38702177
CHST11	-2,38054788
FLRT3	-2,3722138
PDZK1	-2,36519225
AREG	-2,36246849
NT5E	-2,34806287
ADAMTS12	-2,3199437
DDIT4L	-2,27521459
ASS1	-2,26102176
SYK	-2,26085402
ARHGEF6	-2,23613454
ETNK2	-2,22507383
ARHGAP29	-2,2129676
F2RL1	-2,19577271
SLC1A4	-2,18345814
IFFO1	-2,17606843
PRKD1	-2,16944729
NMU	-2,16400109
ARNTL2	-2,16102474
LOXL2	-2,15867104
PAK6	-2,14957934
EFEMP1	-2,13675289
CCN2	-2,13102426
S100A4	-2,11185702
TACC1	-2,09313719
PROCR	-2,05070531
SLC17A9	-2,04232414
PODXL	-2,02796232
TRIM9	-2,01308039
GJB2	-1,99959008
TFPI2	-1,99582949
SOBP	-1,99274117
CD302	-1,98730379
METTL7A	-1,9760744
PTCH1	-1,9746419
MYB	-1,96963916
F3	-1,96861729
CNTNAP2	-1,96782327
S100A9	-1,95994213
GLI3	-1,94955291
CLIC3	-1,94825486
DNAJC6	-1,93825518
PDLIM2	-1,93700025
ITGA2	-1,921673
CMTM8	-1,91786131
EPB41L2	-1,90718991
ABCA12	-1,90677359
FURIN	-1,9063586
GRB10	-1,90561815
FAM83B	-1,88522274
MSX2	-1,87966306
S100A16	-1,87004155
TSPAN5	-1,86860342
HHIPL2	-1,85080682
PLK2	-1,83947971
JDP2	-1,82164494
PALM2AKAP2	-1,80556917
SAMD12	-1,79728435
GALNT7	-1,77517382
DOK7	-1,75259115
CARD6	-1,7448487
RUNDC3B	-1,73957364
MDGA1	-1,71568607
FGFR1	-1,65160009
FAM83A	-1,64755498
HSD17B11	-1,64158575
APBB2	-1,63370528
RASGEF1B	-1,61359389
FAT4	-1,60311148
ARNT2	-1,58857737
PLEKHG3	-1,57026251
PAPSS2	-1,56990202
PTAFR	-1,56257618
ST8SIA4	-1,55459977
FAM171A1	-1,54176876
IL1RN	-1,53600237
ANXA6	-1,52823226
SERPINE2	-1,46948749
BASP1	-1,46941004
LMO2	-1,46376835
GPAT3	-1,44612342
LAMA3	-1,44533633
LIMCH1	-1,44479009
LAT2	-1,43886493
DSC2	-1,43421778
RIMKLA	-1,42520177
SULT2B1	-1,4215135
EPHB1	-1,41467873

CEMIP2	-1,41217399
GPX8	-1,41176017
SMOX	-1,39667427
BMP4	-1,37151343
UCHL1	-1,36135274
OVOL2	-1,3523198
RNFT2	-1,34445402
DUBR	-1,34186242
FAM13A	-1,33431196
COL16A1	-1,3334633
SH3TC2	-1,33289965
NEK9	-1,33175645
PAM	-1,33043954
LRRC8C	-1,33002333
GMPR	-1,32606142
TGFB1	-1,32405475
KRT17	-1,3173422
CRISPLD2	-1,31679037
CAPRIN2	-1,30904337
MAP1B	-1,29906262
ZDHHC11	-1,29180912
C5AR1	-1,28985766
SLC27A2	-1,28982726
PPTC7	-1,28719243
ADGRF4	-1,27795225
CADM1	-1,26769312
OAS2	-1,26265135
SLC6A16	-1,25604602
ABCG1	-1,24253212
DAB2IP	-1,24059239
FZD8	-1,23710169
PLEKHH1	-1,23642572
AKR1B10	-1,23431143
PDGFB	-1,23410262
PKIB	-1,23227918
ARHGEF2	-1,23162922
ABCC3	-1,22536235
BICDL1	-1,2208223
CLIP4	-1,20557795
ETV4	-1,20478462
OAS3	-1,20255351
SGCB	-1,20157347
MAGEE1	-1,19598114
CTDSPL	-1,19410072
MRPS6	-1,19195177

NSFL1C	-1,19113685
CBR1	-1,18567386
ID2	-1,17370562
FBN2	-1,1651703
EREG	-1,1621843
AHNAK	-1,15994439
EEF1AKMT1	-1,15907623
ACSL4	-1,15353254
MERTK	-1,15205731
MAPK13	-1,14198459
MRC2	-1,14153145
PKD2	-1,13919449
PPARA	-1,12242809
MFSD6	-1,11931591
RAPGEF5	-1,10742863
SLC9A6	-1,10556095
TRIB3	-1,10087343
MCAM	-1,09162357
EID3	-1,08495739
NXN	-1,07857874
GSN	-1,07780701
BMP7	-1,06846905
GNB5	-1,06285294
ITGB5	-1,05210222
PMEPA1	-1,04335552
MGLL	-1,03075141
NRSN2	-1,03006479
PIK3R1	-1,02806629
RBM24	-1,02295156
ENTPD8	-1,02035519
CELSR1	-1,01859671
RAPGEFL1	-1,01800572
PAQR3	-1,0159005
CRIP2	-1,01529379
COL18A1	-1,01459625
FSTL3	-1,00554105
CA11	-1,00226736

Supplementary Table S 10: Genes encoding kinases with increased expression in resistant CTC-ITB-01 cells.

Gene ID	Log2FC
HCK	4.52651435
EphA6	3.17134183
PIK3C2G	2.6859474
PDGFRB	2.21074835
DCLK1	2.06167815
TNIK	2.05820768
FRK	1.95993895
LRRK2	1.94763577
CAMK1D	1.74935123
DIPK2A	1.70068295
CAMK2B	1.51174808
MAST1	1.48970885
BMPR1B	1.32737032
SGK1	1.31537077
LYN	1.2748514
PIP5K1B	1.25347052
MAP3K3	1.24860977
PLK2	1.1851595
NIM1K	1.14885529
PXK	1.12241029
GASK1B	1.1077671
BRSK1	1.05769753
TK1	1.05174391
CDK14	1.04173125
GRK3	1.01262906

Supplementary Table S 11: Genes encoding kinases with increased expression in resistant MCF7 cells.

Gene ID	Log2FC
MYO3B	4.55250864
BMPR1B	3.56934613
PDK4	3.10017794
GRK1	2.82378829
EphA7	2.66702439
PIK3C2G	2.15798159
PRKG1	2.12077144
CDK6	2.05033917
ERBB4	1.97926814
BLK	1.97518717
NIM1K	1.811804
PKDCC	1.67033708
HK2	1.63671716
AXL	1.59113647
LYN	1.58799098
GASK1B	1.50839252
DCLK1	1.19622412
JAK3	1.13467673
BRSK1	1.10746607
NME4	1.08741861
CDKL5	1.07720953
LRRK2	1.05934608
CAMK2D	1.03085064
DAPK2	1.00289078
SGK3	1.06592686
STK32A	4.10310085
TESK2	1.50847543
TPK1	2.1665378
TTBK1	1.04337166
TTBK2	1.03916115

Abbreviations

°C	Degree Celsius
%	Percent
µL	Microliter
ABC	ATP-binding casette
AI	Aromatase inhibitor
AJCC	American Joint Comittee
Alp	Alpelisib
AML	Accute myeloid leucemia
APC	Allophycocyanin
APS	Ammoniumpersulfat
ATP	Adenosine triphosphate
BC	Breast cancer
BCA	Bicinchoninic acid
bp	Base-pair
BSA	Bovine serum albumin
CAM	Cell adhesion molecule
CCK-8	Cell Counting Kit - 8
CDK4/6i	CDK4/6 inhibitor
cDNA	Complementary DNA
CFA	Colony formation assay
cfRNA	Cell-free RNA
circRNA	Circular RNA
cm^2	Square centimeter
Cq	Quantification cycle
CSCs	Cancer stem cells
CTCs	Circulating tumor cells
ctDNA	Circulating tumor DNA
DAPI	4',6-diamidino-2-phenylindole
ddH_2O	Double distilled water
DEG	Differentially expressed gene
DMSO	Dimethyl sulfoxide
DoRothEA	Discriminant regulon expression analysis
DTT	Dithiothreitol
ECM	Extracellular matrix
EDTA	ethylenediaminetetraacetic acid
EGF	Epidermal growth factor
EMT	Epithelial-mesenchymal-transition
ER	Estrogen receptor
EV	Extracellular vesicle
FCS	Fetal calf serum

FDA	Food and Drug Administration
FDR	False discovery rate
FGF	Fibroblast growth factor
FITC	Fluorescein isothiocyanate
Fulv	Fulvestrant
GnRH	Gonadotropin-releasing hormone Agonist
GO	Gene Ontology
GO BP	Gene ontology biological process
GPCR	G-protein coupled receptor
h	Hours
HR+	Hormone receptor-positive
HUVEC	Human umbilical vein endothelial cells
IC50	concentration of an inhibitor where the response is reduced by half
IDC	Invasive ductal carcinoma
IF	Immunofluorescence
IGF	Insulin growth factor
ILC	Invasive lobular carcinoma
ISH	*In-situ* hybridization
lncRNA	long non-coding RNA
log2FC	log2-fold change
mBC	metastatic breast cancer
MET	Mesenchymal-epithelial-transition
min	Minutes
miR	microRNA
miRNA	microRNA
MISH	miRNA *in situ* hybridization
mL	Mililiter
mM	Milimolar
mRNA	Messenger RNA
MSigDB	Molecular signature database
MTT	3-(4,5-dimethylthiazol-2-yl)-2,5-diphenyltetrazolium bromide
ncRNA	non-coding RNA
NES	Normamlized enrichment score
ng	Nanogramm
NGS	Next generation sequencing
nm	Nanometer
NSCLC	Non-small cell lung cancer
ORA	Over representation analysis
OS	Overall survival
PAGE	Polyacrylamide protein electrophoresis
par	Parental
PARP	Poly-ADP-ribosyl polymerase

PBS	Phosphate buffered saline
PCA	Prinicipal component analysis
PDX	Patient derived xenograft
PE	Phycoerythrin
PerCP	Peridinin Chlorophyll
PFA	Paraformaldehyde
PFS	Progression free survival
PI	Propidium iodide
pM	Picomolar
PMSF	Phenylmethylsulfonyl fluoride
PR	Progesterone receptor
PVDF	Polyvinylidendifluoride
qPCR	Quantitaive polymerase chain reaction
res	Resistant
Ribo	Ribociclib
RNA	Ribonucleic acid
RNA-seq	RNA-sequencing
rpm	Rounds per minute
RT	Room temperature
SDS	Sodium dodecyl sulfate
SDS	Sodium dodecyl sulfate
sec	Seconds
SERD	Selective estrogen receptor degrader
SERM	Selective estrogen receptor modulator
TBS-T	Tris buffered saline and Tween
TEMED	N,N,N',N'-Tetramethyl ethylenediamine
TF	transcription factor
TNBC	Triple negative breast cancer
UKE	University Medical Center Hamburg-Eppendorf
v/v	Volume per volume
v/v	Volt
vs	versus
w/v	Weight per volume
WST	Water-soluble tetrazolium
x g	Times gravity
XTT	(2,3-Bis-(2-Methoxy-4-Nitro-5-Sulfophenyl)-2H-Tetrazolium-5-Carboxanilide)

Gene	Description
AARD	Alanine and arginine rich domain containing protein
ABCA	ATP binding cassette subfamily A
ABCB	ATP binding cassette subfamily B
ABCC	ATP binding cassette subfamily C
ABCG	ATP binding cassette subfamily G
ABL	ABL proto-oncogene 1, non-receptor tyrosine kinase
ACAT1	Acetyl-CoA acetyltransferase 1
AKT	AKT Serine/Threonine Kinase 1
ALDH1	Aldehyde dehydrogenase 1 family member A1
AR	Androgen receptor
ARFIP2	ADP ribosylation factor interacting protein 2
ARHGAP10	Rho GTPase activating protein 10
ATP6V0A2	ATPase H+ transporting V0 subunit A2
AXIN2	Axin 2
AXL	AXL receptor tyrosine kinase
BCL2	BCL2 Apoptosis Regulator
BCR	Breakpoint cluster region protein
BRCA1/2	Breast cancer genes 1/2
BRSK1	BR serine/threonine kinase 1
C16orf87	Chromosome 16 open reading frame 87
CALD1	Caldesmon 1
CBLC	Cbl proto-oncogene C
CCND1	Cyclin D1
CCND3	Cyclin D3
CCNE1	Cyclin E1
CCNE2	Cyclin E2
CD24	Cluster of differentiation 24
CD44	Cluster of differentiation 44
CD45	Cluster of differentiation 45
CDH1	E-Cadherin
CDH2	N-Cadherin
CDK2	Cyclin dependent kinase 2
CDK4/6	Cyclin dependent kinases 4 and 6
CDK6	Cyclin dependent kinase 6
CDKN1A	Cyclin dependent kinase inhibitor 2A
CDKN2A	Cyclin dependent kinase inhibitor 2A
CDKN2B	Cyclin dependent kinase inhibitor 2B
CEP170	Centrosomal protein 170
CHMP4A	Charged multivesicular body protein 4A
CLDN1	Claudin 1
CLEC2B	C-Type lectin domain family 2 member B

COL18A1	Collagen type XVIII alpha 1 chain
COL3A1	Collagen type III alpha 1 chain
COSMIC	Catalogue of somatic mutations in cancer
CXCR4	C-X-C Motif Chemokine Receptor 4
DAB2	DAB adaptor protein 2
DCLK1	Doublecortin like kinase 1
DLC1	DLC1 Rho GTPase Activating Protein
DNAH3	Dynein axonemal heavy chain 3
DPYD	Dihydropyrimidine dehydrogenase
EpCAM	Epithelial cell adhesion molecule
ERBB	HER2
ESR1	Estrogen receptor
FAT1	FAT atypical cadherin 1
FGFR	Fibroblast growth factor receptor
FN1	Fibronectin
FOXO3	Forkhead box O3
FZD4	Frizzled class receptor 4
GASK1B	Golgi associated kinase 1B
GLCE	Glucuronic acid epimerase
GPC4	Glypican 4
GPC6	Glypican 6
GRHL2	Grainyhead like transcription factor 2
GUF1	GTP binding elongation factor GUF1
HNRNPA1	Heterogeneous nuclear ribonucleoprotein A1
HNRNPH2	Heterogeneous nuclear ribonucleoprotein H2
HOXB-AS1	HOXB cluster antisense RNA 1
HS6ST3	Heparan sulfate 6-O-sulfotransferase 3
ICAM1	Intercellular adhesion molecule 1
IFI44	Interferon induced protein 44
IGFR1	Insulin like growth factor 1
IL6	Interleukin 6
JUN	Jun proto-oncogene, AP-1 transcription factor subunit
KRT15	Keratin 15
KRT17	Keratin 17
KRT4	Keratin 4
L1CAM	L1 cell adhesion molecule
LAMB1	Laminin subunit beta 1
LHFPL6	LHFPL tetraspan subfamily member 6
LRRK2	Leucine rich repeat kinase 2
LYN	LYN proto-oncogene, Src family tyrosine kinase
MAP3K5	Mitogen-activated protein kinase 5
ME2	Malic enzyme 2

MICALL1	MICAL like 1
MMP3/9	Matrix metallopeptidase 3/9
MT-ND5	Mitochondrially encoded NADH:Ubiquinone oxidoreductase core subunit 5
mTOR	Mechanistic target of rapamycin kinase
MUC1	Mucin 1
MUC13	Mucin 13
NF1	Neurofibromin 1
NFKB1	Nuclear factor kappa B subunit 1
NIM1K	NIM1 serine/threonine protein kinase
NOTCH3	Notch receptor 3
OVOL2	Ovo Like Zinc Finger 2
PCDH17	Protocadherin 17
PECAM	Platelet and endothelial cell adhesion molecule 1
PEG10	Paternally Expressed 10
PI3K	Phosphatidylinositol-3-kinase
PI3KC2G	Phosphatidylinositol-4-phosphate 3-kinase catalytic subunit type 2 gamma
PI3KCA	Phosphatidylinositol-3-kinase α
PJA2	Praja ring finger ubiquitin ligase 2
PLEKHH3	Pleckstrin Hhomology, MyTH4 and FERM domain containing H3
PLK1	Polo-like kinase 1
PLK4	Polo like kinase 4
PRR11	Proline rich 11
PRRX1	Paired Related Homeobox 1
PSCK9	Proprotein convertase subtilisin/kexin type 9
PTEN	Phosphatase And Tensin Homolog
PTEN	Phosphatase And Tensin Homolog
RAD51C	RAD51 paralog C
RB1	Retinoblastoma protein
RELA	RELA proto-oncogene, NF-KB subunit
RELB	RELB proto-oncogene, NF-KB subunit
RNF128	Ring finger protein 128
RUNX2	RUNX family transcription factor 2
SALL4	Sal-like protein 4
SAMD11	Sterile alpha motif domain containing 11
SCNN1A	Sodium Channel Epithelial 1 Subunit Alpha
SERPINB1	Serpin family B member 1
SNAI1	Snail Family Transcriptional Repressor 1
SNAI2	Snail Family Transcriptional Repressor 2
SORL1	Sortilin related receptor 1
SOX2	SRY-box transcription factor 2
SOX9	SRY-box transcription factor 9
STEAP1	STEAP family member 1

TCGA	The cancer genome atlas
TGFBR	TGF-beta receptor 1
TGFBR	TGF-beta receptor 2
TIMM17A	Translocase of inner mitochondrial membrane 17A
TK1	Thymidine kinase 1
TLNRD1	Talin rod domain containing 1
TUBA1A	Tubulin alpha 1a
TWIST	Twist Family BHLH Transcription Factor 1
UHRF1BP1L	UHRF1 binding protein 1 like
VCAM1	Vascular cell adhesion molecule 1
VCAN	Versican
VGLL3	Vestigial like family member 3
VIM	Vimentin
VWDE	Von willebrand factor D and EGF domains
WNT5B	WNT family member 5B
XIST	X Inactive Specific Transcript
ZEB1	Zinc Finger E-Box Binding Homeobox 1
ZNF654	Zinc finger protein 654
ZNF671	Zinc finger protein 671
ZSCAN31	Zinc finger and SCAN domain containing 31

Table of figures

List of tables

List of supplementary material

Danksagung

An dieser Stelle möchte ich die Gelegenheit nutzen und allen Beteiligten danken, die diese Arbeit möglich gemacht und mich auf meinem Weg hierher begleitet haben.

An erster Stelle bedanke ich mich bei Herrn Prof. Dr. Klaus Pantel, Direktor des Instituts für Tumorbiologie, für die Überlassung des Themas und die Möglichkeit, die Doktorarbeit im Institut für Tumorbiologie anfertigen zu können. Besonders danke ich ihm für seine kontinuierliche Unterstützung, wertvolle fachliche Hinweise sowie für anregende wissenschaftliche Diskussionen. Des Weiteren möchte ich mich dafür bedanken, dass ich einen Teil meiner Zeit als Doktorandin am MDAnderson Cancer Center in Houston verbringen durfte. Diese Zeit war trotz der Corona-bedingten Einschränkungen für mich sehr prägend, und die Zusammenarbeit mit Prof. Dr. George Calin hat meinen wissenschaftlichen Horizont außerordentlich erweitert.

Des Weiteren möchte ich mich bei meiner Betreuerin Prof. Dr. Sabine Riethdorf bedanken, die mir dieses hoch-interessante, aktuelle und vielfältige Promotionsprojekt zur Verfügung gestellt hat. Dabei stand Sie mir jederzeit mit wissenschaftlichem Rat, neuen Ideen und Motivation zur Seite. Hab vielen Dank für die vielen wissenschaftlichen Diskussionen sowie die immer konstruktive und inspirierende, aber auch entspannte Arbeitsatmosphäre.

Ein großer Dank geht auch an Frau Prof. Dr. Julia Kehr, die sich freundlicherweise dazu bereit erklärt hat, als Zweitgutachterin für diese Arbeit zu fungieren. Herzlichen Dank richte ich auch an alle Mitglieder meiner Prüfungskommission, Frau Prof. Dr. Julia Kehr, Herrn Prof. Dr. Tim Gilberger, Herrn Prof. Dr. Klaus Pantel und Frau Prof. Dr. Sabine Riethdorf, die sich freundlicherweise umgehend dazu bereit erklärt haben, Mitglied meiner Prüfungskommission zu sein.

Weiterhin möchte ich mich ganz herzlich bei Dr. Malik Alawi, Leiter der Core Facility Bioinformatik am UKE, für die außerordentlich kompetente Unterstützung bei der Auswertung meiner RNA-Sequenzierungs-Daten sowie die vielen anregenden Diskussionen und die wertvollen Ideen bedanken.

Mein Dank gilt des Weiteren Prof. Dr. Volkmar Müller und Dr. Elena Laakmann, Klinik für Gynäkologie im UKE für die freundliche Zusammenarbeit sowie die Organisation und die Bereitstellung der Blutproben und klinischen Informationen.

Des Weiteren möchte ich mich ganz herzlich bei Prof. Dr. Andreas Trumpp und seinem Team (HiStem/DKFZ Heidelberg) sowie Prof. Dr. Andreas Schneeweiss, Prof. Dr. Markus Wallwiener, Dr. Laura Michel, Dr. Verena Thewes, Dr. Thomas M. Deutsch und Dr. Hannah Clemente (Universitätsklinikum Heidelberg) für die Bereitstellung von Blutproben und klinischen Informationen bedanken.

An dieser Stelle möchte ich auch ein herzliches Dankeschön an alle Patientinnen, die der Blutentnahme und -bearbeitung zu Studienzwecken zugestimmt haben, richten.
Danke an alle Mitglieder des DETECT-Konsortiums, es hat mir große Freude bereitet, Teil eines solches multizentrischen Projektes zu sein. Mein großer Dank gilt der Stiftung Deutsche Krebshilfe, die meine Doktorarbeit im Rahmen eines Verbundprojektes finanziell unterstützt hat.

Yuanyuan Wang und Dr. Christian Gorzelanny (Klinik für Dermatologie und Venerologie, UKE) danke ich herzlich für die Durchführung der Bioflux-Experimente.

Herzlich bedanken möchte ich mich auch bei Malgorzata, Conny, Antje und Sonja. Ihr habt mich nicht nur tatkräftig bei der Laborarbeit und bei technischen Fragen im Labor unterstützt, sondern habt ganz wesentlich zu der schönen Zeit meiner Doktorarbeit beigetragen, ob mit netten Gesprächen, Naschis oder Kanufahren.

Ein besonderer Dank geht an die ITB „girls und boys", Sonja, Johanna, Katharina, Svenja, Pari, Lucija, Ines, Sebastian, Yassine und Thomas. Auch wenn sich manche Wege kurz nach meinem Start im ITB wieder getrennt haben, habt ihr meine Zeit dort ganz wesentlich geprägt und unvergessen gemacht. Ganz besonders danke ich Sonja, mit der ich lange Zeit den wissenschaftlichen Nachwuchs in der AG Riethdorf bilden durfte. Ich danke Dir für deine stetige Diskussionsbereitschaft, die Sonnenpausen, die guten Ratschläge und die vielen lustigen Gespräche.

Ebenso danke ich all den großartigen Menschen, mit denen ich das Büro teilen durfte, ihr habt mitgeholfen, meinen Arbeitsplatz zu einem tollen Ort zu machen. Besonders hervorheben möchte ich Laura, mit der ich am gleichen Tag dort „eingezogen" bin. Du hast mich nicht nur immer wissenschaftlich unterstützt, wenn ich wieder Rat suchend zu Dir kam, sondern hast mir auch einige der lustigsten und schönsten Momente in den 4 gemeinsamen Jahren am ITB geschenkt. Merci beaucoup.

Vielen Dank auch an meinen Lieblingshamster und der Schickse, die immer ein offenes Ohr für mich hatten und mich aufgebaut und mit Kaffeepausen und rosigen Abenden über die Runden gebracht haben.

Ein Riesendank gilt meinen Eltern, die mir schon immer jeglichen Raum zur Selbstentfaltung gegeben und mich auf meinem Weg zu einer wissenschaftlichen Karriere unterstützt haben. Dank Euch konnte ich meinen Wunsch in Hamburg zu studieren verwirklichen und auch während der Promotion konnte ich jederzeit auf eure Unterstützung und Eure motivierenden Worte bauen. Auch wenn ich Euch viel zu selten gesehen habe, war es immer wahnsinnig lustig und erholsam, wenn wir mal Zeit zusammen hatten. Auch meinem Bruder Maximilian bin ich für seine immerwährende Unterstützung, den Austausch lustiger reels und schöne Besuche in Hamburg und Köln ein großes Dankeschön schuldig.

Abschließend möchte ich mich natürlich bei Marvin bedanken. Seit dem Lateinunterricht bei Ulf gehen wir durch dick und dünn und Du hast mich auch während meiner Promotion stets unterstützt. Selbst in schlechten Zeiten hast Du mich dauernd zum Lachen gebracht, immer für gute Stimmung gesorgt, und dafür, dass ich die Arbeit auch mal hinter mir lassen konnte. (:p)

Eidesstattliche Versicherung

Eidesstattliche Versicherung Hiermit erkläre ich an Eides statt, dass ich die vorliegende Dissertationsschrift selbst verfasst und keine anderen als die angegebenen Quellen und Hilfsmittel benutzt habe.

Hamburg, 27. März 2022

Leonie Florence Ott